U.S.NRC
United States Nuclear Regulatory Commission
Protecting People and the Environment

NUREG/CR-7031
ORNL/TM-2009/175

A Compilation of Elevated Temperature Concrete Material Property Data and Information for Use in Assessments of Nuclear Power Plant Reinforced Concrete Structures

Office of Nuclear Regulatory Research

U.S.NRC
United States Nuclear Regulatory Commission
Protecting People and the Environment

NUREG/CR-7031
ORNL/TM-2009/175

A Compilation of Elevated Temperature Concrete Material Property Data and Information for Use in Assessments of Nuclear Power Plant Reinforced Concrete Structures

Manuscript Completed: October 2010
Date Published: December 2010

Prepared by
D.J. Naus

Oak Ridge National Laboratory
Managed by UT-Battelle, LLC
Oak Ridge, TN 37831-6283

H.L. Graves, NRC Project Manager

NRC Job Code N6511

ABSTRACT

The objective of this limited study was to provide a compilation of data and information on the effects of elevated temperature on the behavior of concrete materials for use in assessments of nuclear power plant reinforced concrete structures that are subjected temperatures in excess of the current American Society of Mechanical Engineers Code limitations. In meeting this objective the physicochemical processes in Portland cement concrete as a function of temperature are noted. The general behavior of Portland cement, aggregate, and concrete materials under elevated temperatures is summarized. Data and information on the effect of elevated temperature and testing conditions on the mechanical and physical properties of concrete are presented. Mechanical property-related items addressed include: stress and strain characteristics, Poisson's ratio, modulus of elasticity, compressive strength, thermal cycling, tensile strength, shrinkage and creep, concrete-steel reinforcement bond strength, fracture energy and fracture toughness, long-term exposure, radiation shielding effectiveness, and multiaxial conditions. Physical properties and thermal effects addressed include: porosity and density, coefficient of thermal expansion, thermal conductivity, thermal diffusivity, specific heat, heat of ablation and erosion rates, moisture diffusion and pore pressure, and simulated hot spots. A general description of heavyweight concrete materials utilized for radiation shielding is provided and the effect of elevated temperature on properties of several shielding concretes is identified. Design codes and standards that address concrete under elevated temperature conditions are described. Examples of methods that can be utilized for assessment of concrete exposed to high temperatures are identified. Temperature-dependent properties of mild steel and prestressing materials for use with Portland cement concretes are provided.

FOREWORD

Under normal conditions most nuclear plant concrete structures are subjected to a range of temperature no more severe than that imposed by ambient environmental conditions. However, there are cases where these structures may be exposed to much higher temperatures (e.g., building fires and chemical and metallurgical applications in which the concrete is in close proximity to furnaces). Also designs of some new generation reactor concepts indicate that concrete may be exposed to long-term steady-state temperatures in excess of the present American Society of Mechanical Engineers Boiler and Pressure Vessel Code (ASME Code) limit of 65^0C. Under such an application the effect of elevated temperature on certain mechanical and physical properties may determine whether the concrete will maintain its structural integrity.

The purpose of this research was to provide an overview of the effects of elevated temperature on the behavior of concrete materials. The effects of elevated temperatures on the properties of ordinary Portland cement concretes and constituent materials are summarized. The effects of elevated temperature on high-strength concrete materials are noted and the performance compared to normal strength concretes. A limited discussion of elevated temperature on radiation shielding concrete is also provided. Nuclear power plant and general civil engineering design codes are described. Finally, design considerations and analytical techniques for evaluating the response of reinforced concrete structures to elevated-temperature conditions are presented.

The major findings contained in this NUREG/CR are: 1) deterioration of concrete's mechanical properties can be attributed to physiochemical changes in cement paste, physiochemical changes in aggregate, and thermal incompatibility of cement paste and aggregate; 2) although a large amount of data and information on effects of elevated temperature on concrete properties are available, many of the elevated temperature tests on concrete did not use representative materials nor representative nuclear power plant environmental conditions, and quantitative comparison of results can be difficult because of different test procedures, constituents and proportions, and testing conditions; and 3) several research projects have been conducted to investigate the behavior of reinforced concrete structures at elevated temperature, however, the overall level of effort has not been sufficient for establishment of widely accepted elevated-temperature concrete design procedures.

On the basis of these findings, if a nuclear plant concrete structure in one of the proposed advanced reactors is required to maintain its functional and performance requirements at temperatures in excess of ASME Code limits, or at moderately elevated temperatures (e.g., 200-300˚C) for extended periods of time, techniques for optimizing the design of structural elements to resist these exposures should be investigated (i.e., the material selection and design).

CONTENTS

LIST OF FIGURES

List of Tables

Acknowledgment

The author would like to acknowledge the continuing support and guidance throughout the program provided by the U.S. Nuclear Regulatory Commission Technical Monitor, Mr. Herman L. Graves, III.

1 INTRODUCTION

Under normal conditions, most concrete structures are subjected to a range of temperature no more severe than that imposed by ambient environmental conditions. However, there are important cases where these structures may experience much higher temperatures (e.g., jet aircraft engine blasts, building fires, chemical and metallurgical industrial applications in which the concrete is in close proximity to furnaces, and some nuclear power-related postulated accident conditions). Under elevated temperature exposure reinforced concrete structures can fail in a number of different ways [1.1,1.2]. For load-bearing slabs, if the strength of the steel reinforcement is lost due to heating then there may be bending or tensile strength failure. Reinforced members may also fail when the bond between the concrete and reinforcement is lost, with associated concrete tensile failure. Shear or torsion failures are also influenced by concrete tensile strength, but are poorly defined experimentally. Finally, compressive failures are usually associated with temperature-related loss of concrete compressive strength in the compression zone. In practice, failure is related to structural performance in situ (e.g., restraint effects).

Of primary interest in the present study is the behavior of reinforced concrete elements in designs of new-generation reactor concepts in which the concrete may be exposed to long-term steady-state temperatures in excess of the present *American Society of Mechanical Engineers Pressure Vessel and Piping Code (ASME Code)* limit of 65°C [1.3]. Secondary interests include performance of concrete associated with radioactive waste storage and disposal facilities and postulated design-basis accident conditions involving unscheduled thermal excursions. Under such applications the effect of elevated temperature on certain mechanical and physical properties of concrete may determine its ability to maintain structural integrity as well as its ability to continue to provide adequate structural margins.

The performance of Portland cement-based materials under elevated temperature exposure is very complicated and difficult to characterize. Concrete's thermal properties are more complex than for most materials because not only is the concrete a composite material whose constituents have different properties, but also its properties depend on moisture and porosity. Exposure of concrete to elevated temperature affects its mechanical and physical properties. The changes in properties result from three processes that take place at elevated temperature: (1) phase transformations (e.g., loss of free water at about 100˚C, decomposition of calcium hydroxide at about 450˚C, and crystal transformation of quartz at 573˚C from the α- to the β-form), (2) pore structure evolution (e.g., volume and surfaces of pores increase up to a temperature of about 500˚C and then decrease with further temperature increase, and (3) coupled thermo-hygro-chemo-mechancial processes (e.g., temperature gradients leading to thermal stresses, multiphase transport of water, and chemical changes that affect pore pressure and structure) [1.4]. Figure 1.1 provides a summary of the physiochemical processes in Portland cement concrete during heating [1.1]. Under thermal loading elements could distort and displace, and, under certain conditions, the concrete surfaces could spall due to the build up of steam pressure. Because thermally-induced dimensional changes, loss of structural integrity, and release of moisture and gases resulting from the migration of free water could adversely affect plant operations and safety, a complete understanding of the behavior of concrete under long-term elevated-temperature exposure as well as both during and after a thermal excursion resulting from a postulated design-basis accident condition is essential for reliable design evaluations and assessments. Because the properties of concrete change with respect to time and the environment to which it is exposed, an assessment of the effects of concrete aging is also important in performing safety evaluations.

Bonded reinforcement (i.e., deformed bars) is provided to control the extent and width of cracks at operating temperatures, resist tensile stresses and computed compressive stresses for elastic design, and provide structural reinforcement where required by limit condition design procedures. Bonded reinforcement in nuclear power plant structures is often used in conjunction with prestressed steel. The prestressed steel provides the structural rigidity and the major part of the strength while the bonded reinforcement distributes cracks, increases ultimate strength and reinforces those areas not adequately strengthened by the prestressed steel, and provides additional safety for unexpected conditions of loading. Steel reinforcement is normally protected by the concrete against significant elevated temperature exposure because of concrete's low thermal diffusivity that results in slow propagation of thermal transients. However, under certain conditions such as long-duration thermal exposure, thin-section members, or occurrence of concrete spalling, exposure the reinforcement to elevated temperature can occur. If the temperatures experienced by the steel are high enough, phase transformations can occur that produce changes in its physical and mechanical properties.

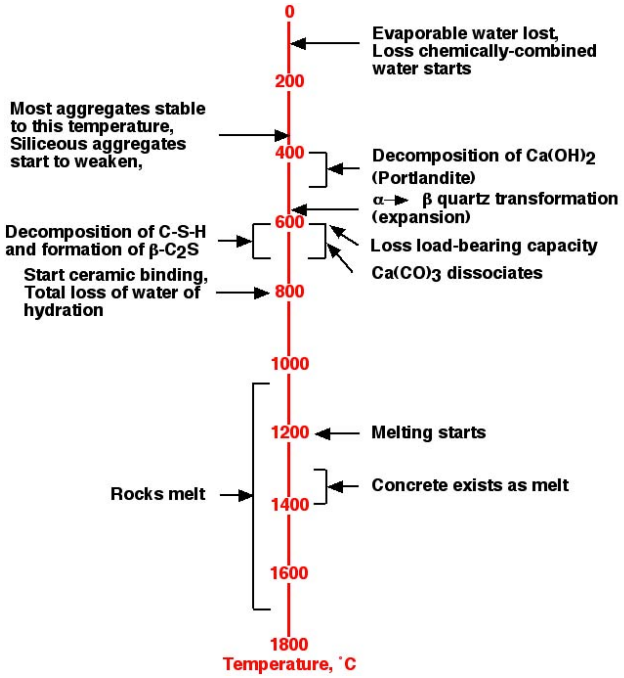

Figure 1.1 Physiochemical processes in Portland cement concrete during heating.

Source: Adaptation of Figure 2 in G.A. Khoury, "Effect of Fire on Concrete and Concrete Structures," *Progress in Structural Engineering Materials* **2**, pp. 429-447, 2000.

This report contains physical and mechanical property data and information on effects of thermal loadings on reinforced concrete materials that either have been used to construct existing plants or that could be used for fabrication of future plants (e.g., high performance concretes). This report supplements previous information provided in NUREG/CR-6900 [1.5] by providing additional material properties data, relationships between properties and temperature for use in analytical assessments, information and mateial properties data on shielding concretes, identification of codes and standards that address concrete under elevated temperature conditions, and identifies several potential methods for assessment of concrete exposed to high temperatures. The primary application of this information is to assessments of nuclear power plants that have concrete structures experiencing concrete temperatures above ASME Code limits or structures that have experienced temperatures above the Code limits. Although not a primary objective of this activity, limited information is provided to assist in the assessment of the response of concrete structures under thermal loadings representative of accident conditions.

References

1.1 G.A. Khoury, "Effect of Fire on Concrete and Concrete Structures," *Progress in Structural Engineering Materials* **2**, pp. 429-447, 2000.

1.2 I.A. Fletcher, S. Welch, J.L. Torero, R.O. Carvel, and A. Usmani, "Behaviour of Concrete Structures in Fire," *Thermal Science* **11**(2), pp. 37-52, 2007.

1.3 "Code for Concrete Reactor Vessels and Containments," Nuclear Power Plant Components, *ASME Boiler and Pressure Vessel Code*, Section III, Division 2, American Society of Mechanical Engineers, New York, July 2007.

1.4 K. Willam and I. Rhee, "Thermal Degradation Effects in Concrete Material Systems," *NSF-FHWA Workshop on Imaging and Simulation of Concrete Structures*, Northwestern University, Evanston, Illinois, July 30-31, 2003.

1.5 D.J. Naus, "The Effects of Elevated Temperature on Concrete Materials and Structures – A Literature Review," NUREG/CR-6900, U.S. Nuclear Regulatory Commission, Washington, DC, March 2006.

2 EXPERIMENTAL RESULTS ON TEMPERATURE-DEPENDENT PROPERTIES AND PERFORMANCE OF PORTLAND CEMENT CONCRETE MATERIALS

Portland cements are manufactured by mixing finely divided calcareous materials (i.e., lime containing) and argillaceous materials (i.e., clay). The four compounds that make up more than 90% of the dry weight of the cement are tricalcium silicate ($3CaO•SiO_2$), dicalcium silicate ($2CaO•SiO_2$), tricalcium aluminate ($3CaO•A1_2O_3$), and tetracalcium aluminoferrite ($4CaO•A1_20_3•Fe_2O_3$). When water is added to Portland cement, an exothermic reaction occurs, and new compounds are formed (i.e., hydrated cement paste): tobermorite gel [$(Ca_5Si_6O_{16}(OH)_2•4H_2O)$], calcium hydroxide, calcium aluminoferrite hydrate, tetracalcium aluminate hydrate, and calcium monosulfoaliminate. Mature cement paste is normally composed of 70–80% layered calcium-silicate-hydrate (C-S-H) gel, 20% $Ca(OH)_2$, and other chemical compounds [2.1]. The C-S-H gel structure is made up of three types of groups that contribute to bonds across surfaces or in the interlayer of partly crystallized tobermorite material: calcium ions, siloxanes, and water molecules. Bonding of the water within the layers (gel water) with other groups via hydrogen bonds determines the strength, stiffness, and creep properties of the cement paste. Tobermorite gel is the primary contributor to the cement paste structural properties.

Concrete is a heterogeneous multiphase material with relatively inert aggregates that is held together by the hydrated Portland cement paste. When concretes are exposed to high temperatures, changes in mechanical properties and durability occur. It has been noted that there are two schools of thought on causes of thermal damage to Portland-cement-based materials when exposed to elevated temperature [2.2]. The first attributes the irreversible loss of strength and stiffness to microcracking induced by thermal mismatch of some mesoscopic properties and interfaces [2.3,2.4]. The second attributes thermal damage to the dehydration of the primary hydration products in the hardened cement paste matrix [2.5,2.6].

Under elevated-temperature exposure, Portland cement paste experiences physical and chemical changes that contribute to development of shrinkage, transient creep, and changes in strength. Nonlinearities in material properties, variation of mechanical and physical properties with temperature, tensile cracking, and creep effects affect the buildup of thermal forces, the load-carrying capacity, and the deformation capability (i.e., ductility) of the structural members. Property variations are due largely to changes in the moisture condition of the concrete constituents and the progressive deterioration of the cement paste-aggregate bond, which is especially critical where thermal expansion values for the cement paste and aggregate differ significantly. Concrete at room temperature may contain 15-20% water (by vol.) of which 10-12% can evaporate with the remainder chemically bound. The correlation between moisture change and properties is demonstrated in Figure 2.1 which provides a comparison of the weight change and residual compressive strength results for siliceous gravel and limestone coarse aggregate concretes as a function of temperature [2.7]. Weight change and residual compressive strength for siliceous gravel and limestone concretes both changed significantly at temperatures above about 800˚C. The bond region is affected

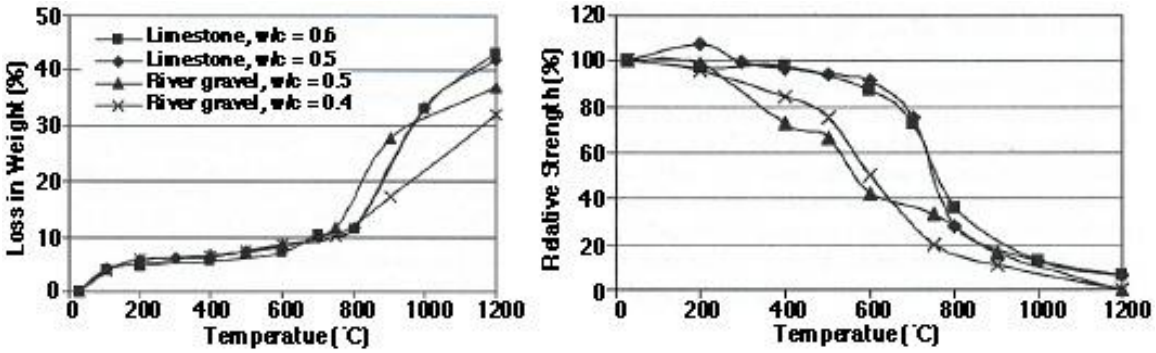

Figure 2.1 Weight change and residual compressive strength of siliceous gravel and limestone concretes as a function of temperature.

Source: O. Arioz, "Effects of Elevated temperatures on Properties of Concrete," *Fire Safety Journal* **42**, pp. 516-522, 2007.

by the surface roughness of the aggregate and its chemical/physical interactions [2.8]. Chemical interaction relates to the chemical reactions between the aggregate and cement paste that can be either beneficial or detrimental. Physical interaction relates to dimensional compatibility between aggregate materials and cement paste. Behavior of concrete at high temperature depends on exposure conditions (i.e., temperature-moisture-load-time regime) [2.8]. Curing influences the degree of hydration, while the temperature and load history prior to exposure to elevated temperature could have a significant effect on the behavior of the Portland cement paste and therefore the concrete.

Concrete at elevated temperature is sensitive to the temperature level, heating rate, thermal cycling, and temperature duration (as long as chemical and physical transformations occur). Deterioration of mechanical properties of concrete due to thermal loading involves three material factors: (1) physicochemical changes in the cement paste, (2) physicochemical changes in the aggregate, and (3) thermal compatibility between the aggregate and the cement paste (e.g., pure cement paste exhibits two to three times greater thermal expansion than limestone) ; and are influenced by environmental factors such as temperature level, heating rate, applied loading, and external sealing influencing moisture loss from the surface [2.9]. Information presented in Table 2.1 provides more detailed

Table 2.1 Influence of environmental factors on heated concrete

Factor	Influence	Comment
Temperature Level	***	• Chemical-physical structure (see Chapter 2) & most properties (see Chapters 6-14).
	**	• The properties of some concrete (e.g. compressive strength and modulus of elasticity) when heated under 20-30% load can vary less with temperature - up to about 500°C - than if heated without load (see Chapters 6 & 14).
Heating Rate	**	• *< 2°C/min:* Second order influence.
	***	• *> about 5°C/min:* Becomes significant ⇒ explosive spalling.
Cooling Rate	*	• *< 2°C/minute:* Negligible influence.
	**	• *> 2°C/minute:* Cracking could occur.
	***	• *Quenching*: Very significant influence.
Thermal Cycling	**	• *Unsealed Concrete:* Significant influence mainly during first cycle to given temperature.
	**	• *Sealed concrete:* Influence in so far as it allows longer duration at temperature for hydrothermal transformations to develop.
Duration at Temperature	**	• *Unsealed concrete*: Only significant at early stages while transformations decay.
	***	• *Sealed concrete*: Duration at temperature above 100°C ⇒ Continuing hydrothermal transformations.
Load-Temp. Sequence	***	• Very important - not usually appreciated
Load Level	***	• < 30%: Linear influence on Transient Creep (Chapter 9) at least in range up to 30% cold strength.
	***	• >50%: Failure could occur during heating at high load levels.
Moisture Level	**	• *Unsealed*: Small influence on thermal strain and transient creep particularly above 100°C.
	***	• *Sealed*: Very significant influence on the structure of cement paste and properties of concrete above 100°C.

*** First order influence, ** Second order influence, * Third order influence.

Source: G. A. Khoury, *Performance of Heated Concrete—Mechanical Properties*, Contract NUC/56/3604A with Nuclear Installations Inspectorate, Imperial College, London, United Kingdom, August 1996.

information on environmental factors that affect heated concrete and an indication of their relative influence [2.8]. Although information in this table indicates that there are several negative effects of elevated temperature exposure, there are two potential positive aspects of elevated temperature exposure of concrete [2.9]. First, transient creep, or load-induced thermal strain, is much larger than elastic strain and contributes to a significant relaxation that helps to minimize stress gradients originating from thermal incompatibilities and temperature gradients in heated concrete [2.10]. Second, concrete in service generally is under load, which has a beneficial effect during heating in that it confines the concrete and tends to inhibit crack development [2.11].

Research has been conducted on the thermal behavior of concrete in connection with the development of prestressed concrete pressure vessels for nuclear power plants (i.e., 20°C to 200°C) and to study the behavior of reinforced concrete members under fire conditions (i.e., 20°C to 1000°C) [2.12]. Interpretation of these results can be difficult however because (1) test materials and curing conditions were different, (2) descriptions of materials are incomplete, (3) different test procedures were utilized (e.g., heating rates and exposure times), (4) test conditions are not comparable (e.g., tested at temperature or permitted to cool to room temperature prior to testing, and loaded or unloaded while heating), and (5) shape and size of the test articles were different (e.g., cube and cylindrical). Factors such as these can combine during first heating to influence the properties of concrete (e.g., measurements of concrete compressive strength at 150˚C have yielded results that can range from as low as 30% to as high as 150% the concrete initial cold strength) [2.13]. Figure 2.2 presents a global diagram of dependence of concrete's thermo-hydral-mechanical properties dependence on the load-heat-time sequence [Note: influence of moisture boundary conditions (i.e., totally sealed, semi-sealed, or unsealed) is not shown; LITS = load-induced thermal strain)] [2.14].

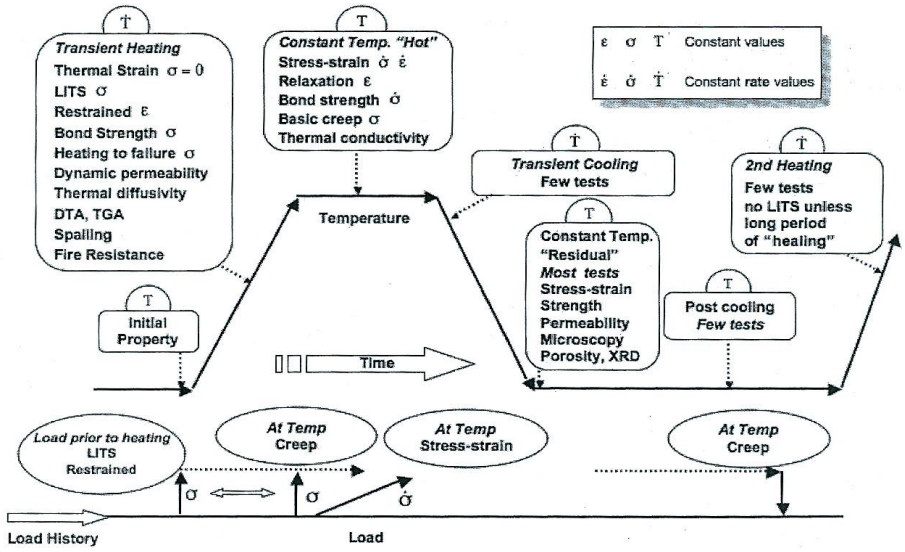

Figure 2.2 Examples of dependence of concrete's thermo-hydral-mechanical properties on heat-load-time sequence of the test regime (moisture boundary conditions not shown).

Source: G.A. Khoury, *Effect of Heat on Concrete*, Department of Civil and Environmental Engineering Report, Imperial College, London, United Kingdom, 1995.

Concrete structural members are to be designed to satisfy the requirements of serviceability and safety limit states for various environmental conditions. Elevated temperature exposure is one of the environmental conditions that may need to be addressed for some of the new advanced reactor designs. Contained in the following sections of this chapter is a summary of literature that has been identified addressing the general behavior and pertinent mechanical and physical properties of concrete materials under elevated-temperature conditions.

2.1 General Behavior

If concrete made with Portland cement or blast furnace slag cement is subjected to heat, a number of transformations and reactions occur, even if there is only a moderate increase in temperature [2.15,2.16]. As aggregate materials

normally occupy 60 to 80% of the concrete volume, the behavior of concrete at elevated temperature is strongly influenced by the aggregate type. The thermal stability of the concrete depends largely on the thermal stability of the aggregate (i.e., thermal strain depends on aggregate used). Commonly used fine and coarse aggregate materials are thermally stable up to 300°– 350°C as noted in Figure 2.3 where thermal expansion data for 20 – 30 mm prisms of gravel, limestone, and basalt aggregate materials is presented showing residual expansion after cooling.

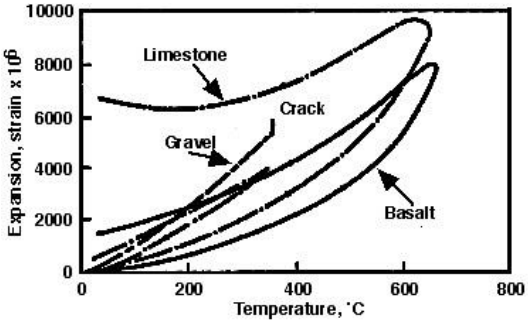

Figure 2.3 Thermal strains of aggregate prisms during heat cycle to 600˚C at 2˚C/min.

Source: G. A. Khoury, *Performance of Heated Concrete—Mechanical Properties*, Contract NUC/56/3604A with Nuclear Installations Inspectorate, Imperial College, London, August 1996.

Thermal instability and breakup temperatures reported for a gravel, limestone, and basalt are 300˚C+, 400˚C+, and 500˚C+, and 350˚C+, 600-700˚C+, and >600˚C, respectively [2.8]. Figure 2.4 presents information on the thermal stability and processes that take place on heating in several aggregate types. Aggregate characteristics of importance to behavior of concrete at elevated temperature include physical properties (e.g., thermal conductivity and thermal expansion), chemical properties (e.g., chemical stability at temperature), and thermal stability/integrity.

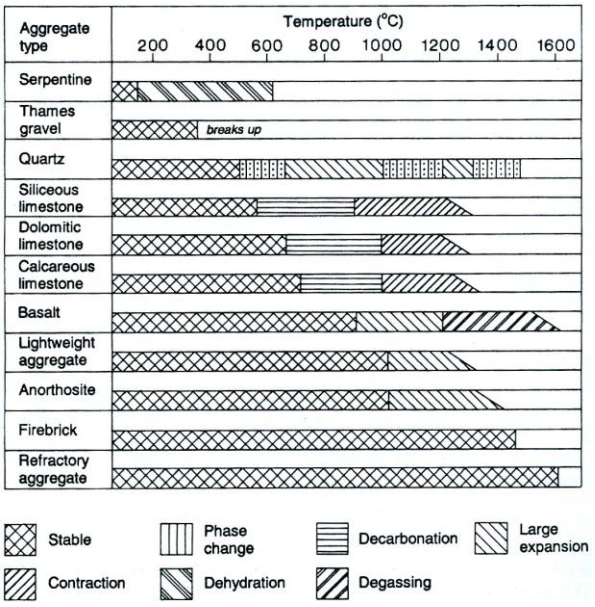

Figure 2.4 Examples of range of thermal stabilities and processes that take place in aggregates during heating.

Source: G.A. Khoury, *Effect of Heat on Concrete*, Department of Civil and Environmental Engineering Report, Imperial College, London, United Kingdom, 1995.

Aggregate materials may undergo crystal transformations leading to significant increases in volume [e.g., crystalline transformation of α-quartz (trigonal) to β-quartz (hexagonal) between 500 and 650°C with an accompanying

increase in volume of ~5.7%]. Some siliceous or calcareous aggregates with some water of constitution exhibit moderate dehydration with increasing temperature that is accompanied by shrinkage (i.e., opal at 373°C exhibits shrinkage of ~13% by volume) [2.17]. Most nonsiliceous aggregates are stable up to about 600°C. At higher temperatures, calcareous aggregates (calcite – $CaCO_3$), magnesite ($MgCO_3$), and dolomite ($MgCO_3/CaCO_3$) dissociate into an oxide and CO_2 ($CaO + CO_2$). Calcium carbonate dissociates completely at 1atm pressure at 898°C with partial dissociation occurring at temperatures as low as 700°C [2.18]. Aggregates produced from crystalline rocks may progressively disintegrate at high temperatures because of thermal incompatibility of aggregate itself and possible dehydration of any chemically combined moisture that is present. Above 1200°C and up to 1300°C some aggregates, such as igneous rocks (e.g., basalt), show degassing and expansion. Lightweight and refractory aggregates can be utilized to produce significant improvements in the heat resistance of Portland cement concretes. However, aggregate porosity of some lightweight aggregates varies from 0 to 50% or more and any water present in the aggregate is evaporable and can be expelled on heating to contribute to pore pressure build up in concrete [2.19]. It has been noted that the thermal stability of aggregates increases in order of gravel, limestone, basalt, and lightweight [2.20]. Hydrous aggregates (e.g., serpentine, limonite, and goethite) containing chemically combined water of crystallization (e.g., 4 -12%, by weight) used in concrete for radiation shielding have dehydration temperatures ranging from 175˚ to 500˚C depending on the aggregate type [2.21]. The descending order of fire endurance of aggregates is expanded slags, shales, slates, and clays; air-cooled slag; basic, finely grained igneous rocks such as granite and basalt; calcareous; siliceous aggregates; and lastly flint [2.19]

Apart from the crystalline transformations occurring mainly in the aggregate materials during heating, a number of degradation reactions occur, primarily in the cement paste, that result in a progressive breakdown in the structure of the concrete. Loss of concrete structural quality (e.g., strength and fracture) under elevated temperature exposure is dependent in large measure on alteration of the physico-chemical composition of the hardened cement paste which affects its phase composition and pore structure (i.e., specific surface of hydration products reduces and pore structure becomes coarser) [2.22,2.23]. An increase in temperature produces significant changes in the chemical composition and microstructure of the hardened Portland cement paste. At low temperatures these reactions mainly take the form of dehydration and water expulsion reactions. Changes in the chemical composition and microstructure of unsealed hardened Portland cement paste occur gradually and continuously over a temperature range from room temperature to 1000°C. At room temperature, between 30 and 60% of the volume of saturated cement paste and between 2 and 10% of the volume of saturated structural concrete are occupied by evaporable water. At temperatures up to 80˚C the hydration products of ordinary Portland cement essentially remain chemically unaltered and changes in the properties can be attributed to physical effects (e.g., changes in van der Waals cohesive forces, porosity, surface, energy, and cracking) [2.14]. As the temperature to which the cement paste is subjected increases, evaporable water is driven off until at a temperature of about 105°C all evaporable water will be lost, given a sufficient exposure period.* At temperatures above 105°C, the strongly absorbed and chemically combined water (i.e., water of hydration) are gradually lost from the cement paste hydrates. This represents the dominant process affecting performance as temperatures increase above about 100˚C [2.9] (Fig. 2.8 presents the influence of temperature on compressive strength and modulus of a cement paste). Dehydration of the calcium hydroxide is essentially zero up to about 400°C, increases most rapidly around 535°C, and becomes complete at about 600°C [2.24], and thus impacts concrete performance at higher temperatures. This is illustrated in Figure 2.5 where multiple x-ray diffraction patterns are presented for samples removed from the surface and interior of mortar specimens after exposure to temperatures up to 1000˚C (i.e., $Ca(OH)_2$ reduces from 6.01% at ambient to 2.52% at 500˚C to nil at 800˚C)** [2.25]. The calcium hydroxide and calcium carbonate results correspond to the diffraction lines of d = 4.90 Å and d = 3.03 Å, respectively. Results for $Ca(OH)_2$ show a gradual reduction with increase in temperature indicating a minor effect on concrete performance at lower temperatures where loss of strongly absorbed and chemically combined water dominates, but has increasing importance at temperatures where decarbonation occurs. Results for $Ca(CO)_3$ indicate negligible carbonation of the sample has occurred.

---

* Relatively immature sealed cement paste tends to accelerate hydration and improve strength on heating, but at temperatures above 80˚ to 100˚C any hydration of cement paste could be beneficial or detrimental to strengthening depending on the CaO/SiO_2 ratio of the gel [2.19]. When heated above 80˚ to 100˚C in sealed condition hydrothermal reactions occur that result in significant changes in its chemical/physical microstructure.

** It has been noted that $Ca(OH)_2$ content change with depth may be used as an indicator of exposure temperature at the concrete surface as well as depth of damage [2.26].

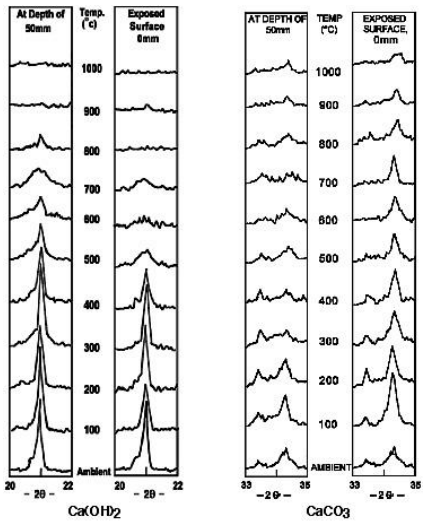

Figure 2.5 X-ray diffraction results for mortar samples of concrete monitoring $Ca(OH)_2$ and $Ca(CO)_3$ fired at different temperatures.

Source: S.K. Handoo, S. Agarwal, and S.K. Agarwal, "Physiochemical, Mineralogical, and Morphological Characteristics of Concrete Exposed to Elevated temperatures," *Cement and Concrete Research* **32**(7), pp. 1009-1018, 2002.

The behavior of unsealed cement paste during, and after, cooling is dominated by absorption of moisture from the surrounding medium [2.19]. Changes that take place during heating are somewhat irreversible, and rewetting of the cement paste after cooling can lead to some restoration of bonds partly due to rehydration. The CaO produced during previous heating from the dehydration of $Ca(OH)_2$ (above 400˚C) and decarbonation of the $CaCO_3$ (above 700˚C) absorbs water on cooling and rehydrates into $Ca(OH)_2$ with a corresponding 44% increase in volume that can lead to development of cracks and a weakening of the paste. It has been noted that 400˚C is a critical temperature for breakdown of the ordinary Portland cement (OPC) pastes due to dehydration of the calcium hydroxide followed by expansive rehydration of lime after cooling that occurs with time that can lead to cracking [2.13, 2.27]. The potential damaging effect of rehydration is illustrated by a study conducted using an ordinary Portland cement paste and an ordinary Portland cement/blast furnace slag paste to investigate the short- and long-term effects of rehydration of lime [2.28]. Three combinations of OPC/ground granulated blast furnace slag materials were studied [i.e., 30, 50, and 65% (by weight) replacement of OPC with slag]. Cylindrical specimens 50-mm diameter by 100-mm long were demolded 24 hours after casting and cured for 14 days in lime-saturated water at 23˚C followed by oven drying for 2 hours at 60˚C. The specimens were subjected to 800˚C for 1 hour, permitted to cool to room temperature, and placed into sealed plastic bags until testing. Two different ages of paste specimens were investigated: one set of OPC and OPC blast furnace slag paste specimens was examined 1 week after thermal exposure and a second set 1 year after thermal exposure. Figure 2.6 presents the evolution of rehydration in the OPC paste specimens for times representing immediately after heating to 800˚C and 2 days after heating. The OPC paste specimens exhibited a large quantity of visible cracks on removal from the furnace and essentially completely disintegrated 2 days after heating. The OPC/blast furnace slag paste specimens exhibited few to no visible cracks upon removal from the furnace and 2 days after removal indicating that replacement of OPC with slag can be beneficial with respect to reducing the harmful effects of rehydration of CaO when exposed to temperatures above 400˚C. After 1 year the OPC pastes had disintegrated and thus exhibited no residual compressive strength while the OPC/slag specimens exhibited similar behavior to the 2 day results with few visible cracks and no visible distinction between 2 day and 1 year results while maintaining similar residual compressive strength. Differential thermogravimetric analysis results for unheated OPC pastes (reference specimens) showed initial weight loss between 100˚ and 200˚C (loss of capillary water), secondary weight loss between 400˚ and 500˚C [dehydration of $Ca(OH)_2$], and tertiary weight loss at temperatures above 750˚C [decarbonation of $Ca(CO)_3$]. Samples of OPC that had been heated did not exhibit initial weight loss, secondary weight loss occurred between 400˚ and 500˚C indicating that CaO rehydration took place with $Ca(OH)_2$ amounts being greater than observed for the reference specimens indicating CaO rehydration results from dissociation of $Ca(OH)_2$ and from decarbonation of $Ca(CO)_3$, and tertiary weight loss above 750˚C did not occur. Differential thermogravimetric results for the 50% slag

specimens exhibited similar behavior to the reference OPC paste specimens. For the specimens tested after 1 week, the peak representing dehydration of the $Ca(OH)_2$ was significantly greater for the OPC pastes than the OPC/slag pastes indicating rehydration of CaO is greater in OPC pastes. For specimens tested after 1 year, results indicated that rehydration of the CaO throughout 1 year had a more significant effect in OPC pastes than OPC/slag pastes. The study results concluded that OPC pastes are more affected by the long-term effect of CaO rehydration than OPC/slag pastes.

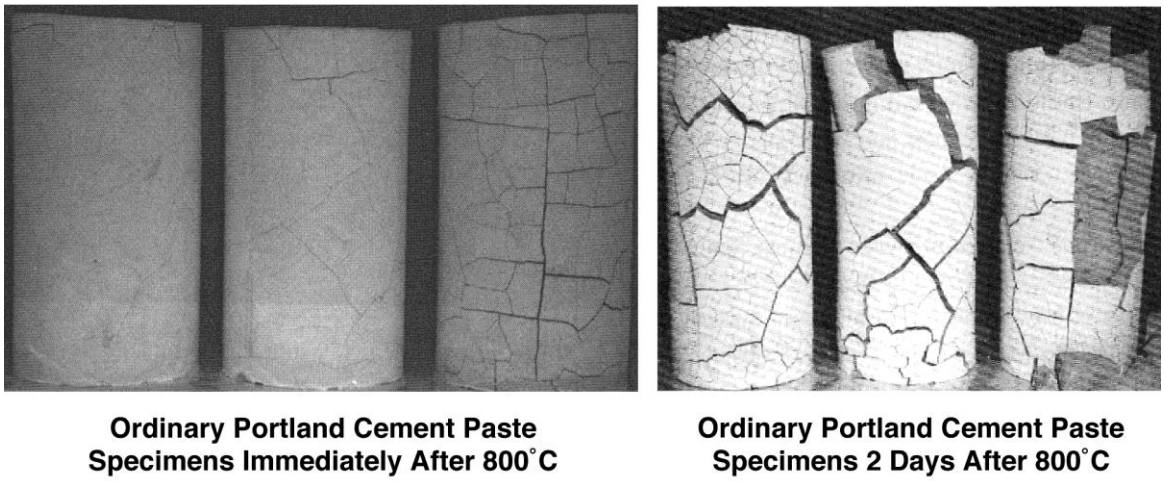

Figure 2.6 OPC paste specimens immediately after and two days after 800˚C heat treatment.

Source: A. Mendes, J. Sanjayan, and F. Collins,, "Long-Term Progressive Deterioration Following Fire Exposure of OPC Versus Slag Blended Cement Pastes," *Materials and Structures* **42**, pp. 95-101, 2009.

Key material features of Portland cement paste that influence properties of concrete at high temperature are its moisture state (i.e., sealed or unsealed), chemical structure (i.e., loss of chemically-combined water from C-S-H in unsealed condition, CaO/SiO_2 ratio of hydrate in sealed condition, and amount $Ca(OH)_2$ crystals in sealed and unsealed condition), and physical structure (i.e., total pore volume, average pore size, and amorphous/crystalline structure of solid) [2.8]. Figure 2.7 provides thermal strain data for Portland cement pastes fabricated from ordinary Portland cement, ordinary Portland cement and fly ash, and sulfate-resisting Portland cement demonstrating the

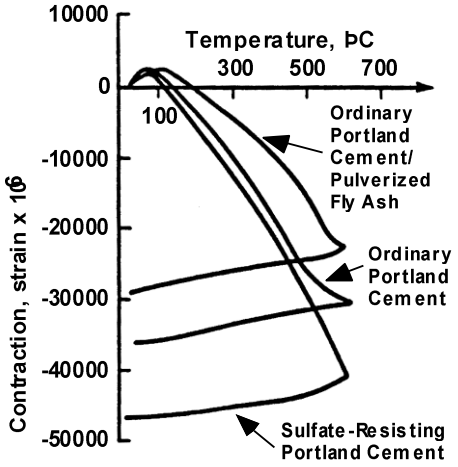

Figure 2.7 Thermal strain during first heat cycle to 600˚C of initially moist cementitious materials.

Source: G. A. Khoury, *Performance of Heated Concrete—Mechanical Properties*, Contract NUC/56/3604A with Nuclear Installations Inspectorate, Imperial College, London, August 1996.

influence of type of Portland cement as well as partial cement replacement. Figure 2.8 indicates the influence of temperature on the ultimate compressive strength and modulus of elasticity of a Portland cement paste (Type I Portland cement; water-cement = 0.33) [2.29]. Figure 2.9 presents a comparison of the relative strength of Portland cement paste (w/c = 0.3) tested either at temperature or after cooling to room temperature prior to testing [2.30]. Initial drop in hot strength was attributed to thermally energized swelling of physically bound water layers causing disjoining pressures, with regain of strength resulting from relief of these pressures due to drying giving rise to greater van der Waal's forces as cement gel layers move closer together [2.30]. Scanning electron microscopy

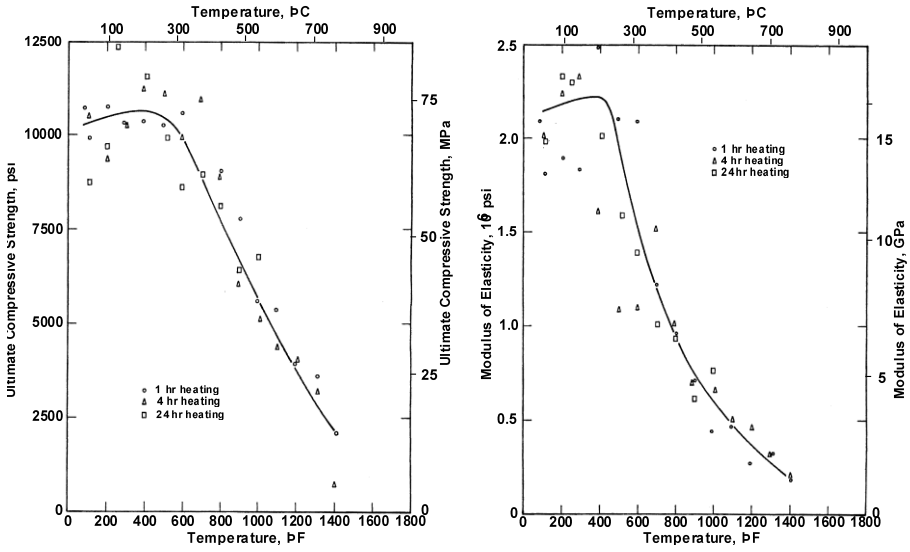

Figure 2.8 Ultimate compressive strength and modulus of elasticity of hydrated Portland cement paste (w/c = 0.3) at elevated temperature.

Source: T.Z. Harmathy and J.E. Berndt, "Hydrated Portland Cement and Lightweight Concrete at Elevated Temperature," *J. American Concrete Institute* **63**, pp. 93-112, January 1966.

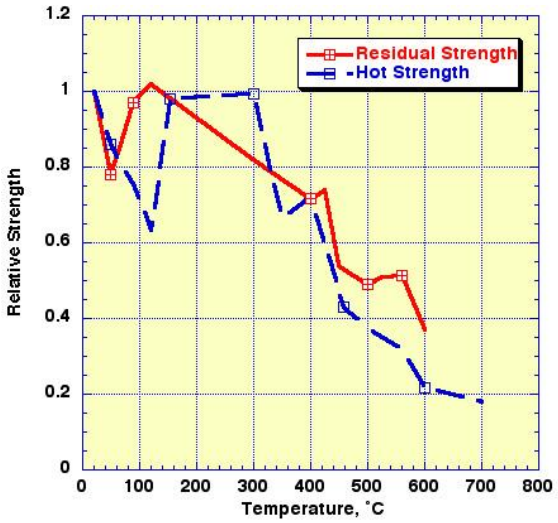

Figure 2.9 Residual and hot strength of Portland cement paste as a function of temperature.

Source: W.P.S. Dias, G.A. Khoury, and P.J.E. Sullivan, "Mechanical Properties of Hardened Cement Paste Exposed to Temperatures Up To 700˚C," ACI *Materials Journal* 87(2), March-April 1990.

results indicate that microcracking increases significantly beyond 300˚C, first around $Ca(OH)_2$ crystals and then around grains of unhydrated cement [2.31]. Figure 2.10 compares the effect of temperature on residual strength of ordinary Portland cement paste (100% OPC) and blends of cement (90% OPC + 10% Silica fume, 70% OPC + 30% pulverized fly ash, and 35% OPC + 65% slag) [2.32]. The 100% OPC exhibited a decline in residual compressive strength at temperatures above 200˚C with the decline significant at temperatures above 300˚C. Results in which silica fume replaced 10% of the OPC were similar to those obtained from the 100% OPC specimens. However, the specimens in which slag and pulverized fly ash were used as partial replacements for OPC retained their strength much better than either the specimens with 100% OPC or silica fume as a partial replacement for OPC. The reason for this was attributed to lower $Ca(OH)_2$ contents of these specimens [2.33]. It was further noted that cement paste and concrete containing 100% OPC tend to lose significant residual compressive strength above 300˚C, but the loss is not quite as significant if the specimens are tested at temperature. Figures 2.11 and 2.12 provide a comparison of

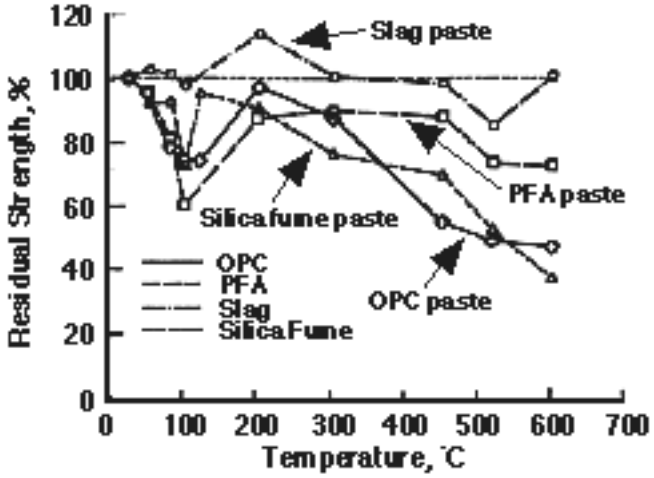

Figure 2.10 Effect of temperature on residual compressive strength of cement paste materials.

Source: P.J.E. Sullivan and R. Sharahar, "The Performance of Concrete at Elevated Temperatures (As Measured by the Reduction in Compressive Strength)," *Fire Technology* **28**(2*)*, pp. 240-250, August 1992.

residual compressive and flexural strength results, respectively, for a plain Portland cement paste and a Portland cement paste containing polypropylene fibers (~0.08%, by volume) after elevated temperature exposures up to 1000˚C (700˚C for fiber-reinforced paste) [2.34]. Water-cement ratio was 0.32 for both materials. As noted in the figure, the temperature range from 30˚ to 120˚C was characterized by strength losses, but after temperature exposures at 150˚ and 440˚C the residual compressive strengths equaled the reference strength at 20˚C. After higher exposure temperatures from 520˚ to 1000˚C the residual compressive strength of the plain paste decreased. Incorporation of the polypropylene fibers decreased both the reference and residual compressive strengths. The reference flexural strengths at 20˚C were identical in the test specimen with and without the polypropylene fibers. At a moderate temperature exposure of 50˚C, the residual flexural strength of the plain cement paste decreased significantly to about 47% its reference strength and at 120˚C it further reduced to about 26% its reference strength. Then in the temperature range from 150˚ to 440˚C the residual strengths increased before decreasing as the exposure temperature increased. Addition of polypropylene fibers improved residual flexural strength at low temperatures.

The aggregate-cement paste bond region has been shown to be the weakest link because it is normally weaker that the cement paste which is normally weaker than the aggregate [2.35]. The reactivity of the aggregate can be beneficial to bond strength or it can be harmful depending on the nature of the chemical reaction that takes place. Studies of bond strength at ambient temperatures have shown that, everything else being equal, variations in bond strength of up to 300% or more can occur depending on preconditioning of the aggregate (e.g., lubricating or polymer coating) [2.36,2.37]. If the aggregate-cement paste bond fails on heating, chemically or as a result of thermal incompatibility between the aggregate and cement paste, the concrete will exhibit a significant reduction in strength, even if both the aggregate and surrounding mortar matrix remain intact [2.19]. Interaction between the aggregate and cement paste can be physical or chemical. Physical interaction results from the differential thermal expansion between the aggregate and cement paste leading to weakening and disruption of the concrete at elevated

temperature (i.e., on heating to 80˚ to 100˚C the cement paste expands slightly as water escapes and the aggregate expands, while at higher temperatures the cement paste continues to shrink and the aggregate expands leading to a large differential strain). Chemical interaction, as influenced by temperature, can occur in the form of the reaction between $Ca(OH)_2$ crystals released by hydration of ordinary Portland cement and magnesium carbonate component of some limestone aggregates that is expansive leading to weakening and disruption of the concrete [2.19].

In general, during first heating concrete is a highly unstable and complex material. A good summary of the degradation reactions that occur in Portland cement concrete is available [2.12] and Figure 2.13 presents an illustration of the deterioration process during heating and cooling phases [2.38]. Changes in the microstructure of concrete occur as temperature rises. The thermal-hydral-mechanical properties also change with time and temperature depending upon factors such as the heating rate, initial moisture condition, boundary conditions, geometry and size of the heated member, loading condition, type of constituents, and chemico-physico interactions [2.26]. Upon first heating, substantial water evaporation occurs from the larger pores close to the concrete surface. Then, from 100˚C onward, the evaporation proceeds at a faster rate with water being expelled from the concrete near the surface as a result of above-atmospheric vapor pressure (i.e, steam flow). At 120˚C the expulsion of water physically bound in the smaller pores, or chemically combined, initiates and continues up to about 500˚C where the

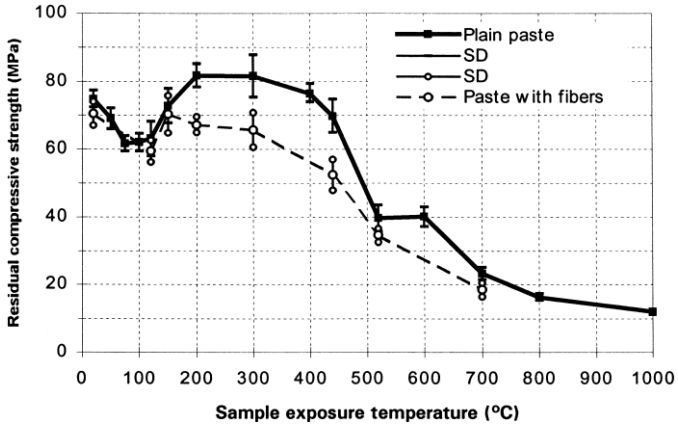

Figure 2.11 Residual compressive strengths of cement paste and cement paste with polypropylene fibers.

Source: J. Komonen and V. Penttala, "Effects of High Temperature on the Pore Structure and Strength of Plain and Polypropylene Fiber Reinforced Cement Pastes," *Fire Technology* **39**(1), pp. 23-34, 2003.

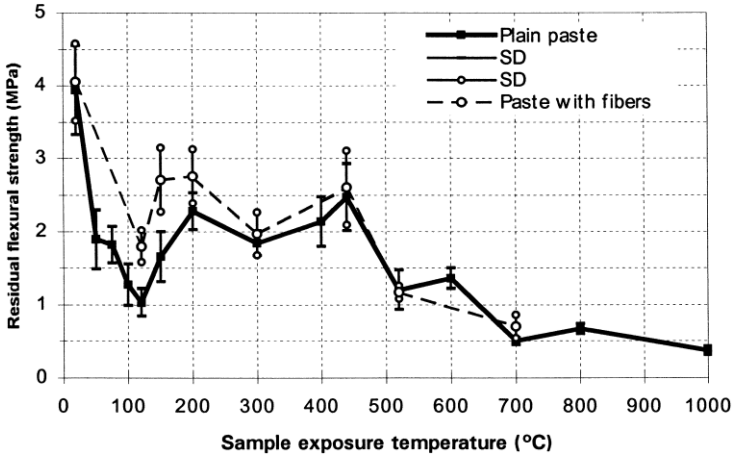

Figure 2.12 Residual flexural strengths of cement paste and cement paste with polypropylene fibers.

Source: J. Komonen and V. Penttala, "Effects of High Temperature on the Pore Structure and Strength of Plain and Polypropylene Fiber Reinforced Cement Pastes," *Fire Technology* **39**(1), pp. 23-34, 2003.

process is essentially complete. From 20˚ to 300˚C, in conjunction with evaporation, dehydration of the hardened cement paste occurs (first stage) with the maximum rate of dehydration occurring at about 180˚C {Tobermorite gel is stable up to a temperature of 150˚C [2.39]}. In the temperature range from 450˚ to 550˚C there is decomposition of the Portlandite {i.e., $Ca(OH)_2 \rightarrow CaO + H_2O$ [2.36]}. At 570˚C the $\alpha \rightarrow \beta$ inversion of quartz takes place with the transformation being endothermic and reversible. A further process of decomposition of the hardened cement paste takes place between 600°C and 700°C with the decomposition of the calcium-silicate-hydrate phases and formation of β-C_2S. Between 600°C and 900°C the limestone begins to undergo decarbonation (i.e., $CaCO_3 \rightarrow CaO + CO_2$). The rate of decomposition and the temperature at which it occurs are not only dependent on temperature and pressure, but also on the content of SiO_2 present in the limestone. Above 1200°C and up to 1300°C, some components of the concrete begin to melt. Above 1300°C to 1400°C concrete exists in the form of a melt.

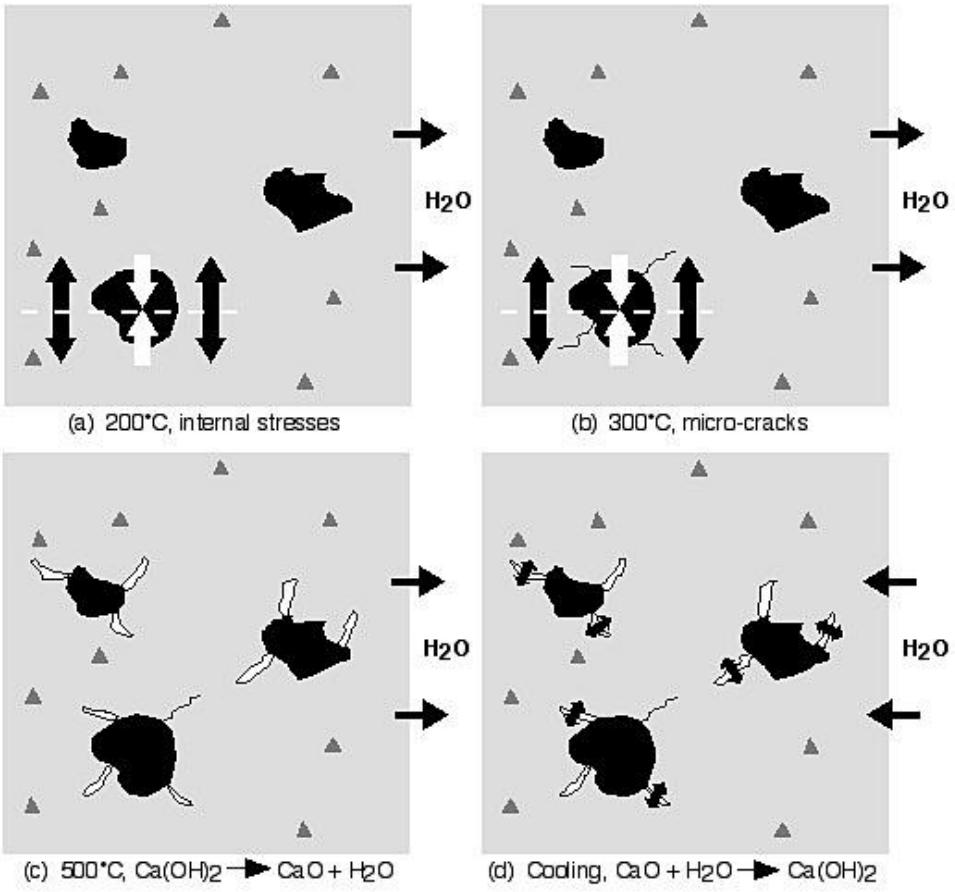

Figure 2.13 Schematic of concrete deterioration under moderate heating and cooling.

Source: Adaptation of figure in K.D. Hertz, "Concrete Strength for Fire Safety Design," *Magazine of Concrete Research* **57**(8), pp. 445-453, 2005.

Apparently liquefaction of the concrete commences with melting of the hardened cement paste followed by melting of the aggregates [2.40-2.42]. The melting points of aggregates vary greatly. At 1060°C basalt is at the lower limit of all types of rock, with quartzite not melting below 1700°C [2.15]. Figure 2.14 presents scanning electron micrographs showing the changes in concrete morphology as temperature increases from ambient to 800˚C (i.e, well developed hydrated phases of $Ca(OH)_2$ intermixed with calcium-silicate-hydrate and calcium aluminate at ambient, and presence of microcracks, voids increasing the porosity of deformed $Ca(OH)_2$ crystals, and disrupted calcium-silicate-hydrate phase boundaries at 800˚C). Figure 2.15 presents differential thermal analysis results for normal weight concrete indicating effects of elevated temperature exposure.

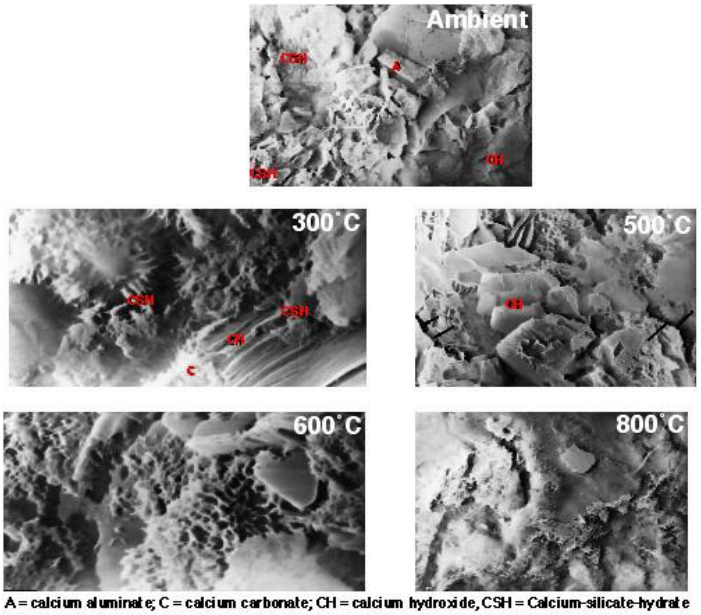

Figure 2.14 Change in morphology of hardened concrete after exposure to elevated temperature.

Source: S.K. Handoo, S. Agarwal, and S.K. Agarwal, "Physiochemical, Mineralogical, and Porphological Characteristics of Concrete Exposed to Elevated temperatures," *Cement and Concrete Research* **32**(7), pp. 1009-1018, 2002.

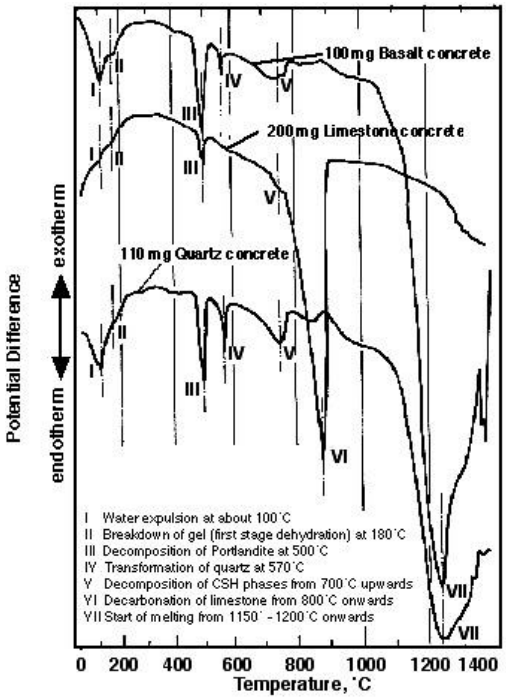

Figure 2.15 Differential thermal analysis of selected normal weight concretes.

Source: U. Schneider, *Behaviour of Concrete at High Temperature*, HEFT 337, Deutscher Ausschuss für Stahlbeton, Wilhelm Ernst & Sohn, Munich, Germany, 1982.

2.2 Mechanical and Physical Properties

Material properties are closely related to the specific test method employed. The properties of concrete at elevated temperature can be defined from a number of viewpoints (e.g., ranging from transient such as representing fire conditions to steady-state such as a structure operating at elevated temperature). To interpret results, knowledge of the test condition(s) employed is required. Three main test parameters are involved in the development of data: heating, application of load, and control of strain [2.43]. These parameters can be fixed at constant values or be varied during testing to provide transient conditions. Six regimes or "idealized" testing methods have been identified for determining properties of concrete at elevated temperature [2.12,2.43,2.44]:

1. Stress-rate controlled test: specimen is heated without load to a specified temperature, temperature is stabilized, load is applied at a controlled rate of stress with strain measurements made until ultimate load is reached. Data can be used to establish compressive or tensile strength, modulus of elasticity, and ultimate strain at collapse. Stress-strain relationship up to ultimate strength at different temperatures can be established.
2. Strain-rate controlled test: specimen is heated without load to a specified temperature, temperature is stabilized, load is applied at a controlled rate of strain and measurement made of stress level in specimen. Data can be used to establish compressive or tensile strength, modulus of elasticity, ultimate strain at collapse, and dissipation of energy. Complete stress-strain curve can be developed.
3. Steady-state creep test: specimen is heated to a specified temperature and then loaded with load held constant and measurements of strain made over a long time period. Measurements provide relationship between strain and time at different temperatures over long time periods.
4. Relaxation test: specimen is heated to a specified temperature, loaded with initial strain held constant, and load monitored as function of time. Data provides relationship between reduction of stress and time at temperature.
5. Transient creep test: load is applied to specimen before heating, heating proceeds at a specified rate, and strain measurements taken until failure occurs when strain rate approaches infinity. Data provide a relationship between strain and time and enable critical temperature values for different stress levels to be established. Family of strain versus time curves corresponding to different applied loads can be developed.
6. Restraint forces test: load is applied to the specimen to establish initial strain before heating at a specified rate while maintaining initial strain by adjusting load until the applied stress level falls to zero. Data provide a relationship between stress and time for different initial stress/strain levels and can be expressed as a relationship between restraint forces and temperature developed as a consequence of heating.

Each of these methods or regimes determines a specific feature of material behavior. Regimes 1 through 4 are related to steady-state tests and regimes 5 and 6 transient tests.

Figure 2.16 provides a schematic representation of testing procedures commonly used to evaluate concrete response to elevated temperature: stressed tests, unstressed tests, and unstressed residual. Stressed tests are a modified version of stress- or strain-controlled experiments performed under isothermal temperature conditions. A preload, generally in the range of 20 to 40 percent of the ultimate compression strength at room temperature, is applied to the concrete specimen prior to heating, and the load is sustained during the heating period. After the specimen reaches a steady-state temperature condition, the stress or the strain is increased at a prescribed loading rate until the specimen fails. Unstressed tests are carried out identically to the stress- or strain-controlled experiments of the steady-state type. Unstressed residual strength tests are experiments where the specimen is first cooled to room temperature after one or several cycles of heating without preloading. The load is then applied at room temperature under stress or strain control until the specimen fails.

2.2.1 Mechanical Properties

It has been established that the mechanical properties of concrete can be adversely affected by elevated-temperature exposure [2.44-2.48]. Deterioration of concrete's mechanical properties can be attributed to three material factors: (1) physicochemical changes in the cement paste, (2) physicochemical changes in the aggregate, and (3) thermal incompatibility between the aggregate and the cement paste; and the properties are influenced by environmental factors such as temperature level, heating rate, applied loading, and external sealing influencing moisture loss [2.9]. Several studies have been conducted to evaluate these factors, however, quantitative interpretation of available data is difficult because (1) samples were either tested hot or cold, (2) moisture migration was either free or restricted,

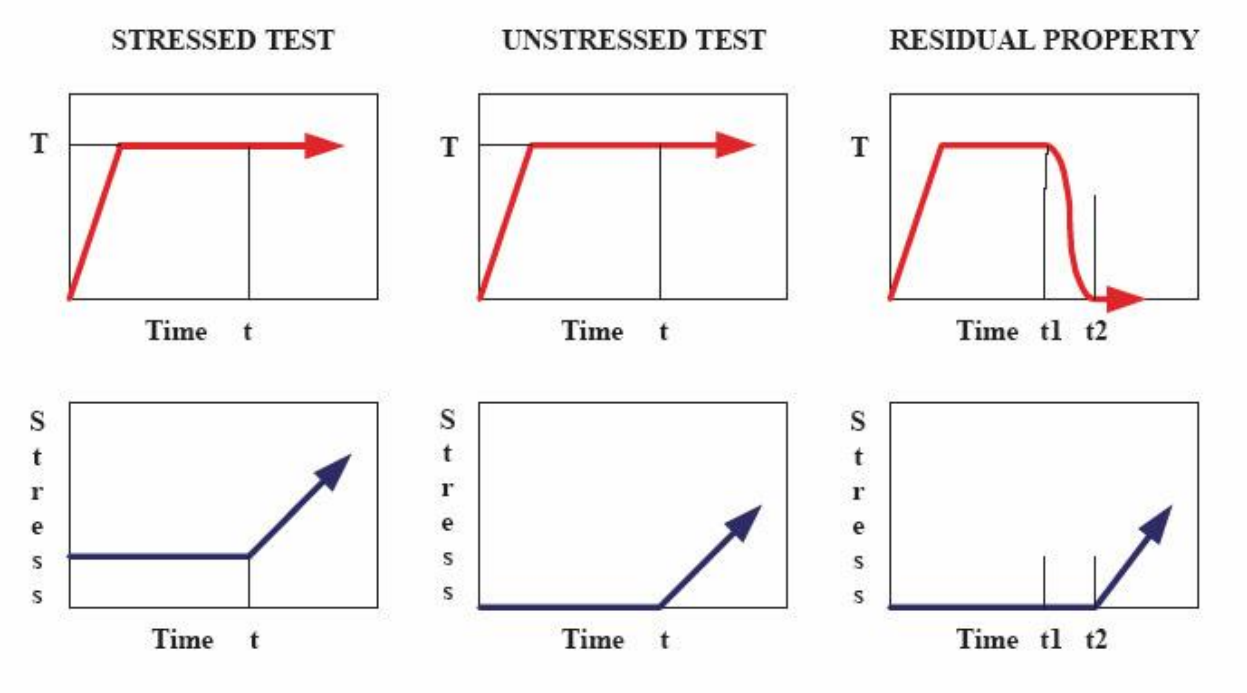

Figure 2.16 Schematic of temperature and loading histories.

Source: K. Willam, Y. Xi, K. Lee, J. Lee, and H. Basche, "Confirmatory Analytical Research on Phenomena Associated with Structural Response to Aircraft Attack – Letter Report," *Appendix A – A Literature Review of Concrete Structures Subjected to High Temperatures, University of Colorado*, Boulder, January 6, 2005.

(3) concrete was either loaded or unloaded while heated, (4) mix constituents and proportions varied, (5) test specimen size and shape were not consistent, (6) specimens were tested at different degrees of hydration, and (7) heat-soak duration varied from test to test. To provide a consistent basis for evaluation of data, it is recommended that several factors be taken into account [2.49]: (1) concrete strength class; (2) test specimen size; (3) thermal compatibility of aggregate and cement paste matrix; (4) cement and concrete composition; (5) level of temperature; (6) degree of hydration; (7) moisture content; (8) moisture gradients, rate of drying or wetting; (9) temperature gradient, rate of heating or cooling; (10) duration of temperature exposure; (11) loading during temperature exposure; (12) temperature-activated transformations in microstructure and chemical composition of cement; (13) state of specimens tested—hot or cold; (14) strength testing procedure; and (15) reference strength selected—wet, moist, or dry. Therefore great attention should be paid by the researcher who produces the data in unraveling and understanding the complexities in order to present the subject to the practicing engineer in whatever form (e.g., texts, diagrams, tables, and numerical modeling input) that are readily usable, as close to reality as possible, and as reliable as possible [2.26].

A review of methods used by various investigators for elevated-temperature testing of concrete indicates that, generally, the tests can be categorized according to cold or hot testing. In cold testing, specimens are gradually heated to a specified temperature, permitted to thermally stabilize at that temperature for a prescribed period of time, permitted to slowly cool to ambient, and then tested to determine residual mechanical properties. In hot testing, specimens are gradually heated to a specified temperature, permitted to thermally stabilize at the temperature for a prescribed period of time, and then tested at temperature to determine relative mechanical properties. During testing, specimens are maintained in either an open environment where water vapor can escape (unsealed) or a closed environment where the moisture is contained (sealed). The closed environment represents conditions for mass concrete where moisture does not have ready access to the atmosphere, and the open environment represents conditions where the element is either vented or has free atmospheric communication. During heating and cooling, the specimens may be either loaded or unloaded. Mechanical properties in which the specimens have been permitted to return to room temperature prior to testing are referred to as residual properties, and when properties are obtained from specimens tested at temperature they are referred to as relative properties.

The performance of concrete can be measured by the change of its stiffness, strength, or some other property that would affect its main function in service. Because concrete has a relatively low tensile strength, it is normally relied upon to take compressive forces, with tensile forces taken by steel reinforcement. As a consequence, much of the research conducted on concrete at elevated temperature has concentrated on compressive strength as the fundamental property in examining its deterioration. However, it has been noted that the compressive strength may not be as good an indicator of deterioration at elevated temperature as tensile or flexural strength under short-term loading [2.50].

2.2.1.1 Stress and Strain Characteristics

Information and Data. Evaluation of structures for small strain conditions involves elastic analysis procedures for which knowledge of the concrete modulus of elasticity and strength is sufficient. When large strains are involved, such as could occur when a structure is subjected to elevated temperature, elastic-plastic analysis procedures are required that involve use of the load-deformation or stress-strain relations developed for concrete at the temperature level of interest. The stress-strain relationship is one of the basic mechanical properties required for prediction of the overall response of concrete structures under thermal loadings [2.51]. Elevated temperature is one of the main factors that can have a significant effect on the concrete stress-strain relationship.

Uniaxial Compression Testing

The majority of stress-strain data reported in the literature are for concrete heated to test conditions without load or loaded under stress-controlled conditions. Figure 2.17 presents stress-strain diagrams for sealed and unsealed limestone aggregate concretes tested at temperature [2.52]. These results indicate that the unsealed specimens are stiffer than the sealed specimens, but strains at ultimate load were reduced. Figure 2.18 presents the influence of test temperature on the stress-strain relationship of a quartz aggregate concrete in a stress-rate controlled test conducted at test temperature [2.53] and a sandstone aggregate concrete with testing performed after specimens cooled to room temperature [2.54]. These data show a significant increase in ultimate strain and a loss of stiffness with increasing temperature. Figure 2.19 shows that specimens made from quartz aggregate concrete that are tested at temperature are stiffer and stronger than identical companion specimens heated to the same temperatures and then permitted to cool to room temperature before testing (i.e., up to 450°C the stress-strain curves of specimens tested at temperature do not change appreciably) [2.55]. It was also concluded from this study that the type of cement and the duration of thermal treatment had a minor effect on the slope of the stress-strain curve. Figure 2.20 presents results for basalt aggregate concrete derived under strain-rate controlled test conditions [2.56]. Figure 2.21 provides stress-strain results for a lightweight masonry concrete tested at several temperatures. Results show that as temperature increases the ultimate stress decreases and the ultimate strain increases.

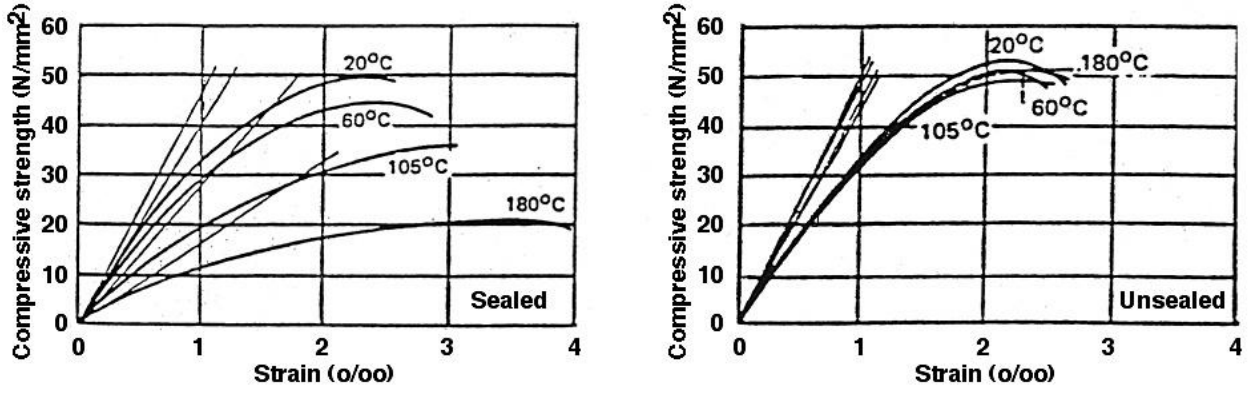

Figure 2.17 Stress-strain diagrams for sealed and unsealed limestone concrete.

Source: R. Kottas, J. Seeberger, and H.K. Hilsdorf, "Strength Characteristics of Concrete in Temperature Range of 20˚ to 200˚C," Paper H01/4 in *5th International Conference on Structural Mechanics in Reactor Technology*, Elsevier Publishers, North-Holland, The Netherlands, August 1979.

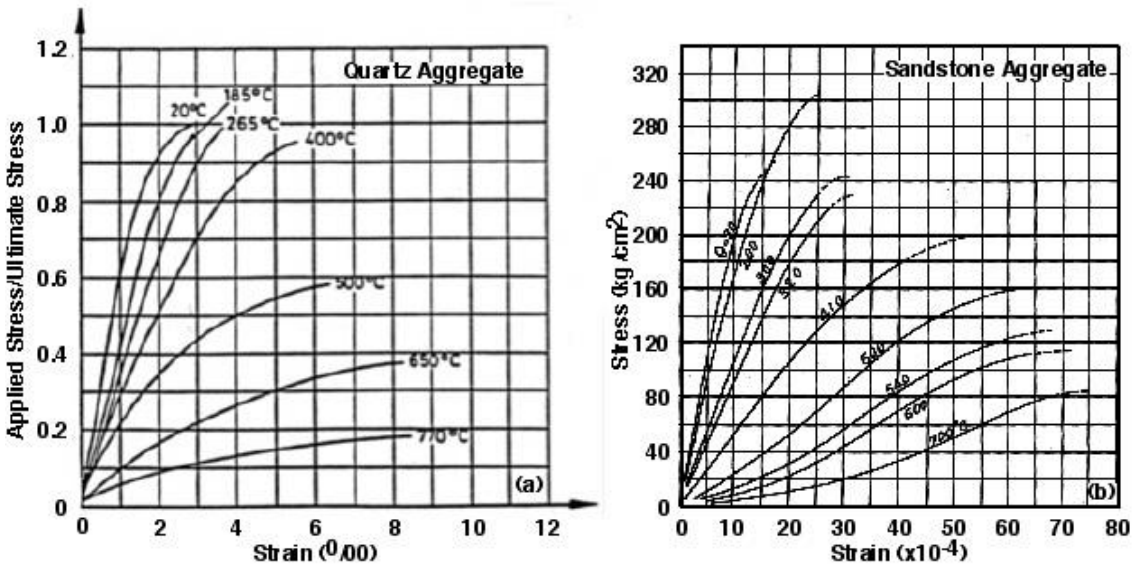

Figure 2.18 Influence of temperature on the stress-strain relation of unsealed quartz aggregate and sandstone aggregate concrete.

Sources: (a) Y. Anderberg and S. Thelanderson, "Stress and Deformation Characteristics of Concrete at High Temperatures, 2-Experimental Investigation and Material Behaviour Model," Bulletin 54, Lund Institute of Technology, Lund, Sweden, 1976.

(b) T. Harada, T. Takeda, S, Yamane, and F, Furumura, "Strength, Elasticity and Thermal Properties of Concrete Subjected to Elevated Temperatures," Paper SP-34-21 in *Concrete for Nuclear Reactors*, pp. 377-406, American Concrete Institute, Farmington Hills, Michigan, 1972.

Currently, utilization of high strength (e.g., $f_c' \geq 55$ MPa)* or high performance concretes (e.g., improved durability) has become an option to the use of traditional normal strength concrete. This is due to significant economic,

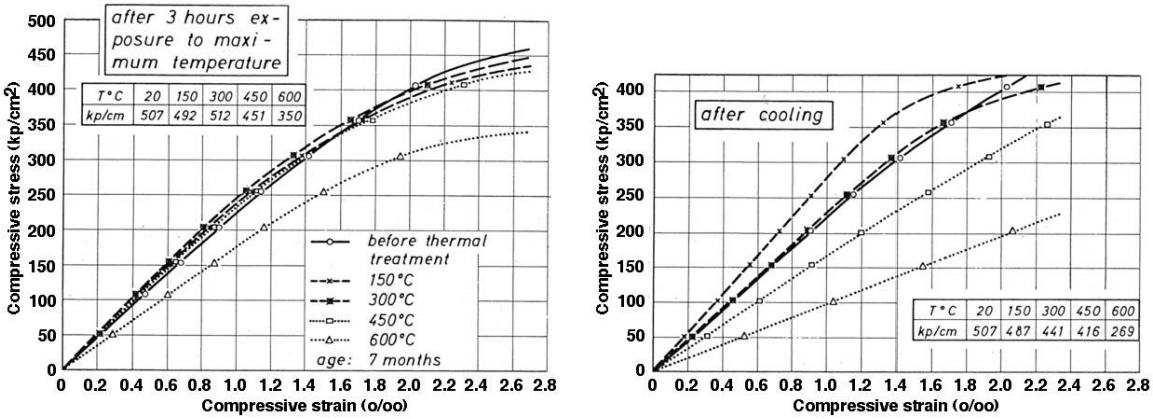

Figure 2.19 Effect of elevated temperature on stress-strain behavior of a quartz concrete.

Source: H. Weigler and R. Fischer, "Influence of High Temperatures on Strength and Deformations of Concrete," Paper SP 34-26 in *Special Publication SP-34*, Vol. I–III, American Concrete Institute, 1972.

* Technical Committee 363, "High-Strength Concrete," *Seventh International Symposium on Utilization of High Strength/High Performance Concrete*, ACI Special Publication 228, pp. 79-80, American Concrete Institute, Farmington Hills, Michigan, June 1, 2005. Does not include concretes produced using exotic materials or techniques.

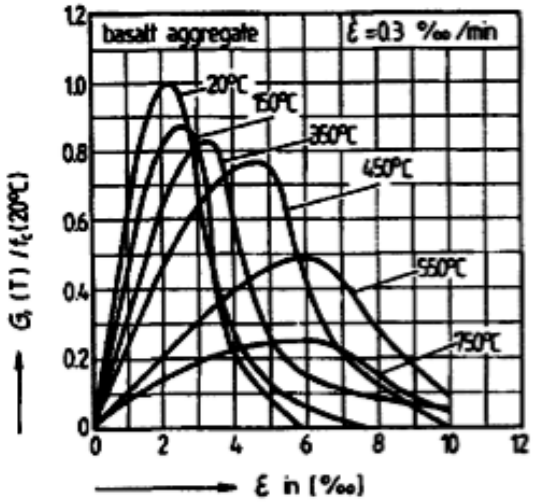

Figure 2.20 Stress-strain relationship for basalt concrete derived in strain-rate controlled tests.

Source: U. Schneider, "Concrete at High Temperatures – A General Review," *Fire Safety Journal* 13, pp. 55-68, 1988.

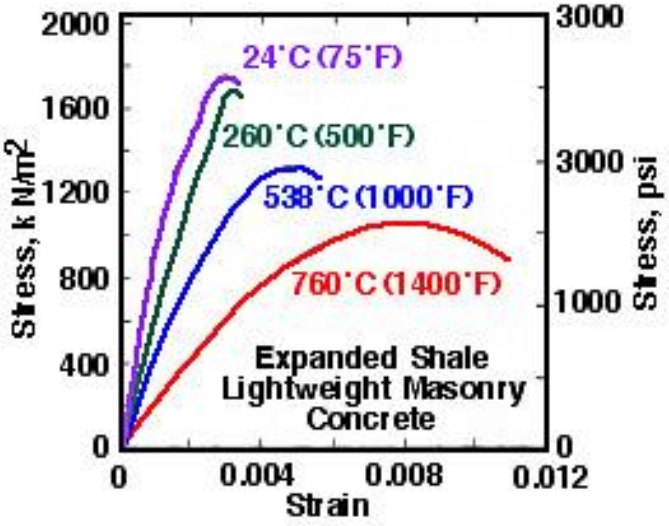

Figure 2.21 Stress-strain curves for expanded shale lightweight masonry concrete tested at temperature.

Source: M.S. Abrams, "Behavior of Inorganic Materials in Fire," *Design of Buildings for Fire Safety*, ASTM STP 685, American Society for Testing and Materials, West Conshohocken, Pennsylvania, 1979.

architectural, and structural advantages that high-strength concrete can provide relative to normal-strength concrete (e.g., high-strength concrete used for primary load-bearing members such as structural framing consisting of beams and columns) [2.57]. The improved strength and performance is obtained by reducing the amount of water in the mix and use of chemical or mineral admixtures to reduce permeability and impart improved workability. However, with the use of lower water-cement ratios and admixtures the concretes become more brittle and exhibit reduced permeability that can make the concretes more susceptible to spalling under rapid thermal loadings. Stress-strain results for a high-strength (91.8 MPa) and a normal-strength (32.9 MPa) concrete tested at temperature are presented in Figure 2.22 and indicate that the high-strength concrete has steeper and more linear stress-strain curves and tends to fail in a more brittle manner than normal-strength concrete. [2.58]. In order to address the potential limitations of high-strength concretes under thermal loadings, polypropylene or steel fibers have been incorporated into the mixes. Additions of

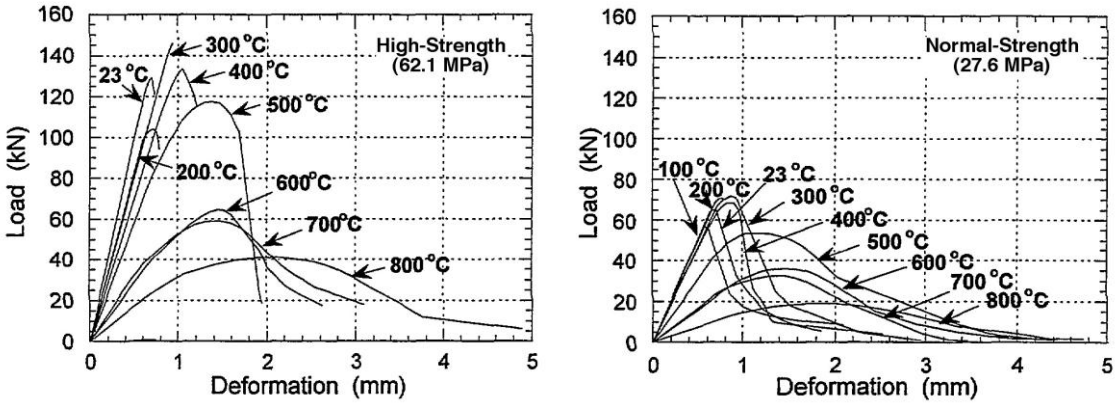

Figure 2.22 Comparison of high-strength and normal-strength concrete load-deformation curves.

Source: C. Castillo and A.J. Durrani, "Effect of Transient High Temperature on High-Strength Concrete," *ACI Materials Journal* **87**(1), American Concrete Institute, pp. 47-53, January-February 1990.

relatively small amounts (e.g., 0.3%, by volume) of polypropylene fibers to the concrete mix improves the resistance to spalling as the polypropylene fibers melt at around 165˚C to relieve the vapor pressure [2.59]. Steel fiber additions (e.g., 1 to 2%, by volume) enhance the mechanical behavior of high-strength concrete at elevated temperature and significantly improve the concrete ductility [2.60]. Figure 2.23 presents a comparison of stress-strain curves for specimens containing polypropylene fibers with several concretes tested at room temperature

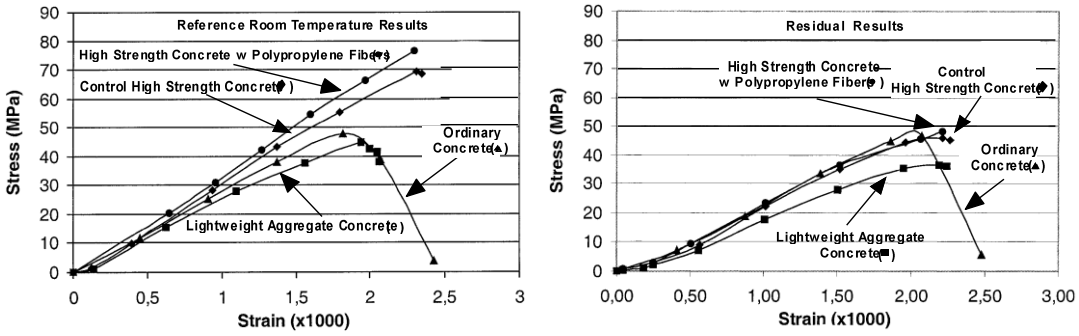

Figure 2.23 Stress-strain relationships for several concrete types before and after exposure to 200˚C.

Source: A. Noumowé and C. Galle, "Study of High Strength Concretes at Raised Temperature up to 200˚C: Thermal Gradient and Mechanical Behaviour," *Transactions of the 16th Structural Mechanics in Reactor Technology*, Paper #1580, Washington, DC, August 2001.

(reference) and after exposure for 7 days at 200˚C (residual) [2.61]. Types of concrete tested included control high strength concrete, concrete incorporating polypropylene fibers (0.22%, by volume), lightweight aggregate concrete (expanded clay), and ordinary concrete. Reference compressive strengths for the concretes were 70, 72, 45, and 48.5 MPa, respectively. Data indicate that the results for the mix with polypropylene fiber and the reference high strength concrete mix were similar, addition of lightweight aggregate reduced the slope of the stress-strain curve but improved the heat resistance, and ordinary concrete endured the effect of temperature better than high strength and lightweight concretes. Figures 2.24 and 2.25 present examples of stress-strain curves obtained at temperature for high-strength siliceous (granite) and carbonate (limestone) aggregate concretes, respectively, with and without steel fiber additions. Ninety-one-day compressive strengths of all mixes were in the range of 78 to 86 MPa. High-strength fiber-reinforced mixes contained about 0.5% steel fibers by volume. Results indicate that aggregate type has an effect on ultimate strain under high temperature conditions (i.e., carbonate aggregate concrete strain at peak strength was up to 40% greater than that for siliceous aggregate concrete) and addition of steel fibers increased ductility at elevated temperature of both concretes.

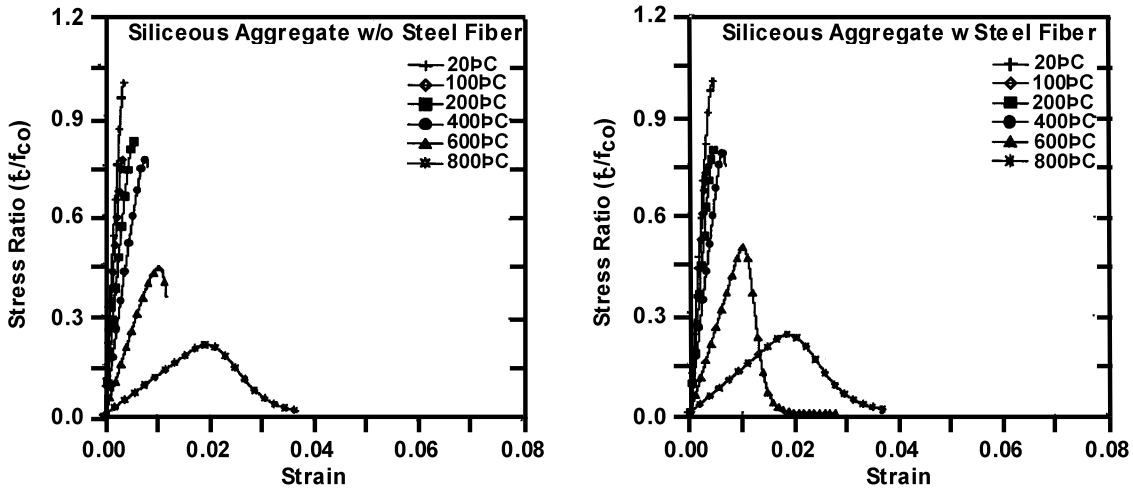

Figure 2.24 Stress-strain curves for high-strength siliceous aggregate concrete without and with steel fiber reinforcement.

Source: F-P. Cheng, V.K.R. Kodur, and T-C. Wang, "Stress-Strain Curves for High Strength Concrete at Elevated Temperatures," Report NRCC-46973, Institute for Research in Construction, National Research Council Canada, March 15, 2004 (http://irc.nrc-cnrc.gc.ca/ircpubs).

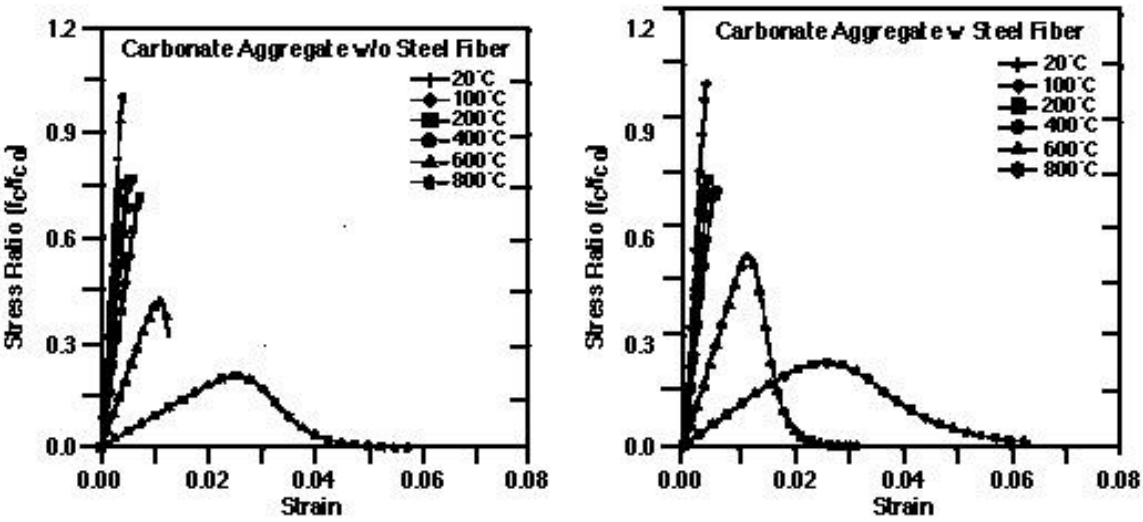

Figure 2.25 Stress-strain curves for high-strength carbonate aggregate concrete without and with steel fiber reinforcement.

Source: F-P. Cheng, V.K.R. Kodur, and T-C. Wang, "Stress-Strain Curves for High Strength Concrete at Elevated Temperatures," Report NRCC-46973, Institute for Research in Construction, National Research Council Canada, March 15, 2004 (http://irc.nrc-cnrc.gc.ca/ircpubs).

Limited data are available on the effect of strain rate on concrete stress-strain characteristics at temperatures of 20˚, 65˚, and 90˚C [2.62]. Nominal concrete compressive strengths were either 30 or 35 MPa after 60 days. Specimens 10-cm diam by 20-cm long were cured for five weeks in a water bath followed by five weeks at either 65˚ or 90˚C prior to testing. A comparison of compressive stress-strain curves at 20˚ and 65˚C for strain rates from 10^{-5}/sec to 10^{1}/sec is presented in Figure 2.26. Results indicate that initial elastic modulus is degraded as a result of elevated temperature exposure and increases with strain rate gradually approaching an upper shelf.

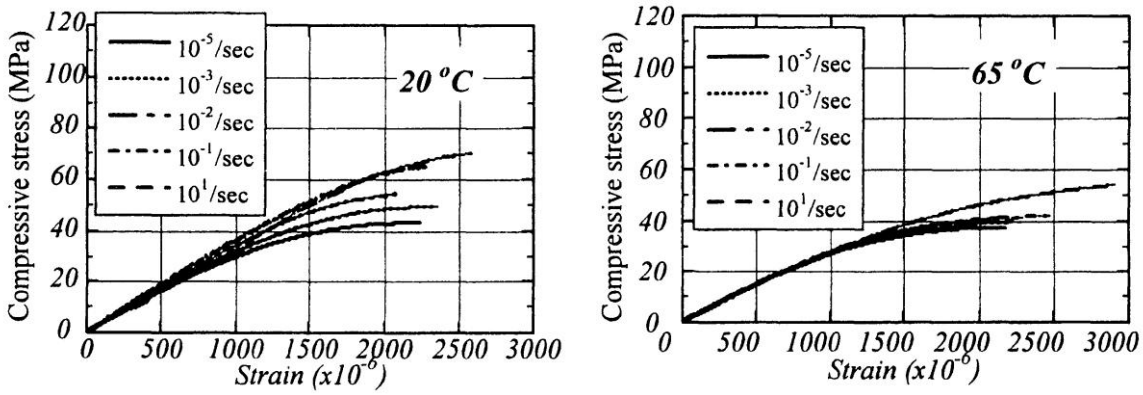

Figure 2.26 Comparison of compressive stress-strain curves for different strain rates at 20˚C and 65˚C.

Source: T. Yagashita, K. Shirai, C. Ito, and H. Shiojiri, "Effect of Strain Rate on Concrete Strength Under High Temperature," *International Conference on Structures Under Shock & Impact VI*, pp. 539-548, Cambridge, United Kingdom, WIT Press, July 2000.

Many nuclear power plant structures, such as prestressed concrete pressure vessels, will be under a compressive load prior to heating. Figure 2.27 demonstrates the beneficial effect of applied preload load (0, 10, or 30% the reference strength) during exposure to temperatures of either 250°C or 450°C on the normalized stress-strain curves [2.12].

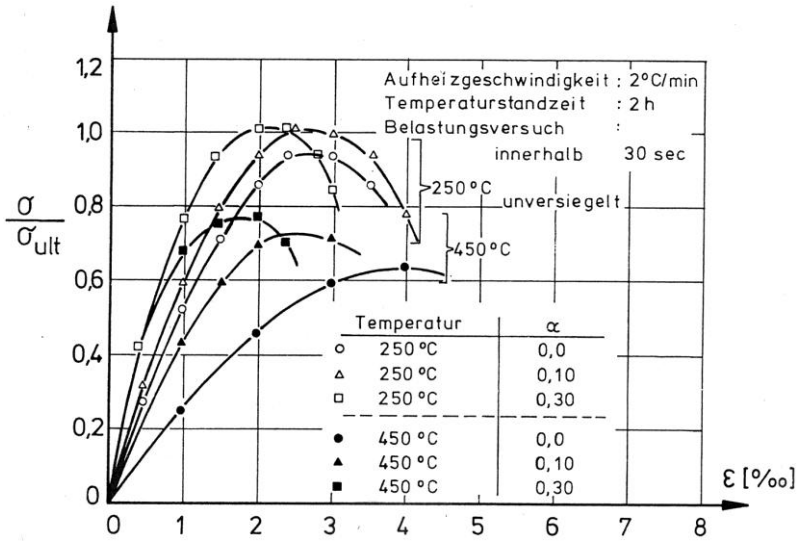

Figure 2.27 Stress-strain relationship of normal concrete with specimens loaded during the heating period.

Source: U. Schneider, *Behaviour of Concrete at High Temperature*, HEFT 337, Deutscher Ausschuss fur Stahlbeton, Wilhelm Ernst & Sohn, Munich, Germany, 1982.

Figure 2.28 provides data on the effect of preloading during heating on the concrete compressive stress-strain behavior for a 70 MPa ordinary Portland cement concrete and Figure 2.29 presents results for an ultra high-performance concrete (> 100 MPa) [2.63]. The unsealed specimens were tested at temperatures from room temperature to 500˚C (700˚C for ultra high-performance concrete) while either unloaded or preloaded to 20% of the specimen's compressive strength. Results indicate that the elastic modulus decreased as the test temperature increased for the specimens not preloaded and that the modulus of the specimens under sustained loading was larger than the modulus of the specimens without sustained loading at the same test temperature. The extent of linearity of the stress-strain curve for the ultra high-performance concrete was greater than that for the lower strength concrete (i.e., 80% of maximum stress versus 50%).

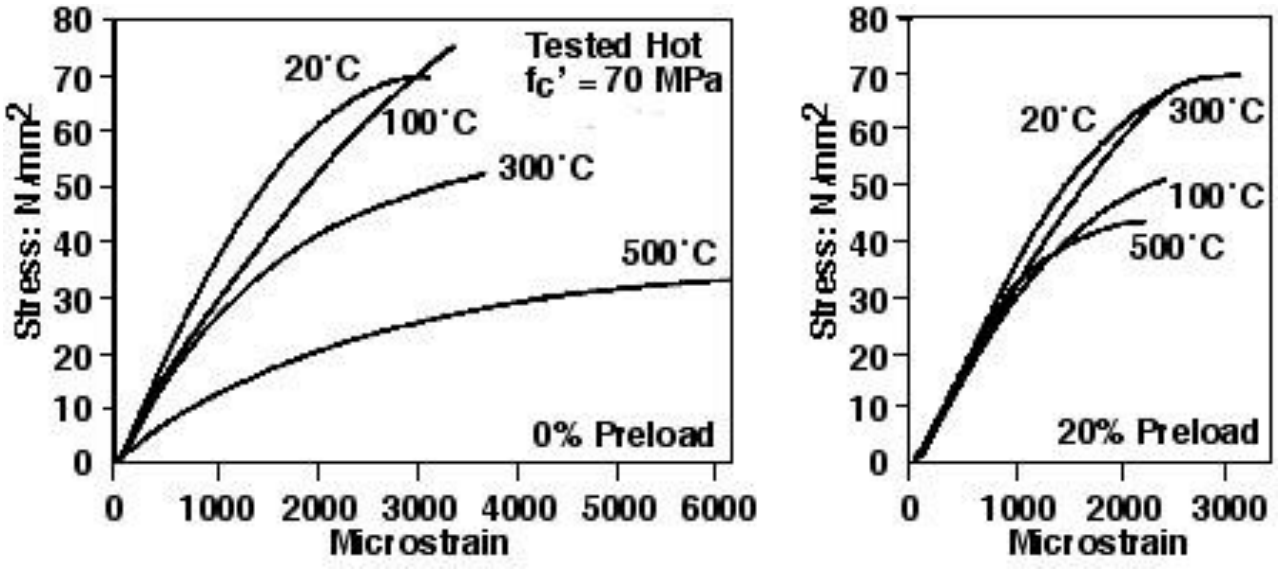

Figure 2.28 The effects of temperature and preloading on unsealed specimens tested at temperature: 70 MPa concrete.

Source: G.A. Khoury, C.E. Majorana, F. Pesavento, and B.A. Schrefler, "Modelling of Heated Concrete," *Magazine of Concrete Research* **54**(02), pp. 77-101, April 2002.

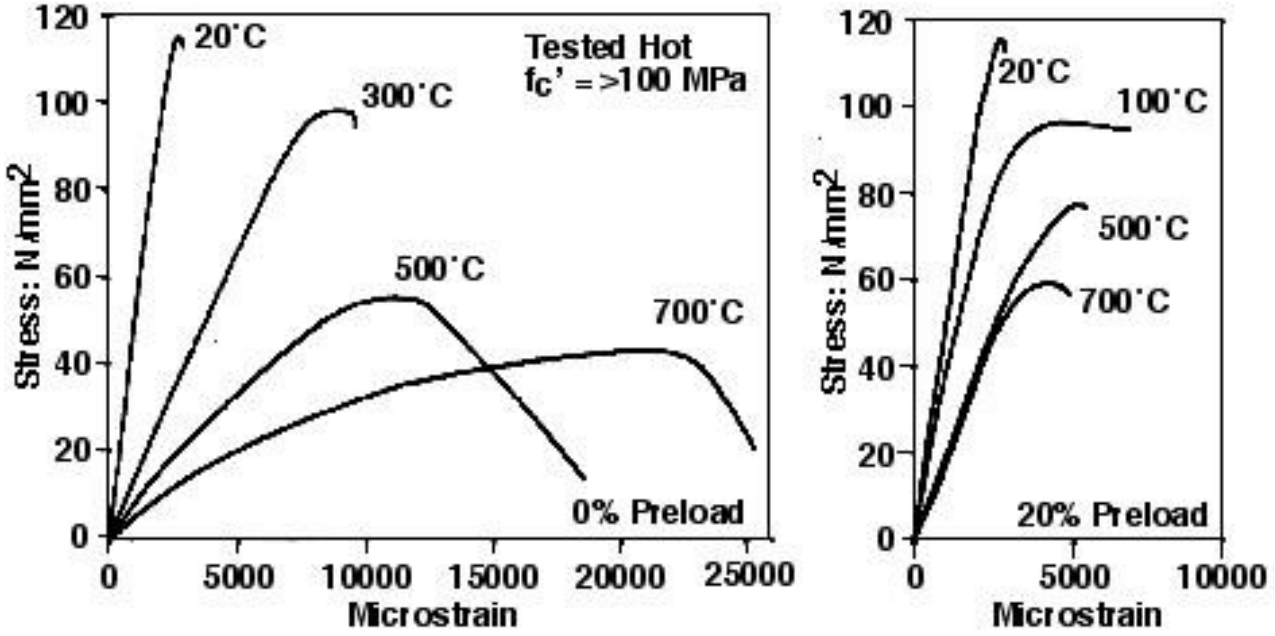

Figure 2.29 The effects of temperature and preloading on unsealed specimens tested at temperature: ultra high-performance concrete.

Source: G.A. Khoury, C.E. Majorana, F. Pesavento, and B.A. Schrefler, "Modelling of Heated Concrete," *Magazine of Concrete Research* **54**(02), pp. 77-101, April 2002.

Additional stress-strain results for specimens either unstressed or stressed (40% preload applied) during heating are presented in Figures 2.30 and 2.31, respectively [2.64]. Four concretes were investigated: normal-strength ordinary

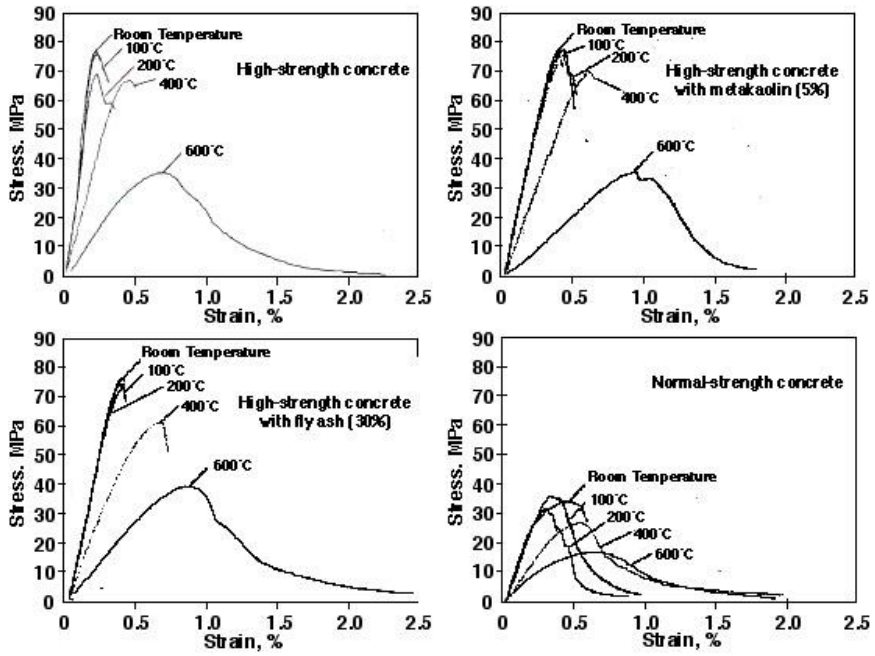

Figure 2.30 Temperature-dependent stress-strain curves in unstressed condition for specimens tested at temperature.

Source: Y.F. Fu, Y.L. Wong, C.S. Poon, and C.A. Tang, "Stress-Strain Behaviour of High-Strength Concrete at Elevated Temperature," *Magazine of Concrete Research* **57**(9), pp. 535-544, 2005.

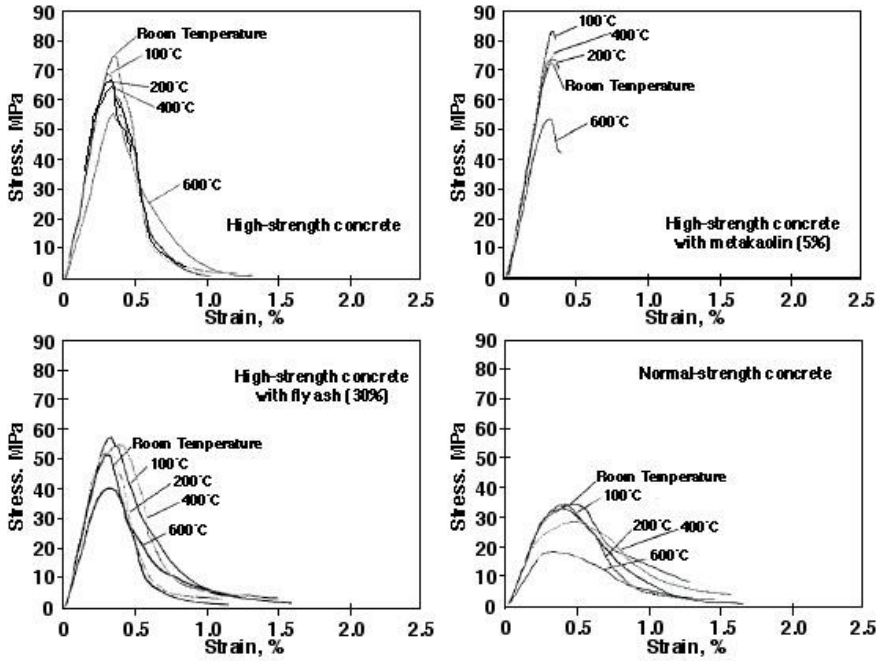

Figure 2.31 Temperature-dependent stress-strain curves in stressed condition for specimens tested at temperature.

Source: Y.F. Fu, Y.L. Wong, C.S. Poon, and C.A. Tang, "Stress-Strain Behaviour of High-Strength Concrete at Elevated Temperature," *Magazine of Concrete Research* **57**(9), pp. 535-544, 2005.

Portland cement concrete, high-strength ordinary Portland cement concrete, ordinary Portland cement concrete in which 30% of cement was replaced by fly ash, and ordinary Portland cement concrete in which 5% of cement was replace by metakaolin.* Granite aggregate having a 20-mm-maximum size was used in all the mixes. Specimens were permitted to thermally stabilize 60 minutes prior to testing. For the unstressed condition (Figure 2.30) the ascending branch of the curves consists of two components: (1) an elastic recoverable strain component, that is temperature dependent and is affected principally by the thermal load level during initial heating to the test temperature; and (2) an irrecoverable plastic strain component. For the normal strength concrete the ascending branch remained linear till about 40% peak strength while it was linear till about 60% for the high-strength concretes indicating that irrecoverable components of strain were small. Above 400˚C the stress-strain curves became increasingly nonlinear as the temperature increased and the peak strains corresponding to peak strength increased by up to a factor of two. For the stressed condition (Figure 2.31) the ascending portions of the stress-strain curves were significantly different than for the unstressed tests with the curves tending to be closer to the room temperature curves for each of the concretes. Nonlinearity increased with temperature but there were no significant increases in peak strain at peak strength. Strain values at peak strength were all less than those obtained for the unstressed condition. Mineral additions were noted to have improved the elevated temperature performance of the concrete.

The effect of cyclic load at elevated temperature and duration of heating has been investigated [2.65]. Specimens utilized were 15.24-cm-diam by 45.7-cm-long cylinders that were sealed in copper jackets after casting (Figure 2.32) and cured for 90-days prior to testing. Type II Portland cement and limestone fine and coarse aggregate (19.05 mm maximum size aggregate) were utilized in the concrete mix that had an average 28-d compressive strength of 44.7 MPa. Strains were determined by wire-resistance strain gages positioned as shown in Figure 2.32 and described elsewhere [2.66]. The effect of several factors on the stress-strain behavior of the concrete was investigated: (1) sustained temperature of 149˚C, (2) number of thermal cycles from 21˚ to 149˚ to 21˚C, (3) influence of permitting moisture to freely escape from concrete during thermal treatment (holes punched in copper sealing jackets), and (4) influence of testing concrete at 149˚C compared to permitting concrete to cool to room temperature prior to testing. Figure 2.33a provides stress-strain results obtained at temperature for specimens that were subjected to 149˚C for periods up to 25 days and Figure 2.33b provides results indicating the effect of

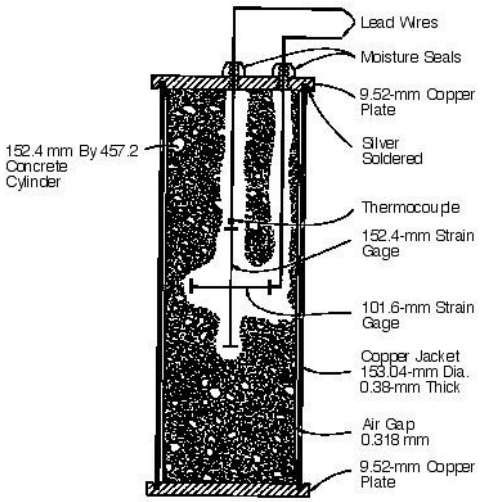

Figure 2.32 Test specimen for evaluation of cyclic and sustained thermal loads on concrete stress-strain curve.

Source: V.V. Bertero and M. Polivka, "Influence of Thermal Exposures on Mechanical Characteristics of Concrete," Paper SP-34-28 in *Concrete for Nuclear Reactors*, pp. 505-531, American Concrete Institute, Farmington Hills, Michigan, 1972.

* Metakaolin is a manufactured pozzolanic mineral admixture, derived from kaolin clay, that significantly enhances many performance characteristics of cement-based mortars, concretes, and related products.

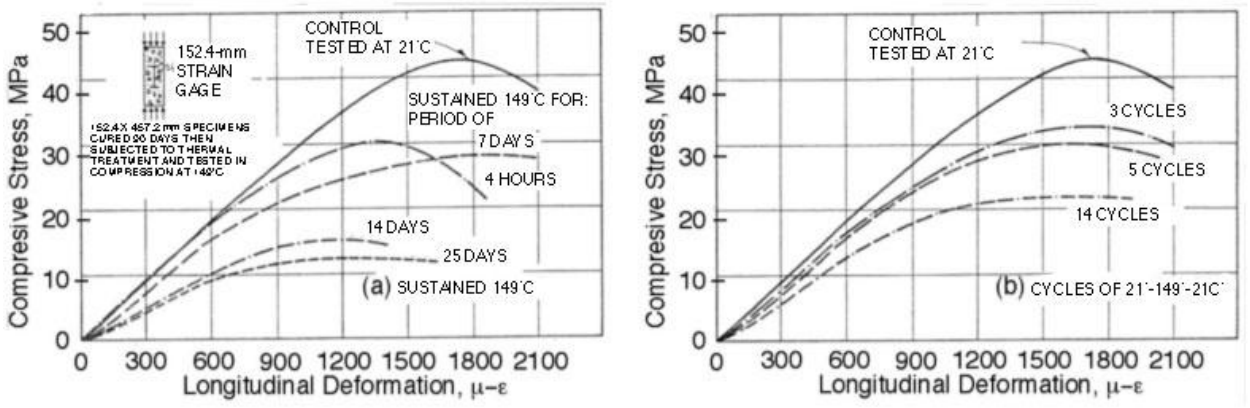

Figure 2.33 Effect of sustained temperature and thermal cycling on concrete stress-strain curve.

Source: V.V. Bertero and M. Polivka, "Influence of Thermal Exposures on Mechanical Characteristics of Concrete," Paper SP-34-28 in *Concrete for Nuclear Reactors*, pp. 505-531, American Concrete Institute, Farmington Hills, Michigan, 1972.

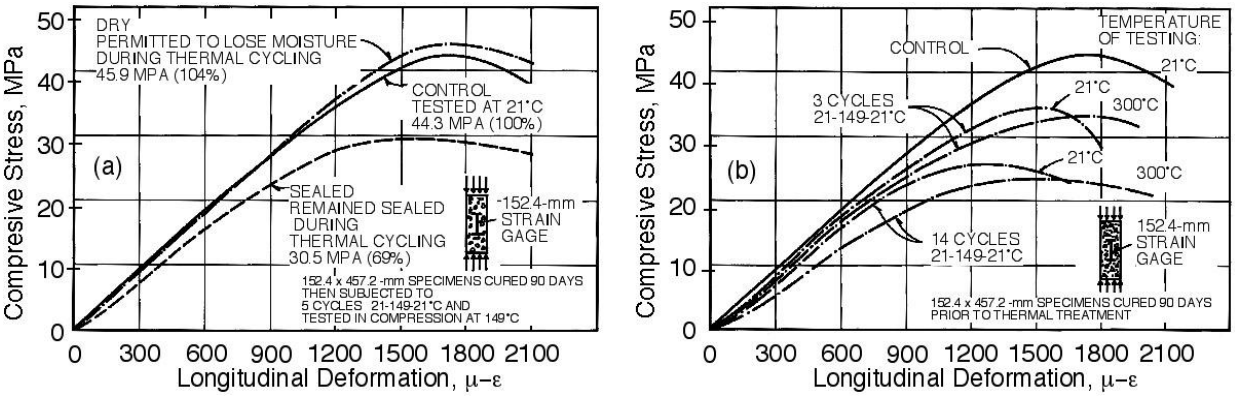

Figure 2.34 Effect of moisture condition and temperature on concrete stress-strain curve.

Source: V.V. Bertero and M. Polivka, "Influence of Thermal Exposures on Mechanical Characteristics of Concrete," Paper SP-34-28 in *Concrete for Nuclear Reactors*, pp. 505-531, American Concrete Institute, Farmington Hills, Michigan, 1972.

number of thermal cycles (one to fourteen) from 21˚ to 149˚ to 21˚C. As the duration of thermal conditioning increased and the number of thermal cycles increased the slope of the stress-strain curve decreased and in general the strain at peak stress decreased. However, if moisture is permitted to freely escape during thermal cycling (five cycles) the stress-strain curve is not significantly affected as noted in Figure 2.34a. Overall, specimens from which moisture was permitted to escape exhibited little difference in characteristics whether tested at 21˚ or 149˚C. Figure 2.34b indicates that for sealed specimens tested at 149˚C the mechanical characteristics of the concrete are somewhat inferior to those obtained when tested at 21˚C. Main parameters that affected the stress-strain relationship at elevated temperature were the moisture condition, the number of thermal cycles, and the temperature at which the concrete is tested.

Limited information is available on the effect of cooling regime (e.g, cooling rate)* on the stress-strain response of concrete. One study has been identified in which stress-strain curves were developed as part of an investigation of

*Cooling regimes are of importance for conditions where concrete has been subjected to thermal loading that is followed by rapid cooling (e.g., accident condition with water quenching).

strength and stiffness characteristics of concrete subjected to various heating and cooling scenarios [2.67]. A granite aggregate ordinary Portland cement concrete having a 28-day reference compressive strength of 21.16 MPa was used to fabricate 101.6-mm-diameter by 203.2-mm-long cylindrical test specimens that were cured for eight weeks in a fog room (23˚C and 93% relative humidity). The specimens were heated in a furnace to 200˚, 400˚, 600˚, or 800˚C with a holding time at temperature of four hours. Following heating, the specimens were cooled slowly (1˚C/minute), naturally (left in furnace and permitted to cool slowly), or rapidly (e.g., specimen removed from furnace and placed into a tank of water initially at 20˚C). Stress-strain curves for slow, natural, and water cooling are presented in Figure 2.35. The initial slope of the stress-strain curves decreased significantly as the temperature increased. The elastic region of the specimens subjected to slow or natural cooling and temperatures of 600˚C and beyond is nonlinear. For water cooling a similar trend was observed at temperatures of 400˚C and beyond. Although the peak stress following thermal exposure was less at each temperature investigated for the water-cooled specimens, the strain at peak stress at each temperature was greater than that for the specimens cooled either slowly or naturally.

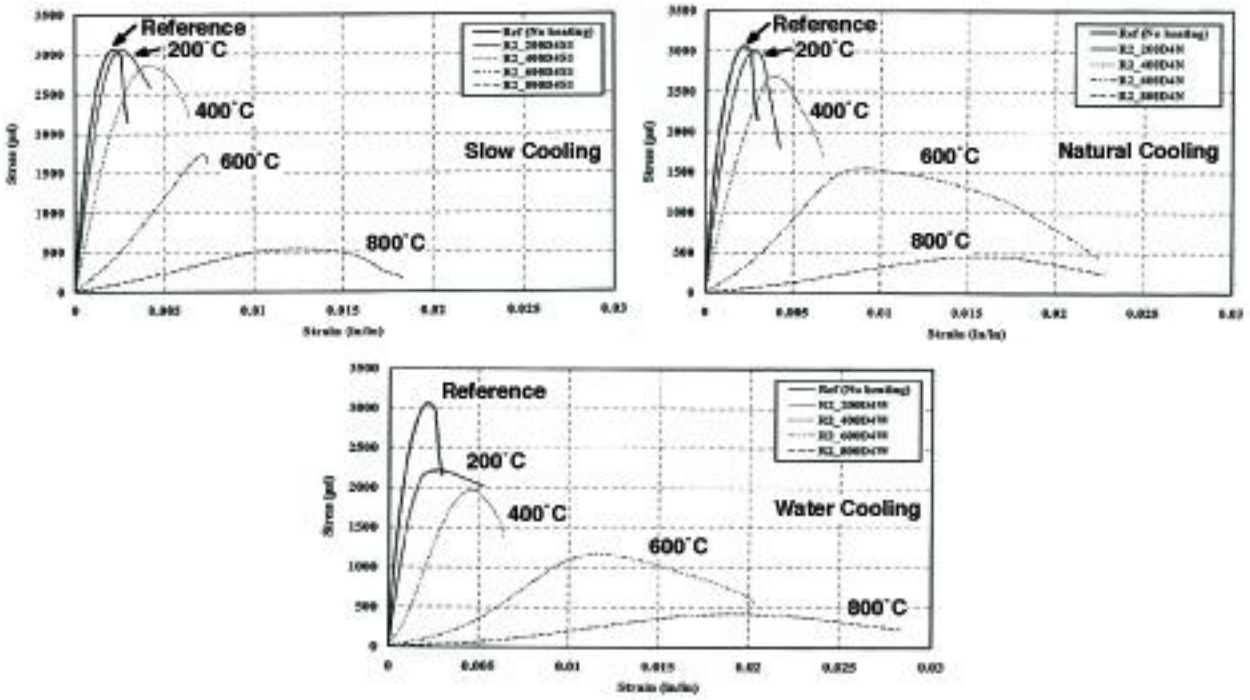

Figure 2.35 Effect of cooling regime on stress-strain curves following thermal exposure.

Source: J. Lee, Y. Xi, and K. Willam, "Concrete Under High Temperature Heating and Cooling," Report SESM No.09/2006, Department of Civil, Environmental, and Architectural Engineering, University of Colorado at Boulder, 2006.

Uniaxial Tension Testing

Results presenting tensile stress-strain curves for concrete at elevated temperature are extremely limited. Figure 2.36 presents the effect of temperature on the tensile stress-strain behavior of a 102 MPa high performance concrete containing silica fume that was tested in direct tension.

Multiaxial Testing

In large structures, such as prestressed concrete pressure vessels, the concrete is stressed either biaxially or triaxially. Unfortunately only limited data at elevated temperature exist for concrete loaded under either biaxial or triaxial conditions.

The test frame presented in Figure 2.37 was used to conduct biaxial tests of 200 by 200 by 50 mm^3 gravel (quartz) concrete specimens [62.0 N/mm^2 (cube strength)] [2.68,2.69]. Load was applied to the specimen using four servohydraulic jacks and brush loading platens. The tests were conducted at temperature using unsealed specimens.

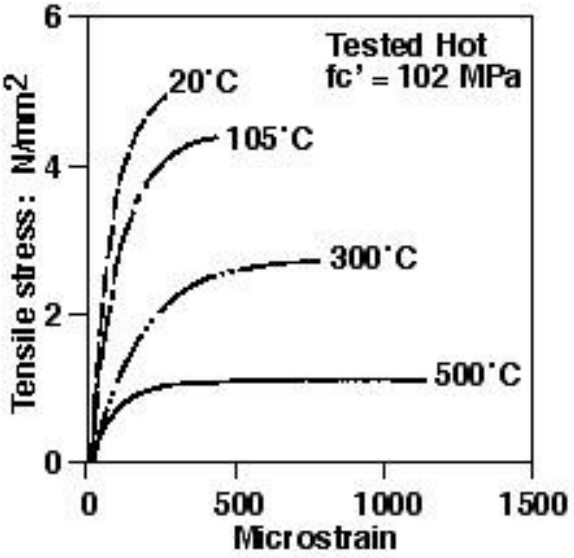

Figure 2.36 Direct uniaxial tensile stress-strain results for an unsealed high performance concrete tested at several temperatures.

Source: G.A. Khoury, C.E. Majorana, F. Pesavento, and B.A. Schrefler, "Modelling of Heated Concrete," *Magazine of Concrete Research* **54**(02), pp. 77-101, April 2002

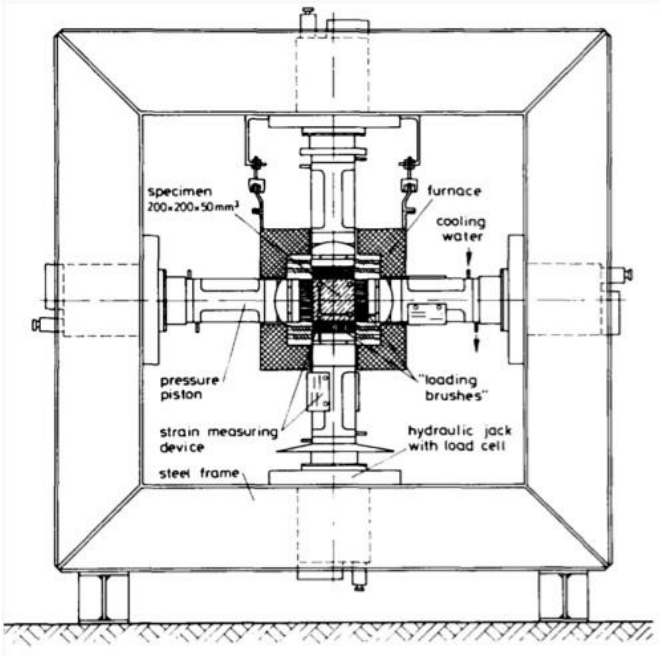

Figure 2.37 Biaxial test system.

Source: C. Ehm and U. Schneider, "The High Temperature Behaviour of Concrete Under Biaxial Load," *Cement and Concrete Research* **25**, pp. 27-34, 1985.

Figures 2.38, 2.39, and 2.40 presents reference uniaxial (σ_1:σ_2 = 1:0), biaxial (σ_1:σ_2 = 1:0.4), and biaxial (σ_1:σ_2 = 1:1), respectively, for test temperatures from 20˚ to 600˚C. The mechanical strains (ε_1, ε_2, and ε_3) were found to be dependent on the stress level, the stress ratio, and the test temperature. The deformations increased with increasing load in all three orthogonal directions and at high stress levels they showed a nonlinear relation in the direction of greatest principal stress. The ultimate strains for all three axes shift to greater values with increasing temperature. At higher temperatures the stress-strain curves were highly nonlinear with the concrete behavior changing from brittle behavior to a soft and plastic behavior. Strains in the unstressed axis (ε_3) reached high values at elevated temperatures and high stress ratios with a maximum value occurring when the stress ratio was 1.0.

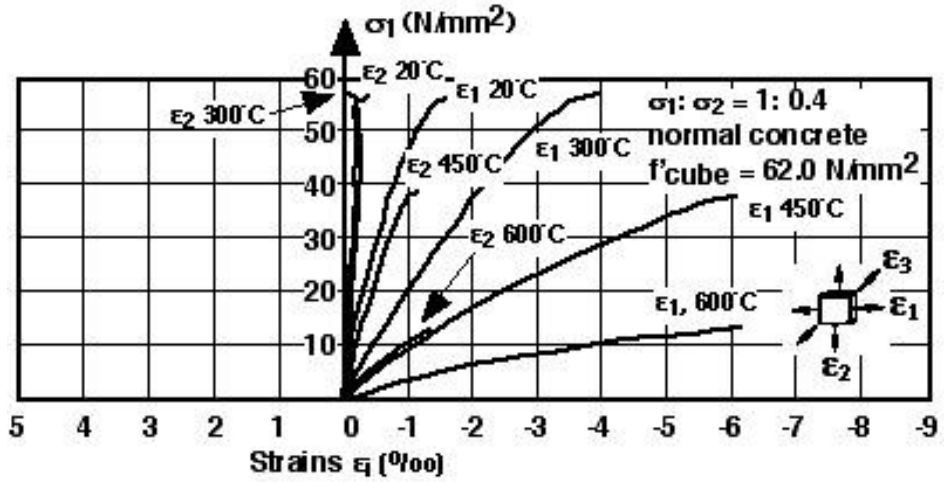

Figure 2.38 Biaxial test results: σ_1:σ_2 = 1: 0 (uniaxial).

Source: C. Ehm and U. Schneider, "The High Temperature Behaviour of Concrete Under Biaxial Load," *Cement and Concrete Research* **25**, pp. 27-34, 1985.

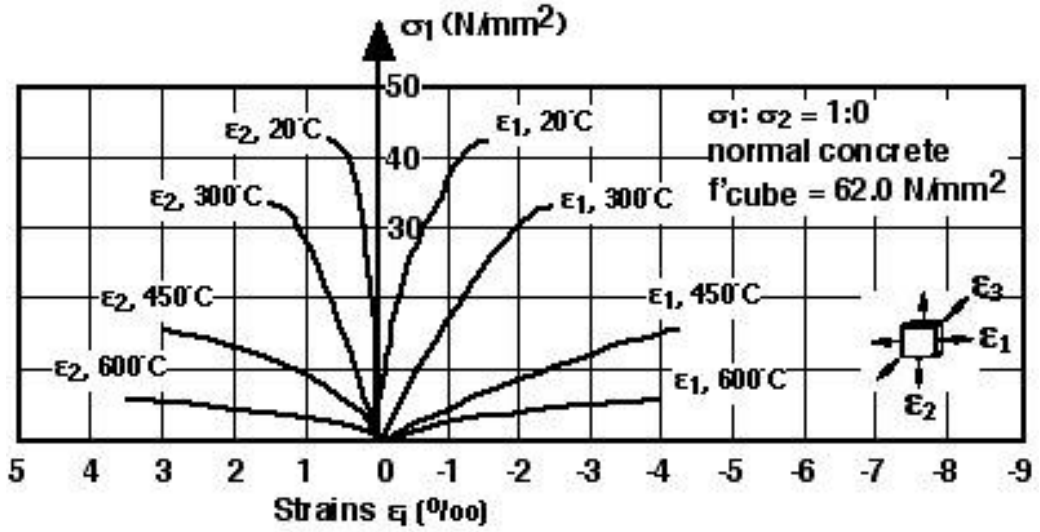

Figure 2.39 Biaxial test results: σ_1:σ_2 = 1: 0.4.

Source: C. Ehm and U. Schneider, "The High Temperature Behaviour of Concrete Under Biaxial Load," *Cement and Concrete Research* **25**, pp. 27-34, 1985.

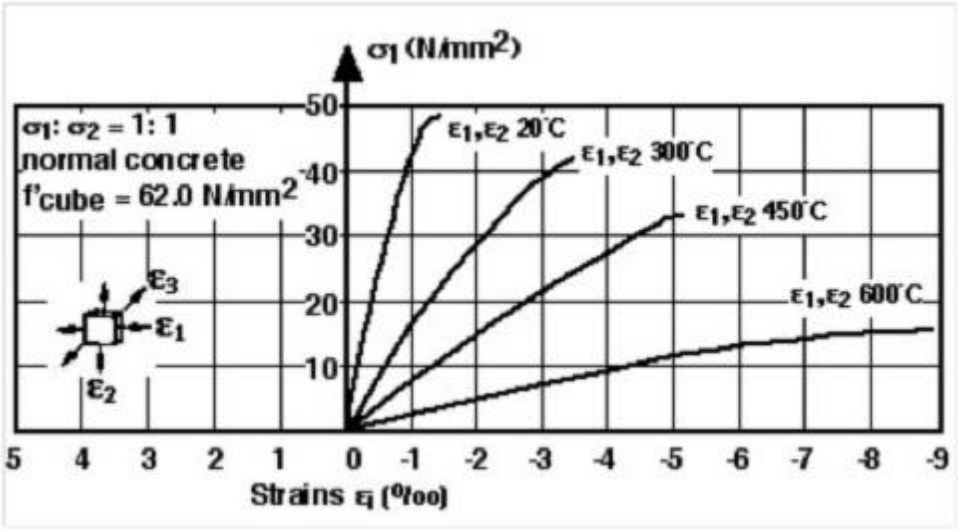

Figure 2.40 Biaxial test results: σ_1:σ_2 = 1: 1.

Source: C. Ehm and U. Schneider, "The High Temperature Behaviour of Concrete Under Biaxial Load," *Cement and Concrete Research* **25**, pp. 27-34, 1985.

When concrete is under a biaxial tension-compression state of stress the capability of concrete to resist cracking is diminished, and both the tensile and compressive strengths are found to decrease rapidly [2.70]. Biaxial tension-compression tests at elevated temperature (i.e., 20˚, 200˚, 300˚, 500˚, and 600˚C) have been conducted using five stress ratios (i.e., 0,0.1, 0.25, 0.50, and 0.75) [2.70]. Specimens 100 by 100 by 100 mm^3 were fabricated using a 20 mm maximum size crushed limestone aggregate concrete having reference compressive and tensile strengths of 32.5 and 3.14 MPa, respectively. The specimens were held at temperature for six hours and then permitted to slowly cool to room temperature prior to testing. Stress ratios (σ_2/σ_3) investigated included 0 (uniaxial), -0.1, -0.25, -0.5, and -0.75. Figure 2.41 presents stress-strain curves for stress ratios of -0.1, -0.2, and -0.25. After high temperature exposure the concrete under tension-compression failed abruptly due to the tensile stress. For every stress ratio the initial elastic modulus and the peak stress values of the stress-strain curves in both principal compressive stress direction and principal tensile stress direction decreased with an increase in exposure temperature. With increasing exposure temperature the strains corresponding to peak stresses decreased, the stress peak inclined toward the strain axis, and the stress-strain curves tended to flatten.

Examples of Stress-Strain Relations for Concrete at Elevated Temperature. Several conceptual models are available for the mechanical behavior of concrete at elevated temperature (e.g., Anderberg and Thelandersson [2.53]; Schneider [2.56]; Terro [2.71]; Khoury, Majorana, Pesavento, and Schrefler [2.63]; Li and Purkiss [2.72]; Gawin, Pesavento, and Schrefler [2.73]; and Khennane and Baker [2.74]). The models were developed in order to establish a general methodology for use in finite-element analysis of concrete structures. In most of these thermomechanical models the strain imposed is broken into four different types: (1) free thermal strain resulting from the change in temperature, (2) creep strain due to the dislocation of microstructures within the material (3) transient strain caused by changes in the chemical composition of the concrete, and (4) stress-related strain resulting from externally applied forces [2.72]. Frequently the creep strain and transient strain are combined as a load-induced thermal strain that at temperatures greater than 100˚C depends mainly on temperature rather than time [2.75]. As noted by results presented previously, the stress-related strain is a function of temperature, stress, and time. A critical review involving several of the stress-strain constitutive models identified above has been completed [2.72]. Formulations identified in the literature that have been used to calculate parameters that affect the stress-strain relationships include:

- concrete compressive strength [2.38]
- strain at peak stress [2.71]
- maximum compressive strain [2.71]
- concrete tensile strength [2.71]

- initial concrete modulus of elasticity [2.53]
- unrestrained thermal strain [2.76]
- yield strength of reinforcing bars [2.77]
- bond strength [2.78]
- transient creep strain (results from changes in the chemical composition of concrete on first heating) [2.53,2.71,2.72].

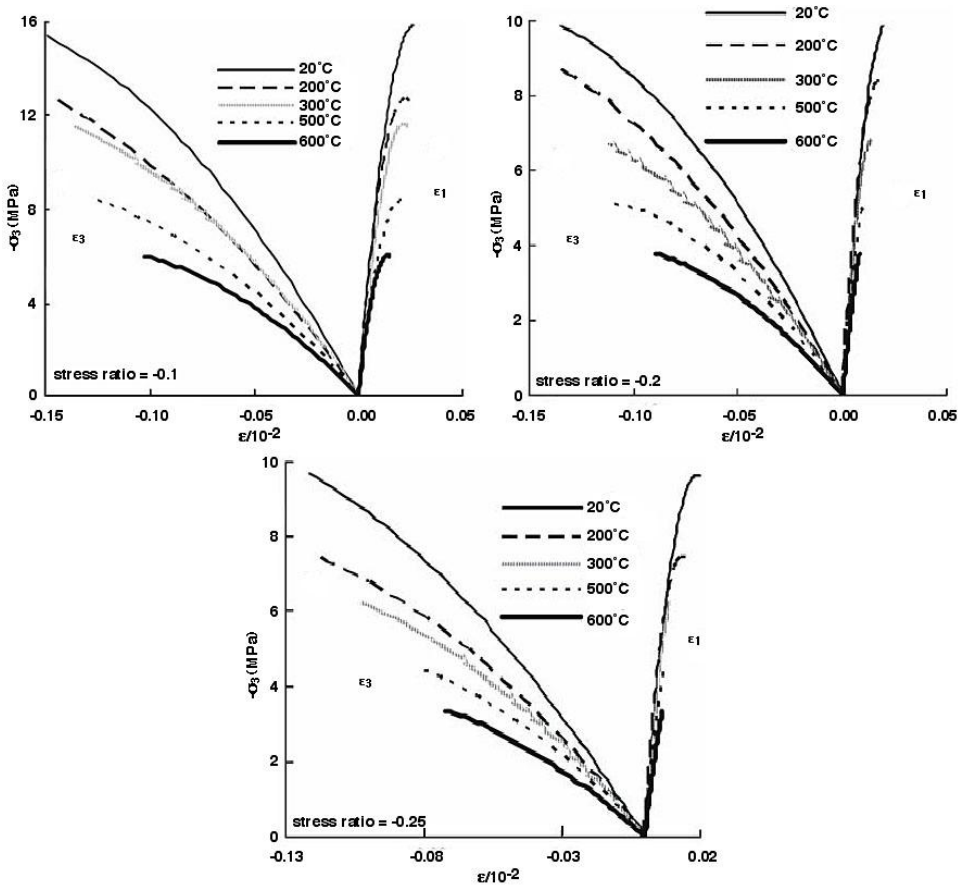

Figure 2.41 Effect of temperature on biaxial stress-strain curves for tension-compression loading.

Source: Y. Song, A. Zhang, L. Qing, and C. Yu, "Biaxial Tensile-cCompressive Experiment on Concrete at High Temperatures," *Frontiers of Architecture and Civil Engineering in China* **1**(1), pp. 94-98, 2007.

Additional information to that referenced above and what is provided below on modeling the strain components of concrete during heating is available [2.8,2.79].

An instantaneous stress-strain relationship for concrete with parabolic ascending and descending branches has been proposed [2.77]*

$$f_{cT} = f'_{cT} \cdot [1 - \left(\frac{(\varepsilon_{0T} - \varepsilon_{cT}}{\varepsilon_{0T}} \right)^2] \qquad \varepsilon_{cT} \le \varepsilon_{0T} \tag{2.1}$$

* A more detailed description of the nomenclature for the instantaneous stress-strain information utilized in this section is provided elsewhere [2.80].

$$f_{cT} = f'_{cT} \bullet [1 - \left(\frac{(\varepsilon_{cT} - \varepsilon_{0T}}{3\varepsilon_{0T}} \right)^2] \qquad \varepsilon_{cT} \geq \varepsilon_{0T} \tag{2.2}$$

Relationships have been proposed that are parabolic for the ascending branch and linear for the descending branch [2.53]

$$f_{cT} = E_{ciT} \bullet [\varepsilon_{cT} - \frac{\varepsilon^2_{cT}}{2 \bullet \varepsilon_{oT}}] \qquad \varepsilon_{cT} \leq \varepsilon_1 \tag{2.3}$$

$$f_{cT}(\text{MPa}) = f_1(\text{MPa}) - 880 \bullet (\varepsilon_{cT} - \varepsilon_1) \qquad \varepsilon_1 \leq \varepsilon_{cT} \tag{2.4}$$

$$f_1 = E_{ciT} \bullet \left(\varepsilon_1 - \frac{\varepsilon_1^2}{2 \bullet \varepsilon_{oT}} \right) \tag{2.5}$$

$$\varepsilon_1 = \varepsilon_{oT} \left(1 - \frac{880\text{MPa}}{E_{ciT}} \right) \tag{2.6}$$

A model has been proposed that accounts for the effect of concrete weight on the shape of the stress-strain curve by using a non-dimensional factor *n*. [2.81]. The recommended value of *n* is between 2.5 and 3.0 for lightweight and normal weight concrete,.

$$\varepsilon_{cT} = \left[1 + \frac{1}{n-1} \bullet \left(\frac{\varepsilon_{cT}}{\varepsilon_{oT}} \right)^n \right] \bullet \frac{f_{cT}}{E_{ciT}} \tag{2.7}$$

Another researcher [2.71] recommended use of n = 2 in the above model.

To account for transient creep effects, each of the above considered the total strain to be composed of separate components [2.80]. The thermal strain is a function of the temperature so it can be separated from the total strain. Calculation of transient creep strain requires an assumption of the corresponding stress which leads to an iterative solution.

Additional compressive and tensile stress-strain relationships have been proposed for concrete [2.80] that are based on two prior models [2.82,2.83]. The models were modified by replacing f'_c and ε_{oc} with the temperature-dependent terms f'_{cT} and ε_{oTc} and modeling transient creep by shifting the strain at maximum stress by the transient creep strain [2.84].

Modification of the first model [2.82] for elevated temperature response is done by changing the strain ε_{50u} for ambient temperature shown in Figure 2.42 to ε_o.

$$f_{cT} = K_{hT} f'_{cT} \left[2.0 \left(\frac{\varepsilon_{cT}}{\varepsilon_{oTc} + \varepsilon_{tr}} \right) - \left(\frac{\varepsilon_{cT}}{\varepsilon_{oTc} + \varepsilon_{tr}} \right)^2 \right] \qquad \varepsilon_{cT} \leq \varepsilon_{oTc} + \varepsilon_{tr} \tag{2.8}$$

$$f_{cT} = K_{hT} f'_{cT} \left[1 - Z(\varepsilon_{cT} - \varepsilon_{oTc} - \varepsilon_{tr}) \right] \geq 0.2 K_{hT} f'_{cT} \tag{2.9}$$

$$K_{hT} = 1 + \frac{\rho_s f_{yT}}{f'_{cT}} \tag{2.10}$$

$$\varepsilon_{oTc} = \varepsilon_{oT} \text{ x } K_{hT} \tag{2.11}$$

$$Z = \frac{0.5}{\varepsilon_{50uT} + \varepsilon_{50h} - \varepsilon_{oTc} - \varepsilon_{tr}} \tag{2.12}$$

$$\varepsilon_{50uT} = \frac{3 + 0.29\ f_c^{'}}{145 f_c^{'} - 1000} \bullet \frac{\varepsilon_{oTc}}{\varepsilon_{oc}} + \varepsilon_{tr} \tag{2.13}$$

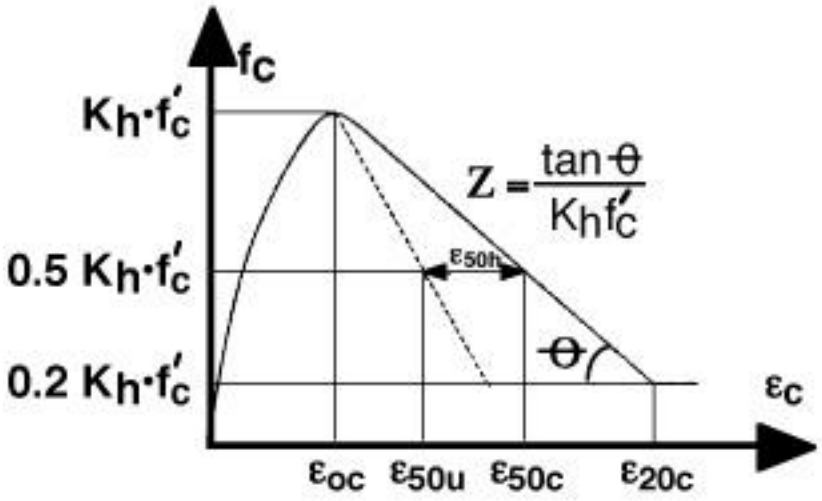

Figure 2.42 Instantaneous stress-strain curve for concrete at ambient temperature.

Source: D.C. Kent and R. Park, "Flexural Members with Confined Concrete," *Journal Structural Engineering* **97**(ST7), pp. 1969-1990, American Society of Civil Engineers, 1971.

Modification of the second model [2.83] is done by estimating E_{ci} by using $2*f'_{cT}/\varepsilon_{oT}$ (r = 2).

$$f_{cT} = \frac{2 \bullet f_{ccT}^{'} \bullet \varepsilon_{cT}}{\left(\varepsilon_{ocT} + \varepsilon_{tr}\right) \bullet \left[1 + \left(\frac{\varepsilon_{cT}}{\varepsilon_{ocT} \bullet \varepsilon_{tr}}\right)^2\right]} \tag{2.14}$$

$$\varepsilon_{ocT} = \varepsilon_{oT} \bullet \left[1 + 5 \bullet \left(\frac{f_{ccT}^{'}}{f_{cT}^{'}} - 1\right)\right] \tag{2.15}$$

f'_{ccT} for circular sections is

$$= f_{cT}^{'} \bullet \left[-1.254 + 2.254 \bullet \sqrt{1 + \frac{7.94 \bullet f_{lT}^{'}}{f_{cT}^{'}}} - \frac{2 \bullet f_{lT}^{'}}{f_{cT}^{'}}\right] \tag{2.16}$$

The value of $f_{lT}^{'}$ can be taken as equal to $K_e \bullet \frac{2 \bullet f_{yT} \bullet A_s}{d_s \bullet S_h}$ and for rectangular sections $f_{ccT}^{'}$ is available based on area of stirrups and their temperature-dependent yield strength [2.83].

A comparison between different instantaneous stress-strain models {[2.53], [2.77], modified model 1 [2.82], and modified model 2 [2.83]} and experimental results [2.12,2.85,2.86] is provided in Figure 2.43. As noted in the

figure, all models did a good job of representing the ascending portion of the stress-strain curve. Reference [2.82] provided the most accurate representation of the descending branch of the curves at different temperatures.

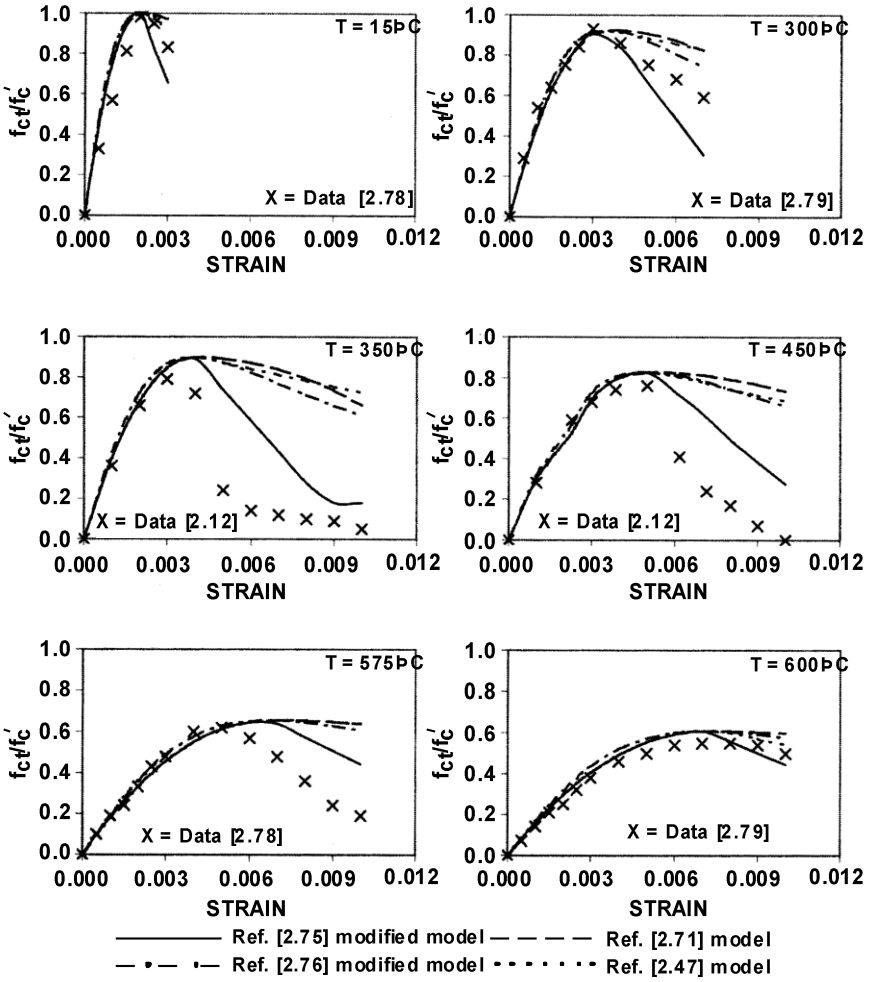

Figure 2.43 Instantaneous stress-strain curves at elevated temperature: comparison of predicted with experimental data.

Source: M.A. Youssef and M. Moftah, "General Stress-Strain Relationship for Concrete at Elevated Temperature," *Engineering Structures* **29**, pp. 2618-2634, 2007.

Additional stress-strain constitutive relationships for concrete at high-temperature have been developed. The American Society of Civil Engineers has proposed the following relationships for normal-strength concrete [2.87]:

$$\sigma_c = f'_{c,T}\left[1-\left(\frac{\varepsilon-\varepsilon_{\varepsilon_{max,T}}}{\varepsilon_{max,T}}\right)^2\right], \varepsilon \le \varepsilon_{max,T} \tag{2.17}$$

$$\sigma_c = f'_{c,T}\left[1-\left(\frac{\varepsilon_{\varepsilon_{max,T}}-\varepsilon}{3\varepsilon_{max,T}}\right)^2\right], \varepsilon > \varepsilon_{max,T} \tag{2.18}$$

$$f'_{c,T} = f'_c, \qquad 20^\circ C \le T \le 450^\circ C \tag{2.19}$$

$$f'_{c,T} = f'_c\left[2.011 - 2.353\left(\frac{T-20}{1000}\right)\right], \quad 450^\circ C \le T \le 874^\circ C \tag{2.20}$$

$$f'_{c,T} = 0, \qquad T > 874^\circ C \tag{2.21}$$

$$\varepsilon_{max,T} = 0.025 + \left(6.0T + 0.04T^2\right)x10^{-6}, \tag{2.22}$$

where:

σ_c = stress in concrete, MPa,
f'_c = 28-day concrete compressive strength in MPa at room temperature,
$f'_{c,T}$ = concrete compressive strength in MPa at temperature,
T = concrete temperature in ˚C,
ε = concrete mechanical strain,
$\varepsilon_{c1,T}$ = concrete strain at maximum stress at temperature T,
$\varepsilon_{cu1,T}$ = concrete ultimate strain at temperature T, and
$\varepsilon_{max,T}$ = concrete strain at maximum stress at temperature T.

This relationship has been modified for high-strength concrete [2.88]:

$$\sigma_c = f'_{c,T}\left[1 - \left(\frac{\varepsilon_{max,T} - \varepsilon}{\varepsilon_{max,T}}\right)^H\right], \varepsilon \le \varepsilon_{max,T} \tag{2.23}$$

$$\sigma_c = f'_{c,T}\left[1 - \left(\frac{30\left(\varepsilon - \varepsilon_{max,T}\right)}{\left(130 - f'_c\right)\varepsilon_{max,T}}\right)^2\right], \varepsilon > \varepsilon_{max,T} \tag{2.24}$$

$$f'_{c,T} = f'_c\left[1.0 - 0.003125\left(T - 20\right)\right], \quad T < 100^\circ C \tag{2.25}$$

$$f'_{c,T} = 0.75f'_c, \qquad 100^\circ C \le T \le 400^\circ C \tag{2.26}$$

$$f'_{c,T} = f'_c\left[1.33 - 0.00145T\right], \qquad 400^\circ C < T \tag{2.27}$$

where,

$$\varepsilon_{max,T} = 0.0018 + \left(6.7f'_c + 6.0T + 0.037T^2\right)x10^{-6}, \text{ and } H = 2.28 - 0.012f'_c.$$

Finally, Eurocode has developed a relationship for the ascending portion of the stress-stain curve for both normal- and high-strength concretes [2.46]:

$$\sigma_{c,\theta} = \frac{3\varepsilon_{c,\theta} f'_{c,\theta}}{\varepsilon_{cu,\theta}\left(2 + \left(\frac{\varepsilon_{c,\theta}}{\varepsilon_{cu,\theta}}\right)^3\right)}, \qquad \text{where } \varepsilon_{c,\theta} \le \varepsilon_{cu,\theta} \text{ and} \tag{2.28}$$

$\sigma_{c,\theta}$ = compressive stress at temperature θ,
$\varepsilon_{c,\theta}$ = compressive strain at temperature θ,
$\varepsilon_{cu,\theta}$ = ultimate concrete strain at temperature θ,
$f'_{c,\theta}$ = compressive strength of concrete at temperature θ, and
$f'_{c,20^\circ C}$ = compressive strength of concrete at room temperature.

Values of $f'_{c,\theta}$ and $\varepsilon_{cu,\theta}$ are obtained from Table 2.2.

Table 2.2 Values for parameters to describe ascending branch of stress-strain relationship for concrete at elevated temperature

Concrete Temperature θ_c (˚C)	$k_{c,\theta} = f'_{c,\theta} / f'_{c,20ºC}$			$\varepsilon_{cu,\theta}$ x 10^{-3} Normal Concrete
	Normal Concrete		Lightweight Concrete	
	Siliceous	Calcareous		
20	1	1	1	2.5
100	0.95	0.97	1	3.5
200	0.90	0.94	1	4.5
300	0.85	0.91	1	6.0
400	0.75	0.85	0.88	7.5
500	0.60	0.74	0.76	9.5
600	0.45	0.60	0.64	12.5
700	0.30	0.43	0.52	14.0
800	0.15	0.27	0.40	14.5
900	0.08	0.15	0.28	15.0
1000	0.04	0.06	0.16	15.0
1100	0.01	0.02	0.04	15.0
1200	0	0	0	15.0

Source: Comité Européen de Normalisation (CEN), *Eurocode 4: Design of Composite Steel and Concrete Structures, Part 1-2: General Rules—Structural Fire Design*, CEN ENV, Commission of European Communities, Brussels, 2004.

The Eurocode permits the use of the linear as well as the nonlinear descending branch in the numerical analysis.

A tensile stress-strain relationship has been proposed [2.80]. Until the cracking stress [f_{crT}] occurs, the ascending portion of the stress-strain curve is represented as a linear branch. Recommended values for [f_{crT}] are

$$\left(0.33\lambda\sqrt{f'_c}\right)\frac{f'_c}{f'_{cT}}\,(\text{MPa}) \qquad \text{direct tension, and} \tag{2.29}$$

$$\left(0.60\lambda\sqrt{f'_c}\right)\frac{f'_c}{f'_{cT}}\,(\text{MPa}) \qquad \text{flexural tension.} \tag{2.30}$$

After cracking, the model in Ref. [2.84] can be modified to account for the reduction in tensile resistance and bond strength [2.80]:

$$f_{tT} = \frac{\alpha_1\alpha_2 f_{crT}}{1+\sqrt{500\varepsilon_{cT}}} \bullet \frac{\tau_{uT}}{\tau_{uo}} \left(\varepsilon_{cT} > \frac{f_{crT}}{E_{ciT}}\right). \tag{2.31}$$

Information on a thermoplasticity model that has been developed for concrete under transient temperature and biaxial stress is available [2.79].

Summary. Relative to temperature effects on concrete's stress-strain curve, several general observations can be made based on information provided above. The ascending branch of the stress-strain curve consists of three components: (1) an elastic recoverable strain that is temperature dependent and is strongly influenced by the load level during initial heating to the test temperature; (2) an irrecoverable plastic strain component; and (3) a time-dependent creep component that is normally small at room temperature but can be significant at high temperatures, particularly above 550˚C [2.63]. The extent of linearity of the stress-strain curve increases as the concrete strength

increases and the slope of the curve tends to decrease as the temperature increases, except if material is under load while heated in which case the curve tends to become more linear and remain closer to its original slope [2.63]. The reduced brittleness of concrete with increasing temperature has been attributed to the evaporation of moisture with evaporation of gel water having a significant influence on the brittleness of concrete [2.89].

Under steady-state conditions, the original concrete strength, water-cement ratio, heating rate, and type of cement have minor influence on the stress-strain behavior. Aggregate-cement ratio, aggregate type, and presence of a sustained load during heating affect the shape of the stress-strain curve [2.46,2.77]. Concretes made with hard aggregates (e.g., siliceous or basalt) generally have a steeper decrease of the initial slope at high temperature (e.g., >550°C) than softer aggregates (e.g., lightweight) [2.56]. Concrete specimens tested at temperature tend to be stiffer and stronger than identical companion specimens heated to the same temperatures and then permitted to cool to room temperature before testing [2.55]. High-strength concrete has a steeper and more linear stress-strain curve and tends to fail in a more brittle manner than normal-strength concrete [2.58]. Curing conditions influence the stress-strain behavior only at relatively low temperatures (<300°C) [2.43]. Addition of fiber reinforcement increases the concrete ductility [2.51].

The mechanical strains in biaxial compression loading were found to be dependent on the stress level, the stress ratio, and the test temperature. The deformations increased with increasing load in all three orthogonal directions and at high stress levels they showed a nonlinear relation in the direction of greatest principal stress. The ultimate strains for all three axes shift to greater values with increasing temperature. At higher temperatures the stress-strain curves for biaxial loading were highly nonlinear with the concrete behavior changing from brittle behavior to a soft and plastic behavior. When concrete is under a biaxial tension-compression state of stress the capability of concrete to resist cracking is diminished, both the tensile and compressive strengths are found to decrease rapidly with increasing exposure temperature, and the concrete fails abruptly due to tensile stress. In addition, the initial elastic modulus and the peak stress values of the stress-strain curves in both principal compressive stress direction and principal tensile stress direction decreased with an increase in exposure temperature and the stress-strain curves tended to flatten.

2.2.1.2 Poisson's Ratio

Information and Data. Poisson's ratio is needed for conducting structural analyses of flat slabs, arch dams, tunnels, tanks, and other statically indeterminate members. At normal ambient conditions Poisson's ratio for concrete can vary from 0.11 to 0.32, but is generally in the range from 0.15 to 0.20. Under uniaxial compression loading, the beginning of matrix cracking occurs at the stress level where there is an apparent increase in the Poisson's ratio value [2.90]. At ambient temperature there appears to be no consistent relationship between Poisson's ratio and concrete characteristics such as water-cement ratio, curing age, and aggregate gradation, but it is generally lower in high-strength concrete and higher for saturated concrete and for dynamically-loaded concrete [2.91].

Data on the effect of elevated temperature on Poisson's ratio are somewhat limited and tend to be inconsistent. Figure 2.44 provides Poisson's ratio results for uniaxially loaded concrete for temperatures from 20° to 750°C [2.92]. At 20°C the Poisson's ratio is constant until the load exceeds about 70% of the ultimate load, while as the temperature increases the deviation of Poisson's ratio increases till in some cases it is >0.5. Figure 2.45 indicates that the Poisson's ratio decreases with increasing temperature from about 0.2 at room temperature to about 0.1 at 400°C [2.93]. This drop was attributed to a change in state due to heating that resulted in water desorption (e.g., weakening of the microstructure caused by breakage of bonds due to heating and by microcracking). When the specimen was permitted to cool after a given change in state the variation of Poisson's ratio with temperature was slight and nil when the evaporable water had been removed. In general, Poisson's ratio values obtained after drying are less than before drying [2.16]. In measurements on sealed cylinders the change in Poisson's ratio with increasing temperature was small (e.g., 0.2 to 0.18) [2.65]. When the concrete is under a confining pressure as it would be in many nuclear power plant concrete structures, it has been hypothesized that Poisson's ratio at elevated temperature would be about the same as at room temperature [2.16].

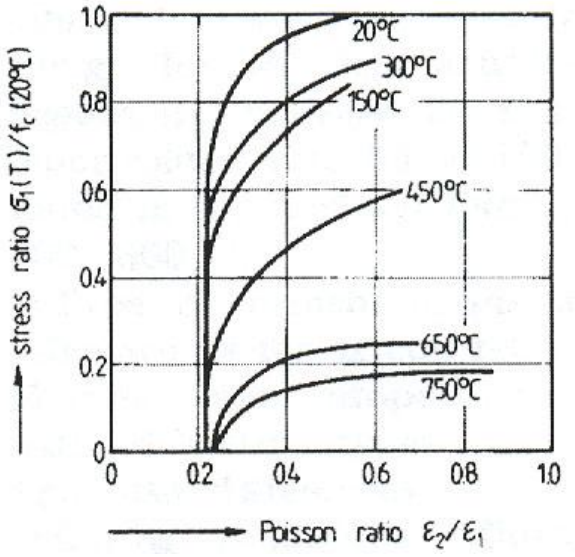

Figure 2.44 Poisson's ratio for uniaxially loaded concrete at high temperature.

Source: C. Ehm, "Experimental Investigations of the Biaxial Strength and Deformation of Concrete at High Temperatures," Dissertation, Technical University of Braunschweig, Germany, 1985.

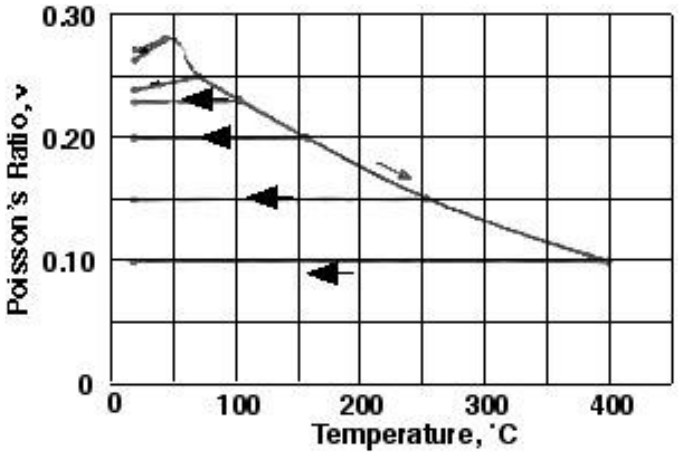

Figure 2.45 Poisson's ratio as a function of temperature for a quartzite concrete.

Source: J.C. Marechal, "Variations in the Modulus of Elasticity and Poisson's Ratio with Temperature," Paper SP 34-27 in *Concrete for Nuclear Reactors*, pp. 495-503, American Concrete Institute, Farmington Hills, Michigan, 1972.

The effect of elevated temperature on elastic properties of concretes containing either a carbonate, siliceous, or lightweight aggregate was evaluated using unsealed specimens [2.94]. A 8.53-mm maximum size aggregate was used in the mixes. All specimens were moist cured for 3 days at 23.9˚C and then stored in air at 50% relative humidity and 23.0˚C for 25 days. Two nominal concrete design compressive strengths were investigated: 27.6-31.0 MPa and 41.4-44.8 MPa. Figure 2.46 presents Poisson's ratio results as a function of temperature for the different aggregate materials and the two nominal concrete compressive strengths. The Poisson's ratio values generally ranged from 0.11 to 0.25. Although results obtained at higher temperature were somewhat erratic and a general trend was not apparent, results did show lower Poisson's ratio values at room temperature for the higher strength concretes.

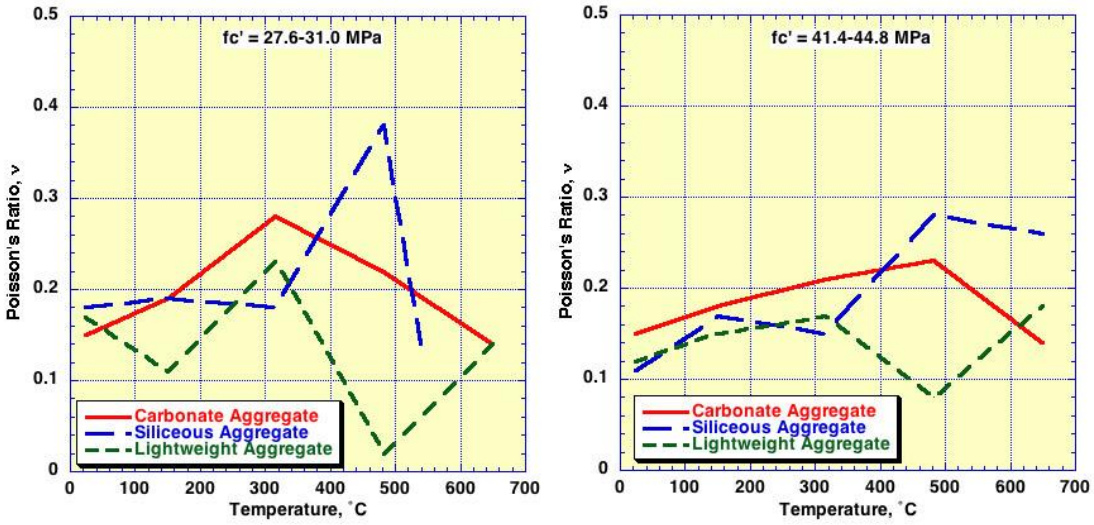

Figure 2.46 Effect of aggregate type and concrete strength on Poisson's ratio.

Source: C.R. Cruz, "Elastic Properties of Concrete at High Temperatures," Department Bulletin 191, *Journal of the Portland Cement Association Research and Development Laboratories* **8**(1), pp. 37-45, January 1966.

Elsewhere Poisson's ratio for high strength concrete has been reported to range from 0.11 at 20°C to 0.25 at 400°C, while above 400°C it increased [2.95]. Additional data for high strength concrete indicated that when the stress did not exceed 50% of peak value, the Poisson's ratio decreased with an increase in temperature [2.96]. Figure 2.47 presents Poisson's ratio results for a hard sandstone aggregate concrete after various heating periods (i.e., 1, 7, 28, and 91 d) at 175°C for specimens that were either sealed or unsealed during heating [2.97]. Poisson's ratio ranged from 0.14 to 0.22 with the trend for it to be larger for the sealed specimens.

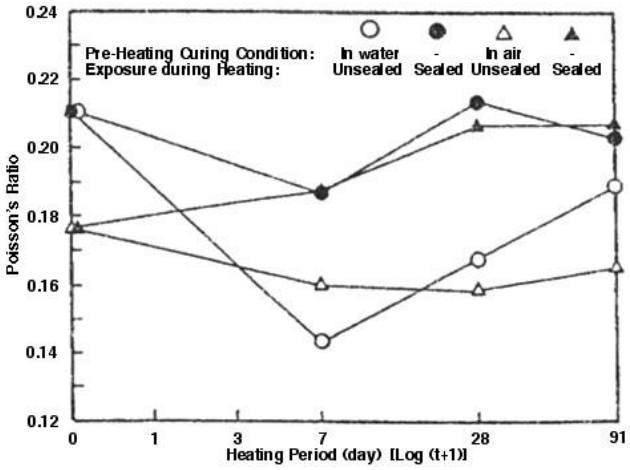

Figure 2.47 Poisson's ratio results for sealed and unsealed concrete specimens.

Source: K. Hirano, K. Ohmatsuzawa, T. Takeda, S. Nakane, T. Kawaguchi, and K. Nagao, "Physical Properties of Concrete Subjected to High Temperature for MONJU," Paper P2-25, Power Reactor and Nuclear Fuel Development Corporation, Tokyo, Japan.

The effect of thermal cycling (ambient to 180˚C to ambient) on Poisson's ratio over a period of 1,024 days was evaluated for a concrete that was similar to that used for the Hanford nuclear underground storage tanks [2.98,2.99]. Two concrete mixes having nominal compressive strengths of 20.7 and 31.0 MPa were utilized in the investigation.

The concrete was fabricated from Type II Portland cement and contained basalt coarse aggregate. Two thermal cycling programs were utilized, either a 14- or 28-day period for cycling from 21˚ to 176.7˚ to 21˚C. Poisson's ratio was determined at room temperature. Figure 2.48 presents Poisson's ratio results as a percentage of initial room temperature value versus number of temperature cycles. Measured values after one 28-day thermal cycle were approximately 35% lower than those obtained from the unheated specimens, however, with increasing number of thermal cycles the Poisson's ratio recovered somewhat. Results for the 14-day thermal cycle series were similar except the minimum in Poisson's ratio occurred later (e.g., after 3 cycles) and the reduction was not as great. The magnitude of longitudinal and lateral strains measured was larger for the long-term heated concrete than for the unheated concrete, though their Poisson's ratio was essentially the same. The variation in Poisson's ratio with length of exposure to 176.7˚C is presented in Figure 2.49. As the length of exposure to the maximum temperature level increased the Poisson's ratio tended to return to the unheated value with the lower strength concrete recovering more than the higher strength concrete.

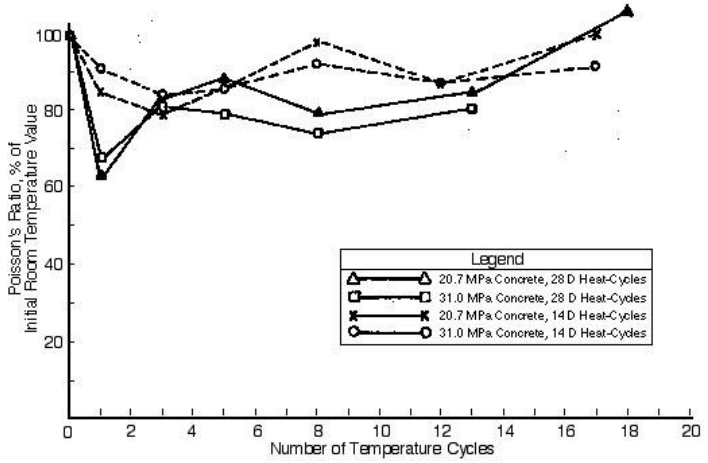

Figure 2.48 Variation of Poisson's ratio of basalt aggregate concrete with number of thermal cycles (ambient to 176.7˚C to ambient).

Source: C. Defigh-Price, "Effects of Long-Term Exposure to Elevated Temperature on the Mechanical Properties of Hanford Concrete," Report RHO-C-54, Construction Technology Laboratories, Portland Cement Association, Skokie, Illinois, October 1981.

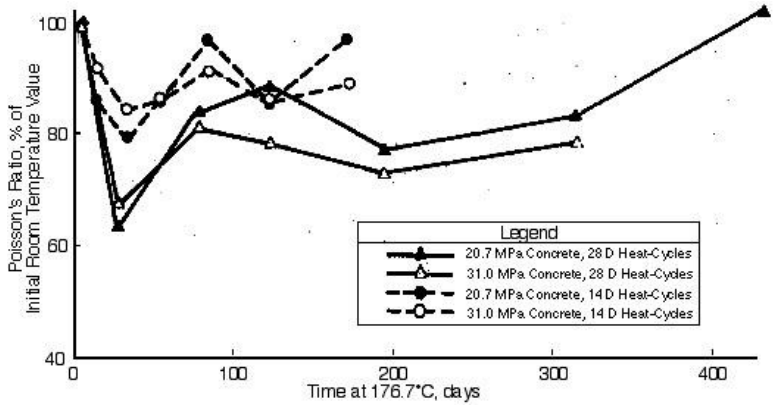

Figure 2.49 Variation of Poisson's ratio of basalt aggregate concrete with length of exposure to 176.7˚C.

Source: C. Defigh-Price, "Effects of Long-Term Exposure to Elevated Temperature on the Mechanical Properties of Hanford Concrete," Report RHO-C-54, Construction Technology Laboratories, Portland Cement Association, Skokie, Illinois, October 1981.

Summary. Poisson's ratio data at elevated temperature are very limited and results tend to be inconsistent and appear to not exhibit a strong dependence on temperature. Values obtained after drying are less than those obtained before drying and for moderate temperatures (e.g., T<180˚C) the values tend to increase with increasing temperature. Thermal cycling (e.g., T<180˚C) reduces Poisson's ratio during the first few cycles, but as the number of cycles increases the Poisson's ratio value tends to recover. The initial reduction in Poisson's ratio with thermal cycling tends to increase as the concrete strength increases.

2.2.1.3 Modulus of Elasticity

Information and Data. Concrete's modulus of elasticity—a measure of its stiffness or resistance to deformation—is used extensively in the analysis of reinforced concrete structures to determine the stresses developed in simple elements and the stresses, moments, and deflections in more complicated structures. Because concrete's stress-strain curve is nonlinear, the modulus of elasticity is determined either by the initial tangent modulus, secant modulus, or tangent modulus method. Most results presented in the literature correspond to static tests conducted under steady-state stress rate or steady-state strain rate control. Temperature can significantly affect the modulus values causing a reduction as a result of the breakage of bonds [2.16]. Drying which increases with temperature reduces the apparent modulus value to produce the bond rupture and it has been observed that fast drying results in a faster decrease in the modulus of elasticity than slow drying [2.100,2.101]. Several potential factors affecting the modulus of elasticity due to elevated temperature exposure have been investigated (e.g., mix proportions, aggregate type, cement type, concrete strength, sealed or unsealed, presence of sustained stress during heating, and duration of thermal exposure). Results addressing several of these factors are provided below.

Normal Weight Concretes

Normal weight concretes are typically concretes used for structural purposes that contain natural sand and gravel or crushed rock aggregates and weigh around 2400 kg/m^3. Figure 2.50 presents results for normal-strength concrete (NSC) and high-strength concrete (HSC) from researchers in China [2.78]. Results show that the elastic modulus for the NSC decreased monotonically with increasing temperature. From the NSC and HSC elastic modulus results obtained at temperature (relative) or after thermal exposure (residual), Reference 2.78 notes that the elastic modulus after high-temperature exposure (residual) was lower than that obtained at temperature and was influenced by type aggregate, the elastic modulus decreased much more for concrete cured in water than for concrete cured in air, and the deterioration in elastic modulus was more related to the maximum temperature during heating than to the heating-cooling cycle.

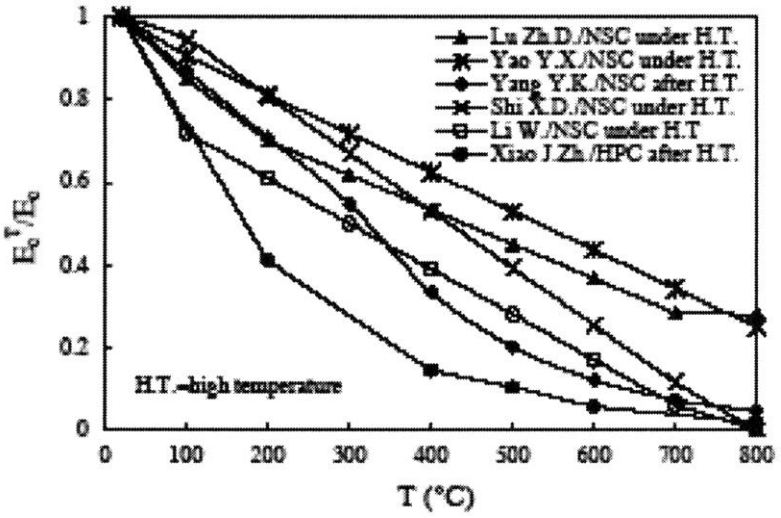

Figure 2.50 Temperature dependence of the concrete modulus of elasticity (normalized).

Source: J. Xiao and G. König, "Study of Concrete at High Temperature in China—An Overview," *Fire Safety Journal* **39**, pp. 89–103, 2004.

Figure 2.51 presents the strong influence of aggregate type on modulus [2.15]. Conclusions from this study were that a sustained stress during heating affects the modulus significantly and the type of cement had little effect. Figure 2.52 illustrates the influence of water-cement ratio on static and dynamic modulus [2.12]. Results presented in Figure 2.53 for a 31-MPa and a 63-MPa limestone aggregate concrete tested at temperature indicate that, when normalized with respect to the room temperature modulus of elasticity, the strength of the concrete does not have a significant effect on the modulus-temperature response [2.58].

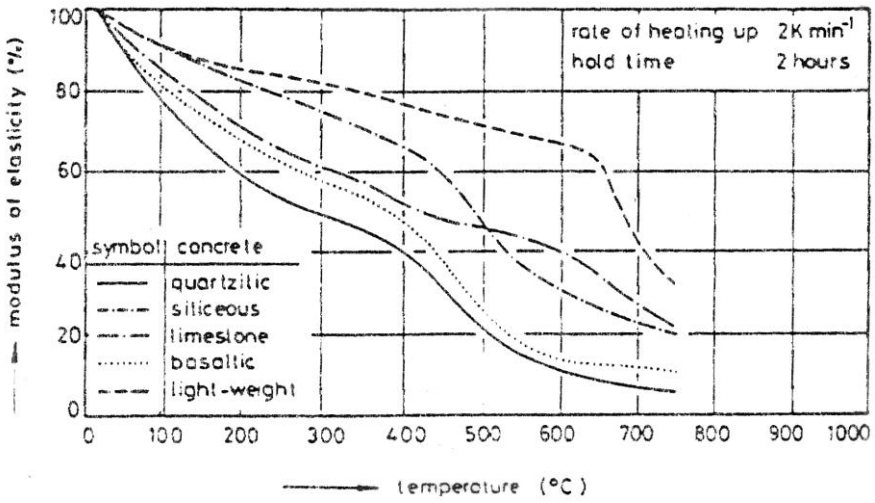

Figure 2.51 Modulus of elasticity of different concretes at elevated temperature.

Source: U. Schneider, C. Diererichs, and C. Ehm, "Effect of Temperature on Steel and Concrete for PCRV's," *Nuclear Engineering and Design* **67**, pp. 245–258, 1981.

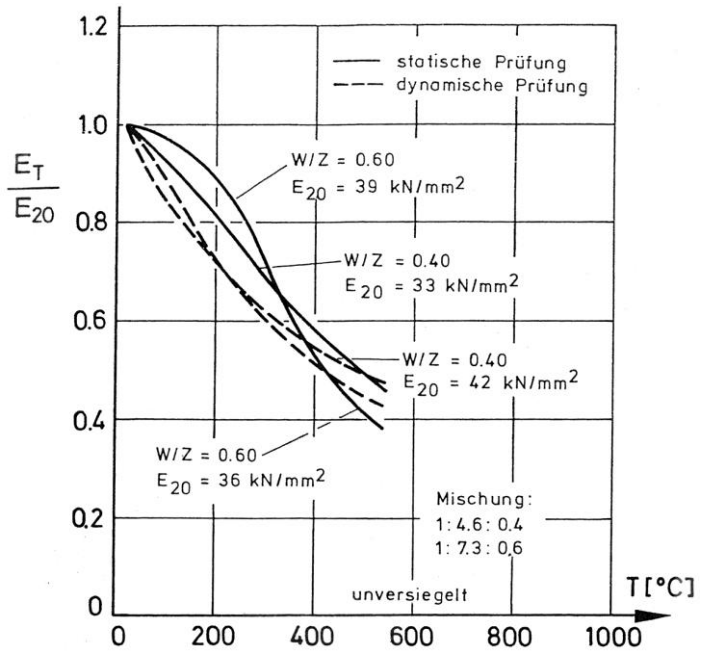

Figure 2.52 Influence of water-cement ratio on modulus of elasticity of concrete at elevated temperature.

Source: U. Schneider, *Behaviour of Concrete at High Temperature*, HEFT 337, Deutscher Ausschuss für Stahlbeton, Wilhelm Ernst & Sohn, Munich, Germany, 1982 (W/Z = water-cement ratio).

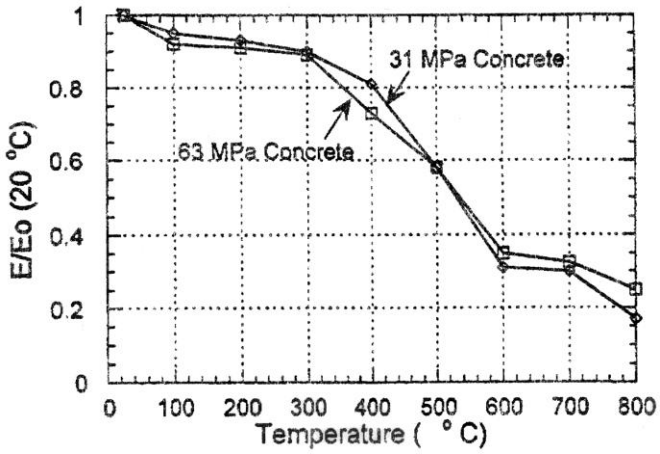

Figure 2.53 Normalized modulus of elasticity vs temperature relationships: NSC and HSC.

Source: C. Castillo and A. J. Durani, "Effect of Transient High Temperature on High-Strength Concrete," *J. American Concrete Institute*, **87**(10), pp. 47-53, January-February 1990.

Results from information presented above as well as those from other researchers have been used to develop a series of figures illustrating the effect of elevated temperature on the modulus of elasticity of concrete materials. References to data sources cited by others or used in figures are identified in Appendix A. Test results are presented in terms of testing procedures identified earlier in the report that are commonly used to evaluate concrete response to elevated temperature: unstressed tests (hot testing), unstressed residual (cold testing), and stressed tests.

Figure 2.54 summarizes results from several researchers on the temperature dependence of the concrete elastic modulus (normalized to reference room temperature value) [2.102]. Also shown in the figure are upper and lower

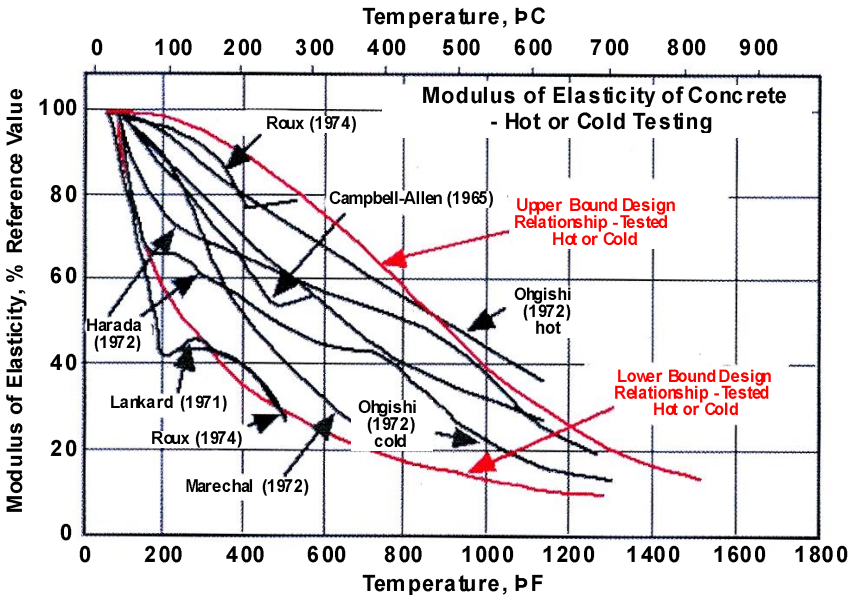

Figure 2.54 Effect of temperature on the modulus of elasticity of concrete: hot and cold test results.

Source: G. N. Freskakis, "Behavior of Reinforced Concrete at Elevated Temperature," Paper 3-4, *Source: ASCE Conf. on Civ. Eng. and Nuclear Power* **1**, Paper 3-5, pp. 3-5-1 to 3-5-21, Knoxville, Tennessee, Sept. 15–17, 1980.

bounds that were established from the data. The results were utilized as part of a study to investigate the behavior of reinforced concrete sections at elevated temperature.

Data on effects of elevated temperature on modulus of elasticity have also been assembled as part of a review of concrete properties for prestressed concrete pressure vessels [2.103]. Figure 2.55 presents a summary of data assembled under this activity for sealed and unsealed specimens that were either tested at temperature (hot) or after returning to room temperature (cold). It was concluded that generally the modulus decreased with increasing temperature for all types of testing, further decreases in modulus occurred with an increase in number of thermal cycles and exposure time, and sealed specimens were more sensitive to these factors with decrease in modulus becoming fairly significant at temperatures above 150˚C.

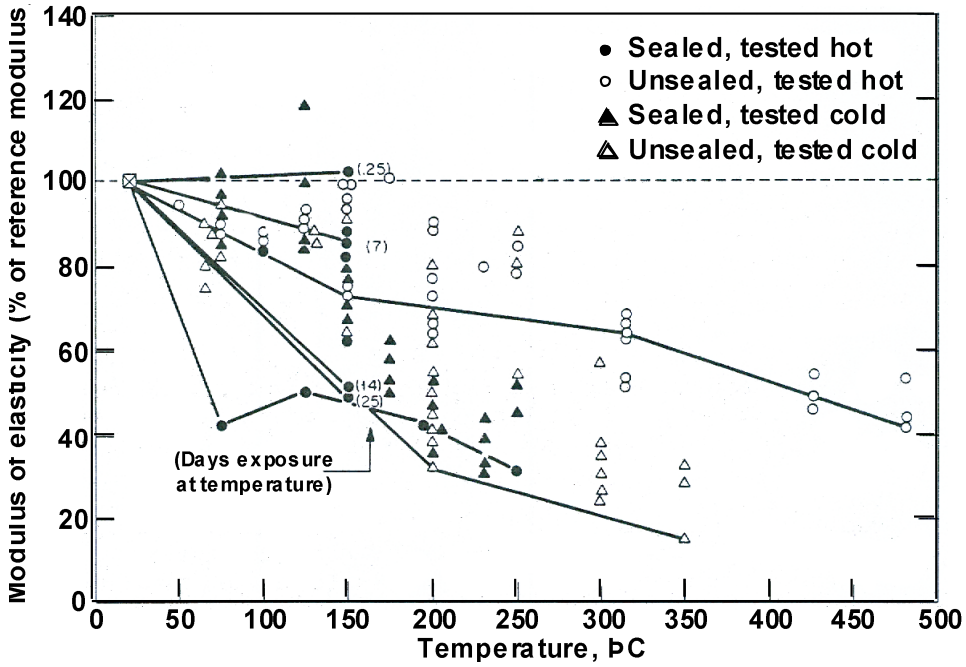

Figure 2.55 Compilation of data on modulus of elasticity vs temperature.

Source: R.K. Nanstad, *A Review of Concrete Properties for Prestressed Concrete Pressure Vessels*, ORNL/TM-5497, Oak Ridge National Laboratory, Oak Ridge, Tennessee, October 1976.

Figure 2.56 presents a compilation developed under the present study on the effect of elevated temperature on the relative modulus of elasticity (i.e., unsealed, hot testing) for a number of different concrete mixtures (i.e., ordinary Portland cement concretes and ordinary Portland cement concretes that also included supplementary cementitious materials). Results obtained for only the Portland cement concretes are provided in Figure 2.57 and results for Portland cement concretes containing supplementary cementious materials are presented in Figure 2.58. The CEB design curve* for unstressed normal weight concretes has been superimposed on the figures to facilitate comparisons. Results indicate similar trends toward a decrease in relative modulus of elasticity with increasing temperature for both the ordinary Portland cement concretes and the Portland cement concretes that contained supplementary cementitious materials. There may be a slight trend for the reductions in modulus to be slightly higher for the Portland cement concretes with supplementary cementitious materials than the ordinary Portland cement concretes, however, the concrete mixes with supplementary cementitious materials were all high-strength concretes ($f_c' \geq 60$ MPa) whereas the vast majority of ordinary Portland cement concretes were normal strength concretes.

* Comites Euro-International Du Beton, *Fire Design of Concrete Structures – in accordance with CEB/FIP Model Code 90*, CEB Bulletin D'Information No. 208, Lausanne, Switzerland, July 1991.

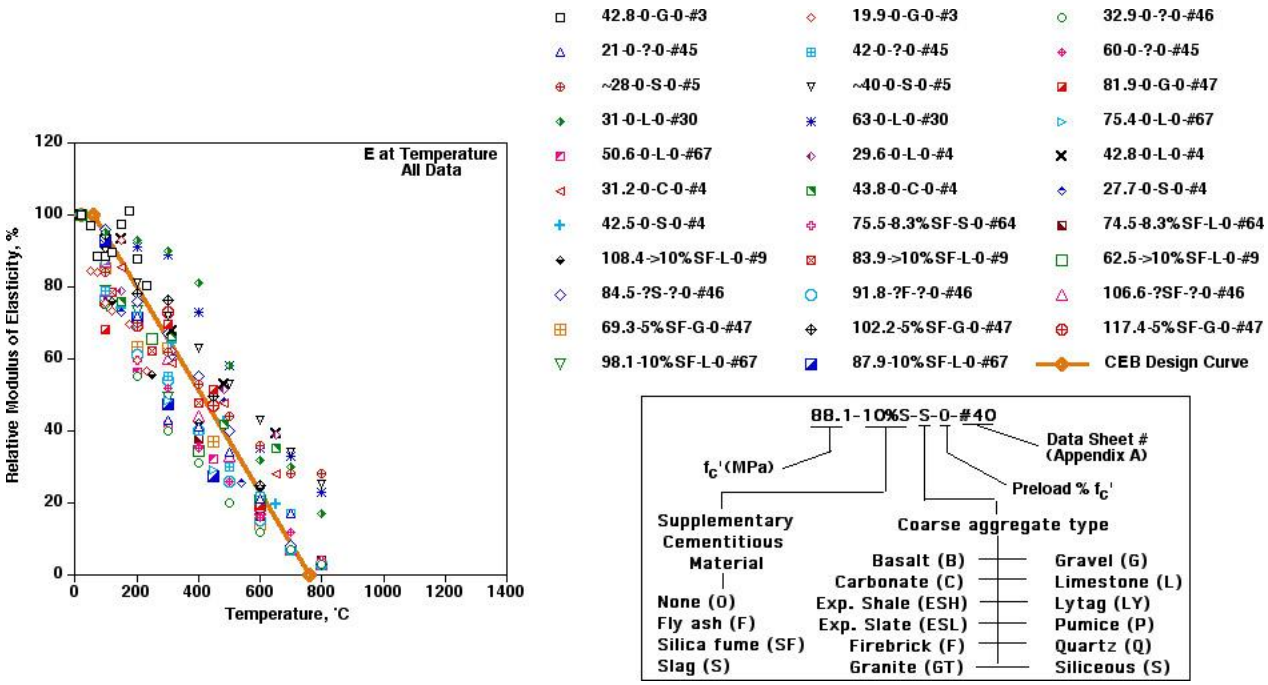

Figure 2.56 Compilation of data on relative modulus of elasticity vs temperature – ordinary Portland cement concretes and concretes containing supplementary cementitious materials.

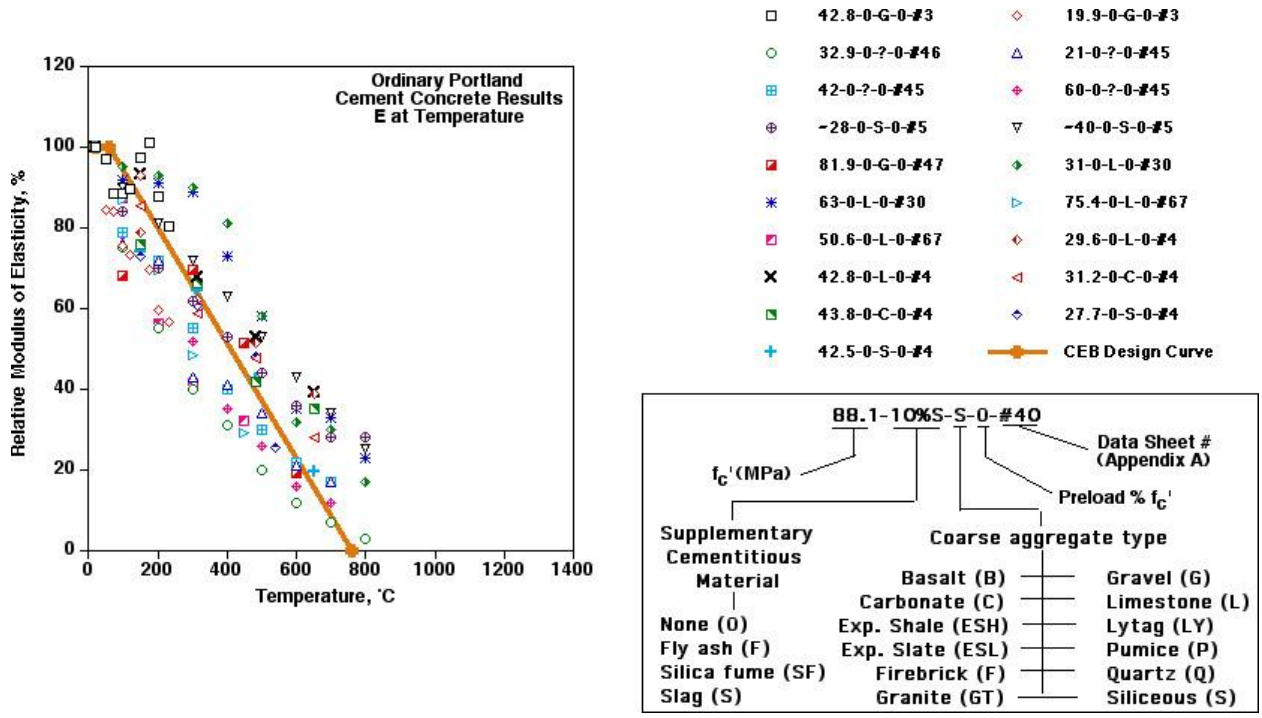

Figure 2.57 Compilation of data on relative modulus of elasticity vs temperature – ordinary Portland cement concretes.

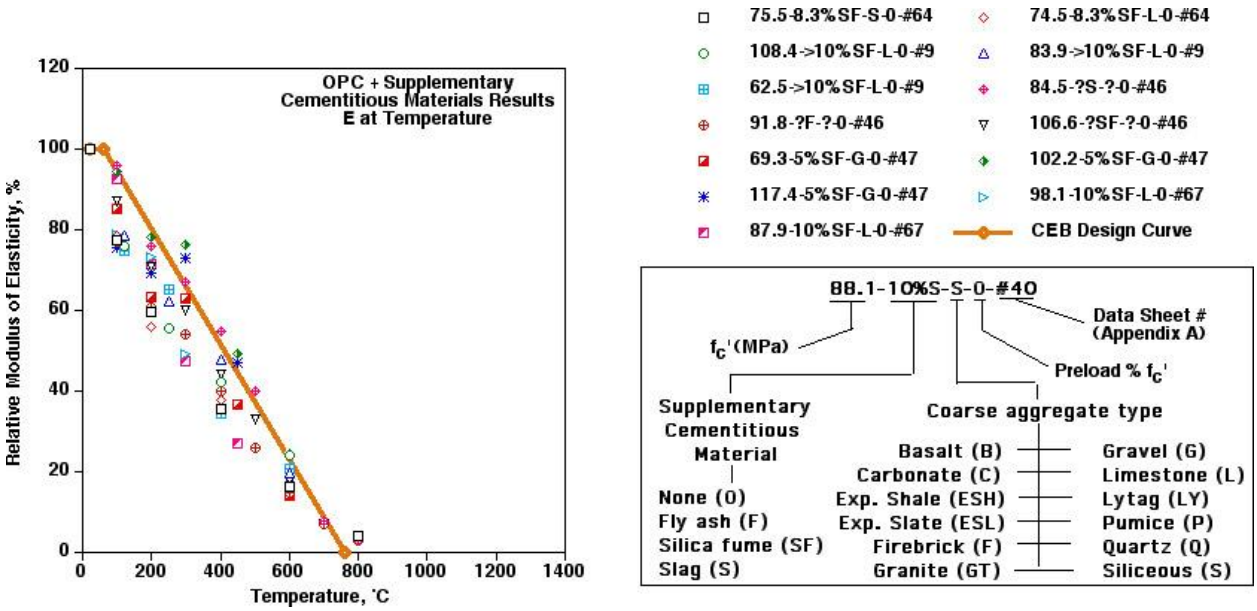

Figure 2.58 Compilation of data on relative modulus of elasticity vs temperature - concretes containing supplementary cementitious materials.

A data compilation developed under the present study on the effect of elevated temperature on the residual modulus of elasticity (i.e., unsealed, cold testing) for a number of different concrete mixtures (i.e., ordinary Portland cement concretes and Portland cement concretes that also included supplementary cementitious materials) is provided in Figure 2.59. Results obtained for only the Portland cement concretes are provided in Figure 2.60 and results for

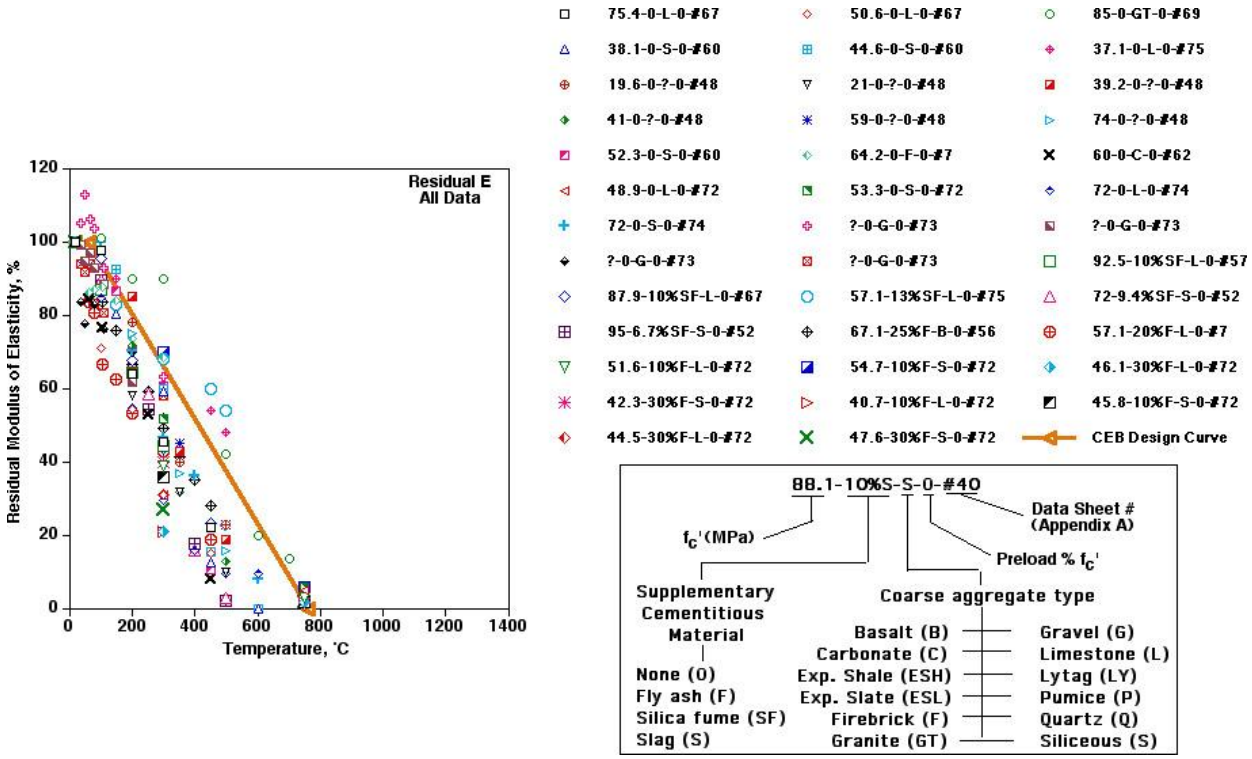

Figure 2.59 Compilation of data on residual modulus of elasticity vs temperature – ordinary Portland cement concretes and concretes containing supplementary cementitious materials.

Portland cement concretes containing supplementary cementious materials are presented in Figure 2.61. The CEB design curve for unstressed normal weight concretes has been superimposed on the figures to facilitate comparisons. Results indicate similar trends toward a decrease in relative modulus of elasticity with increasing temperature for both the ordinary Portland cement concretes and the Portland cement concretes that contained supplementary cementitious materials. Comparing the results to those obtained from specimens tested at temperature, the retained modulus at temperature tends to be higher than that obtained from specimens permitted to cool to room temperature prior to testing.

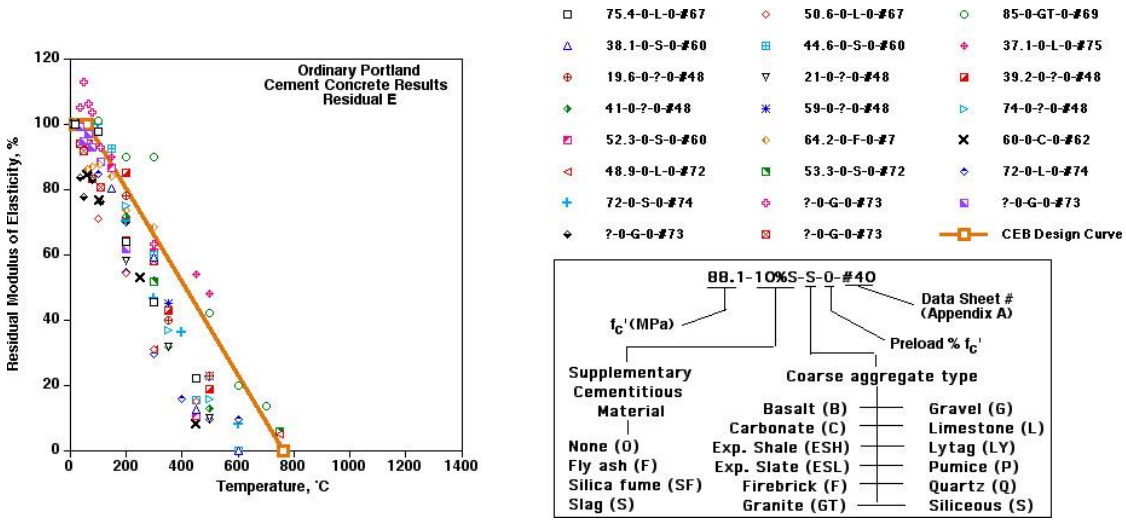

Figure 2.60 Compilation of data on residual modulus of elasticity vs temperature – ordinary Portland cement concretes.

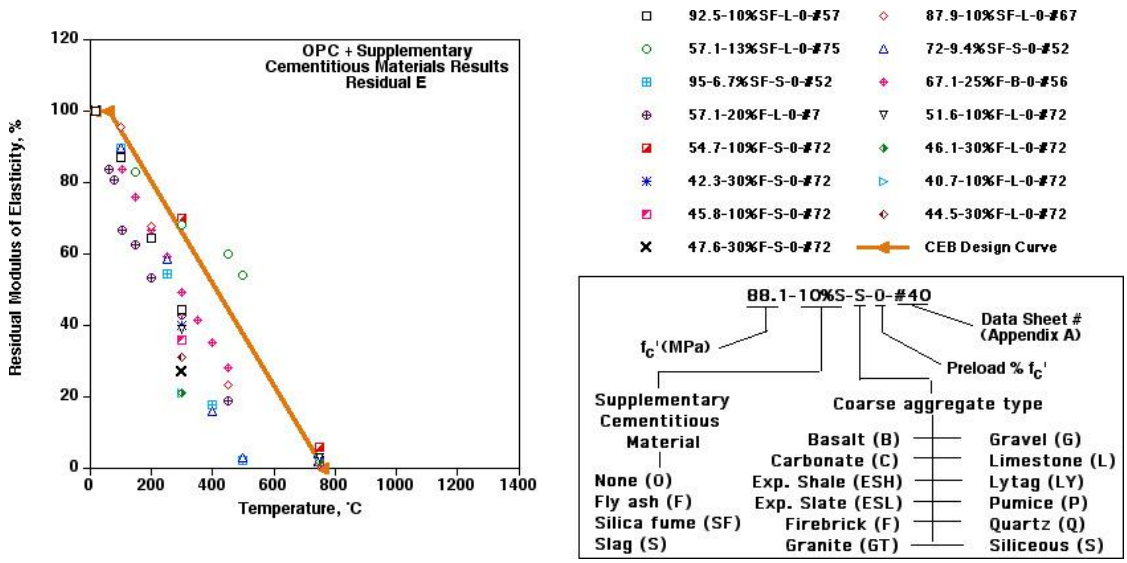

Figure 2.61 Compilation of data on residual modulus of elasticity vs temperature - concretes containing supplementary cementitious materials.

The effect of sustained stress during heating on the relative modulus of elasticity (unsealed, hot testing) is presented in Figure 2.62 for ordinary Portland cement concretes and Portland cement concretes that also included supplementary cementitious materials. Preload levels ranged from 20 to 40% the reference room temperature compressive strength of the concretes. Although results are limited, the presence of preload and its beneficial effects relative to retained modulus is evident.

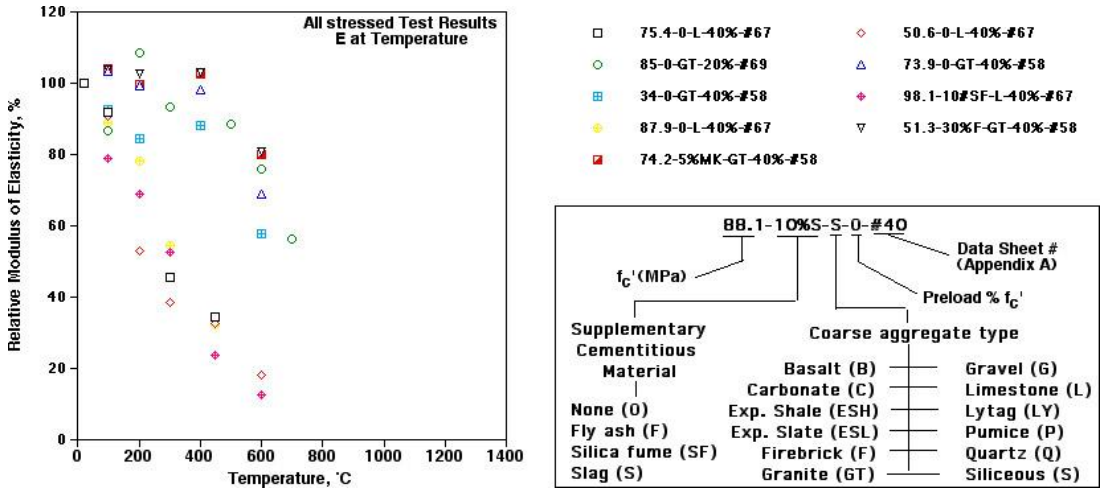

Figure 2.62 Compilation of data on relative modulus of elasticity vs temperature for preloaded specimens – ordinary Portland cement concretes and concretes containing supplementary cementitious materials.

The effect of cooling regime on the residual modulus of elasticity has been studied as part of an overall investigation to evaluate the post-thermal properties of concrete following rapid cooling (e.g., water quenching in conjunction with fire) [2.67]. A granite aggregate ordinary Portland cement concrete having a reference compressive strength of 21.16 MPa and reference initial tangent modulus of 24.8 GPa was used to fabricate 101.6-mm-diameter by 203.2-mm-long cylindrical test specimens that were cured for eight weeks in a fog room (23˚C and 93% relative humidity). The specimens were heated in a furnace to 200˚, 400˚, 600˚, or 800˚C with a holding time at temperature of four hours. Following heating, the specimens were cooled slowly (1˚C/minute), naturally (left in furnace and permitted to cool slowly), or rapidly (e.g., specimen removed from furnace and placed into a tank of water initially at 20˚C). Figure 2.63 presents the effect of cooling regime on the initial relative tangent modulus for concretes subjected to the maximum temperatures up to 800˚C.

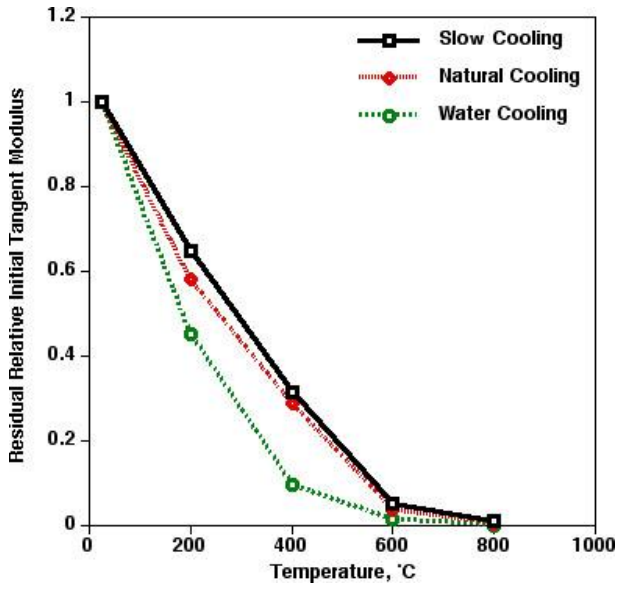

Figure 2.63 Effect of cooling regime on initial tangent modulus following thermal exposure.

Source: J. Lee, Y. Xi, and K. Willam, "Concrete Under High Temperature Heating and Cooling," Report SESM No.09/2006, Department of Civil, Environmental, and Architectural Engineering, University of Colorado at Boulder, 2006.

Additional results on the effect of cooling regime on the residual relative initial tangent modulus are presented in Figure 2.64 for a limestone aggregate ordinary Portland cement concrete [2.104]. The 75-mm-diameter by 200-mm-long cylindrical test specimens were obtained by coring 700 x 500 x 200 mm^3 concrete blocks that had been cast and cured in water at 20˚C for 28 days followed by conditioning in a laboratory environment (20˚C and 65% relative humidity) for several months to permit the moisture content to stabilize. Following curing and conditioning the specimens were placed into an oven and heated to target exposure temperatures of 217˚, 287˚, 320˚, 378˚, or 470˚C where they remained until temperatures at the outer surfaces and centers of the specimens attained uniformity. Following thermal treatment, half the specimens at each temperature were removed from the furnace and permitted to cool in a controlled environment at 20˚C and the other half were taken out of the furnace and sprayed with tap water for a duration of five minutes and then permitted to stabilize in a controlled environment at 20˚C. The cooling regime results show the sensitivity of the tangent modulus to water quenching, particularly in the lower temperature range. The effect of quenching on the tangent modulus decreases somewhat at the higher temperatures, however, the initial tangent modulus already had been severely reduced by exposure to these temperatures.

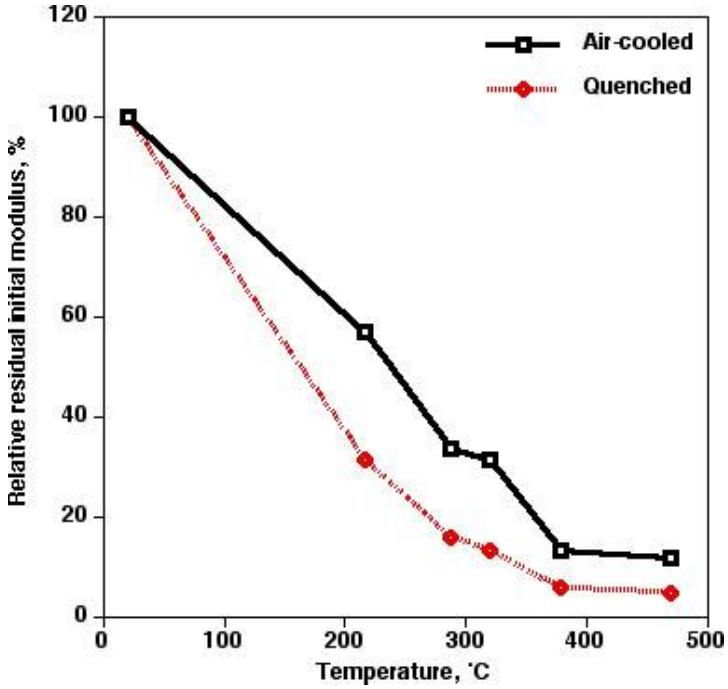

Figure 2.64 Effect of cooling regime on relative residual tangent modulus following thermal exposure.

Source: Y. Nassif, S. Rigden, and E. Burley, "The Effects of Rapid Cooling by Water Quenching on the Stiffness Properties of Fire-Damaged Concrete," *Magazine of Concrete Research* **51**(4), pp. 255-261, August 1999.

The effect of elevated temperature followed by water quenching on the modulus of elasticity* of high-strength concrete containing supplementary cementitious materials such as used in construction of high rise buildings was studied [2.105]. Four mixes were investigated: Mix 1 - 100% general purpose cement, Mix 2 - 62% slag plus 38% cement, Mix 3 - 20% fly ash plus 80% cement, and Mix 4 - 6.6% silica fume plus 93.4% cement. Crushed basalt aggregate having a maximum aggregate size of 10 mm and a water-cement ratio of 0.30 (by weight) was used for all the mixes. Table 2.3 presents reference 28-day properties of the mixes. Specimens used for dynamic modulus of elasticity determinations were 75 x 75 x 305 mm^3 prisms. Specimens were cured by storing in water at 20˚C for 28 days and then placing into the laboratory environment of 20˚C and 65% relative humidity for 2 days. At this time the specimens were heated to temperatures of 200˚, 400˚, 600˚, 800˚, or 1000˚C with a total duration of

* The effect of binder type and water quenching on the relative compressive, flexural, and tensile strengths of these concretes is presented later in this report.

Table 2.3 Properties of concrete mixes at the age of 28 days

Mix	Binder Materials	Cylinder strength, MPa	Tensile strength, MPa	Flexural strength, MPa	Dynamic modulus, GPa
1	100% OPC	61.8	6.58	9.34	46.5
2	62% slag + 38% OPC	40.3	4.28	5.47	39.9
3	20% fly ash + 80% OPC	67.2	5.08	6.94	45.7
4	6.6% silica fume+ 93.4% OPC	76.4	6.93	8.51	55.2

Source: R.S. Ravindrarajah, R. Lopez, and H. Reslan, "Effect of Elevated Temperature on Properties of High-Strength Concrete Containing Cement Supplementary Materials," *9th International Conference on Durability of Building Materials and Components*, 9 p., Brisbane, Australia, 17-20 March 2002.

7 hours (i.e., soak period from 6 to 2 hours depending on maximum temperature). Figure 2.65 presents the normalized residual relative modulus of elasticity results for specimens subjected to elevated temperature followed by quenching in water prior to testing. Elastic modulus decreased as the exposure temperature increased with the results influenced by the binder material type (e.g., silica fume concrete decreased the most followed by the fly ash concrete). At 200˚C the reduction in modulus ranged from 8 to 16%, at 800˚C the reduction ranged from 13 to 20%, and at 1000˚C the reduction ranged from 29 to 40%.

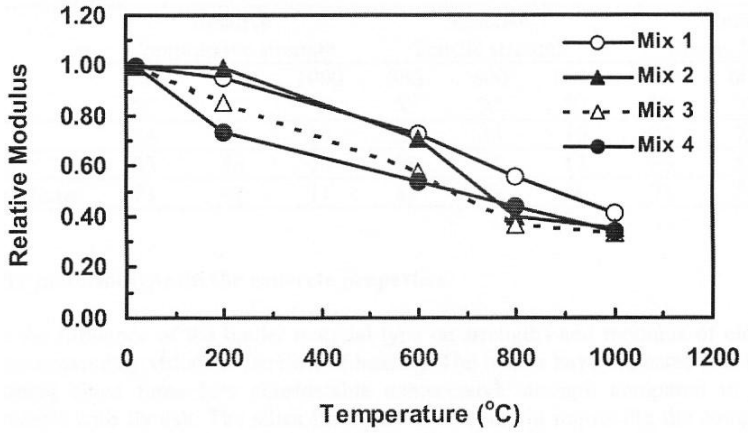

Figure 2.65 Normalized residual modulus of elasticity results for specimens subjected to elevated temperature and quenched in water prior to testing.

Source: R.S. Ravindrarajah, R. Lopez, and H. Reslan, "Effect of Elevated Temperature on Properties of High-Strength Concrete Containing Cement Supplementary Materials," *9th International Conference on Durability of Building Materials and Components*, 9 p., Brisbane, Australia, 17-20 March 2002.

Lightweight and Thermally Stable Aggregate Concretes

Lightweight concrete material systems for structural applications typically contain natural or pyro-processed aggregates with relatively low bulk densities (e.g., expanded shale, slate, or slag) and generally weigh less than 1800 kg/m^3. Relative modulus of elasticity results (unsealed, hot testing) for lightweight/thermally stable aggregate concretes compiled from the literature are presented in Figure 2.66. The CEB design curve for lightweight concrete is superimposed on the data. Results indicate that in general the lightweight/insulating concretes tend to retain their modulus of elasticity at temperature better than normal weight concretes. The improved performance can probably be attributed to the modulus of elasticity of the lightweight aggregates used in the mixes being closer to that of the Portland cement paste [2.19].

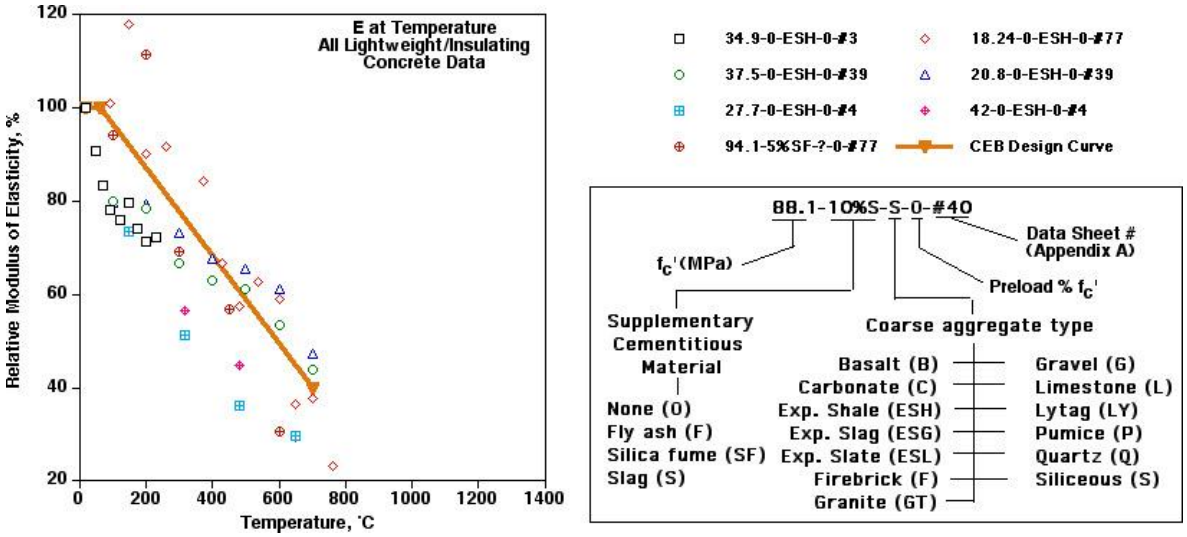

Figure 2.66 Compilation of data on relative modulus of elasticity vs temperature for lightweight/insulating concrete specimens – ordinary Portland cement concretes and concretes containing supplementary cementitious materials.

Fibrous Concretes

Fibrous concretes is made from hydraulic cements containing fine and coarse aggregate materials and discontinuous discrete fibers (e.g., steel, polypropylene, and aramid). Relative modulus of elasticity results (unsealed, hot testing) compiled from the literature for fibrous concretes and the CEB design curve noted earlier are presented in Figure 2.67. Insufficient data are available to draw any definite conclusions relative to incorporation of discontinuous fiber reinforcement in the concrete mixes. However, polypropylene fibers (and steel fibers) have been incorporated into concrete mixes (high strength concretes in particular) to improve fire resistance and enhance resistance of the concrete to thermal spalling. The polypropylene fibers melt at around 170˚C to provide "channels" for the steam pressure that develops in the concrete to escape thus preventing internal pressurization that can produce spalling.

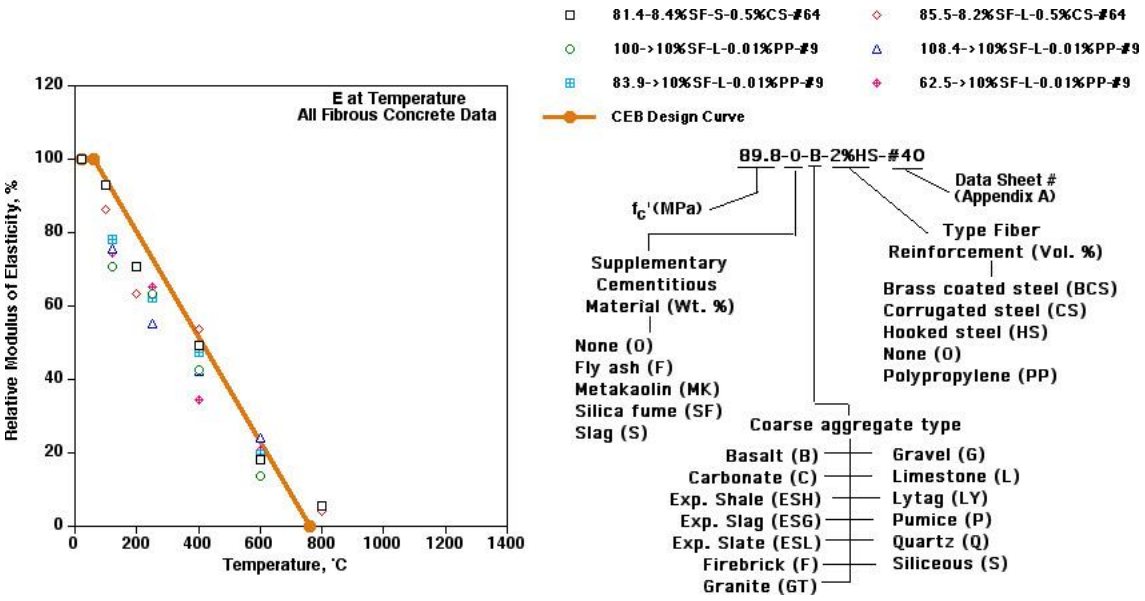

Figure 2.67 Compilation of data on relative modulus of elasticity versus temperature for fibrous concretes.

Examples of Relations for Concrete Modulus of Elasticity at Elevated Temperature. Assuming the secant modulus at a stress of $0.4f_c^T$ is the elastic modulus, the following has been proposed for estimating the modulus at elevated temperature [2.106]:

$$E_c^T = (1 - 0.0015T)E_c \quad \text{for } 20^\circ < T \leq 300^\circ C, \tag{2.32}$$
$$E_c^T = (0.87 - 0.0084T)E_c \quad \text{for } 300^\circ < T \leq 700^\circ C, \text{ and} \tag{2.33}$$
$$E_c^T = 0.28E_c \quad \text{for } T > 700^\circ C. \tag{2.34}$$

A bi-linear equation has also been suggested [2.107]:

$$E_c^T = E_c \quad \text{for } 20^\circ < T \leq 60^\circ C, \text{ and} \tag{2.35}$$
$$E_c^T = (0.83 - 0.0011T)E_c \quad \text{for } 60^\circ < T \leq 700^\circ C. \tag{2.36}$$

A relationship has been developed for the normalized elastic modulus (E_{CR}/E_C) variation with temperature (T) [2.108]:

$$E_{CR}/E_C = -0.00165T + 1.033 \quad \text{for } 20^\circ < T \leq 125^\circ C, \text{ and} \tag{2.37}$$

$$E_{CR}/E_C = \frac{1}{1.2 + 18(0.0015T)^{4.5}} \quad \text{for } 125^\circ < T \leq 800^\circ C. \tag{2.38}$$

Reductions in initial tangent modulus of elasticity E_0 for concrete can be estimated from [2.72]:

$$E(T) = E0 \quad \text{for } T \geq 60^\circ C, \text{ and} \tag{2.39}$$

$$E(T) = \frac{800 - T}{740} E_0 \quad \text{for } 60^\circ < T \leq 800^\circ C. \tag{2.40}$$

The effect of elevated temperature on the concrete secant modulus at a stress corresponding to 40% the room temperature compressive strength of concrete can be estimated from [2.78]:

$$E_C^T = (1 - 0.0015T)E_c \quad \text{for } 20^\circ < T \leq 300^\circ C, \tag{2.41}$$

$$E_C^T = (0.87 - 0.0084T)E_c \quad \text{for } 300^\circ < T \leq 700^\circ C, \text{ and} \tag{2.42}$$

$$E_C^T = 0.28E_C \quad \text{for } T > 700^\circ C, \tag{2.43}$$

where E_C and E_C^T are the concrete elastic moduli at room and elevated temperature.

Summary. An increase in temperature generally leads to a continuous fall in the modulus of elasticity of both sealed and unsealed concrete, with the decrease being larger for sealed concrete. The decrease in elastic modulus with elevated temperature exposure is primarily due to breakage of bonds in the cement paste microstructure. Variations in results from different authors can be caused by a number of factors in addition to the type of aggregate used (e.g., water-cement ratio, method for determination of modulus, testing hot or cold, presence of pre-load, rate of heating and cooling, and rate of loading). Modulus of elasticity at temperature is higher than residual modulus. Variation of modulus values with temperature up to 80˚C is considerable, primarily as a result of use of different aggregate materials, and above 100˚C the decrease in modulus tends to be linear up to a critical temperature at which the concrete experiences severe deterioration [2.19]. Due to thermal incompatibility with the cement paste, concretes containing aggregates with low thermal expansion (e.g., limestone) experience a greater reduction in the modulus of elasticity than those with a higher thermal expansion such as gravels and sandstone [2.19]. The primary

factors affecting the modulus of elasticity at high temperature are the type of aggregate and the presence of sustained stress during heating (sustained stress results in lower decreases in modulus with increasing temperature). Thermal cycling causes a decrease in modulus. Fast drying accompanying heating results in a greater decrease in modulus than slow drying due to increased breakage of bonds. Faster heating rates result in a lower modulus of elasticity. Lightweight aggregate/thermally stable concretes retain their modulus at elevated temperature better than normal weight aggregate concretes. Normal strength concretes (fc' < 60 MPa) retain their modulus better at elevated temperature than high-strength concretes. Duration of temperature exposure, type of cement, water-cement ratio and original concrete strength appear to have little effect on modulus results. The age at test apparently also does not affect the residual modulus as noted for a flint/beach gravel concrete for which results were obtained to 150°C at concrete ages of 3 months and 1 year [2.109].

2.2.1.4 Compressive Strength

Information and Data. The concrete compressive strength is generally considered to be its most important properties and influences the load-carrying capacity of a structure. Thermal loadings in addition to affecting the concrete modulus of elasticity also affect the concrete compressive strength. Most results presented in the literature correspond to static tests conducted under steady-state stress rate or steady-state strain rate control, utilized unsealed specimens, and determined the residual compressive strength (unsealed, cold testing). However, a number of tests are also available in which the relative concrete compressive strength (unsealed, hot testing) was determined. Several potential factors affecting the compressive strength of concrete due to elevated temperature exposure were investigated (e.g., mix proportions, aggregate type, cement type, concrete strength, sealed or unsealed, presence of sustained stress during heating, and duration of thermal exposure). Results addressing several of these factors are provided below.

Cements, Mortars, and Normal Weight Concretes

Figure 2.68, which presents results for unsealed mortars fabricated from ordinary Portland cement, blast furnace slag cement, and truss cement (i.e., mixture of Portland cement, volcanic tuff, and gypsum) indicates little difference in strength-temperature characteristics, except the ordinary Portland cement mortar exhibited a sharper decrease in strength at temperatures greater than 500°C [2.12]. Another study utilizing a number of cementitious materials [e.g., ordinary Portland cement, fly ash, and blast furnace slag cement (cemsave)] also noted that up to 600°C there was little effect of the cement type [2.110]. Results presented in Figure 2.69 indicate that partial replacement of ordinary Portland cement with pulverized fly ash improves the residual strength and may even produce an increase in strength at higher temperatures [2.8,2.11].* Figure 2.70 indicates that for the three water-cement ratios investigated, the residual compressive strengths of unsealed cement paste specimens experienced similar trends [2.8]. These results indicate a peak strength at about 150°C where the residual strengths were 10 to 30% higher than the reference room temperature strength. Although the strength declined at temperatures higher than 300°C to 350°C, at temperatures of 300°C to 350°C it was still higher than the reference strength. Research presented elsewhere involving several aggregate types indicates that the effect of water-cement ratio had little influence on the residual compressive strength up to 600°C [2.111]. For normal strength Portland cement concretes, the concrete strength has a secondary effect on strength-temperature characteristics. Residual compressive strength results are presented in Figure 2.71 for concretes having compressive strengths ranging from 19.6 to 74 MPa [2.112]. This study concluded that a high-strength concrete (e.g, $f_c' > 60$ MPa) has a higher rate of reduction in residual compressive strength (and modulus) than a normal-strength concrete. Figure 2.72 presents results of unstressed tests for ordinary Portland cement concretes having reference compressive strengths either of 21, 42, or 60 MPa [2.113]. Results for each of the concretes were similar in that the compressive strength decreased at 100°C, recovered to the room temperature strength at 200°C, and then decreased monotonically with increasing temperature beyond 200°C. Figure 2.73 shows the effect of curing conditions (e.g., in water unsealed, sealed, in-air unsealed) prior to elevated-temperature exposure [2.97]. After $\geq$ 91 days cure, the specimens, either in a sealed or unsealed condition, were subjected to 175°C for up to 91days. Unstressed and residual compressive strengths were determined periodically over the exposure period. Although differences in compressive strengths occurred at smaller exposure ages, after 91 days exposure to 175°C, similar results were provided under all test conditions.

*A similar effect was achieved through partial replacement of the ordinary Portland cement with ground granulated blast furnace slag. Partial replacement with silica fume was not beneficial and in some cases produced detrimental residual strength results for unsealed specimens.

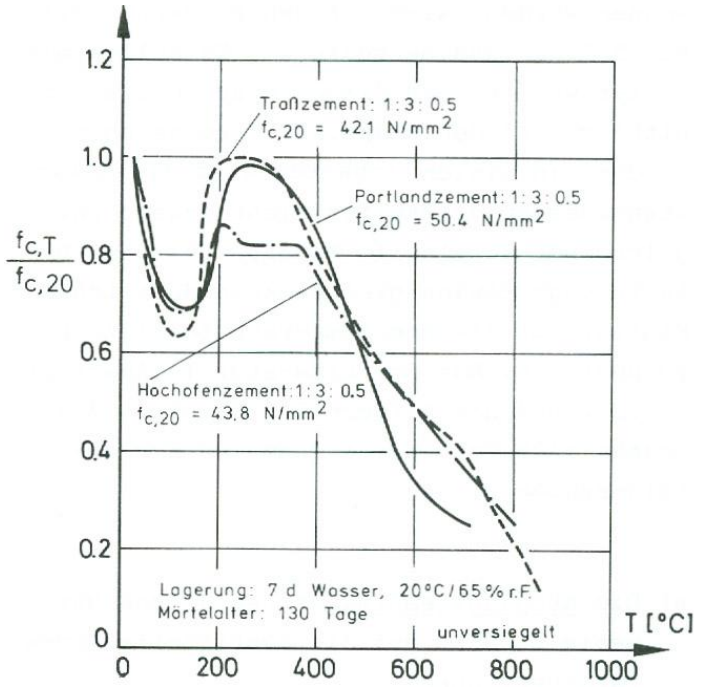

Figure 2.68 Influence of type of cement on strength loss of mortars.

Source: U. Schneider, *Behaviour of Concrete at High Temperature*, HEFT 337, Deutscher Ausschuss fiir Stahlbeton, Wilhelm Ernst & Sohn, Munich, Germany, 1982.

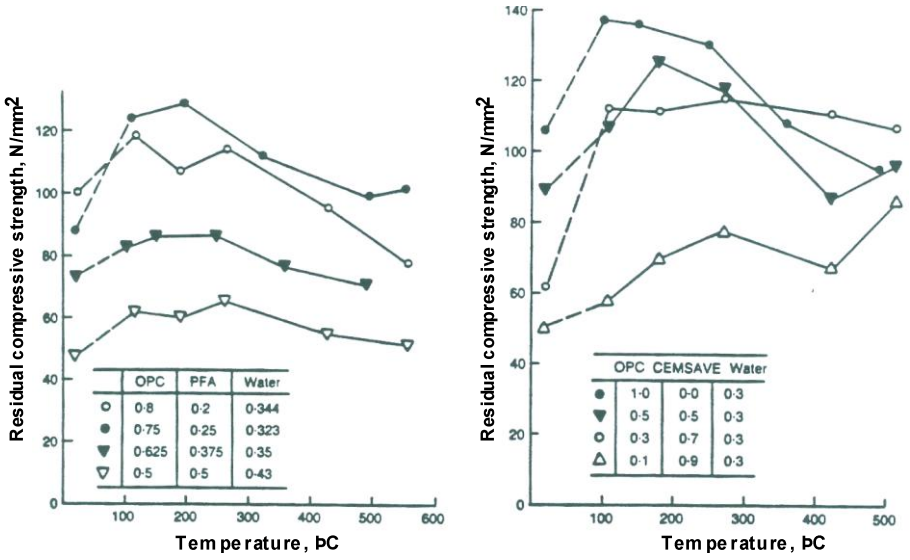

Figure 2.69 Influence of partial replacement of (a) OPC and (b) slag on residual compressive strength.

Source: G. A. Khoury, *Performance of Heated Concrete—Mechanical Properties*, Contract NUC/56/3604A with Nuclear Installations Inspectorate, Imperial College, London, United Kingdom, August 1996.

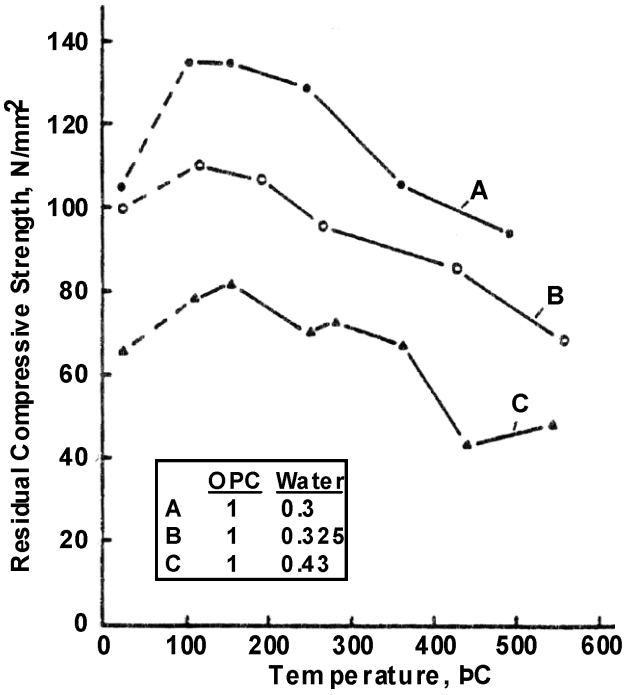

Figure 2.70 Effect of water-cement ratio on residual compressive strength of ordinary Portland cement.

Source: G. A. Khoury, *Performance of Heated Concrete—Mechanical Properties*, Contract NUC/56/3604A with Nuclear Installations Inspectorate, Imperial College, London, United Kingdom, August 1996.

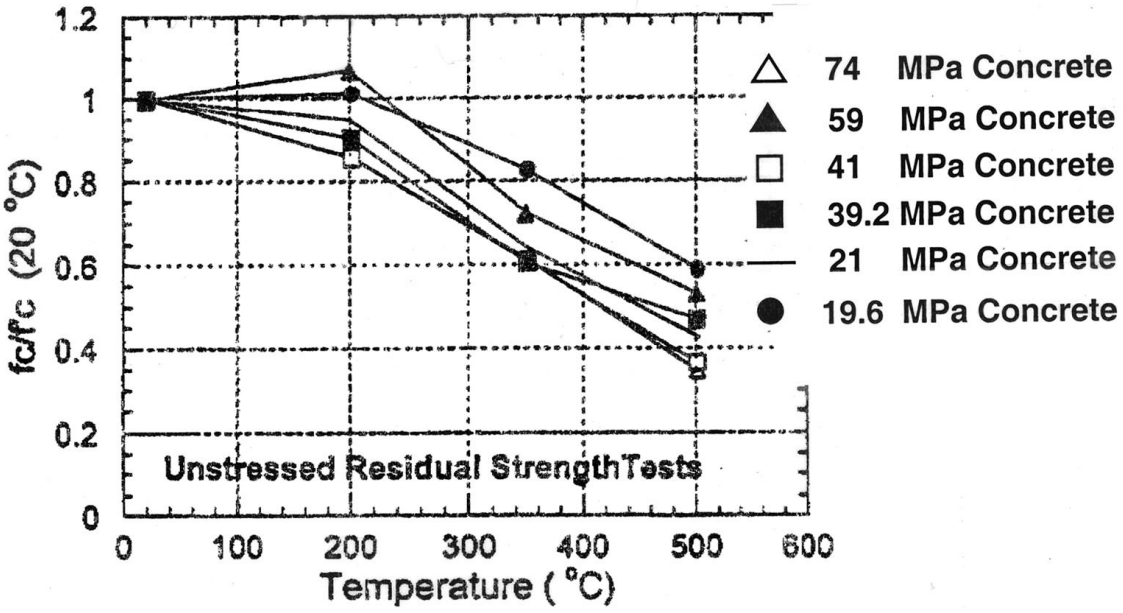

Figure 2.71 Residual normalized strength vs temperature.

Source: T. Morita, H. Saito, and H. Kumajai, "Residual Mechanical Properties of High Strength Concrete Members Exposed to High Temperature—Part 1. Test on Material Properties," *Summaries of Technical Papers of Annual Meeting*, Architectural Institute of Japan, Naiigata, August 1992.

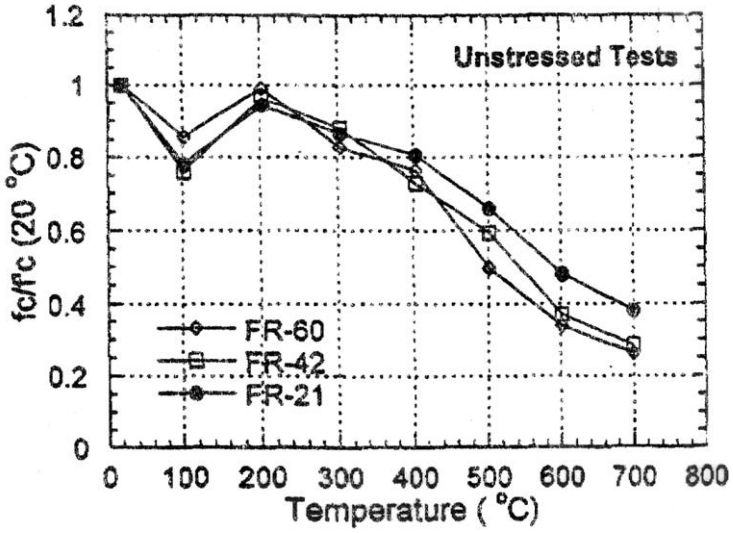

Figure 2.72 Residual compressive strength vs temperature.

Source: T. Furumura, T. Abe, and Y. Shinohara, "Mechanical Properties of High Strength Concrete at High Temperatures," *Proceedings of 4th Weimar Workshop on High Performance Concrete: Material Properties and Design*, held at Hochschule für Architektur und Bauwesen (HAB), Weimar, Germany pp. 237–254, 4–5 October 1995.

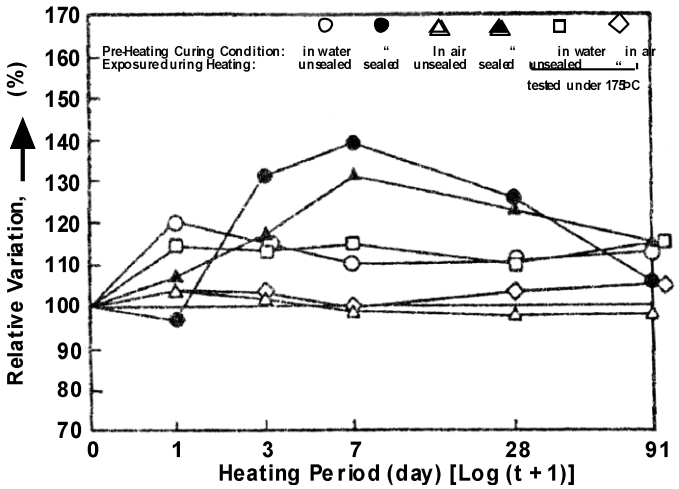

Figure 2.73 Effect of curing conditions prior to elevated-temperature exposure on relative compressive strength.

Source: K. Hirano, K. Ohmatsuzawa, T. Takeda, S, Nakane, T. Kawaguchi, and K. Nagao, "Physical Properties of Concrete Subjected to High Temperature for MONJU," Paper P2-25, Power Reactor and Nuclear Fuel Development Corporation, Tokyo, Japan.

The age at which the concrete is subjected to elevated-temperature exposure has little effect on the strength-temperature response as long as the concrete has adequate curing (e.g., 90 days). Figure 2.74 presents a comparison of residual unstressed compressive strength results for a nuclear power plant concrete (Temelin NPP) at ages of 28-days and 90-days for temperatures to 280°C [2.114]. Figure 2.75 provides residual compressive strength results for sealed and unsealed specimens cast from a nuclear power plant siliceous aggregate concrete at curing ages of 3 months and 1 year [2.109]. These results indicate that some improvement in residual compressive stress due to

more extended curing occurs, but it was not significant, and that the strength of sealed specimens was lower than that of unsealed specimens.

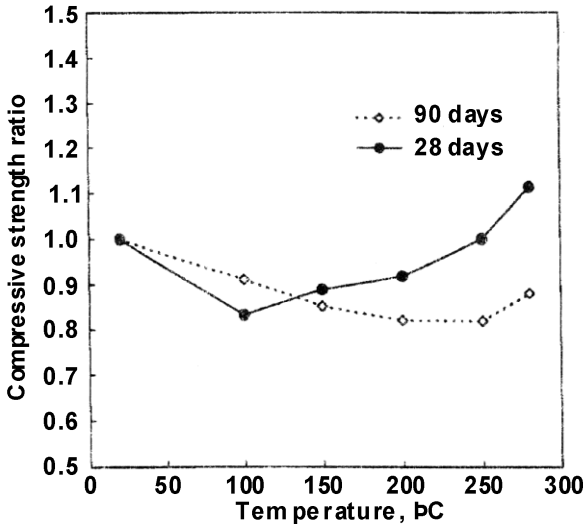

Figure 2.74 Effect of temperature on compressive strength ratio of concrete.

Source: F. Vodak, K. Trtík, O. Kapicková, S. Hisková, and P. Demo, "The Effect of Temperature on Strength—Porosity Relationship for Concrete," *Construction and Building Materials* 18, pp. 529–534, 2004.

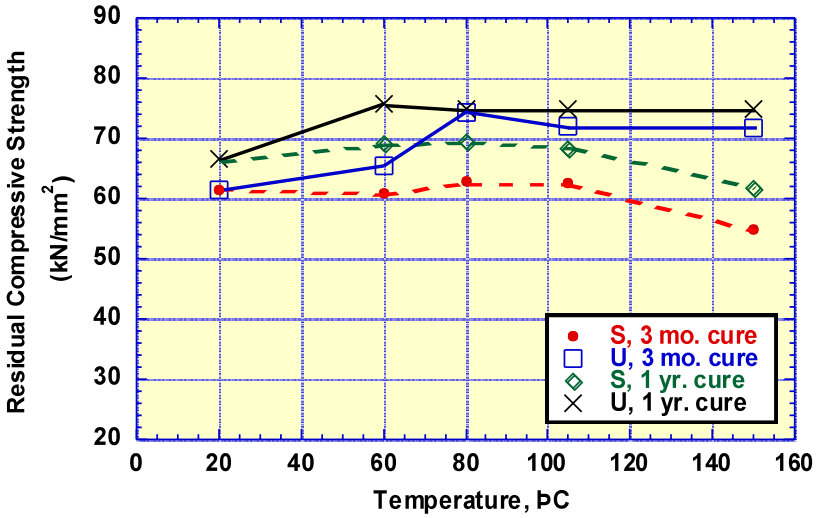

Figure 2.75 Effect of curing age and exposure condition on residual compressive strength (S = sealed, U = unsealed).

Source: J. Guo and P. Waldron, "Deterioration of PCPV Concrete," *Nuclear Engineering and Design* **198**, pp. 211–226, 2000.

As long as the rate of heating does not produce significant thermal gradients, the rate of heating has a secondary effect on the concrete strength-temperature response, particularly at high temperatures. Figure 2.76 indicates the effect of rate of heating on residual strength of a crushed basalt concrete [2.115]. These results indicate that the rate of heating had an insignificant effect on residual strength for temperatures of 600°C and 800°C. However, the heating rate had an effect on the residual compressive strength at lower temperatures. Exposure times at temperature beyond 1 hour had an effect on the residual compressive strength, but this effect diminished as the level

of exposure temperature increased, with the majority of strength loss occurring in the first 2 hours of exposure (Fig. 2.77). Figure 2.78 shows the effect of duration of temperature exposure (exposure periods to 42 days) on the relative strength change of sealed and unsealed gravel and limestone aggregate concretes at exposure temperatures to 180°C. For all temperatures investigated, and for sealed and unsealed conditions, the river gravel concrete generally exhibited a slight strength increase. The compressive strength of the limestone aggregate concrete was relatively constant with increasing exposure period for the unsealed condition, but exhibited a decline in compressive strength with exposure time at 180˚C for the sealed condition. The explanation for this behavior was that the strength loss of the limestone concrete was caused by changes in the microstructure of the hydrated cement paste when exposed to hydrothermal conditions. In the river gravel concrete the strength loss was counteracted by a reaction between the silicates of the fine aggregate particles and the $Ca(OH)_2$ of the hydrated cement paste.

The aggregate type is one of the main factors influencing the compressive strength of concrete at elevated temperature. Figure 2.79 presents a comparison of stressed, unstressed residual, and unstressed compressive strength results for carbonate and siliceous aggregate concretes at temperatures to 871°C [2.116]. Results of this study indicate the influence of the aggregate type, show the beneficial effect of stressing the specimens (within limits) while heated, and indicate that unstressed results obtained at temperature exceed those obtained under unstressed residual conditions (i.e., hot strength results were generally greater than residual strength results). The influence of aggregate type on results is further illustrated in Figure 2.80 where the compressive strength of limestone and other concretes is presented [2.12].* It was noted in this reference that for the temperature range shown in the figure, quartz and basalt aggregate are less sensitive to temperature effects than the limestone aggregate concrete.

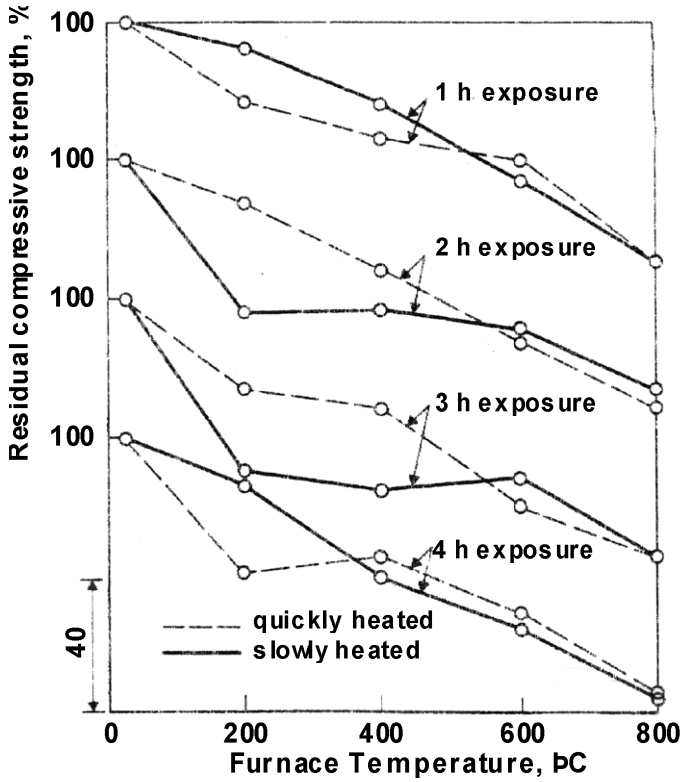

Figure 2.76 Effect of rate of heating on residual strength of slowly cooled concrete.

Source: G. T. C. Mohamedbhai, "Effect of Exposure Time and Rates of Heating and Cooling on Residual Strength of Heated Concrete," *Magazine of Concrete Research* **38**(136), pp. 151–158. September 1986.

*See also Figure 2.207.

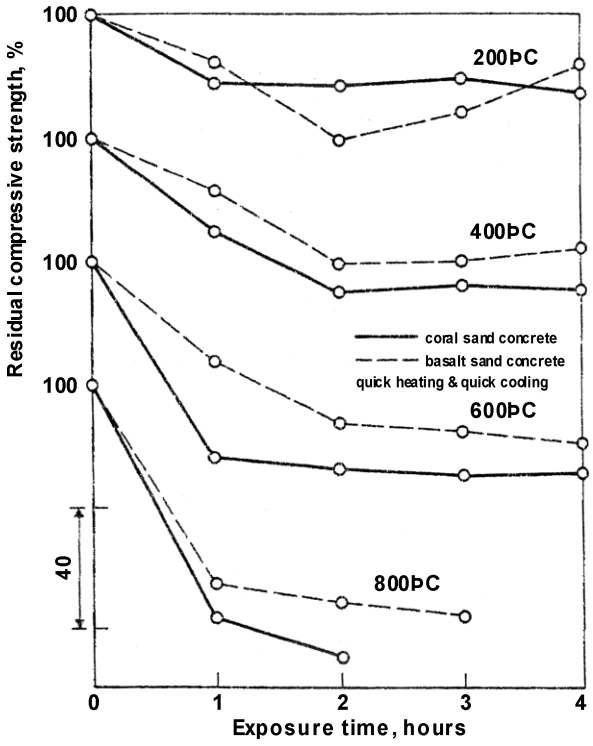

Figure 2.77 Effect of exposure time on residual strength of coral sand and basalt sand concretes.

Source: G. T. C. Mohamedbhai, "Effect of Exposure Time and Rates of Heating and Cooling on Residual Strength of Heated Concrete," *Magazine of Concrete Research* **38**(136), pp. 151–158, September 1986.

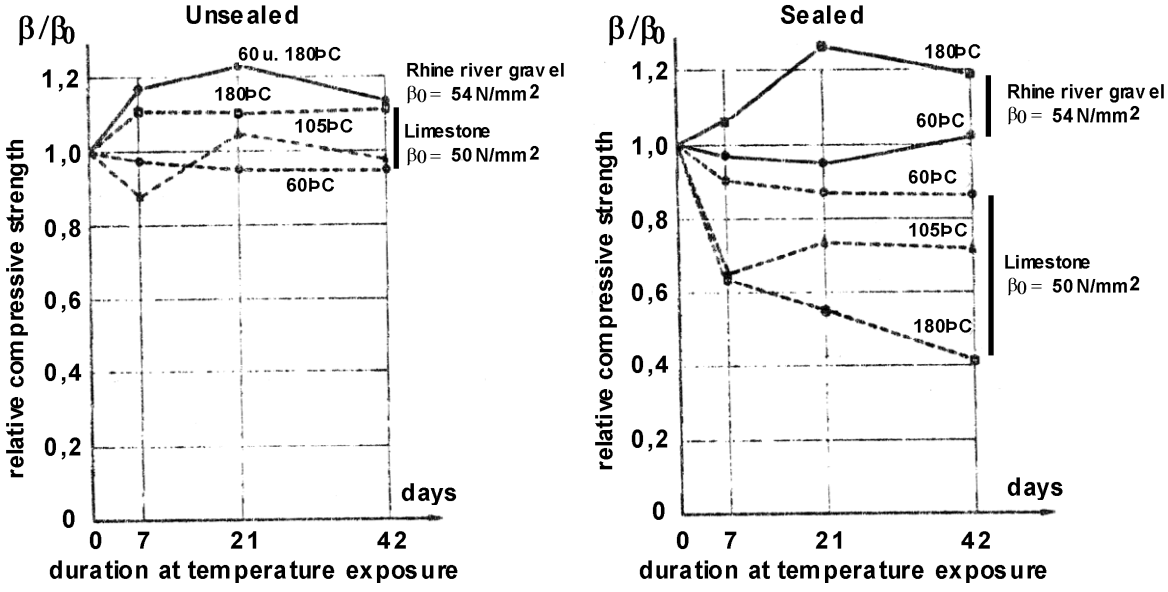

Figure 2.78 Relative strength development of concrete exposed to elevated temperature.

Source: R. Kottas, J. Seeberger, and H. K. Hilsdorf, "Strength Characteristics of Concrete in the Temperature Range of 20° to 200°C," Paper H01/4 in *5th International Conference on Structural Mechanics in Reactor Technology*, 8 p., Elsevier Science Publishers, North-Holland, The Netherlands, August 1979.

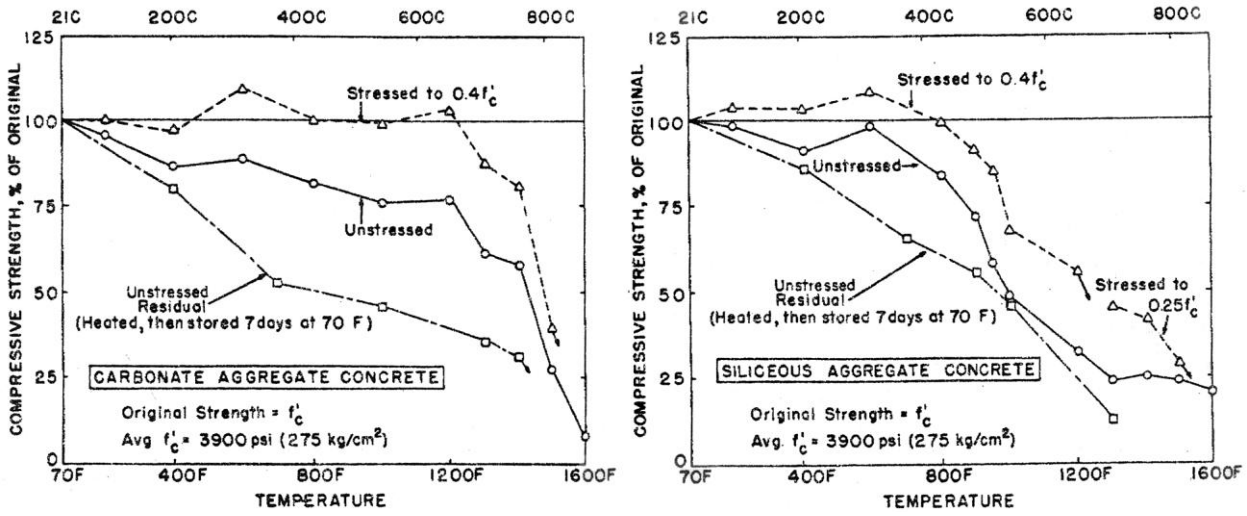

Figure 2.79 Effect of exposure time on residual strength of carbonate and siliceous aggregate concretes.

Source: M. S. Abrams, "Compressive Strength of Concrete at Temperatures to 1600°F," SP-25, *Temperature and Concrete*, American Concrete Institute, pp. 33–58, 1971.

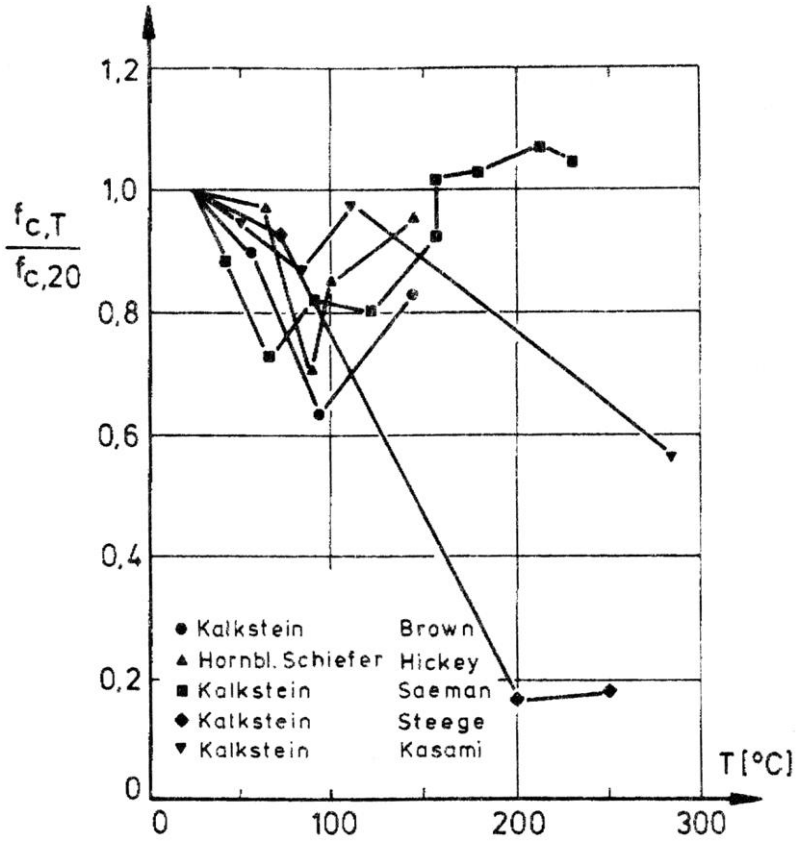

Figure 2.80 Compressive strength of concretes with limestone and other aggregate types.

Source: U. Schneider, *Behaviour of Concrete at High Temperature*, HEFT 337, Deutscher Ausschuss für Stahlbeton, Wilhelm Ernst & Sohn, Munich, Germany, 1982.

Figures 2.81 and 2.82 present normalized compressive strength results for unstressed specimens tested cold (residual) and at temperature (hot), respectively, that are based on results from several investigators. Also shown in the figure are upper and lower bounds that were established from the data. The results were utilized as part of a study to investigate the behavior of reinforced concrete sections at elevated temperature.

Additional information is presented in Figure 2.83 on the effect of elevated-temperature exposure on the compressive strength of unsealed nuclear power plant prestressed concrete pressure vessel-type concretes (limestone, basalt, or gravel aggregate materials) tested either hot (H) or cold (C). This figure plus the previous two figures indicate the influence of the concrete and the test condition on the residual compressive strength after thermal exposure. The general trend for a strength loss with increasing temperature indicates the influence of the cement paste and the increasing role of the aggregate materials at higher temperatures. Factors have been identified that may contribute to the general trend for loss of compressive strength with increasing temperature [2.8]: aggregate damage; weakening of the cement paste-aggregate bond; and weakening of the cement paste due to an increase in porosity on dehydration, partial breakdown of the C-S-H, chemical transformation on hydrothermal reactions, and development of cracking. A number of material and environmental-related factors affect the response of concrete materials to elevated-temperature conditions (e.g., see Table 2.1, p. 4). As many of the aggregate materials are thermally stable up to temperatures of 300°C to 350°C, which includes the temperature range considered for most concrete applications, the compressive strength of concrete at elevated temperature is dependent in large measure on the interaction between the cement paste and aggregate.

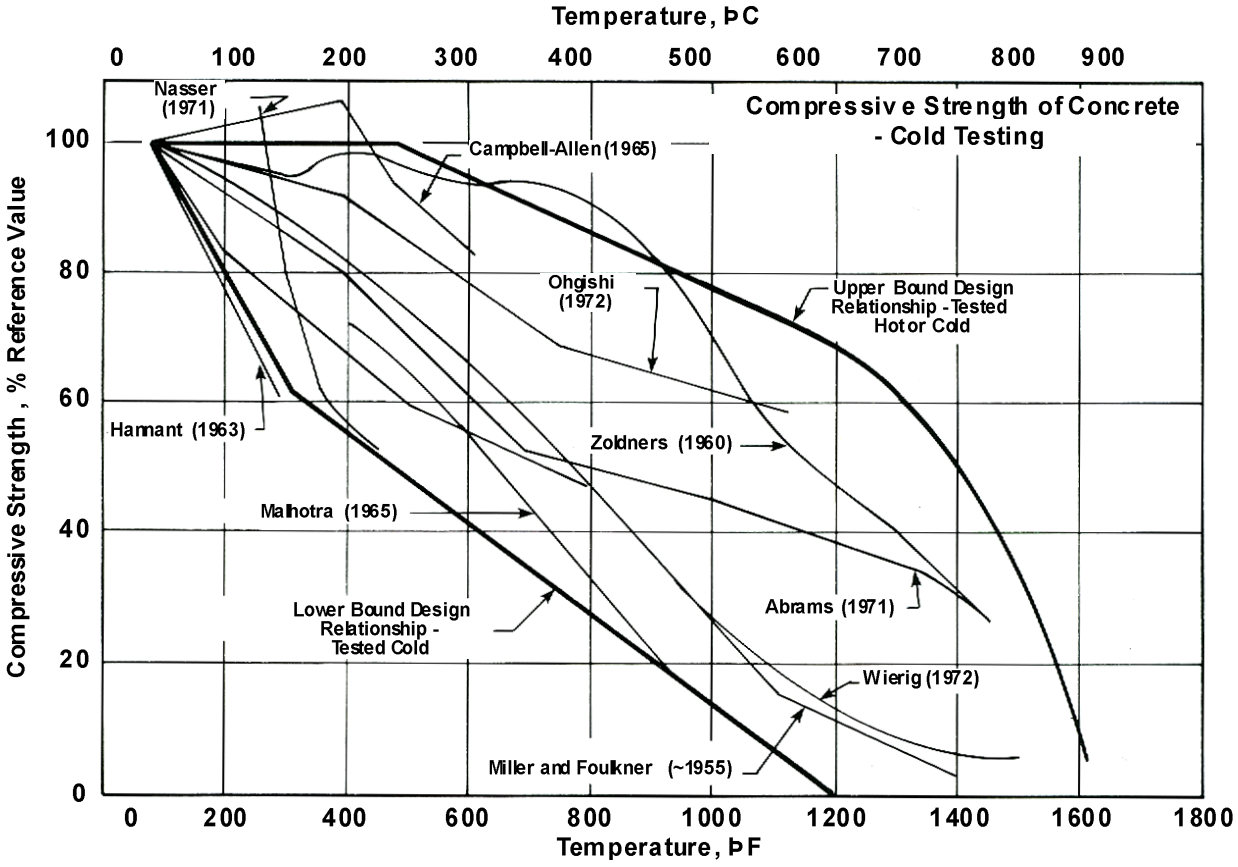

Figure 2.81 Effect of temperature exposure on compressive strength of concrete: tested cold.

Source: G. N. Freskakis et al., "Strength Properties of Concrete at Elevated Temperature," *Civil Engineering Nuclear Power*, Vol. 1, ASCE National Convention, American Society of Civil Engineers, Boston, Massachusetts, April 1979.

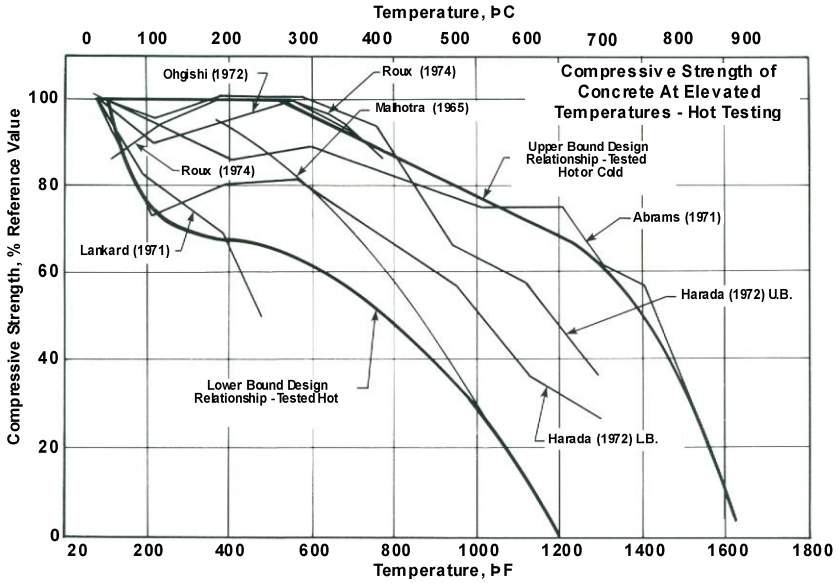

Figure 2.82 Effect of temperature exposure on compressive strength of concrete: tested hot.

Source: G. N. Freskakis et al., "Strength Properties of Concrete at Elevated Temperature," *Civil Engineering Nuclear Power*, Vol. 1, ASCE National Convention, American Society of Civil Engineers, Boston, Massachusetts, April 1979.

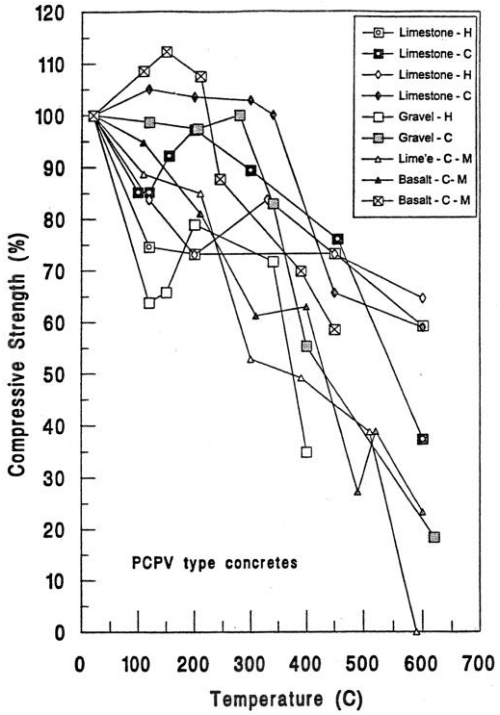

Figure 2.83 Effect of temperature on uniaxial compressive strength of PCPV unsealed concretes (H = hot, C = cold).

Source: G. A. Khoury, *Performance of Heated Concrete—Mechanical Properties*, Contract NUC/56/3604A with Nuclear Installations Inspectorate, Imperial College, London, United Kingdom, August 1996.

Data on effects of elevated temperature on concrete compressive strength have also been assembled as part of a review of concrete properties for prestressed concrete pressure vessels (PCPVs) [2.103]. Figure 2.84 presents a summary of data assembled under this activity for sealed and unsealed specimens that were either tested at temperature (hot) or after returning to room temperature (cold). Results indicate that the reference strength retention of unsealed specimens (open symbols) was better than that for sealed specimens (closed symbols). It was noted that this may be a concern for mass concrete having substantial amounts of retained moisture that experiences thermal loadings and that deleterious effects of elevated-temperature exposure on concrete compressive strength can be considered as significant only for sealed conditions in which significant amounts of free moisture are retained up to 300˚C. Compressive strength was found to decrease with increases of temperature, time of exposure, free-moisture content, and thermal cycling.

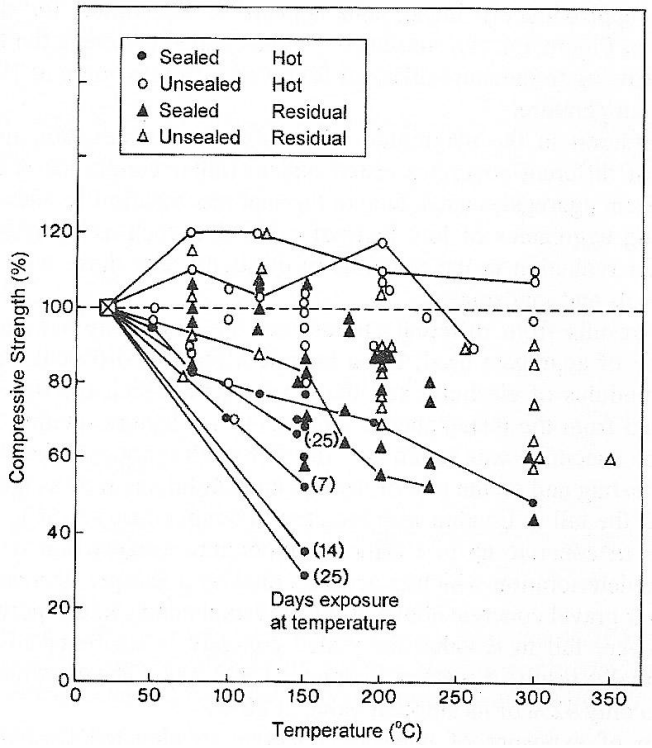

Figure 2.84 Compilation of data on concrete compressive strength vs temperature.

Source: R.K. Nanstad, *A Review of Concrete Properties for Prestressed Concrete Pressure Vessels*, ORNL/TM-5497, Oak Ridge National Laboratory, Oak Ridge, Tennessee, October 1976.

Results from information presented above as well as those from other researchers have been used to develop a series of figures illustrating the effect of elevated temperature on the compressive strength of concrete materials. References to data sources cited by others or utilized in figures are identified in Appendix A. Test results are presented in terms of testing procedures identified earlier in the report that are commonly used to evaluate concrete response to elevated temperature: unstressed tests (hot testing), unstressed residual (cold testing), and stressed tests. All test results presented are for unsealed specimens.

Figure 2.85 presents a compilation of data on the effect of elevated temperature on the relative compressive strength (i.e., unsealed, hot testing) for a number of different concrete mixtures (i.e., ordinary Portland cement concretes and concretes that also included supplementary cementitious materials). The CEB design curve* for unstressed normal weight concretes has been superimposed on the figures to facilitate comparisons.

* Comites Euro-International Du Beton, *Fire Design of Concrete Structures – in Accordance with CEB/FIP Model Code 90*, CEB Bulletin D'Information No. 208, Lausanne, Switzerland, July 1991.

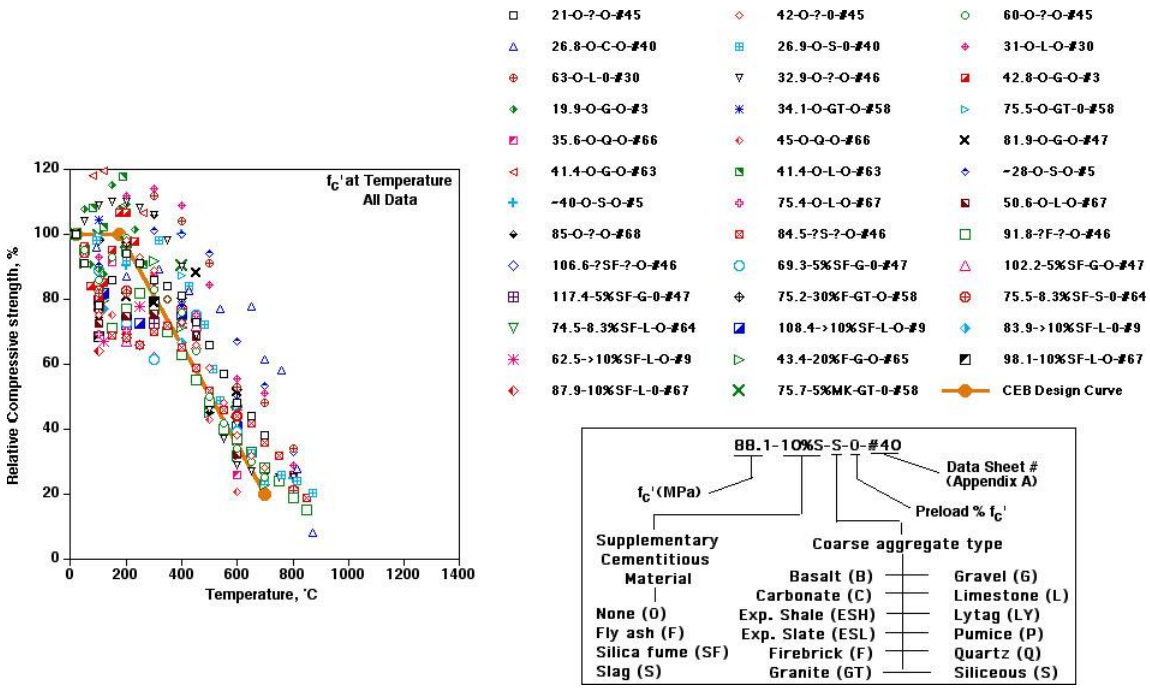

Figure 2.85 Compilation of data on relative compressive strength vs temperature – ordinary Portland cement concretes and concretes containing supplementary cementitious materials.

Results obtained for only the Portland cement concretes are provided in Figure 2.86 with the results subdivided into normal strength concretes (fc' < 60 MPa) and high-strength concretes (fc' $\geq$ 60 MPa) and presented in Figures 2.87 and 2.88, respectively.

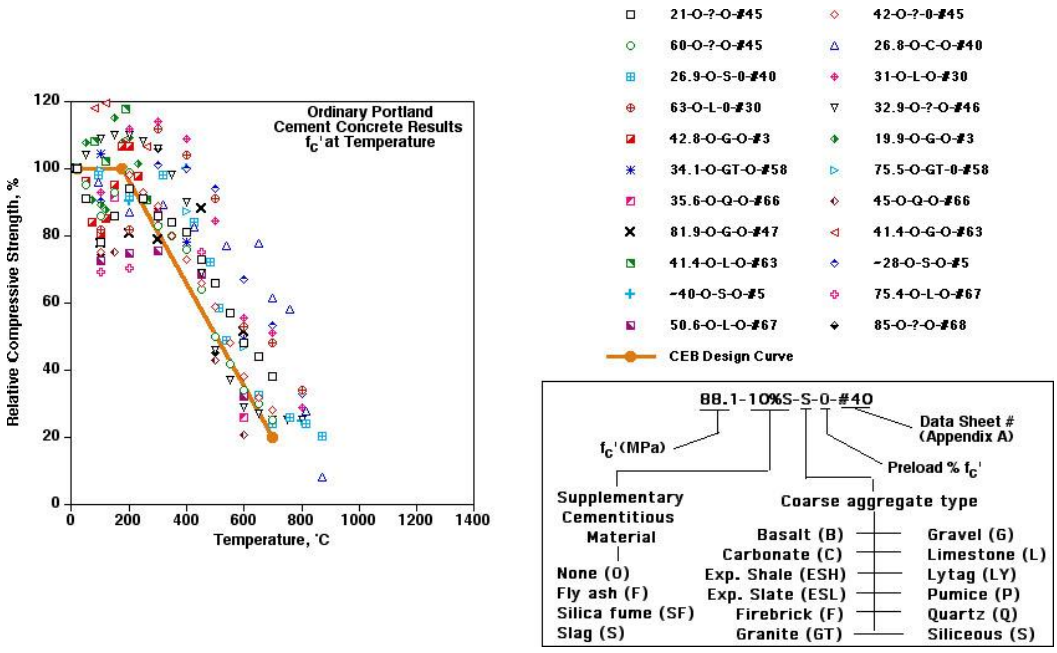

Figure 2.86 Compilation of data on relative compressive strength vs temperature – ordinary Portland cement concretes.

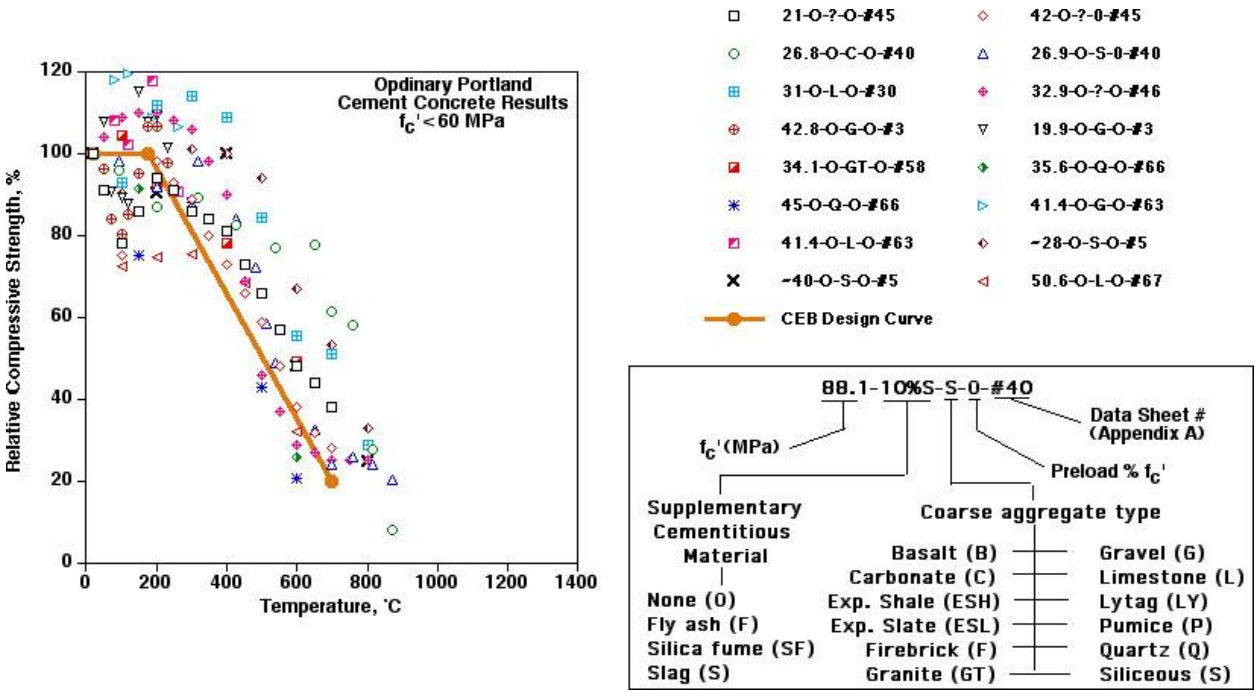

Figure 2.87 Compilation of data on relative compressive strength vs temperature – ordinary Portland cement concretes, $f_c' < 60$ MPa.

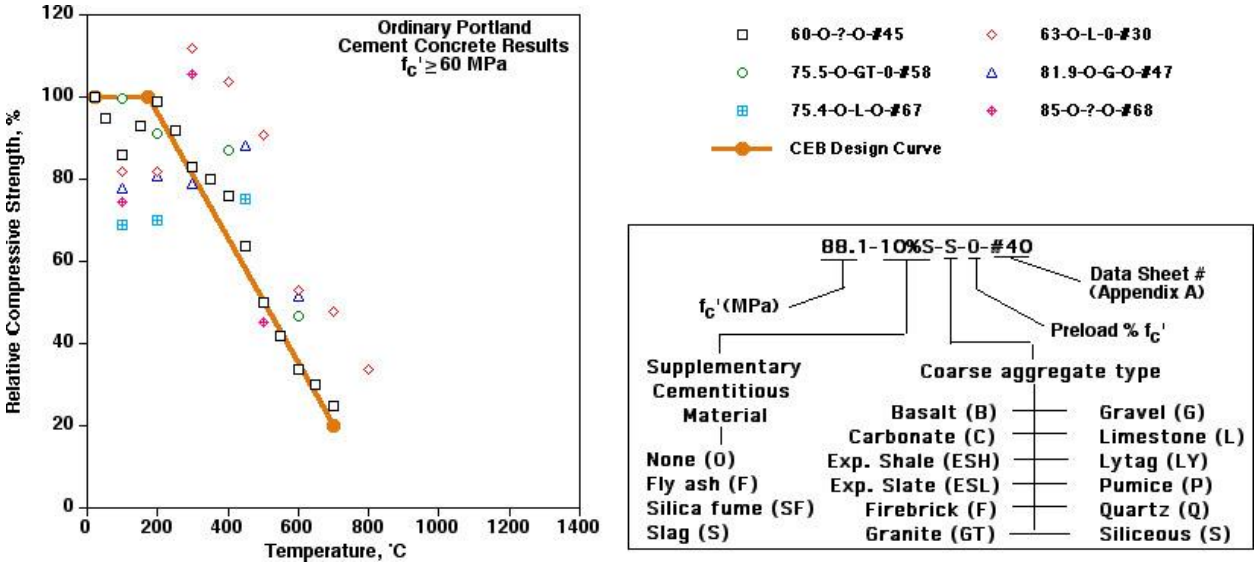

Figure 2.88 Compilation of data on relative compressive strength vs temperature – ordinary Portland cement concretes, $f_c' \geq 60$ MPa.

Results obtained for Portland cement concretes containing supplementary cementious materials are presented in Figure 2.89.

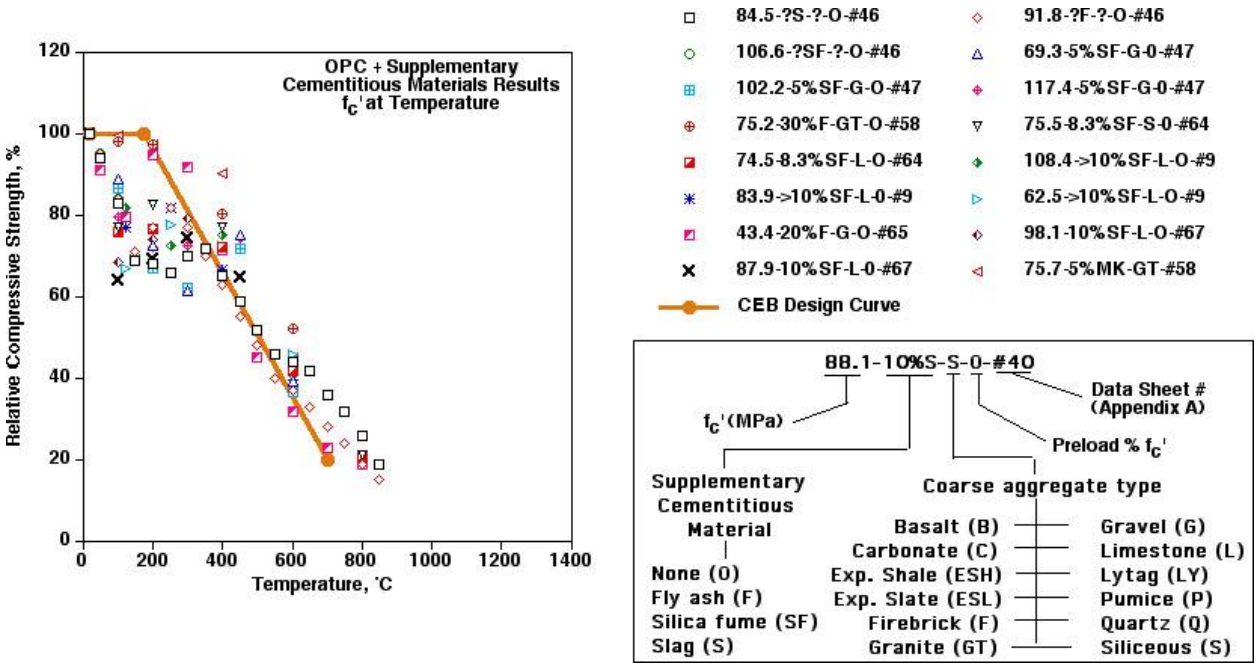

Figure 2.89 Compilation of data on relative compressive strength vs temperature – concretes containing supplementary cementitious materials.

Several general conclusions can be derived based on the relative compressive strength data (unsealed, hot testing). Considerable data scatter is exhibited by the relative compressive strength data particularly at the lower exposure temperatures. Scatter can probably be attributed to different materials and testing conditions utilized in the different studies (e.g., constituents and mix proportions, specimens size and shape, specimens tested at different degrees of hydration and initial moisture contents, and heating rates and thermal stabilization periods). As the exposure temperature increased the loss in relative compressive strength tended to become more linear. Although ordinary Portland cement high-strength concrete data reported are very limited, there may be a slight trend for the high-strength concretes to have increased rates of strength lose at temperatures lower than 400˚C than the normal-strength concretes, but at higher temperatures the rates of strength loss appear to be similar. Results for concretes containing supplementary cementitious materials, which with one exception were all high-strength concretes, also tended to show higher rates of compressive strength loss at temperatures lower than 400˚C than that experienced by the ordinary Portland cement concrete mixes.

Figure 2.90 presents a compilation of data on the effect of elevated temperature on the residual compressive strength (i.e., unsealed, cold testing) for a number of different concrete mixtures (i.e., ordinary Portland cement concretes and concretes that also included supplementary cementitious materials). Results obtained for only the Portland cement concretes are provided in Figure 2.91 with the results subdivided into normal strength concretes ($f_c' < 60$ MPa) and high-strength concretes ($f_c' > 60$ MPa) and presented in Figures 2.92 and 2.93, respectively. Residual compressive strength results for ordinary Portland cement normal-strength concretes utilizing carbonate- or siliceous- and gravel-type aggregate materials are presented in Figures 2.94 and 2.95, respectively. Residual compressive strength results for concretes containing supplementary cementious materials are presented in Figure 2.96, with the results subdivided into normal-strength concretes ($f_c' < 60$ MPa) and high-strength concretes ($f_c' > 60$ MPa) and presented in Figures 2.97 and 2.98, respectively. Residual compressive strength results for concretes containing silica fume, fly ash, metakaolin, and slag as supplementary cementitious materials are presented in Figures 2.99 through 2.102, respectively. The CEB design curve for unstressed normal weight concretes has been superimposed on the figures to facilitate comparisons.

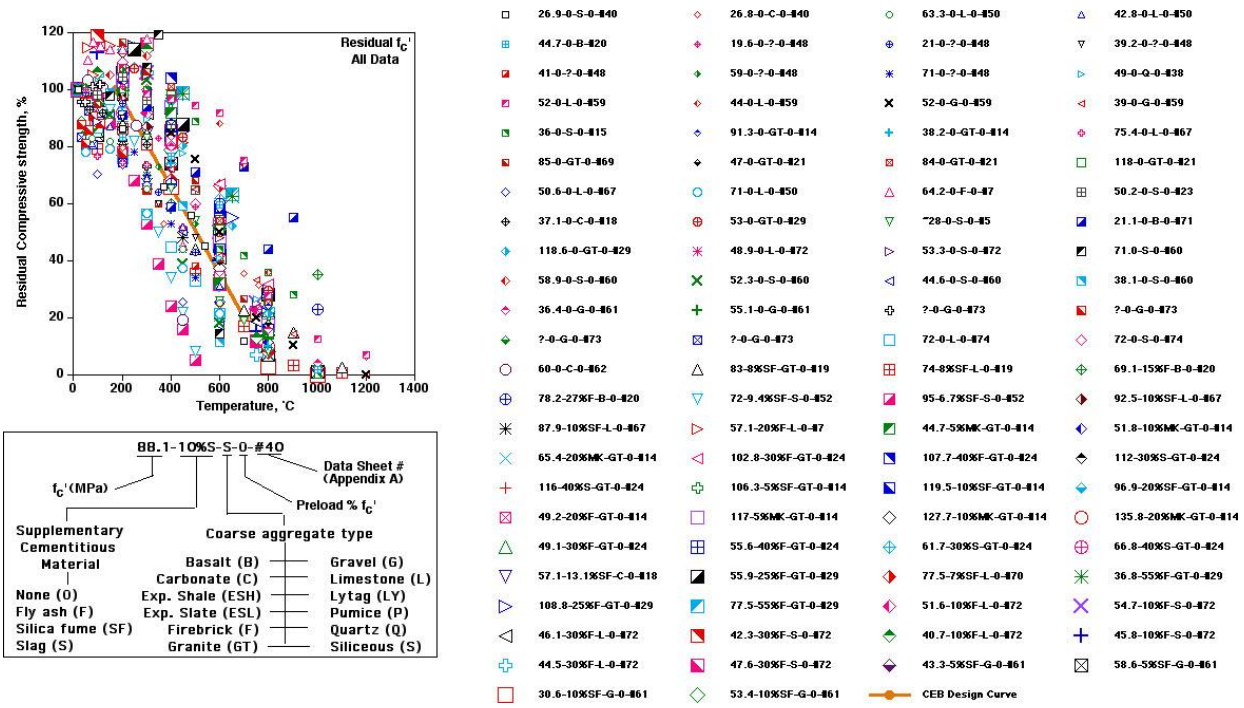

Figure 2.90 Compilation of data on residual compressive strength vs temperature – ordinary Portland cement concretes and concretes containing supplementary cementitious materials.

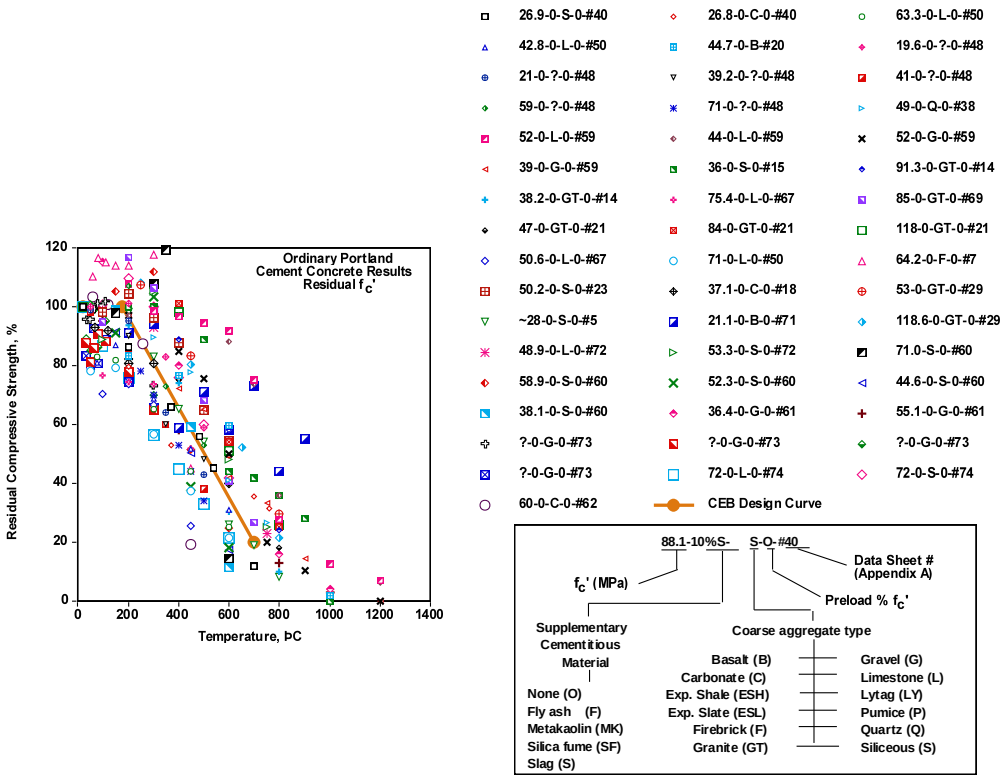

Figure 2.91 Compilation of data on residual compressive strength vs temperature – ordinary Portland cement concretes.

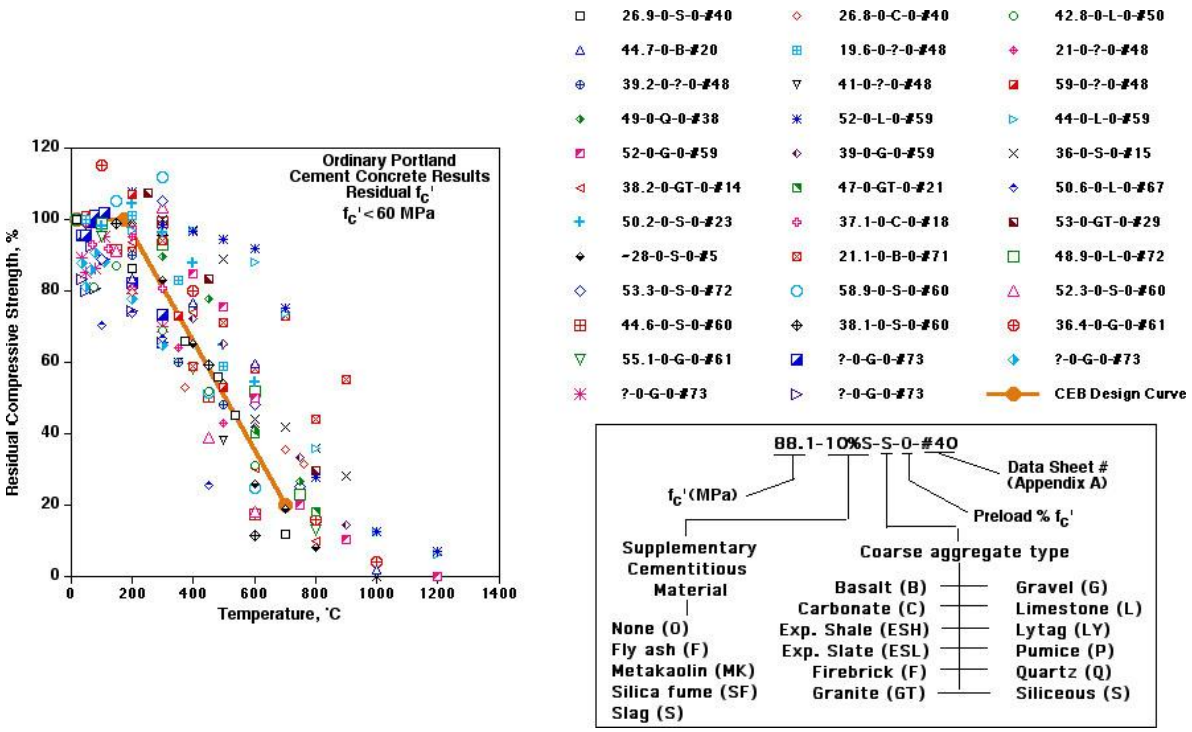

Figure 2.92 Compilation of data on residual compressive strength vs temperature – ordinary Portland cement concretes, $f_c' < 60$ MPa.

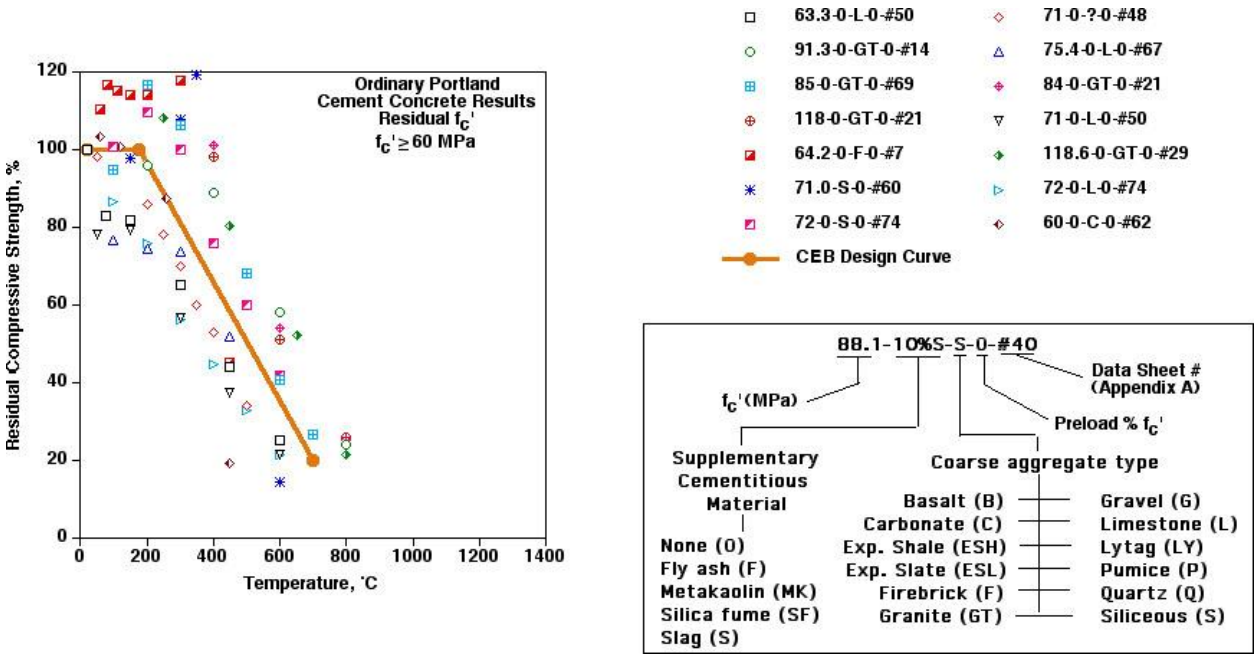

Figure 2.93 Compilation of data on residual compressive strength vs temperature – ordinary Portland cement concretes, $f_c' \geq 60$ MPa.

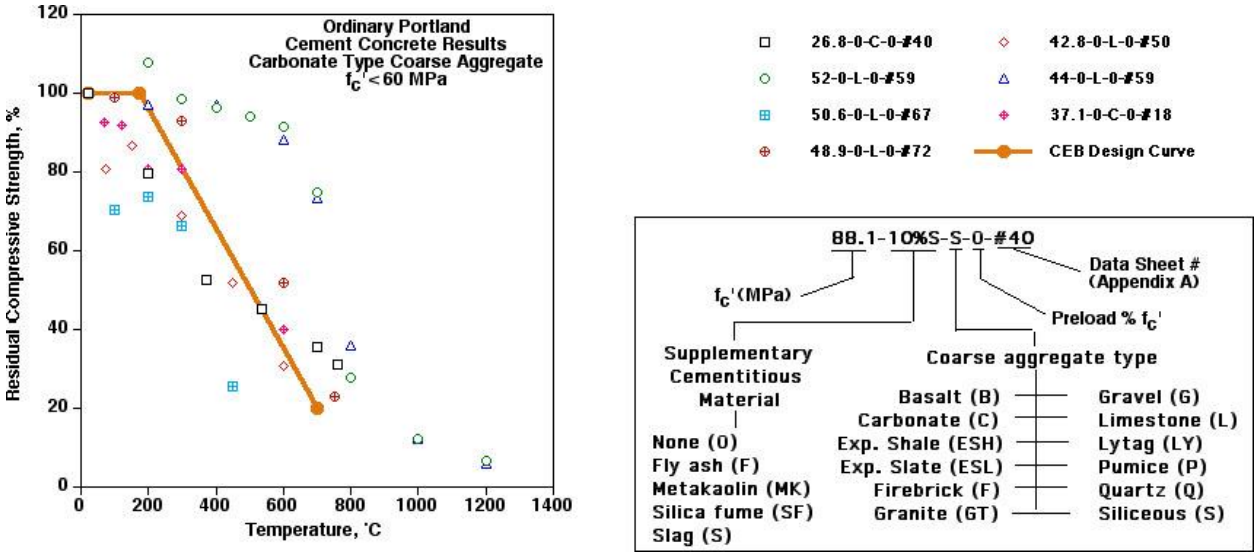

Figure 2.94 Compilation of data on residual compressive strength vs temperature – ordinary Portland cement concretes with carbonate-type aggregates, $f_c' < 60$ MPa.

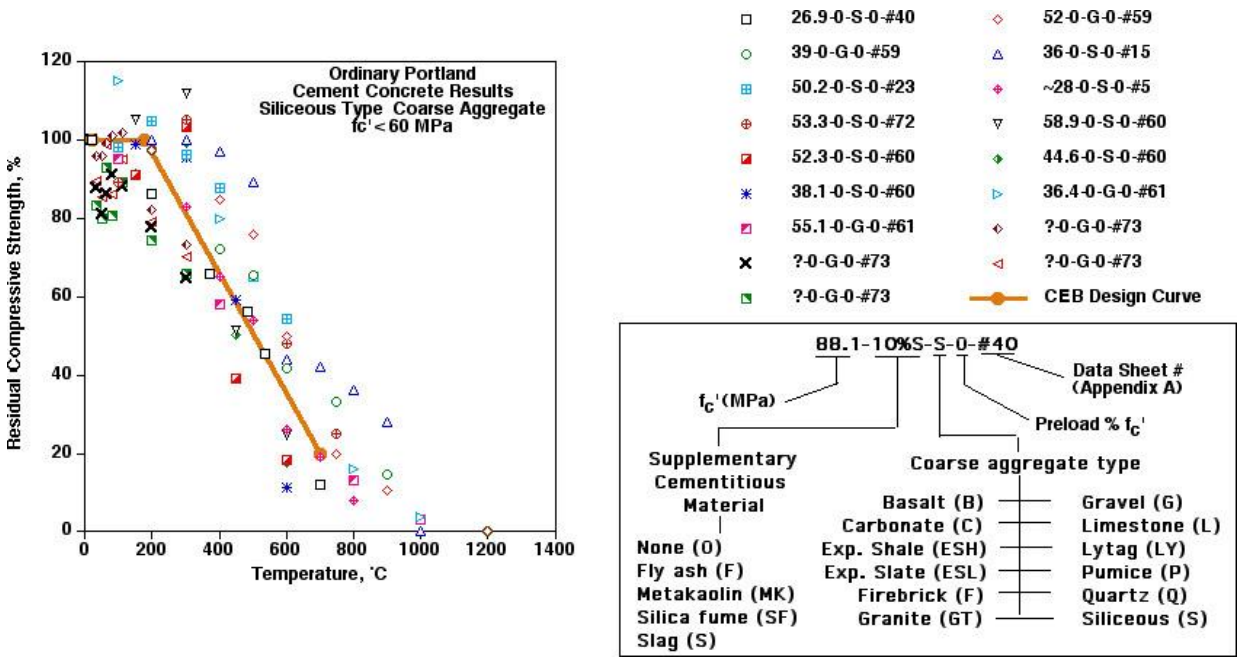

Figure 2.95 Compilation of data on residual compressive strength vs temperature – ordinary Portland cement concretes with siliceous- or gravel-type aggregates, $f_c' < 60$ MPa.

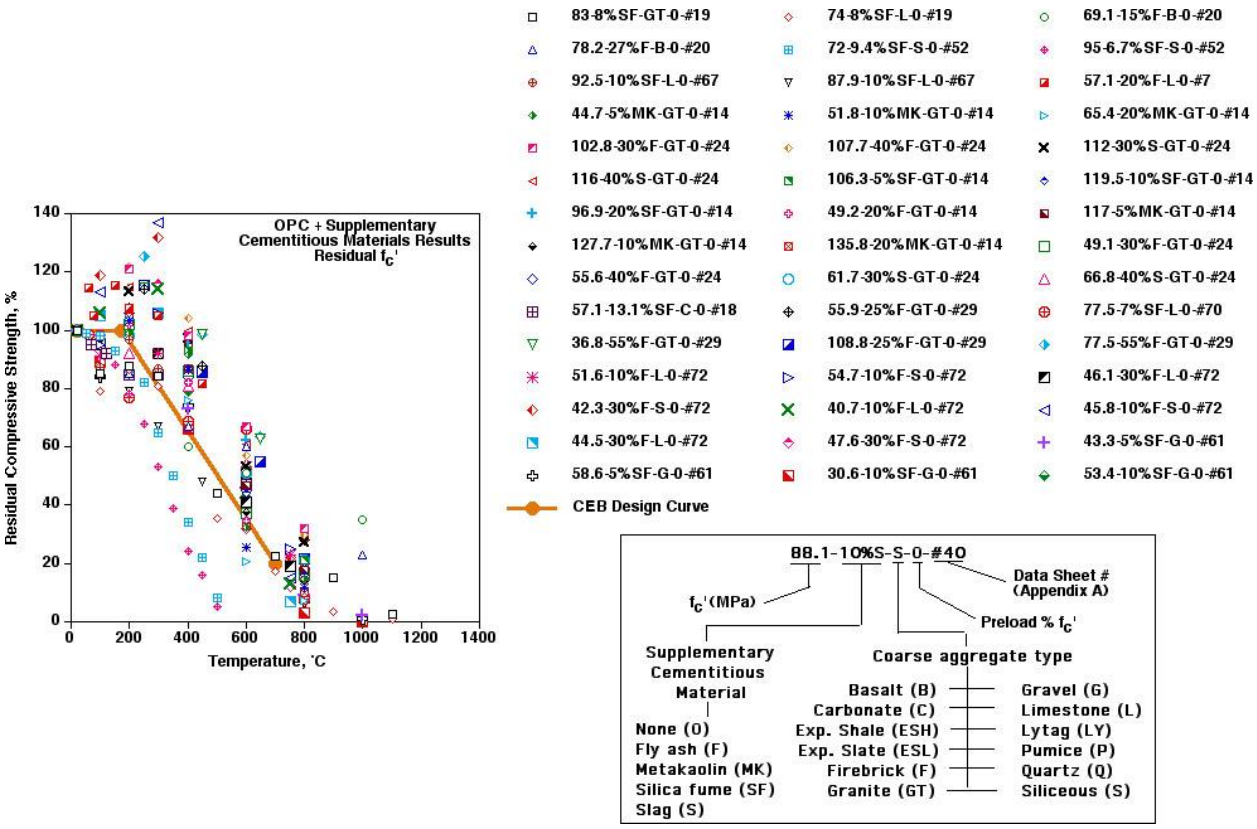

Figure 2.96 Compilation of data on residual compressive strength vs temperature – concretes containing supplementary cementitious materials.

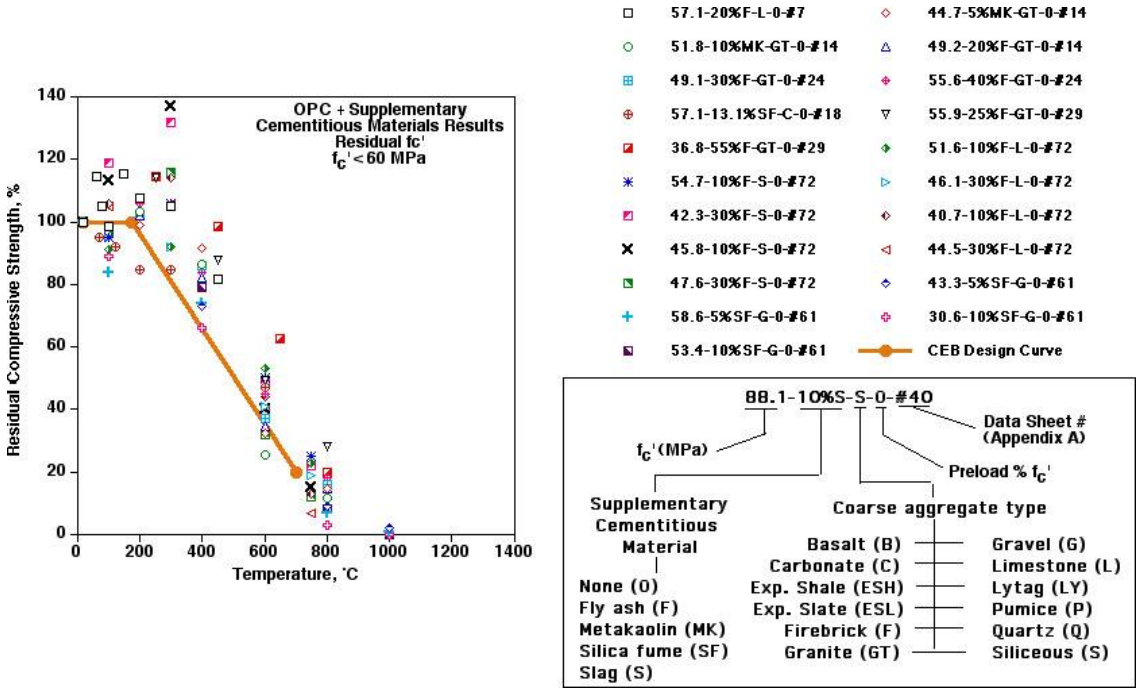

Figure 2.97 Compilation of data on residual compressive strength vs temperature – concretes containing supplementary cementitious materials, fc' < 60 MPa.

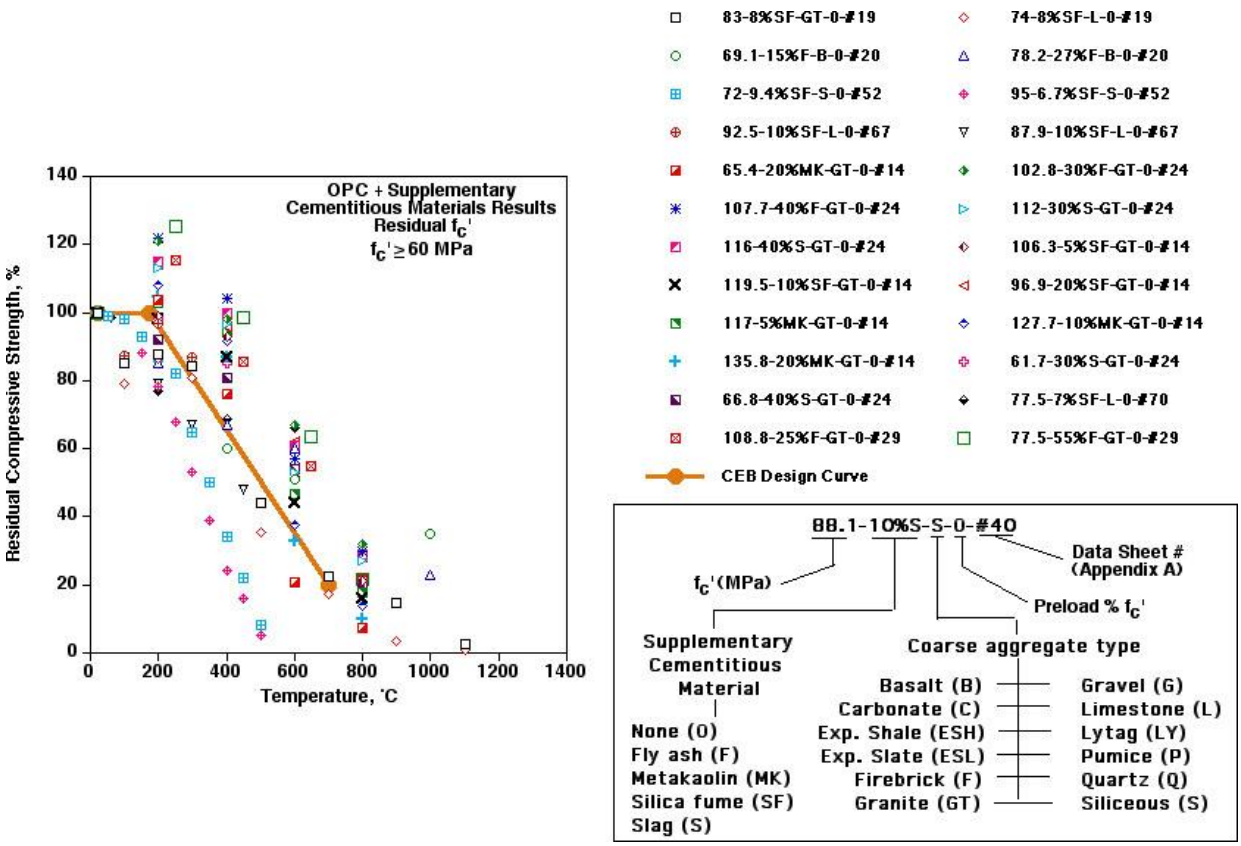

Figure 2.98 Compilation of data on residual compressive strength vs temperature – concretes containing supplementary cementitious materials, fc' $\geq$ 60 MPa.

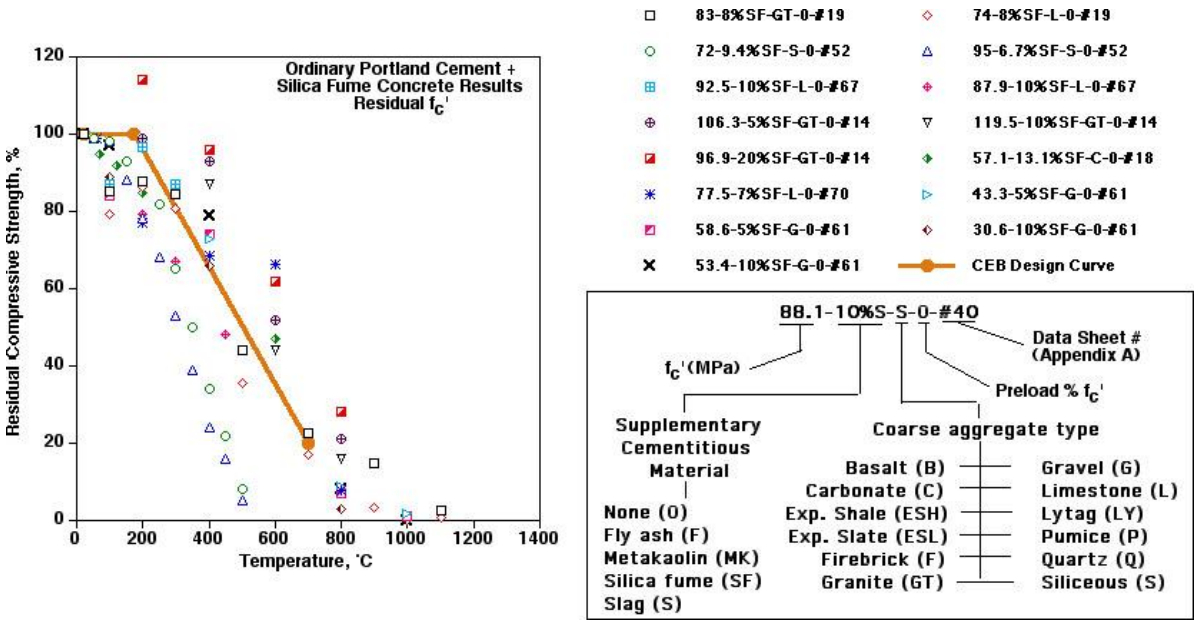

Figure 2.99 Compilation of data on residual compressive strength vs temperature – concretes containing silica fume supplementary cementitious materials.

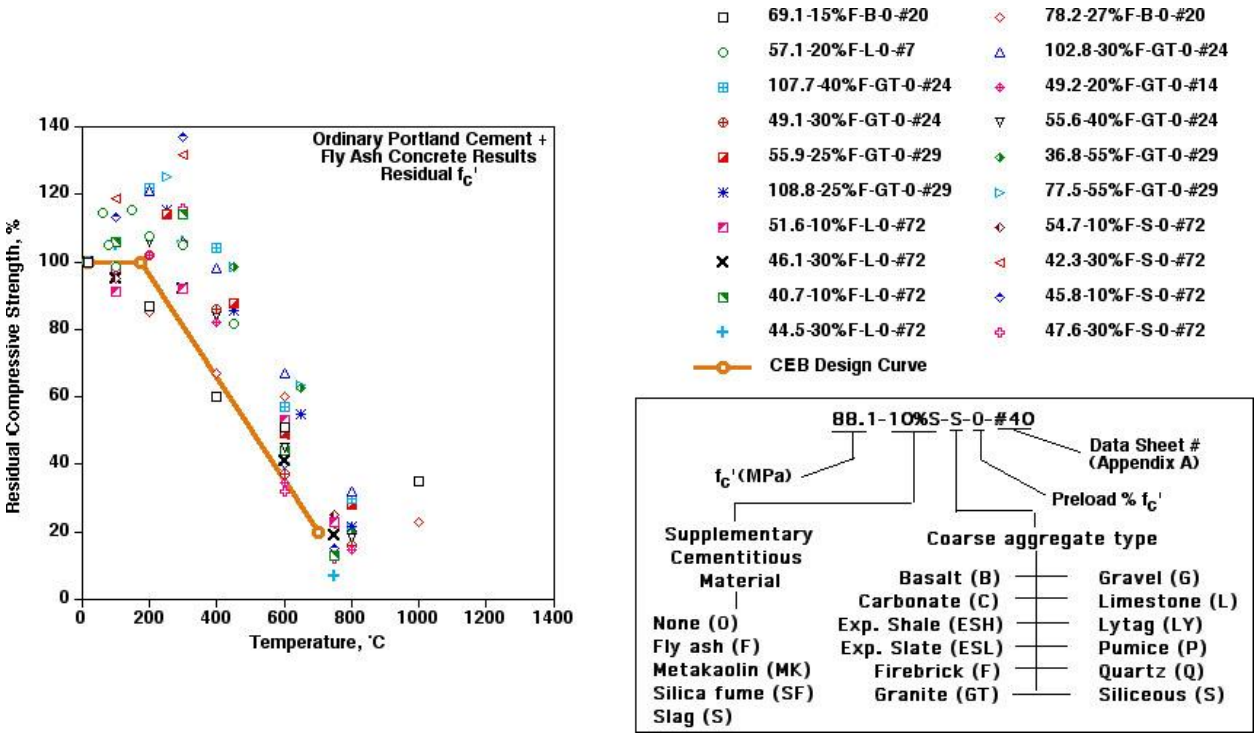

Figure 2.100 Compilation of data on residual compressive strength vs temperature – concretes containing fly ash supplementary cementitious materials.

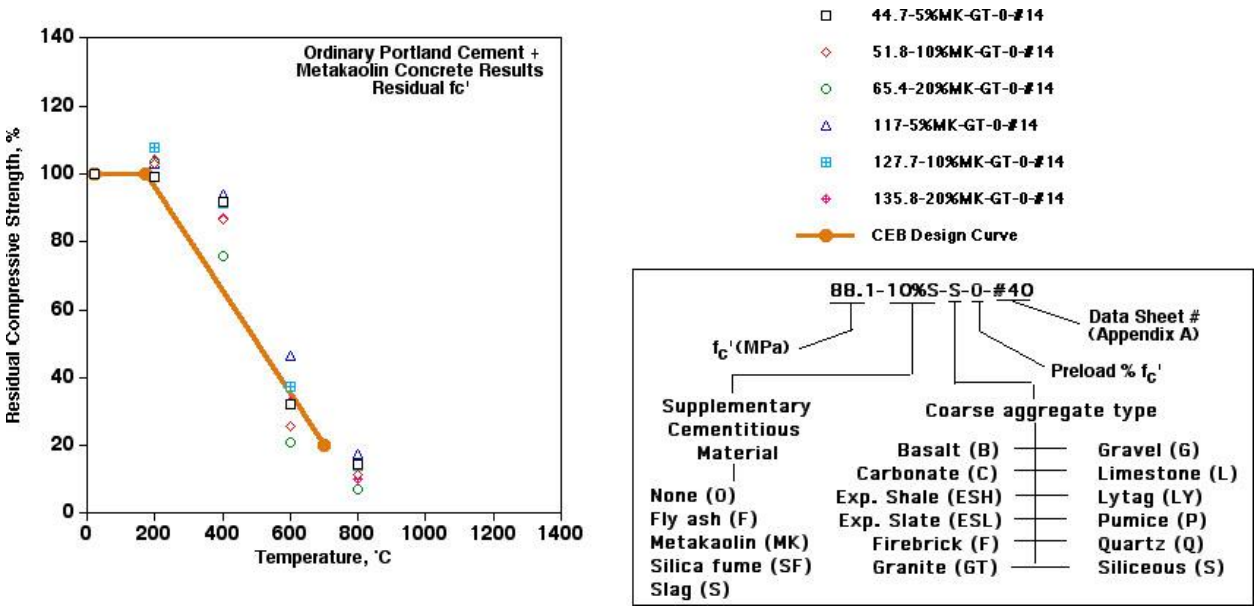

Figure 2.101 Compilation of data on residual compressive strength vs temperature – concretes containing metakaolin supplementary cementitious materials.

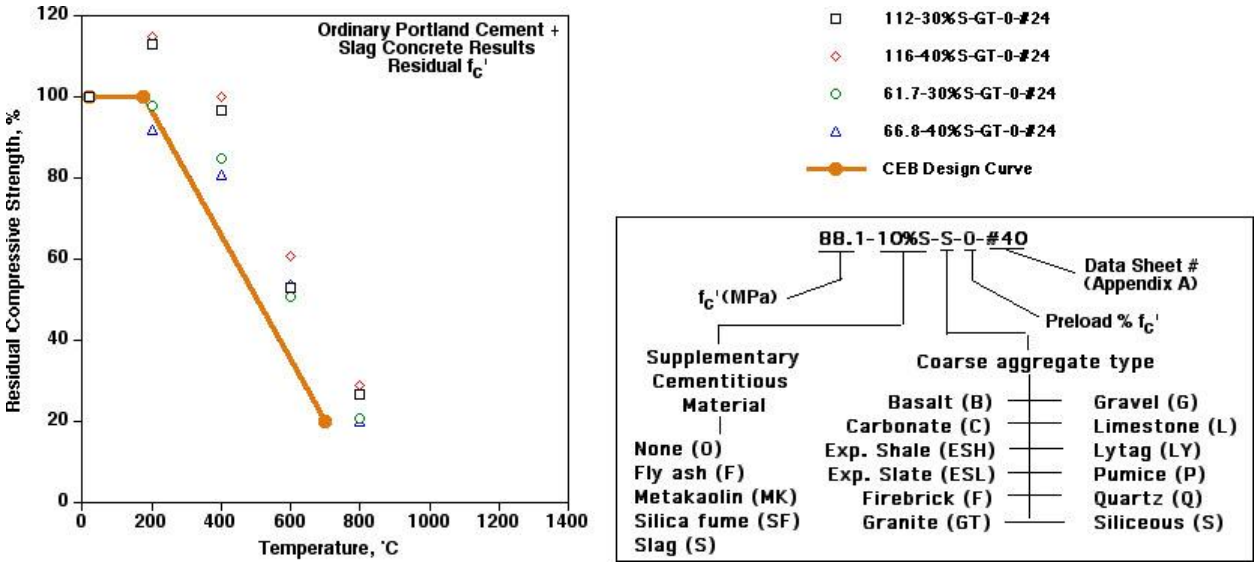

Figure 2.102 Compilation of data on residual compressive strength vs temperature – concretes containing slag supplementary cementitious materials.

Several general conclusions can be derived based on the residual compressive strength data (unsealed, cold testing). Considerable data scatter is exhibited by the residual compressive strength data, particularly at the lower exposure temperatures, which can be attributed to differences in material and environmental factors for the different tests. Comparing the residual (Figure 2.91) to the relative (Figure 2.86) compressive strength results indicates that in general the compressive strength retention of specimens tested at temperature is greater than that obtained from specimens permitted to cool to room temperature prior to testing. Results in Figure 2.91 seem to indicate that for the unsealed specimens the residual compressive strength generally tends to decrease somewhat at temperatures below about 100˚ to 120˚C, that can be followed by an increase in compressive strength as the temperature increases to 200˚ to 250˚C, before again decreasing, with the main decrease occurring as the temperature exceeds about 300˚C. No definite trend could be derived on the effect of initial concrete strength when comparing normal- and high-strength ordinary Portland cement concrete results (Figures 2.92 and 2.93). Although data are limited, there appears to be a slight trend for the siliceous and gravel aggregate-type concretes (Figure 2.95) to exhibit higher residual compressive strengths than carbonate aggregate-type concretes (Figure 2.94) at temperatures below about 400˚C, but at higher temperatures the carbonate-aggregate type concretes may exhibit higher residual compressive strengths. Residual compressive strength results for concretes containing supplementary cementitious materials (Figure 2.96) exhibited a similar trend to that exhibited by the ordinary Portland cement concretes (Figure 2.91). Comparing Figure 2.97 with Figure 2.98 indicates that the residual compressive strength retention of the normal-strength concretes at temperatures above 200˚C may be slightly better than that for the high-strength concretes, but the data are limited. Although results are limited, Figures 2.99 through 2.102 indicates that the residual compressive strength retention is highest for the concretes containing slag and fly ash supplementary cementitious materials, followed by the concrete containing metakaoline, with silica fume concretes exhibiting the lowest residual compressive strength at the higher temperatures.

The effect of sustained stress during heating on the relative compressive strength (unsealed, hot testing) is presented in Figure 2.103 for ordinary Portland cement concretes and concretes that also included supplementary cementitious materials. Preload levels ranged from 20 to 40% the reference room temperature compressive strength of the concretes. Results have been separated into those for ordinary Portland cement concrete materials and those for concretes containing supplementary cementitious materials and are presented in Figures 2.104 and 2.105, respectively. Although results are limited, the presence of preload, within reasonable limits, and its beneficial effects relative to retained compressive strength is evident. Similar effects of pre-loading on the residual compressive strength were noted to that obtained for the ordinary Portland cement concretes, but data were too limited and scatter too great to draw conclusions comparing the relative benefit of preload on ordinary Portland cement concretes and concretes containing supplementary cementitious materials. It has been noted that the beneficial effects on retained compressive strength derived from preload during heating is a result of densification of

the cement paste resulting in a large transient creep component and possibly to a reduction in porosity relative to the unloaded state, and pre-compression can reduce tensile stresses in the concrete, particularly during cooling [2.8].

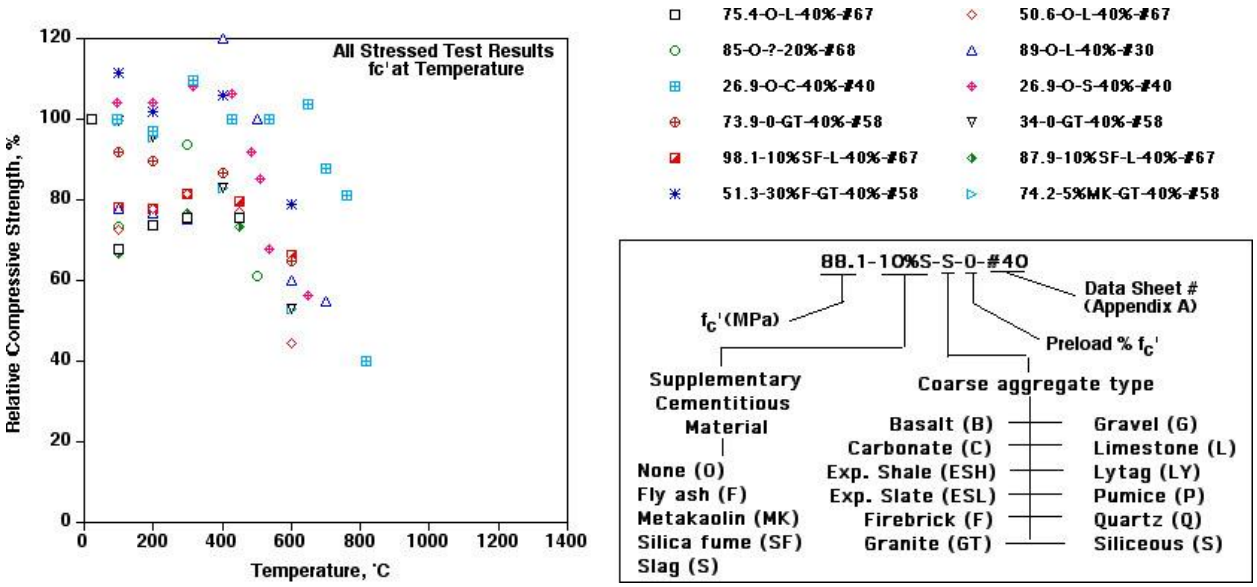

Figure 2.103 Compilation of data on compressive strength vs temperature for preloaded specimens – ordinary Portland cement concretes and concretes containing supplementary cementitious materials.

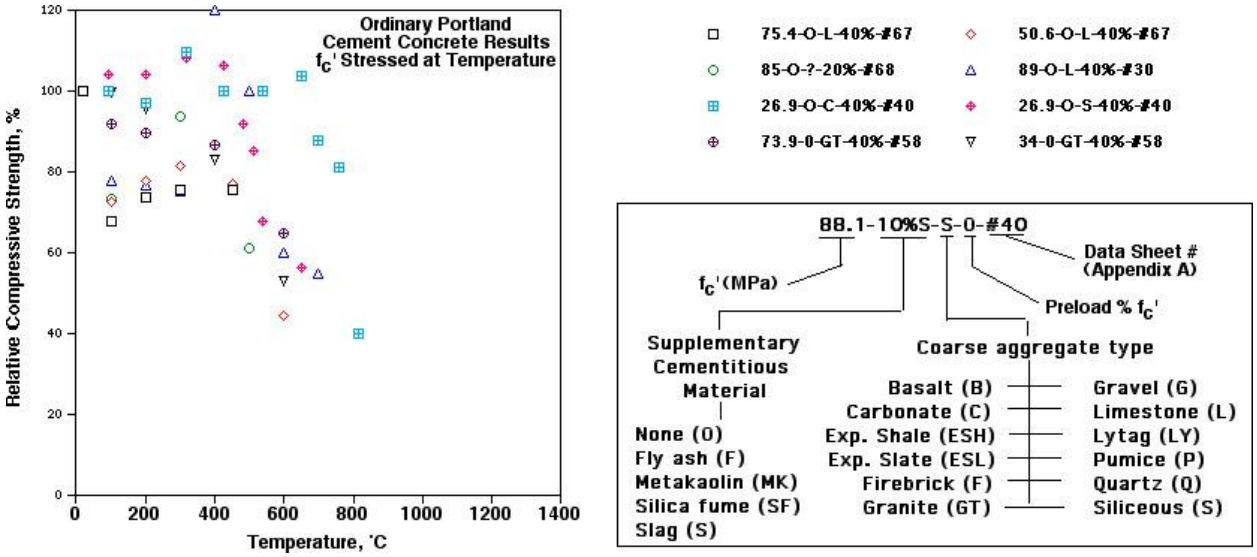

Figure 2.104 Compilation of data on relative compressive strength vs temperature for preloaded specimens – ordinary Portland cement concretes.

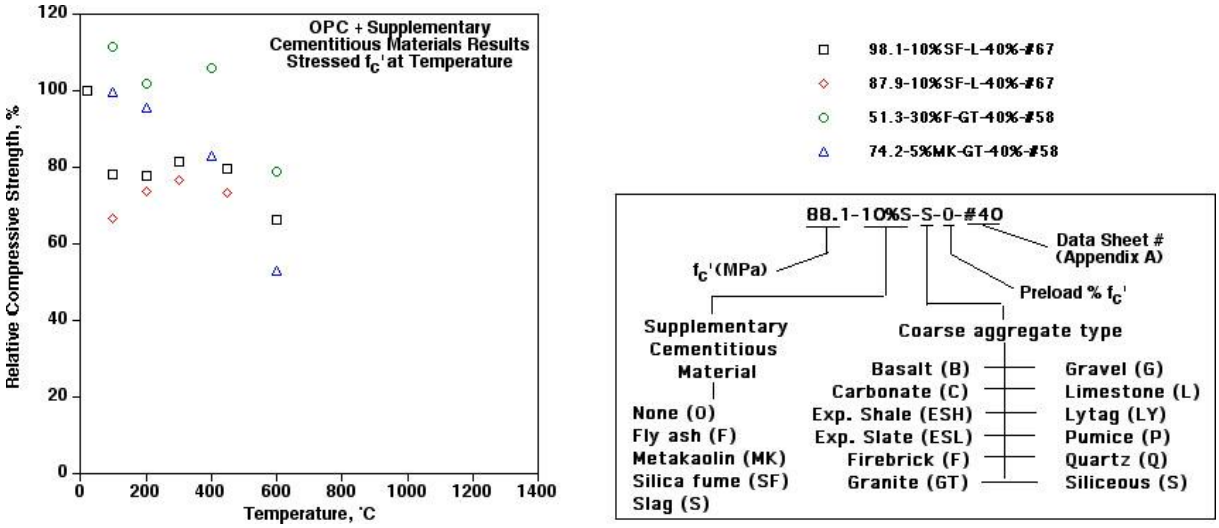

Figure 2.105 Compilation of data on relative compressive strength vs temperature for pre-loaded specimens – concretes containing supplementary cementitious materials.

The effect of cooling regime on the residual compressive strength has been studied as part of an overall investigation to evaluate the post-thermal properties of concrete following rapid cooling (e.g., water quenching in conjunction with fire) [2.67]. A granite aggregate ordinary Portland cement concrete having an initial reference compressive strength of 21.16 MPa was used to fabricate 101.6-mm-diameter by 203.2-mm-long cylindrical test specimens that were cured for eight weeks in a fog room (23˚C and 93% relative humidity). The specimens were heated in a furnace to 200˚, 400˚, 600˚, or 800˚C with a holding time at temperature of four hours. Following heating, the specimens were cooled slowly (1˚C/minute), naturally (left in furnace and permitted to cool slowly), or rapidly (e.g., specimen removed from furnace and placed into a tank of water initially at 20˚C). Figure 2.106 presents the effect of cooling regime on the relative residual compressive strength for concretes subjected to temperatures up to 800˚C.

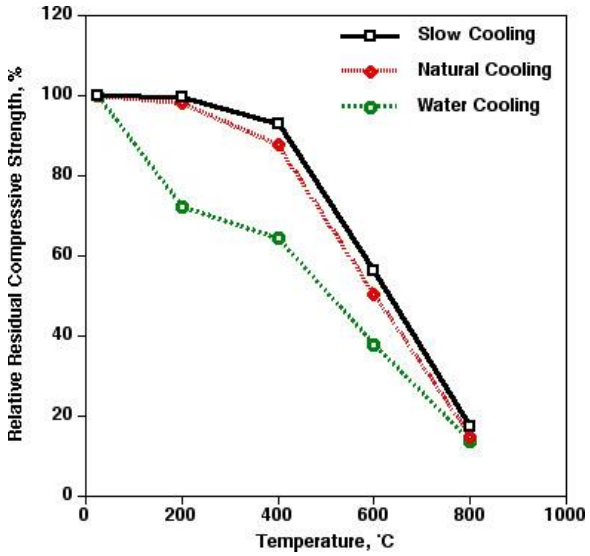

Figure 2.106 Effect of cooling regime on relative residual compressive strength following thermal exposure.

Source: J. Lee, Y. Xi, and K. Willam, "Concrete Under High Temperature Heating and Cooling," Report SESM No.09/2006, Department of Civil, Environmental, and Architectural Engineering, University of Colorado at Boulder, 2006.

The effect of different cooling regimes ranging from natural cooling to water spraying to water quenching on the relative residual concrete compressive strength has been investigated [2.117]. The limestone aggregate concrete utilized in the study contained silica fume, 10.7% (by weight) of the cementitious material, and had a reference compressive strength of 83.5 MPa. The 100 x 100 x 100 mm^3 specimens were cured in water at 20˚C until an age of 58 days and then dried at 105˚C. After drying the specimens were exposed to temperatures either of 200˚, 400˚, 600˚, or 800˚C with the temperature maintained for one hour. After elevated temperature the specimens were exposed to one of several cooling regimes: natural cooling, five-minute spraying with water, 30-minute spraying with water, 60-minute spraying with water, or quenching in water. When the specimens returned to room temperature they were tested. The effect of the cooling regimes on the relative residual compressive strength is presented in Figure 2.107. The cooling regime results show the sensitivity of the relative residual compressive strength to water spraying and quenching, particularly in the lower temperature range. The effect of quenching on the relative residual compressive strength decreases somewhat at the higher temperatures, however, the relative residual compressive strength already had been severely reduced by exposure to these temperatures.

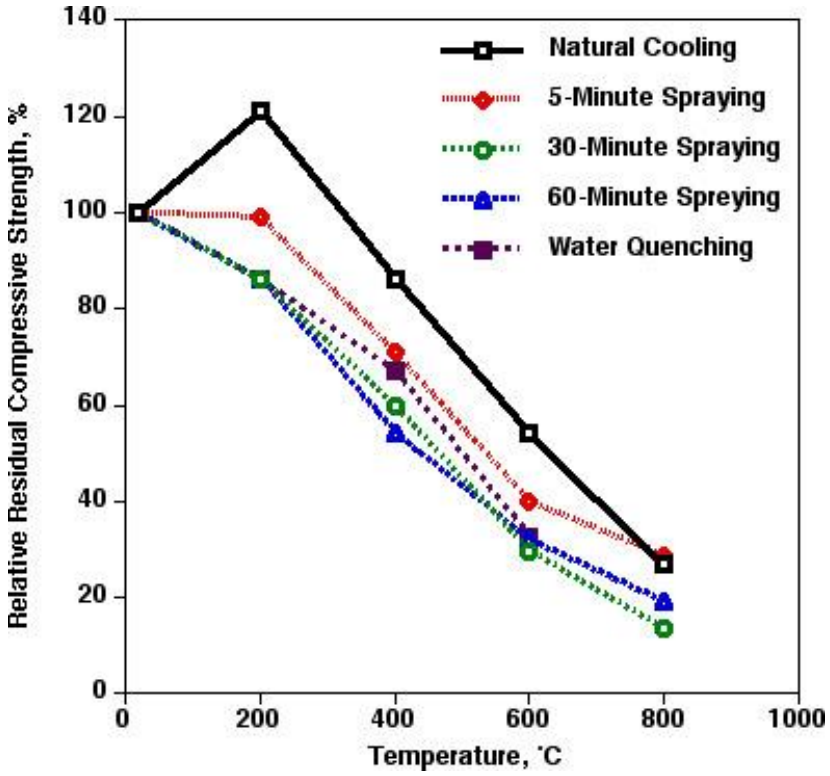

Figure 2.107 Effect of different cooling regimes on relative residual compressive strength following thermal exposure.

Source: G-F. Peng, S-H. Bian, Z-Q. Guo, J. Zhao, X-L. Peng, and Y-C. Jiang, "Effect of Thermal Shock Due to Rapid Cooling on Residual Mechanical Properties of Fiber Concrete Exposed to High Temperatures," *Construction and Building Materials* **22**, pp. 948-955, 2008.

Lightweight and Thermally Stable Aggregate Concretes

Relative compressive strength results (unsealed, hot testing) for lightweight/thermally stable aggregate concretes are presented in Figure 2.108. Relative compressive strength results for lightweight/thermally stable aggregate concretes fabricated using ordinary Portland cement as the binder and ordinary Portland cement plus supplementary cementitious materials as the binder are presented in Figures 2.109 and 2.110, respectively. The CEB design curve for lightweight concrete is superimposed on each of the figures. Residual compressive strength results (unsealed, cold testing) for lightweight/thermally stable aggregate concretes are presented in Figure 2.111. Residual compressive strength results for lightweight/thermally stable aggregate concretes fabricated using ordinary Portland

cement as the binder and ordinary Portland cement plus supplementary cementitious materials as the binder are presented in Figures 2.112 and 2.113, respectively. Specimens tested at temperature (relative strength) in general appear to retain a higher percentage of their compressive strength than that retained by specimens permitted to cool to room temperature prior to testing (residual strength). No definite conclusions could be drawn when comparing results for specimens fabricated using ordinary Portland cement as the binder and specimens fabricated using ordinary Portland cement plus supplementary cementitious materials as the binder.

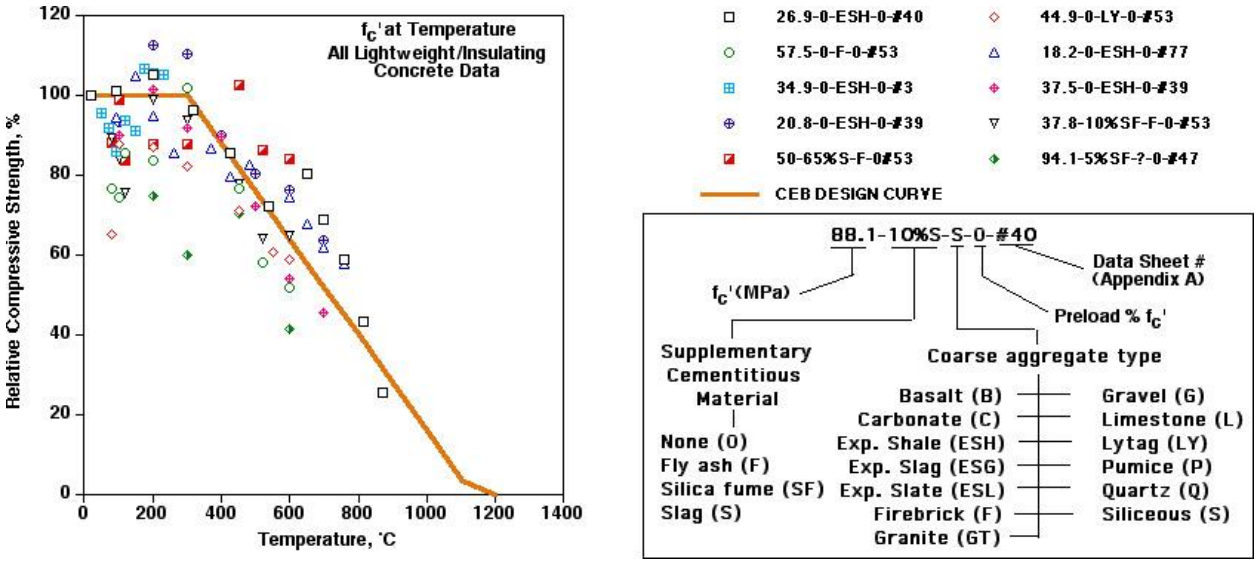

Figure 2.108 Compilation of data on relative compressive strength vs temperature for lightweight/insulating concrete specimens – ordinary Portland cement concretes and concretes containing supplementary cementitious materials.

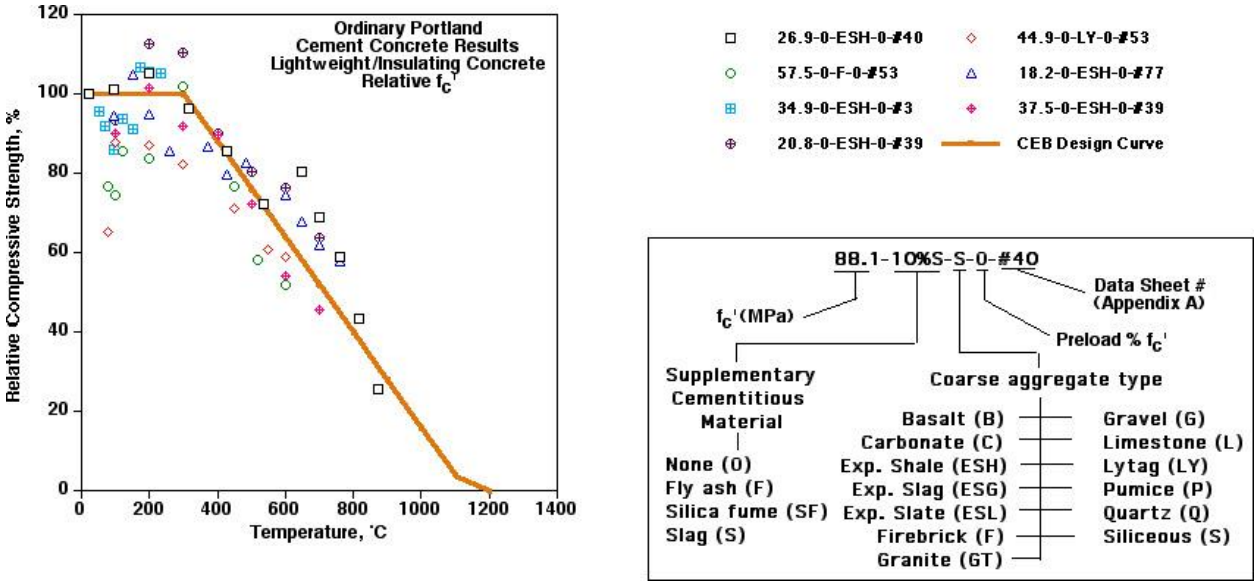

Figure 2.109 Compilation of data on relative compressive strength vs temperature for lightweight/insulating concrete specimens – ordinary Portland cement concretes.

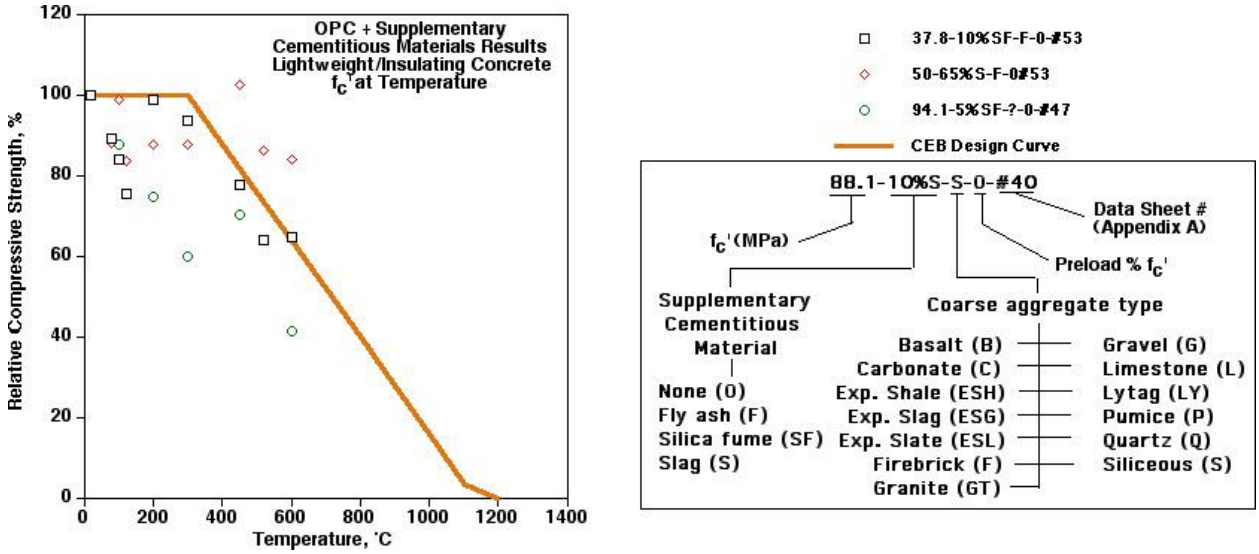

Figure 2.110 Compilation of data on relative compressive strength vs temperature for lightweight/insulating concrete specimens – concretes containing supplementary cementitious materials.

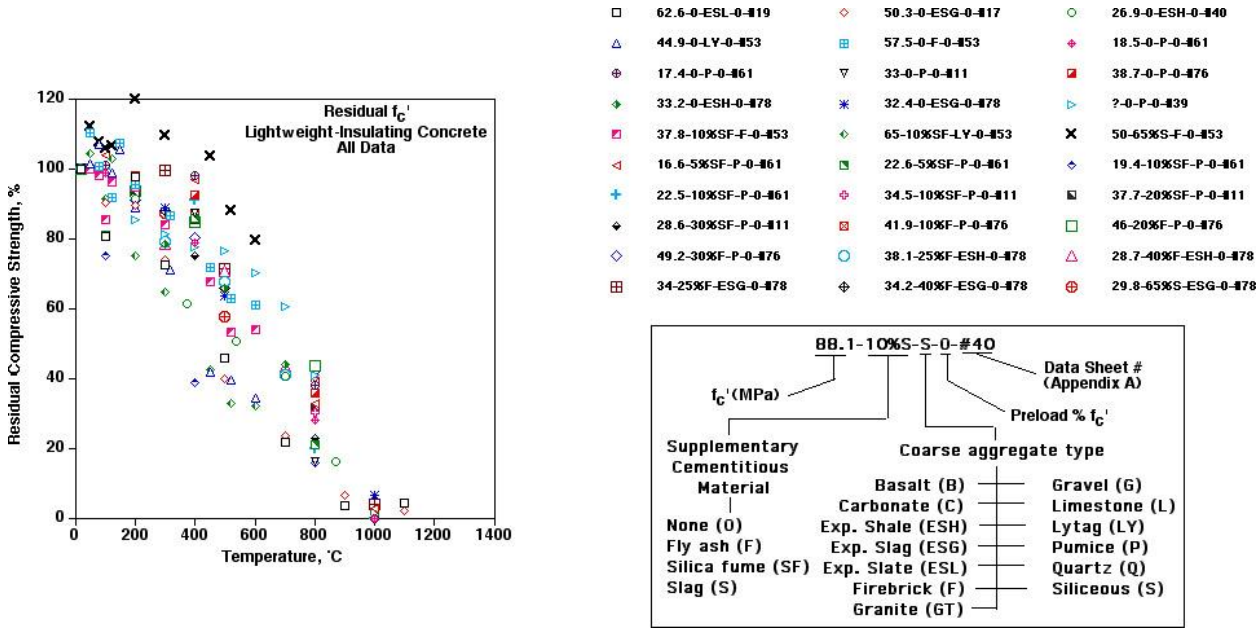

Figure 2.111 Compilation of data on residual compressive strength vs temperature for lightweight/insulating concrete specimens – ordinary Portland cement concretes and concretes containing supplementary cementitious materials.

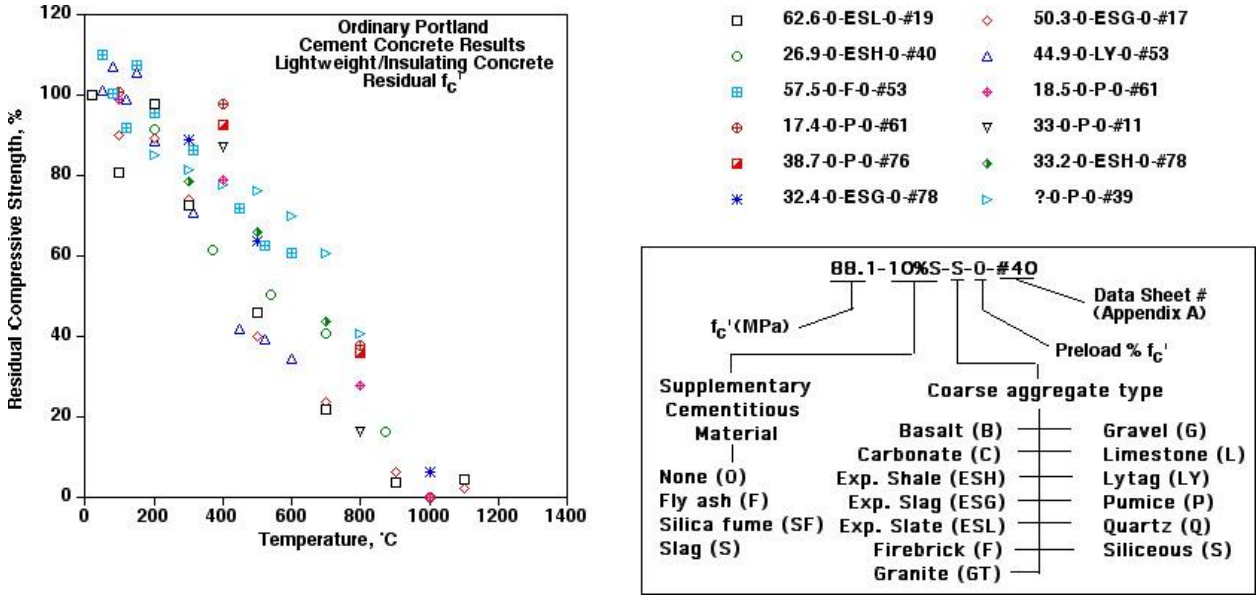

Figure 2.112 Compilation of data on residual compressive strength vs temperature for lightweight/insulating concrete specimens – ordinary Portland cement concretes.

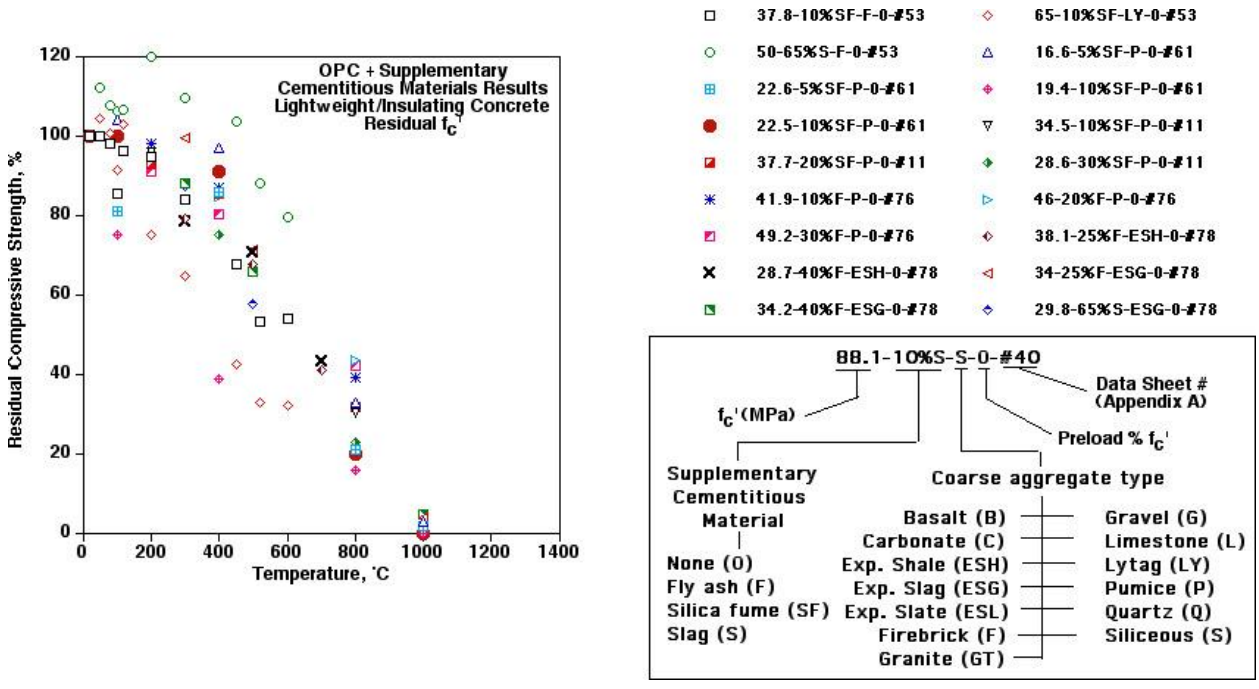

Figure 2.113 Compilation of data on residual compressive strength vs temperature for lightweight/insulating concrete specimens – concretes containing supplementary cementitious materials.

Fibrous Concretes

Relative compressive strength results (unsealed, hot testing) for fiber-reinforced concretes (fibrous concrete) are presented in Figure 2.114. Residual compressive strength results for fibrous concretes are presented in Figure 2.115. At temperatures above about 200˚C the retained compressive strength for the specimens tested at temperature and specimens permitted to cool to room temperature prior to testing both tended to decrease linearly as the temperature increased. Insufficient data are available, especially for relative compressive strength testing, to draw any conclusions when comparing relative and residual compressive strength results.

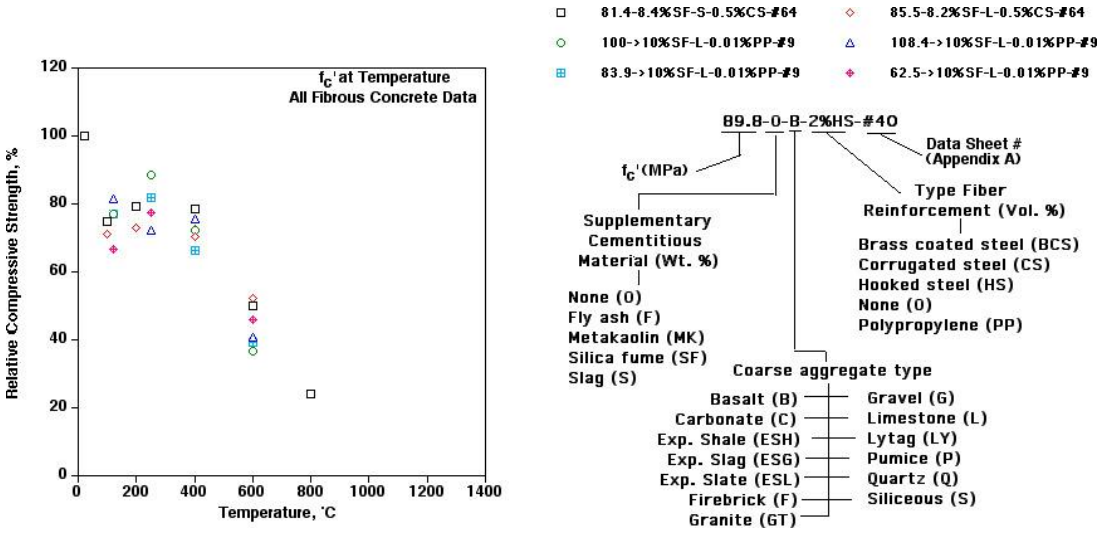

Figure 2.114 Compilation of data on relative compressive strength vs temperature – fibrous concrete.

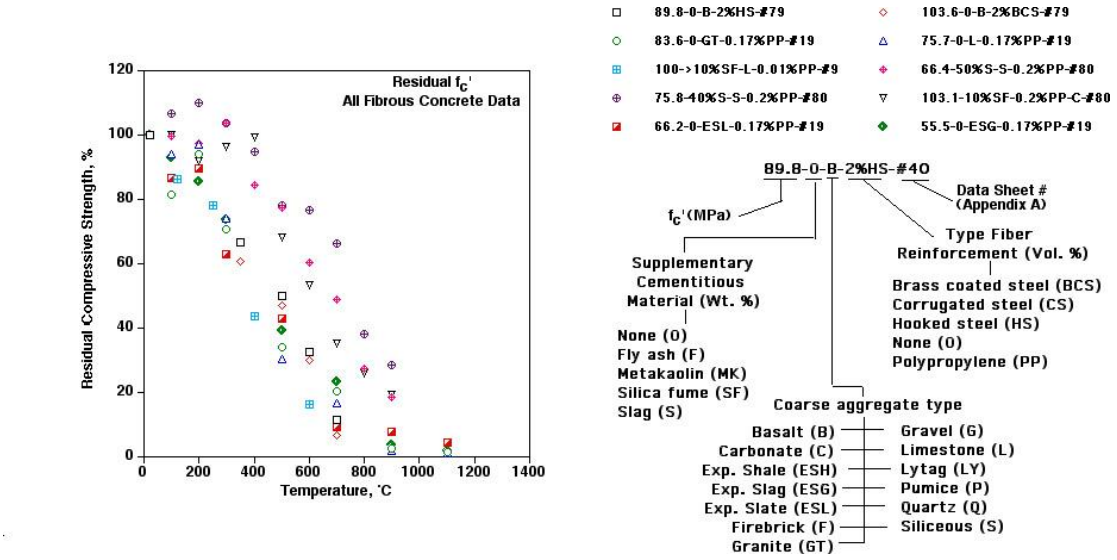

Figure 2.115 Compilation of data on residual compressive strength vs temperature – fibrous concrete.

Some information is available on the effect of different cooling regimes ranging from natural cooling to water spraying to water quenching on the relative residual concrete compressive strength of fibrous concretes [2.117].* The limestone aggregate concretes utilized in the study contained silica fume, 10.7% (by weight) of the cementitious material, and had a reference compressive strengths of 88.6, 83.4 MPa, and 87.2, respectively, for mixes containing

* Companion results for plain concrete subjected to the same cooling regimes were presented earlier in Figure 2.107.

0.1% polypropylene fibers, 0.3% polypropylene fibers, and a combination of 0.07% polypropylene and 1% steel fibers (by volume). The 100 x 100 x 100 mm^3 specimens were cured in water at 20˚C until an age of 58 days and then dried at 105˚C. After drying the specimens were exposed to temperatures of 200˚, 400˚, 600˚, or 800˚C with the temperature maintained for one hour. After elevated temperature exposure the specimens were subjected to one of several cooling regimes: natural cooling, five-minute spraying with water, 30-minute spraying with water, 60-minute spraying with water, or quenching in water. When the specimens returned to room temperature they were tested. The effect of the cooling regimes on the relative residual compressive strengths is presented in Figures 2.116 to 2.118 for the three fibrous concrete materials. Also shown in the figures are companion splitting-tensile strength results that were determined as part of the cooling regime study. Natural cooling retained the highest compressive and tensile strength values for each of the fibrous concretes with water quenching and 30 minute spraying producing the lowest strength retention. The hybrid concrete mix containing polypropylene and steel fibers exhibited improved retention of tensile strength relative to the polypropylene-reinforced concretes while still providing resistance to spalling. Notched beams tested as part of this study indicated that the hybrid fiber reinforced concrete also exhibited significant improvement in fracture energy at room temperature and after elevated temperature exposure compared to companion plain concrete beams.

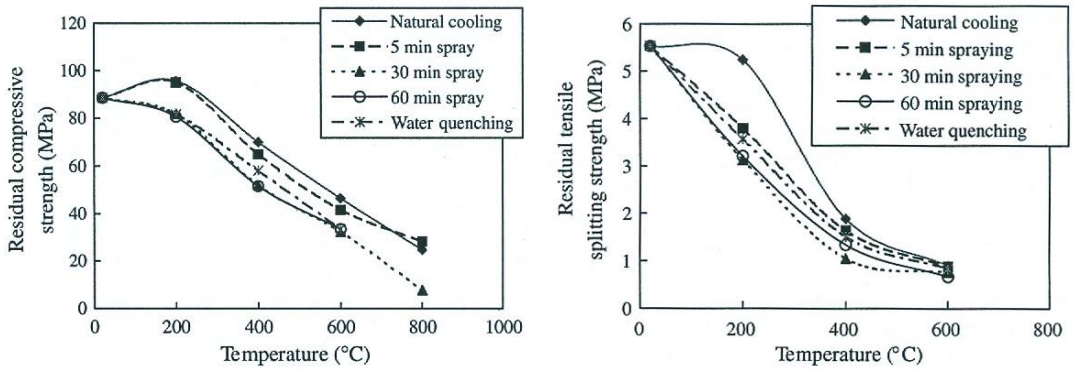

Figure 2.116 Effect of different cooling regimes on residual compressive and tensile strengths of 0.1 % polypropylene fiber reinforced concrete – 88.6 MPa compressive strength.

Source: G-F. Peng, S-H. Bian, Z-Q. Guo, J. Zhao, X-L. Peng, and Y-C. Jiang, "Effect of Thermal Shock Due to Rapid Cooling on Residual Mechanical Properties of Fiber Concrete Exposed to High Temperatures," *Construction and Building Materials* **22**, pp. 948-955, 2008.

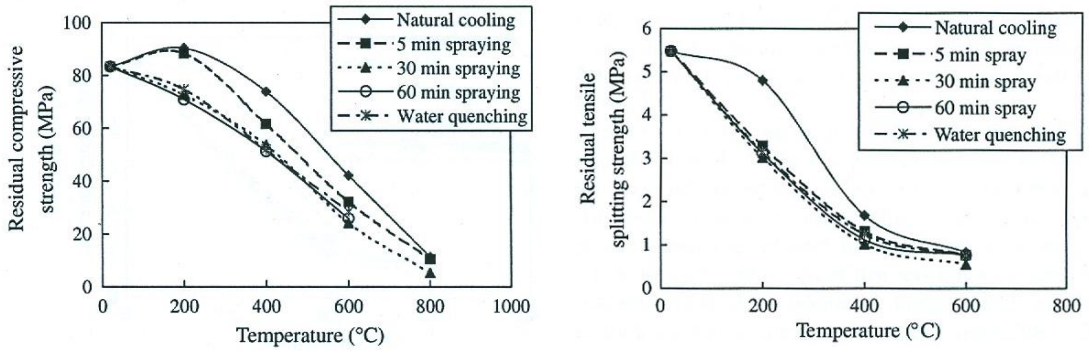

Figure 2.117 Effect of different cooling regimes on residual compressive and tensile strengths of 0.3% polypropylene fiber reinforced concrete – 83.4 MPa compressive strength.

Source: G-F. Peng, S-H. Bian, Z-Q. Guo, J. Zhao, X-L. Peng, and Y-C. Jiang, "Effect of Thermal Shock Due to Rapid Cooling on Residual Mechanical Properties of Fiber Concrete Exposed to High Temperatures," *Construction and Building Materials* **22**, pp. 948-955, 2008.

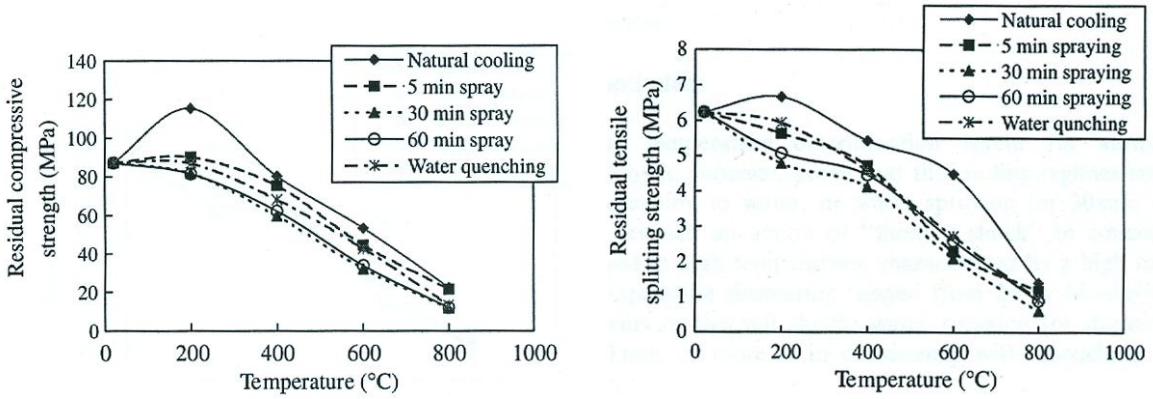

Figure 2.118 Effect of different cooling regimes on residual compressive and tensile strengths of 0.07% polypropylene plus 1% steel fiber reinforced concrete – 87.2 MPa compressive strength.

Source: G-F. Peng, S-H. Bian, Z-Q. Guo, J. Zhao, X-L. Peng, and Y-C. Jiang, "Effect of Thermal Shock Due to Rapid Cooling on Residual Mechanical Properties of Fiber Concrete Exposed to High Temperatures," *Construction and Building Materials* **22**, pp. 948-955, 2008.

Examples of Relations for Concrete Compressive Strength at Elevated Temperature. The following has been proposed for concrete cube compressive strength as a function of temperature [2.107]:

$$f_{cu}^{T} = f_{cu} / \left[1 + 2.4(T-20)^{6} x 10^{-17}\right] \tag{2.44}$$

where f_{cu}^{T} and f_{cu} are the concrete cube compressive strength at elevated temperature and room temperature, respectively.

A relationship has been developed for estimating the peak concrete compressive strength at temperature (f_{UT}) based on temperature (T) and peak compressive strength at room temperature (f_{U0}) of 25 MPa [2.72]:

$$f_{UT}(T) = f_{U0}\left[0.00165\left(\frac{T}{100}\right)^{3} - 0.03\left(\frac{T}{100}\right)^{2} + 0.025\left(\frac{T}{100}\right) + 1.002\right]. \tag{2.45}$$

A relationship has been developed for the normalized residual compressive strength of normal strength concretes ($f_C^{'} < 50$ MPa) following elevated temperature exposure [2.108]:

$$f_{CR}^{'}/f_{C}^{'} = 1.01 - 0.00055T \qquad \text{for } 20^{\circ} \leq T < 200^{\circ}C, \text{ and} \tag{2.46}$$

$$f_{CR}^{'}/f_{C}^{'} = 1.15 - 0.00125T \qquad \text{for } 200^{\circ} \leq T < 800^{\circ}C \tag{2.47}$$

where $f_{CR}^{'}$ is the residual compressive strength, T is the temperature, and $f_{C}^{'}$ is the reference room temperature strength.

The following has been proposed by the American Society of Civil Engineers in their fire protection manual [2.87]:

$$f_{CT}^{'} = f_{C}^{'} \qquad \text{for } 20^{\circ} \leq T \leq 450^{\circ}C, \tag{2.48}$$

$$f'_{CT} = f'_C\left[2.011 - 2.353\left(\frac{T-20}{1000}\right)\right] \qquad \text{for } 450^\circ \leq T \leq 874^\circ C, \text{ and} \qquad (2.49)$$

$$f'_{CT} = 0 \qquad \text{for } T > 874^\circ C \qquad (2.50)$$

where f'_{CT} is the residual compressive strength, T is the temperature, and f'_C is the reference room temperature strength.

The following has been proposed for high strength concrete ($f'_{C0} \geq 55$ MPa) residual compressive strength at elevated temperature [2.118]:

$$f'_c = f'_{C0}\left[1.0625 - 0.003125(T-20)\right] \qquad \text{for } T < 100^\circ C, \qquad (2.51)$$

$$f'_C = 0.75 f'_{C0} \qquad \text{for } 100^\circ \leq T < 400^\circ C, \text{ and} \qquad (2.52)$$

$$f'_C = f'_{C0}(1.33 - 0.00145T) \qquad \text{for } T \geq 400^\circ C \qquad (2.53)$$

where f'_{C0} is the compressive strength at room temperature, T is temperature of interest, and f'_C is the strength at temperature T in MPa.

Summary. From about 22˚ to 120˚C the concrete compressive strength decrease is attributable to thermal swelling of the physically-bound water that causes disjoint pressures. From 120˚C to about 300˚C there is a regain of compressive strength that is generally attributed to greater van der Waal's forces as a result of the cement gel layers moving closer to each other during heating. At temperatures above 300˚C compressive strength losses can become significant probably due to differences in thermal expansion coefficients between the aggregate and cement paste and decomposition of calcium hydroxide. At temperatures above 450˚C concrete compressive strength drops significantly due to loss of bond between the aggregate and cement paste. Residual concrete compressive strength (cold testing) is generally lower than relative concrete compressive strength (hot testing). Moisture content at time of testing has a significant effect on the strength of concrete at elevated temperature with strength of unsealed specimens being higher than strength of sealed specimens. Some regain in compressive strength can occur if specimens are stored in water following thermal exposure. Results in the literature indicate that the original concrete strength of normal strength concrete, type of cement, aggregate size, heating rate, and water-cement ratio have little effect on the relative strength vs temperature characteristics; exposure times at temperatures beyond 1 h had an effect on residual compressive strength, but this effect diminished as the level of exposure temperature increased, with the majority of strength loss occurring in the first 2 h. Age of concrete is important in so far as concretes with relatively incomplete hydration of cement may indicate a strength increase for temperature up to 400° C due to accelerated hydration; maximum test temperature influences the strength recovery in that after exposures to above about 600° C there is no strength recovery; aggregate-cement ratio has a significant effect on strength of concrete exposed to high temperature with the reduction being proportionally smaller for lean mixtures than for rich mixtures. Type of aggregate appears to be one of the main factors influencing concrete strength at high temperature with siliceous aggregate concrete having lower strength (by percentage) at high temperature than calcareous and lightweight concrete; and stressed specimens resulted in higher compressive strength retention at high temperature than unstressed specimens.

2.2.1.5 Thermal Cycling

Data and Information. Thermal cycling, even at relatively low temperatures (65°C), can have some deleterious effects on concrete's mechanical properties (i.e., cyclic heating generally gives lower strengths than a single heating) [2.119]. Figure 2.119 presents the affect of temperature cycling on a limestone aggregate concrete [2.120] and in

Figure 2.120 for a sealed limestone concrete [2.65]. Results indicate that the compressive, tensile, and bond strengths, and the modulus of elasticity are reduced, and the Poisson's ratio increased. As shown in Figure 2.120, the sealed limestone concrete exhibited a 50% loss of strength after 14 cycles at 150˚C. At higher temperatures (200˚ to 300˚C), the first thermal cycle causes the largest percentage of damage, with the extent of damage markedly dependent on aggregate type and is associated with loss of bond between aggregate and cement paste matrix [2.120].

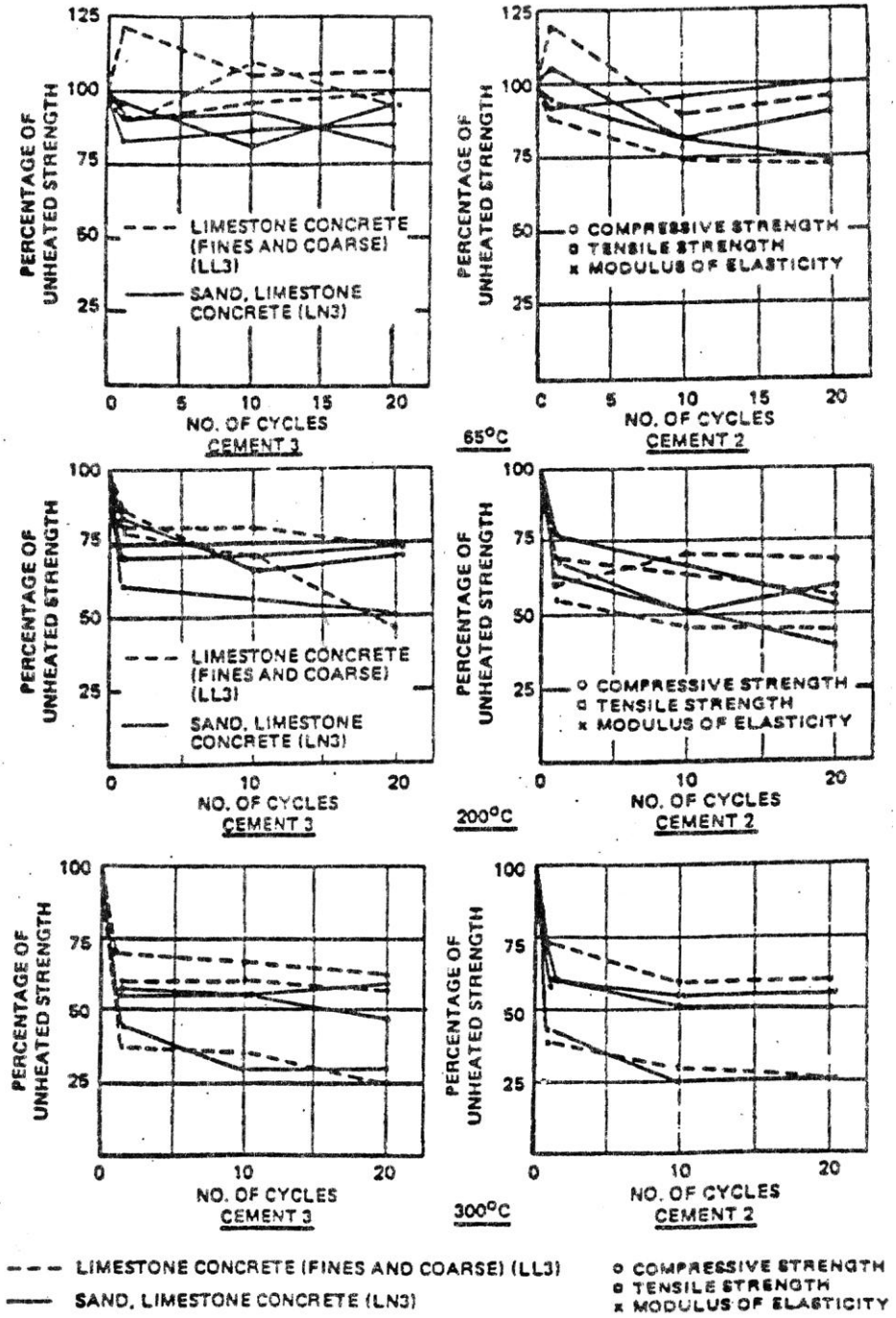

Figure 2.119 Effect of temperature cycles on limestone concretes.

Source: D. Campbell-Allen and P. M. Desai, "The Influence of Aggregate on the Behavior of Concrete at Elevated Temperature," *Nuclear Engineering and Design* **6**(1), pp. 65–77, August 1967.

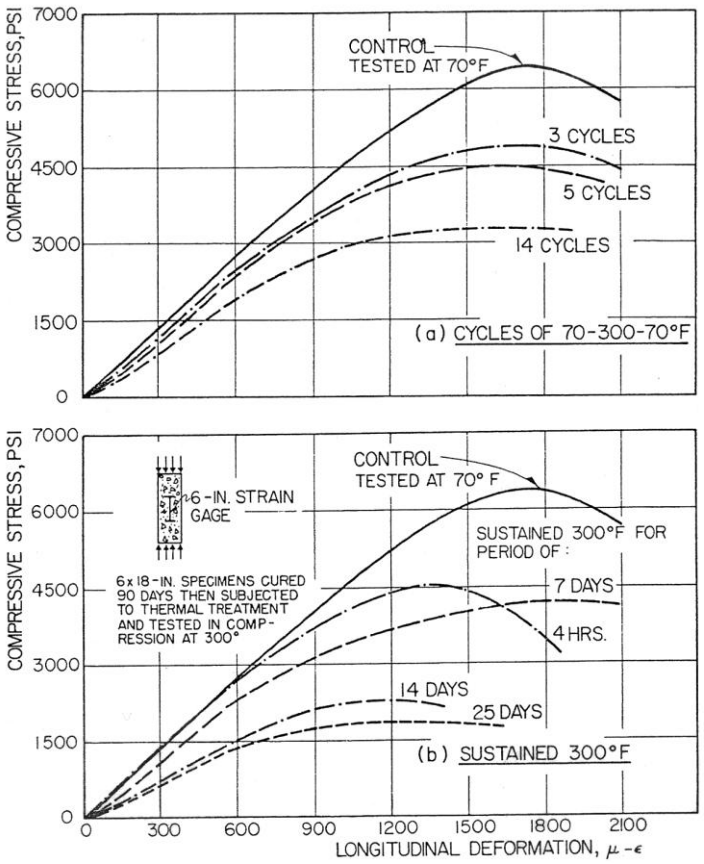

Figure 2.120 Influence of thermal cycling on σ-ε response of sealed concrete tested at 149°C.

Source: V. V. Bertero and M. Polivka, "Influence of Thermal Exposures on Mechanical Characteristics of Concrete," Paper SP 34-28 in *Concrete for Nuclear Reactors*, pp. 505-531, American Concrete Institute, Farmington Hills, Michigan, 1972.

2.2.1.6 Tensile Strength

Information and Data. The tensile strength of concrete is important because it determines the ability of concrete to resist cracking. At room temperature, concrete's tensile strength generally is from 7 to 11% its compressive strength. Direct measurement of concrete's tensile strength is seldom made because of difficulties in gripping the specimen to apply loads. An indication of concrete's tensile strength can be obtained by the splitting-tension and flexure tests. The splitting-tension test is an indirect test for tensile strength of concrete in that a horizontal concrete cylinder is loaded in compression through bearing strips placed along two axial lines that are diametrically opposite on the specimen [2.121]. Flexural strength of concrete is expressed in terms of modulus of rupture that is determined from beam specimens loaded in four-point bending until failure occurs. Because the modulus of rupture is calculated based on linear-elastic conditions, it is a fictitious value, but convenient for comparison purposes. For normal strength concretes tested at room temperature, the modulus of rupture is 60 to 100% higher than the direct tensile strength and 100 to 133% the splitting-tension strength [2.122]. Most tests to determine elevated-temperature effects on concrete tensile strength used splitting-tension tests with the residual tensile strength determined. As noted in Figure 2.121, the effect of elevated temperature on tensile strength shows a similar trend to its effect on compressive strength, but tensile testing of concrete is more sensitive to deterioration at elevated temperature [2.50].

The effect of elevated temperature on the splitting-tensile and direct tension strengths of 10-cm-diameter by 20-cm-long cylindrical test specimens fabricated from ordinary Portland and high alumina cements and different aggregate materials (i.e., sandstone, andesite, limestone, and pumice) was investigated [2.54]. Figure 2.122 presents the effect

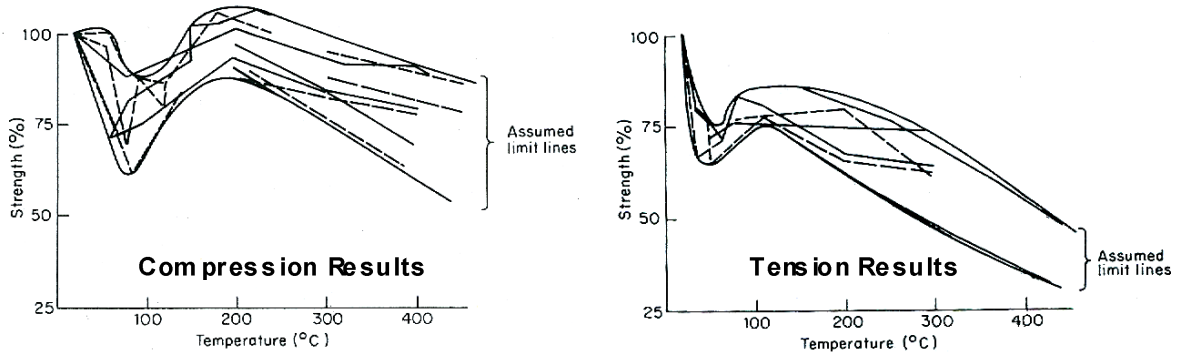

Figure 2.121 Comparison of effect of elevated temperature on compression and tensile strengths of concretes fabricated using different types of conventional aggregate materials.

Source: R. Blundell, C. Diamond, and R. Browne, "The Properties of Concrete Subjected to Elevated Temperatures," Report No. 9, Construction Industry Research and Information Association, Underwater Engineering Group, London, United Kingdom, June 1976.

of short term exposures (1 hour) to temperatures from 100˚ to 800˚C followed by gradual cooling to room temperature prior to testing on the reduction in strength and modulus of elasticity relative to room temperature reference values. All the concrete mixes using ordinary Portland cement exhibited similar compressive strength ratios (i.e., general linear reduction with temperature increase becoming approximately 60% at 400˚C) except for the pumice concrete that retained about 80% its reference strength at 400˚C. The tensile strength ratio of the silica aggregate concrete was close to that exhibited with respect to compressive strength ratio but the tensile strength ratio of the limestone aggregate concrete exhibited a fairly large reduction being about 30% at 400˚C. The modulus of elasticity ratio also decreased with increasing temperature with the rate of reduction increasing in order of andesite, silica, and limestone aggregate concretes. The pumice aggregate maintained a higher modulus ratio at elevated temperature than that for the other aggregate concretes, with the high alumina cement silica aggregate concrete performing the worst. Tensile strength results as a function of exposure period relative to 28-day values for specimens cured at room temperature and residual tensile strength results for specimens subjected to elevated temperature for exposure times from 3 to 12 months at temperatures of 40˚ (direct tension), 60˚ (direct tension), or 80˚C (splitting-tension) using specimens that were either sealed or unsealed during exposure are shown in Figure 2.123. The specimens were fabricated from ordinary Portland cement, river gravel, and had a water-cement ratio of 0.50. The tensile strength for unsealed specimens exhibited a steep drop after 3 months exposure, with the drop being more severe than that obtained for companion compression tests, however the change between 3 and 12 months was not great. Sealed specimens cured at 60˚C exhibited about a 10% loss in strength in direct tension, while sealed specimens cured at 80˚C exhibited an increase in splitting tensile strength of about 20% at 3 months, but decreased with increasing curing time at temperature.

Residual splitting-tensile-strengths were determined at temperatures of 300°C and 600°C for unsealed specimens [2.110]. The specimens were fabricated either from normal Portland cement (N), fly ash cement (F), moderate heat Portland cement (M), blast furnace slag cement (B), or high alumina cement (A). Aggregates investigated included a hard sandstone, basalt, limestone, blast furnace slag, and fire-resistant bricks. Water-cement ratios utilized were either 0.45, 0.55, or 0.65. The 150-mm-diameter by 150-mm-long cylindrical test specimens were cured for 91 days in water prior to heating. Residual results for splitting-tensile, as well as compressive strength, and modulus of elasticity, are summarized in Figure 2.124. The ratio of results after heating to reference room temperature results indicates that the residual ratios decreased with the increase of heating temperature (e.g., results range from approximately 20 to 90% at 300˚C and between approximately 20 and 30% at 600˚C). The high alumina cement mix had a notably lower residual strength ratio (~23%) than that for the other cementitious materials which exhibited a similar effect (~66 to 87%), however there was little difference in tensile strength ratio for all cementitious materials at 600°C. No significant variation in residual tensile strength ratio resulted for the different water-cement ratios.

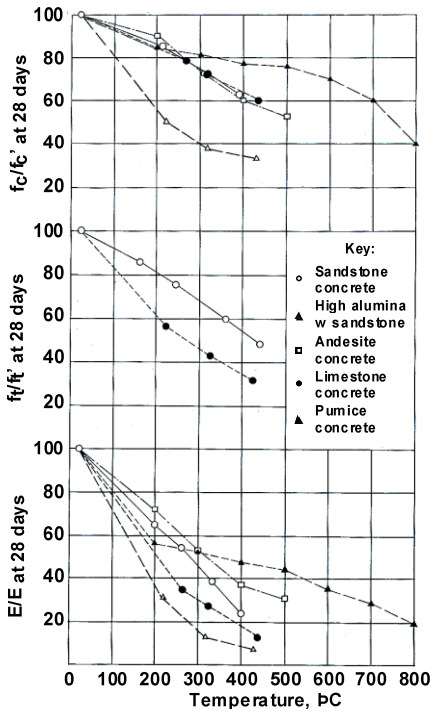

Figure 2.122 Effect of elevated temperature curing on residual compressive and tensile strengths and modulus.

Source: T. Harada, T. Takeda, S, Yamane, and F, Furumura, "Strength, Elasticity and Thermal Properties of Concrete Subjected to Elevated Temperatures," Paper SP-34-21in *Concrete for Nuclear Reactors*, pp. 377-406, American Concrete Institute, Farmington Hills, Michigan, 1972.

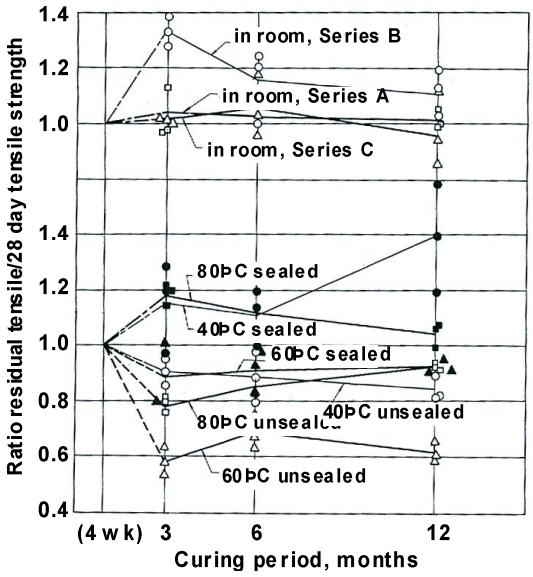

Figure 2.123 Effect of length of room temperature and elevated temperature curing on relative residual tensile strength results for sealed and unsealed specimens.

Source: T. Harada, T. Takeda, S, Yamane, and F, Furumura, "Strength, Elasticity and Thermal Properties of Concrete Subjected to Elevated Temperatures," Paper SP-34-21 in *Concrete for Nuclear Reactors*, pp. 377-406, American Concrete Institute, Farmington Hills, Michigan, 1972.

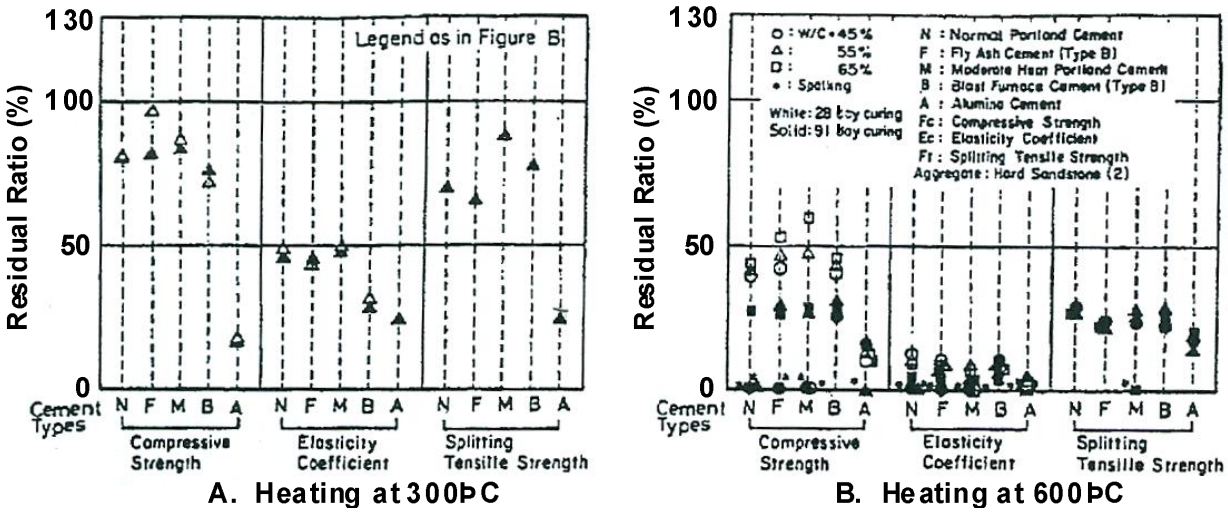

Figure 2.124 Relationship between residual ratios and heating temperatures, cement types, and water-cement ratios.

Source: K. Nagao and S. Nakane, "Influences of Various Factors on Physical Properties of Concretes Heated to High Temperatures," Paper H03/1 in *11th International Conference on Structural Mechanics in Reactor Technology*, pp. 61–66, August 1991.

An investigation was undertaken to determine the changes in mechanical properties of concrete after long-term exposure to sustained temperatures ranging from 75˚ to 600˚C for periods up to eight months [2.123]. Three types of concrete made with normal Portland cement (Type I), normal Portland cement with 35% replacement with blast furnace slag (Type II), and normal Portland cement with 25% replacement with fly ash (Type III) were investigated. Dolomitic limestone was used as the coarse aggregate material. Water-cement ratios ranged from 0.45 to 0.60 (by weight). After moist curing for 28 days the specimens (except for reference specimens) were stored under laboratory conditions at 50% relative humidity for periods from 16 and 30 weeks. After thermal exposure, the specimens were permitted to cool to room temperature prior to testing. Figure 2.125 presents residual splitting-tensile strength results relative to reference room temperature values after one-month exposure to elevated temperatures up to 600˚C. Series A and B, Series C and D, and Series E and F used cementitious materials Type I, Type II, and Type III, respectively. The first series in each group used a water-cement ratio of 0.45 (by weight) and the second series in each group used a water-cement ratio of 0.60 (by weight). After one-month's exposure at 75˚C, the splitting-tensile strength of the 102-mm-diameter by 203-mm-long cylindrical test specimens fabricated with normal cement and slag was relatively unaffected, however, the normal Portland cement concrete and the normal Portland cement plus fly ash concrete residual splitting-tensile strengths were reduced by about 10%. Test results at this temperature after four and eight month's exposure were similar. Concretes exposed to 150˚C for one month produced a decrease in residual splitting-tensile strength from 10% for normal Portland cement concrete with slag to a maximum of about 20% for the Portland cement concrete. After four month's exposure at this temperature virtually all specimens had disintegrated. This behavior was attributed to instability of the limestone aggregate due to the presence of iron sulfide.

Tests were conducted to evaluate the effect of elevated temperature on the residual direct-tensile and splitting-tensile strengths of normal-strength (38.1-MPa) and high-strength (61.1-MPa) calcareous aggregate concretes [2.124]. Direct-tension tests utilized prisms 100 x 100 x 400 mm^3 and splitting-tensile tests were conducted on 160-mm-diameter by 320-mm-long cylindrical test specimens. The specimens were cured at 22˚C and 95% relative humidity until testing at an age of 2 months. The specimens were slowly heated to target test temperatures of 150˚, 300˚, 450˚, or 600˚ C and maintained at the target temperature for one hour prior to permitting to slowly cool to room temperature. Experimental results, shown in Figure 2.126, indicate that the residual tensile strengths for both normal-strength and high-strength concretes decreased similarly and almost linearly with increasing temperature. Tensile strength of the high-strength concrete remained approximately 10-15% higher than that of the normal-strength concrete over the entire temperature range. Also, tensile strengths measured by the splitting-tension test were consistently higher than those obtained by the direct-tension test.

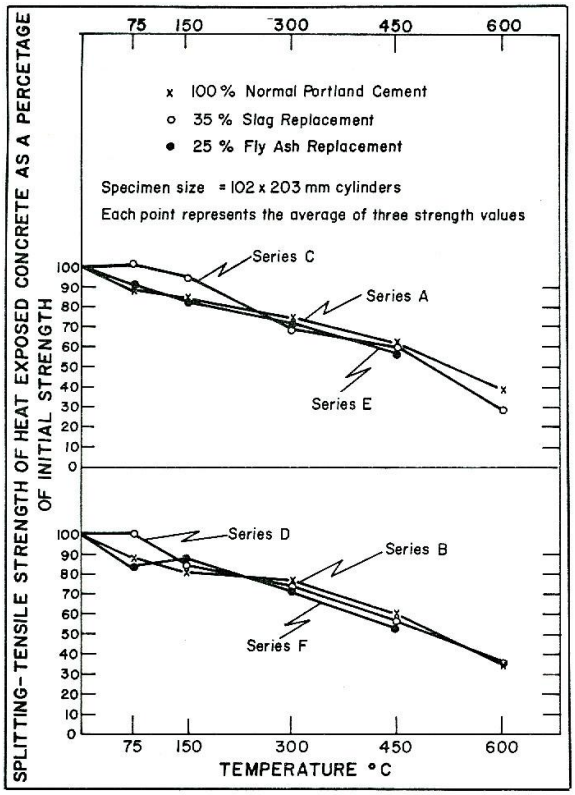

Figure 2.125 Residual splitting-tensile strength of concrete after one month's exposure at various temperatures.

Source: G. G. Carette, K.E. Painter, and V.M. Malhotra, "Sustained High Temperature Effects on Concretes Made with Normal Portland Cement, Normal Portland Cement and Slag, or Normal Portland Cement and Fly Ash," *Concrete International* **4**(7), pp. 41–51, July 1982.

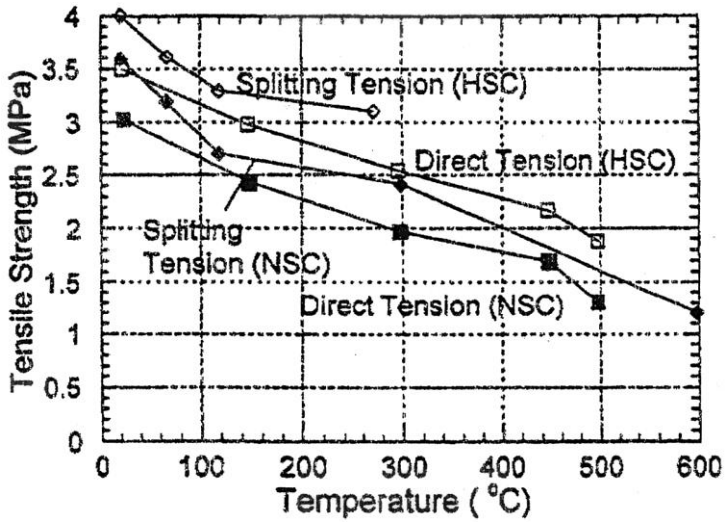

Figure 2.126 Residual tensile strengths of HSC and NSC.

Source: A. N. Noumowe, P. Clastres, G. Debicki, and J-L. Costaz, "Thermal Stresses and Water Vapor Pressure of High Performance Concrete at High Temperature," *Proc. 4th International Symposium on Utilization of High-Strength/High-Performance Concrete*, Paris, 1996.

An experimental study has been conducted to investigate the deterioration of concretes used in the construction of prestressed concrete pressure vessels in the United Kingdom [2.109]. The overall study focused on the dependence of the residual properties of thermally-aged concretes involving representative mix designs, temperature exposure levels from 20˚ to 450˚C, test ages from 3 months to 1 year, and exposure condition (sealed or unsealed). Three prestressed concrete pressure vessel concretes were investigated. Ordinary Portland cement or a combination of ordinary Portland cement and fly ash were used as the cementitious materials. Coarse aggregates included basalt, flint gravel, and dolomitic limestone having a maximum aggregate size up to 20 mm. Water-cement ratios utilized were either 0.43, 0.56, or 0.58. Sealed specimens subjected to temperatures below 100˚C were placed directly in water in a heat-controlled tank and sealed specimens tested at temperature above 100˚C were heated in an autoclave. Residual splitting-tensile strength results for sealed and unsealed specimens cast from a flint gravel aggregate concrete (i.e., w/c = 0.43 and ordinary Portland cement) after curing ages of 3 months and 1 year are presented in Figure 2.127. Results for specimens tested after 1 year curing generally exhibited higher residual splitting-tensile strength than those that were cured for 3 months either in the sealed or unsealed condition. Unlike the residual compressive strength results obtained in the investigation, the tensile strength of sealed concrete specimens that had experienced temperature exposure was higher than that for unsealed specimens (except at 150°C). Comparing compression and tensile results, the splitting-tensile strength appears to be less sensitive to the effect of moisture content (i.e., unsealed specimens did not exhibit a trend of decreasing residual strength with increasing temperature) and were more sensitive to the damage (i.e., microcracking) inside the concrete caused by temperature exposure. Relating the splitting-tensile strength values obtained after thermal treatment to the reference room-temperature values, all three mixes exhibited a trend for the value to decrease with increasing exposure temperature with the decrease being more marked than that exhibited by the compressive strength. In the sealed condition the decrease was greater for the mix using ordinary Portland cement with flint coarse aggregate than for the mixes using a combination of ordinary Portland cement and fly ash with either basalt or dolomitic limestone coarse aggregate.

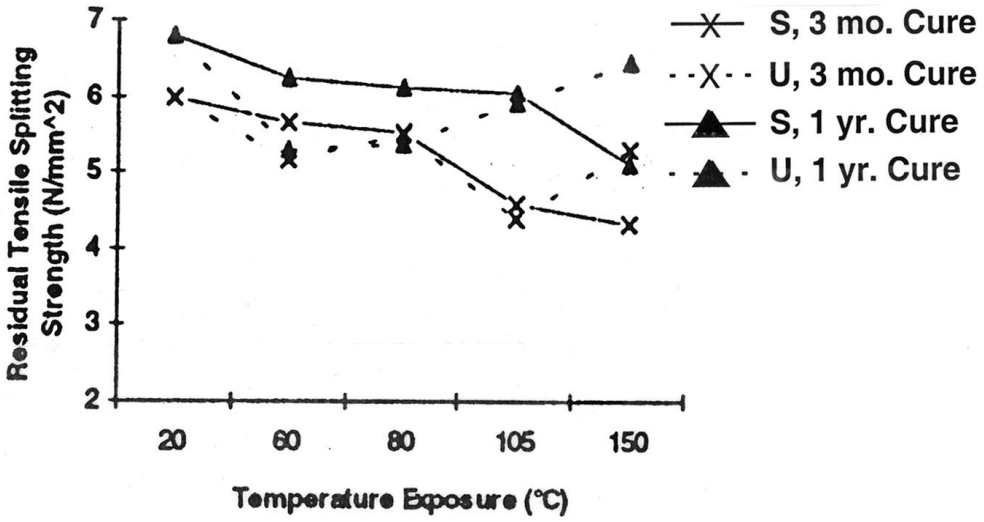

Figure 2.127 Effect of curing age and exposure condition on residual splitting-tensile strength of a flint-gravel aggregate concrete (Solid line = sealed, dashed line = unsealed).

Source: J. Guo and P. Waldron, "Deterioration of PCPV Concrete," *Nuclear Engineering and Design* **198**, pp. 211–226, 2000.

Properties of concrete subjected to high temperature were determined for use in design of the reactor buildings at "Monju" [2.97]. Cylindrical test specimens 10-cm-diameter by 20-cm-long were cast from a hard sandstone aggregate concrete mix that used Type B (fly ash) cementitious material and had a water-cementitious materials ratio of 0.55 (by weight). Preheating conditions investigated included in water (unsealed), in water (sealed), in air (unsealed), and in air (sealed). The heating period started at a concrete age of 91 days and lasted from 1 to 91 days. Specimens were heat treated at 175˚C. Splitting-tensile strength results for the various conditions are summarized in Figure 2.128. Splitting-tensile results indicate that sealed specimens performed better than unsealed specimens. Unsealed specimens exhibited about a 20% reduction, on average, during heating.

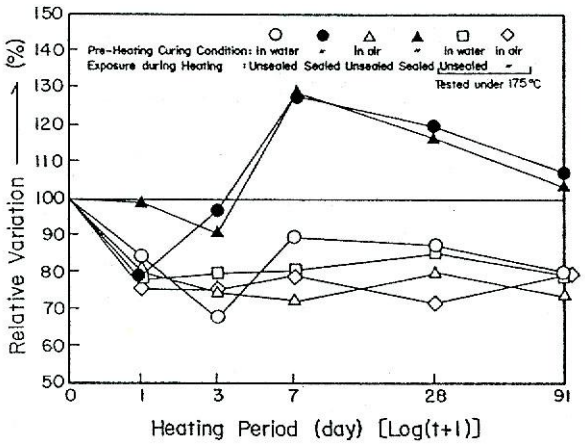

Figure 2.128 Relative variations in splitting-tensile strength.

Source: K. Hirano, K. Ohmatsuzawa, T. Takeda, S. Nakane, T. Kawaguchi, and K. Nagao, "Physical Properties of Concrete Subjected to High Temperature for MONJU," Paper P2-25, Power Reactor and Nuclear Fuel Development Corporation, Tokyo, Japan.

The effect of moisture loss at high temperature on the brittleness of concrete was investigated by conducting three-point bending tests of preheated notched beams 500 x 100 x 100 mm^3 having an effective span of 400 mm and a notch depth of 50 mm [2.89]. The beams were fabricated from a Type III Portland cement, water-cement ratio of 0.54, siliceous river sand, and 20-mm maximum size siliceous gravel aggregate. At an age of 14 days the beams were heated for different exposure periods up to 168 hours and then permitted to cool naturally in air for a period of 12 hours prior to testing. After testing, splitting-tensile and compressive strength100-mm cubes were cut from the broken ends of the beam specimens and tested. A comparison of the effect of elevated-temperature exposure on residual compressive, tensile (splitting-tension), and bend strengths (notched beams) for the siliceous gravel concrete exposed to temperatures up to 600°C is presented in Figure 2.129. Results in the figure indicate that the residual tensile strength, either splitting-tensile or notched beam, is affected more significantly as the temperature increases than the compressive strength.

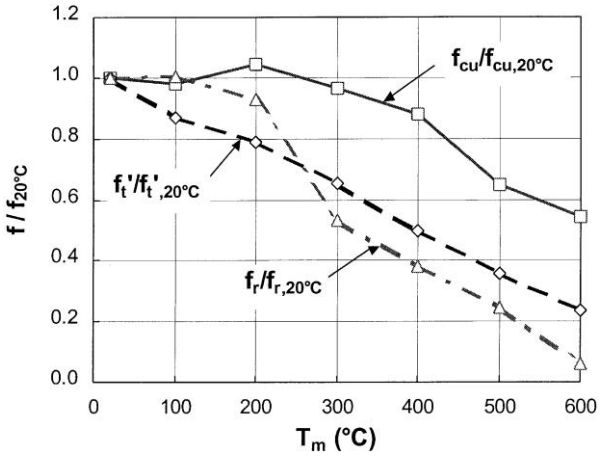

Figure 2.129 Comparison of the effect of elevated-temperature exposure on residual compressive (f_{cu}), tensile (splitting-tension) (f_t), and bend strengths (notched beams) (f_r) of siliceous aggregate concrete.

Source: B. Zhang, N. Bicanic, D.J. Pearce, and D.V. Phillips, "Relationship Between Brittleness and Moisture Loss of Concrete Exposed to High Temperatures," *Cement and Concrete Research* **32**, pp. 363–371, 2002.

The effect of elevated temperature on the splitting-tensile and bending strength of normal- and high-strength concretes has been investigated [2.125]. Specimens were cast from a 20-mm maximum size crushed basalt aggregate concrete mix that incorporated Type II cement and fly ash. Water-cement ratio and proportions of cement and fly ash were varied to produce three concretes (C40, C60,and C70 having 28-day compressive strengths of 42.5, 68.0, and 76.0 MPa, respectively). Splitting-tensile strength specimens were 100-mm cubes and bending strength specimens were 100 x 100 x 415 mm^3. Specimens were cured for 28 days at 20˚C and 90% relative humidity and then heated to temperatures of 200˚, 400˚, 600˚, 800˚, or 1000˚C. After the temperature inside the furnace reached the target temperature on the specimen surface, the specimens were permitted to cool to room temperature prior to testing. Figure 2.130 presents residual splitting-tensile and bending strength results after temperature exposure. The splitting-tensile strength results are presented only for the C70 concrete while the bending results are for all three concrete mixes. Both the splitting-tensile and bending strengths decreased as the exposure temperature increased. The bending strength results for the two higher strength concretes dropped more sharply than that for the normal-strength concrete (C40).

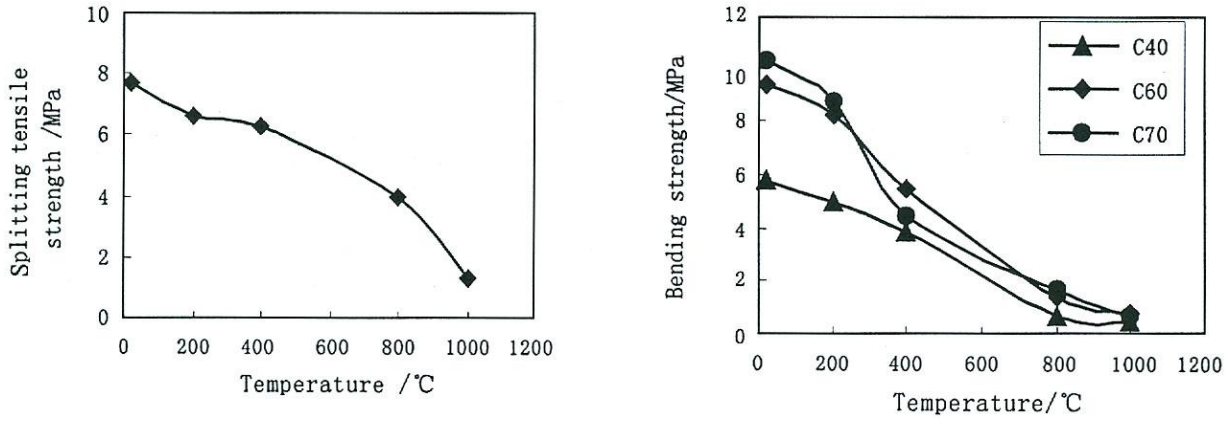

Figure 2.130 Residual splitting-tensile and bending strengths after thermal exposure.

Source: M. Li, C.X. Qin, and W. Sun, "Mechanical Properties of High-Strength Concrete After Fire," *Cement and Concrete Research* **34**, pp. 1001-1005. 2004.

Research related to prestressed concrete pressure vessels has been conducted to investigate the effect of moisture on the properties of Portland cement concrete [2.119]. Two concretes were used in the study, a gravel aggregate concrete and a limestone aggregate concrete. Type II Portland cement was used in the mixes with water-cement ratios of 0.40 and 0.42 for the limestone aggregate and gravel aggregate concretes, respectively. Nominal 28-day compressive strength of the two concretes was 41.4 MPa. Flexural strength specimens were 76.2 x 63.5 x 254 mm^3. Prior to elevated temperature testing the specimens were cured in a fog room for 28 to 200 days. The specimens were subjected to temperatures up to 260˚C for periods ranging from 75 to 109 days both at atmospheric pressure and in an environment in which free moisture was contained in the specimen by a equilibrium saturated steam pressure. Flexural strength results for unsealed specimens as a percentage of reference room temperature value are presented in Figure 2.131 for both sealed and unsealed specimens. For the unsealed specimens both the gravel aggregate and limestone aggregate concretes heated at 79.4˚C and tested at temperature or after cooling to room temperature exhibited slight increases in flexural strength relative to unheated specimens. All specimens tested at 121.1˚ and 260˚C exhibited a loss of flexural strength relative to the unheated specimens. The greatest loss of flexural strength occurred in specimens quenched from 260˚C prior to testing and in specimens cooled slowly from 260˚C and then resaturated with water prior to testing. For the sealed concrete specimens flexural results are presented in Figure 2.132 after autoclaving and cooling to room temperature prior to testing. In general the gravel aggregate concrete exhibited a lesser degree of flexural strength loss that that exhibited by the limestone aggregate concrete, especially at the higher autoclave temperatures.

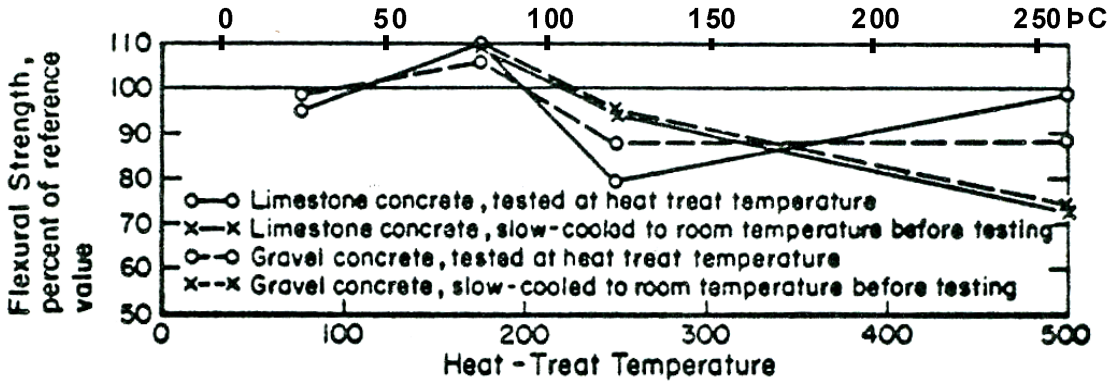

Figure 2.131 Effect of test conditions on flexural strength of gravel and limestone concretes, unsealed.

Source: D. T. Lankard, D.L. Birkimer, F.F. Fondriest, and M.J. Snyder, "Effects of Moisture Content on the Structural Properties of Portland Cement Concrete Exposed to Temperatures Up to 500°F," SP-25 *Temperature and Concrete*, pp. 59–102, American Concrete Institute, Farmington Hills, Michigan, 1971.

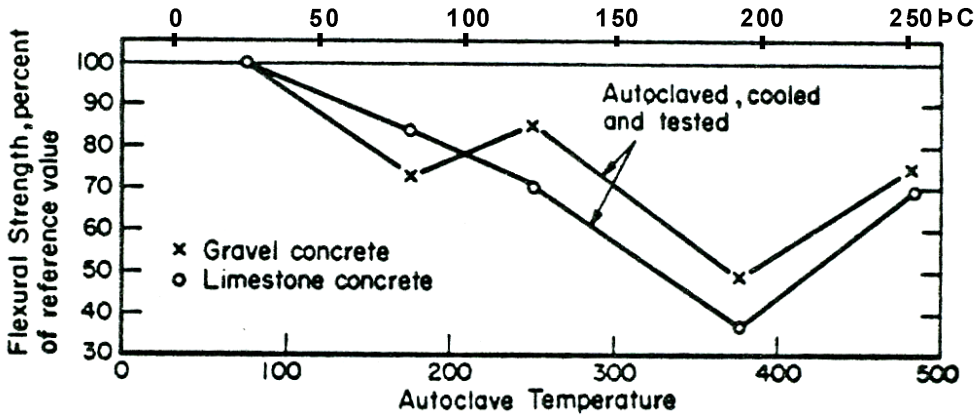

Figure 2.132 Flexural strength of autoclaved gravel and limestone concretes.

Source: D. T. Lankard, D.L. Birkimer, F.F. Fondriest, and M.J. Snyder, "Effects of Moisture Content on the Structural Properties of Portland Cement Concrete Exposed to Temperatures Up to 500°F," SP-25 *Temperature and Concrete*, pp. 59–102, American Concrete Institute, Farmington Hills, Michigan, 1971.

The effect of elevated temperature on the flexural strength of ordinary Portland cement concretes and Portland cement concretes containing fly ash has been investigated [2.126]. Three reference primary mixes (Mix I, Mix II, and Mix III) were prepared in which the cement contents (330.9 to 404.4 kg/m^3) and water-cement ratios (0.55 to 0.45, by weight) were varied to produce concretes having 28-day compressive strengths from 28 to 35 MPa. In addition to each reference mix, three additional mixes were prepared for each of the reference mixes in which fly ash was utilized to replace 10, 20, or 30% (by weight) of the cement content, thus producing a total of 12 concrete mixes. The mixes utilized 20-mm maximum size gravel coarse aggregate. Flexural specimens 100 x 100 x 500 mm^3 were fabricated and subjected to elevated-temperature exposures of 100˚, 200˚, or 250°C for 1-, 2-, or 3-h durations. Figure 2.133 a-c presents the variation of maximum flexural strength with temperature for Mix I, Mix II, and Mix III control specimens and the three mixes with different partial placements of cement with fly ash exposed to elevated temperature for 60 min. Figure 2.133 d-f presents the effect on flexural strength of three different exposure periods for the Mix II test series. Conclusions of this study were that the fly ash consistently showed the same pattern of flexural behavior (i.e., trend) with temperature as that exhibited by concrete without fly ash for thermal exposures up to 250°C; fly ash concrete with fly ash content up to 20% exhibited improved performance relative to concrete without fly ash retaining more of its strength; the exposure time had an effect on the residual flexural strength of concrete, but the majority of strength loss occurred within the first hour of exposure.

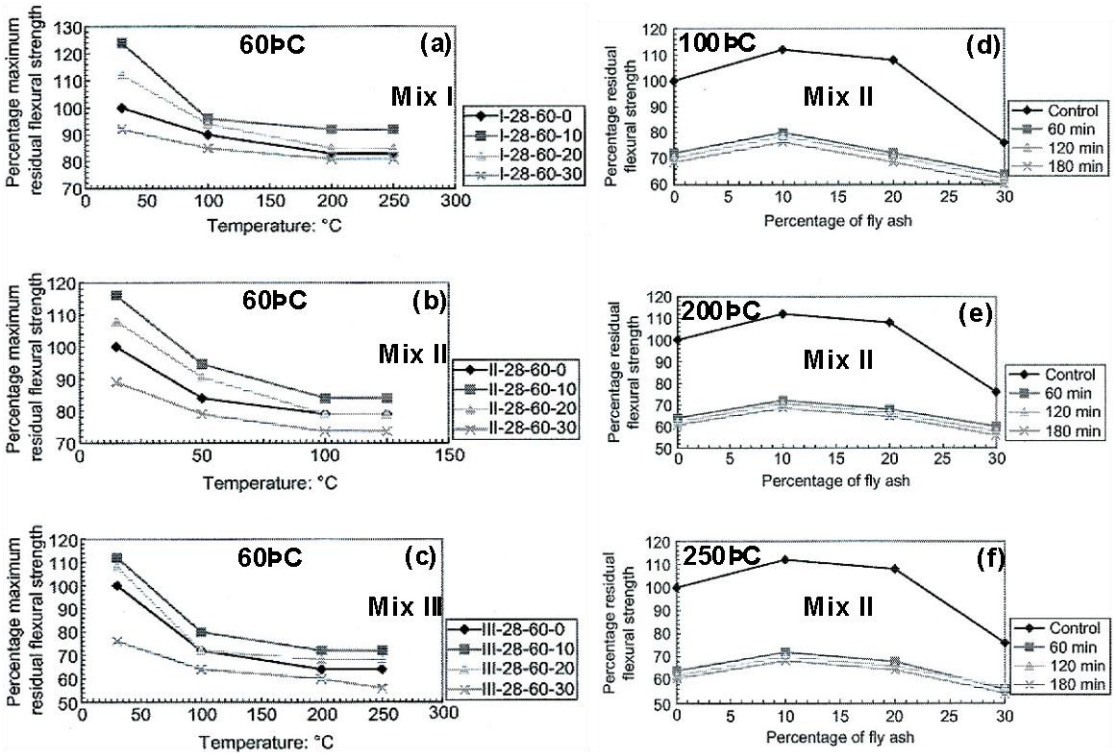

Figure 2.133 Variation of flexural strength with temperature and exposure period for concrete mixes with and without fly ash.

Source: M. P. Raju, M. Shobha, and K. Rambabu, "Flexural Strength of Fly Ash Concrete Under Elevated Temperatures," *Magazine of Concrete Research* **56**(2), pp. 83–88, March 2004.

The effect of elevated temperature followed by water quenching on the properties of high-strength concrete containing supplementary cementitious materials such as used in construction of high-rise buildings was studied [2.105]. Four binder materials were investigated: Mix 1 - 100% general purpose cement, Mix 2 - 62% slag plus 38% cement, Mix 3 - 20% fly ash plus 80% cement, and Mix 4 - 6.6% silica fume plus 93.4% cement. Crushed basalt aggregate having a maximum aggregate size of 10 mm and a water-cement ratio of 0.30 (by weight) was used for all the mixes. Table 2.4 presents reference 28-day properties of the mixes. Specimens used for compression and tensile tests were 100-mm-diameter by 200-mm-long cylinders. The dynamic modulus of elasticity specimens were 75 x 75 x 305 mm^3 prisms. All specimens were cured by storing in water at 20˚C for 28 days and then placing into the laboratory environment of 20˚C and 65% relative humidity for 2 days. The specimens then were heated to temperatures of 200˚, 400˚, 600˚, 800˚, or 1000˚C with a total duration in the furnace of 7 hours (i.e., soak period

Table 2.4 Concrete mix properties at the age of 28 days

Mix	Binder Materials	Cylinder strength, MPa	Tensile strength, MPa	Flexural strength, MPa	Dynamic modulus, GPa
1	100% OPC	61.8	6.58	9.34	46.5
2	62% slag + 38% OPC	40.3	4.28	5.47	39.9
3	20% fly ash + 80% OPC	67.2	5.08	6.94	45.7
4	6.6% silica fume+ 93.4% OPC	76.4	6.93	8.51	55.2

Source: R.S. Ravindrarajah, R. Lopez, and H. Reslan, "Effect of Elevated Temperature on Properties of High-Strength Concrete Containing Cement Supplementary Materials," *9th International Conference on Durability of Building Materials and Components*, 9 p., Brisbane, Australia, 17-20 March 2002.

from 6 to 2 hours depending on maximum temperature). Figure 2.134 presents the normalized residual compressive, splitting-tensile, and flexural strength results for specimens subjected to elevated temperature and quenched in water prior to testing. The strengths of all concretes dropped significantly as the maximum exposure temperature increased. At an exposure temperature of 1000˚C all concretes experienced a significant drop in strength independent of binder type used.

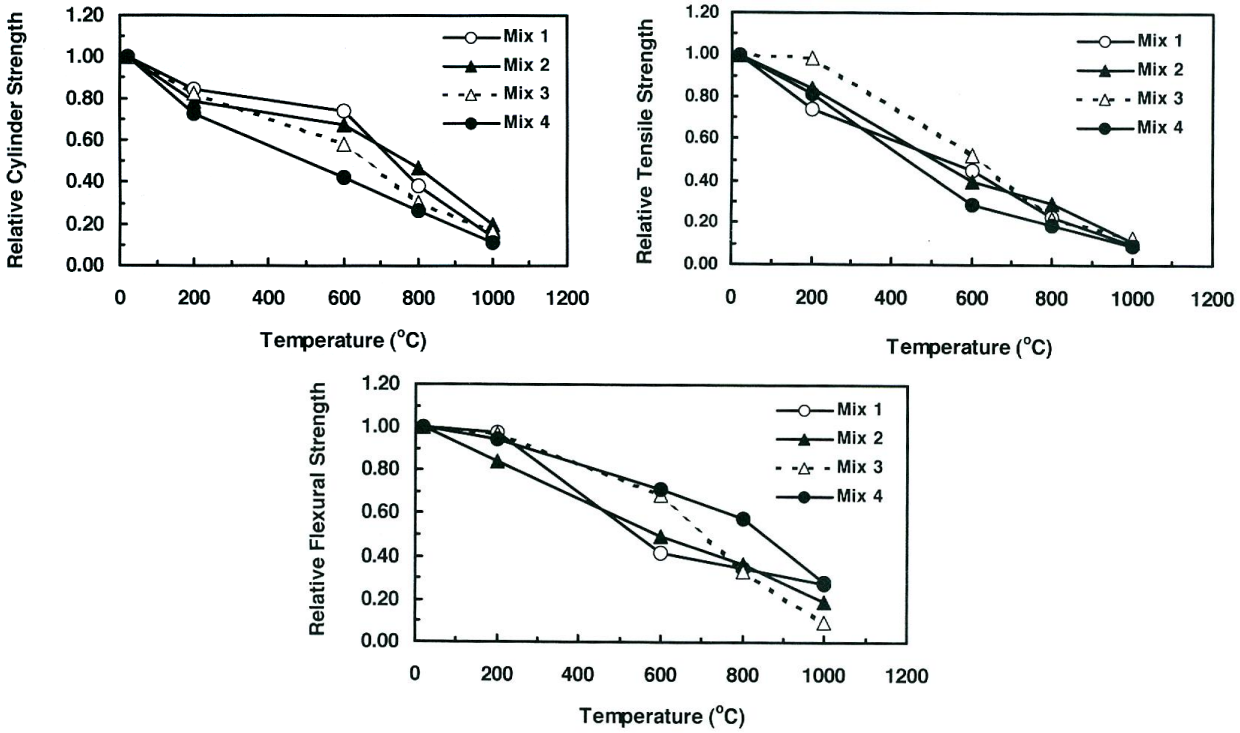

Figure 2.134 Normalized residual property results for specimens subjected to elevated temperature and quenched in water prior to testing.

Source: R.S. Ravindrarajah, R. Lopez, and H. Reslan, "Effect of Elevated Temperature on Properties of High-Strength Concrete Containing Cement Supplementary Materials," *9th International Conference on Durability of Building Materials and Components*, 9 p., Brisbane, Australia, 17-20 March 2002.

The effect of elevated temperature on the flexural and splitting-tensile strengths of high-strength concrete was investigated [2.127]. Four concrete mixes were used in the investigation: ordinary Portland cement having a 28-day compressive strength of 54 MPa, and three concrete mixes containing silica fume with different water-cement ratios that produced concretes having compressive strengths from 91 to 133 MPa. Granite coarse aggregate material having a 10-mm maximum size was used in the mixes to fabricate 100 x 100 x 400 mm^3 beam flexural specimens and 100-mm-diameter by 200-mm-long cylindrical splitting-tensile specimens. The specimens were cured at 27˚C for 27 days in water and then allowed to cure at 25˚C and 60% relative humidity for an additional two months. At an age of about 90 days, the specimens were heated to 200˚ or 400˚C where they remained until the temperature at the center of the specimen was within ±10˚C of the target temperature (about 2-3 hours from start of heat up). Specimens were then slowly cooled by letting the furnace cool to room temperature or quick cooled by removing them from the oven and immediately placing into a water bath. Figure 2.135 presents the variation of residual flexural strength with temperature for slow and quick cooling. The designations G50, G90, G110, and G130 correspond to the nominal compressive strengths (grades) of the four concretes investigated. For each grade concrete the residual flexural strength was lower at 400˚ than 200˚C, with the loss in flexural strength increasing as the concrete grade increased. Residual flexural strengths were lower for specimens cooled rapidly relative to those that were slowly cooled. Figure 2.136 presents the variation of residual splitting-tensile strength with temperature for slow and quick cooling. All grades of concrete exhibited increasing loss of residual splitting-tensile strength with increasing temperature for both slow and quick cooling. Higher strength concretes (G90, G110, and G130) lost

more residual splitting-tensile strength at elevated temperature than the lower strength concrete (G50). Also, specimens cooled quickly exhibited lower residual splitting-tensile strengths than that exhibited by specimens cooled slowly.

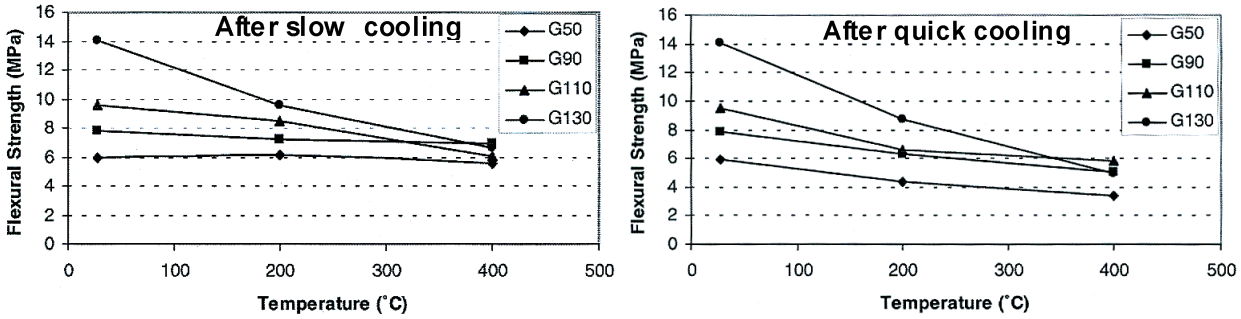

Figure 2.135 Effect of cooling rate on residual flexural strength.

Source: R.V. Balendran, A. Nadeem, T. Maqsood, and H.Y. Leung, "Flexural and Split Cyliner Strengths of HSC at Elevated Temperature," *Fire Technology* **39**, pp. 47-61, 2003.

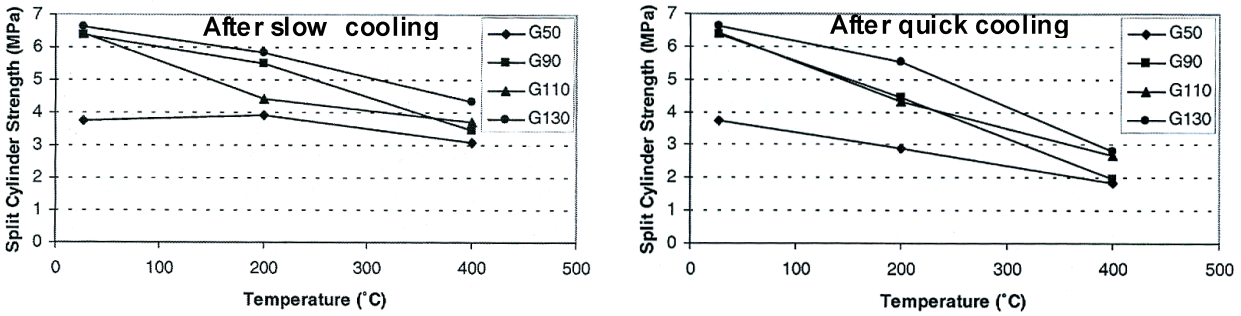

Figure 2.136 Effect of cooling rate on residual splitting-tensile strength.

Source: R.V. Balendran, A. Nadeem, T. Maqsood, and H.Y. Leung, "Flexural and Split Cyliner Strengths of HSC at Elevated Temperature," *Fire Technology* **39**, pp. 47-61, 2003.

The effect of elevated temperature on the splitting-tensile strength of plain and fiber-reinforced concrete has been investigated [2.128]. The concrete utilized ordinary Portland cement, sand, 20-mm maximum size crushed gravel aggregate, and a water-cement ratio of 0.55 (by weight). Fiber reinforcement (0.0, 0.5, 0.7, or 1.0%, by volume) was included in the mixes and consisted of either hooked steel (50-mm long x 0.35-mm diam) or cement fil alkali-resistant glass fibers (50-mm long x 0.25–mm diam). Cylindrical test specimens 100-mm-diameter by 200-mm-long were cast from the mixes and cured for 7 days in water followed by air drying in the laboratory for an additional 21 days before exposing to elevated temperature. The cylinders were exposed to temperatures of 100˚, 200˚, 350˚, 600˚, 700˚, or 800˚C for 90 minutes. Following temperature exposure, six cylinders were removed from the oven and tested immediately, six cylinders were cooled at room temperature for two hours prior to testing, and six cylinders were cooled in water for two hours prior to testing. Figure 2.137 presents results for the plain concrete specimens for the three testing conditions. Results clearly indicate that the splitting-tensile strength of the plain concrete decreases with temperature with the decrease increasing as the temperature increases. Cooling in air and water cooling increased the loss of splitting-tensile strength with temperature. Similar results were obtained for the 1% steel fiber concrete. Figure 2.138 presents the effect of fiber type and volume on the splitting-tensile strength of specimens tested hot. Results show that the splitting-tensile strength of the fiber-reinforced concrete was higher than that of the plain concrete for all temperatures and that the strength of the glass fiber concrete was lower than that of the steel fiber concrete. At temperatures greater than 350˚C, the effect of fiber content was not significant, probably as a result of fiber unbonding.

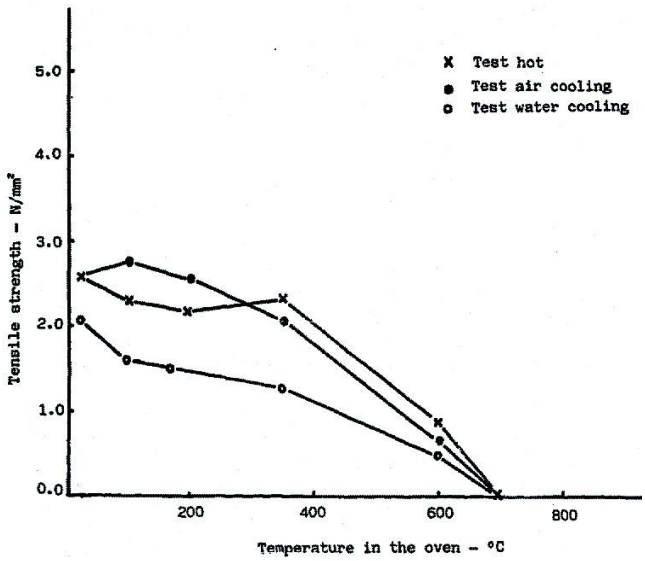

Figure 2.137 Effect of temperature on splitting-tensile strength of plain concrete.

Source: F.I. Faiyadh and M.A. Al-Ausi, "Effect of Elevated Temperature on Splitting Tensile Strength of Fibre Concrete," *International Journal of Cement Composites and Lightweight Concrete* **11**(3), pp. 175-178, August 1989.

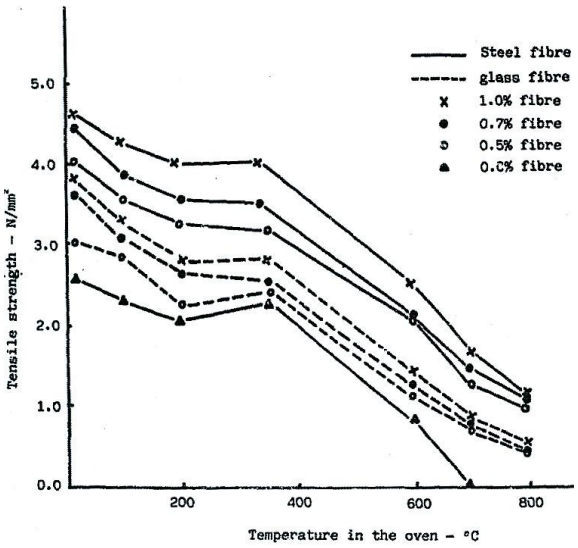

Figure 2.138 Effect of temperature and fiber reinforcement type and quantity on splitting-tensile strength of specimens tested at temperature.

Source: F.I. Faiyadh and M.A. Al-Ausi, "Effect of Elevated Temperature on Splitting Tensile Strength of Fibre Concrete," *International Journal of Cement Composites and Lightweight Concrete* **11**(3), pp. 175-178, August 1989.

Table 2.5 provides additional results on the Effect of elevated temperature on residual splitting-tensile strength of fiber-reinforced concrete [2.129]. Cube specimens 100 x 100 x 100 mm^3 were prepared using high-strength ordinary Type I Portland cement concrete with 19-mm maximum size basalt coarse aggregate, silica sand, and different volumetric mixtures of three types of fibers (i.e., brass-coated steel, hooked steel, and high performance polypropylene) with a total fiber volume of 2%. Reference concrete compressive strengths were 77.3, 89.8, 85.5,

93.75, and 103.6 MPa for plain concrete, hooked steel fibrous concrete (HS), hooked steel- high performance polypropylene fibrous concrete (HSHP), hooked steel-brass coated steel fibrous concrete (HBCS), and brass coated steel fibrous concrete (BCS), respectively. Results in the table indicate that although the splitting-tensile strengths of the fiber-reinforced concrete were generally much higher than those for the plain concrete at temperatures below 500˚C, the percentage loss was larger for the fibrous concretes probably due to differences in thermal expansion coefficient between the fibers and matrix leading to loss of bond. At higher temperatures, the presence of fibers reduced the extent of cracking and spalling.

Table 2.5 Residual splitting-tensile strengths of plain and fibrous concretes after temperature exposure

T (˚C)	Plain	HS	HSHP	HBCS	BCS
23	11.8 (100%)	22.65 (100%)	20.45 (100%)	20.7 (100%)	22.5 (100%)
350	8.85 (75%)	13.4 (59.2%)	11.45 (56%)	13.35 (64.5%)	16.4 (72.9%)
500	5.9 (50%)	7.9 (34.9%)	7 (34.2%)	9.25 (44.7%)	7.8 (34.7%)
600	3.55 (30.1%)	5.18 (22.5%)	4.25 (20.8%)	4.9 (23.7%)	5.55 (24.7%)
700	Spall	1.7 (7.5%)	1.65 (8.1%)	1.7 (8.2%)	1.4 (6.2%)

Source: R.H. Haddad, R.J. Al-Saleh, and N.M. Al-Akhras, "Effect of Elevated Temperature on Bond Between Steel Reinforcement and Fiber Reinforced Concrete," *Fire Safety Journal* **43**(5), pp. 334-343, July 2008.

The effect of silica fume addition on the splitting-tensile and compressive strengths has been investigated for a lightweight concrete [2.130]. The concrete mixes utilized ordinary Type I Portland cement with partial cement replacement by silica fume in amounts representing either 0 (mix M), 10 (mix H), 20 (mix A), or 30% (mix E) the total cementitious materials content. Crushed pumice (16-mm maximum size) was used as the coarse aggregate and the water-cement ratio was 0.77 (by weight). Compressive strength was determined using 100-mm cubes and splitting-tensile strength with cylindrical test specimens 100-mm-diameter by 200-mm-long. Specimens were cured in a water tank for 28 days prior to heating to temperatures of 200˚, 400˚, or 800˚C where they were maintained for one hour prior to permitting them to slowly cool to room temperature. Figure 2.139 presents the effect of elevated temperature on the residual compressive and splitting-tensile strengths. Highest initial compressive and splitting-tensile strengths were obtained for the mix containing 20% cement replacement by silica fume. Starting at a temperature of about 200˚C, the compressive and splitting-tensile strengths started to drop for each of the mixes and exhibited a similar trend in strength reduction with increasing temperature.

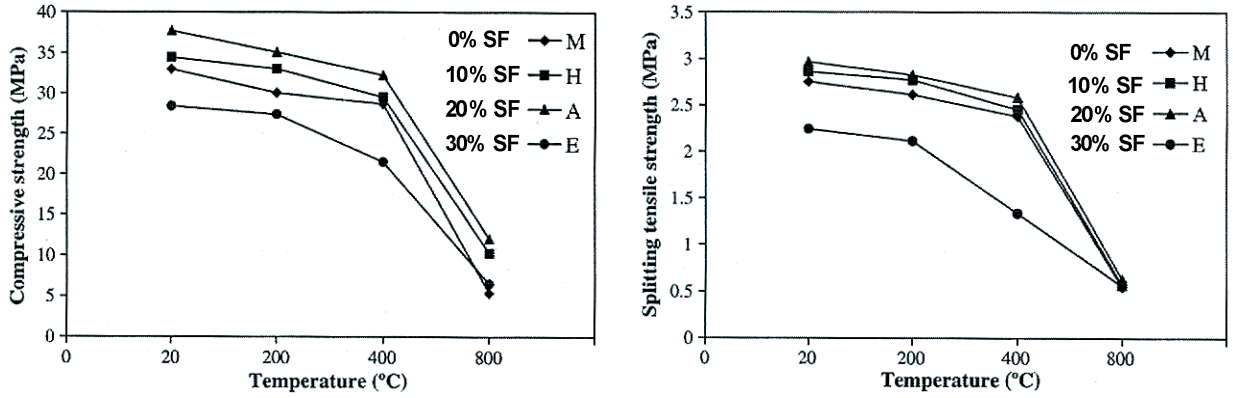

Figure 2.139 Effect of temperature and silica fume content on residual compressive and splitting-tensile strengths of a lightweight concrete.

Source: H. Tanyildizi and A. Coskun, "Performance of Lightweight Concrete with Silica Fume After High Temperature," *Construction and Building Materials* **22**, pp 2124-2129, 2008.

Examples of Relations for Concrete Tensile Strength at Elevated Temperature. Based on test results the following has been proposed for concrete tensile strength as a function of temperature [2.107]:

$$f_t^T = (1- 0.001T)f_t \quad (20^\circ \text{ to } 1000^\circ C) \tag{2.54}$$

where f_t^T and f_t are the tensile strength at elevated temperature and room temperature, respectively. After exposure to elevated temperature the following has been proposed for estimating concrete tensile strength [2.131]:

$$f_t^T = \left[2.08(T/100)^2 - 2.666(T/10) + 104.79\right]f_t \tag{2.55}$$

which has been simplified to a two-part expression

$$f_t^T = [0.58(1- T/300)^2 + 0.42]f_t' \quad \text{for } 20^\circ < T \leq 300^\circ C, \text{ and} \tag{2.56}$$

$$f_t^T = \left[0.42(1.6 - T/300) + 0.42\right]f_t' \quad \text{for } 300^\circ < T < 800^\circ C. \tag{2.57}$$

An expression for the relationship of normalized residual tensile strength (f_{tr}'/f_t') to temperature (T) exposure has been proposed [2.108]:

$$f_{tr}'/f_t' = 1.05 - 0.0025T \quad \text{for } 20^\circ < T \leq 100^\circ C, \tag{2.58}$$

$$f_{tr}'/f_t' = 0.80 \quad \text{for } 100^\circ < T \leq 200^\circ C, \text{ and} \tag{2.59}$$

$$f_{tr}'/f_t' = 1.02 - 0.0011T \geq 0.0 \quad \text{for } 200^\circ < T \leq 800^\circ C. \tag{2.60}$$

Summary. Conclusions from the limited tensile test data available in the literature are that the aggregate type and mixture proportions have a significant effect on the tensile strength vs temperature relationship; the decrease in tensile strength of calcareous aggregate concrete is twice as high as that of siliceous aggregate concrete at 500°C; concretes with lower cement content have lower reduction in tensile strength than those with higher cement content; the rate of heating has minimal effect on tensile strength at high temperature; and the residual tensile strength is somewhat lower than the tensile strength measured at elevated temperature.

2.2.1.7 Shrinkage and Creep

Information and Data. When freshly hardened concrete is exposed to the ambient environment and humidity it will generally undergo thermal shrinkage (shrinkage strain associated with cooling) and drying shrinkage (shrinkage strain associated with moisture loss). Generally for massive structures the drying shrinkage is less important than the thermal shrinkage. Length (or volume) change of concrete under these conditions is important because of its effect on movement of the structure and its tendency to induce cracking.

Shrinkage occurs as a result of two effects: (1) drying or (2) autogeneous volume change. Drying shrinkage results from the loss of absorbed water and is generally the more predominant of the two effects. The rate and magnitude of drying shrinkage generally increase with temperature. Several factors affect concrete drying shrinkage: (1) cement and water contents (shrinkage varies directly with water-cement ratio) [2.132]; (2) composition and fineness of cement; (3) type and gradation of aggregate (shrinkage inversely proportional to size and amount of coarse aggregate - sandstone, slate, basalt and trap rock produce concretes having greater shrinkage than quartz, limestone, dolomite, granite, and feldspar aggregate concretes); (4) admixtures (those that reduce water requirement reduce shrinkage); (5) moisture and temperature conditions; and (6) amount and distribution of reinforcement. Although shrinkage can take place over long periods of time,* the shrinkage rate decreases with time (e.g., 14 to 34% of the 20-year shrinkage occurring in two weeks, 40 to 80% in three months, and 66 to 85% in one year). [2.133].

* Long-term shrinkage may be due to carbonation.

Autogeneous shrinkage is more prevalent in mass concrete structures where the total moisture content remains relatively constant; it results from continued cement hydration reducing the free-water content (products of hydration occupy less volume than the sum of the separate volumes of the components) [2.134]. Autogeneous shrinkage (linear) varies between approximately 40 x 10^{-6} at one month and 100 x 10^{-6} at five years [2.122]. Figure 2.140 presents the effects of several variables influencing autogeneous shrinkage [2.122].

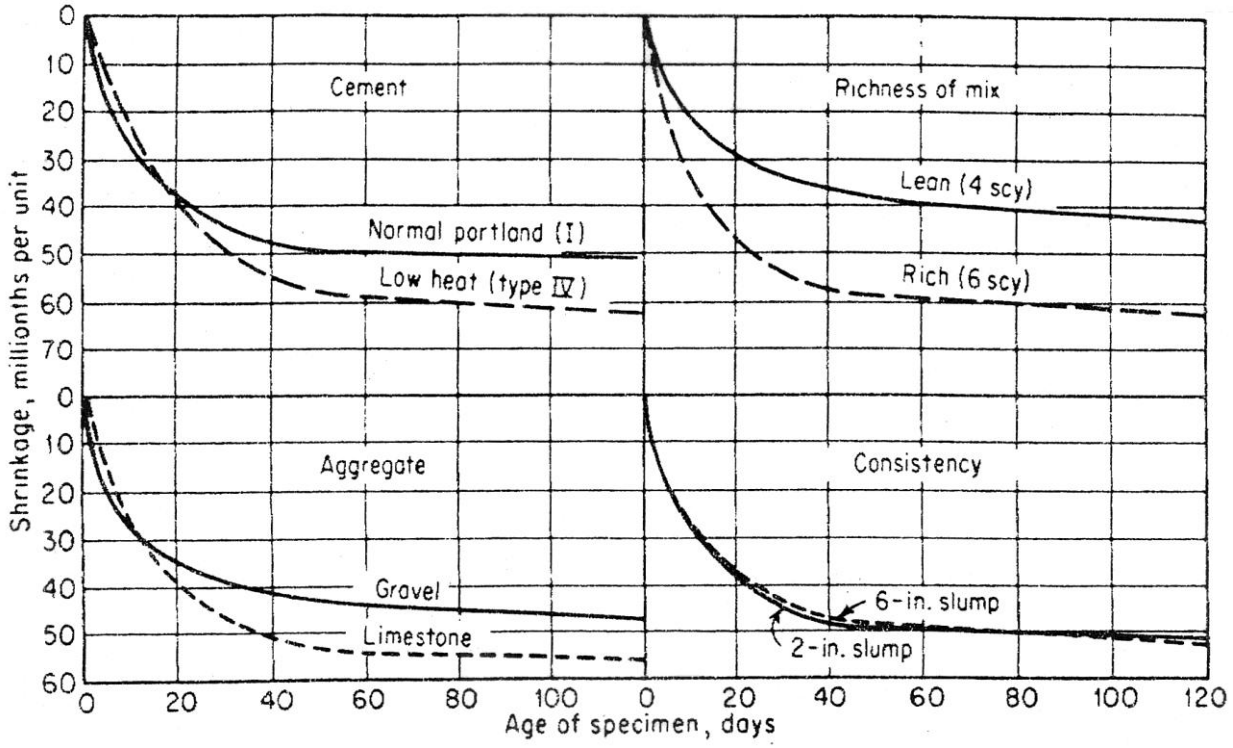

Figure 2.140 Effect of several factors on autogenous shrinkage of concrete.

Source: G. E. Troxell, H. E. Davis, and J. W. Kelly, *Composition and Properties of Concrete*, 2nd Ed., McGraw-Hill, New York, 1968.

In mass structures where the concrete is maintained below 100°C, shrinkage will not be a significant factor over the 30- to 40-year design life of a structure such as a PCPV [2.135]. The shrinkage in the main body of mass concrete remote from the outside environment is caused by self-desiccation of the hardened cement paste component [2.136]. After the initial period where the heat of hydration results in thermal movement, even over long periods of time, the shrinkage is low in comparison to that of smaller members where moisture loss to the external environment can be large. Variation of shrinkage of unsealed concrete stored at different relative humidities for 30 years indicates that if the estimated external relative humidity of the mass concrete at normal temperatures does not drop below 85%, shrinkage after 30 years will be less than 400 microstrain as noted in Figure 2.141. High shrinkage begins when the main bulk of capillary-held water in concrete is lost [2.133], which is only likely to occur if the water-cement ratio of the concrete mix is less than 0.40 [2.137]. Other results indicate shrinkage values for sealed specimens at room temperature of 65 microstrain after 5 years and less than 35 microstrain for sealed specimens at 45°C after 9.5 months [2.136]. Shrinkage results obtained from eight 15.2-cm-diam by 30.5-cm-long sealed cylinders cast using the Wylfa concrete mix design are presented in Figure 2.142 and, on average, appear to be linear with log time. Initial high strains resulted from chemical reactions of the cement. Extrapolation of results over 30 years (Figure 2.143) indicates an expected minimum shrinkage of 100 microstrain. The maximum shrinkage limit shown in the figure was obtained by doubling the sealed shrinkage up to commissioning (i.e., when heating would commence) and then increasing the shrinkage to provide a value of 400 microstrain. This was to account for site mix variations and the uncertain effects of prolonged heating.

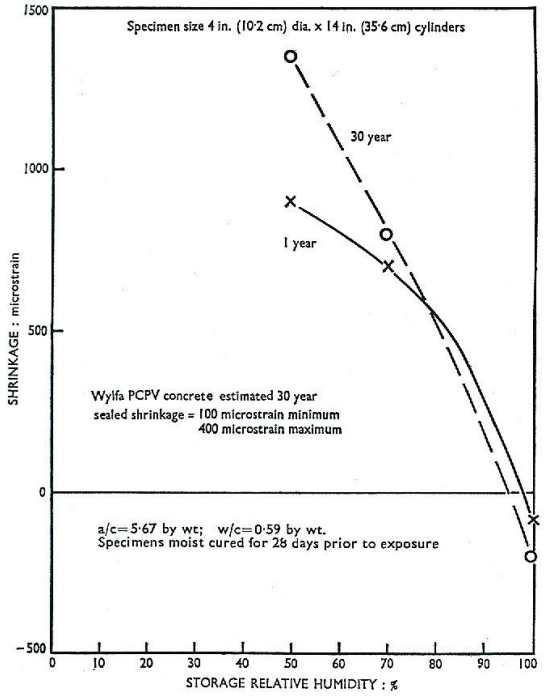

Figure 2.141 Variation of long-term shrinkage of concrete with relative humidity of storage.

Source: R.D. Browne, "Properties of Concrete in Reactor Vessels," *Proceedings of the Conference on Prestressed Concrete Pressure Vessels*, Group C, Paper 13, pp. 131-151, Institute of Civil Engineers, London, United Kingdom, 1967.

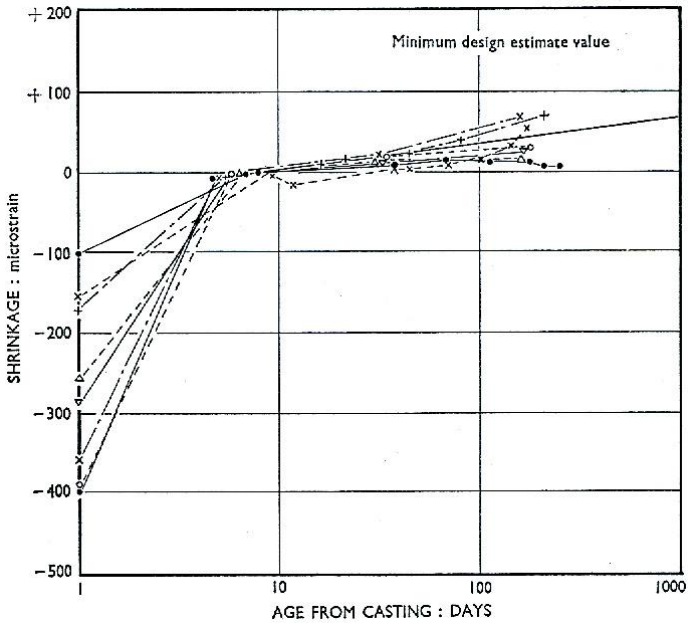

Figure 2.142 Shrinkage measurements obtained from sealed cylinders cast from Wylfa concrete mix.

Source: R.D. Browne, "Properties of Concrete in Reactor Vessels," *Proceedings of the Conference on Prestressed Concrete Pressure Vessels*, Group C, Paper 13, pp. 131-151, Institute of Civil Engineers, London, United Kingdom, 1967.

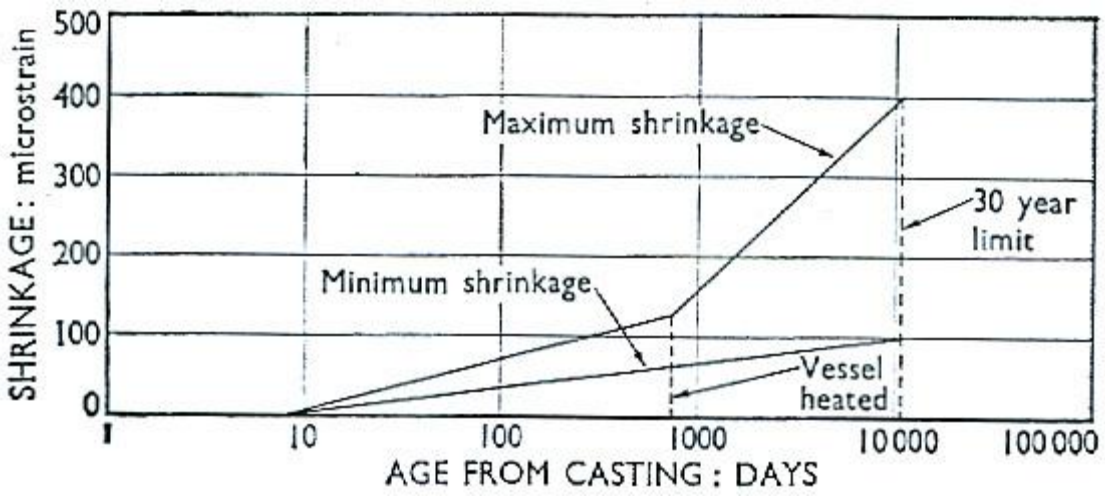

Figure 2.143 Shrinkage design limits for Wylfa PCPV.

Source: R.D. Browne, "Properties of Concrete in Reactor Vessels," *Proceedings of the Conference on Prestressed Concrete Pressure Vessels*, Group C, Paper 13, pp. 131-151, Institute of Civil Engineers, London, United Kingdom, 1967.

Creep can be defined as the increase in strain in a structural member with time due to sustained stress. Creep and drying shrinkage have a number of commonalities: (1) both originate from same source (hydrated cement paste), (2) stress-strain curves are very similar, (3) factors that influence one generally influence the other in the same way, (4) in concrete the magnitude of both (on the order of 400 to 1000 x 10^{-6} microstrain) is large and can not be ignored in design, and (5) both are partially reversible [2.91]. Because creep affects strains, deflections, and stress redistribution, it is important with respect to structural analysis. Creep may also be viewed from another standpoint: if a loaded specimen is restrained from movement (constant net strain), creep will manifest itself as a progressive decrease in stress with time (stress relaxation). Figure 2.144 summarizes the various combinations of loading, restraint, and humidity conditions associated with drying shrinkage and creep. The magnitude of creep and drying shrinkage is also affected by the size and shape of the concrete element [2.91].*

Several theories for the creep mechanism have been proposed: viscous flow of the cement-water paste, closure of internal voids, crystalline flow of aggregate, and seepage into internal voids of colloidal (adsorbed) water formed by cement hydration [2.122]. Some investigators divide creep into two types: (1) basic and (2) drying creep [2.138]. Basic creep has been defined as the load-induced, time-dependent deformation of a specimen which is loaded after achieving thermal, hygral, chemical, and dimensional stability at first heating to a given temperature [2.139]. Drying creep is a function of the moisture loss from the concrete and is related to drying shrinkage. In sealed concrete, drying creep is absent and it is usually the practice to describe the creep during first heating simply as transitional thermal creep. Total creep is the sum of basic and drying creep. Under typical service conditions concrete is most likely drying while under load resulting in creep deformations greater than if the concrete had been dried prior to loading [2.90]. Figure 2.145 illustrates concrete creep under simultaneous drying and loading. A description of the strains that develop for loaded and unloaded concrete during first heat-up, at constant temperature, during cooling, and residual strains is available as well as a method for isolating individual strain components and performing an assessment of their magnitude [2.8].+ Although creep is generally considered only for specimens loaded in compression, creep of concrete in tension also occurs and is on the same order of magnitude as creep in compression [2.140].

---

* A method for predicting the long-term behavior of prestressed concrete containments is provided in Regulatory Guide 1.35.1, "Determining the Prestressing Forces for Inspection of Prestressed Concrete Containments," U.S. Nuclear Regulatory Commission, Washington, D.C., July 1990.

+ Also included in this reference is a method for isolating individual strain components and performing an assessment of their magnitude.

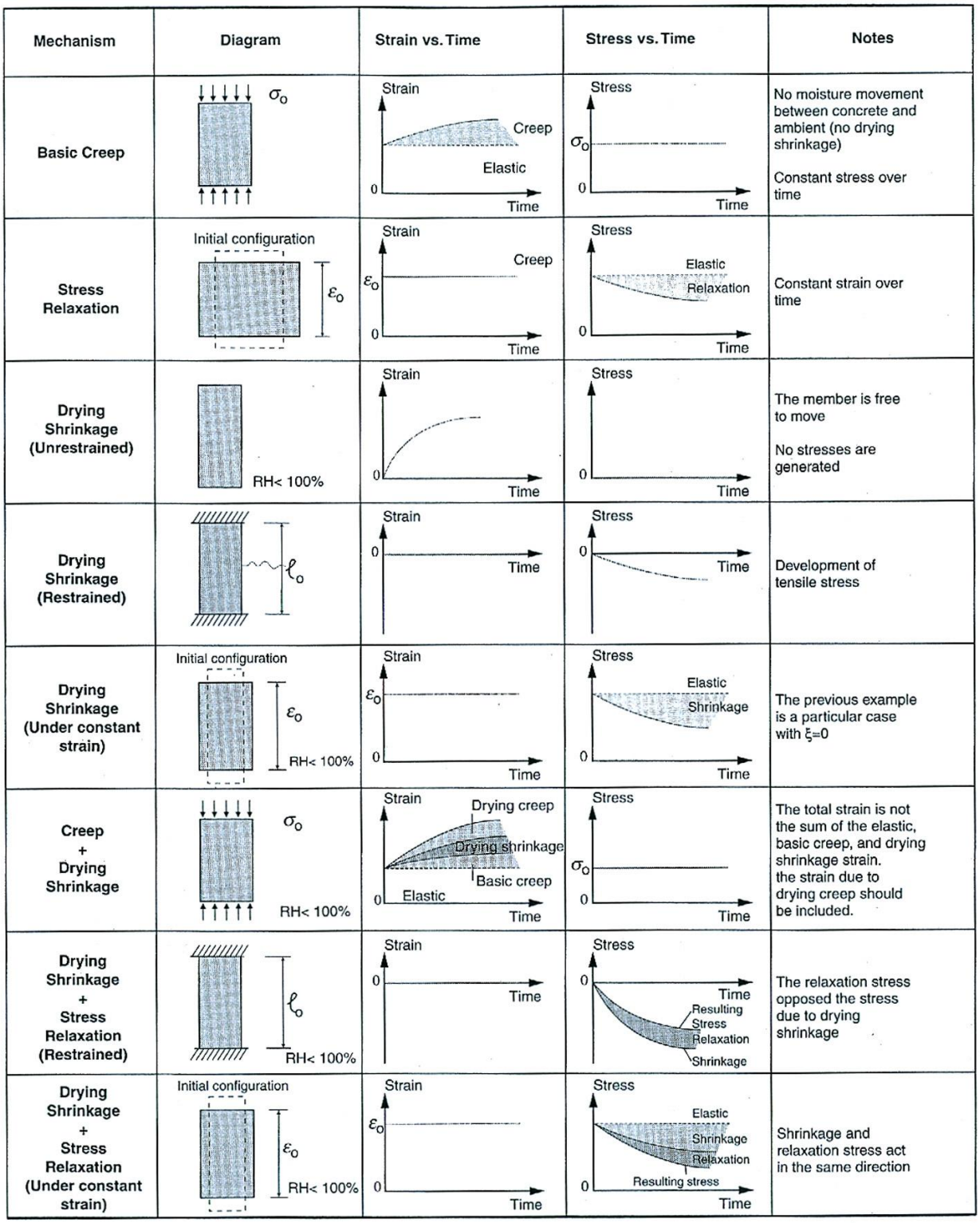

Figure 2.144 Interaction of loading, restraint, and humidity conditions.

Source: P.K. Mehta and P.J.M. Monteiro, *Concrete – Microstructure, Properties, and Materials*, McGraw Hill, New York, New York, 2006.

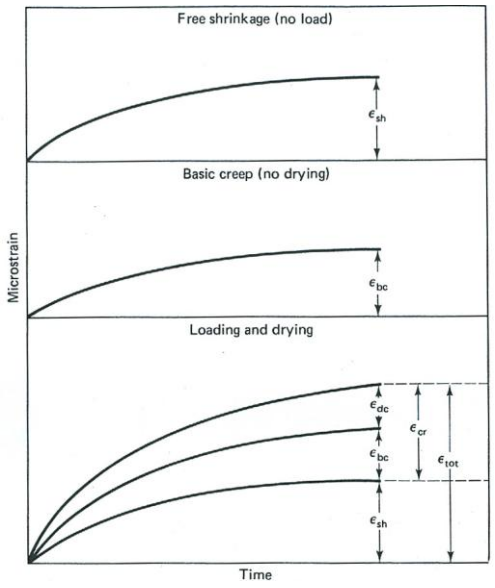

Figure 2.145 Illustration of concrete creep under simultaneous drying and loading.

Source: S. Mindess and J.F. Young, *Concrete*, Prentice-Hall, Inc., Englewood Cliffs, New Jersey, 1981.

Several physical and environmental parameters affect creep deformations of normal weight concrete. Physical parameters inherent to the particular concrete mix include: (1) cement type (degree of hydration); (2) cement paste proportions and content (creep proportional to volume fraction of cement paste in mix); (3) aggregate properties and volume fraction {(a) aggregate restrains creep, (b) mineral character effects are presented in Figure 2.146, and (c) creep tends to be inversely proportional to maximum aggregate size for uniformly graded mixes [2.122,2.141]}; (4) strength and stage of hydration [(a) creep decreases with degree of cement hydration of a mix, and (b) generally the amount of creep is inversely proportional to the concrete strength]; (5) moisture conditions of storing {creep is generally inversely proportional to the relative humidity of the medium surrounding the concrete (Figure 2.147) [2.133]}, and (6) size of mass (the larger the mass, the lower the creep).

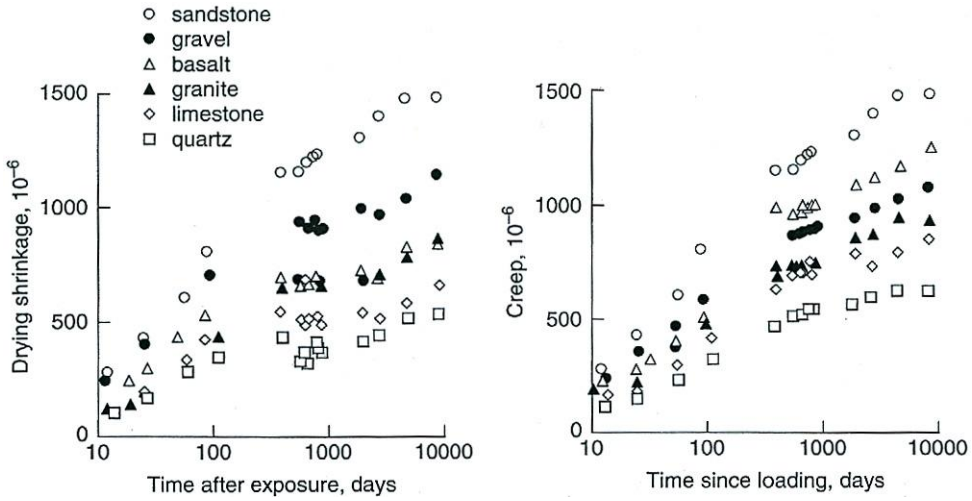

Figure 2.146 Effect of aggregate type on drying shrinkage and creep of concrete.

Source: G. E. Troxell, H.S. Davis, and J.W. Kelly, *Composition and Properties of Concrete,* 2nd Ed., McGraw-Hill, New York, 1968.

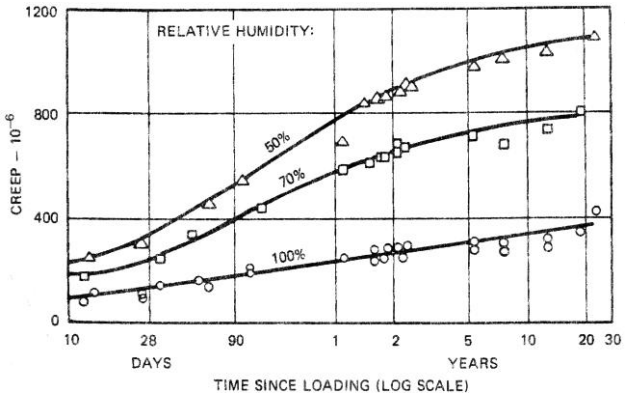

Figure 2.147 Creep of concrete stored at different relative humidities.

Source: A. M. Neville, *Properties of Concrete*, Pitman, London, United Kingdom, 1970.

Mechanical parameters affecting creep include: (1) state of stress: {(a) under uniaxial compressive stress for stress/strength ratio < 0.4, creep is proportional to applied stress; (b) at high stress-strength levels (>0.85), creep can lead to failure; (c) creep under multiaxial compression is less than under uniaxial compression of the same magnitude in the given direction (Figure 2.148); (d) creep occurs under hydrostatic compression [2.142-2.144]}; (2) age at loading [specific creep, or creep strain per unit stress, decreases for increased loading age]; and (3) temperature [(a) creep follows the same general pattern as creep at room temperature – being an exponential

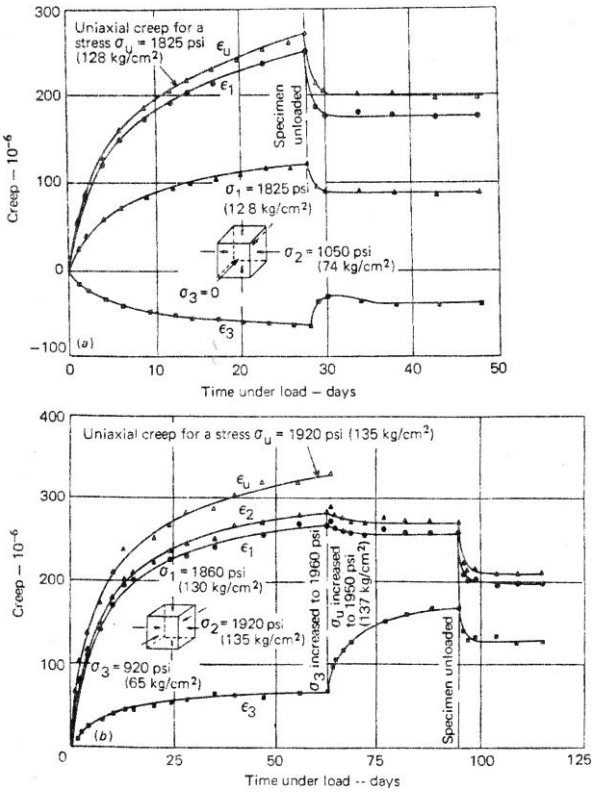

Figure 2.148 Typical creep-time curves under multiaxial compression: (a) biaxial, and (b) triaxial.

Source: A. M. Neville, *Creep of Concrete: Plain, Reinforced and Prestressed*, North-Holland Publishing Company, Amsterdam, The Netherlands, 1970.

function of time under load and a relatively linear function of stress up to a stress-strength ratio of ~0.4; (b) sealed specimens exhibit less creep than unsealed; (c) creep definitely increases with temperature up to at least 50°C and probably increases with temperature up to 150°C; and (d) the degree of creep recovery appears to be more dependent on stress level than temperature] [2.145,2.146].

Upon release of the sustained load, an initial elastic recovery of strain occurs followed by creep recovery that can continue for several days. The magnitude of creep recovery is greater for concrete specimens that were loaded later in their cure cycle, and is inversely proportional to the period of sustained stress. The reversibility of drying shrinkage and creep is illustrated in Figure 2.149. Both the drying shrinkage and creep of concrete exhibit a degree of reversibility. Figure 2.149a relates to drying shrinkage and Figure 2.149b represents a plain concrete specimen subjected to sustained uniaxial compression for 90 days and then unloaded resulting in instantaneous or elastic recovery approximately of the same order of magnitude as the elastic strain on first loading. Creep recovery occurs more rapidly than creep but is not complete.

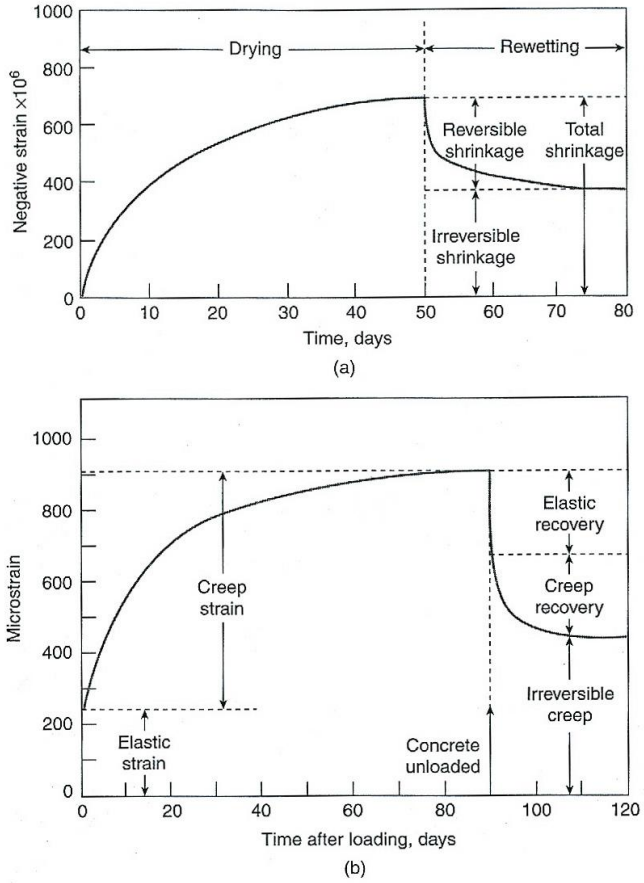

Figure 2.149 Reversibility of drying shrinkage and creep: (a) drying and rewetting, and (b) loading and unloading under uniaxial compression.

Source: P.K. Mehta and P.J.M. Monteiro, *Concrete – Microstructure, Properties, and Materials*, McGraw Hill, New York, New York, 2006.

Additional data and information on concrete shrinkage and creep under uniaxial sustained compressive stress is available in a comprehensive database on the subject that has been developed at Northwestern University in Evanston, Illinois [2.147]. The database contains results for 621 creep tests and 426 shrinkage tests. Potential applications of the database include development of prediction models, reevaluation, recalibration, and mutual comparisons of the existing creep and shrinkage prediction models (e.g., RILEM [2.148] and ACI Committee 209 [2.149]). The database can be downloaded freely from http://www.iti.northwestern.edu.

The effects of temperature on the creep of hardened cement paste can be broadly classified as thermal and structural [2.150]. The thermal effect is that due to the temperature at loading, being seated in the molecular agitation caused by temperature. The structural effect will depend on the maximum exposure temperature, on the assumption that cooling down to the loading temperature does not reverse any structural changes caused by heating or cause structural changes of its own. The above assumption regarding the cooling will be true only if differential thermal strains within the specimen are minimized by a slow rate of cooling and if hydration is not allowed to take place. It was shown that (1) the thermal effect of temperature on creep can be modeled by an Arrhenius-type rate theory, (2) the structural effect of temperature on creep can be classified as that due to loss in strength and that due to a stabilization process, and (3) in the range 300°C to 635°C, the above two processes are opposed to each other (i.e., strength is reduced causing an increase in creep potential, while stabilization, reflected by percentage weight loss, is increased causing a decrease in creep potential) [2.150].

Like all solid materials, creep of concrete increases with temperature. An example of the effect of temperature (21.1˚, 71.1˚, and 96.1˚C) and stress level (35%, 60%, and 70%) on creep of is presented in Figure 2.150. Below 100°C, concrete creep at moderate stress levels originates in the cement paste, probably because of the mutual approach of adjacent laminar particles of cement gel, which is facilitated by the presence of water in gaps between the particles [2.16]. In unsealed specimens the influence of drying becomes significant in the temperature range of 70 to 100˚C [2.16]. At moderate temperature levels hydration (aging) accelerates, but as the temperature increases the reverse of this effect takes place (dehydration accelerates creep). Above 100°C drying of the concrete is very rapid with an associated increase in the creep rate until a stable moisture condition is reached [2.151]. After the moisture is lost and a stable moisture content at a given temperature is reached, the creep rate becomes less than that before loss of moisture [2.16]. In addition to the moisture content and drying effects, the size and shape of the structural member are also important in that they affect the time and rate of moisture loss [i.e., large section members such as walls or a base mat in a nuclear power plant require extended periods of time (days or years) for the moisture to diffuse out of the structure]. Results indicate that when the magnitudes of creep strains in unsealed concrete are compared with the magnitudes of sealed ones (mass concrete), the creep of sealed concrete is greater with it being 0.7 to 5 times greater than the corresponding values for unsealed concrete above a temperature of about 71°C [2.152]. Figures 2.151 and 2.152 present examples of the effect of temperature on creep rate and creep. Temperature accelerates the diffusion of the solid components and water along gaps between the particles.

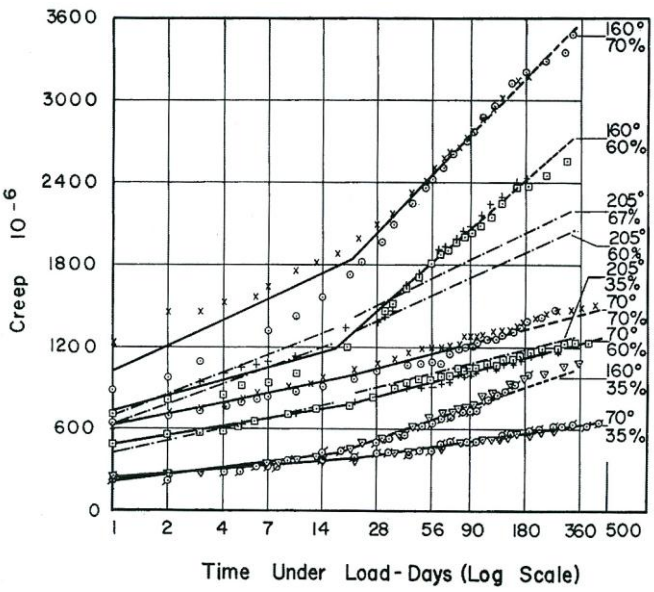

Figure 2.150 Relation between creep and logarithm of time under load for concretes stored at different temperatures and loaded to different stress levels. (Temperatures are in˚F and data points for 205˚F not shown).

Source: K.W. Nasser and A.M. Neville, "Creep of Concrete at Elevated Temperatures," *Journal of the American Concrete Institute*, Title 62-87, pp. 1567-1579, Farmington Hills, Michigan, December 1965.

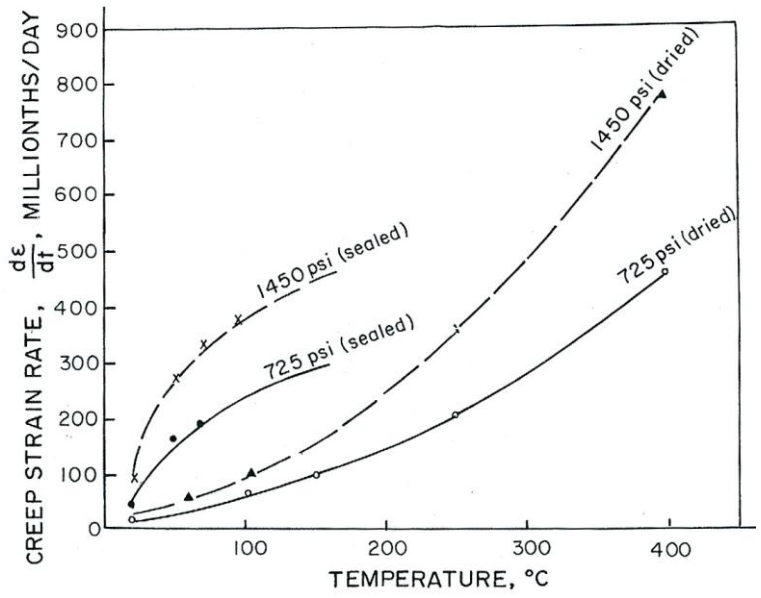

Figure 2.151 Variation of creep rate of Portland cement/porphyry aggregate concrete with temperature.

Source: J.C. Marechal, "Creep of Concrete as a Function of Temperature," Paper SP 34-30 in *Concrete for Nuclear Reactors*, pp. 547-564, American Concrete Institute, Farmington Hills, Michigan, 1972**.**

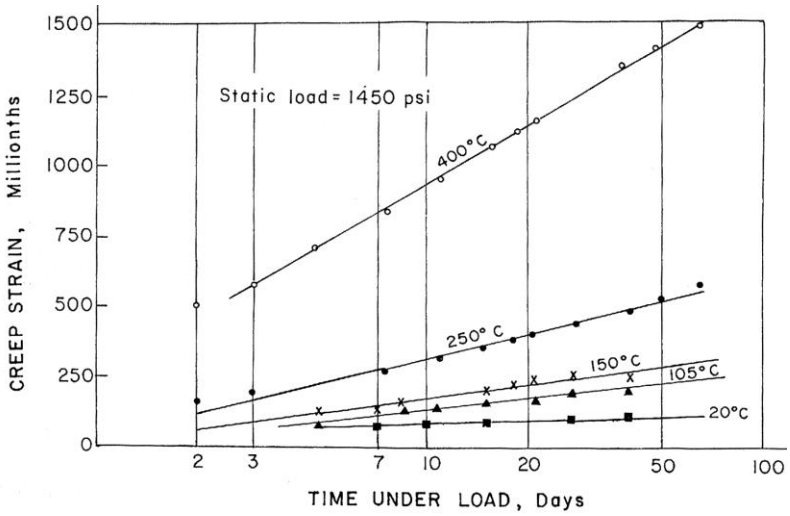

Figure 2.152 Creep of Portland cement/porphyry concrete at various temperatures.

Source: J.C. Marechal, "Creep of Concrete as a Function of Temperature," Paper SP 34-30 in *Concrete for Nuclear Reactors*, pp. 547-564, American Concrete Institute, Farmington Hills, Michigan, 1972**.**

Tests have been carried out to investigate the effect of age of concrete at loading (i.e., at 3, 8, 12, 18, 32, 90, 300, or 365 days) and its water-cement ratio (i.e., 0.5 or 0.7) [2.153]. Eight-day compressive strengths for the two mixes were 11.9 and 29.1 MPa for the higher and lower water-cement ratio mixes, respectively. Prismatic concrete specimens 20 x 20 x 60 cm^3 fabricated from Type II Portland cement and granite aggregate were used in the study. Specimens were either water soaked at room temperature or simulated mass concrete. Test temperatures were either room temperature (21.5˚C) or 45˚C. Figure 2.153 presents specific creep strains (total) for specimens tested at either

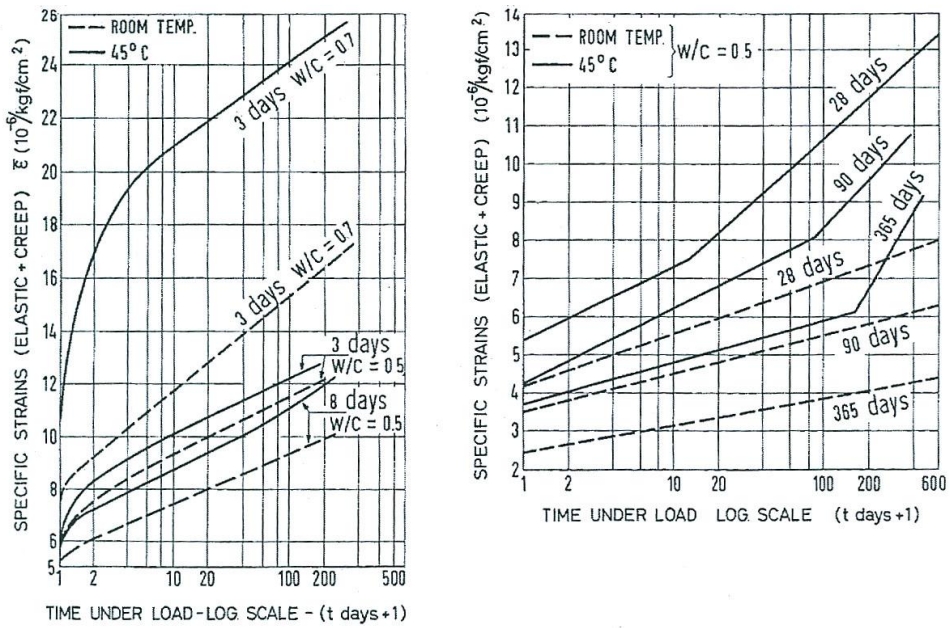

Figure 2.153 Specific creep strains at room temperature and 45˚C for young (left) and mature (right) concretes.

Source: A.F. da Silveira and C.A. Florentino, "Influence of Temperature on the Creep of Mass Concrete," Paper SP 25-7 in *Temperature and Concrete*, pp. 173-189, American Concrete Institute, Farmington Hills, Michigan, 1970.

room temperature or 45˚C and either loaded early (i.e., 3 or 8 days) or at later ages (i.e., 28, 90, or 365 days). Specific creep strains in concrete loaded at age τ at 45˚C could be fit reasonably well by an expression developed by McHenry [2.154]:

$$\bar{\varepsilon} = Ae^{-\alpha\tau}\left(1 - e^{-\beta t}\right) + B\left(1 - e^{-\gamma t}\right), \tag{2.61}$$

where t is the time after loading, and A, B, α, β, and γ are characteristic parameters determined experimentally. Conclusions of the study were that creep strains and creep recovery strains were of the same nature and could be described by the same analytical expression for the temperature range of the study, temperature rise increases creep strains, the greater the temperature the greater the creep recovery strains, influence of temperature is greater for concretes having a higher water-cement ratio, creep strains are on the same order for water-soaked concrete and a similar mass concrete, and ratio of transverse to longitudinal strains remains approximately constant during a creep test and has a value equal to the Poisson's ratio.

Most testing of creep of concrete at temperatures above 100˚C utilized specimens that were unsealed (i.e., freely lose moisture). A review of the literature on the effect of elevated temperature on the time-dependent volume change due to load (i.e., creep) of concrete has been conducted [2.155]. Data from several investigators [2.156-2.162] were compiled and normalized in terms of specific creep or specific creep rate (average slope of creep curve during specified period in semi-log plot), Figures 2.154-2.156. Conclusions derived from these results were:

(1) Creep at elevated temperature follows the same general pattern as creep at room temperatures (i.e., it is approximately an exponential function of the time under load and a fairly linear function of the stress applied at least up to a stress/strength ratio of about 0.50). Sealed or water-stored specimens generally exhibit less creep than unsealed specimens, and creep decreases with increasing maturity and increases with increasing moisture content of the specimen at loading. Poisson's ratio in creep appears to be unaffected by elevated temperatures.

(2) The effect of elevated temperatures (at least up to 50˚ C) is to increase creep, creep at 50˚ C being approximately two to three times as great as creep at room temperature.
(3) For temperatures of 50˚ to about 100˚ C, some controversy exists about whether or not there is a further increase of total creep with increasing temperature. Some investigators have found a definite maximum of total creep in the range of 50˚ to 80˚ C, but most have not and have concluded that creep of concrete increases with temperature up to around 100˚ C, the creep at 100˚ C being on the order of four to six times as great as the creep at room temperature (at the end of a 60- to 100-day loading period).
(4) Conversely, some investigators also have found a definite maximum for the creep rate between 50˚ and 80˚ C if the creep rate is computed for some period between 1 and 107 days under load (Figure 2.156). This seems to indicate that as the temperature increases, a larger portion of the total creep deformation occurs during the first few hours under load with the effect that the creep values at the end of a l00-day loading period, for instance, increase steadily with temperature, in spite of a creep rate maximum at about 50˚ to 80˚ C for the 1- to 100-day loading period.
(5) Few data are available concerning the creep at temperatures exceeding 100˚ C. Tests on unsealed specimens showed no appreciable change in total creep within the temperature range of about 100˚ to 140 ˚C; the creep rate for a 1- to l00-day loading period appeared to decline. Beyond 110˚ C both creep rate and creep magnitude increase with temperature (unsealed specimens) [2.162 and 2.163].
(6) Some controversy apparently exists concerning creep recovery. Although References [2.156,2.157.2.164] found creep recovery to be essentially independent of temperature and stress, Reference [2.165] reported a significantly higher creep recovery at 45˚ C than at room temperature.
(7) The described experimental results concerning the effect of' temperature appears to further support the "seepage theory," while casting some further doubt upon the validity of other concepts.

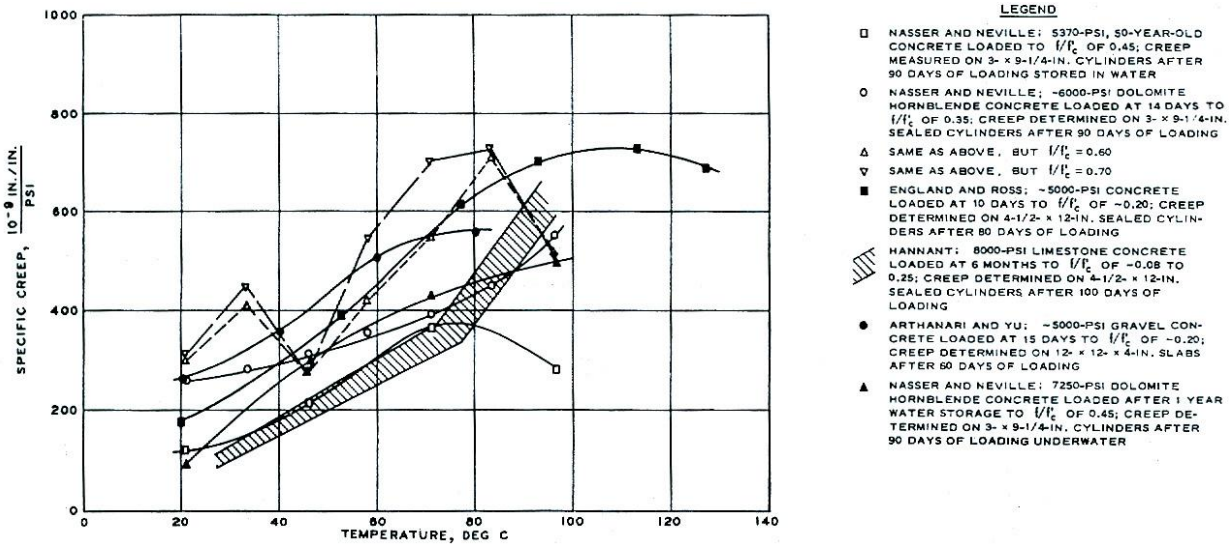

Figure 2.154 Influence of temperature on creep for sealed or water-stored specimens at up to 100 days loading.

Source: H. G. Geymayer, “Effect of Temperature on Creep of Concrete: A Literature Review,” Paper SP-34-31 in *Concrete for Nuclear Reactors*, pp. 565-589, American Concrete Institute, Farmington Hills, Michigan, 1972.

Two series of creep tests have been conducted using quartz aggregate concretes having compressive strengths of 37.9 and 46.2 MPa [2.166]. Cylindrical test specimens 76.2-mm diameter by 152.4-mm long were loaded at an age of 58 days to stress-strength ratios of either 40 or 60% and heated to temperatures of 93.3˚, 204.5˚, 315.6˚, or 426.7˚C. The specimens were first loaded to their test values for a period of one day and then heated to the desired temperature at 1.7˚C/hr. Heating continued for 326 days at which time it was terminated and the specimens were

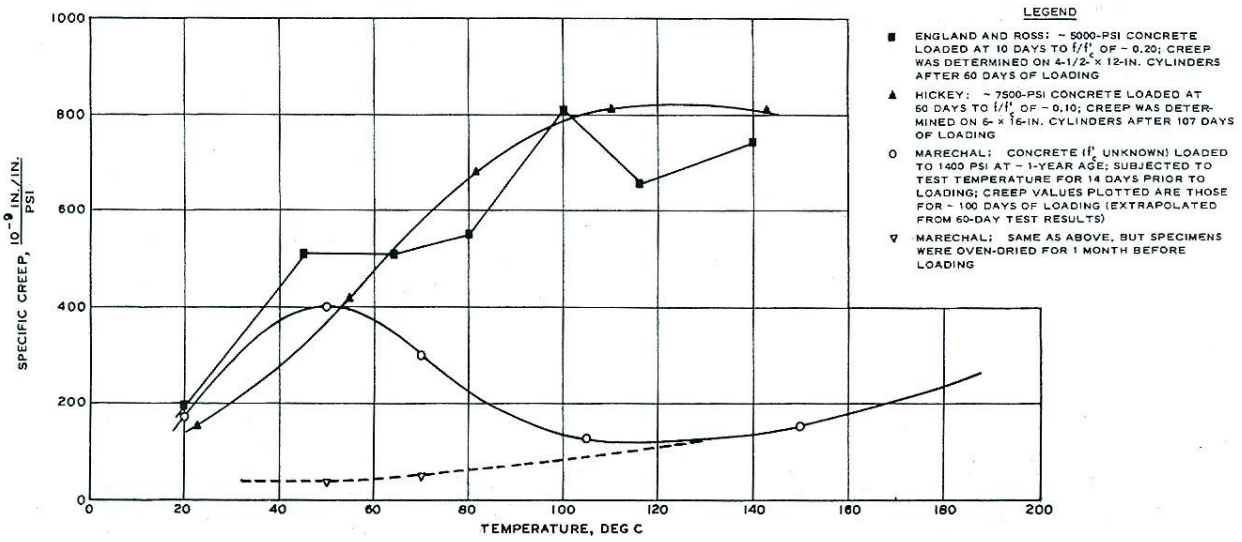

Figure 2.155 Influence of temperature on creep for unsealed specimens at up to 107 days loading.

Source: H. G. Geymayer, "Effect of Temperature on Creep of Concrete: A Literature Review," Paper SP-34-31 in *Concrete for Nuclear Reactors*, pp. 565-589, American Concrete Institute, Farmington Hills, Michigan, 1972.

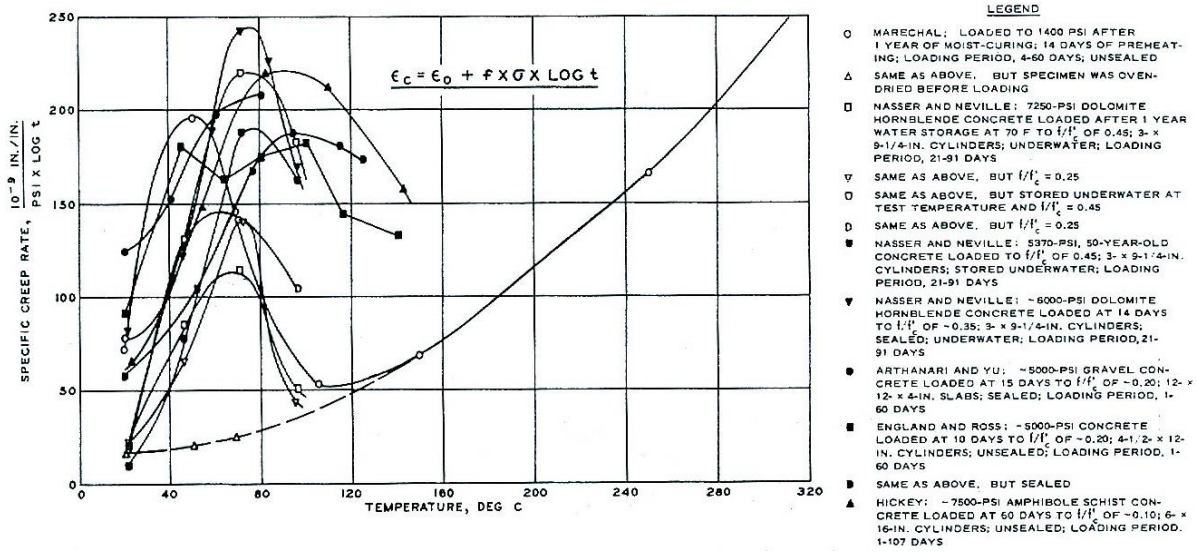

Figure 2.156 Influence of temperature on creep rate ($f_c/f_c' < 0.5$).

Source: H. G. Geymayer, "Effect of Temperature on Creep of Concrete: A Literature Review," Paper SP-34-31 in *Concrete for Nuclear Reactors*, pp. 565-589, American Concrete Institute, Farmington Hills, Michigan, 1972.

permitted to slowly cool to room temperature. Figures 2.157 and 2.158 present creep results for the 37.9 and 46.2 MPa concrete, respectively, for the two stress-strength levels investigated. Conclusions of the investigation were that: (1) the shape of the creep-time curves of concrete at elevated temperature was the same as that at room temperature; (2) creep rate is higher when concrete is subjected to a high temperature and a high stress-strength ratio, with the latter affecting creep more; (3) concrete with lower water-cement ratio has less creep than concrete with higher water-cement ratio, and (4) a nonlinear relationship generally exists between creep and stress-strength ratio.

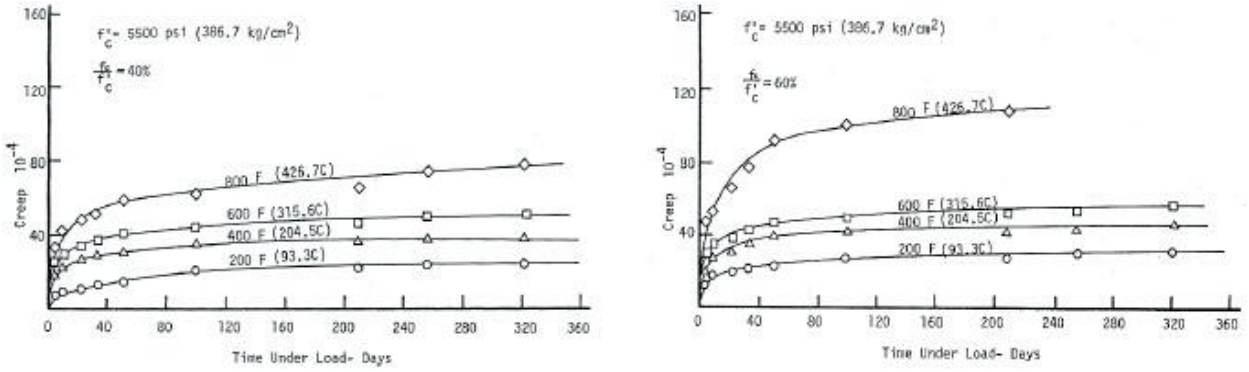

Figure 2.157 Relation between creep and time under load: 37.9 MPa concrete.

Source: C.H. Wang, "Creep of Concrete at Elevated Temperatures," Paper SP 27-19 in *Designing for Effects of Creep, Shrinkage, Temperature in Concrete Structures*," American Concrete Institute, Farmington Hills, Michigan, 1971.

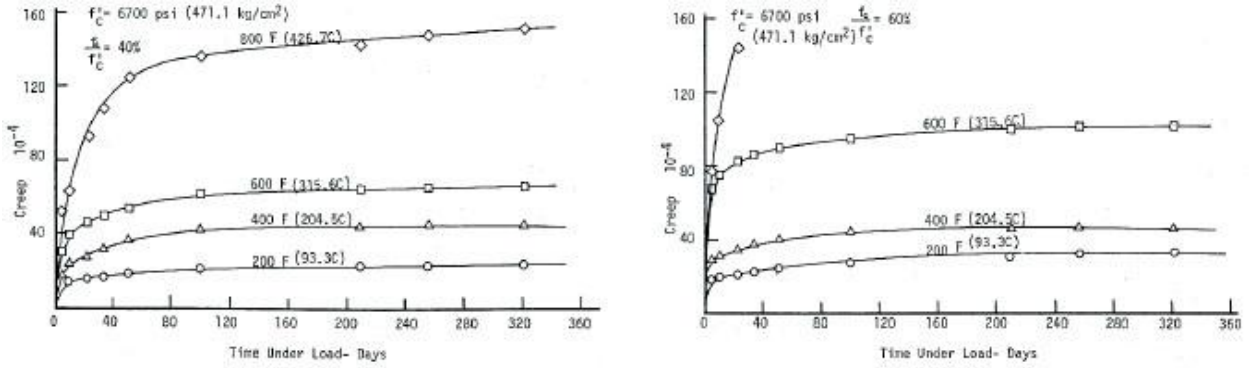

Figure 2.158 Relation between creep and time under load: 46.2 MPa concrete.

Source: C.H. Wang, "Creep of Concrete at Elevated Temperatures," Paper SP 27-19 in *Designing for Effects of Creep, Shrinkage, Temperature in Concrete Structures*, American Concrete Institute, Farmington Hills, Michigan, 1971.

Creep data under elevated-temperature conditions (e.g., $\geq$100˚C) using sealed specimens to represent mass concrete are limited because of the difficulty in sealing the specimens to prevent moisture loss. Several steady-state creep tests have been conducted in support of development of prestressed concrete reactor vessels for high-temperature gas-cooled reactor applications. Test temperatures were generally limited to the ASME Code limit of 65°C, although some data are available at higher temperatures.

Creep data have been developed for limestone or dolerite aggregate concretes loaded to 14.55 MPa at temperatures between 20˚ and 95˚C and ages from 7 and 400 days [2.167]. Although data initially indicated that creep versus log time from loading was linear, the data deviated upward from the straight line for longer times under load. A log-log plot of results showed that for the sealed specimens the experimental creep curves remained linear up to six years. Incorporating data from other investigators [2.156,2.158,2.159,2.162], led to the following expression for the creep curve:

$$\varepsilon = a(t)^n \quad \text{or} \quad \log \varepsilon = \log a + n \log t \tag{2.62}$$

where

ε = specific creep strain,
a = factor decreasing with age at loading, k, and increasing with absolute temperature Θ,
t = time under load in days, and
n = factor decreasing with age at loading, k, and varying with absolute temperature.

Relative to the slope of the straight lines in a log-log plot, it was hypothetically suggested that n can be expressed in terms of a modified Arrhenius activation energy equation such as:

$$n = C \bullet \sigma \bullet e^{\frac{-E}{R\Theta}} \tag{2.63}$$

where

C = a constant,
σ = stress,
E = activation energy, and
R = Boltzman constant.

In a program to observe the creep in mass concrete (sealed specimens) at high temperatures (up to 232.2˚C), 7.62-cm-diam by 22.9-cm-long concrete cylinders were subjected to various stress-strength ratios (20%, 30%, and 60% of 14-d compressive strength) for periods greater than 6 months [2.145]. A Type III cement with 1.9l-cm maximum size aggregate (dolomite and hornblende) and a water-cement ratio of 0.60 were used in all tests. After curing the specimens at test temperature for 13 days, the specimens were loaded and creep strains measured for 6 months. The specimens were then unloaded and creep recovery monitored for about 70 days. At temperatures of 121˚C and above the axial stresses were corrected to account for the steam pressure. Figure 2.159 presents an example of creep versus log time results obtained at a test temperature of 176.7˚C and stress levels of 8.27, 12.41, and 17.24 MPa. The results indicate that two straight lines, one covering 1 to 21 days and one covering 21 to 180 days, can be used to fit the data at each stress level. Figure 2.160 presents an example of the affect of temperature on creep versus time results for specimens loaded to a stress-strength ratio of 20%. Although the shape of the curves was found to be similar, the creep at 148.9˚C was found to be the largest from the 40th day onward (i.e., after 180 days, the creep at temperatures of 176.7˚C and 232.2˚C was less than creep at 148.9˚C). Creep recovery was found to be smaller than the corresponding creep, independent of temperature, dependent on stress, and having a maximum recovery strain of 390 x 10^{-6}. Additional data indicating the effect of load level and temperature on creep of a 42 MPa quartz aggregate concrete loaded to stress-strength levels (α) of either 0.2 or 0.4, and a 39.8 MPa quartz aggregate concrete loaded to a stress-strength level of 0.3 are presented in Figures 2.161 and 2.162, respectively.

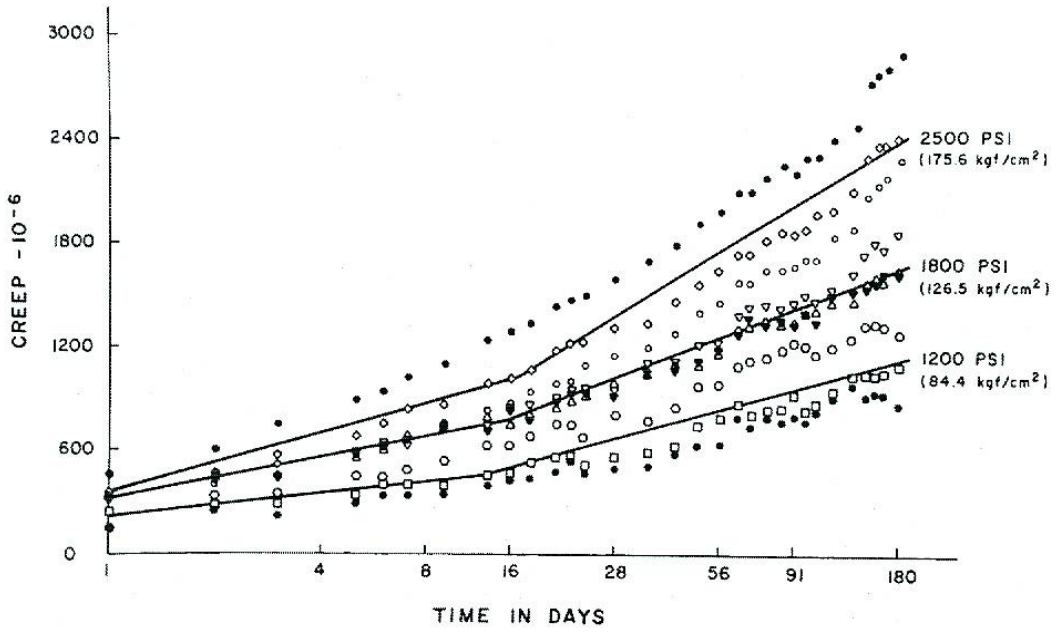

Figure 2.159 Effect of stress level on creep versus log time in days at 176.7˚C.

Source: K.W. Nasser and R.P. Lohtia, "Creep of Mass Concrete at High Temperatures," *Journal of American Concrete Institute* **68**(4), pp. 276-281, Farmington Hills, Michigan, April 1971.

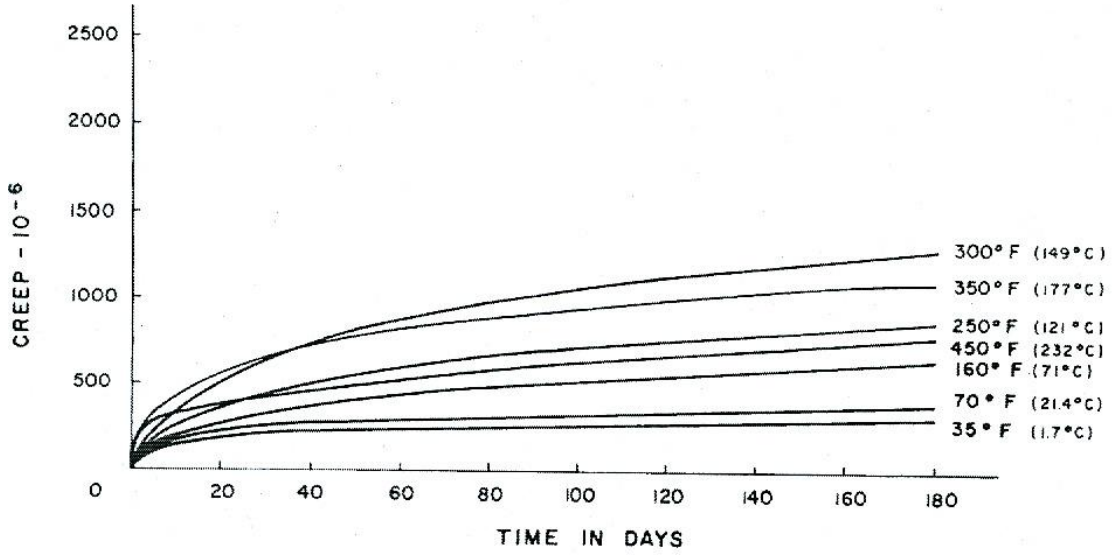

Figure 2.160 Effect of temperature on creep versus time in days for a stress-strength ratio of 20%.

Source: K.W. Nasser and R.P. Lohtia, "Creep of Mass Concrete at High Temperatures," *Journal of American Concrete Institut,* **68**(4), pp. 276-281, Farmington Hills, Michigan, April 1971.

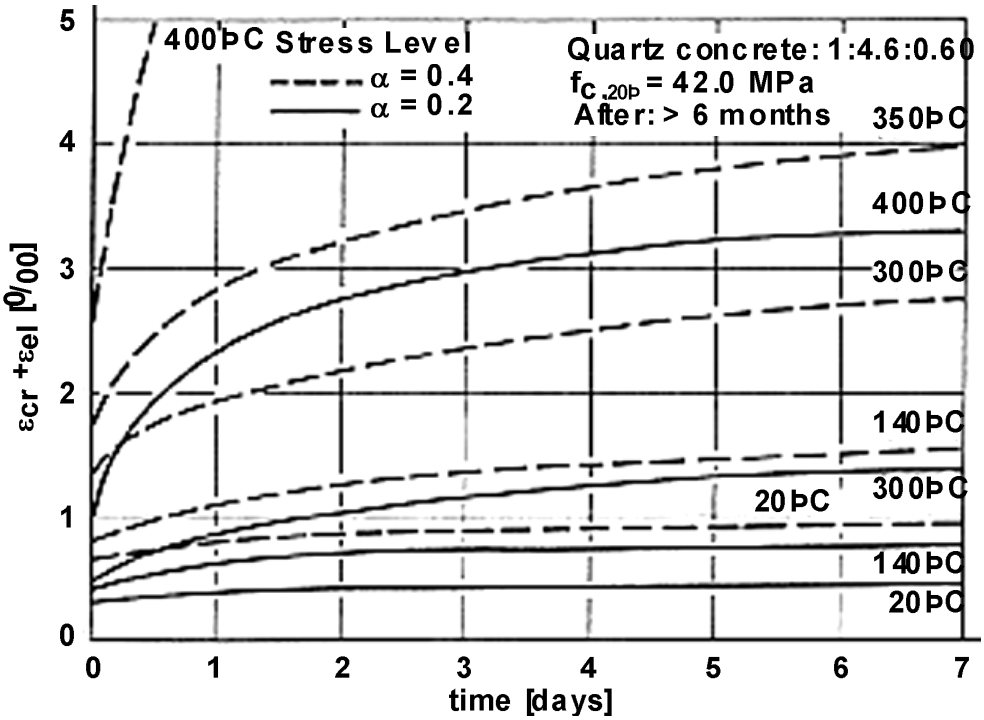

Figure 2.161 Influence of load level and temperature on creep of a quartz aggregate concrete.

Source: H. Gross, "On High Temperature Creep of Concrete," Paper H6/5 in *Proceedings of 2nd International Conference on Structural Mechanics in Reactor Technology*, Elsevier Science Publishers, North-Holland, The Netherlands, 1973.

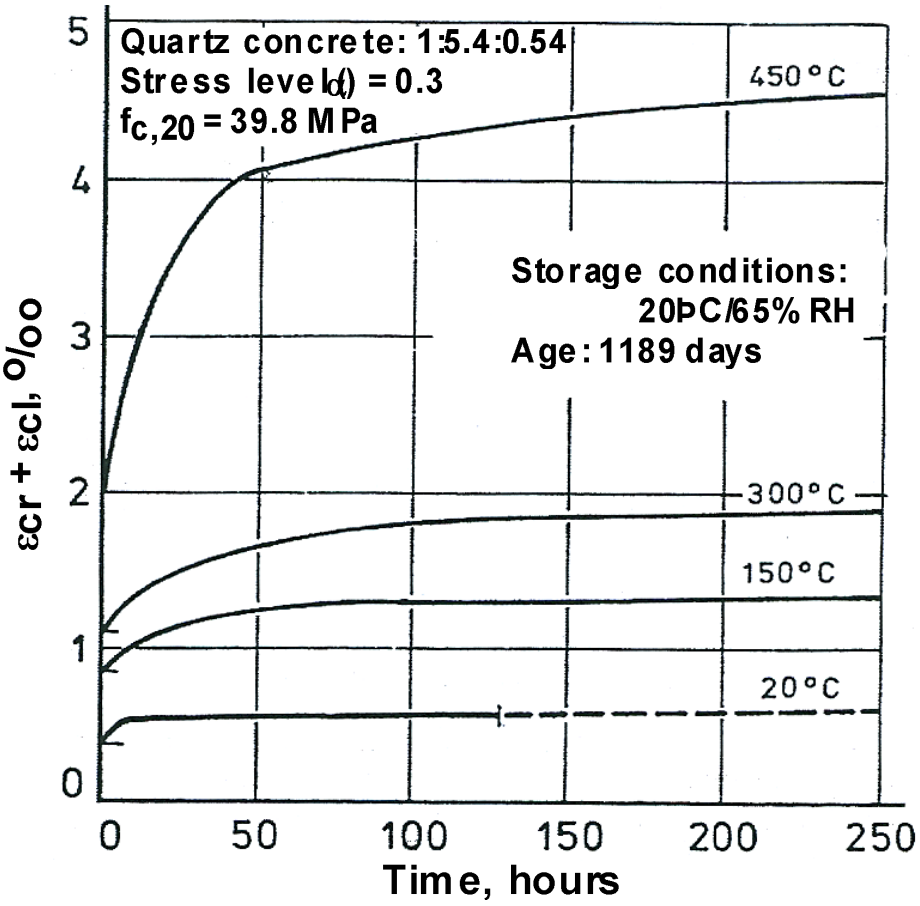

Figure 2.162 High temperature creep of ordinary concrete with quartz aggregate.

Source: U. Schneider, *Behaviour of Concrete at High Temperature*, HEFT 337, Deutscher Ausschuss für Stahlbeton, Wilhelm Ernst & Sohn, Munich, Germany, 1982.

A 5-year investigation on creep and other properties of concrete for prestressed concrete reactor vessels (PCRVs) has been conducted [2.168]. The creep tests were made on sealed concrete specimens to simulate mass concrete. The test parameters included: temperatures of 23˚, 43˚, and 71°C; nominal stress levels of 30%, 45%, and 60% of the reference compressive strength; and ages at loading of 28, 90, and 270 d. Additional tests were conducted to determine autogeneous length change and drying shrinkage of the concrete, the effect of testing temperature (23˚, 43˚, and 71°C) on compressive strength, and the influence of up to five thermal cycles (23° C to 71° C to 23° C) on compressive strength, splitting-tensile strength, modulus of elasticity, and Poisson's ratio. All creep specimens were cast in the vertical position with sealing of the specimen against loss of moisture accomplished by means of steel end plates and a wrapping of 1.59-mm-thick butyl rubber around the specimen. All specimens were stored at 23° C prior to testing. In Figure 2.163 the total strains obtained for Mix No. 1 are plotted for the 13 test conditions investigated. Making a direct comparison of strain data obtained at different levels of stress requires that values of total strain per unit of applied constant stress be computed. The effect of temperature on total strain of concrete per unit of applied stress was for the strain to increase with an increase in temperature. Concrete tested at higher stress levels achieved higher total strains and thus exhibited the highest strains per unit of applied constant stress. Age at loading had a more significant effect on strains of concretes tested at 23°C than for concretes tested at 43°C or 71°C. For the seven groups of specimens for which creep recovery at 23°C or 71°C was obtained, about 39% of the 90-d creep recovery occurred during the first day and 65% within 10 d after unloading, independent of the previous applied stress level. At 71°C creep recovery of only one group of specimens was observed. This group experienced 31% and 52% of the 90-d creep recovery at 1 and 10 d, respectively, after unloading. In general, the drying shrinkage strains leveled off between 400 and 600 microstrains at all test conditions, with the higher drying

shrinkage strains occurring at the higher temperatures where humidities were lowest. Modulus of elasticity of the creep specimens was determined during loading, subsequent unloading, and when testing the creep specimens to failure on completion of the creep phase of the program. The modulus of elasticity of the concretes ranged from 40.7 to 44.8 GPa, with an average Poisson's ratio of 0.22.

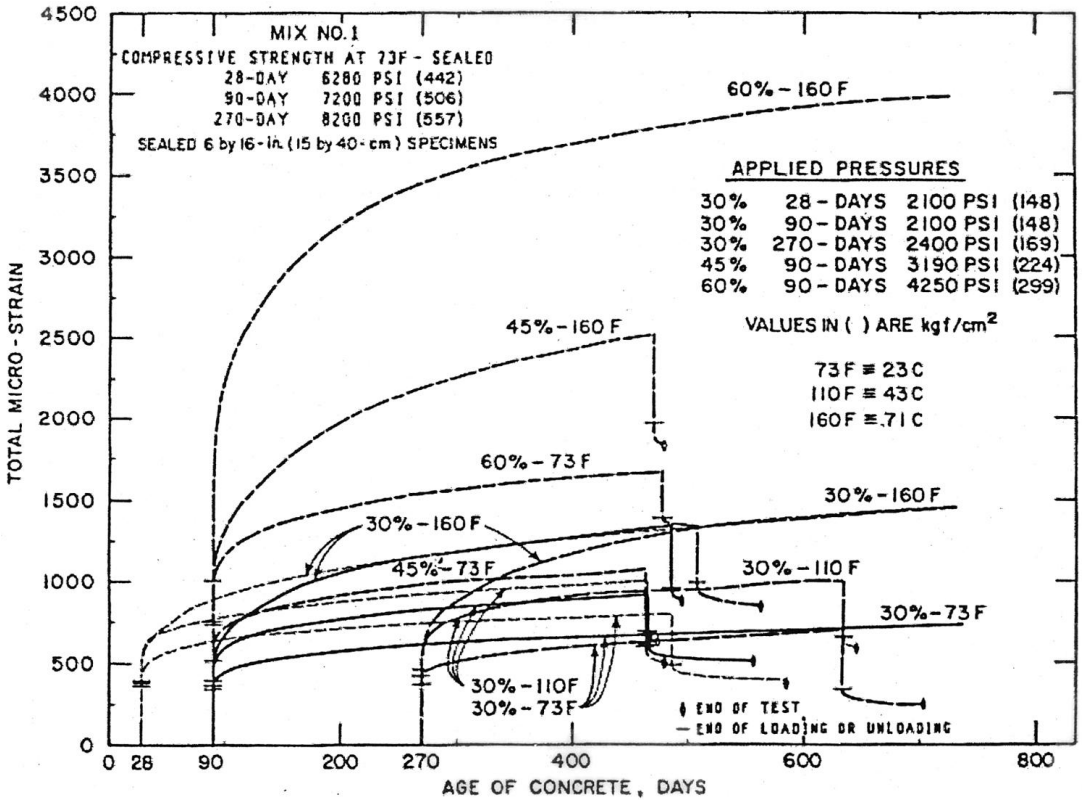

Figure 2.163 Total strains for a number of test parameters.

Source: J. Komendant. V. Nicolayeff, M. Polivka, and D. Pirtz, "Effects of Temperature, Stress Level, and Age at Loading on Creep of Sealed Concrete," Paper SP 55-3 in *Douglas McHenry International Symposium on Concrete and Concrete Structures*, American Concrete Institute, Farmington Hills, Michigan, 1978.

Creep of concrete under multiaxial loading conditions has been investigated [2.169,2.170]. The objective of the study was to develop information on the time-dependent deformation behavior of concrete in the presence of temperature, moisture, and loading conditions similar to those encountered in a prestressed concrete pressure vessel. Four primary factors were addressed in the study: (1) temperature during curing history (23.9˚ and 65.6˚C), (2) curing history (as air-dried or as-cast), (3) several multiaxial load combinations with stress levels varying from 0 to 24.8 MPa, and (4) time covering a period of 18 months after casting. Cylindrical concrete specimens 15.2-cm-diameter by 40.6-cm-long were fabricated from a 41±4.1 MPa concrete mix. One day after casting the as-cast specimens were sealed by coating them with epoxy. One day later a second epoxy coating was applied and the specimens placed into copper jackets that were sealed by soldering. At an age of 83 days, a neoprene jacket was applied to the specimens. Air-dried specimens at an age of 48 hours were submerged and cured in a lime-saturated water solution for five days after which they were stored in a laboratory environment at 22.8˚C and 60% relative humidity until an age of 81 days they were sealed using the same procedure as for the as-cast specimens. Strains were measured using vibrating wire gages. Loading was initiated at an age of 90 days. Compressive loads were applied along the three principal axes of the cylindrical specimens with loads along the longitudinal axis varied independently of the loads applied along the radial axes permitting triaxial, biaxial, and uniaxial states of stress. Figure 2.164 presents a schematic of the multiaxial testing system. Time-creep strain curves illustrating the influence of temperature during loading and time on axial and radial creep strains are presented in Figures 2.165 and

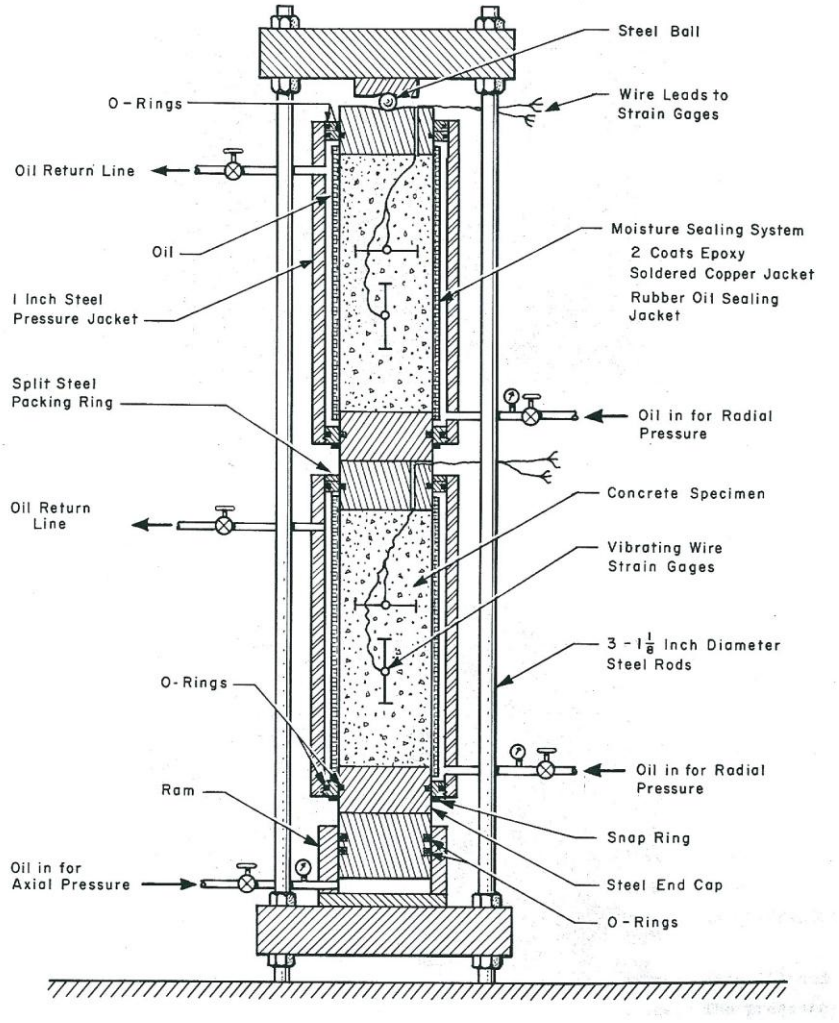

Figure 2.164 Schematic of multiaxial testing system.

Source: G.P. York, T.W. Kennedy, and E.S. Perry, *Experimental Investigation of Creep in Concrete Subjected to Multiaxial Compressive Stresses and Elevated Temperature*, Research Report 2864-2, Department of Civil Engineering, The University of Texas at Austin, June 1970.

2.166, respectively. Results indicate that creep strains for curing histories and temperatures utilized in the study were generally unaffected by time at later ages after loading indicating there was no significant interactions between time and temperature during loading or between time and curing history. Each of the factors addressed affected creep. Compressive and tensile creep strains were generally larger for: (1) a test temperature of 65.6˚ as compared to 23.9˚C, (2) an air-dried concrete than an as-cast concrete (except for low-tensile creep where the opposite was true), (3) increased time after loading, and (4) higher stresses for uniaxial and biaxial states of stress. The effects of major interactions indicated that increasing the stress level increased the creep strains but that the increase was larger for specimens at the higher temperature relative to the lower temperature and for air-dried specimens relative to as-cast specimens, except for specimens exhibiting small tensile creep strains. Also, this increase was larger after longer periods under load.

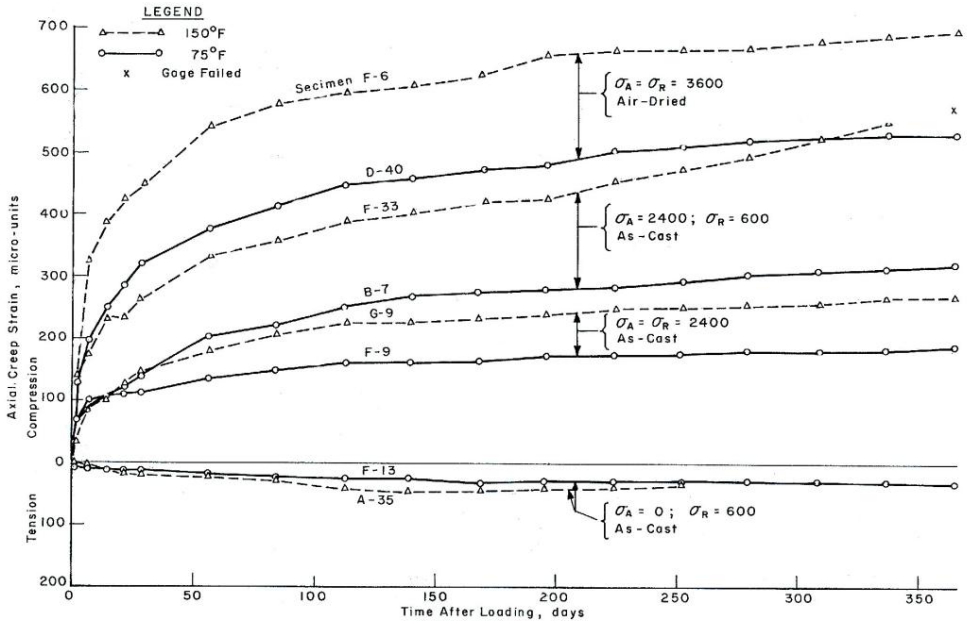

Figure 2.165 Effect of time after loading and temperature on axial creep strain for a variety of stress conditions.

Source: G.P. York, T.W. Kennedy, and E.S. Perry, *Experimental Investigation of Creep in Concrete Subjected to Multiaxial Compressive Stresses and Elevated Temperature*, Research Report 2864-2, Department of Civil Engineering, The University of Texas at Austin, June 1970.

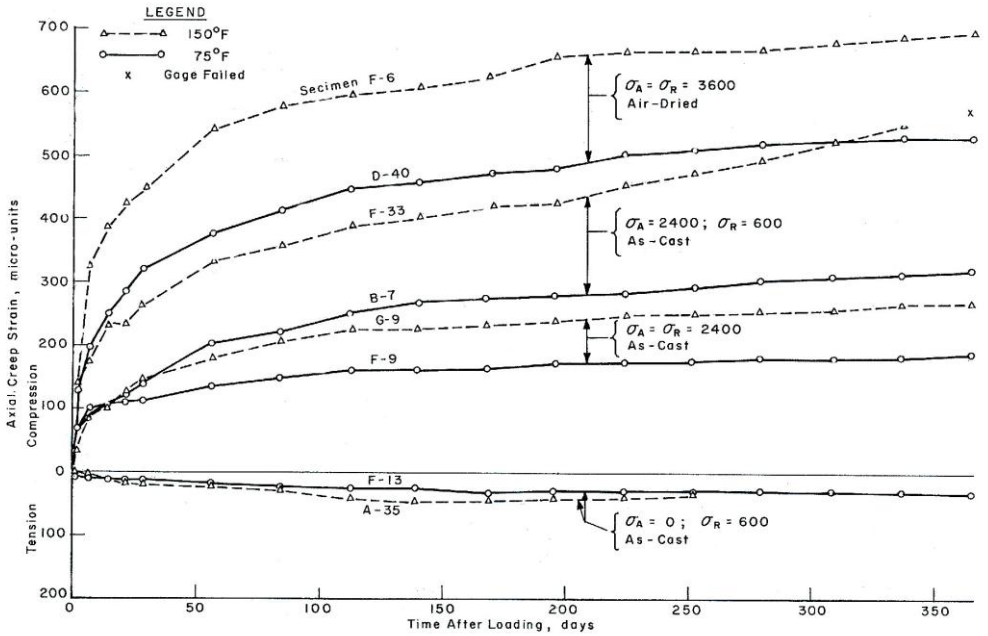

Figure 2.166 Effect of time after loading and temperature on radial creep strain for a variety of stress conditions.

Source: G.P. York, T.W. Kennedy, and E.S. Perry, *Experimental Investigation of Creep in Concrete Subjected to Multiaxial Compressive Stresses and Elevated Temperature*, Research Report 2864-2, Department of Civil Engineering, The University of Texas at Austin, June 1970.

As the confining pressure increased, the overall creep strains decreased. The effect of temperature and time after loading on creep Poisson's ratio are presented in Figure 2.167 for as-cast and air-dried specimens at comparable stress conditions. Within the test conditions of the study, creep Poisson's ratio values ranged from approximately 39% to 84% of the elastic Poisson's ratio values with an overall average value throughout the testing program of 0.16. Creep Poisson's ratio values for air-dried concrete were approximately 30% less than those from as-cast specimens. The magnitude of stress and state of stress influenced creep Poisson's ratio although this influence was less at higher temperature and for air-dried concrete. Creep recovery results indicated from 1 to 46% of the creep strain (average = 17%) at time of unloading was recovered 84 days after release of load with the percentage of creep recovery depending primarily on the curing history (e.g., as-cast specimens recovered more than air-dried specimens). Percentage of creep recovery was not significantly affected by temperature during loading, elastic strain recovery, magnitude of stress, or type of stress applied.

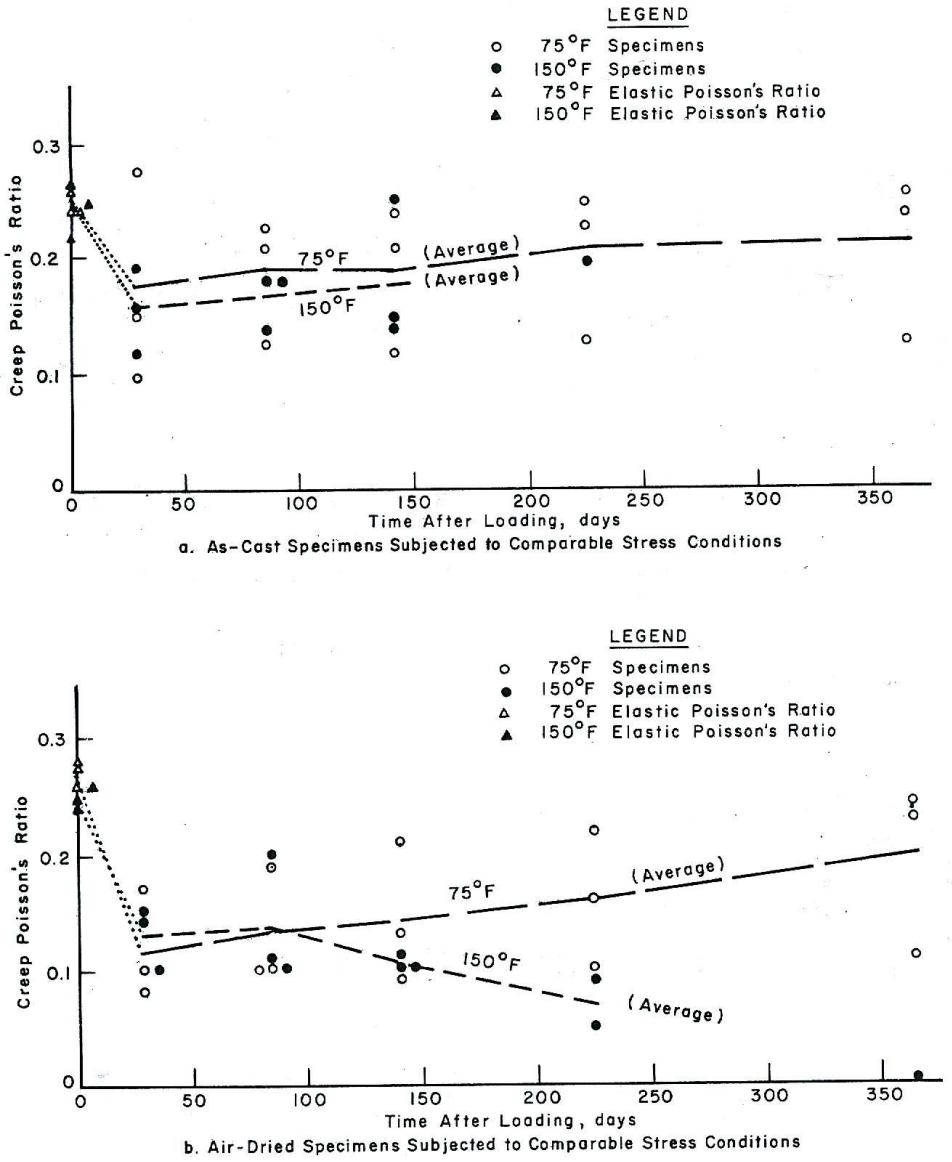

Figure 2.167 Effect of temperature and time after loading on creep Poisson's ratio.

Source: G.P. York, T.W. Kennedy, and E.S. Perry, *Experimental Investigation of Creep in Concrete Subjected to Multiaxial Compressive Stresses and Elevated Temperature*, Research Report 2864-2, Department of Civil Engineering, The University of Texas at Austin, June 1970.

In a related study [2.171], the time-dependent deformation of concrete was investigated by subjecting it to various stress conditions and elevated temperatures using a multiaxial testing system similar to that presented in Figure 2.164. Cylindrical test specimens were 15.2-cm diameter by 40.6-cm long. Factors addressed in the study included modulus of elasticity of aggregate [Tennessee limestone (main), Alabama greywacke (low), and Alabama chert (high)], curing history prior to loading (as-cast and air-dried), temperature during loading (22.7˚C and 65.6˚C), and state of stress during loading (uniaxial, biaxial, hydrostatic, and triaxial stress state) with axial and radial states of stress ranging from 0 to 16.54 MPa. Examples of axial and radial creep strain versus time results for triaxially-loaded specimens (σ_A = 16.54 MPa, σ_R = 4.14 MPa) are presented in Figures 2.168 to 2.171. Results are presented for cure history (as-cast and air-dried specimens), aggregate modulus (high, main, and low), and test temperature (22.7˚C and 65.6˚C). The effect of time after loading on creep Poisson's ratio is presented in Figure 2.172. In the investigation it was found that compressive and tensile total creep strains were generally larger for (1) a test temperature of 65.6°C than for 23.9°C, (2) an air-dried concrete than an as-cast concrete (except for low tensile creep), (3) increased time after loading, and (4) uniaxial than biaxial states of stress, and that the axial creep strains decreased with increasing confining stress (Figure 2.173). Compressive and tensile creep strains were generally proportional to the inverse of the elastic modulus of both the concrete and aggregate. Creep Poisson's ratio was generally smaller than elastic Poisson's ratio. The percentage of creep recovered was essentially the same for variations in curing, temperature, concrete modulus, and stress level investigated, with multiaxial stress states averaging only about 5% more creep recovery than for uniaxial stress states.

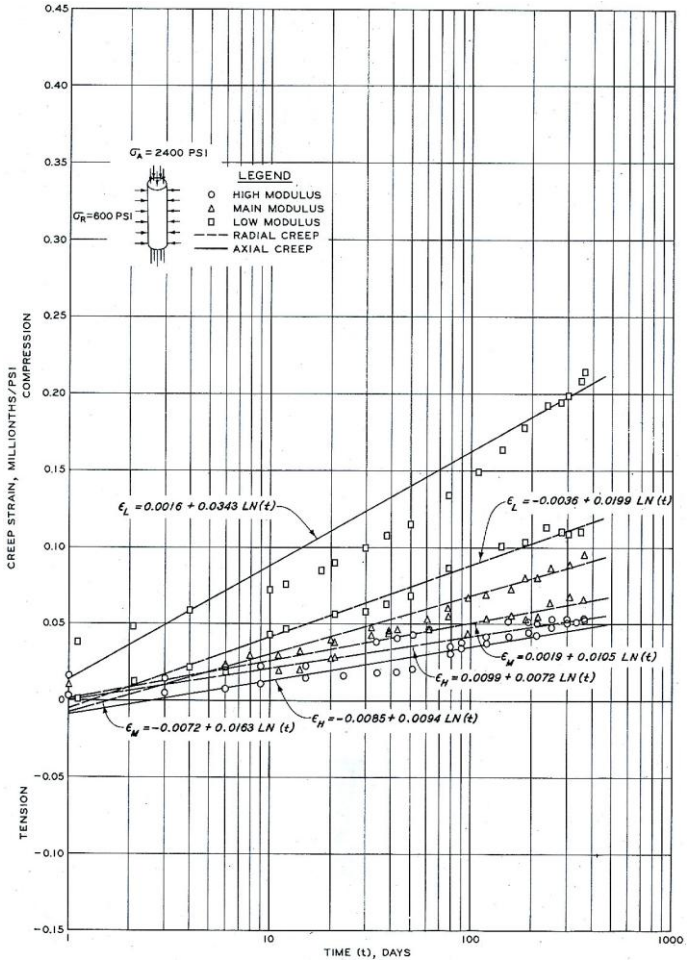

Figure 2.168 Axial and radial creep strain vs time: as-cast specimens at 22.7˚C.

Source: J.E. McDonald, *Time-Dependent Deformation of Concrete Under Multiaxial Stress Conditions*, Technical Report C-75-4, U.S. Army Engineer Waterways Experiment Station, Vicksburg, Mississippi, October 1975.

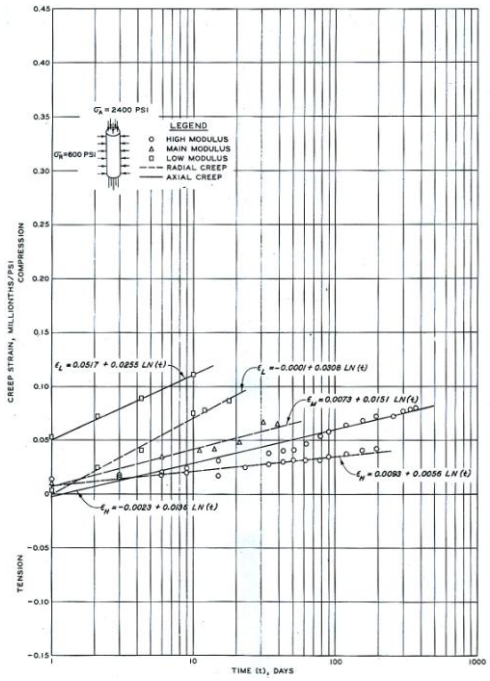

Figure 2.169 Axial and radial creep strain vs time: air-dried specimens at 22.7˚C.

Source: J.E. McDonald, *Time-Dependent Deformation of Concrete Under Multiaxial Stress Conditions*, Technical Report C-75-4, U.S. Army Engineer Waterways Experiment Station, Vicksburg, Mississippi, October 1975.

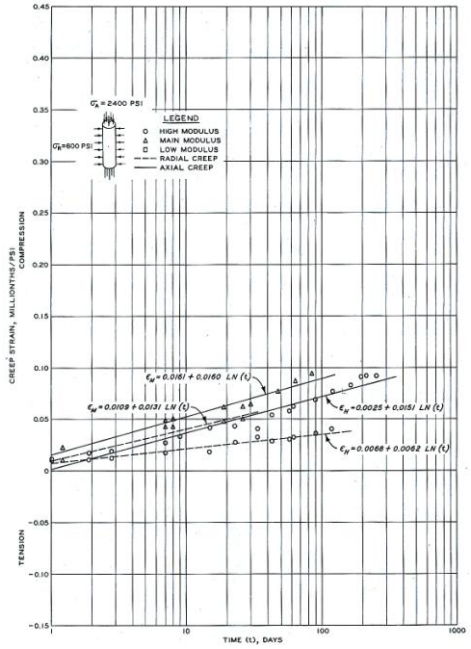

Figure 2.170 Axial and radial creep strain vs time: as-cast specimens at 65.6˚C.

Source: J.E. McDonald, *Time-Dependent Deformation of Concrete Under Multiaxial Stress Conditions*, Technical Report C-75-4, U.S. Army Engineer Waterways Experiment Station, Vicksburg, Mississippi, October 1975.

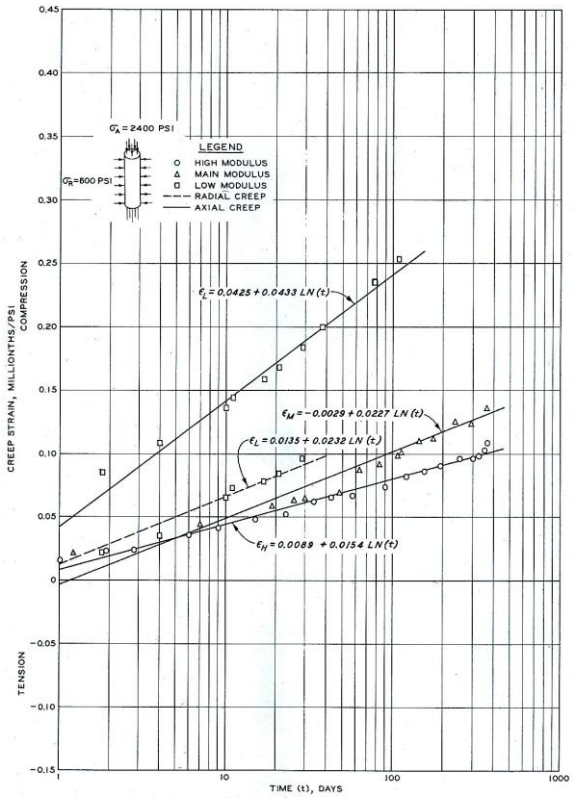

Figure 2.171 Axial and radial creep strain vs time: air-dried specimens at 65.6˚C.

Source: J.E. McDonald, *Time-Dependent Deformation of Concrete Under Multiaxial Stress Conditions*, Technical Report C-75-4, U.S. Army Engineer Waterways Experiment Station, Vicksburg, Mississippi, October 1975.

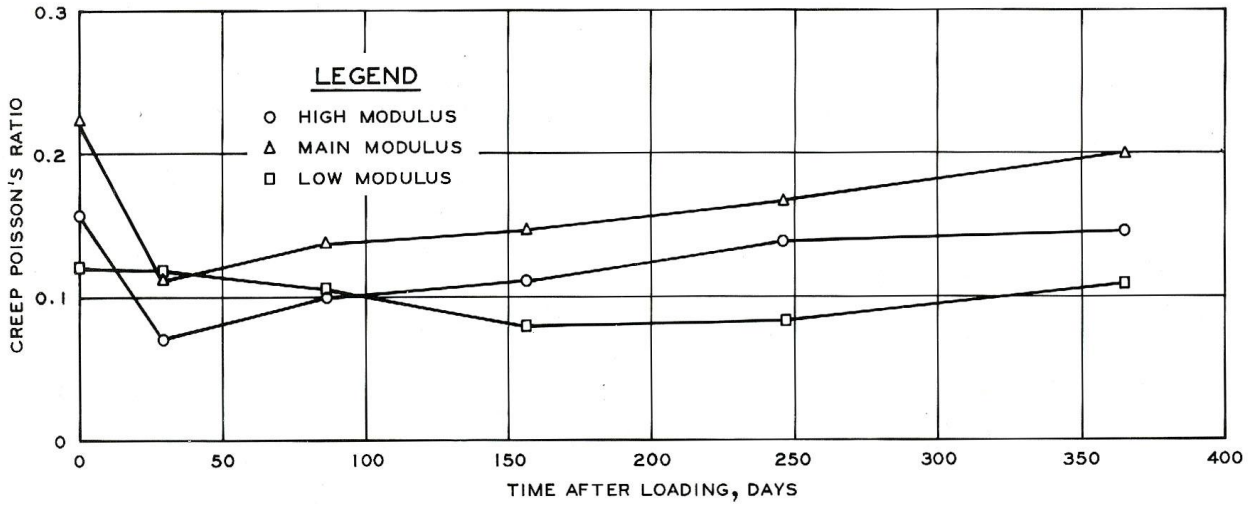

Figure 2.172 Effect of time after loading on creep Poisson's ratio.

Source: J.E. McDonald, *Time-Dependent Deformation of Concrete Under Multiaxial Stress Conditions*, Technical Report C-75-4, U.S. Army Engineer Waterways Experiment Station, Vicksburg, Mississippi, October 1975.

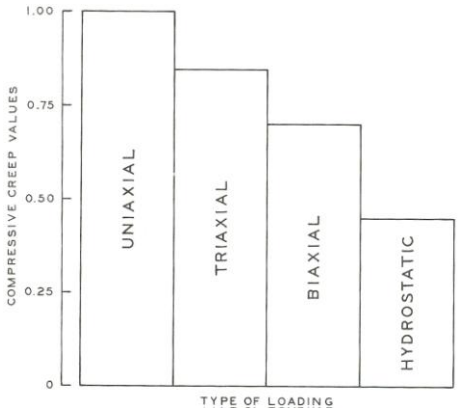

Figure 2.173 Relative effect of type of loading on compressive creep.

Source: J.E. McDonald, *Time-Dependent Deformation of Concrete Under Multiaxial Stress Conditions*, Technical Report C-75-4, U.S. Army Engineer Waterways Experiment Station, Vicksburg, Mississippi, October 1975.

Summary. Investigations of creep behavior at elevated temperature produced the common observation that increasing temperature results in substantially higher creep strains. In general, the specific creep of sealed specimens is shown to be less than that for specimens subjected to some degree of drying. Also, it is apparent that creep will be substantially greater for young concrete in both sealed and unsealed conditions. The phenomenon of a "creep maximum" has been observed by several investigators. This term is somewhat of a misnomer, because the observation is that the specific creep rate reaches a maximum with increasing temperature and is not necessarily accompanied by a corresponding maximum in actual creep strain. The observed maximum has been reported to occur at 50 to 100°C and in one case for a 20% stress-strength ratio at up to 150°C. In fact, not all studies have reported the maximum creep rate effect. Also, in general, most studies have reported that the shape of the curves for creep versus time at high temperatures is similar to those at room temperature. Creep recovery has been observed to be less than the associated creep strain. The degree of creep recovery appears to be independent of temperature but dependent on stress. In addition, shrinkage strains of concrete are reported to be very low for sealed specimens, and, in fact, high temperature exposure has been shown to result in expansion. With regard to the stress-strength ratio, increasing ratios increase creep substantially. Considering the reports on deterioration of compressive strength at temperatures over 100°C for sealed specimens, the stress at which creep becomes structurally significant is substantially decreased. For sustained temperatures above 100°C, the variations in experimental techniques, concrete mixtures, curing, and loading histories prohibit the development of a reliable general conclusion on long-term behavior.

2.2.1.8 Concrete–Steel Reinforcement Bond Strength

Information and Data. In addition to the effect of elevated temperature on the properties of the steel* and concrete, knowledge of the effects of temperature on the bond strength between concrete and steel is important for understanding the response and structural capacity, including residual, of reinforced concrete to thermal loadings. Bond arises primarily from friction and adhesion between concrete and steel and may be affected by the relative magnitude of concrete shrinkage. It is a function of (1) the concrete properties (cement type, admixtures, water-cement ratio), (2) the mechanical properties of the steel (size and spacing of lugs), and (3) rebar position within the concrete member (bond is greater for vertical bars than for horizontal bars). Permissible bond stresses are generally specified as percentages of concrete's compressive strength. Although considerable research has been conducted investigating the bond between concrete and steel at room temperature, results indicating the effect of elevated-temperature exposure are somewhat limited. The general trend for the effect of elevated temperature on the bond strength of concrete to mild steel is shown in Figure 2.174. Concrete aggregates used in the tests were sandstone, andesite, serpentine, and basalt [2.50].

* Appendix B provides information on the effects of elevated temperature on steel reinforcement.

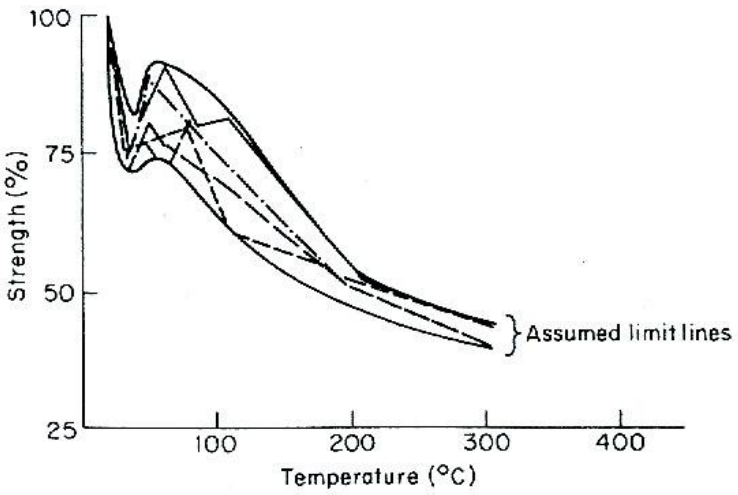

Figure 2.174 Indication of effect of elevated temperature on relative bond strengths of concretes fabricated using different types of conventional aggregate materials.

Source: P.J.E. Sullivan, "The Effects of Temperature on Concrete," Chapter 1 in *Developments in Concrete Technology—1*, F. D. Lydon, Ed., Applied Science Publishers, London, 1979.

Relative residual bond stress was evaluated by testing specimens fabricated from concrete mixes using river gravel and ordinary Portland cement containing embedded plain, round steel bars [2.172]. The specimens were fabricated from four different mixes, moist cured for 28 days at 20˚C, and then stored at 21˚C and 85% relative humidity until tested at an age of 90 days. The specimens were subjected to temperatures from 20˚C to 300˚C for 90 days, permitted to slowly cool to room temperature, and then tested. It was found that the residual bond stress (evaluated at free-end slip of 0.025 mm) after subjecting the specimens to 300°C for 90 d and then cooling to room temperature was only about 50% the reference value before heating (Figure 2.175).

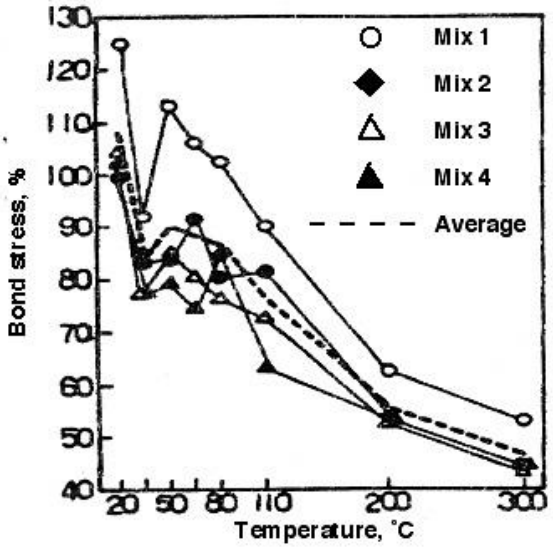

Figure 2.175 Relative residual bond strengths of heated concretes.

Source: H. Kasami, T. Okuno, and S. Yamane, "Properties of Concrete Exposed to Sustained Elevated Temperature," Paper Hl/5 in *Proc. 3rd International Conference on Structural Mechanics in Reactor Technology*, Elsevier Science Publishers, North-Holland, The Netherlands, 1975.

In a similar investigation, normal weight concrete specimens 140 x 140 x 300 mm^3 and fabricated from ordinary Portland cement and river gravel coarse aggregate were tested to investigate the effect of reinforcement type (i.e., 20-mm-diameter plain round bars or ribbed bars) [2.173]. The specimens were heated to temperatures up to 450˚C and then permitted to cool to room temperature prior to testing. Slip at both the loaded and nonloaded ends was measured as a function of load. Figure 2.176 presents bond stress versus temperature results for the ribbed and plain round bars and shows that the ribbed bars experienced a loss of bond strength only above 400°C, but the smooth bars lost strength after only a small temperature increase.

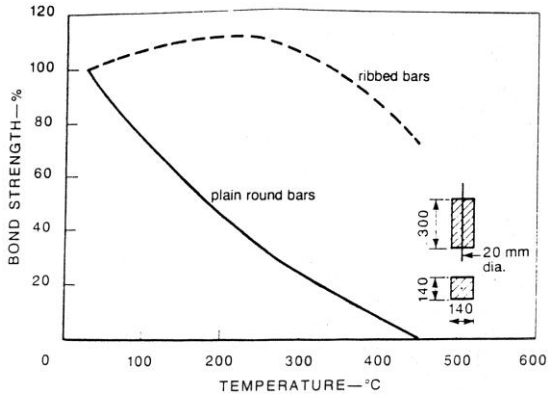

Figure 2.176 Relative residual bond strength of ribbed and plain round bars.

Source: A. F. Milovanov and G. D. Salmanov, "The Influence of High Temperature Upon the Properties of Reinforcing Steels and Upon Bond Strength Between Reinforcement and Concrete," *Issledovanija po zharoupornym betonu I zhelezobetonu,* pp. 203–223, 1954.

A comparison of the effects of elevated temperature on the bond of 14-mm-diameter ribbed and plain round bars embedded in 15 x 15 x 45 cm^3 prisms for two different concrete strengths (17 and 33 MPa) is presented in Figure 2.177 where results are presented relative to those obtained from unheated specimens [2.174]. The concrete mixes consisted of ordinary Portland cement in combination with an aggregate mixture of 60% river gravel and 40% crushed granite. Residual bond strengths after exposure to 500˚C and 700˚C and then cooling for 24 hours at room temperature ranged from about 80% to 50% the unheated values for the ribbed steel bars and about 45% to 25% for the plain round bars.

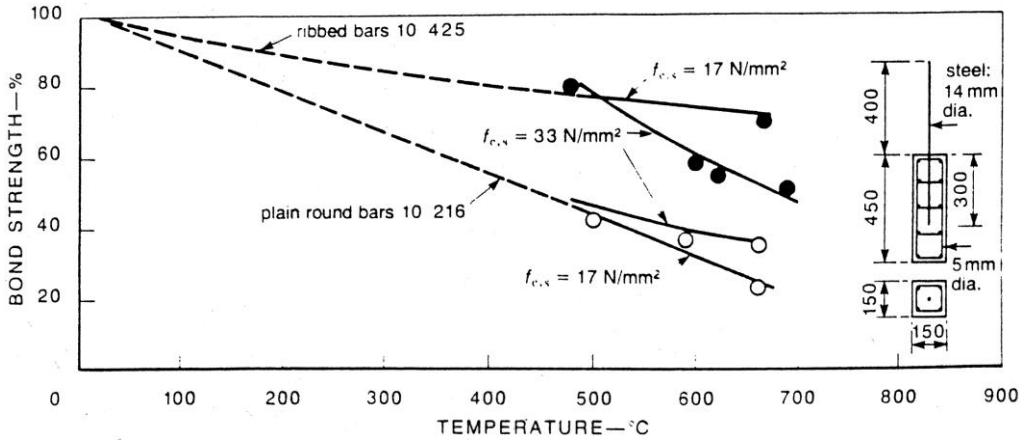

Figure 2.177 Relative residual bond strength of ribbed and plain round bars for different concrete compressive strengths.

Source: H.V. Reichel, "How Fire Affects Steel-to-Concrete Bond," *Building Research and Practice* **6**(3), pp. 176–186, May/June 1978.

Figure 2.178 presents the effect of bar diameter on bond strength after elevated temperature exposure for ribbed and plain round bars [2.175]. The results were obtained from a series of tests involving 280 specimens with varied bar diameters from 8 to 25 mm that were heated to temperatures up to 800˚C, maintained at temperature for 2 hours, and then permitted to slowly cool to room temperature prior to testing. The concrete was fabricated from Danish sea gravel (mixture of quartz, granite, and limestone) and had a compressive strength of 20 MPa. The bond strength as a percentage of the concrete compressive strength was higher for the ribbed bars than the plain round bars, and at temperatures up to 400˚C was about 65% the concrete compressive strength.

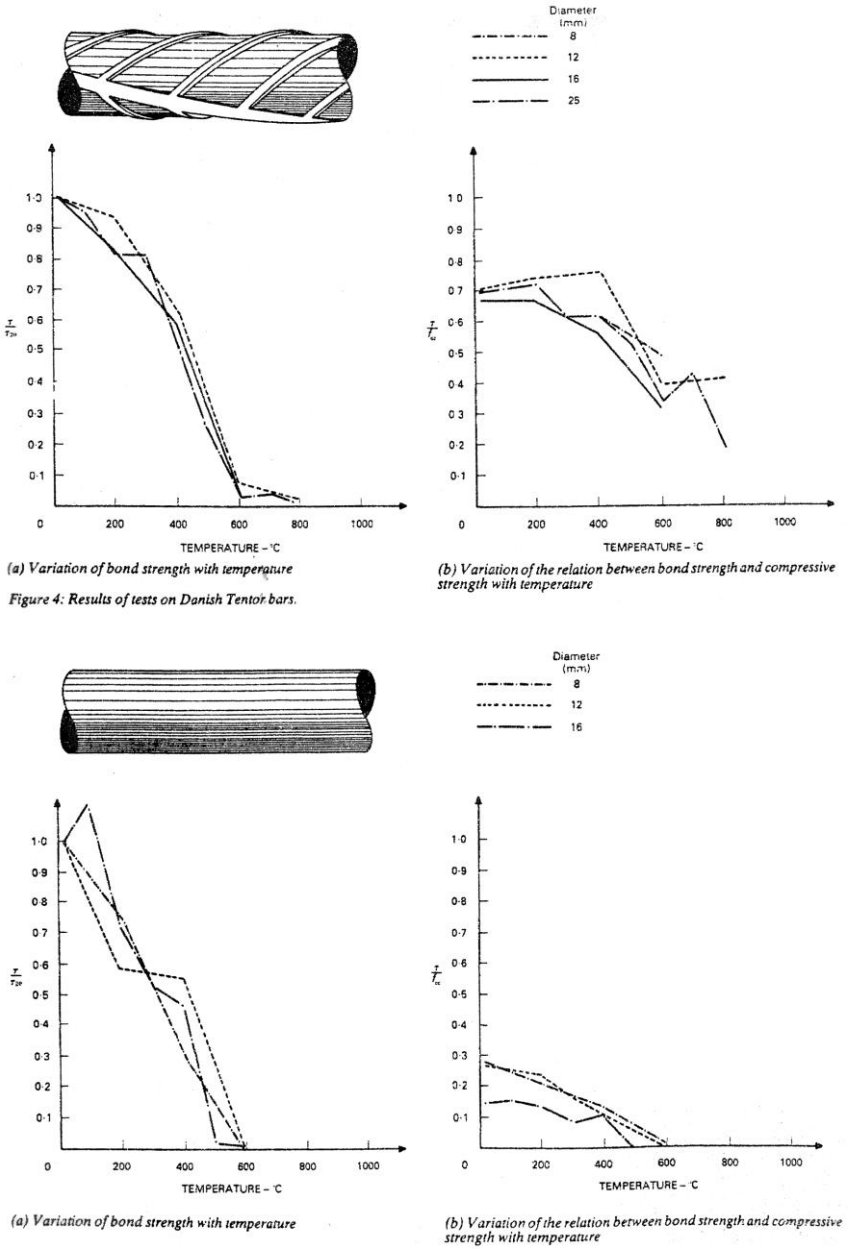

Figure 2.178 Effect of bar diameter on bond strength after elevated-temperature exposure for ribbed and plain round bars.

Source: K. Hertz, "The Anchorage Capacity of Reinforcing Bars at Normal and High Temperatures," *Magazine of Concrete Research* **34**(121), pp. 213–220, December 1982.

In another investigation the bond strength at high temperature for ribbed steel bars, plain round bars, and deformed prestressing bars was evaluated by testing cylindrical concrete pull-out specimens 191-mm-high by 172-mm-diameter [2.176]. The 16-mm maximum size siliceous aggregate concrete mix had cube compressive strengths of 48.0 to 60.9 N/mm^2 at 28-days and 50.7 to 63.9 N/mm^2 at testing (150 to 600 days age). The specimens were heated to the desired test temperature, held at temperature for 3 hours, and then tested. Slip at both the loaded and nonloaded ends was measured as a function of applied load. Bond stress-slip results as a function of temperature are presented in Figure 2.179 for 16-mm diameter cold deformed steel and 7.5-mm diameter prestressing steel reinforcement. Figure 2.180 presents bond stress-slip results for heavily rusted plain 8-mm diameter round bars of cold-deformed steel, and relative bond strength-temperature results for plain round mild steel bars, cold deformed steel, and shaped prestressing steel. Results of the investigation indicate that loss of bond strength for ribbed bars at constant elevated temperature is of the same order of magnitude as loss of high-temperature compressive strength and at same temperatures round plain bars exhibit a sharper decrease in bond strength than ribbed bars. Results for the rusted plain mild steel round bars were not significantly affected by elevated temperatures up to 200˚C, but at temperatures of 300˚C and above the bond stress at a given slip decreased significantly.

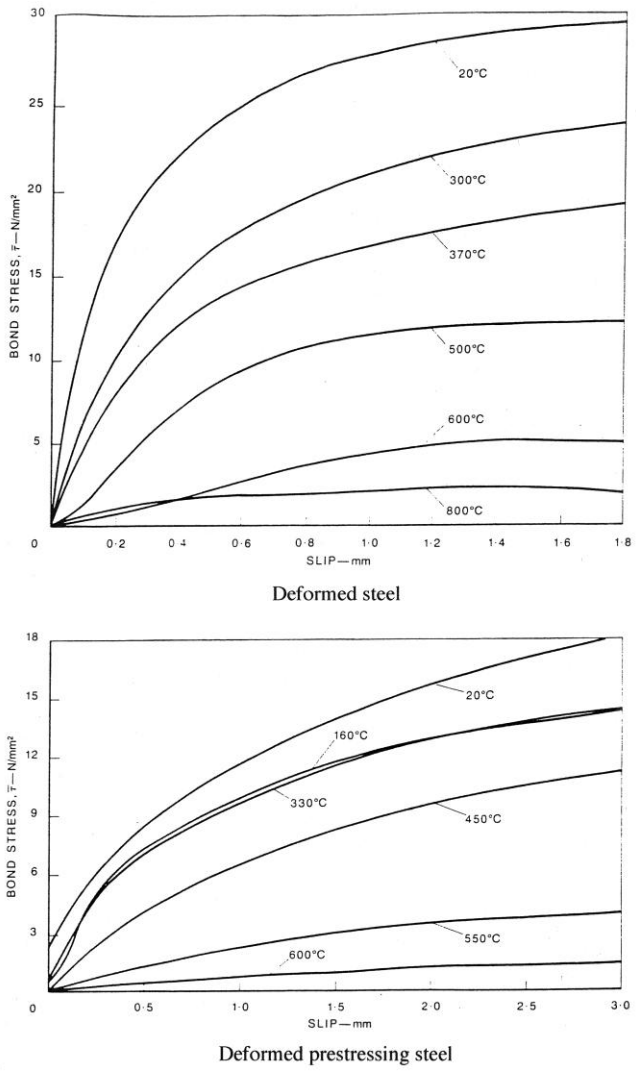

Figure 2.179 Bond-slip relationship at elevated temperature for cold deformed steel and prestressing steel.

Source: U. Diederichs and U. Schneider, "Bond Strength at High Temperature," *Magazine of Concrete Research* **33**(115), pp. 75–83, June 1981.

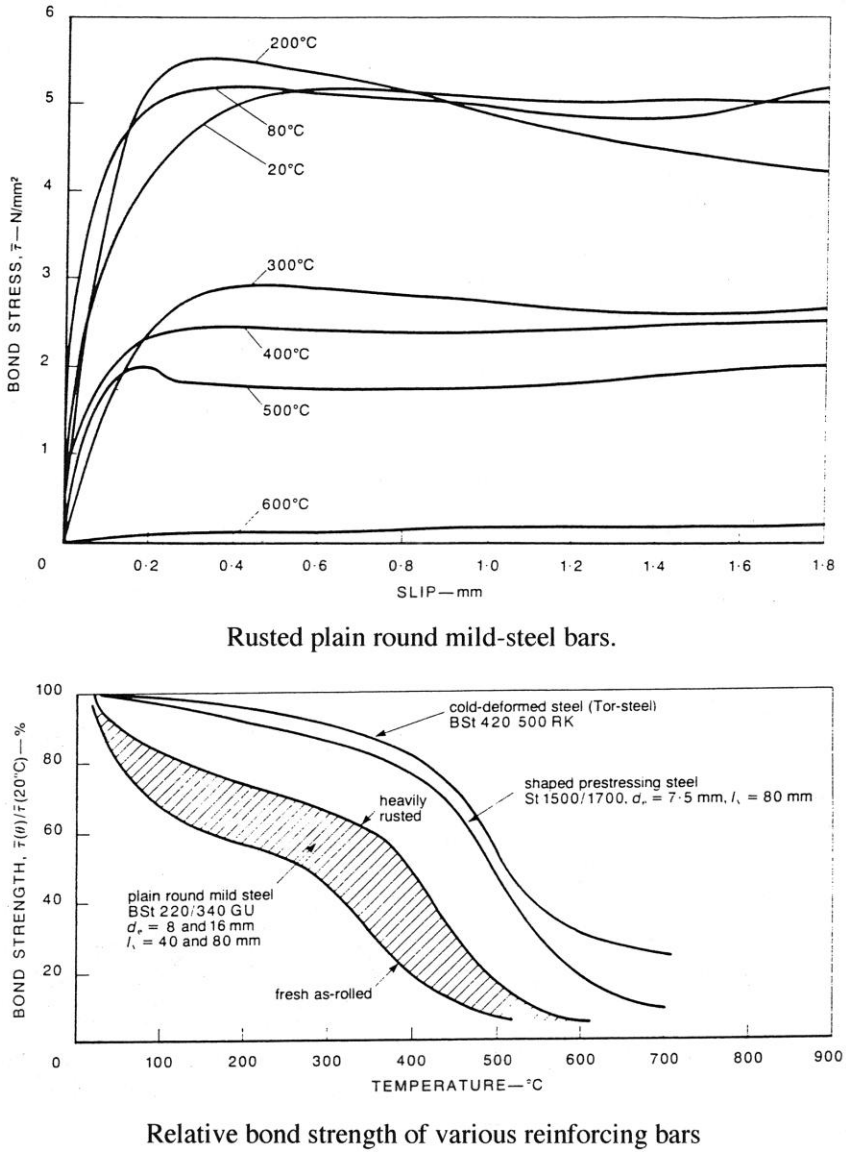

Figure 2.180 Relative bond strength as a function of temperature.

Source: U. Diederichs and U. Schneider, "Bond Strength at High Temperature," *Magazine of Concrete Research* **33**(115), pp. 75–83, June 1981.

Concrete specimens 15 x 15 x 20 cm^3 were used to evaluate rebar bond strength [2.177]. The concrete mix used ordinary Type I Portland cement and had a compressive strength of 49.2 MPa after water curing for 28 days. Two No. 3 reinforcing bars were embedded vertically in each specimen from both ends with embedded lengths of 6 and 8 cm, respectively. After water curing the specimens were air dried for a week and then subjected to elevated temperatures up to 550˚C. After attaining the desired soak temperature, the specimens were maintained at this temperature for different periods ranging from 30 minutes to 180 minutes, after which they were permitted to slowly cool to room temperature. Testing was initiated 24 hours after reaching room temperature. Figure 2.181 presents relative residual bond strength results as function of exposure time for several different soak temperatures. A substantial decrease in bond strength was observed at temperatures greater than 200°C, and the bond strength decreased with increasing exposure time. A procedure for experimentally and numerically relating the ratio of residual bond strength to temperature and exposure time, and a procedure for integrating changes in bond strength due to temperature fluctuations to predict final residual bond strength was proposed.

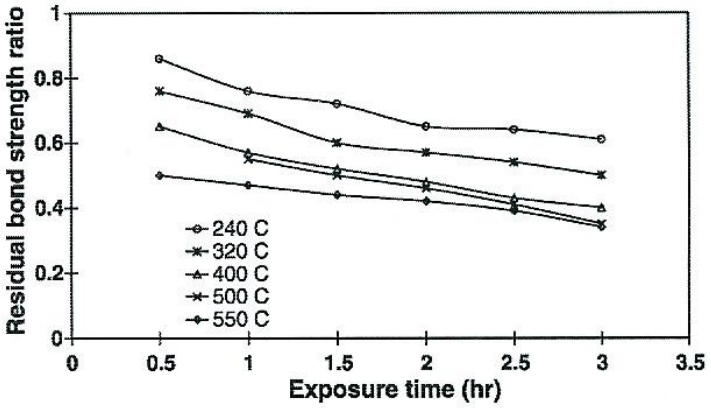

Figure 2.181 The effect of elevated-temperature exposure time on the relative residual bond strength of No. 3 bars embedded in a concrete cube.

Source: C-H. Chiang and C-L. Tsai, "Time-Temperature Analysis of Bond Strength of a Rebar After Fire Exposure," *Cement and Concrete Research* **33**, pp. 1651–1654, 2003.

Figure 2.182 presents the influence of type aggregate on the relative bond strength [2.178]. The type of aggregate is one of the main factors determining the high temperature bond strength. The lower the thermal strain of concrete the higher the bond strength at elevated temperature.

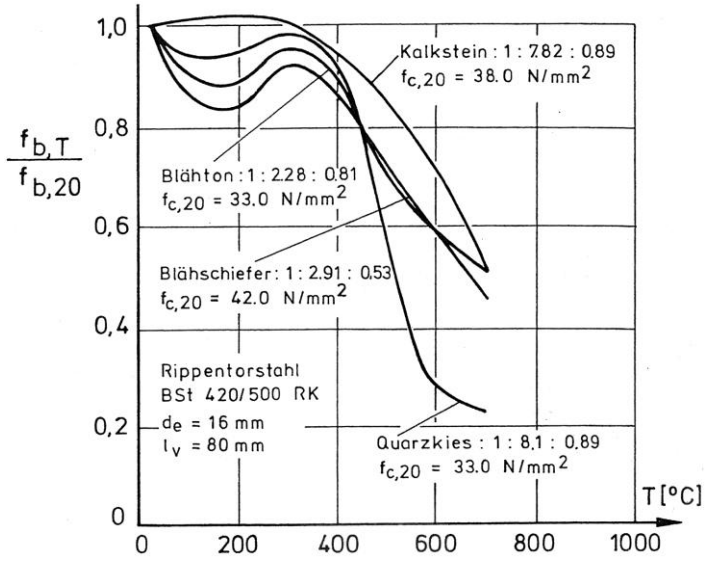

Figure 2.182 Bond between concrete and deformed bars exposed to high temperature.

Source: H. Sager and F.S. Rostasy, "High Temperature Behavior of Reinforcing and Prestressing Steels," *Sonderforschungs-Bereich* **148**, Part II, pp. 51–53, Technical Universitat Braunschweig, Germany, 1980.

Figure 2.183 presents the affect of curing conditions (e.g., in water unsealed, sealed, in air unsealed) prior to elevated-temperature exposure on the relative variation in bond strength at start of pull-out for a hard sandstone aggregate concrete after various heating periods at 175°C [2.97]. Specimens 150 x 150 x 150 mm^3 containing a D25 rebar embedded 10 cm were used for the tests. The bond strength of specimens unsealed during heating exhibited up to about a 30% decline for heating exposures of 3 d or less, but specimens that were sealed exhibited practically

no reduction as a result of temperature exposure. Prolonged elevated-temperature exposure for sealed specimens exhibited a positive effect on the bond strength, and for the unsealed specimens a recovery in bond strength to the point that after 91-d exposure it was reduced by 10 to 15% relative to control results. Other results also indicate that the loss in bond strength between concrete and steel reinforcement at temperatures < 65°C is small (≤15%) [2.176,2.179].

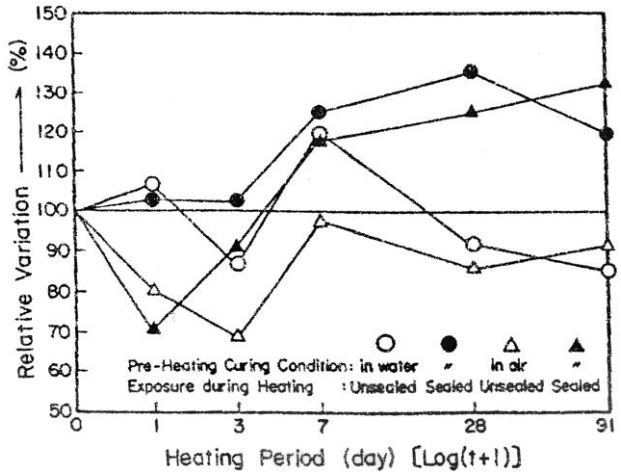

Figure 2.183 Relative variation in bond strength at start of pull-out for a hard sandstone aggregate concrete after various heating periods at 175°C.

Source: K. Hirano, K. Ohmatsuzawa, T. Takeda, S. Nakane, T. Kawaguchi, and K. Nagao, "Physical Properties of Concrete Subjected to High Temperature for MONJU," Paper P2-25, Power Reactor and Nuclear Fuel Development Corporation, Tokyo, Japan.

The effect of elevated temperature on the residual bond strength of a siliceous aggregate ordinary Portland cement concrete was evaluated by testing 10-cm-diameter by 20-cm-long cylindrical bond pull-out specimens [2.54]. The concrete strength just prior to initiation of heating (age of about 26 months) was 46.7 MPa. The specimens were heated to soak temperatures of 100˚, 300˚, or 450˚C, maintained at temperature for 72 hours, and then slowly cooled to room temperature prior to testing. Figure 2.184 presents residual bond strength results relative to those for unheated specimens, as well as residual results for weight, compressive strength, dynamic modulus of

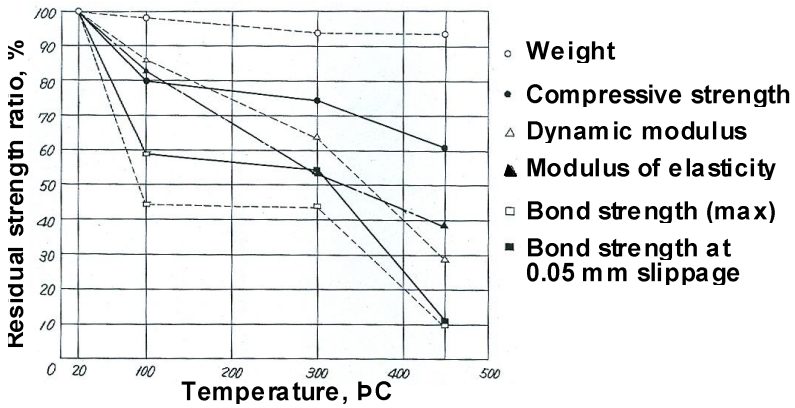

Figure 2.184 Effect of elevated temperature on residual strength ratios.

Source: T. Harada, T. Takeda, S, Yamane, and F, Furumura, "Strength, Elasticity and Thermal Properties of Concrete Subjected to Elevated Temperatures," Paper SP-34-21in *Concrete for Nuclear Reactors*, pp. 377-406, American Concrete Institute, Farmington Hills, Michigan, 1972.

elasticity, and static modulus of elasticity. The relative residual bond strength at time of free-end slippage of 0.05 mm was approximately 44% at 100˚ to 300˚C, and 10% at 450˚C. The relative residual maximum bond strength was approximately 50 to 60% at 100˚ to 300˚C, and 10% at 450˚C. It was concluded that the percentage reduction in bond strength due to elevated temperature exposure was greater than that for the compressive strength.

The response of bond in reinforced concrete to high temperature was investigated for four test conditions: (1) stressed during heating (3.7 MPa) and loaded to failure while hot, (2) stressed during heating (3.7 MPa) and loaded to failure after cooling, (3) no applied stress during heating and loaded to failure while hot, and (4) no stress during heating and loaded to failure after cooling [2.180]. The effect of cover depth was also investigated. Cylindrical specimens 300 mm in length by various diameters according to cover depth were fabricated from a 19-mm maximum size natural gravel aggregate, ordinary Portland cement, and had a cube strength of 35.0 MPa after curing in air for 3 months. Bonded within the central portion of each specimen over a 32-mm depth was a 16-mm diameter Tor bar (high yield strength deformed bar). A standard cover depth of 55 mm was used except cover depths of 25, 32, and 46 mm were also investigated for test condition 2. Specimens were heated to temperatures up to 750˚C, held at temperature for one hour, and then tested or permitted to cool to room temperature where they remained for 24 hours prior to testing. Figure 2.185 presents bond stress-slip curves for various temperatures for specimens tested using test condition 2. A comparison of hot and residual maximum bond stress and temperature

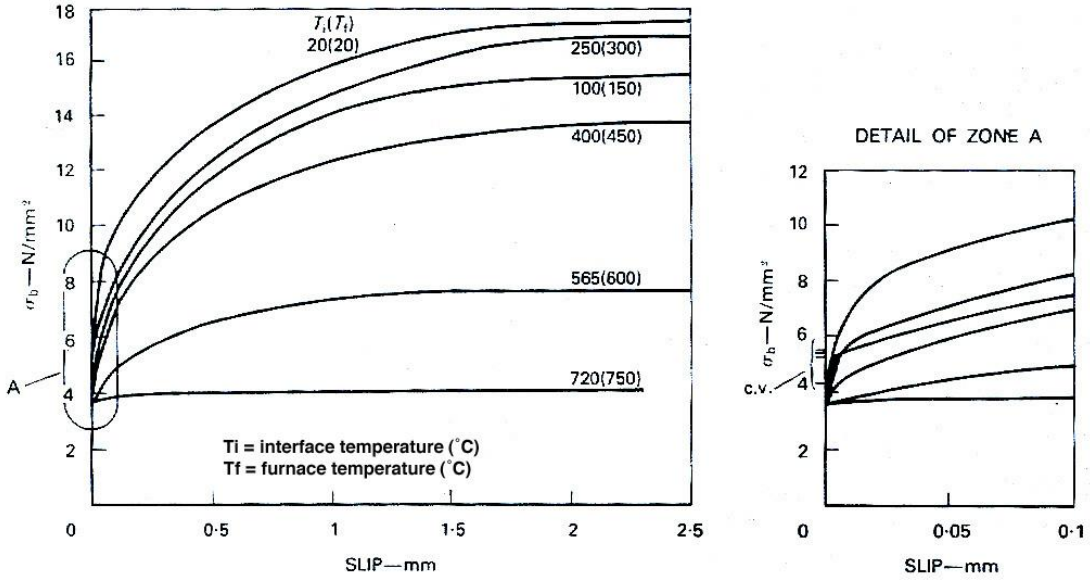

Figure 2.185 Residual bond stress vs slip relationships at various temperatures: 16-mm diameter bars with 55 mm cover and stressed at 3.7 MPa while heated.

Source: P.D. Morley and R. Royles, "Response of the Bond in Reinforced Concrete to High Temperatures," *Magazine of Concrete Research* **35**(123), pp. 67-74, June 1983.

results is presented in Figure 2.186. These results tend to indicate that specimens heated with a steady-state bond stress applied provided a slightly improved performance relative to results obtained from specimens heated under a no-stress condition due to restraint applied by loading. The effect of cover on the ratio of residual maximum bond stress to maximum bond stress at 20˚C with a steady-state stress of 3.7 MPa held for 24 hours while heated is presented in Figure 2.187. The maximum bond stress and the maximum bond slip both decreased as the cover depth decreased. The large difference in slip between smaller and larger cover depths was caused by the difference in mode of failure experienced. Specimens with larger cover depths exhibited a greater resistance to splitting permitting greater slip to take place prior to concrete failure. General conclusions of the study were that the reduction in bond strength with temperature was greater than that for the concrete compressive strength, crushing of concrete immediately beneath the rebar ribs was the cause of a critical value in the bond stress-slip curve, and the bond stress was dependent on concrete strength.

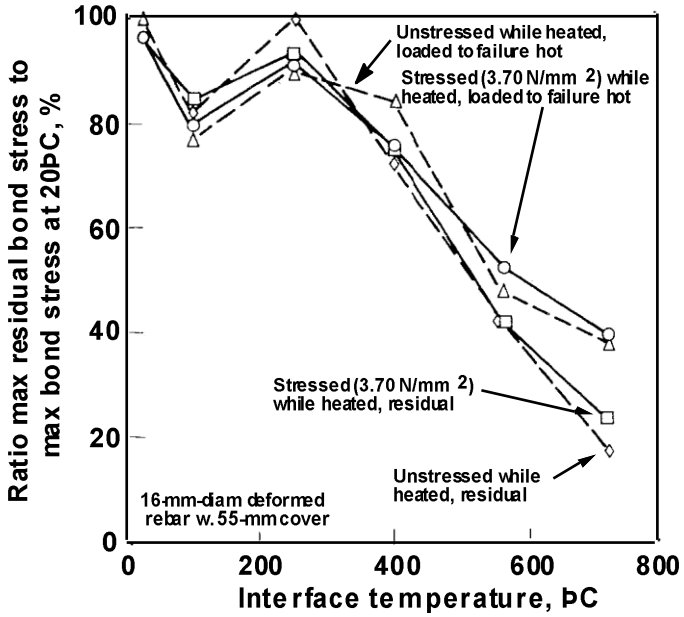

Figure 2.186 Stressed and unstressed hot and residual bond stress results at various temperatures.

Source: P.D. Morley and R. Royles, "Response of the Bond in Reinforced Concrete to High Temperatures," *Magazine of Concrete Research* **35**(123), pp. 67-74, June 1983.

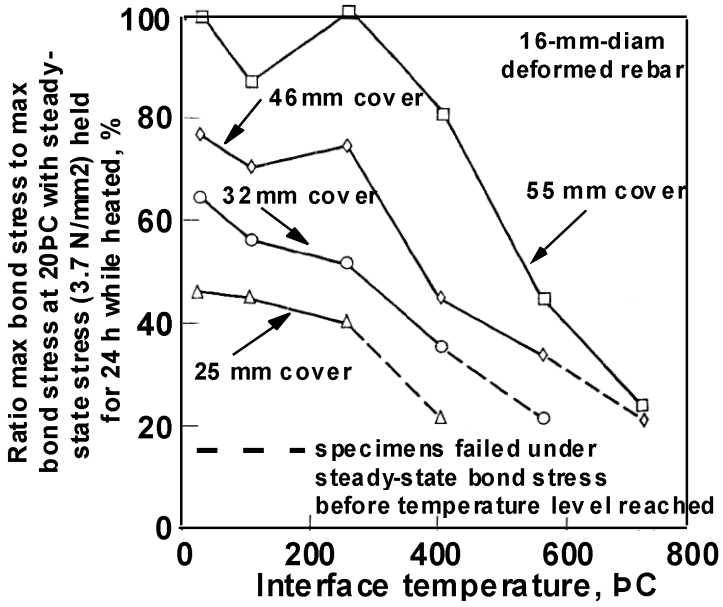

Figure 2.187 Variation of maximum bond stress with temperature for different cover depths.

Source: P.D. Morley and R. Royles, "Response of the Bond in Reinforced Concrete to High Temperatures," *Magazine of Concrete Research* **35**(123), pp. 67-74, June 1983.

The effect of load cycling on the ratio of maximum residual bond stress to maximum bond stress at 20˚C was investigated [2.181]. Cylindrical test specimens 126-mm diameter by 300-mm long containing a 15-mm diameter rebar embedded over a length of 32 mm within the central portion of the cylinder were used. Before loading to failure, the effect of cycling the bond stress twenty times between 1.0 and 3.7 MPa was examined. Figure 2.188

presents the effect of load cycling on residual bond strength for deformed rebar. Increasing the temperature caused the bond stress-slip relationship to decrease and produced irreversible slip, particularly in the temperature range 250˚ to 450˚C indicating a significant decrease in bond performance. The dashed line in the figure to 720˚C indicates that these specimens failed before the sequence of twenty load cycles and loading to failure had been completed.

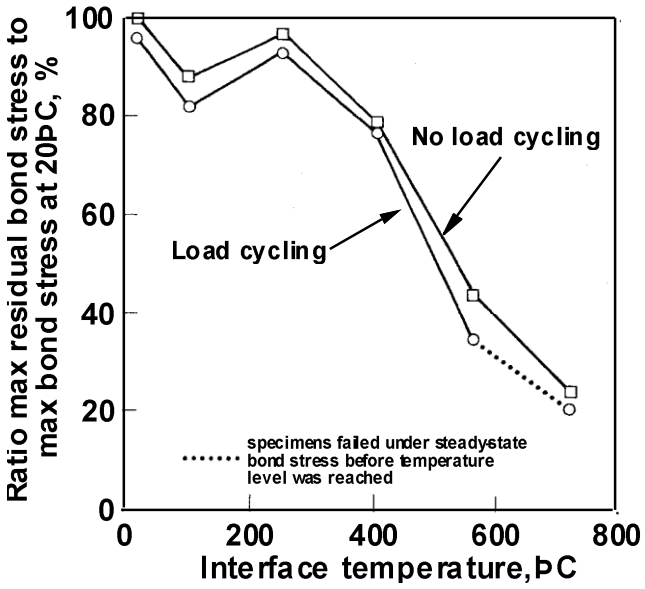

Figure 2.188 Effect of load cycling on the residual bond strength for 16-mm-diameter deformed rebar.

Source: R. Royles and P.D. Morley, "Further Responses to the Bond in Reinforced Concrete to High Temperatures," *Magazine of Concrete Research* 35(124), pp. 157-163, September 1983.

The residual performance of bond between high-strength pozzolanic concrete and reinforcing steel has been investigated [2.182]. Cylindrical pullout specimens either 82- or 100-mm diameter by 150-mm long were cast with an 18-mm diameter Grade 60 deformed steel rebar embedded along the entire specimen length. Concrete mixes used a 19-mm maximum size limestone coarse aggregate and ordinary Portland cement or a combination of ordinary Portland cement and natural pozzolan. Four concrete mixes were used in which the ordinary Portland cement was replaced with natural pozzolan in weight percentages of either 0, 10, 15, or 25. Concrete compressive strengths for these mixes were 73.1, 66.0, 67.0, and 66.1 MPa, respectively. After curing in water at 23˚C for 40 days, the specimens were heated to temperatures of either 600˚ or 800˚C where they remained for 1 hour prior to permitting them to slowly cool to room temperature over about a 26 hour period. The bond behavior of the pullout specimens was evaluated using a fixture that applied a constant displacement rate of 0.01 mm/s with slippage monitored by two LVDTs. Compressive strength results obtained from companion 100-mm-cube test specimens exhibited almost equal strength reduction percentages (i.e., 39.2 to 40.8%) at 600˚C, except for the specimens in which 25% of the ordinary Portland cement was replaced by natural pozzolans (48.2% reduction). At 800˚C, however, the percentage reduction in compressive strength increased as the percentage of pozzolan increased. Post-test examination of specimen surfaces indicated that cracking and the maximum crack widths at 800˚C were greater than that observed at 600˚C. Figure 2.189 presents residual bond stress versus free-end slip results obtained after exposure to either 600˚ or 800˚C for concretes having different natural pozzolan contents. The curves corresponding to unheated specimens exhibited almost linear response at low slip ranges before becoming nonlinear near failure. Bond strength was significantly reduced after exposure to temperatures of 600˚ and 800˚C, with the reduction higher for the 800˚C value (e.g., up to 74% versus up to 24%). Curves for the specimens that had been heated exhibited nonlinear behavior over the entire slip range with a varying rate of stress change. This was attributed to cracks that formed at low to medium pullout loads that due to heating tended to close permitting greater slippage. Once the cracks closed resistance to slippage increased as did the pullout load required for further slippage. Near failure local crushing of the concrete occurred near the rebar ribs resulting in significant slippage followed by a sudden splitting failure of the concrete along the rebars, Relative to natural pozzolan content, at 600˚C the percentage reduction in bond strength increased as the natural pozzolan content increased.

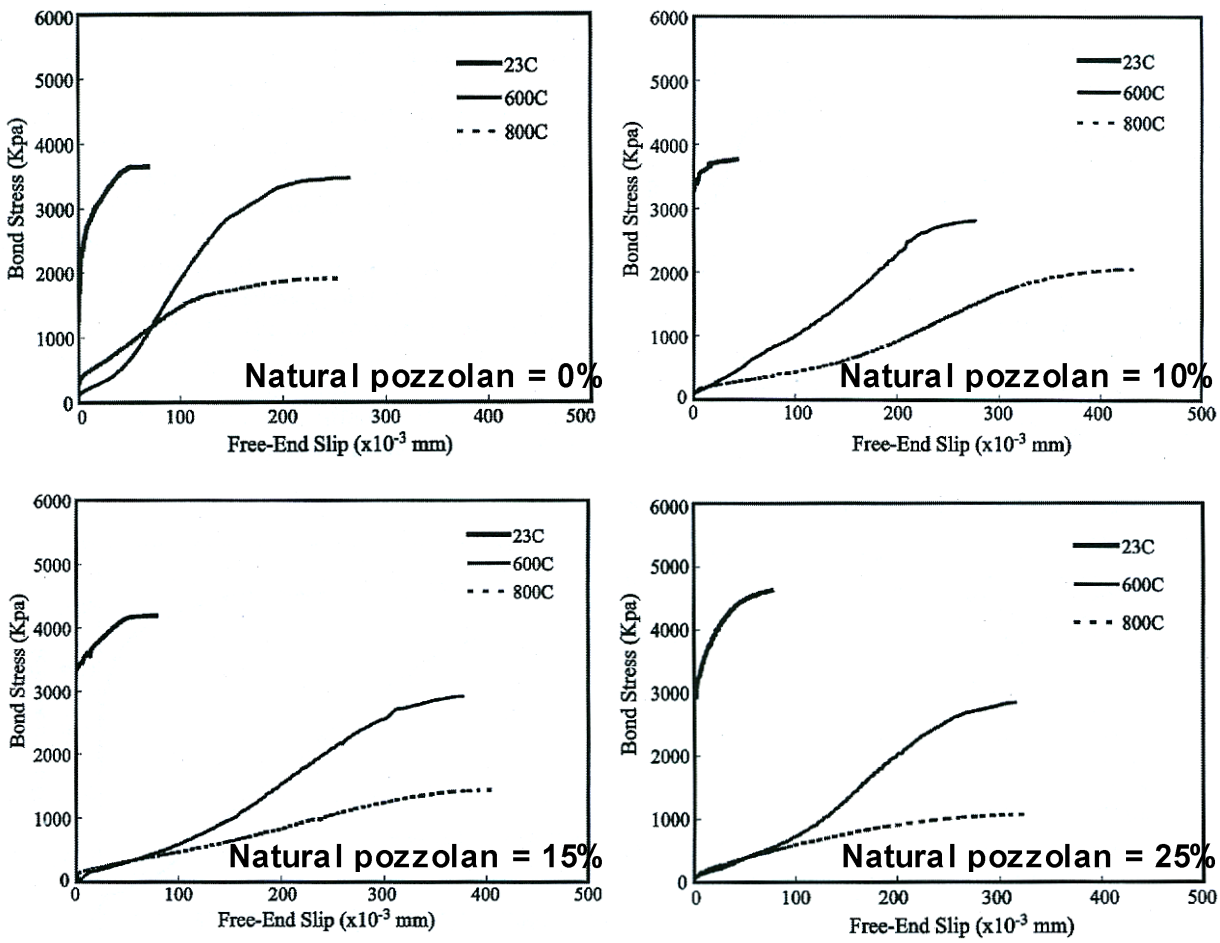

Figure 2.189 Effect of natural pozzolan content on residual bond stress versus slip results.

Source: R.H. Haddad and L.G. Shannis, "Post-Fire Behavior of Bond Between High Strength Pozzolanic Concrete and Reinforcing Steel," *Construction and Building Materials* **18**, pp. 425-435, 2004.

The bond behavior between fiber-reinforced concrete and 20-mm diameter reinforcing steel bars under elevated temperature exposure has been investigated [2.129]. Modified pullout specimens 100 x 100 x 400 mm^3 were prepared using high-strength ordinary Type I Portland cement concrete with 19-mm maximum size basalt coarse aggregate, silica sand, and different volumetric mixtures of three types of fibers (i.e., brass-coated steel, hooked steel, and high performance polypropylene) with a total fiber volume of 2%. Reference concrete compressive strengths were 77.3, 89.8, 85.5, 93.75, and 103.6 MPa for plain concrete, hooked steel fibrous concrete (HS), hooked steel-high performance polypropylene fibrous concrete (HSHP), hooked steel-brass coated steel fibrous concrete (HBCS), and brass coated steel fibrous concrete (BCS), respectively. Pullout specimens contained Grade 60 deformed rebars having a diameter of 20 mm. Specimens were cured for 28 days at 40˚C and then placed into laboratory air at 60% relative humidity and 23˚C prior to heat treatment. Heat-treated specimens were then subjected to temperatures ranging from 350˚ to 700˚C for 2 hours and then permitted to slowly cool to room temperature prior to testing. The presence of fibers in the concrete mix reduced the length and intensity of cracks in the temperature range of 350˚ to 500˚C, but had limited effect at higher temperatures because of loss of bond to the concrete matrix. The contribution of fibers to maintaining residual compressive and tensile strengths was limited in the temperature range of 350˚ to 600˚C but was significant at 700˚C. Figure 2.190 presents bond stress versus free-end slip results for plain concrete, hooked steel fiber concrete, hooked steel-high performance polypropylene fibrous concrete, hooked steel-brass coated steel fibrous concrete, and brass coated steel fibrous concrete. Results exhibit linear behavior up to about 40% of ultimate bond stress, and from then on a nonlinear response. Exposure of the

modified bond pullout specimens fabricated using different combinations of fibers to temperatures in the range of 500˚ to 700˚C resulted in softening of the bond stress versus free-slip curves. Response was determined by the state of the fibrous concrete materials with negligible effect provided by steel rebars. At elevated temperatures cracks increased to reduce the confinement around the rebars resulting in a reduction in bond stress and an increase in free-end slip relative to lower temperatures (e.g., 350˚C). Figure 2.191 summarizes relative residual bond strength versus temperature results obtained for the plain and fibrous concrete mixes. As noted in the figure, the residual bond strength decreases with increasing exposure temperature with the largest decrease occurring at 500˚C. The decrease in bond strength resulted from an increase in intensity, width, and extension of cracks with temperature resulting in reduced confinement of steel rebar. In the temperature range of 350˚ to 600˚C the fibrous concrete mixes exhibited greater relative residual bond strength relative to the plain concrete mix.

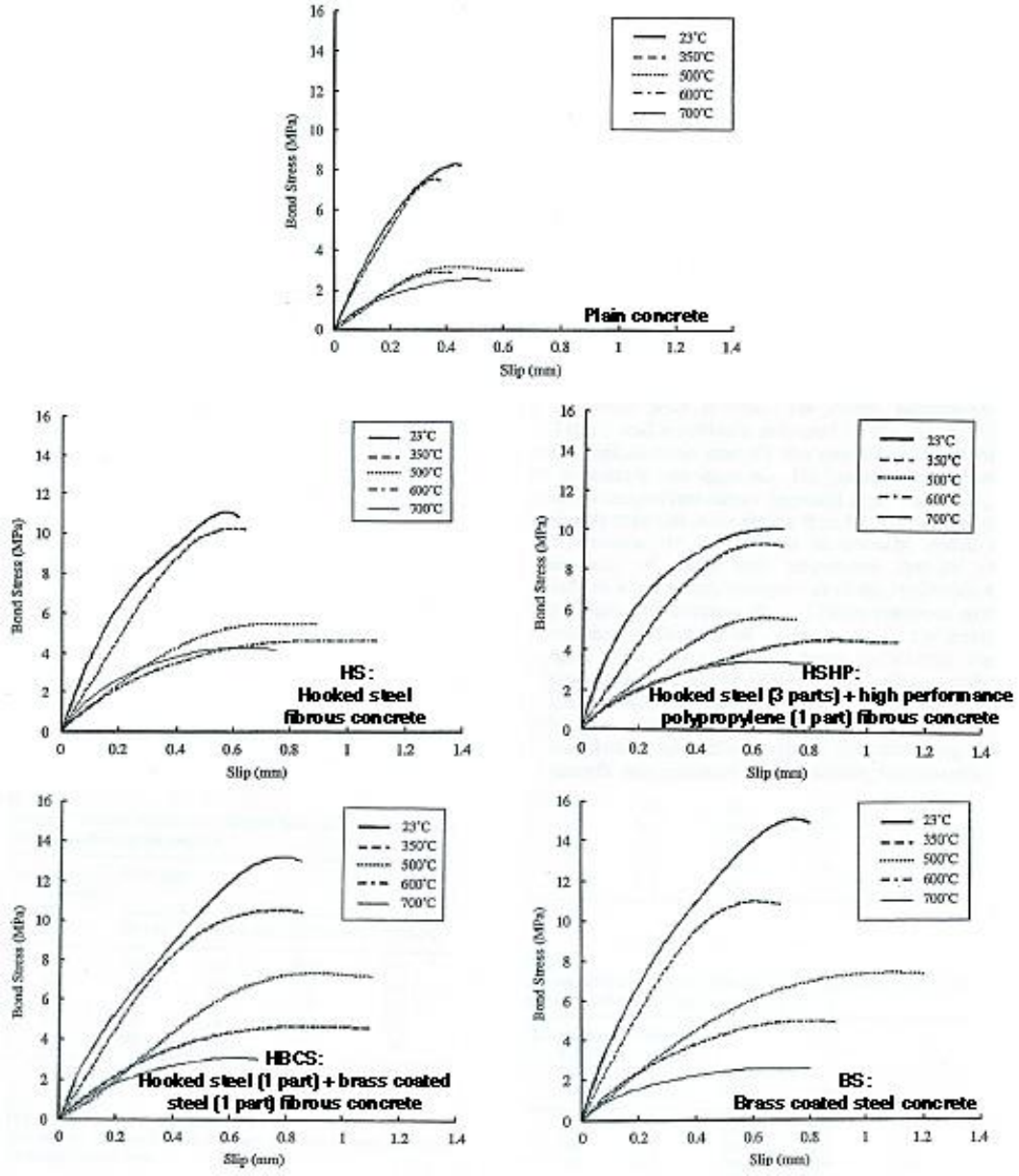

Figure 2.190 Effect of fiber type on residual bond stress versus slip results.

Source: R.H. Haddad, R.J. Al-Saleh, and N.M. Al-Akhras, "Effect of Elevated Temperature on Bond Between Steel Reinforcement and Fiber Reinforced Concrete," *Fire Safety Journal* **43**(5), pp. 334-343, July 2008.

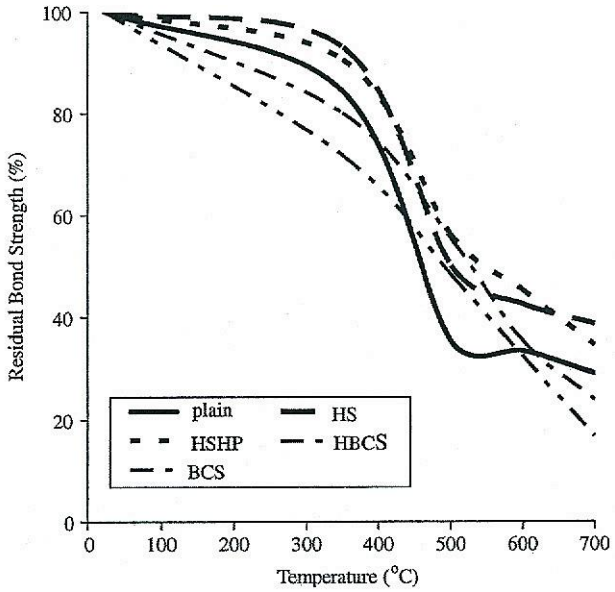

Figure 2.191 Effect of fiber type on residual bond stress versus temperature results.

Source: R.H. Haddad, R.J. Al-Saleh, and N.M. Al-Akhras, "Effect of Elevated Temperature on Bond Between Steel Reinforcement and Fiber Reinforced Concrete," *Fire Safety Journal* **43**(5), pp. 334-343, July 2008.

Examples of Constitutive Relationships for Bond Stress Between Concrete and Steel. The bond strength between concrete and steel decreases with increasing temperature. The magnitude of the loss is a function of the type of concrete and the reinforcement sttl surface condition (i.e., smooth, deformed, or degree of rusting) [2.183]. An estimate of the ultimate bond stress as a function of temperature can be obtained from [2.184]:

$$\tau_u^T = [2.7438(T/100)^2 - 3.322(T/10) + 105.881]x10^{-2}\tau_u \tag{2.64}$$

where τ_u^T and τ_u represent the ultimate bond strength at elevated and room temperature, respectively.

An analytical model has been developed for bond stress versus free-end slip [2.129]. It is proposed that the ascending part of the bond stress versus free-end slip curve can be described by:

$$\frac{\tau}{\tau_1} = \left(\frac{S}{S_1}\right)^n, \tag{2.65}$$

where τ_1 is the ultimate bond strength, S_1 the corresponding slip, and n is a curve-fitting parameter that must be less than 1. A nonlinear empirical model has been developed that relates the percentage residual bond to exposure temperature for the data presented in Figure 2.191 [2.129]:

$$RBS = k\frac{\left\lfloor 1-\left(-0.0035\sqrt{T}-0.52\right)^2\right\rfloor}{\left[1+\left(-0.0035T-0.52\right)^2\right]}, \tag{2.66}$$

where RBS is the residual bond strength, T the exposure temperature for T > 23˚C, and k a constant depending on the type of concrete mixture.

Summary. Conclusions from results presented in the literature specific to concrete-reinforcing steel bond at elevated temperature are that the test procedure and shape of specimen have a significant influence on test results, ribbed bars

exhibit improved performance relative to plain round bars, surface roughness increases the performance for plain round bars, the bond strength decreases as the exposure temperature increases, at high temperatures (≥200°C) the time at temperature affects the bond strength, the diameter of ribbed steel reinforcement (8 to 25 mm) does not have a significant effect on bond strength, residual bond strengths of specimens sealed during temperature exposure perform better than unsealed specimens (≤175°C), curing conditions are important at moderate elevated-temperature exposures (≤400°C), residual bond strength is lower than bond strength obtained at temperature, a clear influence of the water-cement ratio and concrete strength on bond strength at elevated-temperature exposure has not been observed, the type of aggregate has a significant effect on the high-temperature bond strength, at temperatures < 65°C the bond strength is relatively unaffected, the smaller the aggregate size in relation to the bar diameter the more workable will be the concrete and the greater the chances of obtaining good adhesion between the cement paste and steel, the maximum bond stress and the maximum bond slip decrease as the cover depth decreases (tensile strength of the concrete surrounding a reinforcing bar is enhanced as the concrete cover increases because a larger amount of concrete can be compacted more readily and the large difference in slip between smaller and larger cover depths is caused by the difference in mode of failure experienced), load cycling causes a decrease in the maximum bond stress, reduction in bond strength due to elevated temperature exposure appears to be greater for concretes having ordinary Portland cement contents replaced by natural pozzolans in amounts greater than 10% the weight, incorporation of fibers into the concrete mix has been shown to provide improved bond stress versus free-end slip results by limiting concrete cracking and reducing spalling, and the reduction in bond strength with temperature is greater than that for the concrete compressive strength.

2.2.1.9 Fracture Energy and Fracture Toughness

Information and Data. The effects of elevated temperature related to exposure period and curing age on the residual fracture properties of a normal- and a high-strength concrete were investigated using three-point bending tests of preheated beams [2.185]. The 500 x 100 x 100 mm^3 beams were notched with a diamond saw to a depth of 50 mm prior to heating. Rapid-hardening Portland cement in conjunction with a 20-mm maximum size graded gravel and sand were used to fabricate the test specimens. Water-cement ratios (by weight) used for the normal- and high-strength concretes were 0.54 and 0.30, and 29-day compressive strengths were 57.4 and 77.6 MPa, respectively. Specimens were cured in water for seven days and then placed into the laboratory environment until testing. Most beams were exposed to temperatures from between 100˚ and 600˚C for 12 hours at 14 days, while some of the normal-strength beams were heated either for various exposure periods up to 168 hours at 14 days age or for 12 hours at ages of 7, 28, and 90 days. Residual fracture energy (G_f), defined as total energy dissipated over a unit crack area, as a function of exposure temperature is presented in Figure 2.192 for both concretes (heating for 12 hours at an age of 14 days). Results show that the residual fracture energy increases up to about 300˚C and then decreases with increasing temperature. The initial increase was attributed to additional cement hydration and the

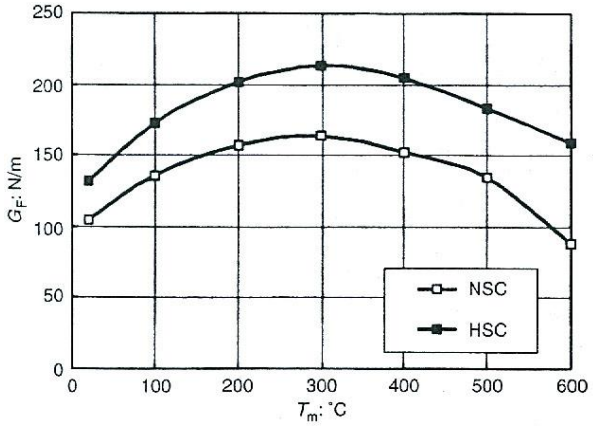

Figure 2.192 Effect of temperature on fracture energy (G_f).

Source: B. Zhang, N. Bicanic, C.J. Pearce, and G. Balabanic, "Residual Fracture Properties of Normal- and High-Strength Concrete Subject to Elevated Temperatures," *Magazine of Concrete Research* **52**(2), pp. 123-136, April 2000.

decrease in fracture energy at temperatures above 300˚C to increased microcracking and dehydration of cement. Figure 2.193 presents the effect of exposure period (t_h) starting at a concrete age of 14 days. When the heating temperature was below 300˚C, G_f monotonically increased with exposure period as a result of additional cement

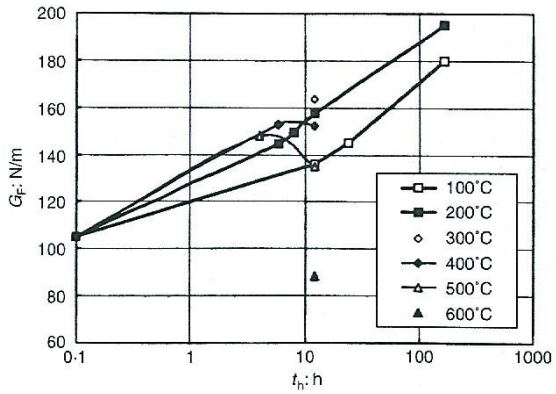

Figure 2.193 Effect of exposure period (t_h) on fracture energy (G_f) of normal strength concrete.

Source: B. Zhang, N. Bicanic, C.J. Pearce, and G. Balabanic, "Residual Fracture Properties of Normal- and High-Strength Concrete Subject to Elevated Temperatures," *Magazine of Concrete Research* **52**(2), pp. 123-136, April 2000.

hydration. At the higher temperatures G_f increased initially, but as the exposure period increased (t > ~8 hours) it decreased as shown in the figure. The effect of different curing times on the fracture energy is shown in Figure 2.194 for specimens that were unheated and specimens that had been heated at 300˚C for 12 hours at the designated curing time. As shown in the figure, G_f continued to increase as the curing age increased due to continued cement hydration, but appeared to level off at 90 days.

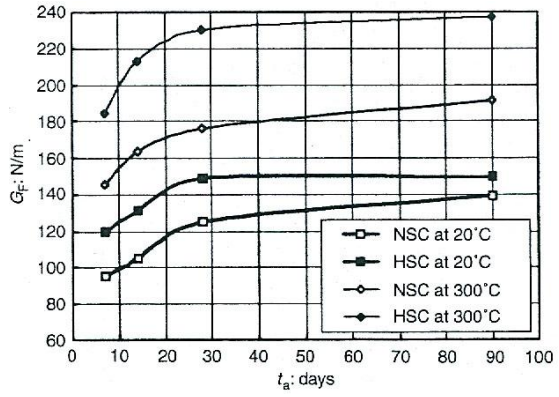

Figure 2.194 Effect of curing period on fracture energy (G_f).

Source: B. Zhang, N. Bicanic, C.J. Pearce, and G. Balabanic, "Residual Fracture Properties of Normal- and High-Strength Concrete Subject to Elevated Temperatures," *Magazine of Concrete Research* **52**(2), pp. 123-136, April 2000.

Figure 2.195 presents temperature dependence of residual fracture energy for an ordinary concrete and a high-strength concrete [2.186]. Both concretes were fabricated using 20-mm maximum size calcareous aggregate. Silica fume (5.7% by weight of total cementitious materials) was incorporated into the high-strength concrete mix. Compressive strengths for the ordinary and high-strength concretes at 28 days were 30 and 75 MPa, respectively. Tests were conducted using three-point bend specimens 100 x 100 x 400 mm^3 containing a 50-mm-deep notch. Prior to testing, specimens were heated to temperatures of 120˚, 250˚, or 400˚, held at temperature for three hours,

and then permitted to slowly cool to room temperature. Results for the ordinary and high-strength concretes exhibited similar trends in that generally the fracture energy increased with increasing exposure temperature. Fracture energies for both concretes at 400˚C were about two and a half times the reference unheated values.

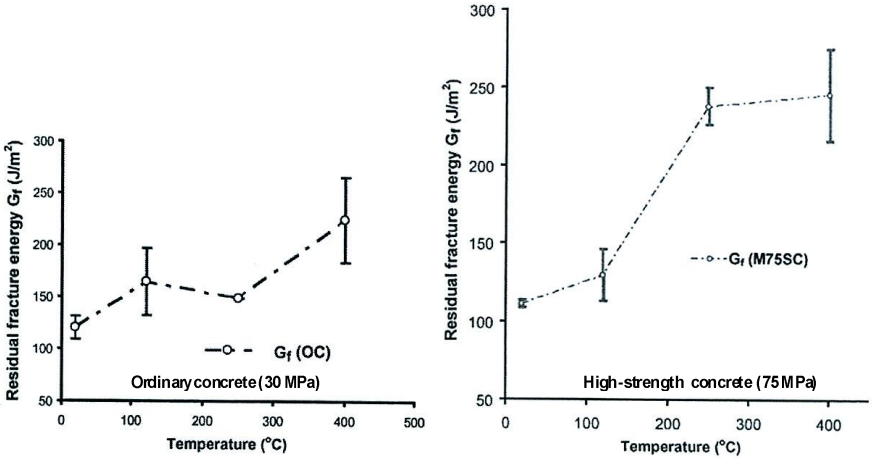

Figure 2.195 Effect of exposure temperature on residual fracture energy of ordinary and high-strength concretes.

Source: A. Menou, G. Mounajed, H. Boussa, A. Pineaud, and H. Carre, "Residual Fracture Energy of Cement Paste, Mortar and Concrete Subject to High Temperature," *Theoretical and Applied Fracture Mechanics* **45**, pp. 64-71, 2006.

Beams 150 x 150 x 750 mm^3 were tested under three-point bending to investigate the effect of elevated temperature on concrete fracture toughness [2.187]. Half the beams had a 25-mm initial notch at midspan and half the beams had a 60-mm notch at midspan. The notch thickness was 2.5 mm and was cast into the beams by placing a piece of Plexiglas with the desired crack dimension in the beam mold prior to casting the concrete. The 36 MPa compressive strength concrete was fabricated using Type I Portland cement, gravel coarse aggregate having a maximum aggregate size of 12.7 mm, and a water content corresponding to a water-cement ratio of 0.45 (by weight). Prior to testing, the beams were placed into a curing room at 21˚C and 95% relative humidity for 28 days. After curing the beams were removed from the curing room and heated to temperatures of 50˚, 100˚, 150˚, 200˚, 250˚, or 300˚C where they remained for 24 hours prior to slowly cooling to room temperature and testing. Figure 2.196 presents the variation of residual fracture toughness with temperature for the beams. Also shown in the figure are analytical results obtained from an expression presented in the reference. Results indicate a steady decline in residual fracture

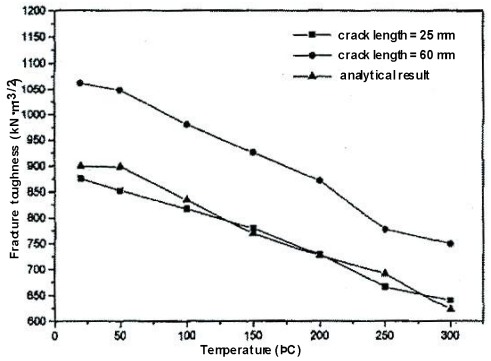

Figure 2.196 Effect of temperature on residual fracture toughness of a concrete.

Source: H. Abdel-Fattah and S.A. Hamoush, "Variation of the Fracture Toughness of Concrete with Temperature," *Construction and Building Materials* **11**(2), pp. 105-108. 1997.

toughness with an increase in exposure temperature with the decrease increasing for exposure temperatures above 50˚C. The effect of number of thermal cycles, one to three from room temperature to exposure temperature to room temperature, on the concrete residual fracture toughness is shown in Figure 2.197. Results indicate that each thermal cycle leads to a reduction in the residual fracture toughness with the reduction being about 20% for each thermal cycle at temperatures above 50˚C. The effect of thermal cycling becomes more significant at temperatures greater than 100˚C.

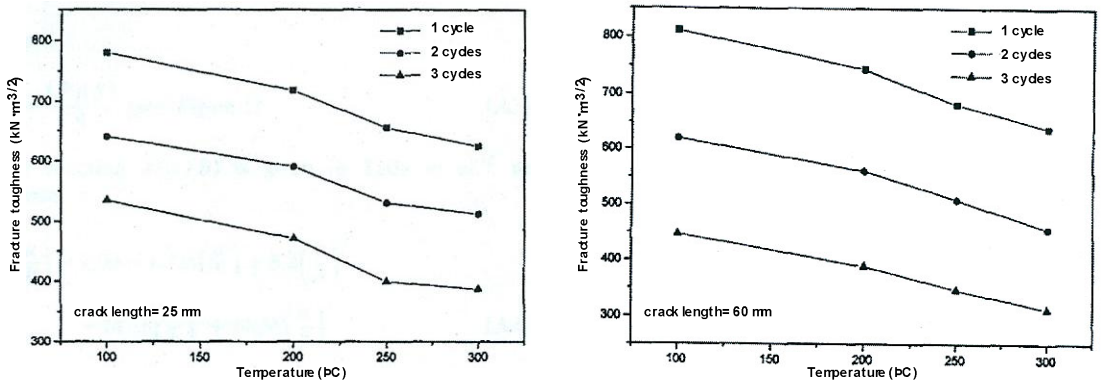

Figure 2.197 Effect of thermal cycling on residual fracture toughness of a concrete.

Source: H. Abdel-Fattah and S.A. Hamoush, "Variation of the Fracture Toughness of Concrete with Temperature," *Construction and Building Materials* **11**(2), pp. 105-108. 1997.

Summary. The residual fracture energy of both normal- and high-strength concretes increased as the exposure temperature increased for temperatures up to about 300˚ or 400˚C due to increased cement hydration; however, as the temperature further increased the residual fracture energy decreased due to increased microcracking and cement dehydration. The residual fracture energy of normal-strength concrete tended to increase with thermal exposure period for temperatures below 300˚C; however, at higher exposure temperatures the residual fracture energy increased at first for a few hours (t_h < 10 hours) and then decreased. The residual fracture energy increased with increased curing age in the first 28 days due to additional cement hydration, but after that it tended to be stable. The residual fracture toughness of concrete decreased as the exposure temperature increased with the decrease being relatively significant at temperatures greater than 50˚C. As the number of heating cycles increased the residual fracture toughness decreased, with the decrease being about 20% for each additional cycle (up to three total thermal cycles).

2.2.1.10 Long-Term Exposure (Aging)

Information and Data. During the nominal 40-year design life of nuclear power plants,* certain concrete components may be subjected to moderately elevated temperatures that could affect the concrete's properties. In conducting safety evaluations for these components, the significance of concrete component aging needs be taken into account. Unfortunately, only limited data have been identified related to the effects of long-term elevated-temperature exposure on concrete properties. Surprisingly, although Portland cement concretes have been in existence for more than 160 years, relatively little documented information is available on the aging of concrete structures that are being acted upon by environmental stressors under well-defined conditions [2.188]. When concrete is fabricated with close attention to the factors related to the production of good concrete (e.g., material selection, production control, desirable properties, and costs), the concrete will have infinite durability unless subjected to extreme external influences (e.g., overload, elevated temperature, industrial liquids, and gases) [2.122].

An investigation has been conducted to determine the changes in mechanical properties of a limestone aggregate concrete after exposure to temperatures of 75°C and 300°C for periods up to 8 months and 600°C for 1 month [2.123]. After 8-month's exposure to 75°C, compressive and splitting-tensile strengths were 98 and 94%,

* Service lives of 60 years and beyond are currently being addressed.

respectively, of their reference values. However, after exposure to 600°C for just 1 month, compressive and splitting-tensile strengths were only 23 and 38%, respectively, of their reference values. In companion mixes where either fly ash or blast furnace slag was used, improvement in retention of mechanical properties occurred after exposure to sustained high temperatures as a result of partial replacement of the cement.

The effect of long-term exposure (up to 13 years) at moderate elevated temperature (65°C) on the mechanical properties of a limestone aggregate concrete was investigated [2.189]. Tests conducted during this study were somewhat unusual because the specimens were first subjected to a simulated temperature-vs-time cement hydration cycle. Also, because the concrete mix was being evaluated for an application that experienced exposure to sulfate-bearing groundwater at elevated temperatures (~65°C), both ordinary and sulfate-resistant Portland cements were investigated. Specimens, after being subjected to the simulated cement hydration cycle, were stored either in water at 19°C (control specimens) or in a sodium sulfate solution (2000 ppm) at 65°C. Frequently during the test program, the sodium sulfate solution was changed, which required cooling to room temperature; the specimens were therefore also subjected to thermal cycling. Results of the study indicated that there was no evidence of long-term degradation in compressive strength for any of the concrete mixes and heat treatments utilized, and that for a given compressive strength the dynamic modulus of elasticity was lower for the concrete that had been heated. Cooling down and reheating the limestone and flint aggregate mixes for a total of 87 cycles did not appear to cause degradation in strength.

A 5-year testing program was conducted to determine the effects of long-term exposure to elevated temperature on the mechanical properties of concrete used in construction of the radioactive underground storage tanks at Hanford Engineering Development Laboratory (HEDL) [2.190]. Tests were conducted using specimens fabricated from the same mix proportions and materials specified for the concrete used to fabricate the tanks (20.7- and 31.0-MPa design compressive strengths). Concrete strength, modulus of elasticity, and Poisson's ratio values were determined from specimens subjected to 121°, 177°, or 232°C for periods of up to 33 months. The effect of thermal cycling was also investigated. Results showed that the compressive strength in general tended to decrease with increasing temperature and also with length of exposure; however, with the exception of the cylinders exposed to 232°C, all compressive strength results obtained after a 900-d exposure period exceeded the design values noted previously. Splitting-tensile strength results also decreased somewhat with increasing temperature and length of exposure. Modulus of elasticity was affected the most by the elevated-temperature exposure; after 920 d of heating at 232°C, it had a value that was only 30% the value obtained from an unheated control specimen. Poisson's ratio, although exhibiting somewhat erratic values, was relatively unaffected by either the magnitude or the length of elevated-temperature exposure. Thermal cycling (~18 cycles) to 177°C produced moderate reductions in compressive strength (5 to 20%), significant reductions in modulus (30 to 50%), and slight reductions in Poisson's ratio (0 to 20%). Time-dependent (creep) and physical property data were also obtained using specimens cast from the concrete mixes.

Associated with the laboratory investigation described in the previous paragraph was a study to confirm the laboratory results by testing samples removed from the underground storage tanks and process buildings at HEDL [2.191]. Cores 76-mm in diameter were obtained over the length of the haunch wall and footing of a single-shell tank that was built in 1953; contained waste for about 8 years; reached temperatures in the range of 127°C to 138°C; and experienced a radiation field of 0.10 to 0.13°C/kg/h (400 to 500 R/h). Although considerable scatter was obtained from the data because of different concrete pours and different environmental exposures, after about 29 years of exposure only one data point fell below the 20.7-MPa design compressive strength. Figure 2.198 presents compressive strength results obtained from cores removed from structures at HEDL and compares the results to values based on the laboratory results.

A study has been carried out to examine the effect of temperature on sealed and unsealed air-entrained concrete containing fly ash, conventional water reducer, and superplasticizer [2.192]. The properties of compressive strength and modulus of elasticity were studied at seven different temperatures ranging from –11°C to 232°C and at seven different exposure periods from 1 to 180 d. Local crushed aggregates of 19-mm maximum size consisting primarily of dolomite and hornblende were used in the concrete mixtures. Figure 2.199 presents the relative strength (ratio of compressive strength at temperature to that obtained from unheated control specimens) as a function of temperature and exposure time that was obtained from testing sealed specimens. The results indicate that up to a temperature of 121°C there was no degradation in compressive strength for exposures up to 180 d. With increasing temperature,

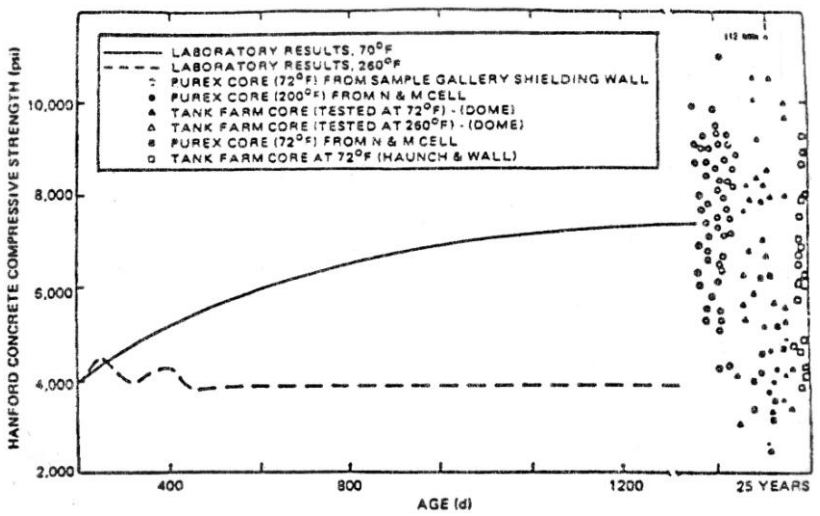

Figure 2.198 Comparison of laboratory and actual sample long-term compressive strength data.

Source: M.P. Gillen et al., "Strength and Elastic Properties of Concrete Exposed to Long-Term Moderate Temperatures with High Radiation Fields," RHO-RE-SA-55 P, Rockwell Hanford Operations, Richland, Washington, 1984.

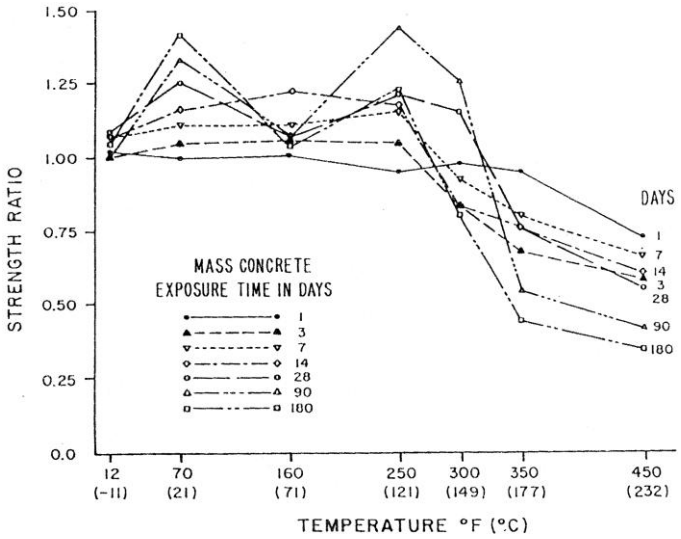

Figure 2.199 Relationship of relative strength and temperature of mass concrete (sealed).

Source: K.W. Nasser and M. Chakraborty, "Temperature Effects on Strength and Elasticity of Concrete Containing Admixtures," *Proceedings of Symposium Temperature Effects on Concrete*, ASTM Special Technical Publication 858, American Society for Testing and Materials, West Conshohocken, Pennsylvania, 1985.

the strength decreased with the extent of strength reduction generally proportional to the exposure temperature and time at temperature (e.g., at 232°C and 180-d exposure the strength was about 50% its reference value). The corresponding relationship of the relative modulus of elasticity (ratio of modulus of elasticity at temperature to that obtained from unheated control specimens) as a function of temperature and exposure time obtained from sealed specimens is presented in Figure 2.200. The modulus of elasticity started to decline monotonically at temperatures $\geq$ 71°C with the decline in modulus proportional to the exposure temperature and time at temperature (e.g., at 232°C and 180-d exposure the modulus was about 25% its reference value). Relative compressive strength and modulus of

elasticity results for unsealed specimens are presented in Figure 2.201 and indicate improved performance relative to the sealed specimens. An explanation of the greater effect of elevated-temperature exposure on sealed (mass concrete) specimens was that in a closed system saturated steam pressure develops at high temperatures, that causes deterioration in structural properties of the cement gel.

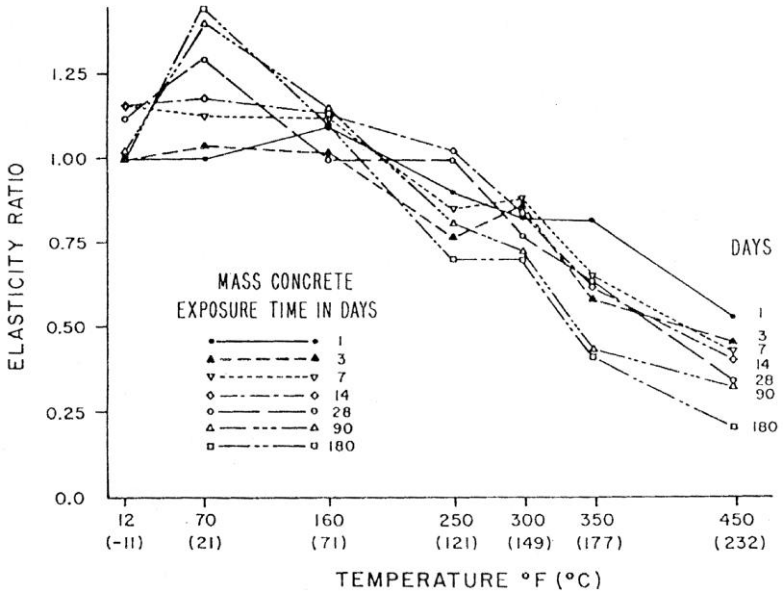

Figure 2.200 Relationship of elasticity ratio and temperature of mass concrete (sealed).

Source: K.W. Nasser and M. Chakraborty, "Temperature Effects on Strength and Elasticity of Concrete Containing Admixtures," *Proceedings of Symposium Temperature Effects on Concrete*, ASTM Special Technical Publication 858, American Society for Testing and Materials, West Conshohocken, Pennsylvania, 1985.

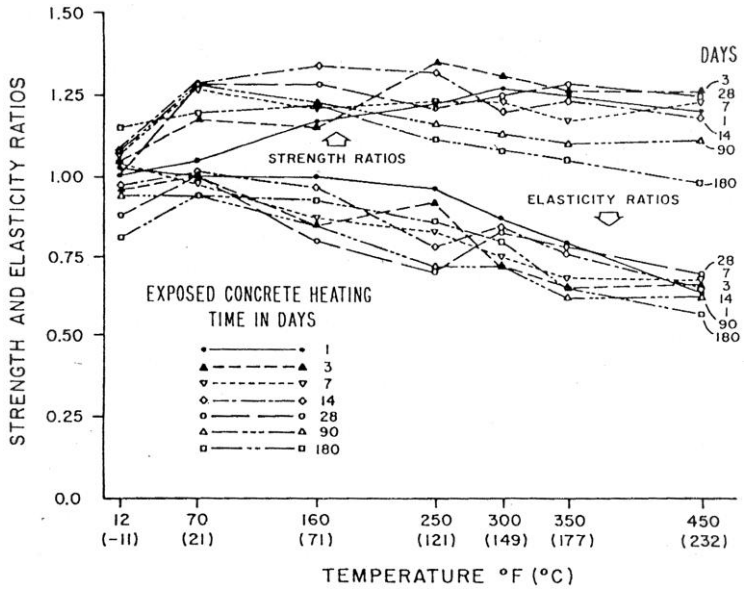

Figure 2.201 Relationship of strength and elasticity and temperature of unsealed concrete.

Source: K.W. Nasser and M. Chakraborty, "Temperature Effects on Strength and Elasticity of Concrete Containing Admixtures," *Proceedings of Symposium Temperature Effects on Concrete*, ASTM Special Technical Publication 858, American Society for Testing and Materials, West Conshohocken, Pennsylvania, 1985.

A laboratory study has been conducted to evaluate the relative performance of limestone and dolostone aggregate ordinary Portland cement concretes under sustained exposure to high temperature [2.193]. After 28-d moist cure followed by 26 weeks of room temperature curing, the test specimens were exposed for up to 4 months to temperatures ranging from 76°C to 450°C, and 1 month for a 600°C exposure. Figure 2.202 presents residual compressive strength versus conditioning temperature (up to 450°C) after 4 months exposure for the limestone concrete.* The loss of compressive strength of specimens exposed to elevated temperature was proportional to the exposure temperature. At temperatures of 150°C and higher, an increase in length of exposure from 48 h to 4 months resulted in further decreases in strength. In all cases, any major loss in strength was found to occur within the first month of exposure. In general the leaner concretes (water-cement ratio = 0.6) were slightly less affected than the richer concretes in terms of relative strength loss after exposure.

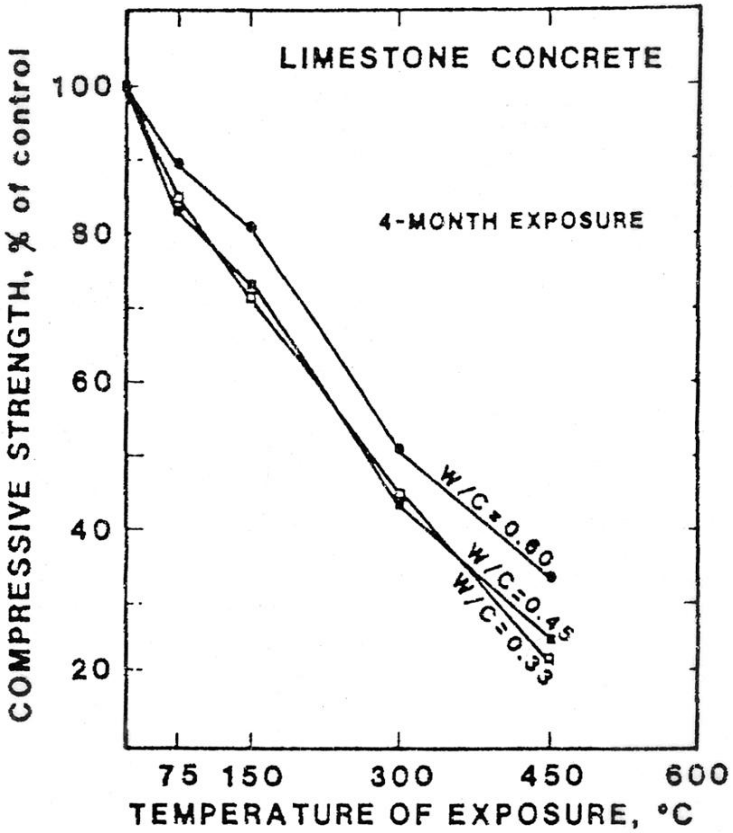

Figure 2.202 Relative residual compressive strength of limestone concrete after 4-month exposure to various temperatures (up to 450°C).

Source: G. G. Carrette and V. M. Malhotra, "Performance of Dolostone and Limestone Concretes at Sustained High Temperatures," *Proceedings of Symposium Temperature Effects on Concrete,* ASTM Special Technical Publication 858, pp. 38–67, American Society for Testing and Materials, West Conshohocken, Pennsylvania, 1985.

The effect of elevated-temperature exposure at 65°C, 90°C, or 110°C for periods up to 3.5 years was investigated in Japan in support of nuclear power plant facilities [2.194]. Either basalt or sandstone coarse aggregates were utilized in the concrete mixtures. Cementitious materials studied included Class B fly ash, moderate heat cement plus fly ash, and normal Portland cement. Heating conditions adopted were: (1) long-term heating tests [allowable temperature except for local areas (long-term) (65°C), allowable local temperature (long-term) (90°C), temperature

*The dolostone aggregate results are not discussed because pyrite was contained in some of the aggregate particles, and it underwent slow oxidation that produced a disintegrating expansion of the aggregate and cracking of the concrete.

at which water is considered to evaporate rapidly (110°C)]; (2) short-term heating tests [allowable temperature (short-term) (175°C)]; and (3) thermal cycling tests for up to 120 cycles [cycled heating temperatures (20°C to 110°C to 20°C) to simulate temperature variations during operational periods]. Three cylindrical specimens were prepared for each test condition and put under either sealed conditions, where evaporation of water was prevented, or unsealed conditions, where evaporation was allowed. Figure 2.203 presents the residual compressive strength and modulus of elasticity results, and Figure 2.204 the effect of thermal cycling for the sealed and unsealed concretes.

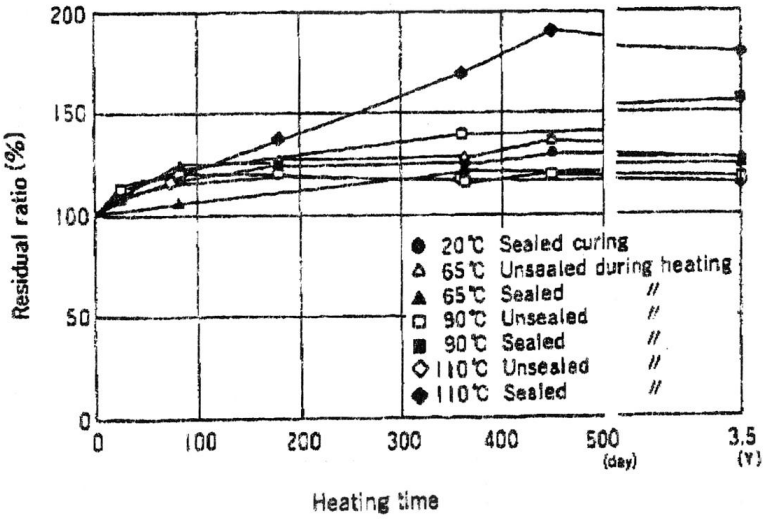

Compressive strength

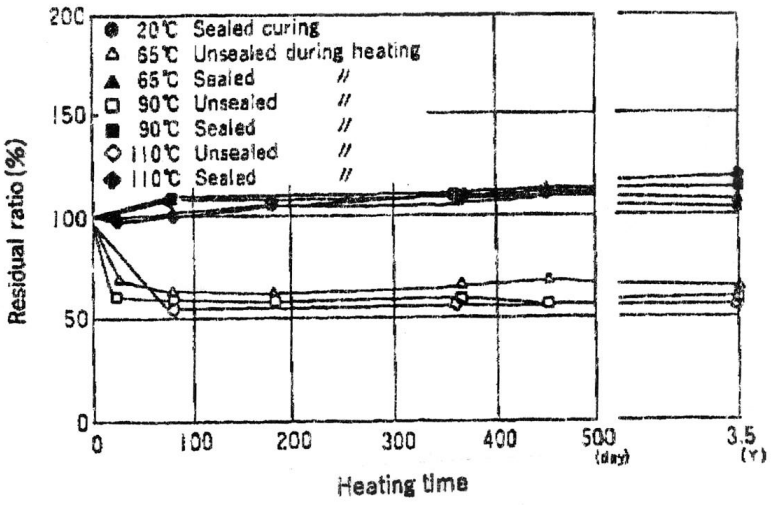

Modulus of elasticity

Figure 2.203 Long-term (3.5-year) heating effect on compressive strength and modulus.

Source: T. Suzuki, M. Tabuchi, and K. Nagao, "Study on the Degradation of Concrete Characteristics in the High Temperature Environment," *Concrete Under Severe Conditions: Environment and Loading*, Vol. 2, pp. 1119–1128, E & FN Spon Publishers, 1995.

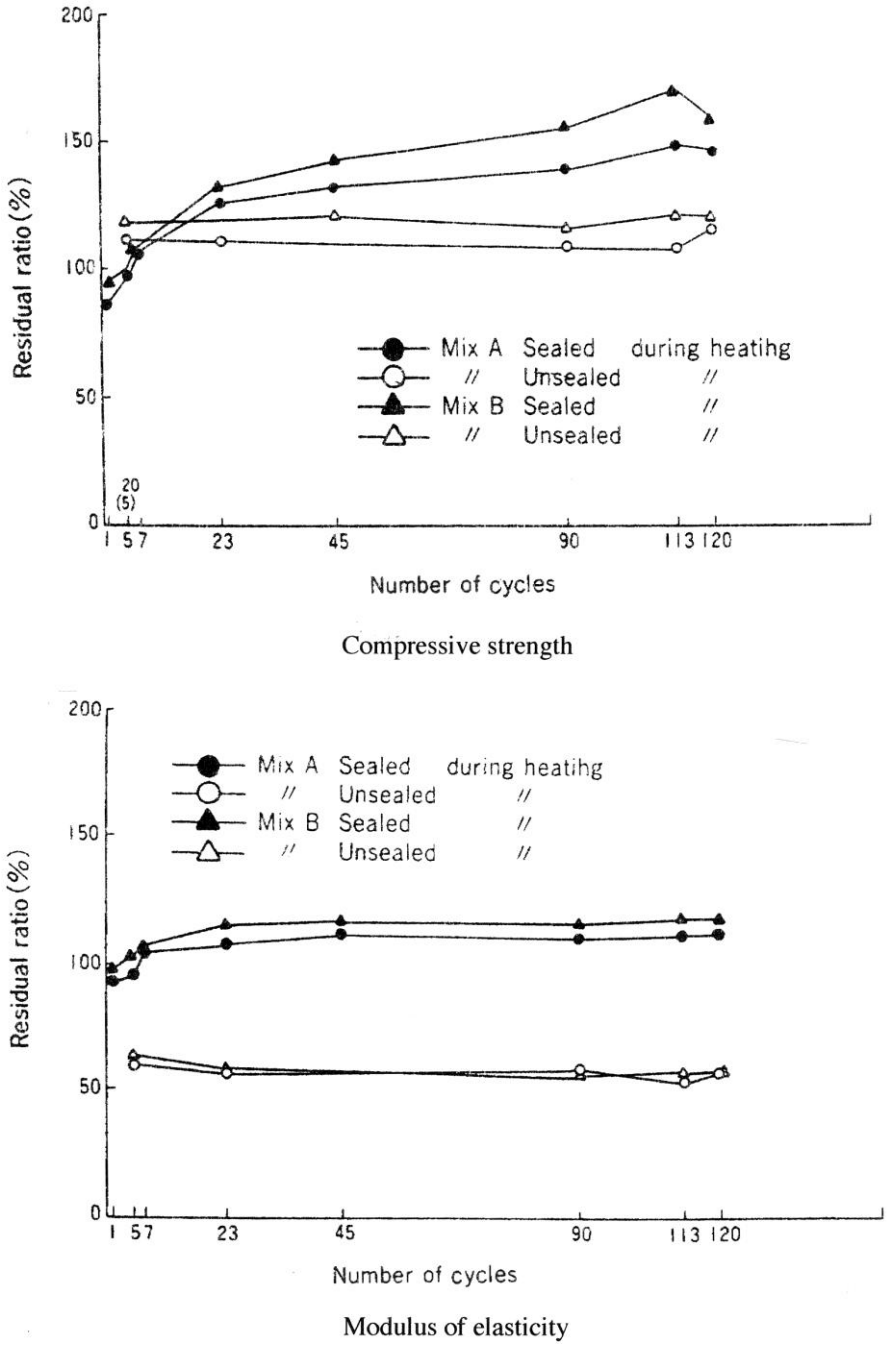

Figure 2.204 Effect of thermal cycling on compressive strength and modulus.

Source: T. Suzuki, M. Tabuchi, and K.Nagao, "Study on the Degradation of Concrete Characteristics in the High Temperature Environment," *Concrete Under Severe Conditions: Environment and Loading*, Vol. 2, pp. 1119–1128, E & FN Spon Publishers, 1995.

Several conclusions were derived from the heating tests results:

1. Under long-term heating at 65°C, 90°C, and 110°C, compressive strength after heating was greater than before heating, under both sealed and unsealed conditions. This was especially true under sealed conditions at 110°C in which the compressive strength increased for 1.5 years reaching approximately 200% that of unheated control specimens. These results are considered to be the effect of autoclave curing. Under unsealed conditions

it was considered that microcracking in concrete, resulting from moisture migration and evaporation under high temperatures, caused a degradation of compressive strength. However, the acceleration of hydration at high temperatures in any nonhydrated sections of the concrete increased the compressive strength more than degradation caused by microcracking. The results after 3.5 years were relatively unchanged from those measured after 1 year. Therefore, it was found that the compressive strength ceased to fluctuate at an early stage.

2. Under sealed conditions during heating, elastic modulus had a tendency to increase slightly, though not as much as the compressive strength. The elastic modulus under sealed conditions remained relatively unchanged under heating, even after 3.5 years. Under unsealed conditions during heating, the modulus of elasticity at temperature relative to that obtained from unheated control specimens was reduced about 50%. The reduction in the elastic modulus under unsealed conditions can be explained by the closing of microcracks at an early stage of stress. Thus, the elastic modulus of concrete heated to high temperatures, with moisture migration and evaporation present, was markedly reduced. In addition, it was found that the elastic modulus became stabilized at an early stage, not changing much from 91 d through 3.5 years, even under heating.
3. During the thermal-cycle heating test, compressive strength after heating was greater than before heating under both sealed and unsealed conditions. However, the ratio of increase was smaller than under constant heating, suggesting the influence of thermal cycling. For the same number of thermal cycles, the compressive strength was consistently higher for the sealed specimens relative to that obtained from unsealed specimens. Under unsealed conditions specimens exhibited little influence of number of cycles on compressive strength for thermal cycle numbers greater than five (i.e., little change in compressive strength value for cycles greater than five). Under unsealed conditions the modulus of elasticity exhibited a similar trend to that obtained for constant heating in that it was reduced by about 50%. A major part of the reduction occurred in the early stages of the thermal cycling. Under sealed conditions during thermal cycling the elastic modulus showed a tendency similar to that of the compressive strength, but the modulus of elasticity did not increase as much as the compressive strength of the sealed specimens.
4. The greater the weight reduction became, the greater the decrease in the elastic modulus tended to be, which indicated that moisture migration and evaporation during heating affected the reduction of elastic modulus. Therefore, to estimate the properties of massive concrete structures subjected to high temperatures accurately, it is necessary to study moisture migration in mass concrete members that are subjected to high temperatures over long periods of time.

A series of studies was conducted to evaluate the drying effect of elevated-temperature exposure on the properties of concrete [2.172]. Specimens made from four concrete mixes of ordinary Portland cement and river-gravel aggregate (Table 2.6) were tested to investigate the compressive, tensile, and bond strengths[*]; moduli of elasticity; and weight loss after 90-d exposure to temperatures of 35˚, 50˚, 65˚, 80˚, 110˚, 200˚, and 300°C. Moisture in the specimens was allowed to evaporate freely. Residual strength tests of unheated and heated concretes were conducted at room temperature on both dried and wet specimens presoaked in water for 2 d. Exposure to sustained elevated temperature higher than 35°C showed remarkable deteriorating effects on the physical properties of concrete when moisture in concrete was allowed to evaporate. Greater reduction of strengths and weights after exposure were associated with the mixes having higher mix water contents. Strengths did not decline linearly as the

Table 2.6 Mix proportions for concrete mixtures

Concrete Mixture	Mix Proportions (kg/m^3)			
	Water	Cement	Sand	River Gravel
Mix 1	165	330	836	1045
Mix 2	195	390	779	974
Mix 3	164	273	895	1035
Mix 4	190	317	849	1036

Source: H. Kasami, T. Okuno, and S. Yamane, "Properties of Concrete Exposed to Sustained Elevated Temperature," Paper H1/5 in *Proc. 3rd International Conference on Structural Mechanics in Reactor Technology*, Elsevier Science Publishers, North-Holland, The Netherlands, 1975.

[*] Bond strength results were discussed in Section 2.2.1.8.

temperature rose and were minimal at around 50°C. Dry compressive strengths of heated concretes indicated approximately 10% loss when heated at 50°C with practically no change when heated at higher temperatures up to 110°C, 20% loss at 200°C, and 30% loss at 300°C. Wet compressive strengths of heated concretes indicated larger losses than dry strengths, and more than 20% loss when heated at only 35°C. Reductions in tensile and bond strengths and modulus of elasticity of heated concretes were greater than that obtained for compressive strengths. Tensile strength tests indicated approximately 30% loss upon exposure to temperatures of 50°C to 65°C, and less strength loss at higher temperatures. Bond strengths showed approximately 15% loss when heated at only 35°C, and smaller loss for higher temperatures of 50°C to 80°C, 25% loss at 110°C, and more than 50% loss at 300°C. Moduli of elasticity of heated concretes indicated a tendency to decline linearly with increasing temperature, experiencing a 15% loss at 50°C, 25% loss at 110˚C, and 50% loss at 300˚C. The unusual deterioration at around 50˚C in compressive, tensile, flexural and shear strengths was also indicated in subsequent investigations regardless of the kind of aggregates. However, the influence of aggregate on the properties of heated concrete was significant. Sandstone and basalt aggregate concretes indicated smaller reductions, while limestone, andesite, and serpentine aggregate concretes showed greater reductions in strengths after exposure. Changes in chemical composition in the cement paste were not noticeable below 100°C; however, the porosity was found to be affected by the exposure temperature. The unusual deterioration in strengths at around 50°C can be due to either the expansion of cement paste or to the change in porosity caused by evaporation of free water. Figure 2.205 presents the effect of exposure temperature on residual compressive strength, tensile strength, and modulus of elasticity results after 90-day

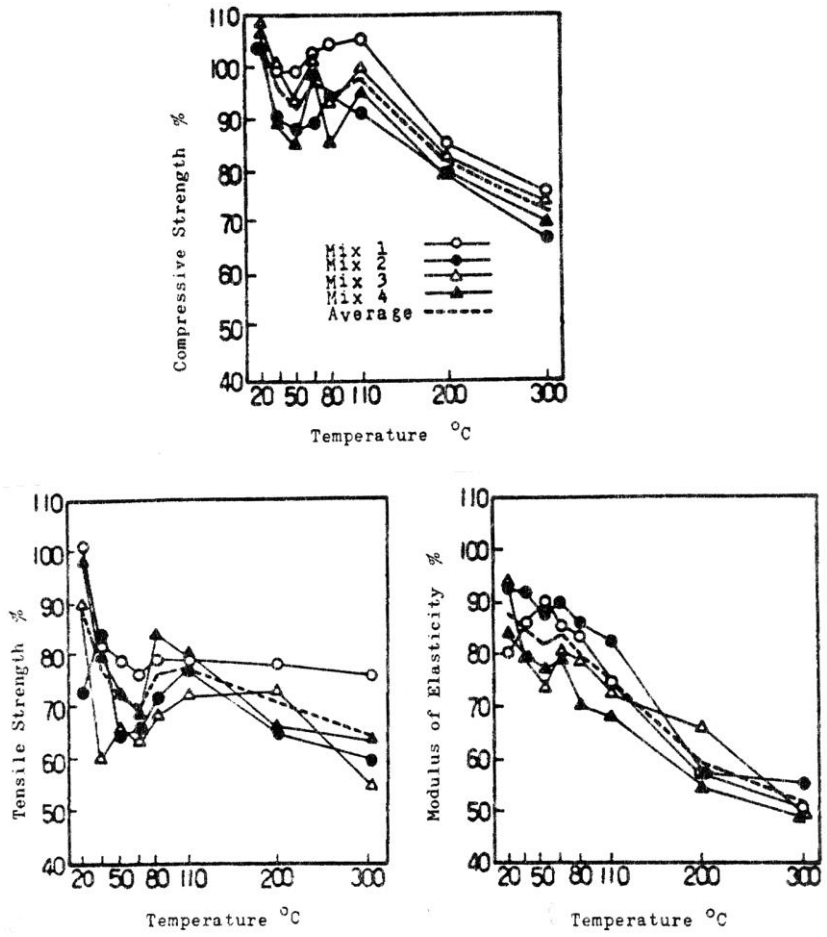

Figure 2.205 Effect of exposure temperature on residual compressive strength, tensile strength, and modulus of elasticity after 90-d exposure.

Source: H. Kasami, T. Okuno, and S. Yamane, "Properties of Concrete Exposed to Sustained Elevated Temperature," Paper Hl/5 in *Proc. 3rd International Conference on Structural Mechanics in Reactor Technology*, Elsevier Science Publishers, North-Holland, The Netherlands, 1975.

exposure for each of the concrete mixtures investigated. Figures 2.206 presents weight loss results for the different concrete mixtures. Residual compressive strength and moduli of elasticity results showing the effect of aggregate material type are presented in Figure 2.207. The effect of aggregate type and temperature exposure level on shear strength* is presented in Figure 2.208.

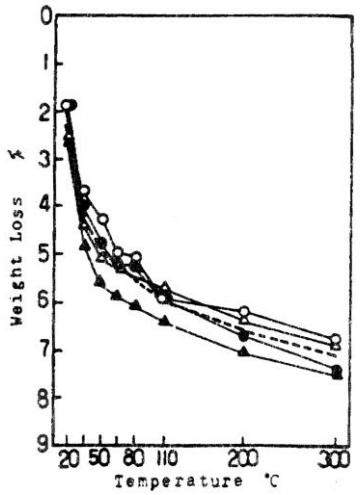

Figure 2.206 Weight loss of heated concrete.

Source: H. Kasami, T. Okuno, and S. Yamane, "Properties of Concrete Exposed to Sustained Elevated Temperature," Paper Hl/5 in *Proc. 3rd International Conference on Structural Mechanics in Reactor Technology*, Elsevier Science Publishers, North-Holland, The Netherlands, 1975.

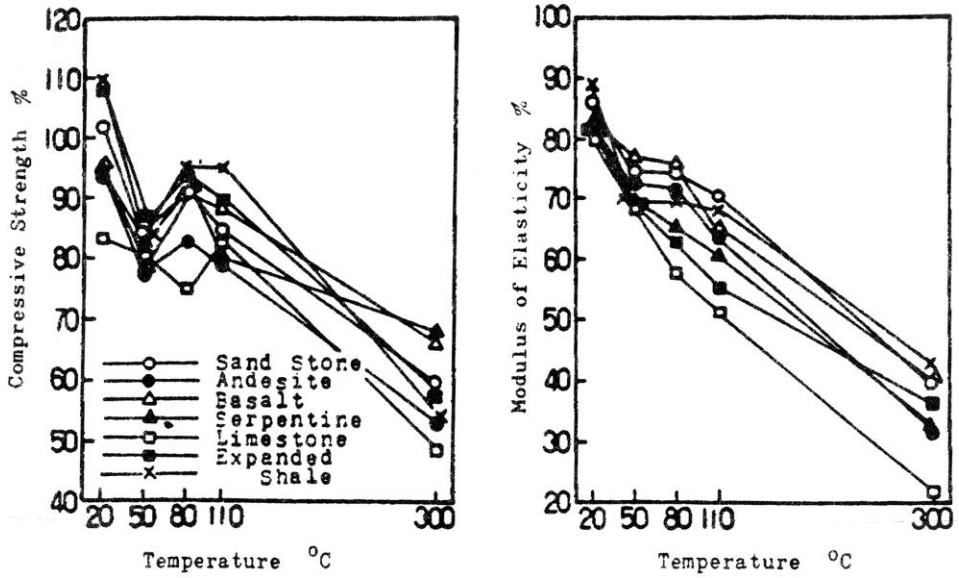

Figure 2.207 Compressive strength and modulus of elasticity of heated concretes.

Source: H. Kasami, T. Okuno, and S. Yamane, "Properties of Concrete Exposed to Sustained Elevated Temperature," Paper H1/5 in *Proc. 3rd International Conference on Structural Mechanics in Reactor Technology*, Elsevier Science Publishers, North-Holland, The Netherlands, 1975.

*Shear is the action of two equal and opposite parallel forces applied in planes a short distance apart. Shear stresses cannot exist without accompanying tensile and compressive stresses (pure shear is applied only through torsion).

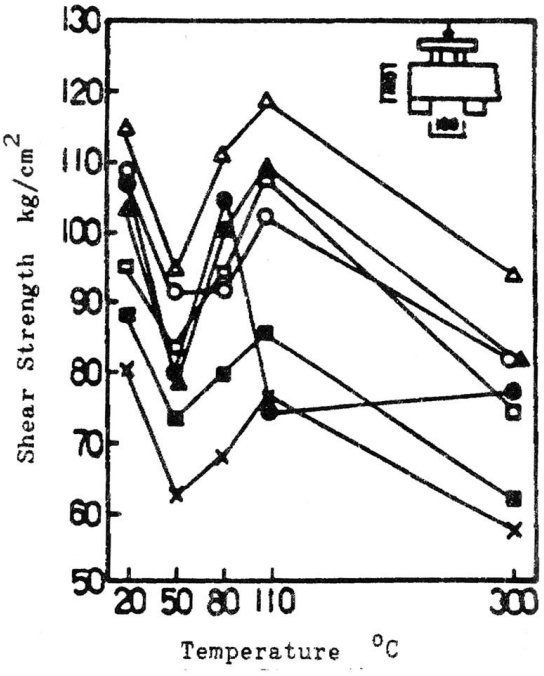

Figure 2.208 Shear strength of heated concrete.

Source: H. Kasami, T. Okuno, and S. Yamane, "Properties of Concrete Exposed to Sustained Elevated Temperature," Paper H1/5 in *Proc. 3rd International Conference on Structural Mechanics in Reactor Technology*, Elsevier Science Publishers, North-Holland, The Netherlands, 1975.

An experimental study has been conducted to rationalize the design method for facilities used to store spent fuel and to obtain fundamental data for estimating the long-term safety of the facilities under elevated temperature exposure conditions [2.195]. Four concrete mixes, listed in Table 2.7, were employed in the study: two ordinary Portland cement concretes having design compressive strengths of 24 and 40 MPa, and two concrete mixes having design compressive strength of 40 MPa in which 55% (by weight) of the ordinary Portland cement was replaced by blast furnace slag. Shale and limestone coarse aggregate were used in the concrete mixes. Cylindrical test specimens 10-cm diameter by 20-cm long[+] were cured by soaking for 28 days in water and then air drying at 20±3˚C and 60%

Table 2.7 Concrete mixture proportions

Concrete Mixture	Mix Proportions (kg/m^3)						Reference Values*	
	Water	Cement	Blast Furnace Slag	Coarse Aggregate	Fine Aggregate	Water Reducer	Compressive Strength (MPa)	Modulus of Elasticity (GPa)
No. 1	160	370	0	1103	789	0.925	56.5	35.3
No. 2	162	250	0	1082	908	0.625	32.3	28.6
No. 3	160	167	203	1103	789	0.416	58.6	33.3
No. 4	160	167	203	1103	789	0.416	54.9	34.3

*Room temperature (unheated, unsealed) reference values for mixes used in 110˚C test series.

Source: T. Kanazu, T. Matsumura, and T. Nishiuchi, "Changes in the Mechanical Properties of Concrete Subjected to Long-Term Exposure to High Temperatures," Report No. U95037, Abiko Research Laboratory, Central Research Institute of Electric Power Industry, Japan, March 1996.

[+] Cylindrical test specimens 20-cm diameter by 40-cm long were used for splitting-tensile strength tests.

relative humidity for about two months. Both sealed and unsealed specimens were used in the study. Sealed specimens were sealed by placing into metal containers and soldering the seams. At an age of about 3 months, heating of the specimens initiated. Exposure temperatures investigated were 65˚, 85˚, and 110˚C. After thermal exposures of 1 month, 1 year, 1.5 years, 2 years, 3 years, and 8 years* specimens were removed from the ovens and permitted to cool to room temperature prior to testing. Compressive strength, modulus of elasticity, weight change, and splitting-tensile strength data were obtained and compared to reference 3-month baseline results. Figures 2.209 and 2.210 present residual compressive strength results for unsealed and sealed specimens, respectively. Residual moduli of elasticity results for unsealed and sealed specimens are presented in Figures 2.211 and 2.212, respectively. Change in specimen weight with exposure time is presented in Figures 2.213 and 2.214 for unsealed and sealed specimens, respectively. Figure 2.215 presents splitting-tensile strength results. Conclusions derived from the study were that: the decrease in compressive strength at temperatures of 65˚ and 110˚C basically ended after three months under unsealed conditions and after 1 to 2 years exposure for sealed conditions as the moisture condition stabilized, the decrease in compressive strength was somewhat greater for sealed specimens than for unsealed specimens, decreases in compressive strength were somewhat greater for specimens containing blast furnace slag, modulus of elasticity for sealed and unsealed specimens exhibited similar decreases with increasing exposure temperature, the decrease in modulus for unsealed specimens tended to stabilize after about 2 years exposure, the decrease in modulus was somewhat larger for specimens containing blast furnace slag, weight loss increased as the temperature increased, weight loss for unsealed specimens tended to stabilize after 1 month exposure while for sealed specimens the weight loss increased for about 1.5 years before stabilizing, weight loss results seemed to correlate well with decrease in modulus of elasticity in that as the weight loss increased the modulus decreased, specimens containing blast furnace slag tended to exhibit a slightly higher weight loss than that exhibited by reference concrete, and the tensile strength ratio tended to decrease for exposures up to 2 years and then increase slightly. The study recommended that consideration should be given to increasing the current temperature limit (65˚C) for concrete utilized in facilities for storage of spent nuclear fuel. A limit of up to about 110˚C for the physical properties is possible as long as the temperature dependence of the mechanical properties is taken into consideration. Since evaporation of gel water increases markedly at temperatures greater than 110˚C and elevated temperature considerations for design of reinforced concrete structures (e.g., creep and bond between concrete and steel reinforcement) become more pronounced at temperatures greater than 100˚C, it was considered reasonable to raise the limit to 85˚C.

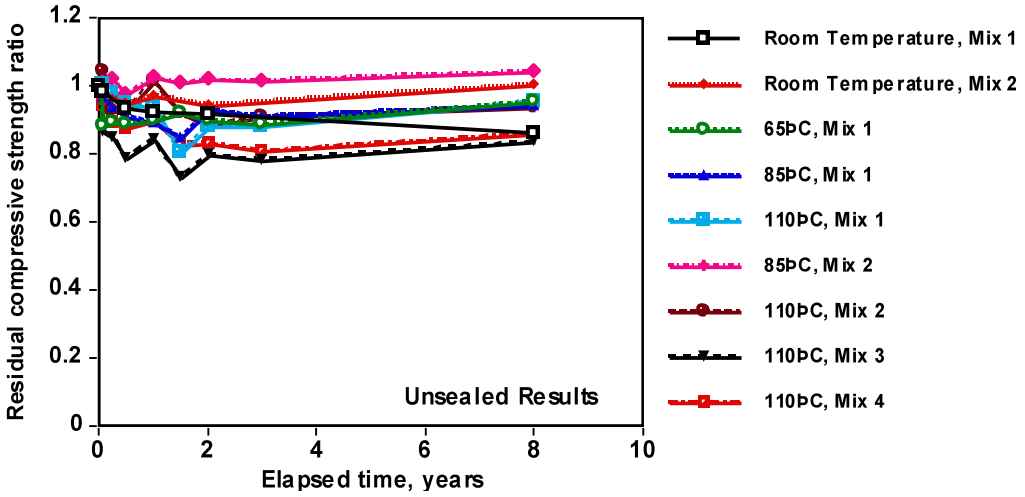

Figure 2.209 Residual compressive strength vs exposure time: unsealed specimens.

Source: T. Kanazu, T. Matsumura, and T. Nishiuchi, "Changes in the Mechanical Properties of Concrete Subjected to Long-Term Exposure to High Temperatures," Report No. U95037, Abiko Research Laboratory, Central Research Institute of Electric Power Industry, Japan, March 1996.

*No 8-year results were obtained for the sealed specimens.

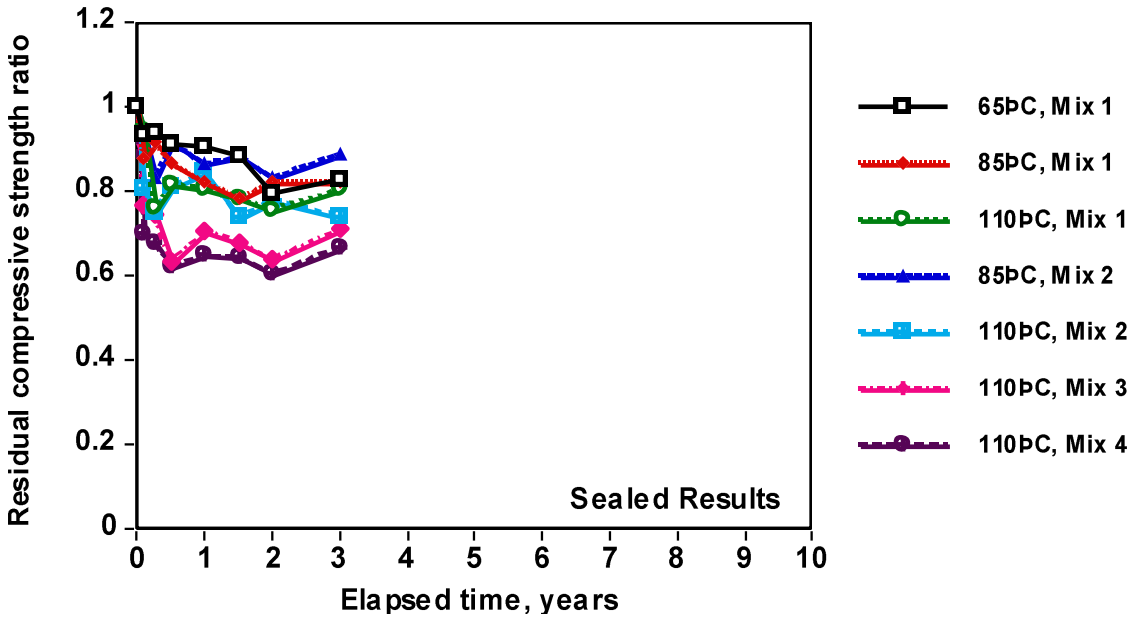

Figure 2.210 Residual compressive strength vs exposure time: sealed specimens.

Source: T. Kanazu, T. Matsumura, and T. Nishiuchi, "Changes in the Mechanical Properties of Concrete Subjected to Long-Term Exposure to High Temperatures," Report No. U95037, Abiko Research Laboratory, Central Research Institute of Electric Power Industry, Japan, March 1996.

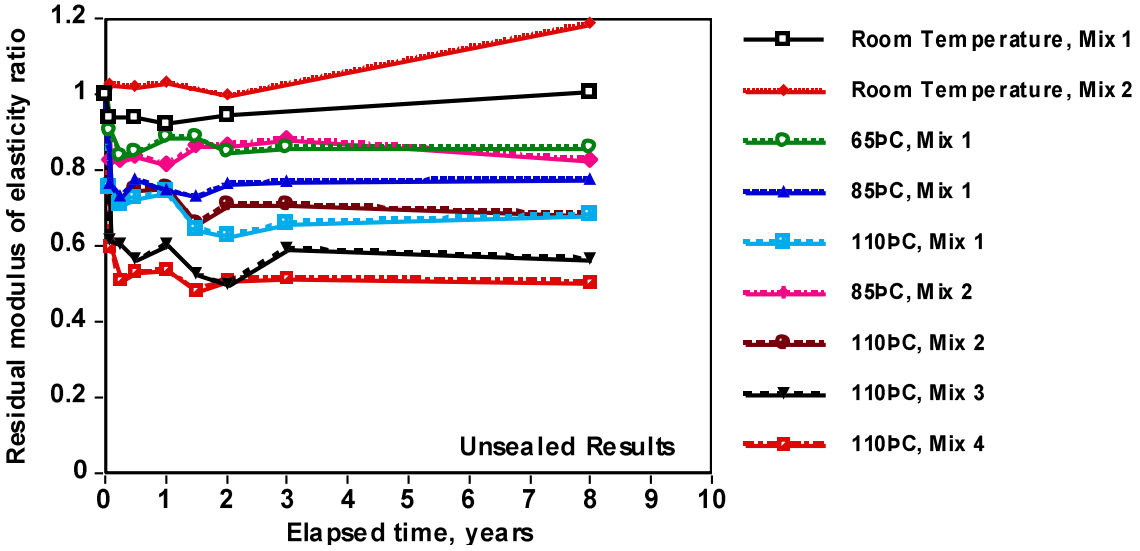

Figure 2.211 Residual modulus of elasticity vs exposure time: unsealed specimens.

Source: T. Kanazu, T. Matsumura, and T. Nishiuchi, "Changes in the Mechanical Properties of Concrete Subjected to Long-Term Exposure to High Temperatures," Report No. U95037, Abiko Research Laboratory, Central Research Institute of Electric Power Industry, Japan, March 1996.

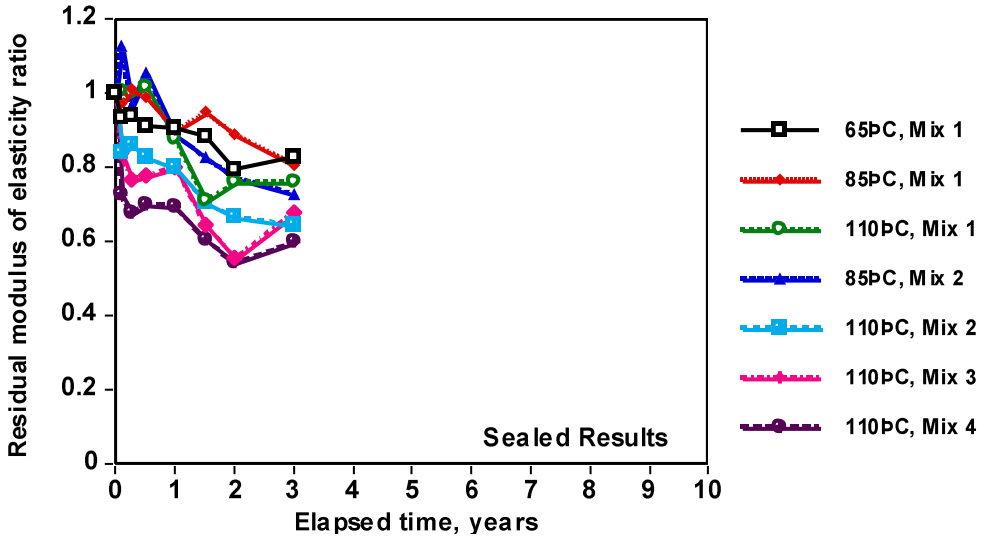

Figure 2.212 Residual modulus of elasticity vs exposure time: sealed specimens.

Source: T. Kanazu, T. Matsumura, and T. Nishiuchi, "Changes in the Mechanical Properties of Concrete Subjected to Long-Term Exposure to High Temperatures," Report No. U95037, Abiko Research Laboratory, Central Research Institute of Electric Power Industry, Japan, March 1996.

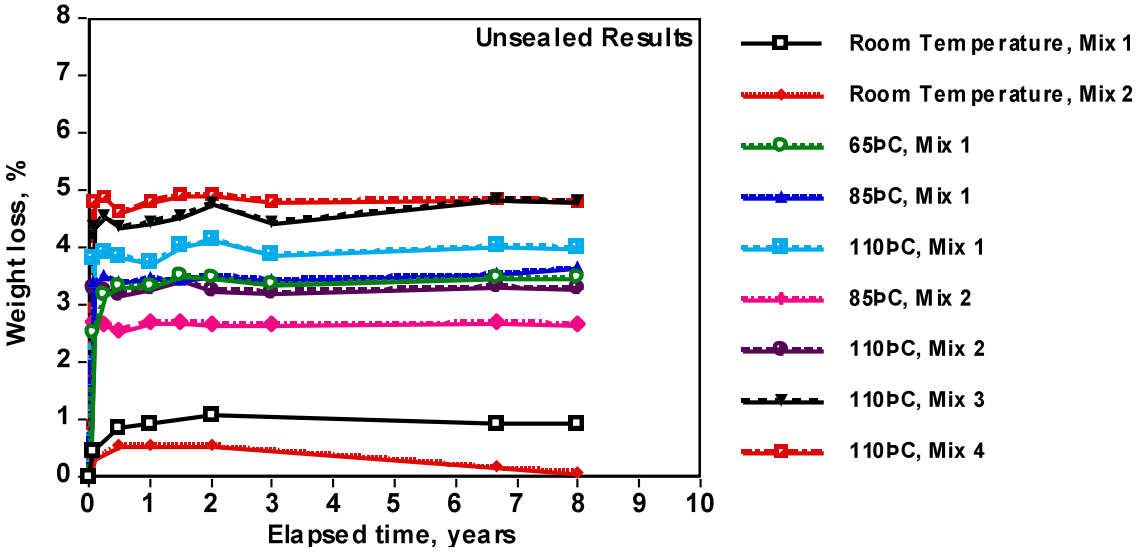

Figure 2.213 Change in weight vs exposure time: unsealed specimens.

Source: T. Kanazu, T. Matsumura, and T. Nishiuchi, "Changes in the Mechanical Properties of Concrete Subjected to Long-Term Exposure to High Temperatures," Report No. U95037, Abiko Research Laboratory, Central Research Institute of Electric Power Industry, Japan, March 1996.

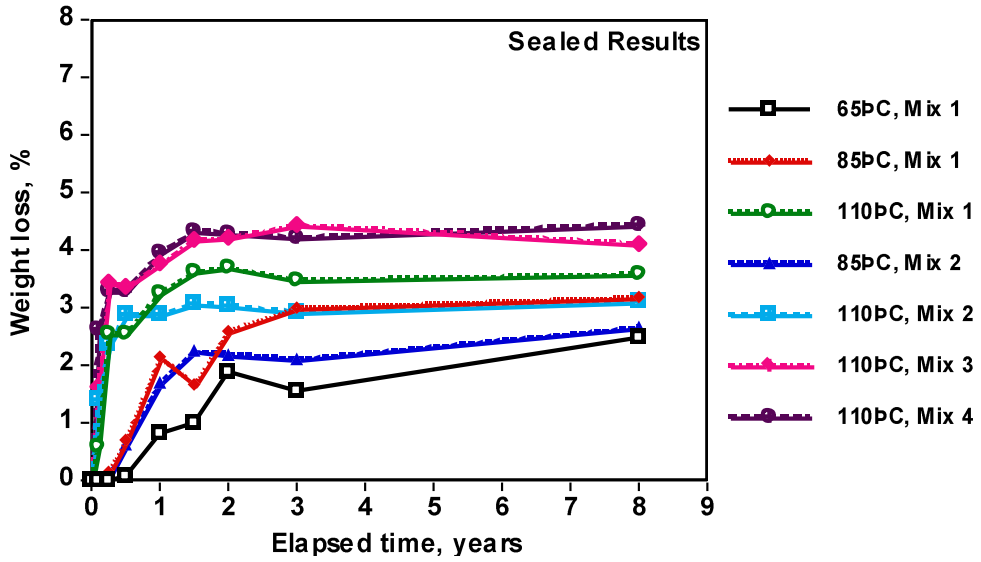

Figure 2.214 Change in weight vs exposure time: sealed specimens.

Source: T. Kanazu, T. Matsumura, and T. Nishiuchi, "Changes in the Mechanical Properties of Concrete Subjected to Long-Term Exposure to High Temperatures," Report No. U95037, Abiko Research Laboratory, Central Research Institute of Electric Power Industry, Japan, March 1996.

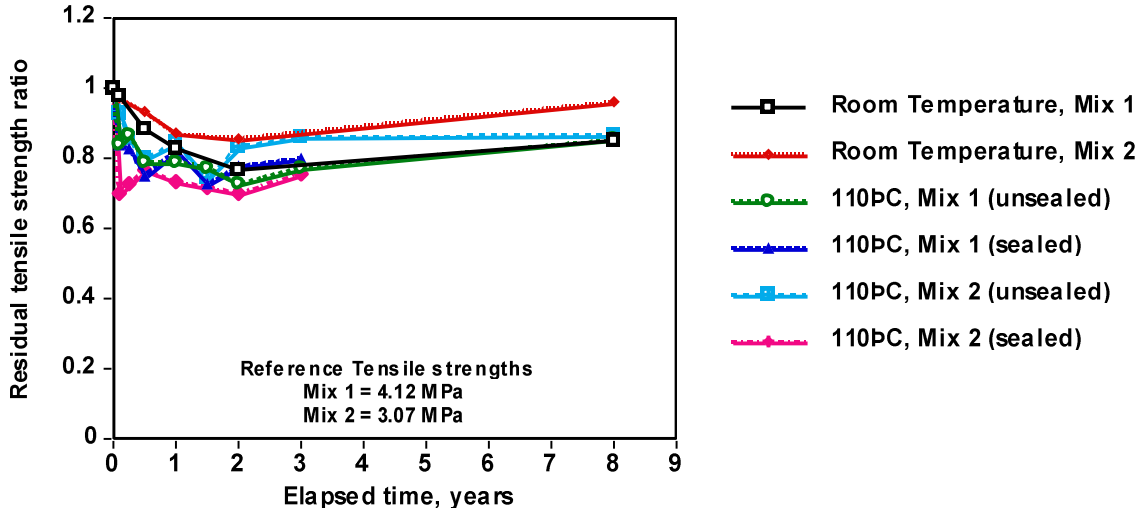

Figure 2.215 Change in splitting-tensile strength ratio vs exposure time: sealed specimens.

Source: T. Kanazu, T. Matsumura, and T. Nishiuchi, "Changes in the Mechanical Properties of Concrete Subjected to Long-Term Exposure to High Temperatures," Report No. U95037, Abiko Research Laboratory, Central Research Institute of Electric Power Industry, Japan, March 1996.

Summary. Results for exposure of concrete to elevated temperature for relatively long periods of time are limited and tend to indicate that strength and modulus of elasticity decrease with increasing exposure time at elevated temperature (T > 110˚C), with most of the decrease occurring relatively soon. Modulus of elasticity is affected more than compressive strength. At relatively low elevated temperatures (T < 110˚C) the elevated temperature exposure can result in an increase in compressive strength, especially for sealed conditions due to autoclave curing, with the modulus of elasticity being relatively unaffected for sealed conditions but dropping for unsealed conditions. At

moderate elevated temperatures (e.g., 230˚C) unsealed specimens exhibited improved performance relative to sealed specimens, possibly due to saturated steam pressure that develops in a closed system to cause deterioration of structural properties of cement gel. Partial replacement of the cement with fly ash or blast furnace slag appears to impart improved performance at elevated temperature. Sealed specimens performed better under thermal cycling than unsealed specimens, and thermal cycling has a greater effect on modulus of elasticity than compressive strength.

2.2.1.11 Radiation Shielding Effectiveness

Information and Data. Portland cement concrete possesses many of the physical qualities of an ideal radiation shield. It is a polyphase material consisting of particles of aggregate contained in a matrix of Portland cement paste. Gamma rays are absorbed by the high-density-aggregate materials and neutrons are attenuated by hydrogen atoms in the cement paste. A concrete shield is exposed to two sources of heat: heat transferred from hot parts of the reactor system and heat produced internally by the attenuation of neutrons and gamma rays [2.196]. Energy captured from slowed down fast neutrons and gamma rays entering the shield from the reactor core is deposited within the shield material and liberated as heat. The total amount of heat generated can be considerable. The heat generated may have detrimental effects on the physical, mechanical, and nuclear properties of the concrete. Different types of concrete perform differently under radiation exposure, although if heated to relatively high temperatures they all will lose waters of crystallization and become somewhat weaker and less effective in neutron attenuation [2.197]. Provided below is a brief summary of the effect of elevated temperature exposure on shielding effectiveness.

The effectiveness of concrete as a shield may be reduced under service conditions (elevated temperature) as drying reduces the hydrogen content or cracking occurs. Figure 2.216 presents results of elevated-temperature exposure on shielding of heavyweight aggregate (iron limonite and magnetite limonite) concretes [2.198]. Significant changes in

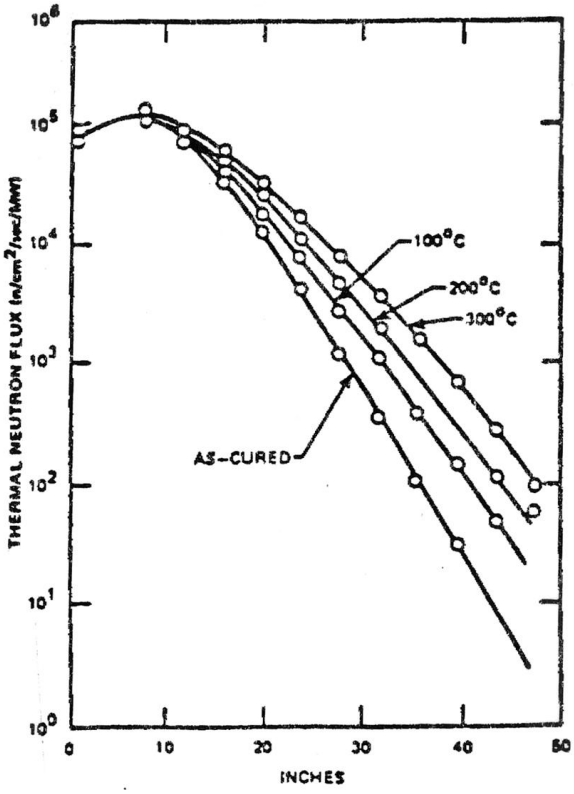

Figure 2.216 Thermal neutron distribution in ordinary concrete as a function of temperature.

Source: E. G. Peterson, "Shielding Properties of Ordinary Concretes as a Function of Temperature," HW-65572, Hanford Atomic Products Operation, Richland, Washington, August 2, 1960.

attenuation effectiveness were found as the concrete was heated to 100°C and 200°C, with little additional change as a result of heating to 300°C. Despite the loss of neutron and gamma attenuation efficiency with increasing temperature, it was concluded that the concrete would serve as a satisfactory shield material. If increasing efficiency were required at higher temperatures, it could be accounted for in the design.

Shielding effectiveness of concrete is also reduced if through-cracks develop. The effect of straight and crooked cracks through a concrete shield on gamma ray attenuation has been investigated [2.199]. In the immediate vicinity of the concrete surface, leakage of gamma rays through a slit contributed significantly to γ-dose rate, but diminished rapidly with distance from the surface as a result of shield thickness and scattering effects. The shielding effectiveness of cracked concrete has been investigated and formulas developed to define the resulting effects [2.200]. Guidelines developed to compensate for cracking note that it might be economically advantageous to allow a concrete shield to crack and then shield the resulting radiation by other means.

Additional information on attenuation, materials for radiation-shielding concrete, nuclear properties of concrete, water content and its effect on nuclear properties of concrete, and basic design of radiation shields is available [2.21].

Summary. The presence of hydrogen in a concrete radiation shield is important, particularly with respect to neutron attenuation. Thermal loadings that can affect the concrete water content can reduce the concrete's radiation shielding effectiveness. Temperature limits have been recommended to protect ordinary and heavyweight concrete shields against water loss, the effect of elevated temperature, radiation-absorption effects, and thermal stress conditions [2.201]. For neutron shields maximum internal and ambient temperatures are noted as 88˚ and 71˚C, respectively, and for gamma shields the maximum internal and ambient temperatures are noted as 177˚ and 149˚C, respectively,

2.2.1.12 Multiaxial Conditions

Information and Data. In large structures such as prestressed concrete pressure vessels, once the post-tensioning is applied, the concrete is stressed either biaxially or triaxially, with the biaxial case, particularly tension-compression, being of most concern. Regulatory documents in the United States, United Kingdom, France, and Germany generally consider multiaxial stress states by allowing use of stresses that are somewhat higher than would be permitted for uniaxial loading conditions. A summary of guidelines provided in these codes is available [2.202].

As most of the multiaxial testing of concrete has been conducted at room temperature, a brief review of this information is presented first to provide an indication of the effect of multiaxial loading on concrete behavior. More details on these results are available [2.103,2.202]. This is followed by information on more recent results and multiaxial loading of concrete at elevated temperatures.

A number of studies have been conducted investigating the behavior of concrete at room temperature under multiaxial loading, primarily using unsealed specimens [2.203-2.217]. A review of information contained in many of these documents is available [2.103]. In the review it is noted that it is generally accepted that the ultimate strength of concrete increases when sustaining multiaxial stresses are imposed. The method of load application is a primary topic of research, and results obtained with steel-brush platens, ball-bearing platens, fluid-cushion platens, and deformable platens have shown promise for reducing end restraints to tolerable levels so that the true ultimate strength can be measured (see Figure 2.217). The most reliable data indicate a maximum biaxial compressive strength of 1.25 times the uniaxial strength when measured with the same apparatus. Triaxial tests indicate strengths up to four to six times the uniaxial strength. Tests with sealed specimens are very limited. Results indicate that the sealed specimens are weaker than dry concrete, but that wet concrete gives a greater relative increase in strength under multiaxial stress conditions. An important observation concerns that of a supposed critical stress level under biaxial loading, a stress that may occur as low as 50% of the ultimate and at which severe permanent damage takes place within the specimen. Since uniaxial strength is generally used as a material property for design, one may suppose that the actual vessel conditions involving biaxial stresses will make that data conservative by 25%. However, tests conducted with steel platens, the common method, indicate a strength measurement that is 25% too high, meaning that there may be, essentially, no additional margin for strength data obtained with steel platens. The additional observation of a critical stress below ultimate for short- and long-term loading may be more realistic for design purposes. The review concludes noting that additional work needs to be done to develop a better

understanding of multiaxial behavior as well as development of improved methods of providing accurate strength data, especially with regard to sealed concrete and elevated temperatures.

Since the above review, an international program involving researchers from the Federal Republic of Germany, Italy, United Kingdom, and United States has been conducted [2.218]. The program's objective was to provide insight into the significance of systematic effects on concrete multiaxial test results. All participants in the program used specimens from the same concrete and mortar mix that were: (1) mixed, cast, and cured at one laboratory; (2) shipped under controlled conditions to the other laboratories; and (3) tested at an identical age. The testing program was divided into two parts: (1) deformations and strength of concrete under biaxial loading, applied monotonically and proportionally, with stress ratios σ_2/σ_1 = 0/3, 1/3, 2/3, and 3/3; and (2) deformations and strength of concrete under triaxial loading with stress increased hydrostatically up to one of several specified octahedral shear planes ranging from 75 to 200% of the uniaxial strength and then deviated within that plane along one of three stress paths - triaxial compression, constant intermediate principal stress, or triaxial extension to failure. Uniaxial mortar cylinder compressive strengths ranged from 29.9 to 37.2 MPa and concrete compressive strengths from 29.7 to 34.7 MPa. Figure 2.217 presents schematics of the different multiaxial test methods used in the investigation.

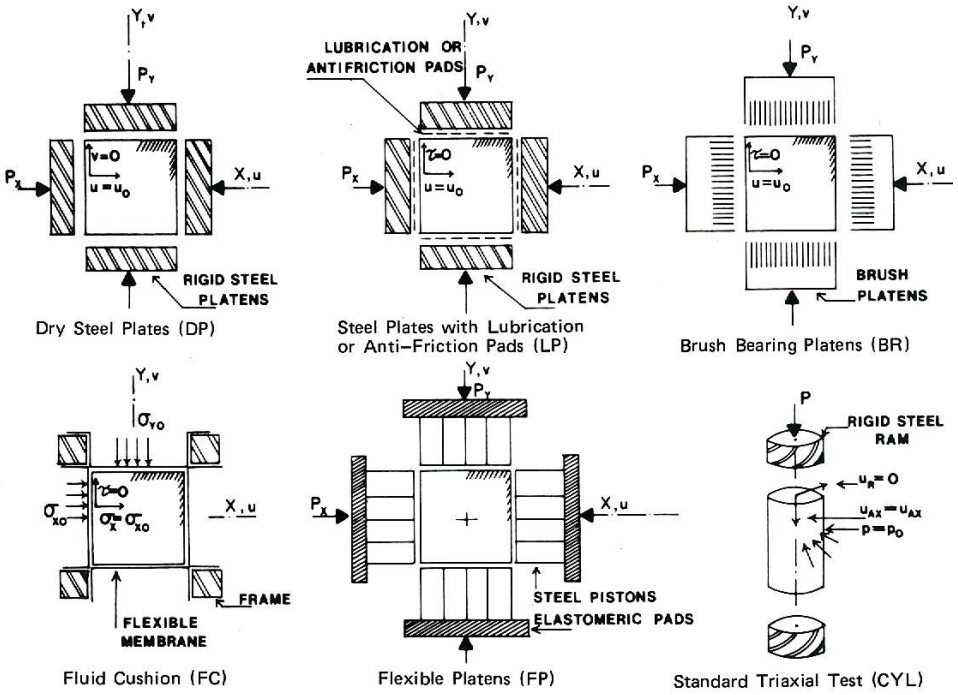

Figure 2.217 Multiaxial test methods.

Source: K.H. Gerstle, D.L. Linse, P. Bertacchi, M.S. Kotosovos, H-Y. Ko, J.B. Newman, P. Rossi, G. Schickert, M.A. Taylor, L.A. Traina, R.M. Zimmerman, and R. Bellotti, "Strength of Concrete Under Multiaxial Stress States," Paper SP 55-5 in *Douglas McHenry International Symposium on Concrete and Concrete Structures*, pp. 103-131, American Concrete Institute, Farmington Hills, Michigan, 1978.

Biaxial and triaxial results for concrete cube specimens are presented in Figure 2.218. Figure 2.218b presents triaxial failure envelopes within the octahedral plane σ_0 = 34.5 MPa. Most of the triaxial tests were performed by first subjecting the specimen to a specified hydrostatic pressure, ranging from 20.7 to 55.2 MPa, followed by deviating within the octahedral plane along one of the three stress paths shown in the figure. The following conclusions were derived from the investigations: (1) a systematic relationship exists between the degree of constraint of the loading system and the uniaxial and multiaxial strengths (differences in strength found in previous investigations at least partially can be ascribed to differences in loading systems) and (2) decomposition of the failure stress state into hydrostatic and deviatoric portions appears to offer a systematic approach to the development

of failure criteria for concrete and mortar under mu1tiaxia1 stresses (establishment of a common failure criterion for uniaxial, biaxial, and triaxial loading conditions that is path-independent seems possible on the basis of test results).

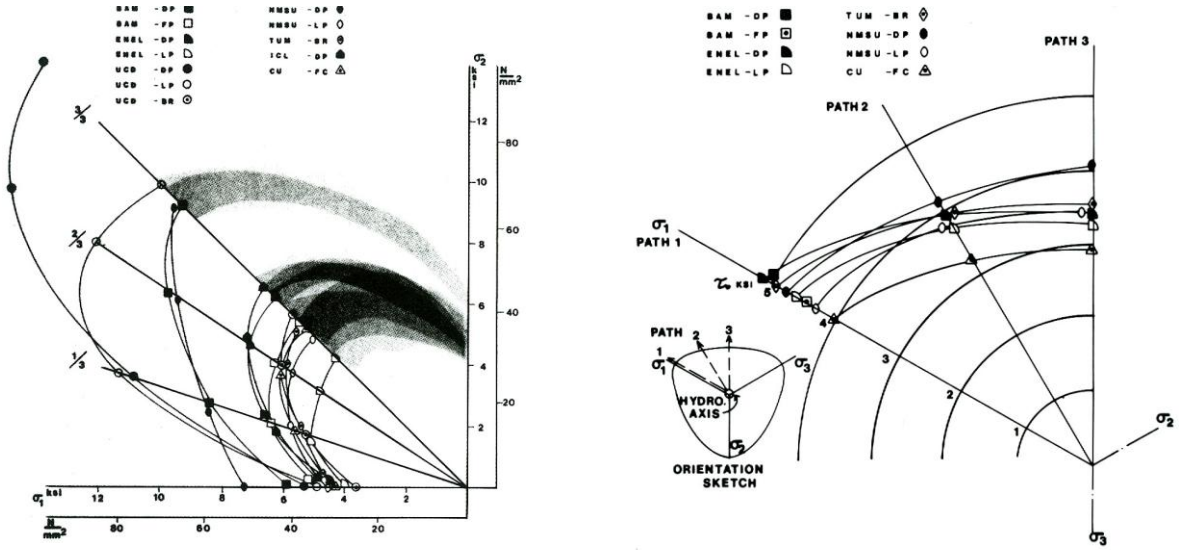

(a) Biaxial loading.

(b) Triaxial loading.

Figure 2.218 Multiaxial test results: (a) strength of concrete under biaxial loading and (b) triaxial failure envelopes within octahedral plane σ_0 = 34.5 MPa.

Source: K.H. Gerstle, D.L. Linse, P. Bertacchi, M.S. Kotosovos, H-Y. Ko, J.B. Newman, P. Rossi, G. Schickert, M.A. Taylor, L.A. Traina, R.M. Zimmerman, and R. Bellotti, "Strength of Concrete Under Multiaxial Stress States," Paper SP 55-5 in *Douglas McHenry International Symposium on Concrete and Concrete Structures*, pp. 103-131, American Concrete Institute, Farmington Hills, Michigan, 1978.

The behavior of high-performance concrete under biaxial loading has been investigated [2.219]. The concrete mix (f_c' = 71.3 MPa at 28d) incorporated limestone coarse aggregate, siliceous sand, and three cementitious materials: Type I cement, fly ash, and ground granulated blast furnace slag. The test specimens were 150 x 150 x 50 mm^3. Interfaces between the loading platens and specimens were lubricated to avoid restraint. Figure 2.219 presents typical complete stress-strain curves for biaxial compression loading and tension-compression loading for different nominal strain ratios. The shape of the biaxial compression stress-strain curves was found to be similar to results for the uniaxial curves in that they both had ascending and descending parts. The biaxial tension-compression stress-strain curves in the tensile direction were found to be similar to those observed under uniaxial tension loading. The multiaxial strength and the strength envelope are an important basis for the analysis and design of concrete structures. Specimens under tension-compression loading were found to be only damaged in the tensile direction with a split developing parallel to the compression direction. Figure 2.220 presents biaxial strength envelopes in stress space and strain space. The biaxial peak strains for most cases were found to be lower than those obtained for uniaxial compression loading, primarily due to the strength increase in the compression region under biaxial loading and an associated reduction in deformation capacity. It was concluded that the strength increase in the biaxial compression region is accompanied by strain softening which needs to be considered in the analysis and design of concrete structures.

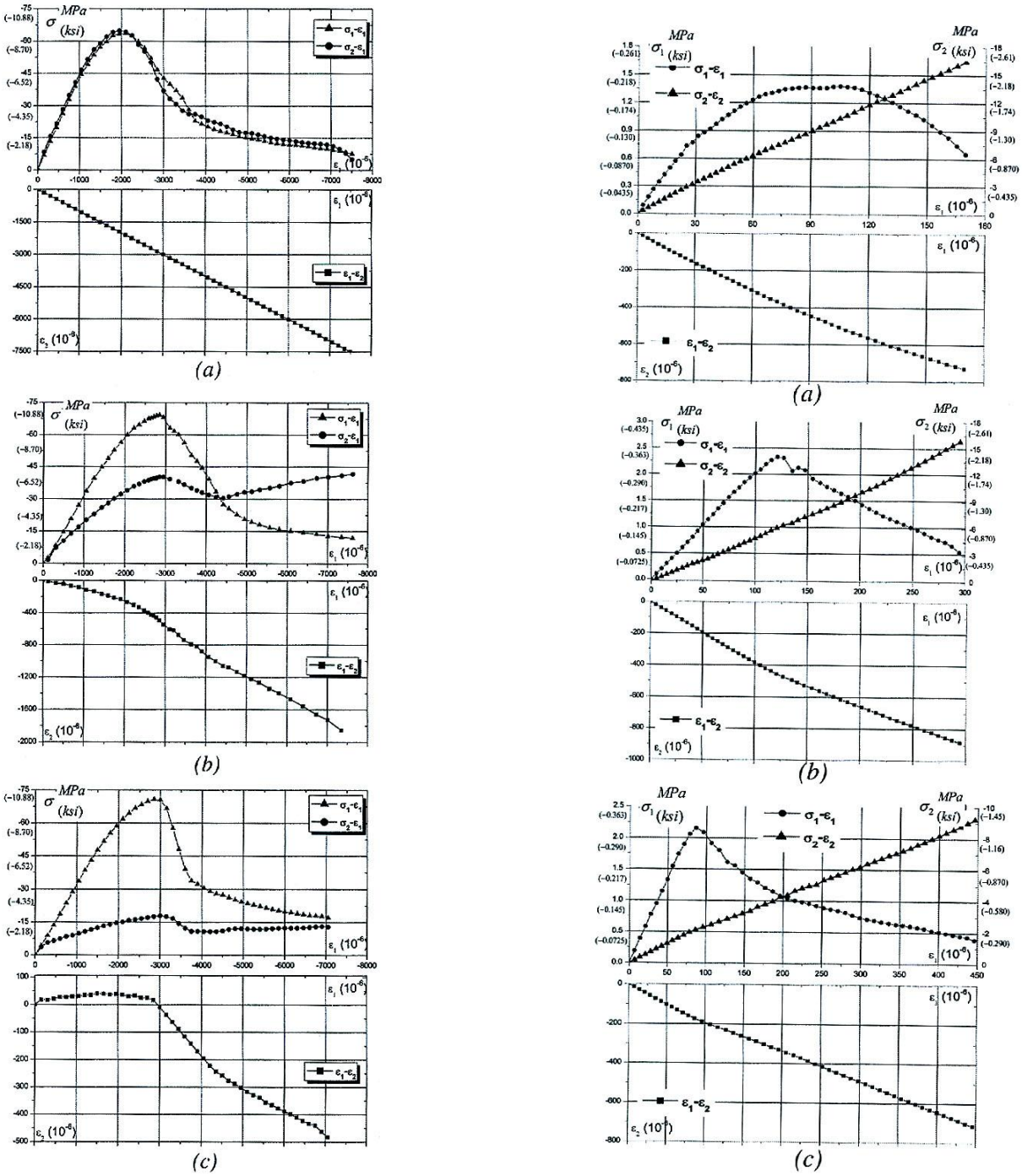

Biaxial compression
(a) $\alpha = 1$, (b) $\alpha = 0.3$, (c) $\alpha = 0.1$

Tension-compression
(a) $\alpha = -0.167$, (b) $\alpha = -0.25$, (c) $\alpha = -0.5$

Figure 2.219 Complete stress-strain curves for biaxial compression for different strain ratios (α).

Source: W. Ren, W. Yang, Y. Zhou, and J. Li, "Behavior of High-Performance Concrete Under Uniaxial and Biaxial Loading," Title No. 105-M62, *ACI Materials Journal*, American Concrete Institute, Farmington Hills, Michigan, November-December 2008.

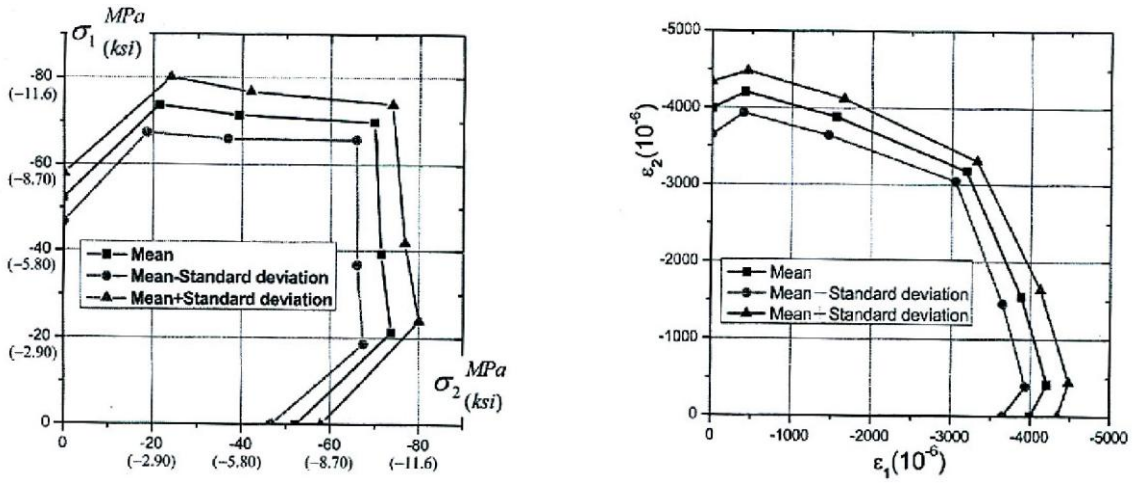

Stress Space Strain Space

Figure 2.220 Biaxial strength envelopes in stress space and strain space.

Source: W. Ren, W. Yang, Y. Zhou, and J. Li, "Behavior of High-Performance Concrete Under Uniaxial and Biaxial Loading," Title No. 105-M62, *ACI Materials Journal*, American Concrete Institute, Farmington Hills, Michigan, November-December 2008.

In another study, an investigation was conducted to provide experimental failure behavior characteristics under biaxial stresses for plain concrete of a Korean nuclear containment building [2.220]. Type I Portland cement concretes of two strength were investigated: (1) 37.8 MPa corresponding to design strength of wall and dome concrete of containment and (2) 27.5 MPa corresponding to base concrete. Three combinations of biaxial loading (compression-compression, compression-tension, and tension-tension) and four stress-ratio levels ($\alpha = f_2/f_1$) were considered in each loading regime as noted in Figure 2.221. Concrete plate specimens 200 x 200 x 60 mm^3 were used in the study. Teflon pads were placed at the interfaces between the loading system and specimen to minimize frictional effects. Tensile loading was applied by epoxying the platens to the specimen surfaces. Biaxial tests were performed under constant stress ratio. Figure 2.222 presents the biaxial strength envelopes for the two concretes

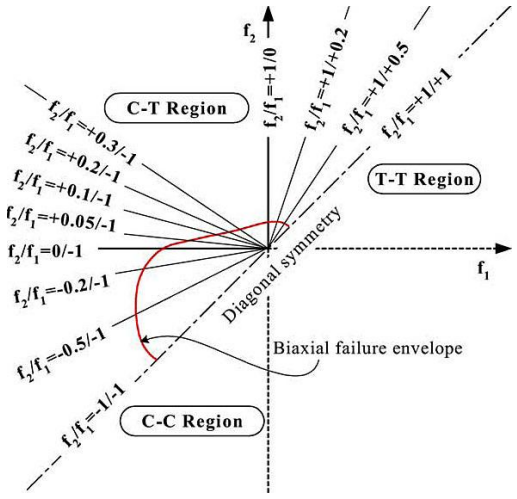

Figure 2.221 Stress ratios considered(f_2/f_1).

Source: S-K. Lee, Y-C. Song, and S-H. Han, "Biaxial Behavior of Plain Concrete of Nuclear Containment Building," *Nuclear Engineering and Design* **227**, pp. 143-153, 2004.

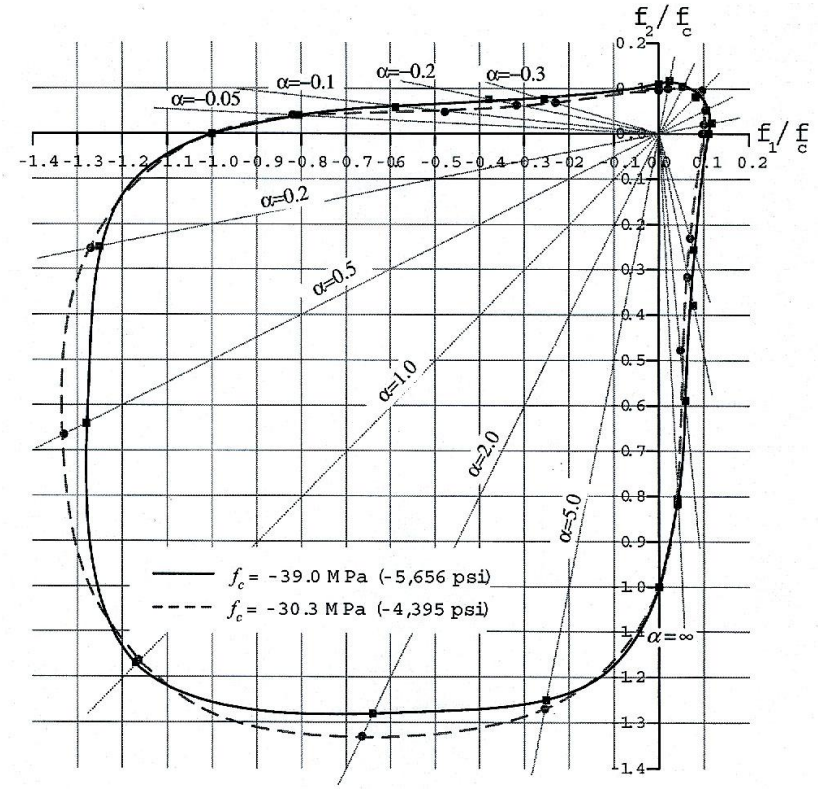

Figure 2.222 Biaxial strength envelopes.

Source: S-K. Lee, Y-C. Song, and S-H. Han, "Biaxial Behavior of Plain Concrete of Nuclear Containment Building," *Nuclear Engineering and Design* **227**, pp. 143-153, 2004.

investigated. Figure 2.223 presents biaxial stress-strain curves that were developed for the three different loading conditions for the wall and dome concrete materials. The stress-strain curve for specimens subjected to equal biaxial compression (f_2/f_1 = -1/-1) tends to have an initial slope that is relatively steep whereas for uniaxial compression (f_2/f_1 = 0/-1) the slope is much less indicating the effect of increased confinement under biaxial loading. Stress-strain curves for combined tension-compression show that the principal stress in the compressive direction (f_1) decreases as the absolute value of the stress ratio (f_2/f_1) increases due to the principal tensile stresses in the orthogonal direction increasing more due to the increase of absolute value of f_2/f_1 (principal compressive stress decrease). Typical crack patterns and failure modes are presented in Figure 2.224 and are similar to those obtained by other researchers. The fracture of concrete under uniaxial compression, Figure 2.224a, was determined by formation of a major crack. As the stress ratio increased, Figures 2.224b-d, the major cracks become inclined at increasing angles to the direction of applied loading. In the compression-tension region three different fracture mode patterns occurred. In Figure 2.224e a major crack formed at a 45˚ angle to the direction of applied compressive load, as well as many tensile cracks perpendicular to the direction of applied load. As the stress ratio increased, Figure 2.224f, fewer cracks formed perpendicular to the direction of applied load. Figures 2.224g and h exhibit only one apparent tensile crack. Figure 2.224i presents results for uniaxial tension in which the specimen failed by development of one major crack perpendicular to the direction of applied load. Figures 2.224j to l show a major crack developed at an approximate 45˚ inclination to the direction of maximum principal stresses as the stress ratio decreases to 1.0.

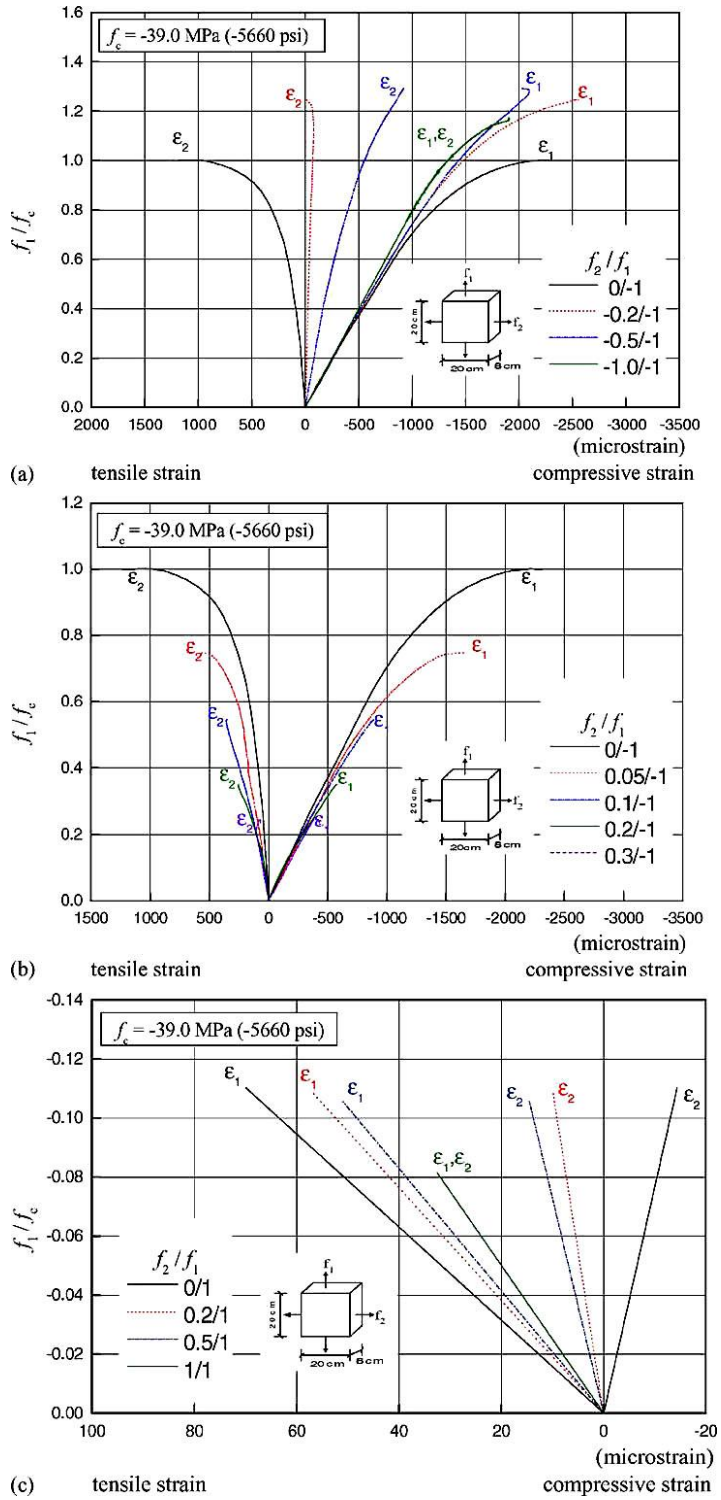

Figure 2.223 Stress-strain relationships for wall and dome concrete under: (a) biaxial compression, (b) combined compression and tension, and (c) biaxial tension.

Source: S-K. Lee, Y-C. Song, and S-H. Han, "Biaxial Behavior of Plain Concrete of Nuclear Containment Building," *Nuclear Engineering and Design* **227**, pp. 143-153, 2004.

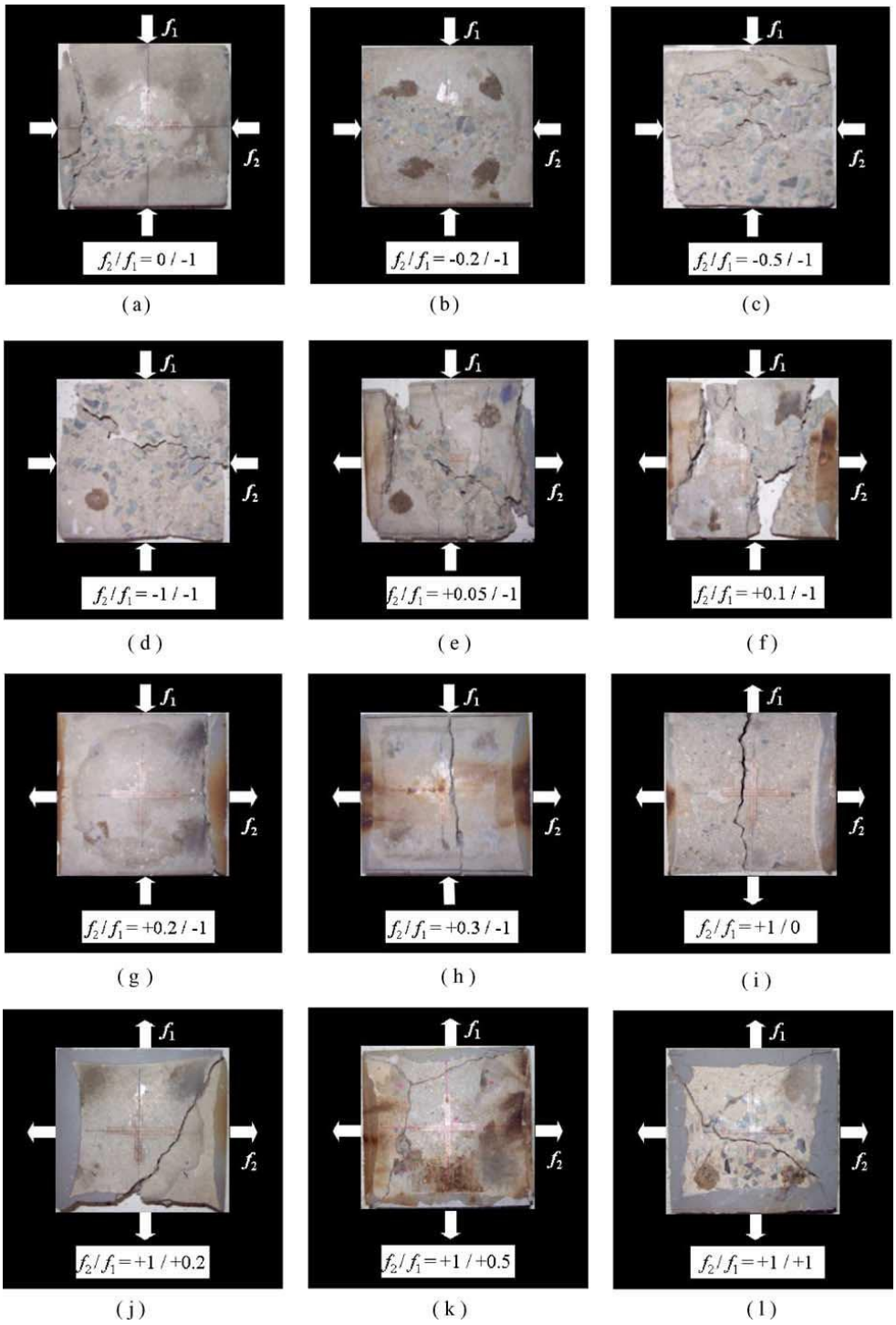

Figure 2.224 Failure modes under biaxial loading for different stress ratios.

Source: S-K. Lee, Y-C. Song, and S-H. Han, "Biaxial Behavior of Plain Concrete of Nuclear Containment Building," *Nuclear Engineering and Design* **227**, pp. 143-153, 2004.

Other researchers indicated that concrete under different biaxial loading conditions (e.g., compression-compression, compression-tension, and tension-tension) could be described by relatively simple mathematical relations [2.213]. The relations developed for the different loading regions are:

$$\left(\frac{\sigma_1}{\beta_p}+\frac{\sigma_2}{\beta_p}\right)^2+\frac{\sigma_1}{\beta_p}+3.65\frac{\sigma_2}{\beta_p}=0 \qquad \text{(compression-compression region)} \qquad (2.67)$$

$$\frac{\sigma_2}{\beta_z}=1+0.8\frac{\sigma_1}{\beta_p} \qquad \text{(compression-tension region)} \qquad (2.68)$$

$$\sigma_2=\beta_z=0.64\sqrt[3]{\beta_p^2}=\text{constant} \qquad \text{(tension-tension region)} \qquad (2.69)$$

where,

σ_1, σ_2 = principal stresses,
β_p = uniaxial compressive strength, and
β_z = uniaxial tensile strength.

The equations were obtained by breaking down the stress and strain states into hydrostatic and deviatoric components that could be used in conjunction with finite-element methods and force-deformation relations to provide a means to perform nonlinear analyses of structures.

Biaxial tests of a quartzite concrete (f_c' = 35.5 to 45.0 MPa) and mortar (f_c' = 35.0 MPa) using plate-shaped specimens (200 × 200 × 50 mm^3) were conducted [2.221]. After a 2-h hold time at temperatures of 150˚, 300˚, 450˚, or 600°C, the unsealed specimens were loaded to failure at a constant displacement rate using brush platens. Specimen heating was applied at the free surfaces. A comparison of uniaxial (x = 0) and biaxial (x = 0.7) results for tests at 300°C and 600°C is shown in Figure 2.225. Results have been normalized with respect to

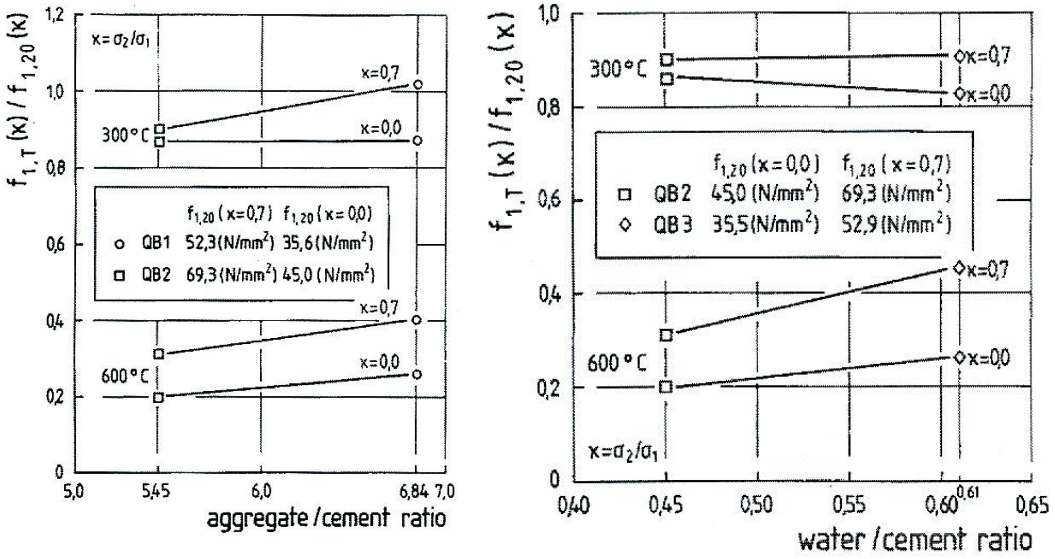

Figure 2.225 Influence of aggregate content and water-cement ratio on uniaxial and biaxial results for tests at 300°C and 600°C.

Source: K.-Ch. Thienel and F. S. Rostásy, "Influences of Concrete Composition on Strength and Deformations Under Uniaxial and Biaxial Loading at Elevated Temperature," Paper H04/6 in *Transactions of the 12th International Conference on Structural Mechanics in Reactor Technology*, pp. 145–150, 1993.

corresponding strength values at room temperature and the same stress ratio. The tests exhibited a smaller decrease in compressive strength for concrete with higher aggregate contents at both temperatures. Under biaxial loading, an increase in strength even appears at 300°C for the leaner mix. The effect of water-cement ratio on strength for uniaxially and biaxially loaded specimens is also presented in Figure 2.225. These results also have been

normalized and indicate that initially the water-cement ratio did not affect the temperature-dependent strength losses at 300˚C. After decomposition of the Portlandite (450˚ to 550˚C) the decrease in strength was at a lower rate for the concrete (QB3) made with a higher water-cement ratio. As the temperature increased, the influence of water-cement ratio decreased resulting in similar strength values for both concretes at 600˚C. The uniaxial strength of mortar was reduced less than that of concrete at temperatures above 300°C. The influence of aggregate content on residual modulus of elasticity at 300˚ and 600˚C is presented in Figure 2.226. At 300˚C the modulus is reduced more for the leaner concrete mix, however, at 600˚C the differences are on the same order for the two mixes. If a higher water-cement ratio is used, Figure 2.226, a similar trend is observed but the difference in modulus for the two concretes is greater at 300˚C. For ultimate strain in the direction of the main loading axis it was noted that the ultimate strain increases with increasing temperature, and at temperatures up to 300˚C there was a tendency for lower strain values for the concrete with higher aggregate contents. Biaxial compression was noted to result in higher strain values throughout the temperature range. The influence of stress ratio on the compressive strength for various temperatures is shown in Figure 2.227. The stress ratio of the compressive strength was varied between 0 and 1, where the stress ratio represents the ratio of the applied stresses in the two principal directions. The solid and dashed lines in the figure represent the mean biaxial behavior (predicted) at each temperature noted. The failure envelopes are similar for each temperature with increasing temperature producing a larger loss of biaxial strength. The difference between uniaxial and biaxial strength increased as the temperature increased. The temperature-dependent decrease in strength was affected by the composition of the concrete in the entire range of biaxial compressive stress. The maximum aggregate size had a significant influence on behavior, while the aggregate content and water-cement ratio were less influential.

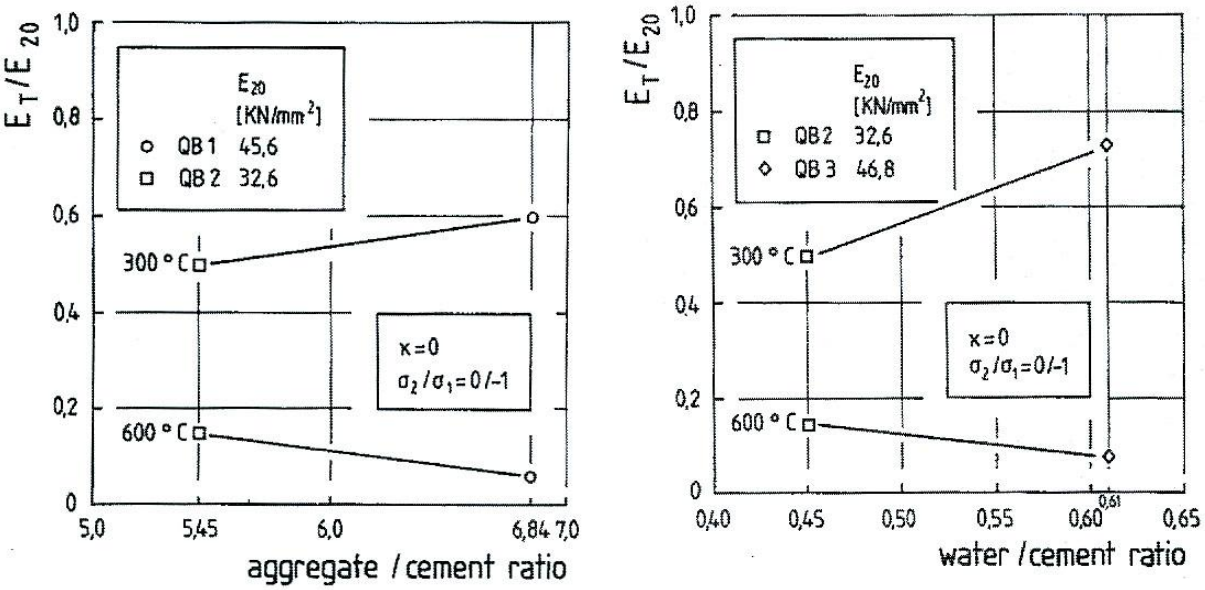

Figure 2.226 Influence of aggregate content and water-cement ratio on modulus of elasticity results for tests at 300°C and 600°C.

Source: K.-Ch. Thienel and F. S. Rostásy, "Influences of Concrete Composition on Strength and Deformations Under Uniaxial and Biaxial Loading at Elevated Temperature," Paper H04/6 in *Transactions of the 12th International Conference on Structural Mechanics in Reactor Technology*, pp. 145–150, 1993.

Experimental investigations at temperatures to 600˚C were made to determine the strengths and deformations of concretes subjected to biaxial compressive stresses [2.68]. Figure 2.37 presents the test frame used to conduct biaxial tests of 200 by 200 by 50 mm^3 gravel (quartz) concrete specimens [62.0 N/mm^2 (cube strength)] [2.68,2.69]. Load was applied to the specimen using four servohydraulic jacks. The tests were conducted at temperature using unsealed specimens. Figure 2.228 presents the effect of loading platen (brush or rigid) on the concrete biaxial strength. The brush platens provided a reduction in strain inhibition and a corresponding decrease in strength compared to rigid platen results. The effect of elevated temperature on concrete biaxial strength is presented in

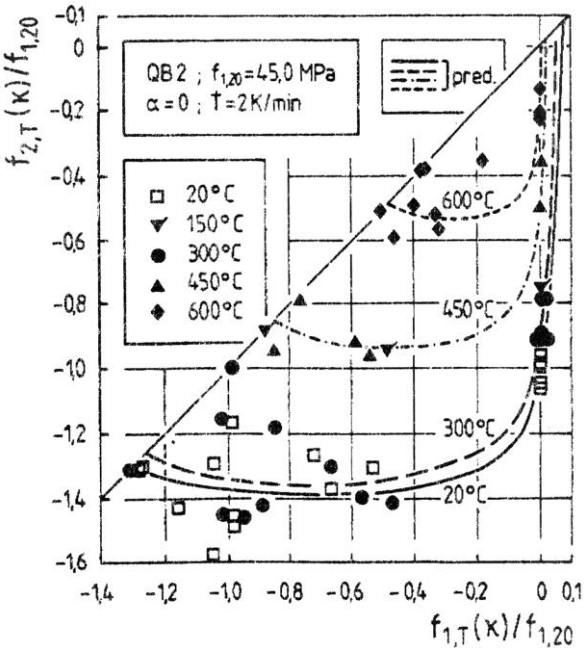

Figure 2.227 Biaxial compressive strength at different temperatures.

Source: K.-Ch. Thienel and F. S. Rostásy, "Strength of Concrete Subjected to High Temperature and Biaxial Stress; Experiments and Modeling," *Materials and Structures* **28**, pp. 575–580, 1995.

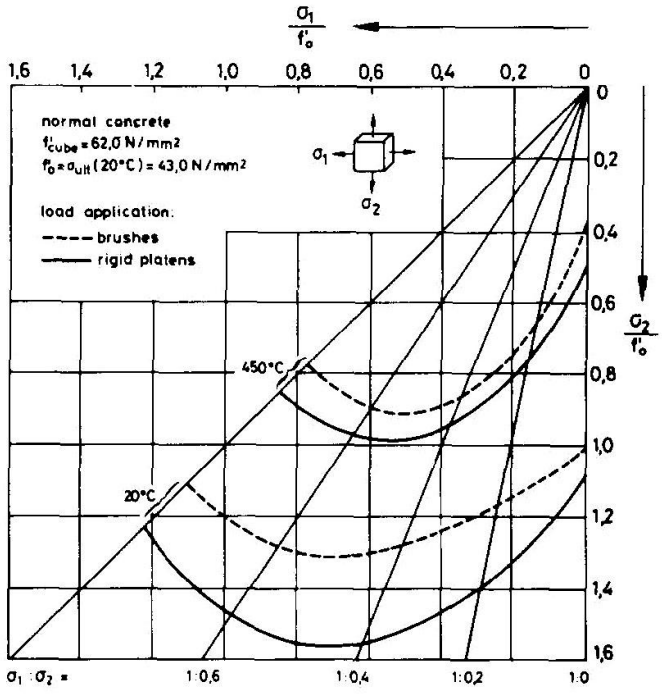

Figure 2.228 Effect of loading platen type on concrete biaxial strength.

Source: C. Ehm and U. Schneider, "The High Temperature Behaviour of Concrete Under Biaxial Load," *Cement and Concrete Research* **25**, pp. 27-34, 1985.

Figure 2.229 where the data are reported as a fraction of the unconfined uniaxial compressive strength at 20˚C. Results show that the strength of concrete under biaxial compression is higher than under uniaxial compression. At 20˚C the strength ratio reaches a maximum of 1.34 with the relative increase in ultimate strength at this stress ratio being more marked at higher temperatures. In uniaxial loading the ultimate failure occurred by splitting in the plane parallel to the load and perpendicular to the specimen face, while in biaxial compression loading the ultimate failure occurred by splitting along planes parallel to the load and parallel to the specimen free surface. Deformation results were presented previously in Section 2.2.1.1.

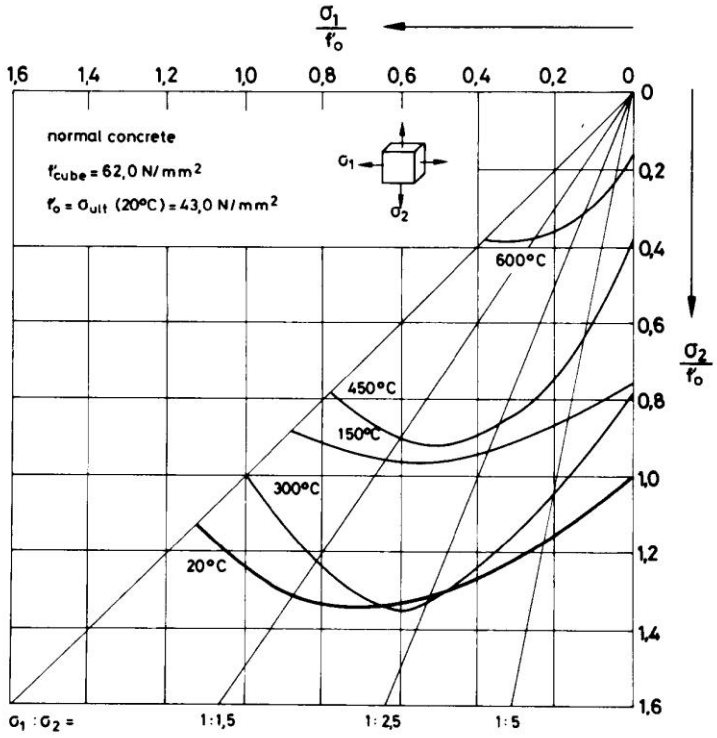

Figure 2.229 Effect of temperature on concrete biaxial strength.

Source: C. Ehm and U. Schneider, "The High Temperature Behaviour of Concrete Under Biaxial Load," *Cement and Concrete Research* **25**, pp/ 27-34, 1985.

Biaxial tension-compression tests (residual) at elevated temperature (i.e., 20˚, 200˚, 300˚, 500˚, and 600˚C) have been conducted [2.70]. Specimens 100 by 100 by 100 mm^3 were fabricated using a 20-mm-maximum-size crushed limestone aggregate concrete having reference compressive and tensile strengths of 32.5 and 3.14 MPa, respectively. The specimens were held at temperature for six hours and then permitted to slowly cool to room temperature prior to testing. Stress ratios (σ_2/σ_3) investigated included 0 (uniaxial), -0.1, -0.25, -0.5, and -0.75. Tensile loads were applied by gluing the specimen surface to the tensile loading platens. Figure 2.230 presents the change in tensile strength with temperature for the stress ratios investigated. For each stress ratio all tensile strengths follow the same pattern. A regression equation between tensile strength and temperature, also shown in the figure, was developed:

$$\sigma_T(t) = \sigma_T(-0.001t + 0.9798), \tag{2.70}$$

where, $\sigma_T(t)$ is the tensile strength for any stress ratio corresponding to temperature t,
σ_T is tensile strength at 20˚C and for any stress ratio, and
t = temperature.

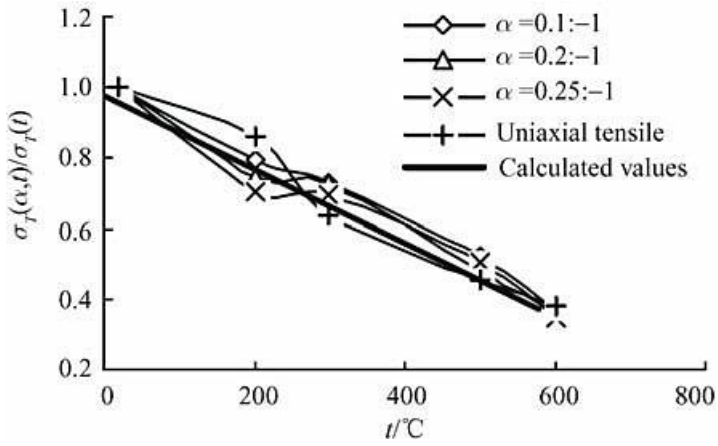

Figure 2.230 Change in tensile strength with temperature.

Source: Y. Song, A. Zhang, L. Qing, and C. Yu, "Biaxial Tensile-Compressive Experiment on Concrete at High Temperatures," *Frontiers of Architecture and Civil Engineering in China* **1**(1), pp. 94-98, 2007.

The relationship between tensile strength and stress ratio and temperature is presented in Figure 2.231 and shows that at each temperature the tensile strength decreases with the decline in absolute values of the stress ratios.

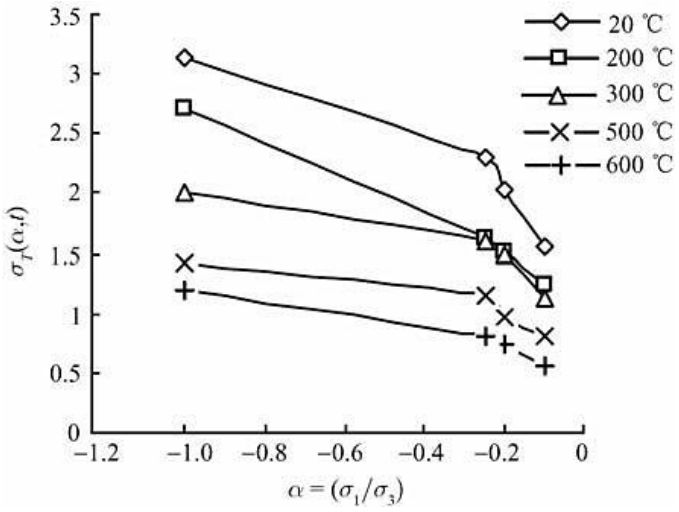

Figure 2.231 Effect of temperature on the relationship between tensile strength and stress ratios.

Source: Y. Song, A. Zhang, L. Qing, and C. Yu, "Biaxial Tensile-Compressive Experiment on Concrete at High Temperatures," *Frontiers of Architecture and Civil Engineering in China* **1**(1), pp. 94-98, 2007.

A two-linear regression equation between tensile strength, stress ratio, and temperature was developed:

$$\sigma_T(\alpha,t)=(-1.518\alpha+0.3659)f_T(t) \qquad -0.4177 \le \alpha \le -0.1 \qquad (2.71)$$

$$\sigma_T(\alpha,t)=f_T(t) \qquad \alpha < -0.4177, \qquad (2.72)$$

where, $\sigma_T(\alpha,t)$ is the tensile strength at t (˚C) for various stress ratios. The failure envelopes under biaxial tensile-compressive stresses derived from the experimental data are presented in Figure 2.232. For every temperature all

envelopes are somewhat concave to the $\sigma_3(t)/\sigma_{c20}$ axis. A linear regression failure equation has been developed from the data:

$$\sigma_{3(t)} = 10.891\sigma_1(t) + 0.01487\sigma_1(t)t + \sigma_c(t), \text{ where} \tag{2.73}$$

$\sigma_3(t)$ and $\sigma_1(t)$ are compressive and tensile strengths, respectively, and $\sigma_c(t)$ is the uniaxial compressive strength for various temperatures whose value can be estimated from

$$\frac{\sigma_{c(t)}}{f_c} = -1.2x10^{-6}t^2 - 1x10^{-5}t + 1.0016, \text{ where} \tag{2.74}$$

f_c is the concrete uniaxial compressive strength at room temperature. Conclusions of the study for concrete under biaxial tension-compression loading were that: at high temperature sudden tensile failure occurs for stress ratios less than or equal to -1.0; both the absolute value of tensile and compressive strengths decrease with increasing temperature with a drop in absolute values of tensile strain (ε_1) and compressive strain (ε_3) being similar to that of strength; and the tensile strength increases with a decrease in stress ratio and reaches a maximum value at the uniaxial tensile stress state, but the absolute value of compressive strength (and compressive strain ε_3) decreases with a decrease in stress ratio and reaches a maximum value at the uniaxial compressive stress state.

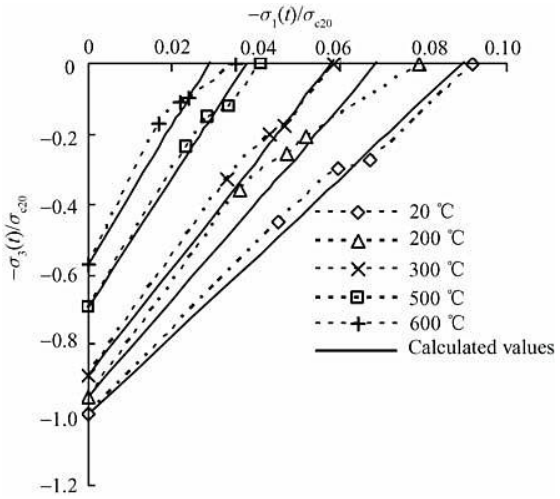

Figure 2.232 Effect of temperature on the concrete biaxial tension-compression failure envelopes.

Source: Y. Song, A. Zhang, L. Qing, and C. Yu, "Biaxial Tensile-Compressive Experiment on Concrete at High Temperatures," *Frontiers of Architecture and Civil Engineering in China* **1**(1), pp. 94-98, 2007.

Elsewhere for biaxial testing of concrete at elevated temperature it was noted that when the principal stress ratio remains constant, the biaxial strength of the concrete decreased with an increase in temperature [2.222]. Loss of strength was observed at 150°C under biaxial conditions but was much lower than that obtained under uniaxial loading. Under the same elevated temperature, the biaxial strength of concrete varied with different values of principal stress ratio. When the principal stress ratio equaled 0.5, the biaxial strength of concrete at high temperature reached a maximum.

Triaxial testing of concrete at elevated temperature was conducted using solid and hollow cylinders [2.223]. The specimens were either in a sealed or unsealed condition after exposure to temperatures up to 150˚C. Triaxial stress was imposed on the specimens by applying a hydrostatic pressure of 3.31 MPa during axial loading. The moisture loss varied directly with the strength after heat exposure. The sealed concrete strengths were reduced to about 70% and 60% of the reference strength at 100˚ and 150˚C, respectively.

An apparatus for testing concrete under multiaxial compression loading at elevated temperature has been recently developed at the University of Sheffield [2.224]. The apparatus (Figure 2.233) can subject 100 mm cubic concrete specimens to true multiaxial compression ($s_1 \neq s_2 \neq s_3$) up to 400 MPa at temperatures to 300˚C. Forces are delivered through three independent loading frames equipped with servo-controlled hydraulic actuators creating uniform displacement boundary conditions via rigid platens. Displacements are measured to an accuracy of 10^{-6} m using a system of six laser interferometers. Complex experiments can be conducted involving (1) load and temperature cycling, (2) small stress probes, and (3) arbitrary (pre-defined) loading paths. The apparatus has been used to investigate uniaxial, biaxial, and hydrostatic compression in partially sealed conditions, at temperatures up to 250˚C of an ordinary Portland cement quartz-diorite concrete [2.225]. The elevated temperature tests were performed in two phases: (1) conditioning and (2) deviatoric loading. In the conditioning phase the specimens were heated to different heat-load regimes [e.g., heated without load and held under constant temperature (HS), loaded then heated and held under steady-state conditions (LHS), heated without load then loaded and held under constant temperature and load (HLS), or loaded first and subjected to a thermal cycle followed by a steady-state period (LHCHS)]. Results of the conditioning phases were used to determine the load-induced thermal strain defined as the difference between the strains recorded in LHS and HS tests. The effects of the different conditioning regimes on the properties of the material under multiaxial compression loading were investigated during the deviatoric loading phase performed at a constant temperature of 250˚C. The reference only presents results of the conditioning phase (i.e., load-induced thermal strain for concrete heated at two different rates under uniaxial, biaxial, and hydrostatic compression of either 13 MPa or 26 MPa). Figure 2.234 provides a summary of the averaged strains recorded in all the tests (i.e., load-induced thermal strain and shrinkage, and load-induced thermal strain). Results indicate that: the load-induced thermal strain is a function of load, temperature, and moisture movement; and only occurs on first heating of loaded concrete to a given temperature and not during cooling or upon second heating to the same temperature, but if the second heating cycle exceeds the first the strains start to increase again at a similar rate to that of the first heating cycle.

Figure 2.233 mac^{2T} apparatus for multiaxial compression of concrete at elevated temperature.

Source: M. Petkovski, R.S. Crouch, and P. Waldron, "Apparatus of Testing Concrete Under Multiaxial Compression at Elevated Temperature (max^{2T})," *Experimental Mechanics* **46**, pp. 387-398, 2006.

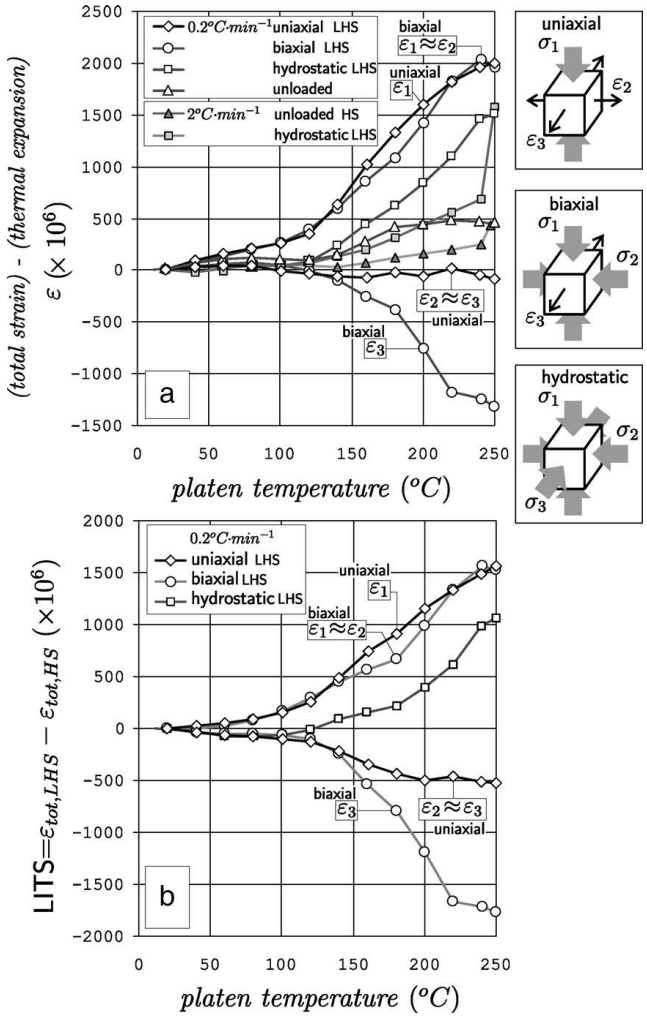

Figure 2.234 Average temperature-strain relationships from all LHS and HS tests: (a) load-induced thermal strain and shrinkage, (b) load-induced thermal strain.

Source: M. Petkovski and R.S. Crouch, "Strains Under Transient Hygro-Thermal States in Concrete Loaded in Multiaxial Compression and Heated to 250˚C," *Cement and Concrete Research* **38**, pp. 586-596, 2008.

Summary. Several conclusions can be derived from the multiaxial strength results. Multiaxial strength and strength envelopes are an important basis for the analysis and design of concrete structures. The platen-interface constraint influences test results (i.e., strength increases as the constraint increases). Ultimate strength of concrete at room temperature increases under multiaxial compressive loading with maximum biaxial compressive strength being about 1.25 times uniaxial compressive strength and triaxial compressive strength being four to six times uniaxial compressive strength. Under essentially biaxial conditions where stresses in two directions are substantially larger than the third, there is little increase in strength and if the stress in the third direction becomes tensile the biaxial strength is reduced below the uniaxial strength [2.135]. Sealed specimens are weaker than dry concrete, but wet concrete gives a greater relative increase in strength under multiaxial stress conditions. For biaxial loading at elevated temperature the maximum aggregate size had a significant influence on results, the aggregate content and water-cement ratio generally had second-order effects, the failure envelopes although similar for each temperature as the temperature increased the loss of biaxial strength increased, and when the principal stress ratio remained constant the biaxial strength of the concrete decreased with an increase in temperature. Difference between uniaxial and biaxial strength increased as the temperature increased. Under elevated temperature biaxial tension-compression loading, the tensile strength decreased with the decline in absolute values of the stress ratios at each temperature.

2.2.2 Physical Properties and Thermal Effects

The physical, or thermal, properties of concrete are important both in the planning of mass concrete construction (thermal changes) and the dissipation of heat build up during operation. The thermal expansion coefficient and modulus of elasticity data are prerequisite to computing the thermoelastic stresses that result from nonuniform heating. Desirable thermal properties identified for a prestressed concrete pressure vessel (PCPV) are summarized in Table 2.8.

Table 2.8 Preferred concrete physical properties

Preferred property	Reason
High density	To provide good neutron and gamma ray absorption properties
Low elastic and creep deformation under load	To reduce movements and the redistribution of stresses under varying load and temperature cycles To reduce prestress losses
Low drying shrinkage	To reduce movements and temperature stresses
Low thermal expansion	To reduce movements and temperature stresses
Resistant to thermal shock	To prevent damage to structure under rapid heating application (i.e., adjacent to steam penetrations)
High thermal conductivity	To minimize the cooling system requirements to keep vessel concrete at a permissible level (PCPVs)

Source: R.D. Browne, "Properties of Concrete in Reactor Vessels," *Proceedings of the Conference on Prestressed Concrete Pressure Vessels*, Group C, Paper 13, pp. 131-151, Institute of Civil Engineers, London, United Kingdom, 1967.

As water is added to cement, an exothermic chemical reaction takes place. If the heat is generated at a faster rate than it can be dissipated, a temperature rise occurs. Factors affecting the amount and rate of heat generated during this reaction are the cement type, temperature at placement, water-cement ratio, and cement content. In mass concrete structures where there can be significant heat build up, cracking can occur upon cooling because the exterior of the structure will cool faster than the interior. However, by using low (Type IV) or moderate (Type II) heat of hydration cements and following the procedures recommended in Ref. 2.226, this problem can be minimized.

Under normal conditions, most concrete structures are subjected to a range of temperature no more severe than that imposed by ambient environmental conditions. However, there are important cases where these structures may experience much higher thermal loadings.* For example, local temperature loadings (hot spots) can develop at internal faces of a structure due to local loss of insulation, jet impingement (following pipe rupture), or hot penetrations. Internal gas temperatures under accident conditions operate on the lined faces of containments and internal structures resulting in a temperature distribution set up across a wall that can lead to significant internal forces and moments as well as affecting material properties of concrete that in turn can affect concrete creep and relaxation of post-tensioning tendon forces (where applicable).

Concrete's thermal properties are more complex than for most materials because not only is the concrete a composite material whose components have different properties, but also its properties depend on moisture content and porosity. Temperature variations produce expansions or contractions of concrete structures. If movement of a structure is restrained, significant internal stresses can develop, thus leading to cracking, distortions, or even destruction. In general, the density, conductivity, and diffusivity of concrete will increase with an increase in temperature. The coefficient of thermal expansion α is used as a measure of the volume change of a material subjected to a temperature differential. Dissipation of heat is important to nuclear power plant structures such as a PCPV because it affects the development of thermal gradients and the resulting thermal stresses. The basic quantities involved are (1) the coefficient of thermal conductivity λ, (2) the thermal diffusivity D, and (3) the specific heat c_p. These quantities are related by the term $D = \lambda/\rho c_p$ (m^2/s).

* Concrete structures that experience radiation also can develop thermal gradients as a result of radiation absorption.

2.2.2.1 Porosity and Density

Information and Data. The loss of evaporable water does not affect porosity, however, dehydration creates additional pore space to effectively increase the porosity as the temperature increases [2.24]. The average pore size increases with temperature as the ultrafine gel structure of the calcium silicate hydrate is progressively destroyed by dehydration [2.16]. At 850˚C porosity is about 40% greater than it was at 105˚C [2.24], as noted in Figure 2.235. As a result of the pore size increase the bulk mass density of the cement paste decreases with temperature (i.e., from 1.45 g/cm^3 at 105˚C to 1.3 g/cm^3 at 850˚C [2.24]).

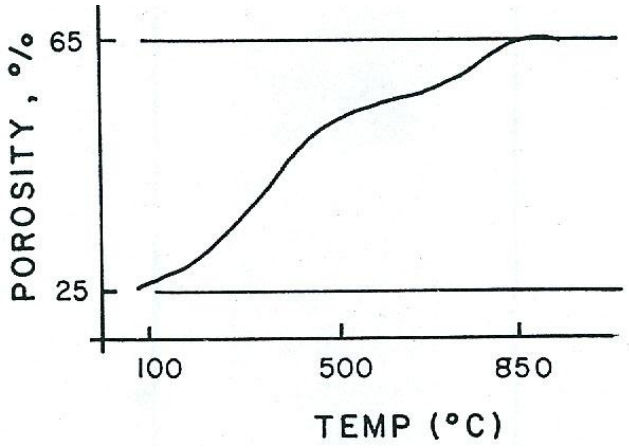

Figure 2.235 Variation of Portland cement paste porosity with temperature.

Source: T. Z. Harmathy, "Thermal Properties of Concrete at Elevated Temperatures," *J. of Materials* **5**, pp. 47–74, 1970.

As the volume of a given mass of concrete changes on exposure to elevated temperature, the mass density will also change. Changes in mass density result from thermal expansion and drying shrinkage, diffusion of water or released gases, and dehydration, melting, or sintering. The density of concrete depends on the density of its aggregate materials and its moisture content in the temperature range from 20°C to 150°C. Figure 2.236 presents variations of true density, bulk density, and porosity for a cement paste [2.24]. In the unsealed condition results reflect the

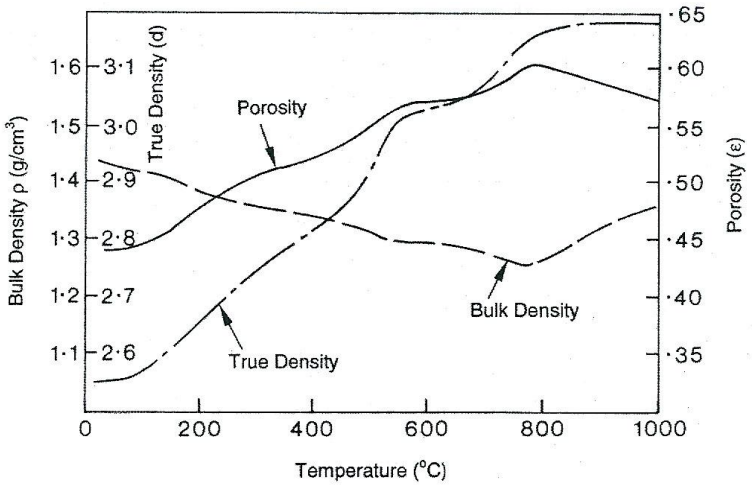

Figure 2.236 True density, bulk density, and porosity of cement paste versus temperature.

Source: T. Z. Harmathy, "Thermal Properties of Concrete at Elevated Temperatures," *J. of Materials* **5**, pp. 47–74, 1970.

influences of chemical transformations that include water dilation up to about 80˚C, the loss of free and physically bound water at 100˚ to 200˚C depending on section size and heating rate, followed by loss of chemically-combined water at temperatures above 100˚C, the dissociation of calcium hydroxide at 400˚ to 500˚C, and decarbonation above 600˚C [2.19]. In concrete the aggregate plays an important role in terms of thermal dilation and the dissociation of some aggregates such as carbonate aggregates that display a significant reduction in density above 600˚C and a marked increase in porosity [2.19]. Figure 2.237 presents the effect of aggregate type on the density of concretes in the temperature range from room temperature to 1000°C [2.19]. Storage (curing or preconditioning) conditions at lower temperature are also important because moist specimens will lose water and thus experience a greater decrease in density upon heating than specimens that have experienced drying. At temperatures from 150°C to 600°C the density of limestone concrete is relatively constant. At temperatures from 600˚ to 900˚C decarbonation of limestone commences and weight loss occurs [2.227] as the concrete porosity increases until at higher temperatures sintering takes place and the density may increase slightly [2.15]. Siliceous aggregates exhibit a somewhat steeper decrease in density with heating in the range from room temperature to 700°C due to the large thermal expansion of the quartz. Basalt exhibits the smallest decline in density because of its lower thermal expansion [2.15]. Figure 2.238 presents bulk density as a function of temperature for a 38-MPa basalt aggregate concrete utilized for Korean nuclear power plants [2.228] and Figure 2.239 provides additional data on the density of normal and lightweight concretes as a function of temperature.

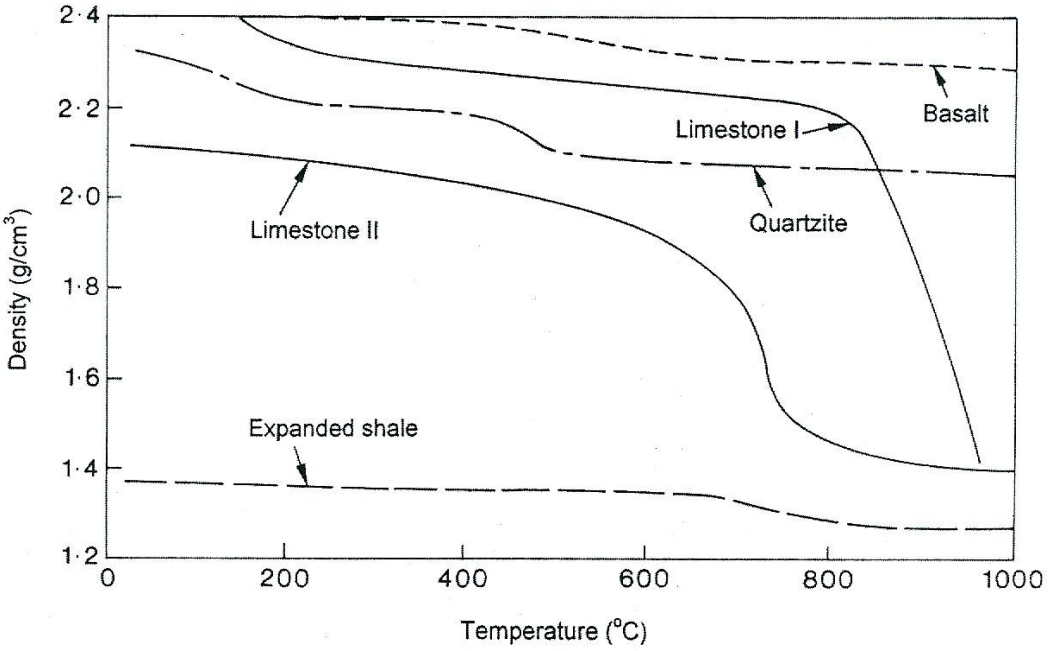

Figure 2.237 Density of concretes having different coarse aggregate types.

Source: *Fire Design of Concrete Structures – Materials, Structures and Modelling*, Bulletin 38, International Federation for Structural Concrete, Lausanne, Switzerland, April 2007.

Summary. The loss of evaporable water does not affect porosity, however, as the temperature increases dehydration creates additional pore space to effectively increase the porosity. The average pore size increases with temperature as the ultrafine gel structure of the calcium silicate hydrate is progressively destroyed by dehydration, with porosity being about 40% greater at 850˚C than it was at 105˚C. Changes in density are related to weight changes, thermal dilation, and changes in porosity. In temperature range 20˚ to 150˚C the density of concrete depends on the density of the aggregates and their moisture content, and is affected by storage conditions, with water-stored specimens changing most. At temperatures greater than 150˚ to ~600˚C there is a minor change in density of limestone aggregate concretes, however, at temperatures greater than 600˚C decomposition of limestone leads to a porous material. Siliceous aggregate concretes exhibit a steeper decline in density than calcitic aggregate concretes for temperatures from 20˚ to 700˚C. Basalt aggregate concretes exhibit a smaller decrease in density with temperature because they have relatively low thermal expansion.

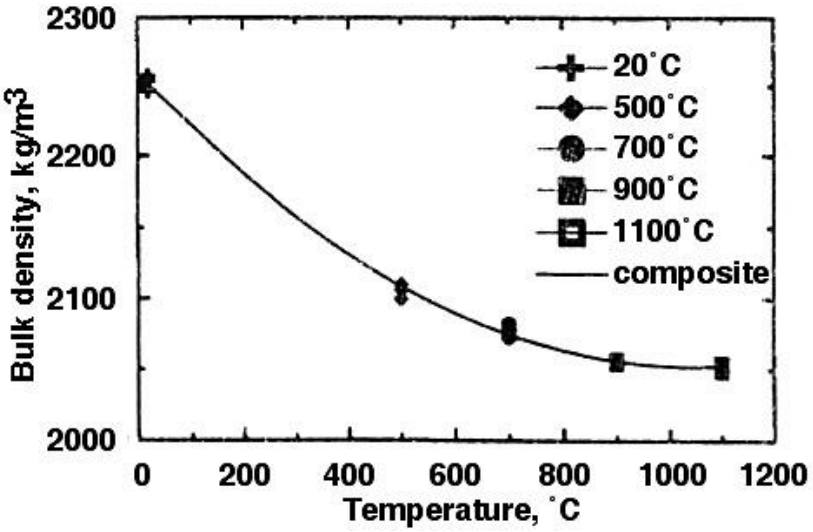

Figure 2.238 Density of a nuclear power plant concrete vs temperature.

Source: K-Y. Shin, S-B. Kim, J-H. Kim, M. Chung, and P-S. Jung, "Thermo-Physical Properties and Transient Heat Transfer of Concrete at Elevated Temperatures," *Nuclear Engineering and Design* 212, pp. 233–241, 2002.

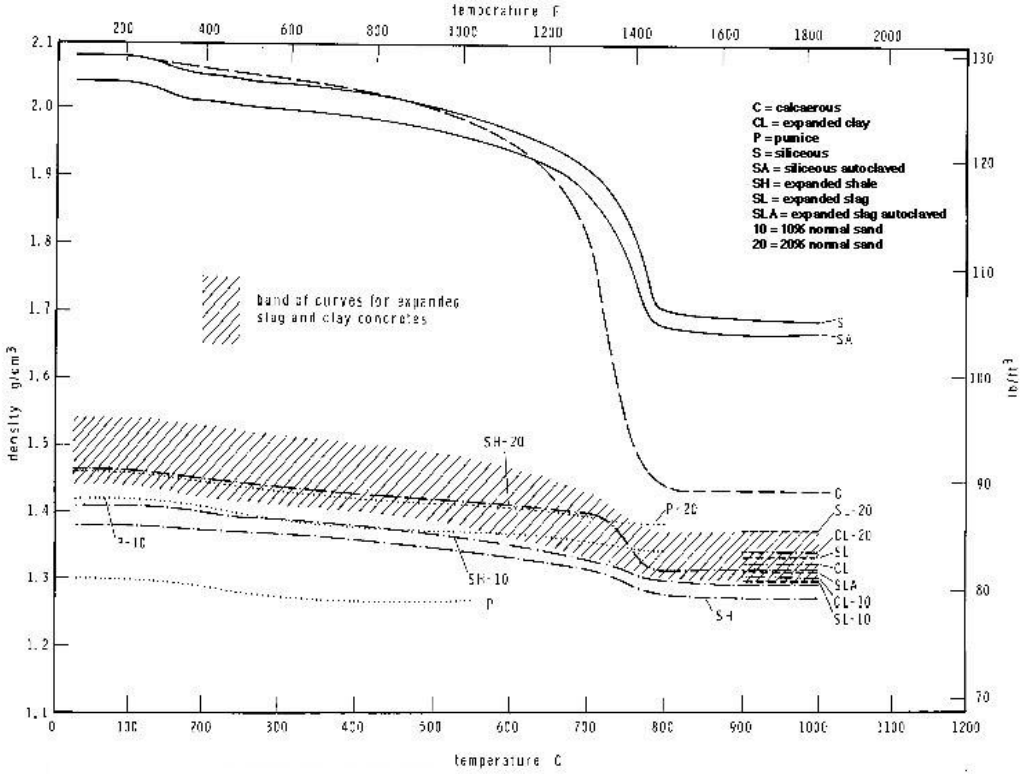

Figure 2.239 Density of normal and lightweight concretes versus temperature.

Source: T. Z Harmathy. and L.W. Allen, "Thermal Properties of Selected Masonry Unit Concretes," *Journal of American Concrete Institute* **70**, pp. 132–142, 1973.

2.2.2.2 Coefficient of Thermal Expansion

Information and Data. The coefficient of thermal expansion represents the volume change of a material due to temperature change and is expressed as a change in length per degree of temperature change. The coefficient is important as a measure of the structural movement and thermal stresses resulting from a temperature change that can lead to cracking and spalling.

Concrete's thermal expansion is a complicated phenomenon because of the interaction of its two main components - cement paste and aggregate - which each have their own coefficients of thermal expansion. When differences in the thermal expansion between the hardened cement paste and aggregate are large, heating causes microstresses and microcracking that can disrupt the concrete microstructure. Observations of thermal expansion are complicated by various extraneous effects that accompany the temperature change (e.g., additional volume changes caused by changes in moisture content, chemical reactions leading to dehydration and conversion, and creep and microcracking resulting from non-uniform thermal stresses) [2.5].

Figure 2.240 presents data on the change of length of hardened Portland cement paste at elevated temperature. Initially the hardened cement paste expands on heating up to approximately 150˚C, the maximum expansion being on the order of 0.2% [2.5]. Expansion ceases between 150˚ and 300˚C and then between 300˚ and 800˚C the hardened cement paste shrinks with the shrinkage being 1.6 to 2.2% at 800˚C. The initial expansion has been

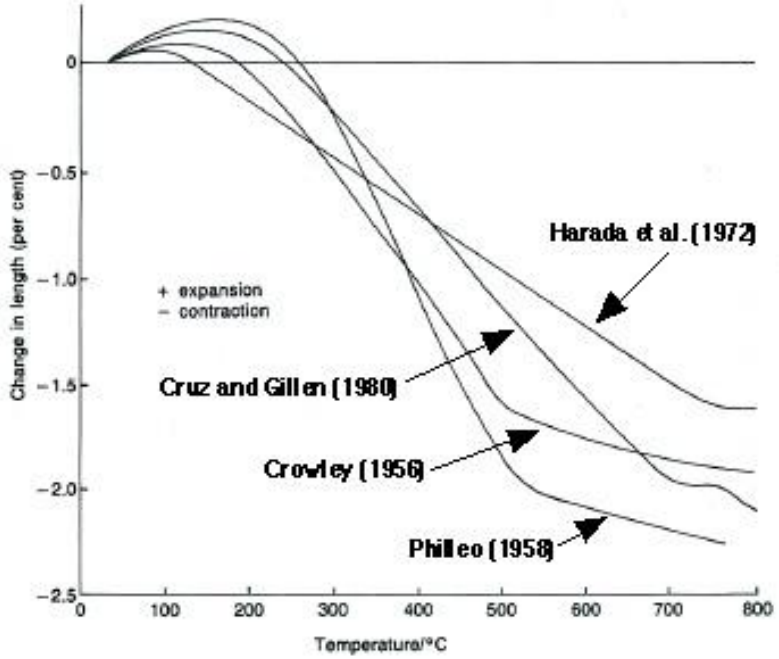

Figure 2.240 Length change of Portland cement paste specimens at elevated temperature.

Source: Z.P. Bazant and M.F. Kaplan, *Concrete at High Temperatures: Material Properties and Mathematical Models*, Longman, London, United Kingdom, 1996.

attributed to kinetic molecular movements in the cement paste plus swelling pressures caused by a decrease in capillary tension of water as the temperature rises [2.229]. Up to about 300˚C thermal shrinkage and thermal expansion both occur to produce a net expansion of the cement paste and at higher temperatures thermal shrinkage exceeds thermal expansion. Shrinkage of the cement paste results from loss of evaporable and chemically-combined water.

Because the aggregate generally constitutes a major proportion of the mix, it primarily influences the resultant coefficient of thermal expansion. Selection of an aggregate with a low coefficient of thermal expansion may help in crack prevention in mass concrete. The main factor affecting the coefficient of thermal expansion of aggregate

materials is the percentage by weight of silica present in the aggregate [2.230]. Aggregates with little or no silica (e.g., limestone) have the lowest coefficients of thermal expansion. Table 2.9 presents typical values for coefficients of thermal expansion for different rocks and concretes at normal temperatures. Scatter within an aggregate (rock) type is due to the anisotropic nature of most rocks relative to exhibiting differing expansions in different directions. Processed lightweight aggregates (e.g., expanded slag, shale, or clay) have lower coefficients of thermal expansion than naturally-occurring rocks. Table 2.10 presents the effect of temperature on the coefficient of thermal expansion values and Figure 2.241 presents examples of linear thermal expansion of various rocks with temperature.

Table 2.9 Coefficients of thermal expansion of different rocks and concrete at normal temperature

Rock Group	Typical silica content by wt. %	Coefficient of thermal expansion (10^{-6} °C^{-1})			
		Rock		Concrete	
		Range	Average	Range	Average
Chert	94	7.4-13.0	11.8	11.4-12.2	-
Quartzite	94	7.0-13.2	10.3	11.7-14.6	12.1
Quartz				9.0-13.2	-
Sandstone	84	4.3-12.1	9.3	9.2-13.3	11.4
Marble	Negligible	2.2-16.0	8.3	4.1-17.4	10.7
Siliceous limestone	45	3.6-9.7	8.3	8.1-11.0	10.7
Granite	66	1.8-11.9	6.8	8.1-10.3	9.6
Dolerite	50	4.5-8.5	6.8	-	9.6
Basalt	51	4.0-9.7	6.4	7.9-10.4	9.3
Limestone	Negligible	1.8-11.7	5.5	4.3-10.3	8.6
Gravel	5-95			9.0-13.7	

Source: R.D. Browne, "Properties of Concrete in Reactor Vessels," *Proceedings of the Conference on Prestressed Concrete Pressure Vessels*, Group C, Paper 13, pp. 131-151, Institute of Civil Engineers, London, United Kingdom, 1967.

Table 2.10 Effect of elevated temperatures on the coefficient of thermal expansion on selected rocks

Temperature range (˚C)	Coefficient of thermal expansion (10^{-6} °C^{-1})			
	Sandstone	Limestone	Granite	Anorthsite
20-100	10.0	3.0	4.0	4.0
100-300	15.0	9.0	13.5	8.5
300-500	21.5	17.0	26.0	10.0
500-700	25.0	33.0	47.5	12.5

Source: Z.P. Bazant and M.F. Kaplan, *Concrete at High Temperatures: Material Properties and Mathematical Models*, Longman, London, United Kingdom, 1996.

The resultant coefficient of thermal expansion for concrete is dominated by the aggregate material, however, the resulting coefficient tends to be somewhat higher due to the larger thermal expansion coefficient of the hardened cement paste, and will increase in proportion to the cement content [2.231]. It has been indicated that up to 700˚C the concrete expansion is very similar to that for the aggregate used in the concrete [2.54]. In theory, the coefficient of thermal expansion of concrete can be calculated based on knowledge of the relative volumetric proportions, the relative elasticities, and the thermal expansion coefficients of its constituents [2.136]. Figure 2.242 presents thermal coefficient of expansion values for neat cements, mortars, and concretes [2.232]. As shown, values of the coefficient for concretes range from ~2.2×10^{-6} to 3.9×10^{-6} per °C with 3.1×10^{-6} per °C being a typical value. The coefficient of thermal expansion of hardened cement paste and concrete tend to initially increase slightly with age due to a decrease in internal relative humidity and then decrease slowly [2.233]. The coefficient is influenced by the moisture condition (applies to paste component) and has minimum values for the two extremes: dry and saturated [2.227].

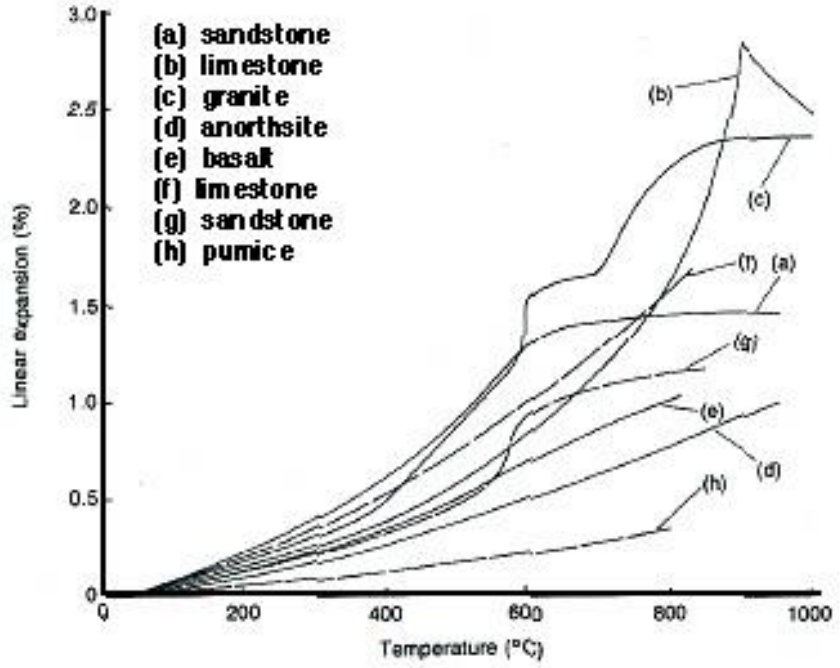

Figure 2.241 Linear thermal expansion of various rocks with temperature.

Source: Z.P. Bazant and M.F. Kaplan, *Concrete at High Temperatures: Material Properties and Mathematical Models*, Longman, London, United Kingdom, 1996.

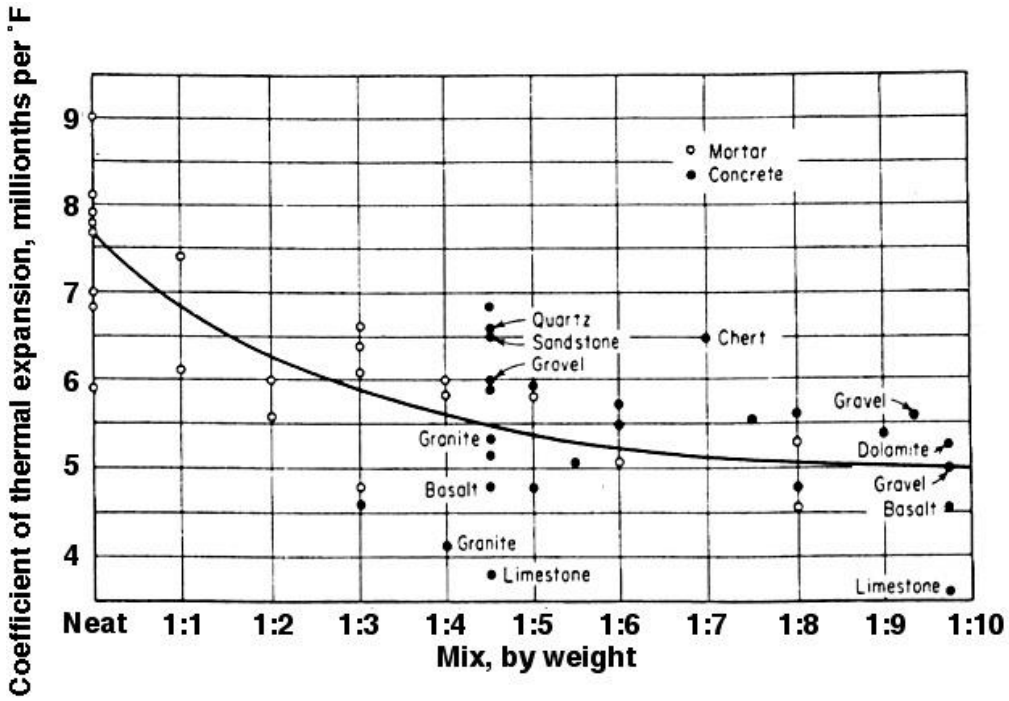

Figure 2.242 Coefficients of thermal expansion of neat cements, mortars, and concretes.

Source: *Concrete Manual*, 7th Ed., U.S. Bureau of Reclamation, Denver, Colorado, 1963.

Figure 2.243 presents a comparison of thermal strain results for Portland cement paste, mortars, and concretes for temperatures to 871˚C [2.234]. The coefficient of linear expansion increases with increasing temperature due to the aggregate expansion dominating over contraction of the cement paste, however, the effects of specimen moisture

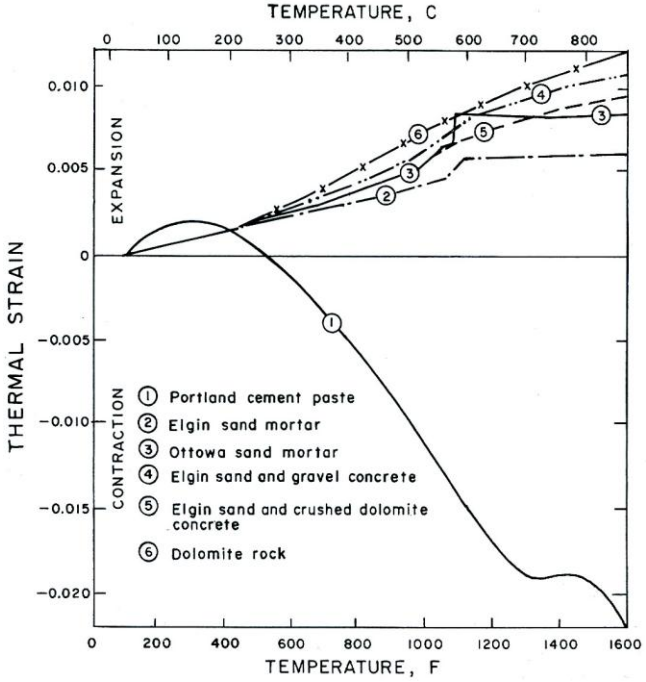

Figure 2.243 Thermal strain of Portland cement, mortar ,and concrete on heating.

Source: C.R. Cruz and M. Gillen, "Thermal Expansion of Portland Cement Paste, Mortar, and Concrete at High Temperature," *Fire and Materials* **4**(2), 1980.

condition at test initiation (i.e., the number of thermal cycles that have been applied to the specimen) also has to be taken into consideration in determining the net specimen length change with temperature [2.235]. Table 2.11 presents coefficient of thermal expansion values at elevated temperatures for concretes made with different aggregates, including heavyweight aggregate materials. Results have been presented that indicate that lightweight aggregate concretes (e.g., pumice and expanded shale aggregates) may shrink at temperatures greater than 300˚C [2.18]. Tests of sealed concrete indicate that under thermal cycling (20˚ to 149˚ to 20˚C) permanent expansive set occurs after one cycle and the permanent expansion increases with increasing number of cycles, but at a decreasing rate [2.65]. Also the coefficient decreased as the number of cycles increased and specimens permitted to dry after initial heating showed less expansion during subsequent thermal cycles.

Table 2.11 Coefficients of thermal expansion at elevated temperature for concretes made with different aggregates

Type of aggregate in concrete	Coefficient of thermal expansion (10^{-6} ˚C^{-1})		
	Below 300˚C	300˚-600˚C	600˚-800˚C
Granite	0.71	10.4	15.9
Serpentine	4.14	4.1	1.3
Limonite	4.86	4.5	4.2
Haematite	5.94	11.5	16.2
Steel shot	4.20	8.5	16.2
Iron and steel scrap	5.1	7.2	8.6

Source: A.N. Komarovskii, *Design of Nuclear Plants*, 2nd Edition, Atomizdat, Moscow, Chapter 7 (Translated from Russian by Israel Program for Scientific Translations, Jerusalem), 1968.

Additional thermal expansion coefficients for limestone and siliceous aggregate concretes are presented in Figs. 2.244 and 2.245, respectively. Results indicate an almost monotonic increase in thermal expansion

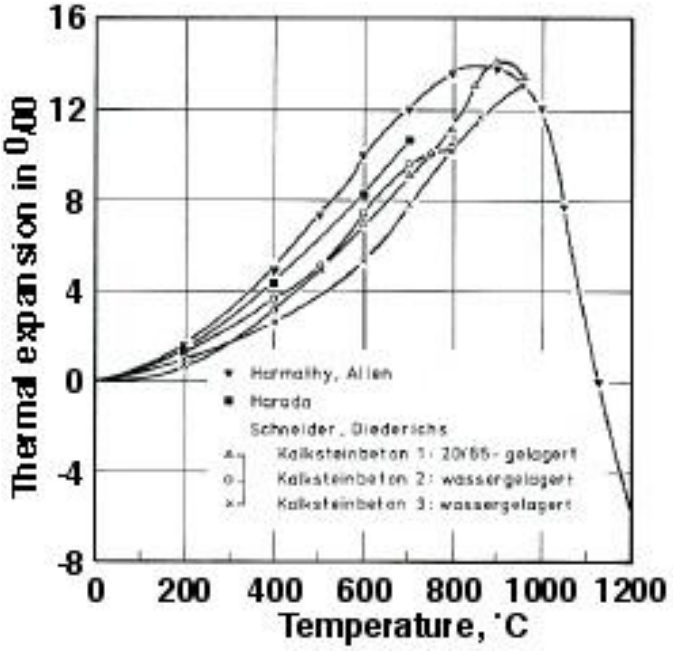

Figure 2.244 Thermal expansion of limestone aggregate concretes.

Source: U. Schneider, *Behaviour of Concrete at High Temperature*, HEFT 337, Deutscher Ausschuss für Stahlbeton, Wilhelm Ernst & Sohn, Munich, Germany, 1982.

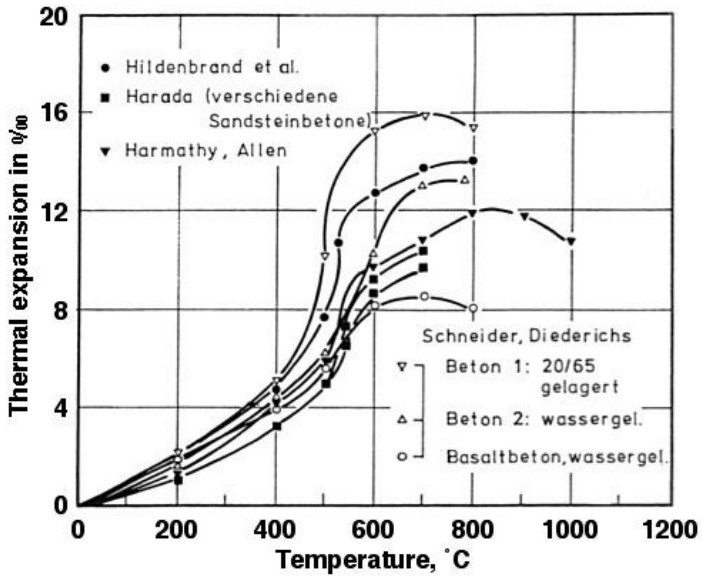

Figure 2.245 Thermal expansion of siliceous aggregate concretes.

Source: U. Schneider, *Behaviour of Concrete at High Temperature*, HEFT 337, Deutscher Ausschuss für Stahlbeton, Wilhelm Ernst & Sohn, Munich, Germany, 1982.

coefficient for the limestone concrete until decarbonation ($CaCO_3 \rightarrow CaO + CO_2$) leads to a decrease in the coefficient. The thermal expansion of the siliceous concrete is greater than that for the limestone concrete. Basalt, due to its fine crystalline structure, exhibits a lower expansion than the siliceous concrete. The presence of load reduces the thermal expansion as noted in Figure 2.246.

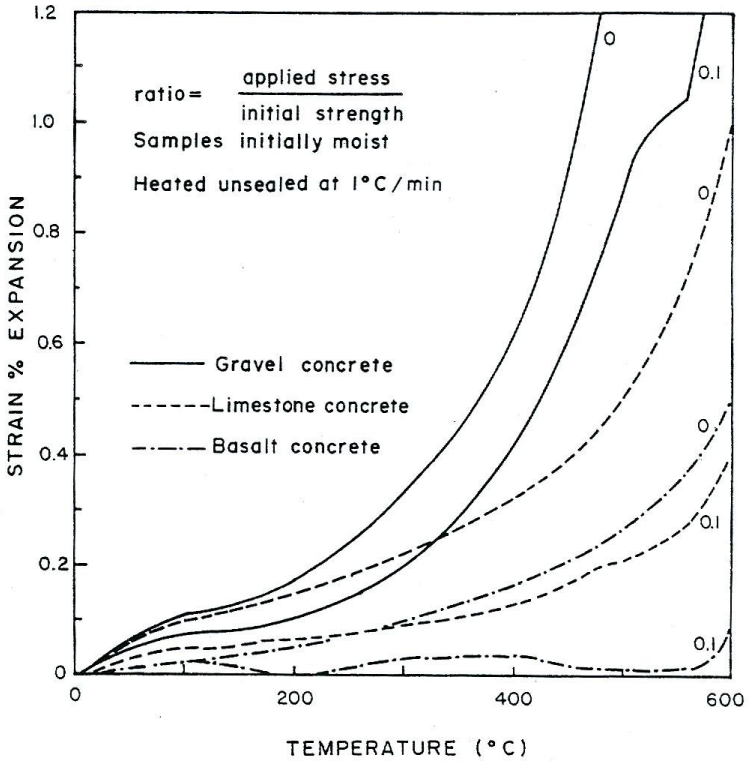

Figure 2.246 Variation of thermal strain with temperature and load for Portland cement concretes: 0 = no load, 0.1 = load corresponding to 10% f_c'.

Source: P.J.E. Sullivan, G.A. Khoury, and B.N Grainger, "Strain Behavior Under Uniaxial Compression of Three Concretes During First Heating to 600˚C," *Proceedings of 6th International Conference on Structural Mechanics in Reactor Technology*, Vol. G-H, Paper 1/3, Paris, France, 1981.

Examples of Relations for Concrete Thermal Expansion. Traditionally the free thermal strain is expressed as a linear function of temperature by employing a thermal expansion coefficient such as

$$\varepsilon_{th} = \alpha(T - T_0) \tag{2.75}$$

where α is the thermal expansion coefficient and T_0 is the initial temperature. For normal weight concrete with siliceous aggregate α can be approximated by [2.72]:

$$\alpha = (0.008T + 6)x10^{-6}. \tag{2.76}$$

This same expression has also been recommended for high strength ($f_C^{'}$ > 55MPa) siliceous and carbonate aggregate concretes [2.118].

Additional relationships for concrete thermal expansion at high-temperature of siliceous and carbonate aggregate high-strength concretes have been developed [2.236].

For siliceous aggregate concrete

$$\alpha = -0.0002 + 0.000011T \quad \text{for } 0^\circ \leq T \leq 450^\circ C \tag{2.77}$$

$$\alpha = -0.0115 + 0.000036T \quad \text{for } 450^\circ < T \leq 650^\circ C \tag{2.78}$$

$$\alpha = 0.0119 \quad \text{for } 650^\circ < T \leq 1000^\circ C \tag{2.79}$$

For carbonate aggregate concrete

$$\alpha = -0.0002 + 0.000008T \quad \text{for } 0^\circ \leq T \leq 450^\circ C \tag{2.80}$$

$$\alpha = -0.0061 + 0.000021T \quad \text{for } 450^\circ < T \leq 920^\circ C \tag{2.81}$$

$$\alpha = 0.0242 - 0.000012T \quad \text{for } 920^\circ < T \leq 1000^\circ C. \tag{2.82}$$

Summary. Thermal expansion represents the volume change of a material due to temperature change and is important in that it can result in thermal stresses and structural movement that can lead to concrete cracking and spalling. Thermal expansion is a non-linear function of temperature. The main factors influencing the coefficient of thermal expansion of concrete are the aggregate type and coarse aggregate fraction. Moisture content, water-cement ratio, and type cement only affect thermal expansion at relatively low temperatures (e.g., T < 200˚C). The coefficient of thermal expansion decreases slightly with age. Although Portland cement paste experiences contraction at temperatures above 150˚ to 400˚C, naturally-occurring aggregates always expand with increasing temperature to produce a net expansion. When differences in thermal expansion between Portland cement paste and aggregate materials are large, microstresses can occur resulting in microcracking of the concrete. Considerable differences exist relative to expansion of aggregate materials with the largest expansion occurring for aggregates having the highest percentage of silica by weight (e.g., quartz expansion > limestone expansion). Processed lightweight aggregate materials have lower thermal expansion coefficients than naturally-occurring aggregate materials and can show residual contraction after heating. Under elevated temperature conditions there is no significant difference for concretes that are dry and those that are completely saturated. The presence of load reduces the thermal expansion with increasing temperature. The thermal expansion is not fully reversible on subsequent cooling due to irreversible chemical changes and changes in microstructure. At high temperatures (600°C to 800°C) most concretes no longer exhibit an expansion and in some cases contract.

2.2.2.3 Thermal Conductivity

Information and Data. Thermal conductivity gives the heat flux transmitted through a unit area of a material under a unit temperature gradient (i.e., ability to conduct heat). For prestressed concrete pressure vessels, concrete with a high thermal conductivity is generally desirable so thermal gradients through the thickness will be minimal. At normal temperatures the thermal conductivity of concrete depends primarily on the thermal conductivity of the aggregate and the moisture content at the time of heating (e.g., increase in aggregate-to-cement ratio and decrease in water-cement ratio tends to increase the coefficient). Table 2.12 presents typical thermal conductivity values for concrete constituents and saturated concretes. Other factors influencing the thermal conductivity of concrete are the

Table 2.12 Thermal conductivities at ambient temperature of concrete constituents

Material	Thermal conductivity (W/m˚C)
Aggregates	0.7-4.2
Saturated concretes	1.0-3.6
Saturated hardened cement paste	1.1-1.6
Water	0.515
Air	.0034

Source: G.A. Khoury, *Transient Thermal Creep of Nuclear Reactor Pressure Vessel Type Concretes*, Ph.D. Dissertation, University of London, Vol. 1, pp. 1126; Vol. 2, pp. 418; Vol. 3, pp. 895, 1983.

hardened cement paste, and the pore volume and distribution. Age does not appear to affect the coefficient of thermal conductivity [2.136]. At low temperatures and with moist concrete very high values for thermal conductivity exist [2.15]. At higher temperatures the thermal conductivity increases slightly, but decreases as it approaches 100°C. Up to 300°C to 400°C, the thermal conductivity decreases further, and as the temperature increases beyond 300°C increasing cracking develops. Figure 2.247 presents the effect of temperature on thermal conductivity of an initially saturated concrete.

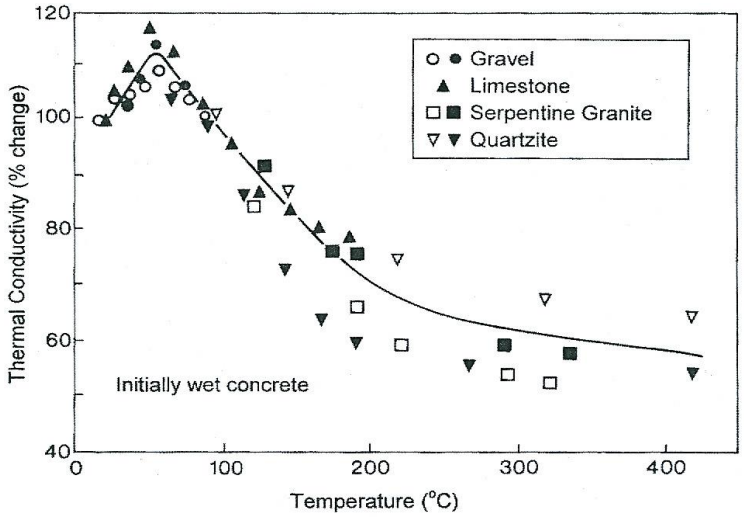

Figure 2.247 Effect of temperature on thermal conductivity of initially saturated concrete.

Source: R. Blundell, C. Diamond, and R. Browne, *The Properties of Concrete Subjected to Elevated Temperatures*, Report No. 9, Construction Industry Research and Information Association, Underwater Engineering Group, London, United Kingdom, June 1976.

Although thermal conductivity of concrete depends on all its constituents, it is largely determined by the type of aggregate used since aggregate makes up 60 to 80% the concrete volume. Table 2.13 lists thermal conductivity values for concrete with different aggregate types. Lightweight aggregates have lower thermal conductivities due to their porosity. Because the conductivity of water is approximately half that of cement paste, the lower the mix-water content, the higher the conductivity of the hardened concrete [2.24]. As shown in Figure 2.248, thermal conductivities of concrete made with highly crystalline aggregate decrease with temperature up to 1000°C, while those of concrete made with amorphous aggregate are essentially constant [2.18]. Figure 2.249 presents thermal conductivities for normal concretes having different aggregate types. Figures 2.250 and 2.251 presents thermal conductivities of concrete as a function of density and moisture content and the variation of thermal conductivity

Table 2.13 Typical values of thermal conductivity

Aggregate Type	Thermal conductivity	
	Btu in./hr•ft^2•F	W/m•K
Quartzite	24	3.5
Dolomite	22	3.2
Limestone	18-23	2.6-3.3
Granite	18-19	2.6-2.7
Rhyolite	15	2.2
Basalt	13-15	1.9-2.2

Source: P.K. Mehta and P.J.M. Monteiro, *Concrete – Microstructure, Properties, and Materials*, McGraw Hill, New York, New York, 2006.

as a function of temperature for several mortars and concretes, respectively. The thermal conductivity on cooling depends on the temperature level at the start of cooling, and after cooling to ambient conductivity falls to a level still below the original unheated level [2.19].

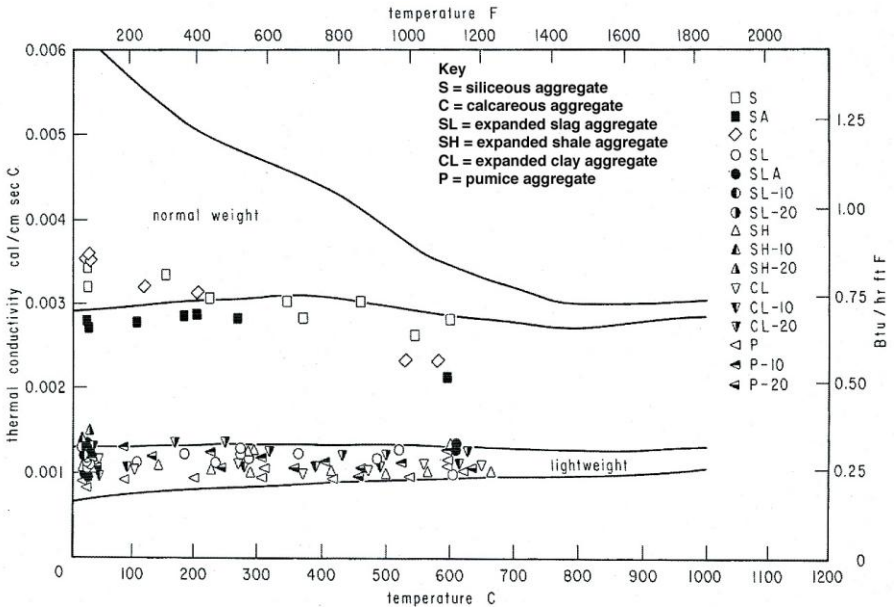

Figure 2.248 Thermal conductivity of normal and lightweight concretes.

Source: T. Z. Harmathy and L.W. Allen, "Thermal Properties of Selected Masonry Unit Concretes," *J. American Concrete Institute* **70**, pp. 132–142, 1973.

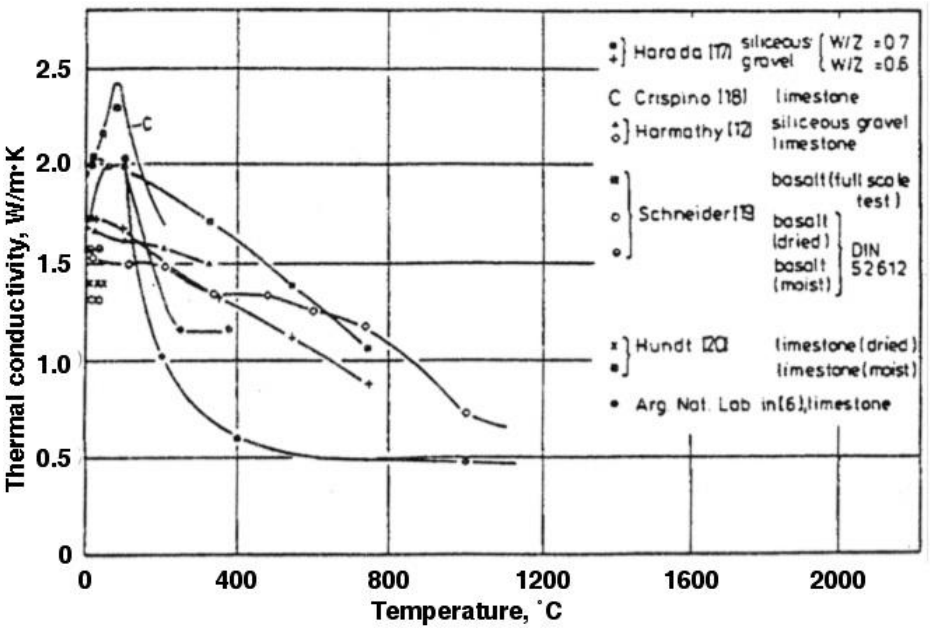

Figure 2.249 Thermal conductivity of ordinary concretes with different aggregates.

Source: U. Schneider, C. Diererichs, and C. Ehm, "Effect of Temperature on Steel and Concrete for PCRV's," *Nuclear Engineering and Design* **67**, 245–258, 1981.

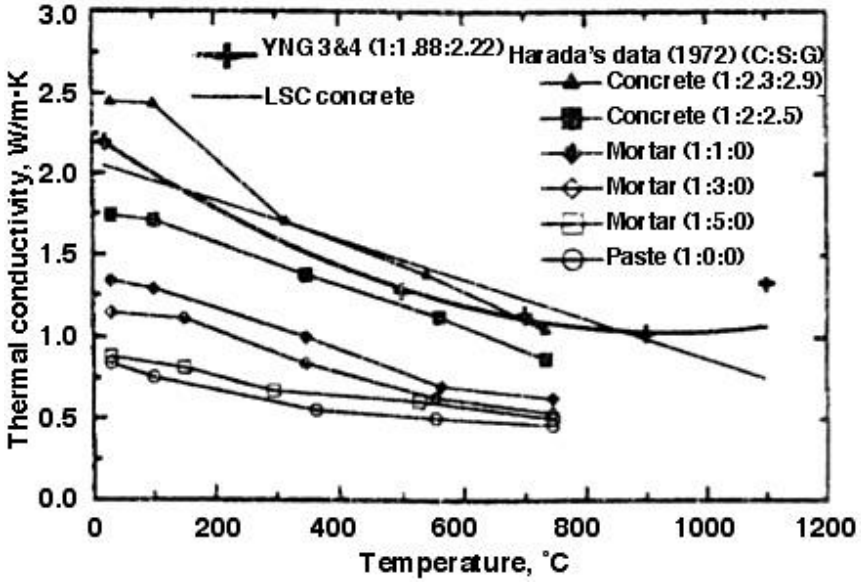

Figure 2.250 Thermal conductivity as a function of density and moisture content.

Source: K-Y. Shin, S-B. Kim, J-H. Kim, M. Chung, and P-S. Jung, "Thermo-Physical Properties and Transient Heat Transfer of Concrete at Elevated Temperatures," *Nuclear Engineering and Design* **212**, pp. 233–241, 2002.

Figure 2.251 Thermal conductivity as a function of temperature.

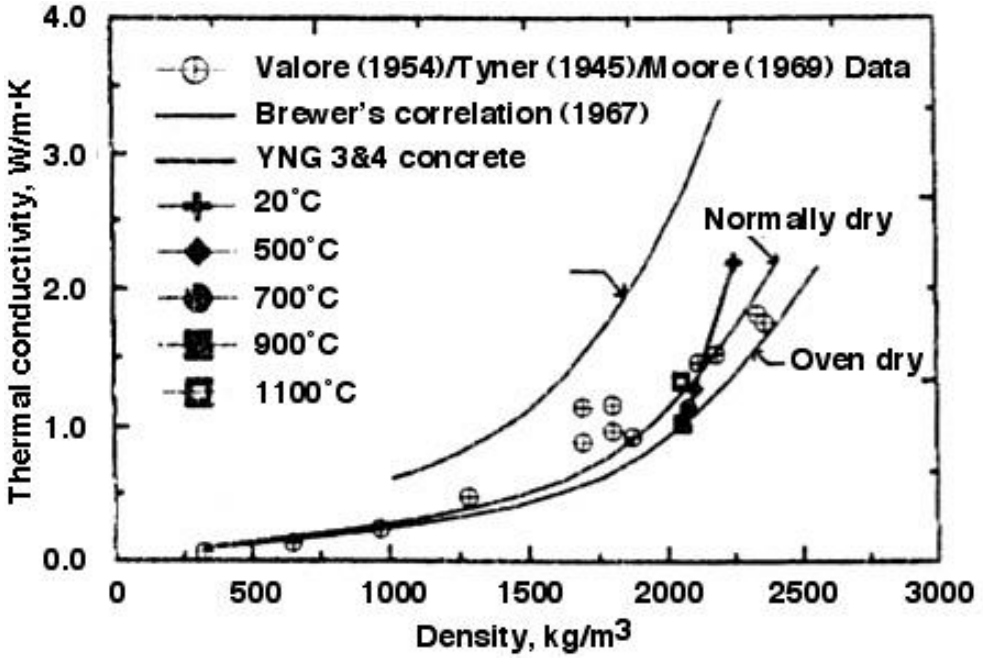

Source: K-Y. Shin, S-B. Kim, J-H. Kim, M. Chung, and P-S. Jung, "Thermo-Physical Properties and Transient Heat Transfer of Concrete at Elevated Temperatures," *Nuclear Engineering and Design* **212**, pp. 233–241, 2002.

Figure 2.252 presents the influence of temperature on thermal conductivity of a siliceous aggregate concrete from the French Penly Nuclear Power Plant [2.237]. Results presented in the figure are based on 40 measurements at each of the test temperatures (30˚, 60˚, 90˚, 150˚, and 200°C) and are comparable to those obtained by other researchers for siliceous aggregates in this temperature range [2.24,2.238].

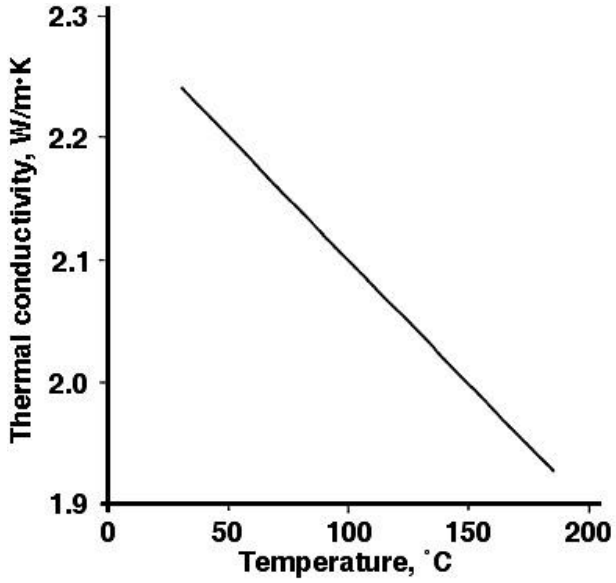

Figure 2.252 Thermal conductivity of a nuclear power plant concrete.

Source: F. Vodak, R. Cerny, J. Drchalová, S. Hosková, O. Kapicková, O. Michalko, P. Semerák, and J. Toman, "Thermophysical Properties of Concrete," *Cement and Concrete Research* **27**(3), pp. 415-426,1997.

Examples of Relations for Concrete Thermal Conductivity. Constitutive relationships for concrete thermal conductivity at high-temperature have been developed. The American Society of Civil Engineers has proposed the following relationships for normal-strength concrete [2.87]:

Siliceous aggregate concrete

$$k_c = -0.000625T + 1.5 \qquad 20^\circ C \le T \le 800^\circ C \qquad (2.83)$$

$$k_c = 1.0 \qquad 800^\circ C < T \qquad (2.84)$$

Carbonate aggregate concrete

$$k_c = 1.355 \qquad 20^\circ C \le T \le 293^\circ C \qquad (2.85)$$

$$k_c = -0.001241T + 1.7162 \qquad 293^\circ C < T \qquad (2.86)$$

This relationship has been modified for high-strength concrete [2.88]:

Siliceous aggregate concrete

$$k_c = 0.85(2 - 0.0011T) \qquad 20^\circ C < T \le 1000^\circ C \qquad (2.87)$$

Carbonate aggregate concrete

$$k_c = 0.85(2 - 0.0013T) \qquad 20^\circ C \le T \le 300^\circ C \qquad (2.88)$$

$$k_c = 0.85(2.21 - 0.002T) \qquad 300^\circ C < T \qquad (2.89)$$

Finally, Eurocode has developed relationships for both normal- and high-strength concretes [2.46]:

Upper limit all concrete types

$$k_c = 2 - 0.2451(T/100) + 0.0107(T/100)^2 \qquad 20^\circ C \le T \le 1200^\circ C \tag{2.90}$$

Lower limit all concrete types

$$k_c = 1.36 - 0.136(T/100) + 0.0057(T/100)^2 \qquad 20^\circ C \le T \le 1200^\circ C \tag{2.91}$$

Figure 2.253 provides a comparison of thermal conductivity values predicted by ASCE and Eurocode models and test data for siliceous and carbonate aggregate normal-strength concretes [2.88]. Experimental results indicate large variation in thermal conductivity values for normal-strength concretes. The standard deviation of the compiled data ranged from 0.22 W/m•˚C at room temperature to 0.18 W/m•˚C at 800˚C for siliceous aggregate concretes, and from 0.4 W/m•˚C at room temperature to 0.16 W/m•˚C at 800˚C for carbonate aggregate concretes. Variation in test data was attributed to differences in test methods, conditioning procedures, and measurement techniques.

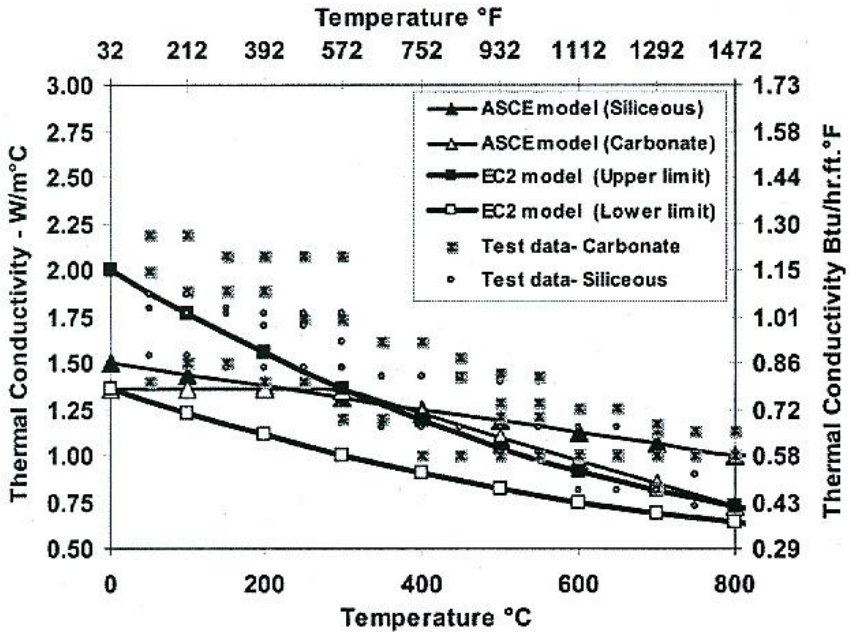

Figure 2.253 Comparison of experimental results and thermal conductivity predicted by different models for normal-strength concretes.

Source: V.K.R. Kodur, M.M.S. Dwaikat, and M.B. Dwaikat, "High-Temperature Properties of Concrete for Fire resistance Modeling of Structures," *ACI Materials Journal* **105**(5), pp. 517-527, American Concrete Institute, Farmington Hills, Michigan, September-October 2008.

Summary. Major factors that influence the concrete thermal conductivity are moisture content, hardened cement paste, pore volume and distribution, and amount and type of aggregate material. The conductivity varies linearly with moisture content. Increasing the water-cement ratio increases the concrete porosity and correspondingly reduces the thermal conductivity, especially when dry, since both water and air have lower thermal conductivity values than cement paste. Type of cement can influence thermal conductivity relative to temperature at which water is released (e.g., occurs at higher temperature for blast furnace slag than ordinary Portland cement concretes). Leaner normal weight concrete mixes have higher thermal conductivities, while the opposite is true for lightweight concrete mixes. Although the thermal conductivity of concrete depends on all its constituents, the concrete thermal conductivity is largely determined by the amount and type of aggregate used since aggregates normally constitute 60

– 80% the concrete volume. At normal temperatures the thermal conductivity increases with increasing aggregate content and moisture content. Crystalline aggregates (e.g., quartz) have higher thermal conductivities at normal temperatures with values decreasing as the temperature increases. Amorphous rocks (e.g., basalt and dolerite) have low thermal conductivity values at normal temperatures. At normal temperatures moist concretes have relatively high thermal conductivity values. Pre-dried siliceous and calcareous aggregate concretes exhibit an approximately linear reduction in thermal conductivity with temperature when heated from 20˚ to 500˚C. In general, at temperatures up to 100˚C the thermal conductivity seems to increase with temperature; at temperatures greater than 100˚C the conductivity decreases and at 300˚ to 400˚C there is a further decrease; at temperatures > 600˚C the thermal conductivity increases slightly: and at temperatures greater than 800˚C up to melting there is only a small change in thermal conductivity. Lightweight aggregate concretes have even lower thermal conductivity values at normal temperatures due to increased porosity. For lightweight aggregate concrete the thermal conductivity is relatively constant or increases slightly for temperatures up to 1000˚C.

2.2.2.4 Thermal Diffusivity

Information and Data. Thermal diffusivity is a measure of the rate at which heat will diffuse through a material in all directions due to a temperature change and is thus an index of the facility with which the material will transfer heat due to a temperature change. It is described as follows:

$$D = \lambda/\rho c_p \quad (m^2/sec) \tag{2.92}$$

where D = diffusivity, ρ = density (kg/m^3), λ = thermal conductivity (W/mK), and c_p = specific heat (J/kgK).

Thermal diffusivity is important to nuclear power plant structures such as prestressed concrete pressure vessels for the same reasons cited for thermal conductivity. Thermal diffusivity of concrete is determined by the thermal properties of its constituents. At normal temperatures the diffusivity of concrete is mainly governed by the diffusivity of the aggregate. Aggregates with increasing values of thermal diffusivity include basalt, rhyolite, granite, limestone, dolerite, and quartzite [2.239]. Table 2.14 presents typical values of thermal diffusivity for concretes made with different types of coarse aggregate.

Table 2.14 Thermal diffusivity values for concrete with different coarse aggregate

Type coarse aggregate	ft^2/h	m^2/h
Quartzite	0.058	0.0054
Dolomite	0.051	0.0047
Limestone	0.050	0.0046
Granite	0.043	0.0040
Rhyolite	0.035	0.0033
Basalt	0.032	0.0030

Source: P.K. Mehta and P.J.M. Monteiro, *Concrete – Microstructure, Properties, and Materials*, McGraw Hill, New York, New York, 2006.

Factors that affect thermal conductivity generally have the same influence on thermal diffusivity. Thermal diffusivity of limestone and siliceous aggregate concretes is presented in Figures 2.254 and 2.255, respectively [2.12]. Figure 2.256 presents the influence of temperature on thermal diffusivity of a siliceous aggregate concrete from the French Penly Nuclear Power Plant [2.237] and is noted to be similar to other results presented in the literature for siliceous aggregate concretes in the temperature range investigated (30°C to 200°C) [2.240]. Figure 2.257 presents the thermal diffusivity of several mortars and concretes as a function of temperature [2.228]. The thermal diffusivity of normal weight concrete falls markedly with increase in temperature as noted in Figure 2.258. This is due to the general decrease of thermal conductivity and increase in specific heat at elevated temperature. Finally, Figure 2.259 presents thermal diffusivity results for three normal weight concretes and thirteen lightweight concretes. As noted in the figure, at about 600˚C the thermal diffusivity of all concretes investigated becomes approximately 0.0033 cm^2/sec.

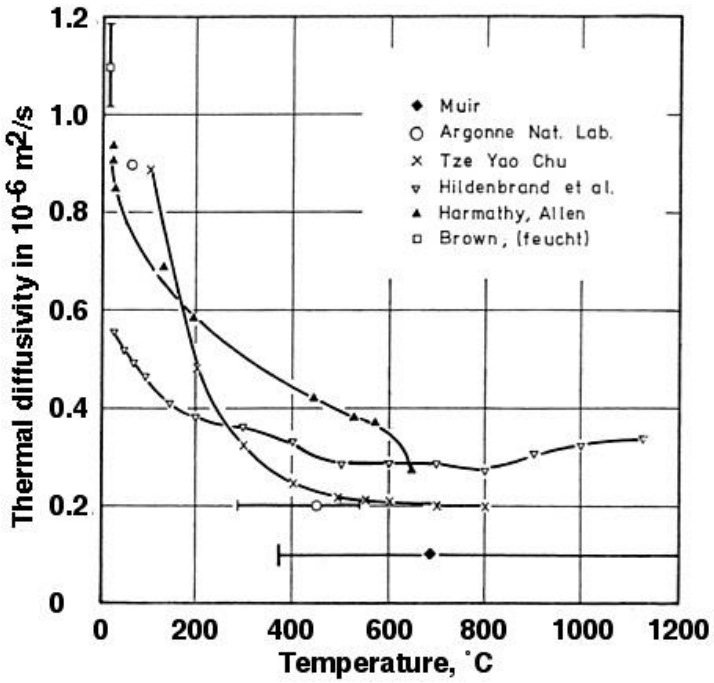

Figure 2.254 Thermal diffusivity of limestone aggregate concrete.

Source: U. Schneider, *Behavior of Concrete at High Temperature*, HEFT 337, Deutscher Ausschuss fur Stahlbeton, Wilhelm Ernst & Sohn, Berlin, Germany, 1982.

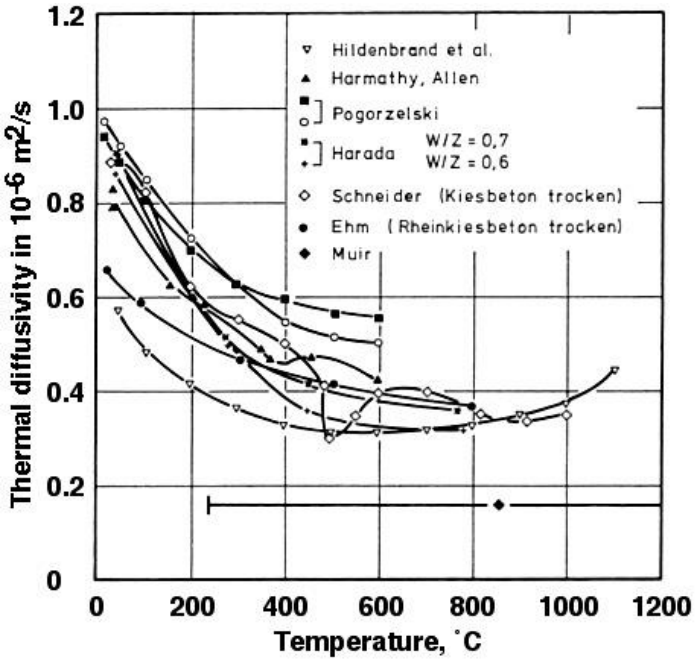

Figure 2.255 Thermal diffusivity of siliceous aggregate concrete.

Source: U. Schneider, *Behaviour of Concrete at High Temperature*, HEFT 337, Deutscher Ausschuss für Stahlbeton, Wilhelm Ernst & Sohn, Munich, Germany, 1982.

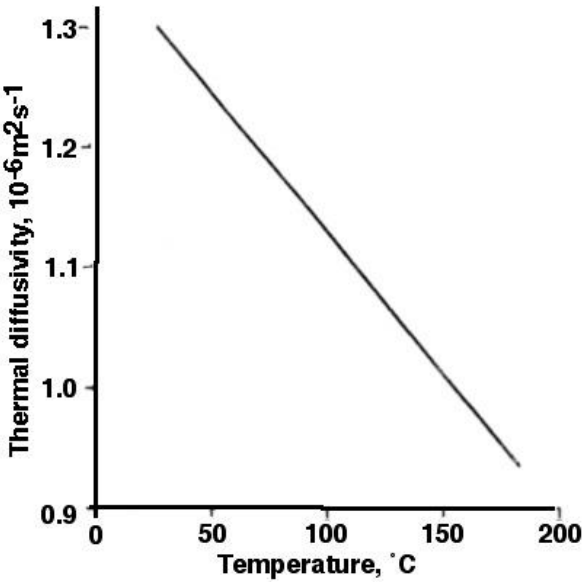

Figure 2.256 Thermal diffusivity of a nuclear power plant concrete.

Source: F. Vodak, R. Cerny, J. Drchalová, S. Hosková, O. Kapicková, O. Michalko, P. Semerák, and J. Toman, "Thermophysical Properties of Concrete," *Cement and Concrete Research* **27**(3), pp. 415-426,1997.

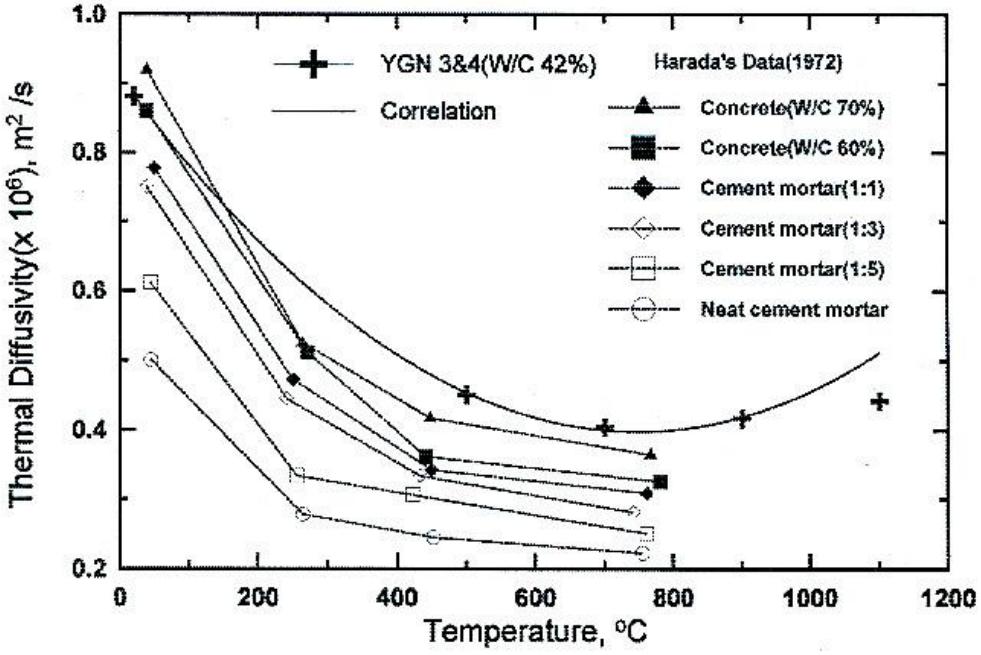

Figure 2.257 Thermal diffusivity variation of a Korean nuclear plant concrete as a function of temperature.

Source: K-Y. Shin, S-B. Kim, J-H. Kim, M. Chung, and P-S. Jung, "Thermo-Physical Properties and Transient Heat Transfer of Concrete at Elevated Temperatures," *Nuclear Engineering and Design* **212**, pp. 233–241 2002.

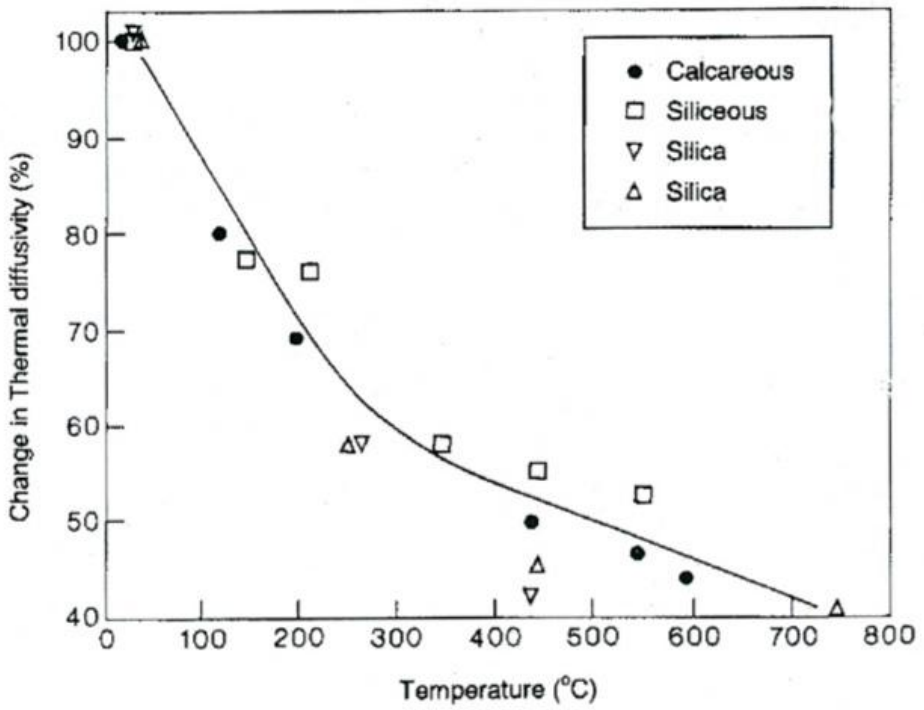

Figure 2.258 Effect of temperature on thermal diffusivity of normal weight concrete excluding latent heat effects.

Source: *Fire Design of Concrete Structures – Materials, Structures and Modelling*, Bulletin 38, International Federation for Structural Concrete, Lausanne, Switzerland, April 2007.

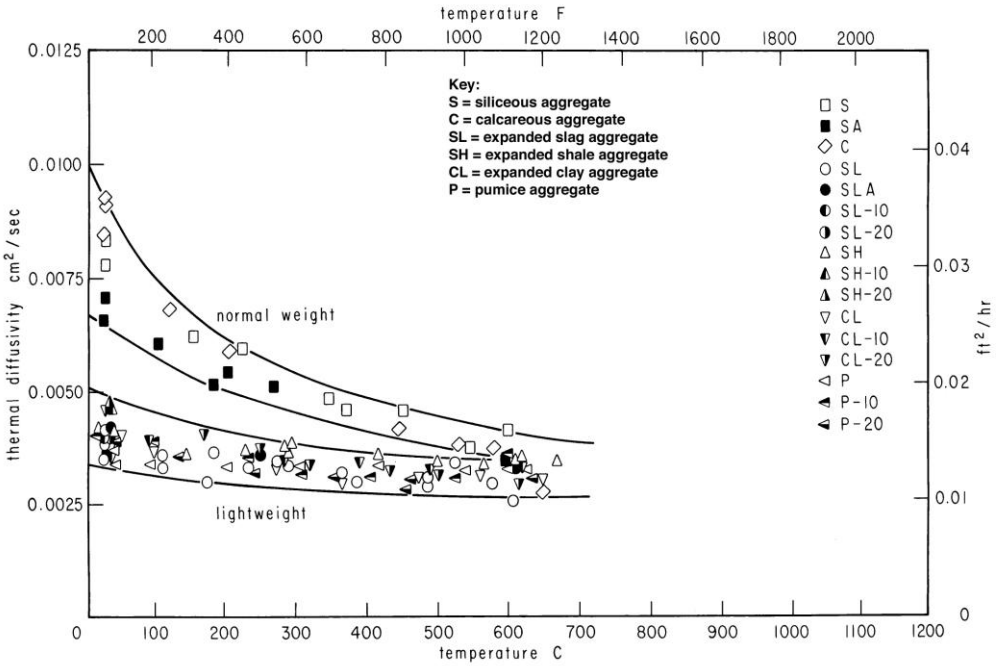

Figure 2.259 Thermal diffusivity of normal and lightweight concretes.

Source: T. Z. Harmathy and L.W. Allen, "Thermal Properties of Selected Masonry Unit Concretes," *J. American Concrete Institute* **70**, pp. 132–142, 1973.

2.2.2.5 Specific Heat

Information and Data. The thermal or heat capacity of a material, or specific heat, is the amount of heat per unit mass required to change the temperature of the material by one degree.

$$c_p = \left(\frac{\partial H}{\partial T_p} \right) \tag{2.93}$$

where H is enthalpy, T is temperature, and *p* is pressure. The specific heat of ordinary concrete at room temperature ranges from 0.5 to 1.13 kJ kg^{-1} K^{-1} while specific heat of hardened cement paste ranges from 0.63 to 1.72 kJ kg^{-1} K^{-1} [2.5]. At room temperature aggregate type, mix proportions, and age do not have a great effect on specific heat of concrete. However, as the moisture content in the concrete increases, the specific heat capacity increases at lower temperatures. The specific heat of aggregate can be calculated from its mineralogical content and the specific heat of concrete determined based on its relative proportions [2.136].

The specific heat of concrete increases with an increase in temperature. At elevated temperature the specific heat value is sensitive to the various transformations that take place in concrete [2.19]. This includes the vaporization of free water at about 100˚C, the dissociation of $Ca(OH)_2$ at about 400˚ to 500˚C and the $\alpha-\beta$ quartz transformation in some aggregates. Heating of initially saturated concrete causes a rapid but temporary rise in the specific heat at about 90˚C due to the rapid release of latent heat of vaporization.

Figure 2.260 presents the effects of temperature on experimentally determined specific heats of various concretes. Figures 2.261 and 2.262 present heat capacities of limestone and siliceous aggregate concretes, respectively. Additional information is provided in Figure 2.263, which presents the influence of temperature on the specific heat of a siliceous aggregate concrete from the French Penly Nuclear Power Plant . Figure 2.264 presents specific heat as a function of temperature for a basaltic aggregate concrete (37.9 MPa, Type V cement) used in construction of Yonggwang Nuclear power plant units 3 and 4 in Korea [2.241]. Results show that the specific heat increased to 500˚C, decreased from 700˚ to 900˚C, and then increased at temperatures above 900˚C. Finally, Figure 2.265 presents specific heat results for three normal weight concretes and thirteen lightweight concretes. It was noted in the reference for this data that generally the specific heat of concrete was somewhat insensitive to the aggregate used and mix ratios [2.18].

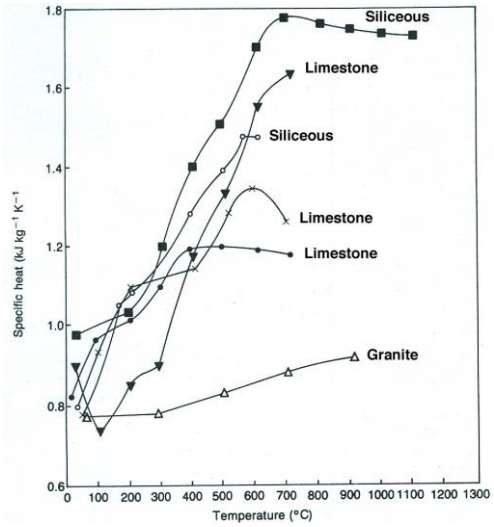

Figure 2.260 Specific heats of various concretes.

Source: Z.P. Bazant and M.F. Kaplan, *Concrete at High Temperatures: Material Properties and Mathematical Models*, Longman, London, United Kingdom, 1996.

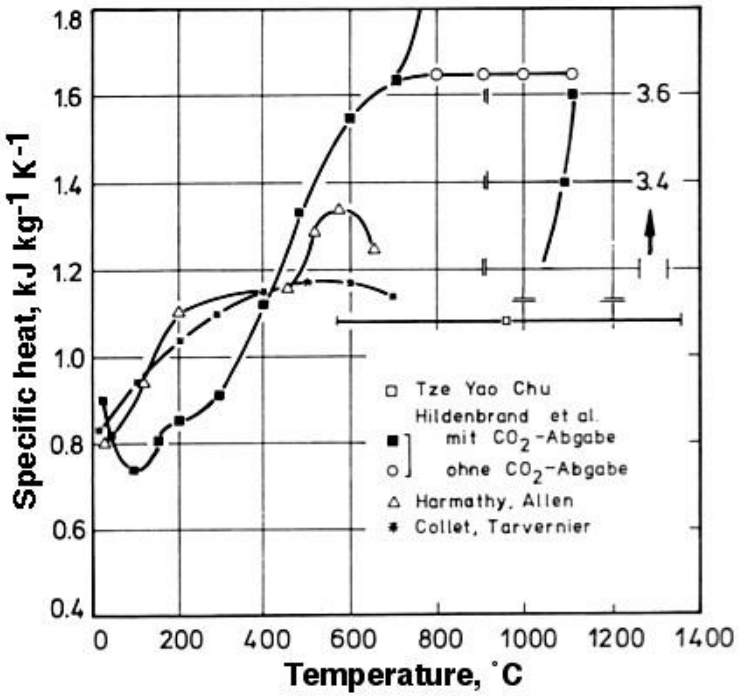

Figure 2.261 Specific heat capacity of limestone aggregate concrete.

Source: U. Schneider, *Behaviour of Concrete at High Temperature*, HEFT 337, Deutscher Ausschuss für Stahlbeton, Wilhelm Ernst & Sohn, Munich, Germany, 1982.

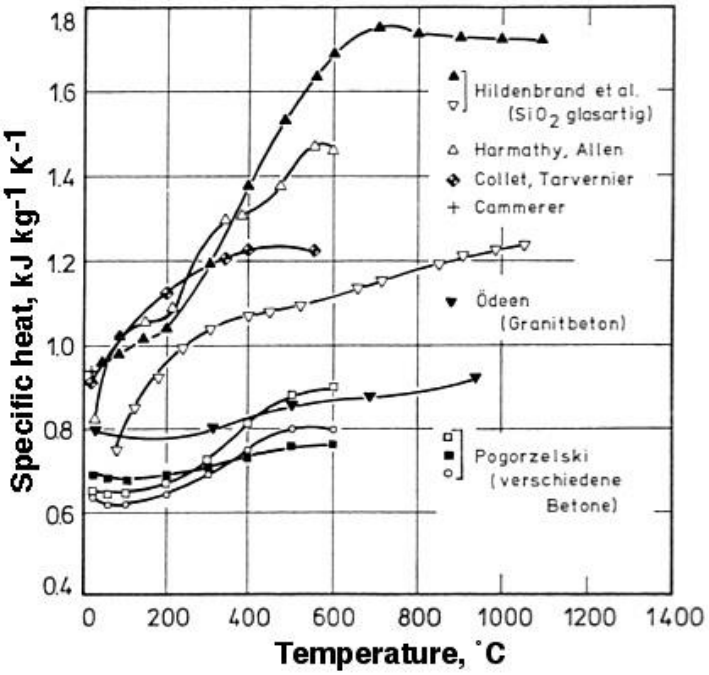

Figure 2.262 Specific heat capacity of siliceous aggregate concrete.

Source: U. Schneider, *Behaviour of Concrete at High Temperature*, HEFT 337, Deutscher Ausschuss für Stahlbeton, Wilhelm Ernst & Sohn, Munich, Germany, 1982.

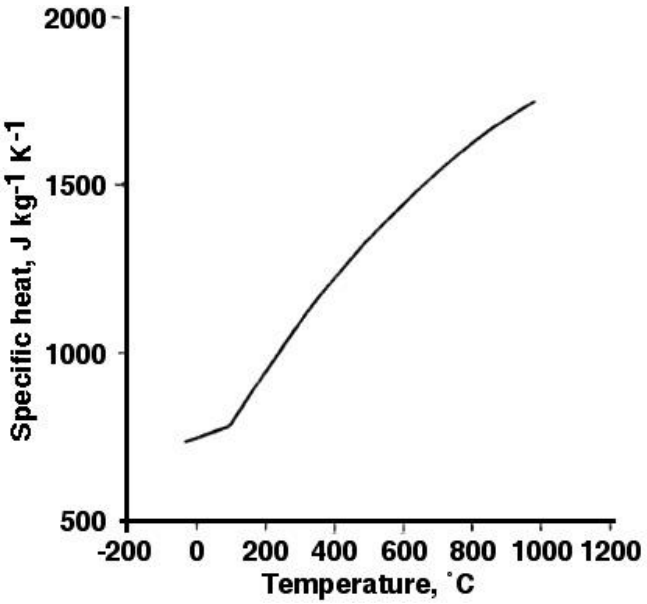

Figure 2.263 Specific heat of a nuclear power plant concrete.

Source: F. Vodak, R. Cerny, J. Drchalová, S. Hosková, O. Kapicková, O. Michalko, P. Semerák, and J. Toman, "Thermophysical Properties of Concrete," *Cement and Concrete Research* **27**(3), pp. 415-426,1997.

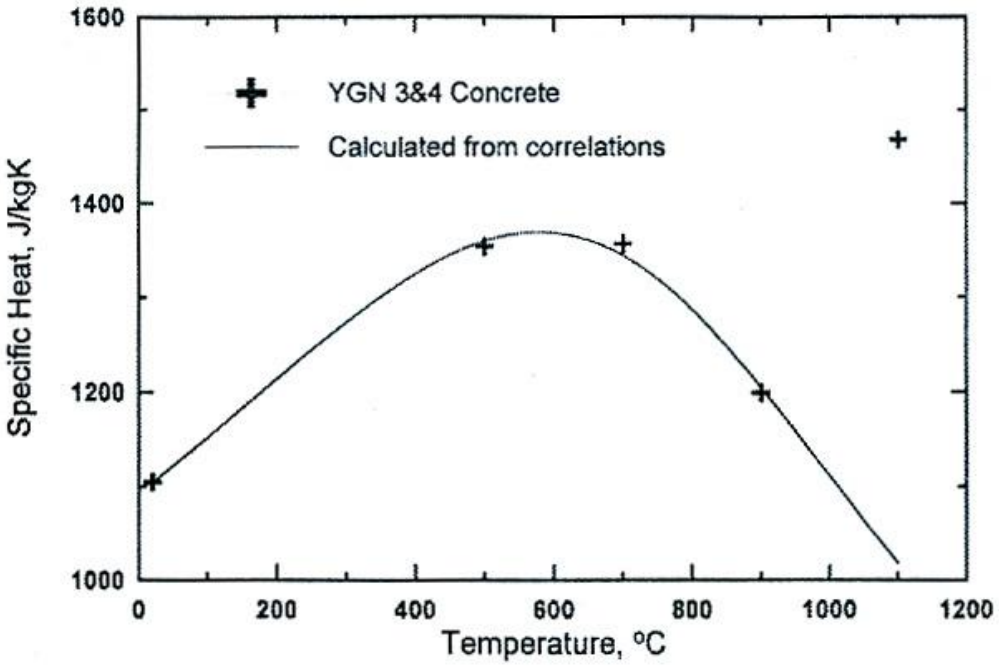

Figure 2.264 Specific heat of a Korean nuclear power plant concrete.

Source: K-Y. Shin, S-B. Kim, J-H. Kim, M. Chung, and P-S. Jung, "Thermo-Physical Properties and Transient Heat Transfer of Concrete at Elevated Temperatures," *Nuclear Engineering and Design* **212**, pp. 233–241 2002.

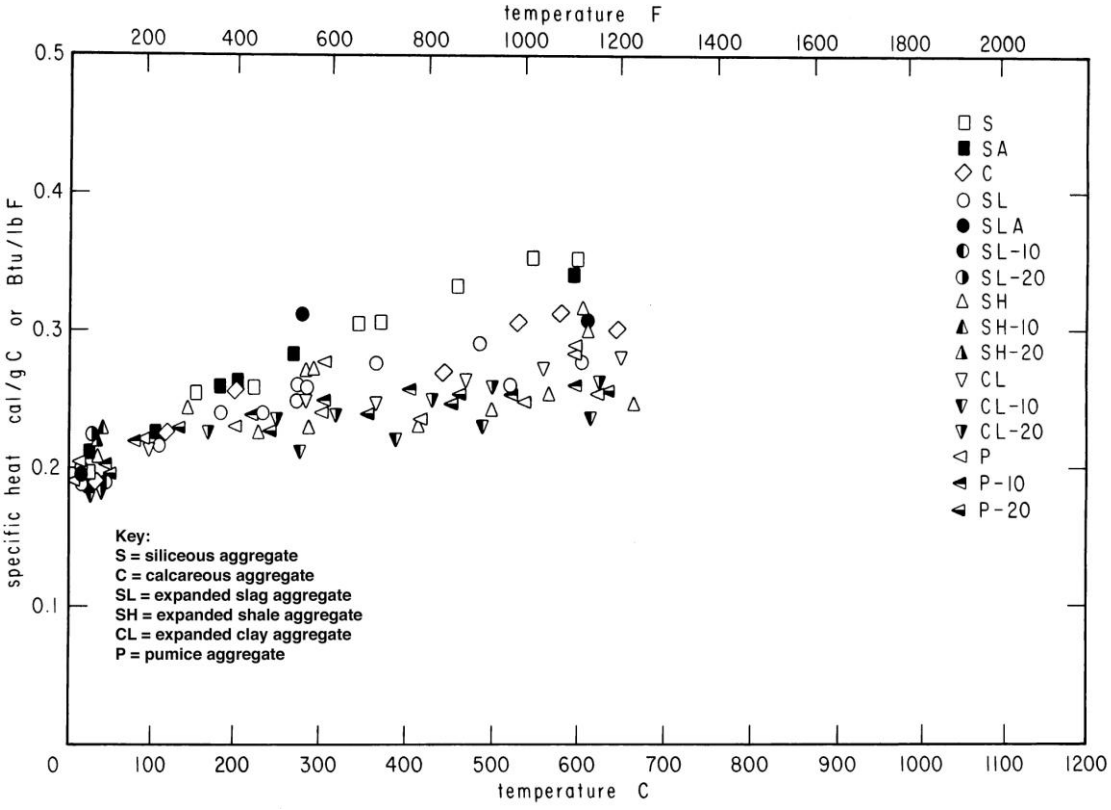

Figure 2.265 Specific heat of normal and lightweight concretes.

Source: T. Z. Harmathy and L. W. Allen, "Thermal Properties of Selected Masonry Unit Concretes," *J. American Concrete Institute* **70**, pp. 132–142, 1973.

Examples of Relationships for Concrete Thermal Capacity. Constitutive relationships for concrete thermal capacity at high-temperature have been developed. The American Society of Civil Engineers has proposed the following relationships for normal-strength concrete [2.87]:

Siliceous aggregate concrete

$$\rho_c = 0.005T + 1.7 \qquad 20^\circ C \le T \le 200^\circ C \qquad (2.94)$$

$$\rho_c = 2.7 \qquad 200^\circ C < T \le 400^\circ C \qquad (2.95)$$

$$\rho_c = 0.013T - 2.5 \qquad 400^\circ C < T \le 500^\circ C \qquad (2.96)$$

$$\rho_c = 10.5 - 0.013T \qquad 500^\circ C < T \le 600^\circ C \qquad (2.97)$$

$$\rho_c = 2.7 \qquad 600^\circ C < T \qquad (2.98)$$

Carbonate aggregate concrete

$$\rho_c = 2.566 \qquad 20^\circ C \le T \le 400^\circ C \qquad (2.99)$$

$$\rho_c = 0.1765T - 68.034 \qquad 400^\circ C < T \le 410^\circ C \qquad (2.100)$$

$$\rho_c = 25.00671 - 0.05043T \qquad 410^\circ C < T \le 445^\circ C \qquad (2.101)$$

$$\rho_c = 2.566 \qquad 445^\circ C < T \le 500^\circ C \qquad (2.102)$$

$$\rho_c = 0.01603T - 5.44881 \qquad 500^\circ C < T \le 635^\circ C \qquad (2.103)$$

$$\rho_c = 0.16635T - 100.90225 \qquad 635^\circ C < T \le 715^\circ C \qquad (2.104)$$

$$\rho_c = 176.07343 - 0.22130T \qquad 715^\circ C < T \le 785^\circ C \qquad (2.105)$$

$$\rho_c = 2.566 \qquad 785^\circ C < T \qquad (2.106)$$

This relationship has been modified for high-strength concrete [2.88]:

Siliceous aggregate concrete

$$\rho_c = 0.005T + 1.7 \qquad 20^\circ C \le T \le 200^\circ C \qquad (2.107)$$
$$\rho_c = 2.7 \qquad 200^\circ C < T \le 400^\circ C \qquad (2.108)$$
$$\rho_c = 0.013T - 2.5 \qquad 400^\circ C < T \le 500^\circ C \qquad (2.109)$$
$$\rho_c = 10.5 - 0.013T \qquad 500^\circ C < T \le 600^\circ C \qquad (2.110)$$
$$\rho_c = 2.7 \qquad 600^\circ C < T \le 635^\circ C \qquad (2.111)$$

Carbonate aggregate concrete

$$\rho_c = 2.45 \qquad 20^\circ C \le T \le 400^\circ C \qquad (2.112)$$
$$\rho_c = 0.026T - 12.85 \qquad 400^\circ C < T \le 475^\circ C \qquad (2.113)$$
$$\rho_c = 0.0143T - 6.295 \qquad 475^\circ C < T \le 650^\circ C \qquad (2.114)$$
$$\rho_c = 0.1894T - 120.11 \qquad 650^\circ C < T \le 735^\circ C \qquad (2.115)$$
$$\rho_c = -0.263T - 212.4 \qquad 735^\circ C < T \le 800^\circ C \qquad (2.116)$$
$$\rho_c = 2 \qquad 800^\circ C < T \le 1000^\circ C \qquad (2.117)$$

Finally, Eurocode has developed relationships for both normal- and high-strength concretes [2.46]:

Specific heat (J/kg˚C)

$$c = 900 \qquad 20^\circ C \le T \le 100^\circ C \qquad (2.118)$$
$$c = 900 + (T - 100) \qquad 100^\circ C < T \le 200^\circ C \qquad (2.119)$$
$$c = 900 + (T - 200)/2 \qquad 200^\circ C < T \le 400^\circ C \qquad (2.120)$$
$$c = 1100 \qquad 400^\circ C < T \le 1200^\circ C \qquad (2.121)$$

Density change (kg/m^3)

$$\rho = \rho(20^\circ C) \text{ = reference density} \qquad 20^\circ C \le T \le 115^\circ C \qquad (2.122)$$
$$\rho = \rho(20^\circ C)(1 - 0.02(T - 115)/85) \qquad 115^\circ C < T \le 200^\circ C \qquad (2.123)$$
$$\rho = \rho(20^\circ C)(0.98 - 0.03(T - 200)/200) \qquad 200^\circ C < T \le 400^\circ C \qquad (2.124)$$
$$\rho = \rho(20^\circ C)(0.95 - 0.07(T - 400)/800) \qquad 400^\circ C < T \le 1200^\circ C \qquad (2.125)$$

Thermal capacity = ρ x c. (2.126)

Figure 2.266 provides a comparison of specific heat values predicted by ASCE and Eurocode models and test data for siliceous and carbonate aggregate normal-strength concretes. The standard deviation of the compiled data ranged from 0.56 MJ/m^3•˚C at room temperature to 1.1 MJ/m^3•˚C at 750˚C for siliceous aggregate concretes, and from 0.6 MJ/m^3•˚C at room temperature to 7.8 MJ/m^3•˚C at 750˚C for carbonate aggregate concretes. Results indicate the significant influence that aggregate type has on specific heat. High heat capacity of carbonate aggregate concrete in temperature range of 600˚ to 800˚C was due to endothermic reaction that absorbs a significant amount of energy. The heat capacity of carbonate aggregate concrete helps to minimize spalling.

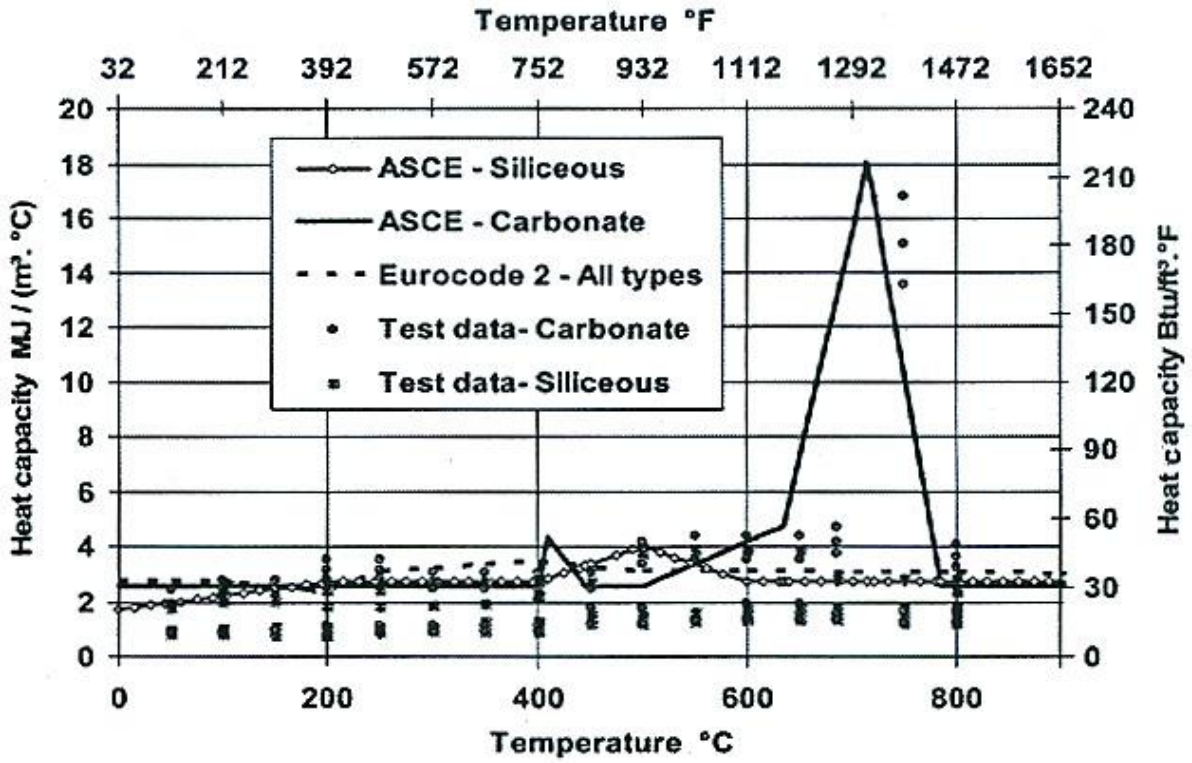

Figure 2.266 Comparison of experimental results and specific heat predicted by different models for normal-strength concretes.

Source: V.K.R. Kodur, M.M.S. Dwaikat, and M.B. Dwaikat, "High-Temperature Properties of Concrete for Fire resistance Modeling of Structures," *ACI Materials Journal* **105**(5), pp. 517-527, American Concrete Institute, Farmington Hills, Michigan, September-October 2008.

Summary. Aggregate type, mix proportions, and age do not have a great effect on specific heat at normal temperatures. Type of aggregate and its proportion have little influence on heat capacity at temperatures below 800˚C. Mix proportions influence heat capacity in that richer mixes indicate a higher latent heat due to dehydration effects. At normal temperatures as the moisture content in the concrete increases the specific heat capacity increases (e.g., at temperatures below 200˚C wet concretes show an apparent specific heat nearly twice that of oven-dried concretes). At elevated temperatures the specific heat value is sensitive to the various transformations that take place in concrete (e.g., vaporization of free water at about 100˚C, the dissociation of $Ca(OH)_2$ at about 400˚ to 500˚C and the $\alpha-\beta$ quartz transformation in some aggregates). Specific heat of siliceous and limestone aggregate concretes increase as temperature increases up to about 700˚C, but the increase for granite aggregate concrete is not as significant.

2.2.2.6 Heat of Ablation and Erosion Rates

Information and Data. Under a hypothetical core disruptive accident involving melting of the reactor core in a nuclear power plant it is of interest to know how much energy is dissipated by the concrete structures designed to contain the core melt. The term heat of ablation is applied in this context and is defined as the heat dissipated per unit mass material during a steady-state erosion process resulting in the removal of a unit mass [2.15]. The heat of ablation is composed of the sensible heat to be provided and the heats of reaction and transformation. It has been calculated that the total amount of heat required to transform a cubic meter of quartzite concrete at normal temperature to a molten state is about 2000 x 10^3 kJ and for limestone concrete the amount of heat is greater (2360 x 10^3 kJ) due to additional heat required to decarbonate limestone aggregate [2.5]. Table 2.15 presents heat of ablation values for different concretes. Note that values in the table are dependent on test conditions and the type of determination.

Table 2.15 Heat of ablation values of different concretes

Type of concrete	Heat of ablation (MJ/kg)	Source with references identified in [2.15]
Basaltic limestone	6±3	Muir (6)
Basaltic limestone	4.5±0.5	Chu (7)
Quartzitic	2.2	Hildenbrand et al. (8)
Calcitic	1.5	Hildenbrand et al. (8)
Quartzitic	2.4	Schneider et al. (5)
Calcitic	3.2	Schneider et al. (5)

Source: U. Schneider, C. Diererichs, and C. Ehm, "Effect of Temperature on Steel and Concrete for PCRV's," *Nuclear Engineering and Design* **67**, pp. 245–258, 1981.

Under a hypothetical core disruptive accident involving melting of the reactor core in a nuclear power plant it is possible that liquid metals such as steel having temperatures up to 3000˚C may penetrate and damage concrete structures. This is the erosion rate and refers to the velocity at which concrete subjected to high temperatures (i.e., ≥1200˚C) is decomposed by mechanical disintegration and by melting process [2.15]. Figure 2.267 presents penetration depth versus time results for simulated molten core (thermite) concrete interactions for a basaltic aggregate concrete (37.9 MPa, Type V cement) used in construction of Yonggwang Nuclear power plant Units 3 and 4 in Korea [2.241]. The peak melt temperature measured was 2230˚C. Figure 2.268 presents the cross section of a concrete specimen after testing. Post-test examination of the cross section showed a 2-3 mm thick crevice between the solidified melt and the erosion front with debris generated during the interaction observed in the solidified melt. The erosion front was irregular and bow-shaped with a maximum depth of 2 cm. Analysis indicated that the maximum concrete erosion rate was 175 cm/h.

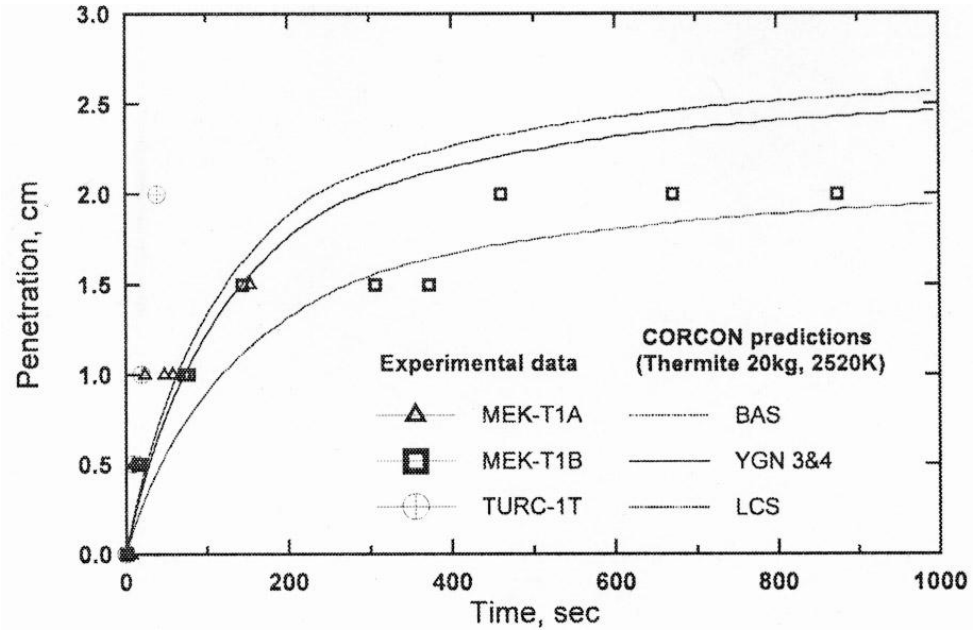

Figure 2.267 Penetration depths vs time for various melt temperature conditions.

Source: K-Y. Shin, S-B. Kim, J-H. Kim, M. Chung, and P-S. Jung, "Thermo-Physical Properties and Transient Heat Transfer of Concrete at Elevated Temperatures," *Nuclear Engineering and Design* **212**, pp. 233–241, 2002.

Table 2.16 presents calculated heats of transformation and decomposition reactions associated with physical and chemical changes that occur in a cubic meter of concrete made with quartzitic and limestone aggregates and Portland blast furnace slag cement [2.242]. Mix proportions by weight for the cement, fine aggregate, coarse

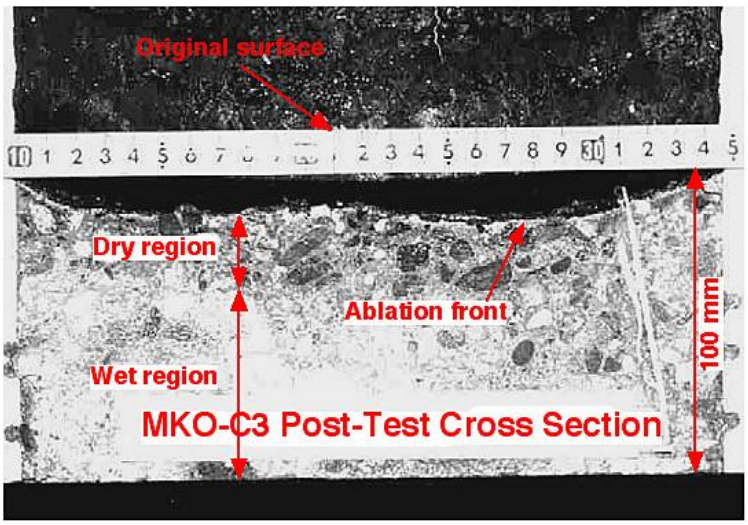

Figure 2.268 Cross section of test specimen after MEK-T1A test.

Source: K-Y. Shin, S-B. Kim, J-H. Kim, M. Chung, and P-S. Jung, "Thermo-Physical Properties and Transient Heat Transfer of Concrete at Elevated Temperatures," *Nucl. Eng. and Design* **212**, pp. 233–241 2002.

Table 2.16 Estimated heats of transformation for quartzitic and limestone aggregate concretes exposed to elevated temperatures

	Temperature (°C)	Transformation or decomposition reaction	Heat of transformation or decomposition reaction per unit mass (kJ kg^{-1}) (a)	Mass of material transformed or decomposed per m^3 of concrete (kg m^{-3}) (b)	Heat of transformation or decomposition per m^3 of concrete (kJ m^{-3}) (a) × (b)
1	30–120	Release of evaporable water	Heat of evaporation of water, 2238 kJ kg^{-1} (endothermic reaction)	130 kg water	290 × 10^3 kJ
2	30–300	Dehydration of non-evaporable or chemically bound water in cement gel	Heat of hydration of β-C_2S, 250 kJ kg^{-1} (endothermic reaction)	78 kg hardened cement paste	20 × 10^3 kJ
3	120–600	Release of remainder of evaporable and non-evaporable water	Heat of hydration not less than 2238 kJ kg^{-1} (endothermic reaction)	About 60 kg water	135 × 10^3 kJ
4	450–550	Decomposition of $Ca(OH)_2$ $Ca(OH)_2 \rightarrow CaO + H_2O$	Heat of decomposition of $Ca(OH)_2$, 1000 kJ kg^{-1} (endothermic reaction)	Not more than 40 kg $Ca(OH)_2$	40 × 10^3 kJ
5	570	Transformation from α- to β-quartz	Heat of transformation of SiO_2, 5.9 kJ kg^{-1} (endothermic reaction)	(c) 1500 kg SiO_2 in quartzite concrete (d) 200 kg SiO_2 in limestone concrete	8.8 × 10^3 kJ 1.2 × 10^3 kJ
6	600–700	Decomposition of CSH and formation of β-C_2S	Heat of decomposition, 500 kJ kg^{-1} (endothermic reaction)	240 kg C_2S in hardened cement paste	120 × 10^3 kJ
7	780	Recrystallization of unhydrated cement	Heat of recrystallization, 50 kJ kg^{-1} (exothermic)	100 kg unhydrated blast furnace slag cement	5 × 10^3 kJ
8	600–900	Decarbonation of limestone aggregate	Heat of decomposition, 1637 kJ kg^{-1} (endothermic)	1440 kg $CaCO_3$	2360 × 10^3 kJ
9	1100–1200	Melting of concrete	Heat of melting, 750 kJ kg^{-2} (endothermic reaction)	(e) 2100 kg quartzite concrete (f) 1500 kg limestone concrete	1575 × 10^3 kJ 1125 × 10^3 kJ

Source: U. Schneider and U. Diederichs, "Physical Properties of Concrete From 20°C Up To Melting," Parts 1 and 2, *Betonwerk & Fertigteiltechnik*, Heft 3, pp. 141-150, and Heft 4, pp. 223-230, 1981.

aggregate and water were approximately 1:1.9:3.5:0.5, respectively. Calculations indicate that the total amount of heat required to transform a cubic meter of quartzitic aggregate concrete at normal temperature to a molten state is approximately 2000 x 10^3 kJ. For limestone concrete the amount can be nearly twice as large due to additional heat required to decarbonate the aggregate.

Table 2.17 presents average rates of erosion by liquid steel for several concretes. Erosion rates in the table were determined either by immersing the specimens in molten steel produced by an induction furnace (1600˚C) or by metallographic reaction (2600˚C) in which thermite was placed into concrete crucibles and ignited. Results indicate that basaltic concrete gave lowest erosion rates, followed by limestone concrete and quartzitic concrete. Variations in data were the result of different concrete mixes and test conditions. From these results it was concluded that concrete could resist very high thermal loadings arising from its interaction with liquid steel, however, very thick concrete foundations would be required to resist a hypothetical core disruptive accident involving melting of the core [2.243].

Table 2.17 Erosion of different concretes by liquid steel

Type of aggregate in concrete	Average rate of erosion (mm/min)	Test method	Source with references identified in [2.15]
Limestone Quartzite	66 44	Immersed in molten steel (about 1600˚C)	Ehm et al. (11)
Basalt Limestone Quartzite	10 20 30	Metallographic reaction (about 2600˚C)	Ehm et al. (11)
Basaltic limestone	20	Metallographic reaction	Sutherland (9)
Quartzite	40	Metallographic reaction	Perinic et al. (10)
Basalt Limestone	22 35	Molten pool Arc-heating	Hildenbrand (8)
Basaltic limestone	12	Plasma jet	Muir (6)

Source: U. Schneider, C. Diererichs, and C. Ehm, "Effect of Temperature on Steel and Concrete for PCRV's," *Nuclear Engineering and Design* **67**, pp. 245–258, 1981.

Summary. Under a hypothetical core disruptive accident involving melting of the reactor core in a nuclear power plant it is of interest to know how much energy is dissipated by the concrete structures designed to contain the core melt. The term heat of ablation is applied in this context and is defined as the heat dissipated per unit mass material during a steady-state erosion process resulting in the removal of a unit mass. For a heat flow between 20 and 200 W•cm^2, the heat of ablation of concrete has been indicated to be 6000 (±3000) kJ•kg^{-1} [2.40]. Others estimates of the heat of ablation are 2227 and 2400 kJ•kg^{-1} for concrete made with siliceous aggregates, 1474 kJ•kg^{-1} for concrete made from calcareous aggregates, and 3200 kJ•kg^{-1} for concretes made from calcareous aggregates [2.242,2.244]. The amount of heat required to transform a given volume of concrete to a molten state is about twice as much for limestone aggregate concrete as for quartzitic concrete due to the additional heat required to decarbonate the limestone aggregate. The rate at which concrete subjected to high temperatures (e.g., > 1200˚C) is decomposed by mechanical disintegration and the melting process is the erosion rate. Experimental results for erosion rates of limestone, quartzitic, and basalt aggregate concretes indicated erosion rates of 20 to 66, 30 to 44, and 10 to 22 mm/min, respectively. Results for a nuclear power plant basaltic concrete mix indicated a rate of about 30 mm/min. The erosion rate does not appear to be that dependent on the type of aggregate used in the concrete mix. Scatter of data presented in the literature is the result of different concrete mixes and test conditions.

2.2.2.7 Moisture Diffusion and Pore Pressure

Information and Data. Movement of moisture in concrete can result by drying from an exposed surface or from temperature gradients. Prediction of moisture migration and pore pressure build up in non-uniformly heated concrete is important for safe operation of concrete containment vessels in nuclear power plants and for assessing the behavior of fire-exposed concrete structures [2.245]. Two main processes are at work when a heat flux is applied to a concrete element: thermo-mechanical and thermal-hydral. The thermo-mechanical process is associated with the temperature field in the concrete element and induces thermal gradients that result in thermal dilation generating tensile stresses perpendicular to the heated face. The thermal-hydral process, illustrated in Figure 2.269, is associated with transfer of mass (water in liquid and vapor phases and air) [2.246]. As the temperature increases water is partly evaporated to generate a pressure in the porous network. The pressure gradient is the major driving force for mass transfer. Vapor and air are partially evacuated to the heated surface but they also migrate to the center of the element where the vapor can condense forming a quasi-saturated layer. After some time the concrete element forms from the heated surface a dry and dehydrated zone, a drying and dehydrated zone, and a quasi-saturated layer that can act as an impermeable wall for gases. Under the right conditions (e.g., low permeability) these processes can result in spalling of the concrete. Transfer of free moisture in concrete can affect the concrete strength, thermal expansion, shrinkage, and creep. Changes in moisture content distribution also can affect the durability and radiation shielding capability of concrete. Pressure build up under postulated accident conditions can potentially lead to failure of the metallic liner.

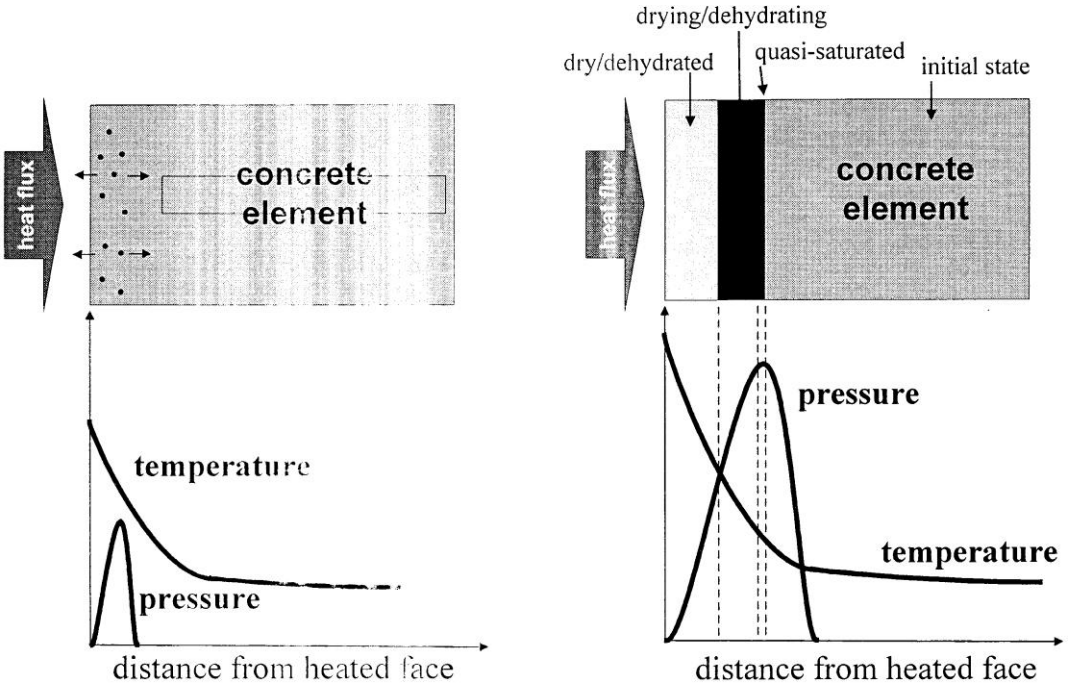

Figure 2.269 Illustration of process of pressure build up in a concrete element under the effect of a pressure gradient.

Source: P. Kalifa, F-D. Menneteau, and D. Quenard, "Spalling and Pore Pressure in HPC at High Temperatures, *Cement and Concrete Research* **30**, pp. 1915-1927, 2000.

At moderate temperatures transfer of moisture in cement paste as well as uncracked concrete is slow (i.e., diffusivity of concrete is approximately 10 $mm^2\ day^{-1}$) [2.247]. Measurements on a thick-wall section (1.52 m) heated on the front face and sealed on all faces except the back face (unheated face) and subjected to a 3.9˚C/m temperature crossfall indicated that even after one year only the inner 0.3 m had lost free water, but shrinkage was large [2.248]. As the temperature increases permeability and diffusivity increase and approximately obey the activation energy concept up to about 100˚C [2.5]. The permeability of concrete depends on the viscosity of water, and to a smaller extent on the density of water (i.e., viscosity drops from 1.00 MPa s at 20˚C to 0.35MPa s at 80˚C, while the density

is reduced from 1.00 to 0.97 kg/m^3) [2.249]. Results obtained by investigating a number of different concretes (44 to 190 MPa compressive strength) indicate that the concrete permeability increases from 13 to 62% when the temperature is raised from 20˚ to 50˚C and by 3 to 55% by an additional increase to 80˚C, with considerable variation in results depending on the type of concrete, and that the increase in permeability and diffusivity can be predicted from theory of thermodynamics [2.249]. Above 100˚C the drying times for concrete become orders of magnitude shorter (i.e., the moisture diffusivity increases significantly as 100˚C is exceeded as the average pore size increases significantly and flow of water probably takes place mainly in a vaporized state as steam) [2.250]. As the temperature increases further the moisture diffusivity continues to increase [2.5].

Heating concrete can produce very large pore pressures that are functions of temperature, temperature history, and size of specimen. The transformation and mass transport of moisture in concrete have a unique influence on concrete's temperature profile and pore pressure development. A general description of the evolution of pore pressure build up in heated concrete is provided in results for a study conducted to quantify the effects of factors influencing pore pressure build up and the potential for explosive spalling of normal- and high-strength concretes [2.251]. A noticeable rise in pore pressure occurred when the concrete reached the temperature range of 105˚C to 160˚C that coincided with the vaporization of free water and the transport of water vapor as evidenced by a drop in the concrete's rate of temperature rise. In the temperature range of 160˚C to 180˚C there was a sharp rise in pore pressure that coincided with the release of chemically-bound water. Beyond 180˚C the concrete pore pressure continued to rise, but with a decreasing rate until peaking occurred in the temperature range from 220˚C to 245˚C. At this point the concrete either spalled explosively or the pore pressure attenuated. General conclusions from this study were that specimens with high water-cementitious materials ratios and lower initial moisture contents have lower pore pressures than their counterparts and that thermal gradients were an influencing factor in the process of pore pressure build up (e.g., higher thermal gradients caused by high heating rates can lead to microcracks that permit moisture to escape resulting in lower pore pressures).

A number of experimental studies were conducted several years ago investigating pore pressures and moisture distributions under thermal gradients in support of development of gas-cooled reactor technology [2.252]. Pore pressure was investigated with regard to concrete spalling and the build up of backpressure behind the liner of a nuclear power plant concrete containment due to thermal gradients. The backpressures between the concrete and liner result from steam and saturated vapor pressures that develop from the free water in the concrete. Additional pressure also develops under elevated temperature from heating of the non-condensable gases that were trapped in the concrete pores during the concrete curing process. A consistent finding of the experimental studies was that the generated pore pressure under elevated temperature was about equal to the sum of the saturated vapor pressure and the partial air pressure for the entrapped pore gases at the temperature of the concrete [2.252]. These results indicate that the pore pressure for a sealed specimen can exceed 414 kN/m^2 (0.414 MPa) at 140˚C as noted in Figure 2.270.*

In unsealed specimens, diffusion and eventual drying leads to lower pore pressures than those obtained for sealed specimens at the same temperature. Additional data are provided in Figure 2.271 which presents temperature and pore pressure distributions in a 30.5-cm-thick wall at 4 and 7 hours after heat-up in a test program to investigate water-release rates in walls [2.254].

Experiments were performed on thick sections of concrete to determine long-term shrinkage, pore pressures, and moisture distributions [2.255]. Pore pressure measurements were made using cylindrical concrete specimens that were 0.6-m-long and either sealed completely or had a pressure release to the atmosphere at the low temperature end. Low and high temperatures for the vented and sealed specimens were 40˚ and 130˚C and 40˚ and 140˚C, respectively. Figure 2.272 presents pressure distributions for the vented and sealed specimen tests at different exposure times. Results indicate that early in the test the behavior of the two specimen types is similar in that differences in sealing become apparent only after 40 days exposure. In both cases the pore pressures dissipate slowly in the hot regions as water migrates toward the cooler parts of the specimen. Additional tests of moisture distribution under thermal gradients were conducted using cylindrical concrete specimens having lengths representing wall thicknesses of 0.6, 0.9, 1.6, or 3.1 m. Each specimen was heated to the same nominal base temperature of 125˚C with the concrete exposed to atmospheric conditions at the cold end. The cylinders were

* Results of an analytical study for the Economic Simplified Boiling Water Reactor indicate that a backpressure of 71.0 kPa can develop at the end of a 72-hour period following a loss-of-coolant accident [2.253].

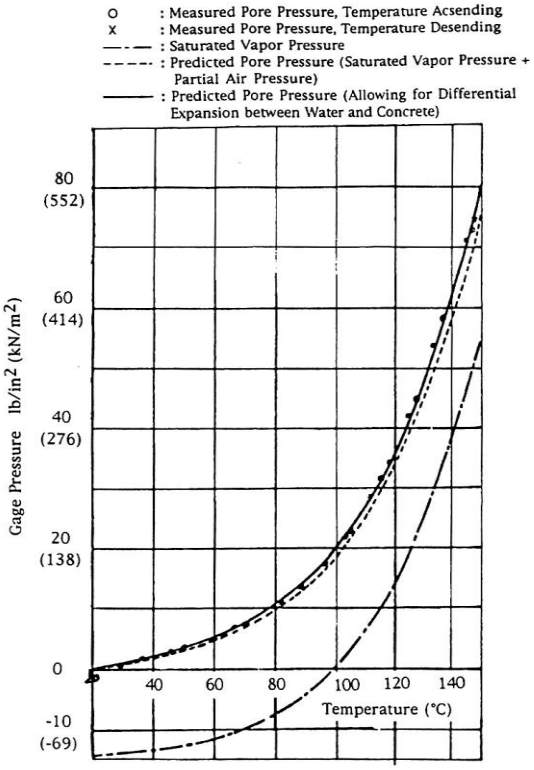

Figure 2.270 Pore pressure build up in sealed concrete specimen.

Source: G.L. England and T.J. Sharp, "Migration of Moisture and Pore Pressures in Heated Concrete," *Proceedings of 1st International Conference on Structural Mechanics in Reactor Technology*, Elsevier Science Publishers, North-Holland, The Netherlands, 1971.

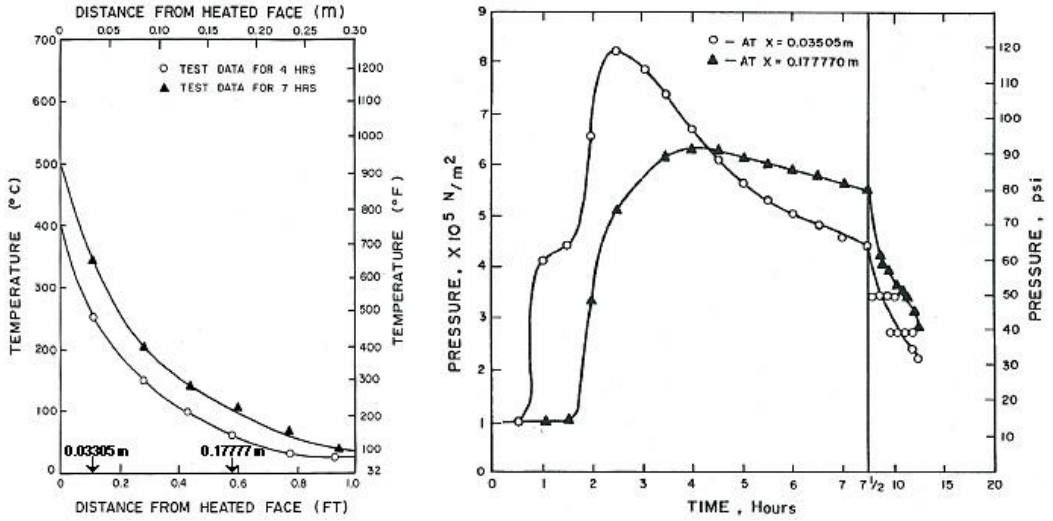

Figure 2.271 Temperature distribution and pore pressure data for 30.5-cm-thick heated concrete wall.

Source: K.H. Chen, E.L. Glueker, E.L. Lam, and V.S. Shippey, "Comparison of Mechanical Codes for Predicting Water Release from Heated Concrete," GEFR-00521, General Electric, April 1980.

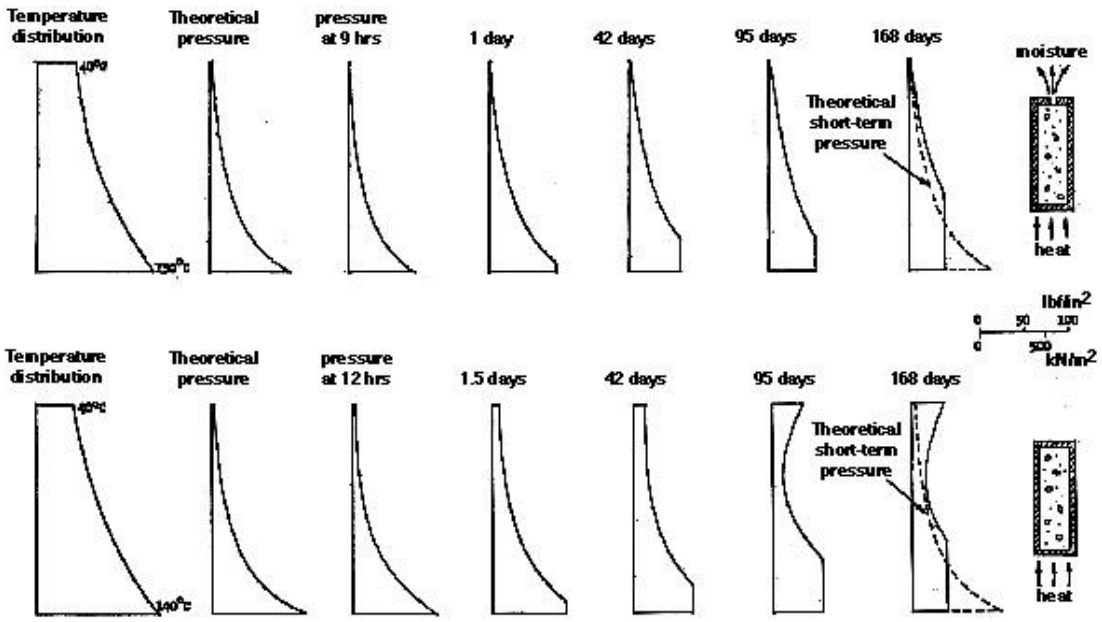

Figure 2.272 Pressure distribution for vented and sealed pore pressure test at given times.

Source: G.L. England and A.D. Ross, "Shrinkage, Moisture, and Pore Pressure in Heated Concrete," Paper SP 34-42 in *Concrete for Nuclear Reactors*, pp. 883-907, American Concrete Institute, Farmington Hills, Michigan, 1972.

sealed along their lengths. Figure 2.273 presents phase diagrams for water in the concrete specimens after 887 days. As shown in the figure, drying has occurred at the two ends of the specimen, and depending on the length of the moisture path, an excess of water may be present in intermediate regions. In other words, for the longer specimens

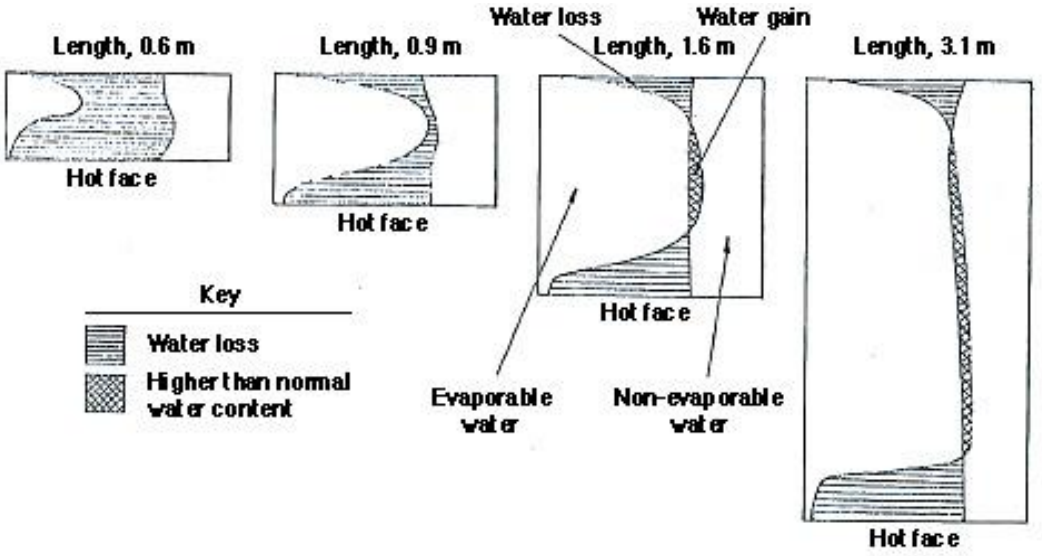

Figure 2.273 Phase diagrams for water in concrete at 887 days for concretes of various lengths and hot face temperature of 125˚C.

Source: G.L. England and A.D. Ross, "Shrinkage, Moisture, and Pore Pressure in Heated Concrete," Paper SP 34-42 in *Concrete for Nuclear Reactors*, pp. 883-907, American Concrete Institute, Farmington Hills, Michigan, 1972.

the temperature gradients have caused more water to migrate into the intermediate regions than to migrate from them to produce a higher than normal water content. Drying depths obtained after 887 days heating for 3.05-m-long specimens that experienced hot-face temperatures of 150˚, 125˚, or 100˚C were 0.914, 0.49, and 0.305 m, respectively. It was concluded from the study that pore pressures are unlikely to be of importance in the bulk of the concrete of a concrete reactor vessel but could become of importance relative to stability of the liner adjacent to the vessel wall. At temperatures below 100˚C results also indicated that drying is not likely to be a very important factor in thick sections because even after many years exposure to such a thermal crossfall drying is unlikely to penetrate more than 0.5 m from either face. As the hot-face temperature increases the depth to which drying penetrates at the cold face remains essentially unchanged while that at the hot face increases. Other research for a prestressed concrete pressure vessel having a 35˚C maximum temperature (i.e., Wylfa) indicates that no significant moisture migration should occur over 30 years except at the outer face [2.136].

More recently, thermally-induced pore pressures and corresponding temperatures in normal- and high-strength concretes were determined in a experimental study to quantify several factors influencing pore pressure build up and the potential for spalling [2.251]. Normal- and high-strength concretes having compressive strengths at 28-days age of 40.6 and 75.3 MPa, respectively, were used to fabricate concrete blocks 100 x 100 x 200 mm^3. In addition to concrete strength, other variables included curing condition (submerged or air-dried), presence of polypropylene fibers (either 13 or 38-mm-long, and amounts of either 1.5 or 3 kg/m^3), and heating rate (either 5˚C/min or 25˚C/min). The concrete blocks contained pore pressure gages located at 25, 50, and 75 mm from the heated face. Prior to heating, all surfaces of the specimens, except the heated surface, were insulated with an insulating blanket to promote one-directional heat flow. Specimens were heated to 600˚C. Results of the study noted the influence of transformation and mass transport of moisture in concrete on its temperature profile and pore pressure development. There was a noticeable increase in pore pressure when the concrete reached the temperature range of 105˚ to 160˚C which coincides with the vaporization of free water and transport of water vapor as evidenced by a drop in the concrete's rate of temperature rise. A sharp increase in pore pressure occurred in the concrete temperature range of 160˚ and 180˚C which coincided with the release of chemically-combined water. At concrete temperatures greater than 180˚C the pore pressure continued to rise, but with a decreasing rate, until peaking at a concrete temperature of 220˚ to 245˚C. After this either the pressure attenuated or explosive spalling occurred. Spalling only occurred for the high-strength concrete that had been cured by submerging and heating at 5˚C/min. Pore pressures measured when spalling occurred averaged 2.05 MPa. Addition of polypropylene fibers significantly reduced pore pressure build up with the pressure build up decreasing as fiber content increased. Normal-strength concrete (high water-cement ratio and lower initial water content) consistently had lower pore pressures compared with the high-strength concretes cured by submerging. Thermal gradient was determined to be an influencing factor in the process of pore pressure build up with higher thermal gradients producing lower pore pressures, possibly due to formation of microcracks that permitted pore pressure to escape.

In an effort to obtain information regarding the mature of moisture movement and rate of moisture loss in a prestressed concrete pressure vessel (PCPV), an experimental study of moisture migration in a pie-shaped specimen representing the flow path through a cylindrical wall of the PCPV was conducted [2.256]. The model was 2.74 m in length with cross-sectional dimensions of 0.61 x 0.61 m^2 on one end by 0.81 x 0.81 m^2 on the other end. It was sealed against moisture loss on the small end (interior) and along lateral surfaces and exposed to the atmosphere at the other end (exterior). Temperature distributions, shrinkage, and moisture distribution were monitored for approximately 17 months prior to application of a 44˚C temperature gradient that was maintained for one year. A series of heating lamps was used to maintain the required temperature on the interior surface. At the end of the test, with the exception of zones nearest the specimen ends, moisture contents were relatively constant as noted in Figure 2.274 (i.e., moisture contents at two ends were approximately 15% less than the average moisture content for the other measuring locations). Concrete strains corrected for thermal effects were small with only about 1 m (that nearest open end) indicating shrinkage strain in excess of 20 millionths, implying that drying shrinkage was minimal. It was concluded that moisture migration in thick sections of concrete, such as a thick-walled prestressed concrete pressure vessel, is a slow process and is not likely to be a significant factor with temperature differences of 44˚C or less.

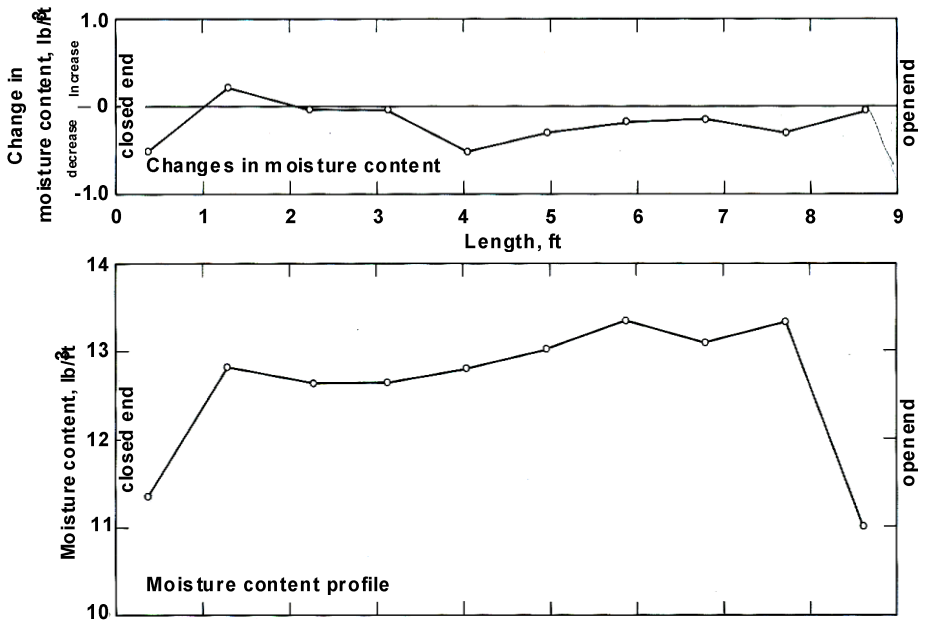

Figure 2.274 Changes in moisture content in specimen after heating and moisture content profile at end of test period.

Source: J. E. McDonald, *Moisture Migration in Concrete*, Technical Report C-75-l, U.S. Army Waterways Experiment Station, Vicksburg, Mississippi, May 1975.

A study has been conducted to investigate the effects on temperature distribution, moisture migration, and strain variation due to heating of a simulated section of a mass concrete wall [2.257]. Cube specimens 1500 mm in dimension, such as shown in Figure 2.275, were tested either with or without venting systems. Five surfaces of each specimen were sealed and insulated with glass wool. During a test the bottom surface of the specimen was heated to175°C over a 2- to 3-h period, and the temperature was maintained at this level for 91 d. Table 2.18 summarizes

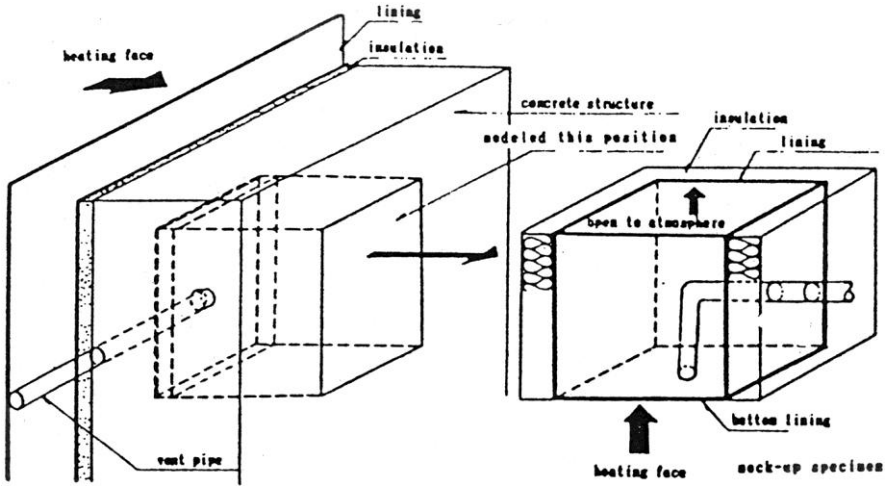

Figure 2.275 Simulated section of mass concrete wall.

Source: T. Takeda, S. Nakane, and K. Nagao, "Experimental Studies on Characteristics of Concrete Members Subjected to High Temperature," *Transactions of 9th International Conference on Structural Mechanics in Reactor Technology*, Vol. H, pp. 195–200, Lausanne, Switzerland, August 17–21, 1987.

the testing conditions for this series of tests. Items measured during a test included temperature, moisture, concrete strain, water discharge from the venting system, and compressive strength and modulus of elasticity of concrete after heating. Figure 2.276 presents details and measurement positions for a typical specimen. Concrete temperature distributions at various times since the start of heating for a vented and nonvented specimen are presented in Figure 2.277. Moisture distributions at various times for the vented and unvented specimens are presented in Figure 2.278. At 91 d after heating, the moisture distribution showed similar conductivities for normal patterns

Table 2.18 Summary of conditions for simulated mass concrete wall section tests

Items	Conditions	Items	Conditions
1) Types of specimen	Specimen with a venting system and without a venting system Two specimen in total	8) Exposure condition during heating	Top surface of the specimen is exposed to air
2) Shape and dimension of specimen	150 ×150 ×150 cm Cube	9) Temperature Control method	Electric capacity controller and temperature controller
3) Age when heated	Greater than 91 days	10) Measuring method	
4) Heating period	3 months	a. Moisuture content	Electrode method
5) Heating temperature	Surface temperature of the concrete of the bottom lining inside is constantly set at 175℃	b. Temperature	C-C thermo-couple for high temparature
		c. Inside strain	Embedment type strain gage
6) Heating method	Electric panel heater	d. Water discharge from vent pipe	Store the cooled vapor discharged from venting system
7) Curing conditions until heating begins	In-situ curing	e. Strength and elastic modulus	Core specimen

Source: T. Takeda, S. Nakane, and K. Nagao, "Experimental Studies on Characteristics of Concrete Members Subjected to High Temperature," *Transactions of 9th International Conference on Structural Mechanics in Reactor Technology*, Vol. H, pp. 195–200, Lausanne, Switzerland, August 17–21, 1987.

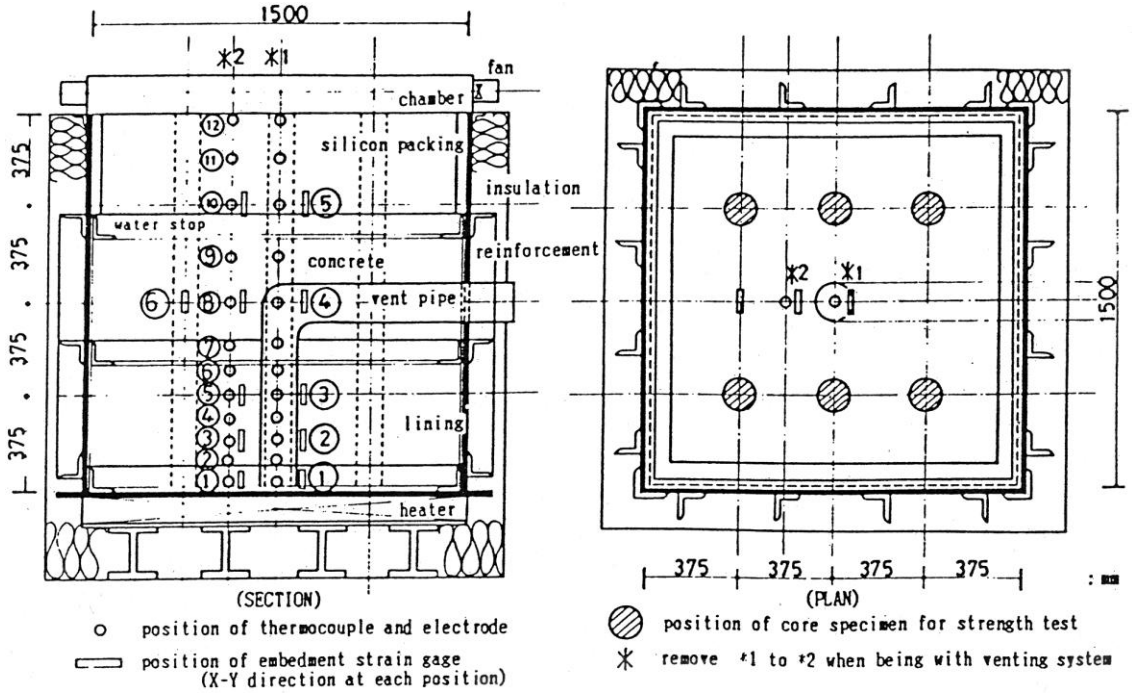

Figure 2.276 Details of simulated section of mass concrete wall and measurement positions.

Source: T. Takeda, S. Nakane, and K. Nagao, "Experimental Studies on Characteristics of Concrete Members Subjected to High Temperature," *Transactions of 9th International Conference on Structural Mechanics in Reactor Technology*, Vol. H, pp. 195–200, Lausanne, Switzerland, August 17–21, 1987

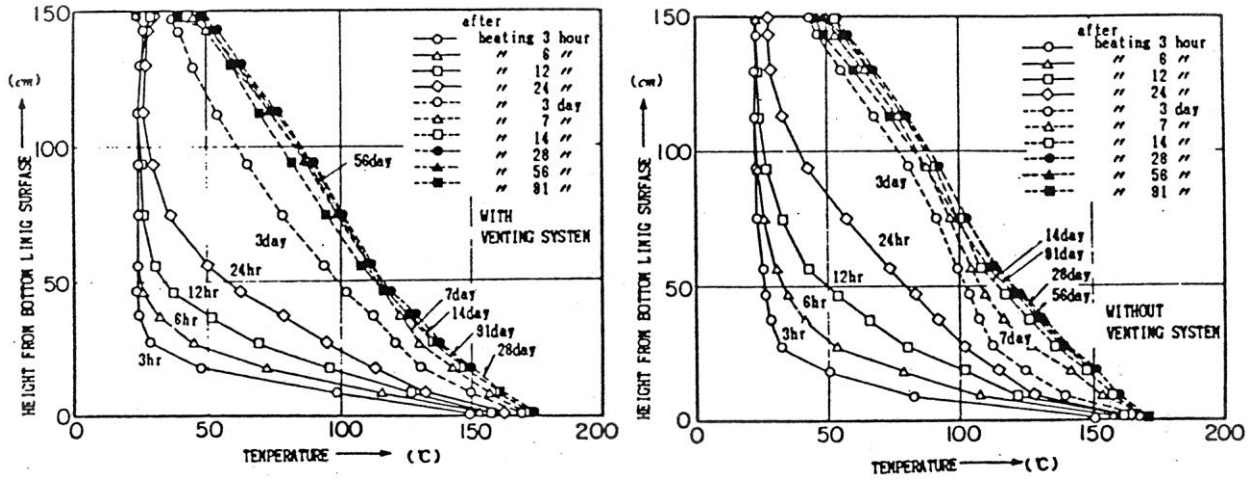

Figure 2.277 Temperature distribution at various times in simulated mass concrete wall with and without a venting system.

Source: T. Takeda, S. Nakane, and K. Nagao, "Experimental Studies on Characteristics of Concrete Members Subjected to High Temperature," *Transactions of 9th International Conference on Structural Mechanics in Reactor Technology*, Vol. H, pp. 195–200, Lausanne, Switzerland, August 17–21, 1987

for the two types of specimens, but the high moisture content zone was greater for the nonvented specimen. Water discharge from the venting system, shown in Figure 2.279, increased relatively rapidly for the first 7 d of heating and then gradually decreased with a total of 150 L (70 L/m^2 of bottom liner) discharged over the 91-d test duration. As the temperature increased, the concrete strains near the bottom liner (heated face) increased, and as heating continued the concrete strains at the unheated face increased with time, Figure 2.280. Core samples removed from the specimens at conclusion of a test and tested at room temperature were used to determine the effect of heating on the concrete's compressive strength and modulus of elasticity. Test results for strength and modulus of elasticity are shown in Figures 2.281 and 2.282, respectively. Reference values for strength and modulus of elasticity obtained from water-cured and sealed control specimens are also shown in the appropriate figure. The effect of the

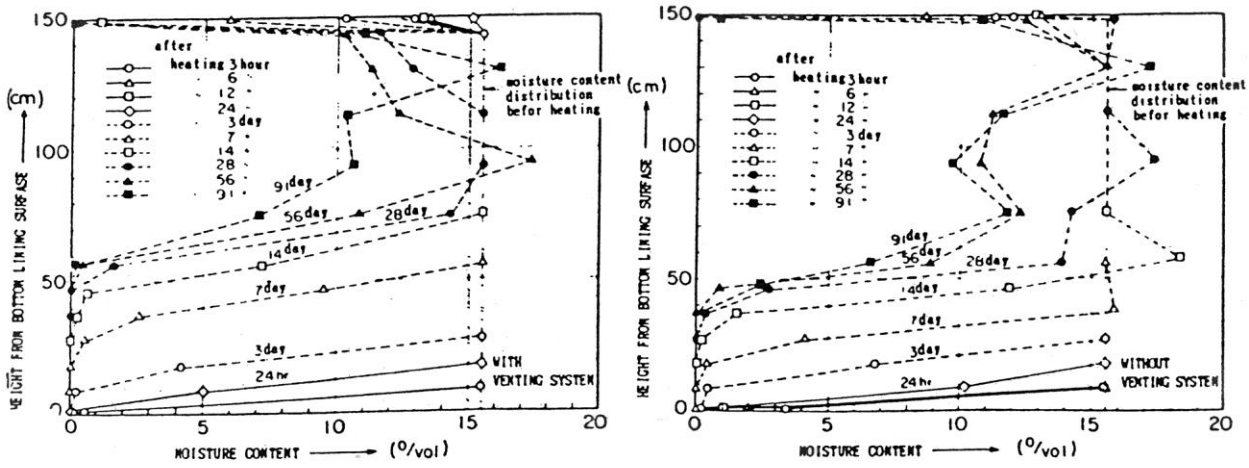

Figure 2.278 Moisture distribution at various times in simulated mass concrete wall section with and without a venting system.

Source: T. Takeda, S. Nakane, and K. Nagao, "Experimental Studies on Characteristics of Concrete Members Subjected to High Temperature," *Transactions of 9th International Conference on Structural Mechanics in Reactor Technology*, Vol. H, pp. 195–200, Lausanne, Switzerland, August 17–21, 1987.

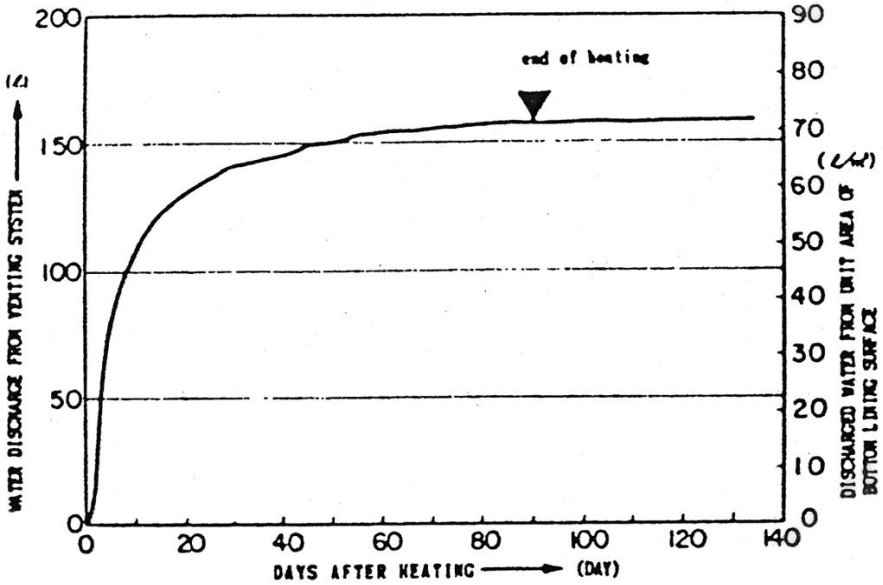

Figure 2.279 Water discharge from vent pipe of simulated mass concrete wall section.

Source: T. Takeda, S. Nakane, and K. Nagao, "Experimental Studies on Characteristics of Concrete Members Subjected to High Temperature," *Transactions of 9th International Conference on Structural Mechanics in Reactor Technology*, Vol. H, pp. 195–200, Lausanne, Switzerland, August 17–21, 1987.

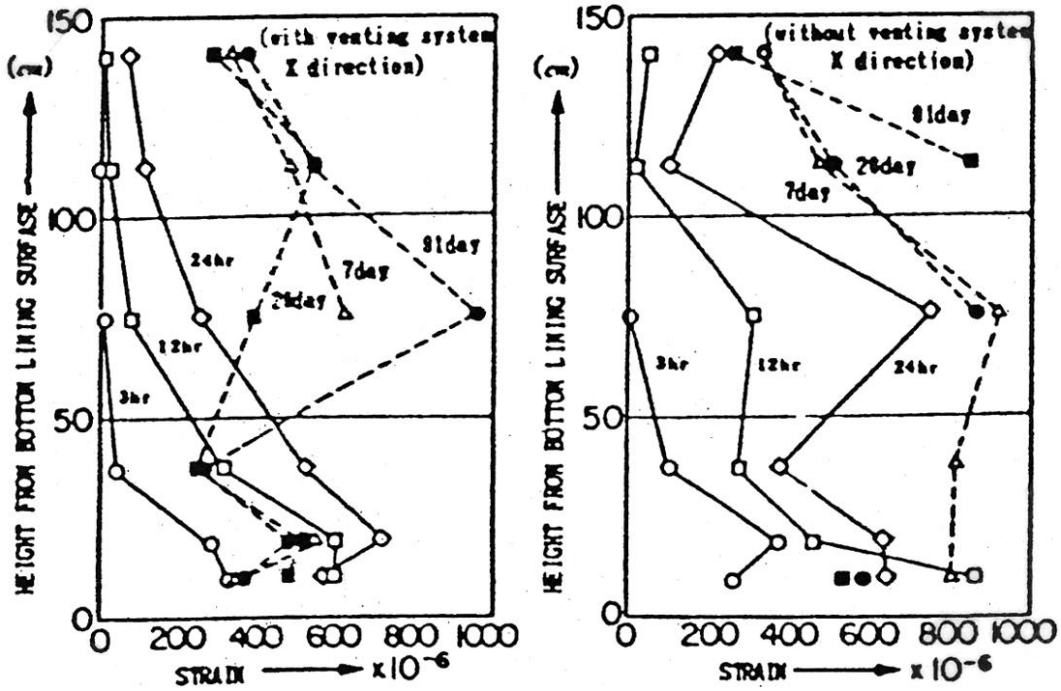

Figure 2.280 Change in strain distribution with time in simulated mass concrete wall section with and without venting.

Source: T. Takeda, S. Nakane, and K. Nagao, "Experimental Studies on Characteristics of Concrete Members Subjected to High Temperature," *Transactions of 9th International Conference on Structural Mechanics in Reactor Technology*, Vol. H, pp. 195–200, Lausanne, Switzerland, August 17–21, 1987.

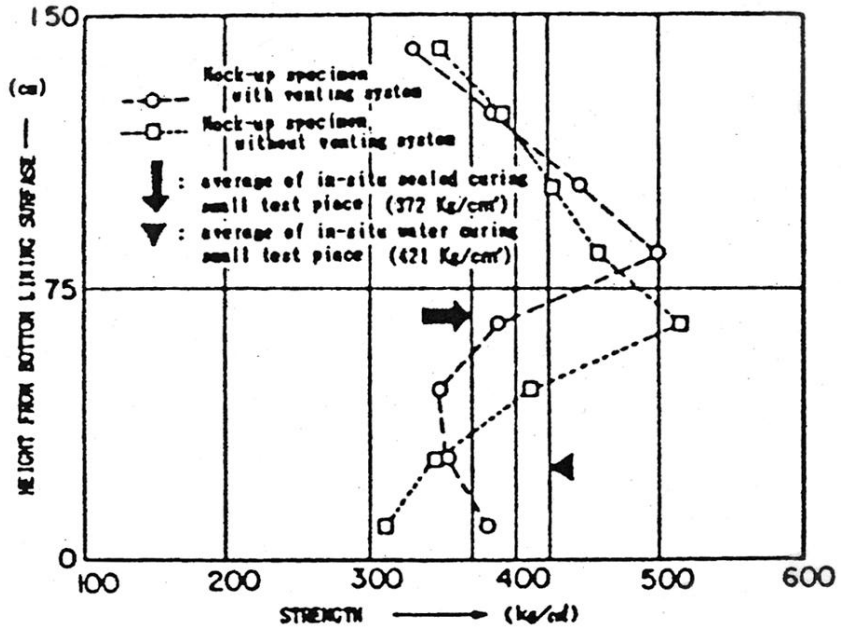

Figure 2.281 Compressive strength test results at selected locations in simulated mass concrete wall section with and without venting.

Source: T. Takeda, S. Nakane, and K. Nagao, "Experimental Studies on Characteristics of Concrete Members Subjected to High Temperature," *Transactions of 9th International Conference on Structural Mechanics in Reactor Technology*, Vol. H, pp. 195–200, Lausanne, Switzerland, August 17–21, 1987.

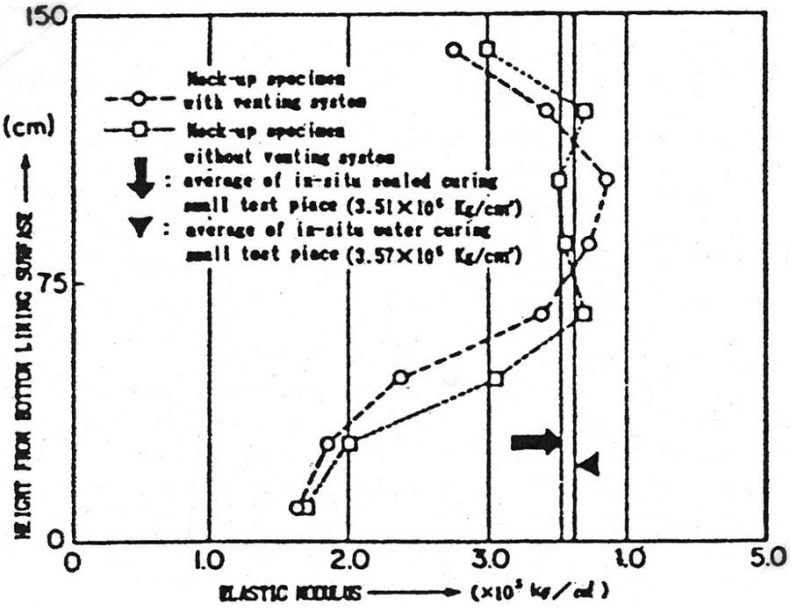

Figure 2.282 Modulus of elasticity test results at selected locations in simulated mass concrete wall section with and without venting.

Source: T. Takeda, S. Nakane, and K. Nagao, "Experimental Studies on Characteristics of Concrete Members Subjected to High Temperature," *Transactions of 9th International Conference on Structural Mechanics in Reactor Technology*, Vol. H, pp. 195–200, Lausanne, Switzerland, August 17–21, 1987.

elevated temperature was most significant on the concrete modulus of elasticity near the bottom face of the specimen, which decreased up to about 40%, relative to sealed control specimens. Compressive strength results at all locations in the test specimens exceeded the design strength (240 kg/cm^2).

Although actual data on moisture distribution in nuclear power plant containments is limited, relative humidity profiles were obtained at two locations in the Barsebäck BWR containment located in Sweden [2.258]. The containment cross-section is somewhat unique in that it consists of an outer 300-mm-thick layer of concrete, a steel liner, and an additional inner 800-mm-thick layer of concrete. Relative humidity measurements were made using two methods: (1) drilling holes and inserting relative humidity probes, and (2) removal and testing of cores. The measurements were made at two locations representing service temperature conditions of 50˚C and 25˚C. Figure 2.283 presents relative humidity results versus distance from the drying surface for the two locations. Since the reactor was out of service the in situ measurements were made when the temperature at both locations was 20˚ to 25˚C, so relative humidity during service was probably slightly higher than that measured. It was concluded from the results that the walls were still drying, even after 30 years, with the drying being extremely slow due to the large thickness and one-sided drying; drying is different in different parts of the containment due to different temperature levels and climatic conditions; and the concrete continued to mature because the moisture conditions in the inner parts permitted further cement hydration. Results were used to develop a method for estimating the moisture conditions in a nuclear containment wall. The method is based on first quantifying the moisture conditions at the outer and inner surfaces, and then describing the moisture fixation and moisture transport within the concrete wall.

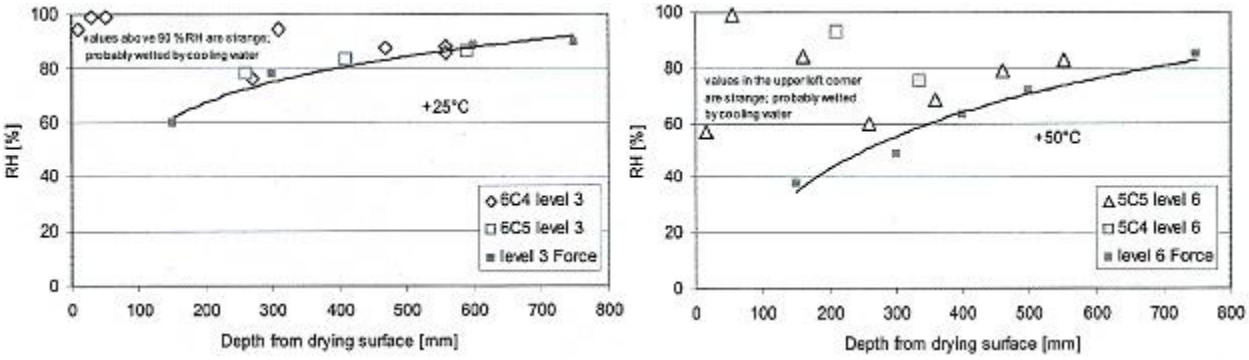

Figure 2.283 Measured relative humidity distributions through Barsebäck containment wall at two locations.

Source: L-O. Nilsson and P. Johansson, "The Moisture Conditions of Nuclear Reactor Containment Walls – An Example for a BWR Reactor," *Proceeding of International Conference on Corrosion and Long Term Performance of Reinforced Concrete in Nuclear Power Plants and Waste Facilities*, NUCPERF 2006, Cadarache, France, March 27-30, 2006.

Several researchers have developed models addressing the behavior of concrete materials when subjected to a temperature field (i.e., potential for concrete spalling based on temperature distribution and pore pressure build up) [2.124,2.259-2.261]. Results of a review of models indicated that although the models are potentially useful for modeling internal stresses and moisture transport, none of the models provided validation of the computed pore pressures using experimental data [2.262]. Since that review several additional models have been proposed that consider the migration of free and bound water, diffusion and migration of dry air and water vapor, and the evaporation of free and bound water [e.g. 2.63,2.73,2.263,2.264]. One of the more recent of these is a mathematical and computational model developed for chemo-hygro-thermal analysis of concrete when it is subjected to thermal load [2.264]. Phase changes of water, changes of material properties caused by temperature and pressure changes, as well as coupling among thermal, hydral, and chemical phenomena are taken into consideration. The model is implemented through a finite-volume code that was developed. High temperature effects are considered by means of temperature and pressure dependence of several parameters. Predicted pore pressure results obtained from the model compared to those obtained during step heating of a concrete slab were quantitatively comparable to the experimental results obtained from a 30 x 30 x 12 cm^3 concrete specimen at high temperature [2.246].

Summary. Transfer of free moisture in concrete can affect the concrete strength, thermal expansion, shrinkage, and creep, as well as potentially affect the concrete durability and radiation shielding capability. Under normal operating conditions (e.g., $T \leq 65^{\circ}C$ as defined by the ASME Code), moisture migration in mass concrete structures is a very slow process and drying is not likely to be an important factor in thick-section concrete structures. Model tests involving simulated mass concrete sections heated at one surface and maintained at room temperature at the opposite surface indicate that when the surface at ambient conditions is vented, the free moisture is lost over only a relatively small length at the heated and unheated surfaces, but shrinkage strains may develop. Above 100˚C the drying time for concrete becomes much shorter and the moisture diffusivity increases. As the temperature at the heated face of a specimen increases, the drying depths increase somewhat. Limited results on moisture distribution in a nuclear power plant containment wall indicate that even after 30 years the walls were still drying, with the drying being extremely slow due to the large thickness and one-sided drying; drying was different in different parts of the containment due to different temperature levels and climatic conditions; and the concrete continued to mature because the moisture conditions in the inner parts permitted further cement hydration. Heating of the concrete can produce relatively large pore pressures that are a function of temperature, temperature history, and size of specimen. The biggest concern relative to pressure build up under postulated accident conditions would be its potential impact on the containment metallic liner (e.g., buckling or failure). The pore pressure generated due to heating is about equal to the sum of the saturated vapor pressure and partial air pressure for the entrapped pore gases at the temperature of the concrete. In unsealed specimens diffusion and eventual drying leads to lower pore pressures than that obtained from sealed specimens at the same temperature. Pore pressures dissipate from the hot region of a concrete specimen as moisture migrates toward the cooler region. Pore pressures in concrete do not increase significantly until the concrete temperature reaches about 105˚C. There have been relatively recent modeling advancements for chemo-hygro-thermal analysis of concrete when it is subjected to thermal load that consider the migration of free and bound water, diffusion and migration of dry air and water vapor, and the evaporation of free and bound water.

2.2.2.8 Simulated Hot Spot Tests

Information and Data. As noted previously, the properties of concrete can be significantly affected by changes in temperature. Concrete's thermal properties are more complex than for most materials because not only is the concrete a composite material whose components have different properties, but concrete's properties depend on moisture content and porosity. While the properties of the steel reinforcement are relatively well understood, the interaction with concrete is not (i.e., at ambient temperatures the bonding between the reinforcement and concrete is considered complete when structural analyses are conducted; however, with an increase in temperature and/or load the bond can deteriorate). Prediction of the performance of concrete structural elements at elevated temperatures is further complicated due to the presence of cracks that form. At high temperatures, correlation of cracking patterns predicted by analytical procedures with experimental results is difficult [2.265]. Due to the problems involved in the analytical treatment of concrete structural members, especially under elevated-temperature conditions, model tests are often used to develop data under representative conditions. The results of these tests are then used to both demonstrate performance and for the validation and refinement of computer codes.

Several research projects have been conducted to investigate the behavior of reinforced concrete structures at elevated temperature; however, the overall level of effort has not been sufficient for establishment of widely accepted elevated-temperature concrete design procedures. Available results have been primarily concerned with testing of specific structural features in support of development of analytical procedures, or model tests related to development of gas-cooled or breeder reactors. A compilation of elevated temperature-related structural features tests, model tests in support of prestressed concrete reactor vessel development, and thermal- and moisture migration-model tests was completed under a prior study [2.266] and will not be repeated. Provided below is information related to tests involving "hot spots" that could develop under conditions such as penetration of steam lines through a containment wall or if localized failure of the liner cooling system of a prestressed concrete reactor vessel occurs.

A thermal cylinder experiment was designed both to provide information for evaluating the capability of analytical methods to predict the time-dependent stress-strain behavior of a 1:6-scale model of the barrel section of a single-cavity prestressed concrete reactor vessel and to demonstrate the structural behavior under design and simulated thermal conditions such as could result from an accident (i.e., hot spot) [2.267]. The model shown in Figure 2.284 was a thick-walled cylinder having a height of 1.22 m, a thickness of 0.46 m and an outer diameter of 2.06 m. It was

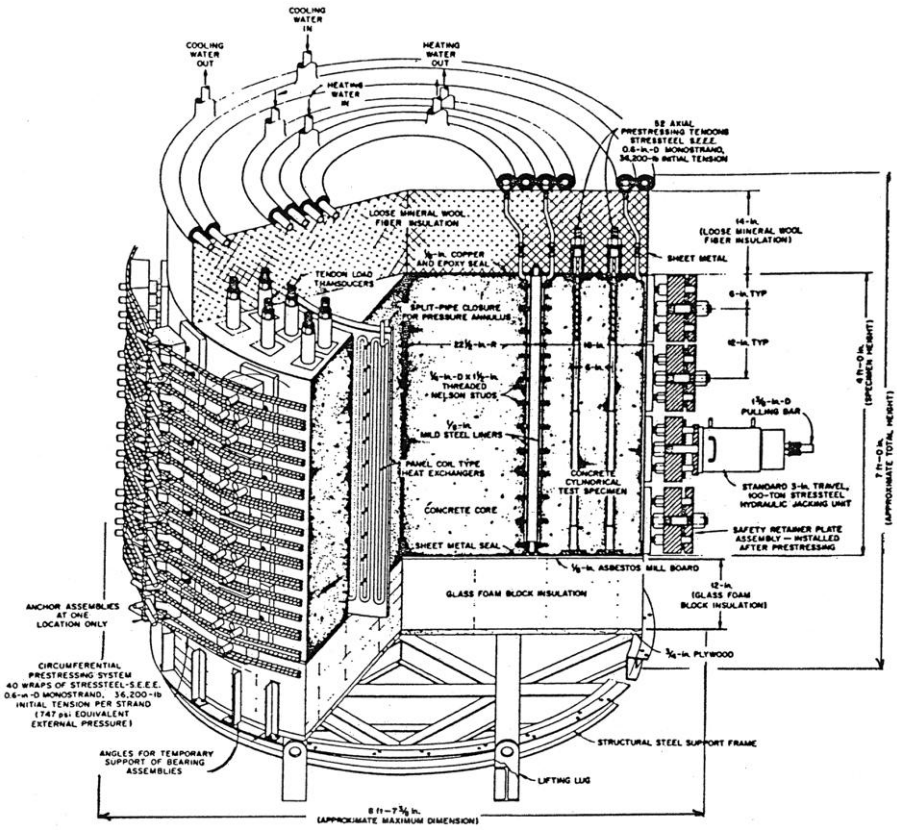

Figure 2.284 Isometric of ORNL thermal cylinder test structure.

Source: J.P. Callahan et al., "Prestressed Concrete Reactor Vessel Thermal Cylinder Model Study," ORNL/TM-5613, Oak Ridge National Laboratory, June 1977.

prestressed both axially and circumferentially and subjected to a 4.83-MPa internal pressure together with a thermal crossfall imposed by heating the inner surface to 65.7°C and cooling the outer surface to 24°C. Because the model was designed to study the behavior of the barrel section of a massive concrete structure, all exposed surfaces were sealed to prevent loss of moisture, and the ends of the cylinder were insulated to prevent heat flow in the axial direction. The experiment utilized information developed from previous studies of concrete material properties, triaxial creep, instrumentation, analysis methods, and structural models. The initial 460 days of testing was divided into time periods that simulated prestressing, heatup, reactor operation, and shutdown. At the conclusion of the simulated operating period, the model was repressurized and subjected to localized heating at 232°C for 84. This temperature excursion was meant to simulate a hot spot condition in which the liner cooling system and/or insulation system is assumed to have failed in an operating nuclear reactor. At the end of this period the inner surface was cooled to 66˚C using the inner water-circulation system, followed by cooling to 24˚C. Comparisons of experimental data with calculated values obtained using the SAFE-CRACK finite-element computer program showed that the program was capable of predicting time-dependent behavior in a vessel subjected to normal operating conditions, but that it was unable to accurately predict the behavior during off-design hot-spot heating. Readings made using a neutron and gamma-ray backscattering moisture probe showed little, if any, moisture migration in the concrete cross-section. Destructive examination (sectioning by saw cutting) indicated that the model maintained its basic structural integrity during localized hot spot heating. No significant defects were seen in the cut surfaces, however, the concrete immediately surrounding the hot-spot heating elements was darkened as shown in Figure 2.285 indicating that some change had occurred in the concrete due to the 232˚C hot-spot heating. A series of impact hammer readings was made in and outside this area and revealed that the relative compressive strength in the hot-spot area was lower (~39%) than that obtained for readings outside the heat-affected zone. As the distance from the heater increased the reduction in compressive strength decreased.

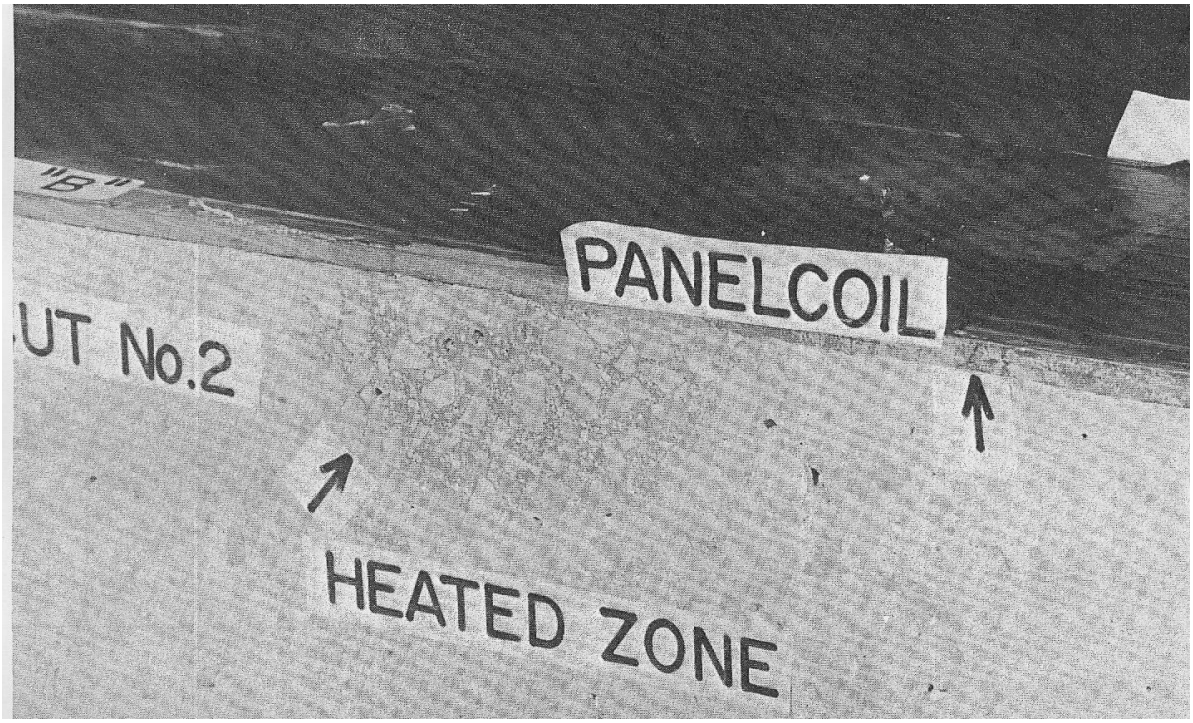

Figure 2.285 Cross section showing discoloration in the vicinity of the hot-spot heating.

Source: J.P. Callahan et al., "Prestressed Concrete Reactor Vessel Thermal Cylinder Model Study," ORNL/TM-5613, Oak Ridge National Laboratory, June 1977.

During commissioning tests of the prestressed concrete reactor vessel at the Oldbury Nuclear Power Station, there were a small number of localized breakdowns of the liner insulation permitting the temperature to reach 180° C in the head penetration region and 90° C in the haunch region at the upper boiler instrument penetration [2.268]. Since hot spots could induce high thermal stresses in the concrete to result in cracking, a theoretical study was conducted that indicated there was no cause for concern about the safety margin against failure of the vessel, but concrete cracking could occur close to the liner. To provide input on concrete cracking, a full-scale model (3.66 m-diameter by 1.52 m thick) of the region of the vessel local to the upper boiler instrumentation where the highest liner temperatures were recorded was fabricated and tested, Figure 2.286. The test procedure included heating of the model over a 24-h period to the steady-state condition achieved in the hot spot region of the prototype, allowing the model to attain thermal equilibrium, and maintaining this condition for 3 months with the prestressing force reduced as the test progressed, and then permitting the model to cool to ambient. Embedded strain instrumentation, dye penetrants, core samples, and ultrasonic testing were used to detect and measure cracking. Results indicated that the hot spot was confined to a small area of the model. Gages indicated that some cracking had occurred during reactor start-up when the penetration liner was only 24°C hotter than the adjacent concrete and was attributed to thermal diffusivity differences between steel and concrete resulting in strain differentials. Cracking was limited to a central region of about 0.46 m where the concrete temperature was 100°C. No cracking of the concrete was observed at heated locations away from steel parts. A second degree of cracking occurred during shutdown that was caused by stress reversals due to residual creep strains. Uncracked regions of the heated concrete showed no loss of strength over control samples stored separately. In addition, measurements of vapor pressure behind the liner showed less severe pressures than those corresponding to the concrete temperatures imposed. This indicated no pressure build up would occur at the hot spot, probably because of pressure relief along the liner-concrete interface. It was concluded that the sustained high hot-spot temperature in the Oldbury vessel did not cause serious damage to the liner or to the concrete.

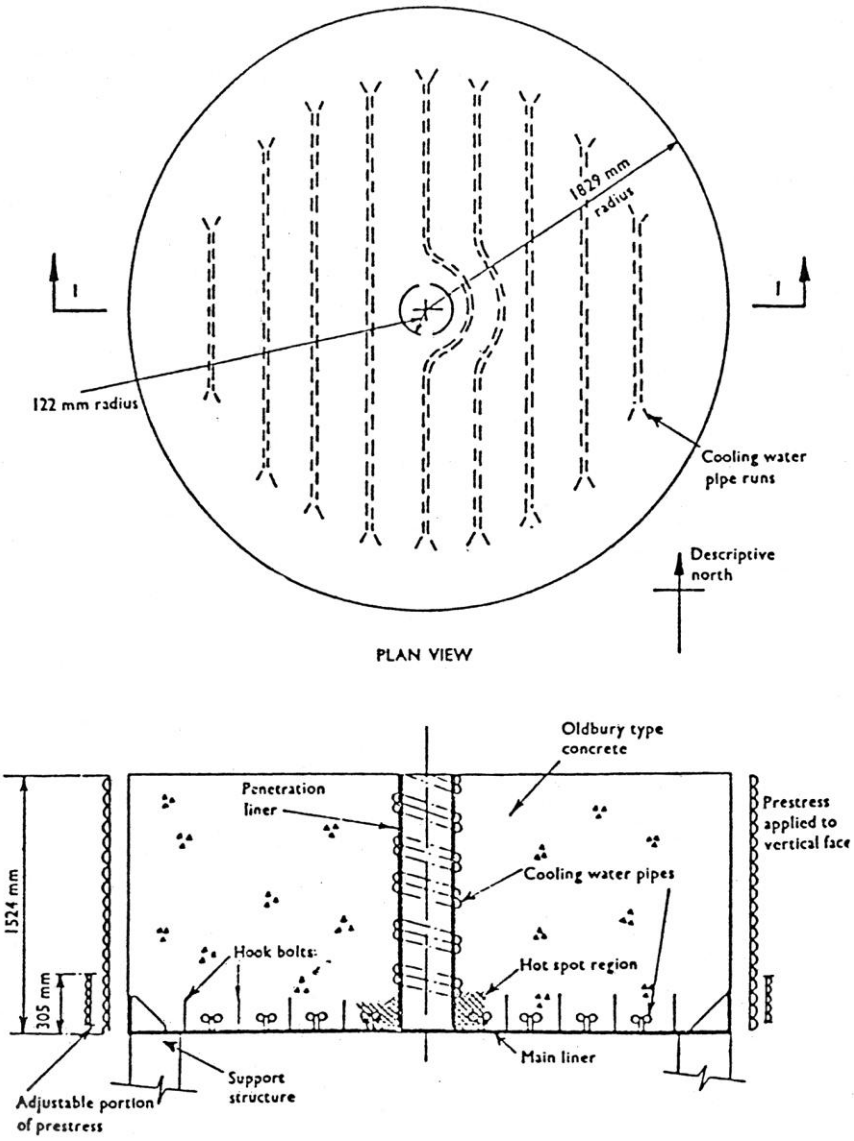

Figure 2.286 Full-scale Oldbury hot-spot model.

Source: J. Irving, G.D.T. Carmichael, and I.W. Hornby, "A Full Scale Model Test of Hot Spots in the Prestressed Vessels of Oldbury Nuclear Power Station," Paper 7699, *Proceedings of Institution of Civil Engineers* **57**, June 1974.

Summary. Due to problems involved in analytical treatment of concrete structural members at elevated temperature (e.g., property changes and cracking), structural features tests have often been used to develop data under representative conditions. The results of these tests are then used to both demonstrate performance and for the validation and the refinement of computer codes. A summary of structural features tests was provided in an earlier study [2.266]. One area of interest is related to hot spots that could develop in the vicinity of hot penetrations or if a localized failure of a liner cooling system occurs in a prestressed concrete reactor vessel. Although results are limited, they tend to indicate that for the conditions investigated (T = 232˚C or 180˚C) the effect was localized. Some loss of concrete strength and cracking will occur in the region of the hot spot, but is not considered to be a threat to structural integrity. Results also seemed to indicate that significant pressure build up behind a liner resulting from a localized hot spot may not occur due to pressure relief along the liner-concrete interface.

2.3 References

2.1 V. S. Ramachandran, R. F. Feldman, and J. J. Beaudoin, *Concrete Science—A Treatise on Current Research*, Hey and Son, London, 1981.

2.2 M.J. DeJong and F-J. Ulm, "The Nanogranular Behavior of C-S-H at Elevated Temperature," *Cement and Concrete Research* **37**, pp. 1-12, 2007.

2.3 A. Khennane and G. Baker, "Plasticity Models for the Biaxial Behavior of Concrete at Elevated temperature," *Computational Methods of Applied Mechanics in Engineering* **100**, pp. 207-223, 1992.

2.4 K. Willam, I. Rhee, and Y. Xi, "Thermal Degradation of Heterogeneous Concrete Materials," *Journal of Materials in Civil Engineering* **100**, pp. 276-285, American Society of Civil Engineers, New York, New York, 2005.

2.5 Z.P. Bazant and M.F. Kaplan, *Concrete at High Temperatures: Material Properties and Mathematical Models*, Longman, London, United Kingdom, 1996.

2.6 F.-J. Ulm, O. Coussy, and Z.P. Bazant, "The 'Chunnel' Fire. I: Chemoplastic Softening in Rapidly Heated Concrete," *Journal of Engineering Mechanics* **125**(3), pp. 272-282, American Society of Civil Engineers, New York, New York, 1999.

2.7 O. Arioz, "Effects of Elevated Temperatures on Properties of Concrete," *Fire Safety Journal* **42**, pp. 516-522, 2007.

2.8 G. A. Khoury, *Performance of Heated Concrete—Mechanical Properties*, Contract NUC/56/3604A with Nuclear Installations Inspectorate, Imperial College, London, August 1996.

2.9 G.A. Khoury, "Effect of Fire on Concrete and Concrete Structures," *Progress in Structural Engineering Materials* **2**, pp. 429-447, 2000.

2.10 G.A. Khoury, P.J.E. Sullivan and B.N. Grainger, "Strain of Concrete During First Heating to 600˚C under Load," *Magazine of Concrete Research* **37**(133), pp. 195-215, 1985.

2.11 G.A. Khoury and S. Algar, "Advanced Mechanical Characterisation of HPC and UHPC Concretes at High Temperatures," *Proceedings of the International Workshop on Durable Concrete Structures*, Weimar, Germany, October 1998.

2.12 U. Schneider, *Behaviour of Concrete at High Temperature*, HEFT 337, Deutscher Ausschuss für Stahlbeton, Wilhelm Ernst & Sohn, Munich, Germany, 1982.

2.13 G.A. Khoury, "Compressive Strength of Concrete at High Temperature: A Reassessment," *Magazine of Concrete Research* **44**(161), pp. 291-309, December 1992.

2.14 G.A. Khoury, *Effect of Heat on Concrete*, Department of Civil and Environmental Engineering Report, Imperial College, London, United Kingdom, 1995.

2.15 U. Schneider, C. Diererichs, and C. Ehm, "Effect of Temperature on Steel and Concrete for PCRV's," *Nuclear Engineering and Design* **67**, pp. 245–258, 1981.

2.16 Z. P. Bazant, J.C. Chern, M.S. Abrams, and M.P. Gillen, *Normal and Refractory Concretes for LMFBR Applications—Vol. 1, Review of Literature on High-Temperature Behavior of Portland Cement and Refractory Concretes*, EPRI Report NP-2437, Northwestern University and Portland Cement Association, Chicago, Illinois, June 1982.

2.17 N. V. Waubke, "On One Physical Aspect of Strength Loss of Portland Cement Concretes at Temperatures up to 1000°C," in *Brandverhalten von Bauteilen, Schriftenreisse der Deutschen Forschungsgemeinschaft*, Heft 2, Technical Universität Braunschweig, Germany, November 1973.

2.18 T. Z. Harmathy and L. W. Allen, "Thermal Properties of Selected Masonry Unit Concretes," *J. American Concrete Institute* **70**, pp. 132–142, 1973.

2.19 *Fire Design of Concrete Structures – Materials, Structures and Modelling*, Bulletin 38, International Federation for Structural Concrete, Lausanne, Switzerland, April 2007.

2.20 G.A. Khoury, B.N. Grainger, and P.J.E. Sullivan, "Transient Thermal Strain of Concrete: Literature Review, Conditions Within Specimen and Behaviour of Individual Constituents," *Magazine of Concrete Research* **37**(132), September 1985.

2.21 M.F. Kaplan, *Concrete Radiation Shielding - Nuclear Physics, Concrete Properties, Design and Construction*, Longman Scientific & Technical, London, United Kingdom, 1989.

2.22 R. Felicetti and P.G. Gambarova, "Effect of High Temperature On The Residual Compressive Strength of High Strength Siliceous Concretes," *Journal American Concrete Institute* **95**, pp. 395-406, 1998.

2.23 V. Vydra, F. Vodak, O. Kapickova, and S. Hoskova, "Effect Of Temperature On Porosity of Concrete for Nuclear Safety Structures," *Cement and Concrete Research* **31**, pp. 1023-1026, 2001.

2.24 T. Z. Harmathy, "Thermal Properties of Concrete at Elevated Temperatures," *J. of Materials* **5**, pp. 47–74, 1970.
2.25 S.K. Handoo, S. Agarwal, S.K. Agarwal, and S.C. Ahluwalia, "Effect of Temperature on the Physico-Chemical and Mineralogical Characteristics of Hardened Concrete," *Proceedings of the 10th International Congress on the Chemistry of Cement*, Gotherburg, Sweden, Paper 4IV067, 4 p., 1997.
2.26 S.K. Handoo, S. Agarwal, and S.K. Agarwall, "Physiochemical, Mineralogical, and Morphological Characteristics of Concrete Exposed to Elevated Temperatures," *Cement and Concrete Research* **32**(7), pp. 1009-1018, 2002.
2.27 A. Mendes, J. Sanjayan, and F. Collins, "Phase Transformations and Mechanical Strength of OPC/Slag Pastes Submitted to Temperature," *Materials and Structures* **41**, pp. 345-350, 2008.
2.28 A. Mendes, J. Sanjayan, and F. Collins,, "Long-Term Progressive Deterioration Following Fire Exposure of OPC Versus Slag Blended Cement Pastes," *Materials and Structures* **42**, pp. 95-101, 2009.
2.29 T. Z. Harmathy and J. E. Berndt, "Hydrated Portland Cement and Lightweight Concrete at Elevated Temperatures," *J. American Concrete Institute* **63**, pp. 93–112, 1966.
2.30 W.P.S. Dias, G.A. Khoury, and P.J.E. Sullivan, "Mechanical Properties of Hardened Cement Paste Exposed to Temperatures Up To 700˚C," ACI *Materials Journal* 87(2), March-April 1990.
2.31 J. Piasta, "Heat Deformations of Cement Paste Phases and the Microstructure of Cement Paste," *Materials and Structures* **17**(102), pp. 415-420, November-December 1984.
2.32 P.J.E. Sullivan and R. Sharahar, "The Performance of Concrete at Elevated Temperatures (As Measured by the Reduction in Compressive Strength)," *Fire Technology* **28**(2*)*, pp. 240-250, August 1992.
2.33 R. Sarshar and G.A. Khoury, "Material and Environmental Factors Influencing the Compressive Strength of Unsealed Cement Paste and Concrete at High Temperature," *Magazine of Concrete Research* **45**(162), pp. 51-61, March 1993.
2.34 J. Komonen and V. Penttala, "Effects of High Temperature on the Pore Structure and Strength of Plain and Polypropylene Fiber Reinforced Cement Pastes," *Fire Technology* **39**(1), pp. 23-34, 2003.
2.35 K.M. Alexander et al., "Aggregate-Cement Bond, Cement Past Strength and the Strength of Concrete," *Proceedings of Conference on Structure of Concrete and Its Behaviour Under Load*, pp. 59-92, Cement and Concrete Association, London, United Kingdom, 1968.
2.36 O. Christensen and T.P.H. Nielsen, "Model Deterioration of the Effect of Bond Between Coarse Aggregate and Mortar on Compressive Strength of Concrete," *Proceedings of American Concrete Institute* **66**(1), pp. 69-72, Farmington Hills, Michigan, 1969.
2.37 R. Lezy and A.A. Pailliere, "The Importance of Concrete Mortars and Grouts by the Addition of Resin," *RILEM Symposium on Synthetic Resins in Building Construction*, Paris, France, 1967.
2.38 K.D. Hertz, "Concrete Strength for Fire Safety," *Magazine of Concrete Research* **57**(8), pp. 445-453, 2005.
2.39 D. H. H. Quon, *Phase Changes in Concrete Exposed to Sustained High Temperatures*, Division Report MRP/MSL 80-111(TR), Mineral Sciences Laboratories, CANMET, Ottawa, Canada, August 1980.
2.40 J. F. Muir, *Response of Concrete Exposed to High Heat Flux on Surface*, Research Paper SAND 77-1467, Sandia National Laboratories, Albuquerque, New Mexico, 1977.
2.41 T. Y. Chu, *Radiant Heat Evolution of Concrete—A Study of the Erosion of Concrete Due to Surface Heating*, Research Paper SAND 77-0922, Sandia National Laboratories, Albuquerque, New Mexico, 1978.
2.42 G. Hildenbrand et al., "Untersuchung der Wechselvirkung von Kernschmelze und Reaktorbeton," *Abschlussbericht Förderungverhaben*, BMFT RS 154, KWU, Erlangen, Germany, May 1978.
2.43 RILEM Committee 44-PHT, *Behaviour of Concrete at High Temperatures*, U. Schneider, Ed., Kassel Universität, Kassel, Germany, 1985.
2.44 Comité Euro International du Beton, *Fire Design of Concrete Structures—In Accordance With CEB/FIP Model Code 90*, CEB Bulletin D'Information No. 208, Switzerland, July 1991.
2.45 Comité Européen de Normalisation (CEN), *prENV 1992-1-2: Eurocode 2: Design of Concrete Structures: Part 1-2: Structural Fire Design*, CEN/TC 250/SC 2, Commission of European Communities, Brussels, 1993.
2.46 Comité Européen de Normalisation (CEN), *Eurocode 4: Design of Composite Steel and Concrete Structures, Part 1-2: General Rules—Structural Fire Design*, CEN ENV, Commission of European Communities, Brussels, 2004.
2.47 *Guide for Determining Fire Endurance of Concrete Elements*, ACI 216R-89, American Concrete Institute, Farmington Hills, Michigan, 1989.

2.48 L. T. Phan and N. J. Carino, "Fire Performance of High Strength Concrete: Research Needs," Applied Technology in Structural Engineering, *Proceedings ASCE/SEI Structures Congress 2000, 8–10 May 2000, Philadelphia, Pennsylvania.*

2.49 S. E. Pihlajavaara, "An Analysis of the Factors Exerting Effect on Strength and Other Properties of Concrete At High Temperature," Paper SP-34-19 in *Concrete for Nuclear Reactors*, pp. 347-354, American Concrete Institute, Farmington Hills, Michigan, 1972.

2.50 P.J.E. Sullivan, "The Effects of Temperature on Concrete, Chapter 1" in *Developments in Concrete Technology—1*, F. D. Lydon, Ed., Applied Science Publishers, London, 1979.

2.51 F-P. Cheng, V.K.R. Kodur, and T-C. Wang, *Stress-Strain Curves for High Strength Concrete at Elevated Temperatures*, Report NRCC-46973, Institute for Research in Construction, National Research Council Canada, March 15, 2004 (http://irc.nrc-cnrc.gc.ca/ircpubs).

2.52 R. Kottas, J. Seeberger, and H. K. Hilsdorf, "Strength Characteristics of Concrete in the Temperature Range of 20° to 200°C," Paper H01/4 in *5th International Conference on Structural Mechanics in Reactor Technology*, p. 8, Elsevier Science Publishers, North-Holland, The Netherlands, August 1979.

2.53 Y. Anderberg and S. Thelanderson, *Stress and Deformation Characteristics of Concrete at High Temperatures, 2-Experimental Investigation and Material Behaviour Model*, Bulletin 54, Lund Institute of Technology, Lund, Sweden, 1976.

2.54 T. Harada, T. Takeda, S, Yamane, and F, Furumura, "Strength, Elasticity and Thermal Properties of Concrete Subjected to Elevated Temperatures," Paper SP-34-21 in *Concrete for Nuclear Reactors*, pp. 377-406, American Concrete Institute, Farmington Hills, Michigan, 1972.

2.55 H. Weigler and R. Fischer, "Influence of High Temperatures on Strength and Deformations of Concrete," Paper SP 34-26 *Concrete for Nuclear Reactors*, pp. 481-493, American Concrete Institute, Farmington Hills, Michigan, 1972.

2.56 U. Schneider, "Concrete at High Temperatures – A General Review," *Fire Safety Journal* 1**3**, pp. 55-68, 1988.

2.57 V.K.R. Kodur and L. Phan, "Critical Factors Governing the Fire Performance of High Strength Concrete Systems, *Fire Safety Journal* **42**, pp. 482-488, 2007.

2.58 C. Castillo and A.J. Durrani, "Effect of Transient High Temperature on High-Strength Concrete," *ACI Materials Journal* **87**(1), American Concrete Institute, pp. 47-53, January-February 1990.

2.59 C-G. Han, Y-S. Hwang, S-H. Yang, and N. Gowripalan, "Performance of Spalling Resistance of High Performance Concrete With Polypropylene Fiber Contents and Lateral Confinement," *Cement and Concrete Research* **35**, pp. 1747-1753, 2005.

2.60 T.T. Lie and V.K.R. Kodur, "Thermal and Mechanical Properties of Steel-Fiber-Reinforced Concrete at Elevated Temperature," *Canadian Journal of Civil Engineering* **23**, pp. 511-517, 1996.

2.61 A. Noumowé and C. Galle, "Study of High Strength Concretes at Raised Temperature up to 200˚C: Thermal Gradient and Mechanical Behaviour," *Transactions of the 16th Structural Mechanics in Reactor Technology*, Paper #1580, Washington, DC, August 2001.

2.62 T. Yagashita, K. Shirai, C. Ito, and H. Shiojiri, "Effect of Strain Rate on Concrete Strength Under High Temperature," *International Conference on Structures Under Shock & Impact VI*, pp. 539-548, Cambridge, United Kingdom, WIT Press, July 2000.

2.63 G.A. Khoury, C.E. Majorana, F. Pesavento, and B.A. Schrefler, "Modelling of Heated Concrete," *Magazine of Concrete Research* **54**(02), pp. 77-101, April 2002.

2.64 Y.F. Fu, Y.L. Wong, C.S. Poon, and C.A. Tang, "Stress-Strain Behaviour of High-Strength Concrete at Elevated Temperature," *Magazine of Concrete Research* **57**(9), pp. 535-544, 2005.

2.65 V.V. Bertero and M. Polivka, "Influence of Thermal Exposures on Mechanical Characteristics of Concrete," Paper SP-34-28 in *Concrete for Nuclear Reactors*, pp. 505-531, American Concrete Institute, Farmington Hills, Michigan, 1972.

2.66 V.V. Bertero, B. Bressler, and M. Polivka, "Instrumentation and Techniques for Study of Concrete Properties at Elevated temperature," Paper SP-34-64 in *Concrete for Nuclear Reactors*, pp. 1377-1419, American Concrete Institute, Farmington Hills, Michigan, 1972.

2.67 J. Lee, Y. Xi, and K. Willam, "Concrete Under High Temperature Heating and Cooling," Report SESM No.09/2006, Department of Civil, Environmental, and Architectural Engineering, University of Colorado at Boulder, 2006.

2.68 C. Ehm and U. Schneider, "The High Temperature Behaviour of Concrete Under Biaxial Load," *Cement and Concrete Research* **25**, pp. 27-34, 1985.

2.69 A. Haksever and C. Ehm, "Application of Biaxial Concrete Data for Bearing Members Under Fire Attack," *Fire Safety Journal* **12**, pp. 109-119, 1987.
2.70 Y. Song, A. Zhang, L. Qing, and C. Yu, "Biaxial Tensile-Compressive Experiment on Concrete at High Temperatures," *Frontiers of Architecture and Civil Engineering in China* **1**(1), pp. 94-98, 2007.
2.71 M.J. Terro, "Numerical Modeling of the Behavior of Concrete Structures in Fire," *Journal American Concrete Institute* **95**(2), pp. 183-193, March 1, 1998.
2.72 L-Y Li and J. Purkiss, "Stress-Strain Constitutive Equations of Concrete Material at Elevated Temperatures," *Fire Safety Journal* **40**, pp. 669-686, 2005.
2.73 D. Gawin, F. Pesavento, and B.A. Schrefler, "Modelling of Hygro-Thermal Behaviour of Concrete at High Temperature with Thermo-Chemical and Mechanical Degradation," *Computer Methods in Applied Mechanics and Engineering* **192**, pp. 1731-1771, 2003.
2.74 A. Khennane and G. Baker, "Uniaxial Model for Concrete Under Variable Temperature and Stress," *Journal of Structural Mechanics* **119**(8), pp. 1507-1525, American Society of Civil Engineers, New York, New York, 1993.
2.75 I.A. Fletcher, S. Welch, J.L. Torero, R.O. Carvel, and A. Usmani, "Behaviour of Concrete Structures in Fire," *Thermal Science* **11**(2), pp. 37-52, 2007.
2.76 Comité Européen de Normalisation (CEN), "Eurocode 2: Design of Concrete Structures," prENV 1992-1-2, Brussels, Belgium, 1992.
2.77 T.T. Lie and T.D. Lin, "Fire Performance of Reinforced Concrete Columns," *Fire Safety: Science and Engineering*, ASTM STP 882, pp. 176-205, American Society for Testing and Materials, West Conshockon, Pennsylvania, 1985.
2.78 J. Xiao and G. König, "Study of Concrete at High Temperature in China—An Overview," *Fire Safety Journal* 39, pp. 89–103, 2004.
2.79 A. Khennane and G. Baker, "Thermoplasticity Model for Concrete Under Transient Temperature and Biaxial Stress," *Proceedings Royal Society of London* **439**(1905), pp. 59-80, 1992.
2.80 M.A. Youssef and M. Moftah, "General Stress-Strain Relationship for Concrete at Elevated Temperature," *Engineering Structures* **29**, pp. 2618-2634, 2007.
2.81 U. Schneider, "Modelling of Concrete Behaviour at High Temperatures," *Proceedings of International Conference on Design of Structures Against Fire*, pp. 53-69, 1986.
2.82 B.D. Scott, R. Park, and M.J.N. Priestly, "Stress-Strain Behaviour of Concrete Confined by Overlapping Hoops at Low and High Strain Rates," *Journal American Concrete Institute* **79**(1), pp. 13-27, 1982.
2.83 J.B. Mander, M.J.N. Priestly, and R. Park, "Theoretical Stress-Strain Model for Confined Concrete," *Journal of Structural Engineering* **114**(8), pp. 1804-1825, American Society of Civil Engineers, New York, New York, 1988.
2.84 M.P. Collins and D. Mitchell, *Prestressed Concrete Basics*, Canadian Prestress Concrete Institute, Ottawa, Ontario, Canada, 1987.
2.85 J.A. Purkiss and J.W. Dougill, "Apparatus for Compression Tests of Concrete at High Temperatures," *Magazine of Concrete Research* **25**(83), pp. 102-108, 1973.
2.86 Z.P. Bazant and J.C. Chern, "Stress-Induced Thermal and Shrinkage Strains in Concrete," *Journal of Engineering Mechanics* **113**(10), American Society of Civil Engineers, New York, New York, pp. 1493-1511, 1987.
2.87 "Structural Fire Protection," *Manual No. 78*, Committee on Fire Protection, Structural Division, American Society of Civil Engineers, New York, New York, 1992.
2.88 V.K.R. Kodur, M.M.S. Dwaikat, and M.B. Dwaikat, "High-Temperature Properties of Concrete for Fire Resistance Modeling of Structures," *ACI Materials Journal* **105**(5), pp. 517-527, American Concrete Institute, Farmington Hills, Michigan, September-October 2008.
2.89 B. Zhang, N. Bicanic, C.J. Pearce, and D.V. Phillips, "Relationship Between Brittleness and Moisture Loss of Concrete Exposed to High Temperature," *Cement and Concrete Research* **32**, pp. 363-371, 2002.
2.90 S. Mindess and J.F. Young, *Concrete*, Prentice-Hall, Inc., Englewood Cliffs, New Jersey, 1981.
2.91 P.K. Mehta and P.J.M. Monteiro, *Concrete – Microstructure, Properties, and Materials*, Third Edition, The McGraw-Hill Company, New York, New York, 2006.
2.92 C. Ehm, *Experimental Investigations of the Biaxial Strength and Deformation of Concrete at High Temperatures*, Dissertation, Technical University of Braunschweig, Germany, 1985.

2.93 J.C. Marechal, "Variations in the Modulus of Elasticity and Poisson's Ratio with Temperature," Paper SP 34-27 in *Concrete for Nuclear Reactors*, pp. 495-503, American Concrete Institute, Farmington Hills, Michigan, 1972.
2.94 C.R. Cruz, "Elastic Properties of Concrete at High Temperatures," Department Bulletin 191, *Journal of the Portland Cement Association Research and Development Laboratories* **8**(1), pp. 37-45, January 1966.
2.95 B. Wu, J. Yuan, and G. Y. Wang, "Experimental Study on the Mechanical Properties of HSC After High Temperature," *Chinese J. Civil Engineering* 33(2), pp. 8–15, 2000.
2.96 J.Zh Xiao, P. Wang, M. Xie, and J. Li, "Experimental Study on Compressive Constitutive Relationship of HPC at Elevated Temperature," *Journal Tongji University* **31**(2), pp. 186–190, 2003.
2.97 K. Hirano, K. Ohmatsuzawa, T. Takeda, S. Nakane, T. Kawaguchi, and K. Nagao, *Physical Properties of Concrete Subjected to High Temperature for MONJU*, Paper P2-25, Power Reactor and Nuclear Fuel Development Corporation, Tokyo, Japan.
2.98 C. Defigh-Price, *Effects of Long-Term Exposure to Elevated Temperature on the Mechanical Properties of Hanford Concrete*, Report RHO-C-54, Construction Technology Laboratories, Portland Cement Association, Skokie, Illinois, October 1981.
2.99 M.S. Abrams, M.P. Gillen, and D.H. Campbell, *Elastic Strength Properties of Hanford Concrete Mixes at Room and Elevated Temperatures*, Final Report to Battelle Pacific Northwest Laboratories, Richland, Washington, from Construction Technology Laboratories, Skokie, Illinois, 1979.
2.100 H. Gross, "On High Temperature Creep of Concrete," Paper H6/5 in *Proc. 2nd International Conference on Structural Mechanics in Reactor Technology*, Elsevier Science Publishers, North-Holland, The Netherlands, 1973.
2.101 P.J.E. Sullivan and J.M. Labani, "Flexural Behaviour of Plain and Reinforced Lightweight Aggregate Concrete Beams up to 600˚C," *Cement and Concrete Research* **4**, pp. 231-237, 1974.
2.102 G. N. Freskakis et al., "Strength Properties of Concrete at Elevated Temperature, *Civil Engineering Nuclear Power*, Vol. 1, ASCE National Convention, American Society of Civil Engineers, Boston, Massachusetts, April 1979.
2.103 R.K. Nanstad, *A Review of Concrete Properties for Prestressed Concrete Pressure Vessels*, ORNL/TM-5497, Oak Ridge National Laboratory, Oak Ridge, Tennessee, October 1976.
2.104 Y. Nassif, S. Rigden, and E. Burley, "The Effects of Rapid Cooling by Water Quenching on the Stiffness Properties of Fire-Damaged Concrete," *Magazine of Concrete Research* **51**(4), pp. 255-261, August 1999.
2.105 R.S. Ravindrarajah, R. Lopez, and H. Reslan, "Effect of Elevated Temperature on Properties of High-Strength Concrete Containing Cement Supplementary Materials," *9th International Conference on Durability of Building Materials and Components*, 9 p., Brisbane, Australia, 17-20 March 2002.
2.106 Z.D. Lu, *A Research on Fire Response of Reinforced Concrete Beams*, PhD Thesis, Tongji University, Shanghai, China, 1973.
2.107 L.W. Li and Z-H. Guo, "Experimental Investigation on Strength and Deformation of Concrete Under High Temperature," *Chinese Journal of Building Society* **14**(1), pp. 8-16, 1993.
2.108 Y.F. Chang, Y.H. Chen, M.S. Sheu, and G.C. Yao, "Residual Stress-Strain Relationships for Concrete After Exposure to High Temperatures," *Cement and Concrete Research* **36**, pp. 1999-2005, 2006.
2.109 J. Guo and P. Waldron, "Deterioration of PCPV Concrete," *Nuclear Engineering and Design* **198**, pp. 211–226, 2000.
2.110 K. Nagao and S. Nakane, "Influences of Various Factors on Physical Properties of Concretes Heated to High Temperatures," Paper H03/1 in *11th International Conference on Structural Mechanics in Reactor Technology*, pp. 61–66, Elsevier Science Publishers, North-Holland, The Netherlands, August 1991.
2.111 G. A. Khoury, *Transient Thermal Creep of Nuclear Reactor Pressure Vessel Type Concretes*, Ph.D. Dissertation, University of London, Vol. 1, pp. 1126; Vol. 2, pp. 418; Vol. 3, pp. 895, 1983.
2.112 T. Morita, H. Saito, and H. Kumajai, "Residual Mechanical Properties of High Strength Concrete Members Exposed to High Temperature—Part 1. Test on Material Properties," *Summaries of Technical Papers of Annual Meeting*, Architectural Institute of Japan, Naiigata, August 1992.
2.113 T. Furumura, T. Abe, and Y. Shinohara, "Mechanical Properties of High Strength Concrete at High Temperatures," *Proc. of 4th Weimar Workshop on High Performance Concrete: Material Properties and Design*, held at Hochschule für Architektur und Bauwesen (HAB), Weimar, Germany, pp. 237–254, October 4–5, 1995.
2.114 F. Vodák, K. Trtík, O. Kapicková, S. Hosková, and P. Demo "The Effect of Temperature on Strength—Porosity Relationship for Concrete," *Construction and Building Materials* **18**, pp. 529–534, 2004.

2.115 G. T. C. Mohamedbhai, "Effect of Exposure Time and Rates of Heating and Cooling on Residual Strength of Heated Concrete," *Magazine of Concrete Research* **38**(136), pp. 151–158, September 1986.
2.116 M. S. Abrams, "Compressive Strength of Concrete at Temperatures to 1600°F," SP-25 *Temperature and Concrete*, American Concrete Institute, pp. 33–58, 1971.
2.117 G-F. Peng, S-H. Bian, Z-Q. Guo, J. Zhao, X-L. Peng, and Y-C. Jiang, "Effect of Thermal Shock Due to Rapid Cooling on Residual Mechanical Properties of Fiber Concrete Exposed to High Temperatures," *Construction and Building Materials* **22**, pp. 948-955, 2008.
2.118 V.K.R. Kodur, T.C. Wang, and F.P. Cheng, "Predicting the Fire Resistance Behaviour of High Strength Concrete Columns," *Cement and Concrete Composites* **26**, pp. 141-153, 2004.
2.119 D. T. Lankard, D.L. Birkimer, F.F. Fondriest, and M.J. Snyder, "Effects of Moisture Content on the Structural Properties of Portland Cement Concrete Exposed to Temperatures Up to 500°F," SP-25 *Temperature and Concrete*, pp. 59–102, American Concrete Institute, Farmington Hills, Michigan, 1971.
2.120 D. Campbell-Allen and P. M. Desai, "The Influence of Aggregate on the Behavior of Concrete at Elevated Temperature," *Nucl. Eng. and Design* **6**(1), pp. 65–77, August 1967.
2.121 "Standard Test Method for Splitting Tensile Strength of Cylindrical Concrete Specimens," Part 14 of *Annual Book of ASTM Standards*, ANSI/ASTM C78-75, American Society for Testing and Materials, West Conshockon, Pennsylvania, 1975.
2.122 G. E. Troxell, H. E. Davis, and J. W. Kelly, *Composition and Properties of Concrete*, 2nd Ed., McGraw-Hill, New York, 1968.
2.123 G. G. Carette, K.E. Painter, and V.M. Malhotra, "Sustained High Temperature Effects on Concretes Made with Normal Portland Cement, Normal Portland Cement and Slag, or Normal Portland Cement and Fly Ash," *Concrete International* **4**(7), pp. 41–51, July 1982.
2.124 A.N. Noumowe, P. Clastres, G. Debicki, and J-L. Costaz, "Thermal Stresses and Water Vapor Pressure of High Performance Concrete At High Temperature," *Proceedings of 4th International Symposium on Utilization of High Strength/High Performance Concrete*, Paris, France, 1996.
2.125 M. Li, C.X. Qin, and W. Sun, "Mechanical Properties of High-Strength Concrete After Fire," *Cement and Concrete Research* **34**, pp. 1001-1005. 2004.
2.126 M. P. Raju, M. Shobha, and K. Rambabu, "Flexural Strength of Fly Ash Concrete Under Elevated Temperatures," *Magazine of Concrete Research* **56**(2), pp. 83–88, March 2004.
2.127 R.V. Balendran, A. Nadeem, T. Maqsood, and H.Y. Leung, "Flexural and Split Cylinder Strengths of HSC at Elevated Temperature," *Fire Technology* **39**, pp. 47-61, 2003.
2.128 F.I. Faiyadh and M.A. Al-Ausi, "Effect of Elevated Temperature on Splitting Tensile Strength of Fibre Concrete," *International Journal of Cement Composites and Lightweight Concrete* **11**(3), pp. 175-178, August 1989.
2.129 R.H. Haddad, R.J. Al-Saleh, and N.M. Al-Akhras, "Effect of Elevated Temperature on Bond Between Steel Reinforcement and Fiber Reinforced Concrete," *Fire Safety Journal* **43**(5), pp. 334-343, July 2008.
2.130 H. Tanyildizi and A. Coskun, "Performance of Lightweight Concrete with Silica Fume After High Temperature," *Construction and Building Materials* **22**, pp. 2124-2129, 2008.
2.131 G.M. Xie and Z.Z. Qian, "Research on Bond and Tension Behaviour of Concrete after High Temperature," *Journal Zhejiang University* **32**(5), pp. 597-602, 1998.
2.132 R. W. Carlson, "Drying Shrinkage of Concrete as Affected by Many Factors," *ASTM Proc*. **38**(II), pp. 419–437, 1938.
2.133 A. M. Neville, *Properties of Concrete*, Pitman, London, 1970.
2.134 F. Goodwin, "Volume Change," Chapter 21" in *Significance and Tests and Properties of concrete & Concrete-Making Materials*, ASTM STP169D, J.F. Lamond and J.H. Pielert Editors, American Society for Testing and Materials, West Conshockon, Pennsylvania, 2006.
2.135 R. D. Browne and R. Blundell, "The Behaviour of Concrete in Prestressed Concrete Pressure Vessels," Paper H11/1 in *Proc. 1st International Conference on Structural Mechanics in Reactor Technology*, Elsevier Science Publishers, North-Holland, The Netherlands, 1971.
2.136 R.D. Browne, "Properties of Concrete in Reactor Vessels," *Proceedings of the Conference on Prestressed Concrete Pressure Vessels*, Group C, Paper 13, pp. 131-151, Institute of Civil Engineers, London, United Kingdom, 1967.
2.137 L.E. Copeland and R.H. Bragg, "Self-Desiccation in Portland Cement Pastes," *Bulletin of American Society for Testing and Materials*, No. 204, pp. 34-39, February 1955.
2.138 I. Ali. And C. E. Kesler, *Creep in Concrete With and Without Exchange of Moisture with the Environment*, TAM Report 641, University of Illinois, Urbana-Champaign, 1963.

2.139 W. P. S. Dias, G. A. Khoury, and P. J. E. Sullivan, "Basic Creep of Unsealed Hardened Cement paste at Temperatures Between 20°C and 725°C," *Magazine of Concrete Research* **39**(139), pp. 93–111, 1987.
2.140 U.S. Bureau of Reclamation, *A 10-Year Study of Creep Properties of Concrete*, Concrete Laboratory Report No. SP-38, Denver, Colorado, July 28, 1953.
2.141 A. M. Neville, "Discussion of the Influence of Sand Concentrations on Deformations of Mortar Bars Under Low Stress," *J. American Concrete Institute* **59**(2), pp. 931–934, June 1962.
2.142 A. M. Neville, *Creep of Concrete: Plain, Reinforced and Prestressed*, North-Holland Publishing Company, Amsterdam, The Netherlands, 1970.
2.143 A. M. Neville, "The Influence of Cement on Creep of Concrete and Mortar," *J. Prestressed Concrete Institute* **66**, pp. 1008–1020, 1969.
2.144 K. S. Gopalarkrishan et al., "Creep Poison's Ratio on Concrete Under Multiaxial Compression," *J. American Concrete Institute* **2**, pp. 12–18, March 1958.
2.145 K.W. Nasser and R.P. Lohtia, "Creep of Mass Concrete at High Temperatures," *Journal of American Concrete Institute*, **68**(4), pp. 276-281, Farmington Hills, Michigan, April 1971.
2.146 H. G. Geymayer, "Effect of Temperature on Creep of Concrete: A Literature Review," Paper SP 34-31 in *Concrete for Nuclear Reactors*, pp. 565-589, American Concrete Institute, Farmington Hills, Michigan, 1972.
2.147 Z.P. Bazant and G-H. Li, "Comprehensive Database on Concrete Creep and Shrinkage," *ACI Materials Journal*, Title No. 105-M72, American Concrete Institute, Farmington Hills, Michigan, November-December 2008.
2.148 RILEM TC 107, "Guidelines for Characterizing Concrete Creep and Shrinkage in Structural Design Cores or Recommendations," *Materials and Structures* **28**, pp. 52-55, 1995.
2.149 ACI Committee 209, "Prediction of Creep, Shrinkage, and Temperature Effects in Structures," *ACI 209R-92*, American Concrete Institute, Farmington Hills, Michigan, 1992
2.150 W. P. S. Dias, G. A. Khoury, and P. J. E. Sullivan, "The Thermal and Structural Effects of Elevated Temperature on the Basic Creep of Hardened Cement Paste," *Magazine of Concrete Research* **23**, pp. 418–425, 1990.
2.151 J. C. Marechal, "Creep of Concrete as a Function of Temperature," Paper SP 34-30 in *Concrete for Nuclear Reactors*, pp. 547-564, American Concrete Institute, Farmington Hills, Michigan, 1972.
2.152 K. W. Nasser and H. M. Mazouk, "Creep of Concrete at Temperatures from 70 to 450°F Under Atmospheric Pressure," *J. American Concrete Institute* **78***(*2), pp. 147–150, March–April 1981.
2.153 A.F. da Silveira and C.A. Florentino, "Influence of Temperature on the Creep of Mass Concrete," Paper SP 25-7 in *Temperature and Concrete*, pp. 173-189, American Concrete Institute, Farmington Hills, Michigan, 1970.
2.154 D. McHenry, "A New Aspect of Creep in Concrete and Its Application to Design," *Proceedings ASTM* **43**, pp. 1069-1084, American Society for Testing and Materials, West Conshockon, Pennsylvania, 1943.
2.155 H. G. Geymayer, "Effect of Temperature on Creep of Concrete: A Literature Review," Paper SP-34-31 in *Concrete for Nuclear Reactors*, pp. 565-589, American Concrete Institute, Farmington Hills, Michigan, 1972.
2.156 K.W Nasser and A.M. Neville, "Creep of Concrete at Elevated Temperatures," *Proceedings Journal of American Concrete Institute* **64**(12), pp. 1567-1579, Farmington Hills, Michigan, 1965.
2.157 K.W Nasser and A.M. Neville, "Creep of Old Concrete at Normal and Elevated Temperature," *Proceedings Journal of American Concrete Institute* **64**(2), pp. 97-103, Farmington Hills, Michigan, 1967.
2.158 G.L. England and A.D. Ross, "Reinforced Concrete Under Thermal Gradients," *Magazine of Concrete Research* **14**(40), pp. 5-12, March 1962.
2.159 D.J. Hannant, *The Strain Behavior of Concrete Under Compressive Stress at Elevated Temperatures*, Laboratory Note RD/L/N 67/66, Central Electricity Research Laboratories, United Kingdom, June 1966.
2.160 S. Arthanari and C.W. Yu, "Creep of Concrete Under Uniaxial and Biaxial Stresses at Elevated Temperatures," *Magazine of Concrete Research* **19**(60), pp. 149-156, September 1967.
2.161 K.B. Hickey, *Creep, Strength, and Elasticity of Concrete at Elevated Temperatures*, Report No. C-1257, Bureau of Reclamation, Washington, DC, December 1967.
2.162 J.C. Marechal, "Causes Physiques et Chimiques du Fluage et du des Béton," RILEM Colloquium on the Physical and Chemical Causes of Creep and Shrinkage of Concrete, *Materials and Structures* **2**(8), pp. 852-855, June 1968.
2.163 J.C. Marechal, "Evolution des Propriétés Thermiques et Méchaniques des Bétons et Autres Matériaux en Fonction de la Température," *Annales Travaux Publics* **21**(246), pp. 852-855, June 1968.

2.164 A.E. Theuer, "Effect of Temperature on the Stress-Deformation of Concrete," *Journal of Research* **18**(2), pp. 195-204, National Bureau of Standards, Gaithersburg, Maryland, February 1937.
2.165 A.F. Da Silveira and C.A. Florentino, "Influence of Temperature on the Creep of Mass Concrete," *American Concrete Institute Symposium on the Effect of Temperature on Concrete*, Memphis, Tennessee, November 5-8, 1968.
2.166 C.H. Wang, "Creep of Concrete at Elevated Temperatures," Paper SP 27-19 in *Designing for Effects of Creep, Shrinkage, Temperature in Concrete Structures*," American Concrete Institute, Farmington Hills, Michigan, 1992.
2.167 R.D. Browne and R. Blundell, "The Influence of Loading Age and Temperature on the Long Term Creep Behavior of Concrete in a Sealed, Moisture Stable, State," *Materials and Structures* **2**(8), pp. 133-144, March 1969.
2.168 J. Komendant. V. Nicolayeff, M. Polivka, and D. Pirtz, "Effects of Temperature, Stress Level, and Age at Loading on Creep of Sealed Concrete," Paper SP 55-3 in *Douglas McHenry International Symposium on Concrete and Concrete Structures*, American Concrete Institute, Farmington Hills, Michigan, 1978.
2.169 G.P. York, T.W. Kennedy, and E.S. Perry, *Experimental Investigation of Creep in Concrete Subjected to Multiaxial Compressive Stresses and Elevated Temperature*, Research Report 2864-2, Department of Civil Engineering, The University of Texas at Austin, June 1970.
2.170 T.W. Kennedy, *An Evaluation and Summary of a Study on the Long-Term Multiaxial Creep Behavior of Concrete*, Research Report 3899-2, Department of Civil Engineering, The University of Texas at Austin, December 1975.
2.171 J.E. McDonald, *Time-Dependent Deformation of Concrete Under Multiaxial Stress Conditions*, Technical Report C-75-4, U.S. Army Engineer Waterways Experiment Station, Vicksburg, Mississippi, October 1975.
2.172 H. Kasami, T. Okuno, and S. Yamane, "Properties of Concrete Exposed to Sustained Elevated Temperature," Paper H1/5 in *Proc. 3rd International Conference on Structural Mechanics in Reactor Technology*, Elsevier Science Publishers, North-Holland, The Netherlands, 1975.
2.173 A. F. Milovanov and G. D. Salmanov, "The Influence of High Temperature Upon the Properties of Reinforcing Steels and Upon Bond Strength Between Reinforcement and Concrete," *Issledovanija po zharoupornym betonu I zhelezobetonu*, pp. 203–223, 1954.
2.174 H. V. Reichel, "How Fire Affect Steel-to-Concrete Bond," *Building Research and Practice* **6**(3), pp. 176–186, May/June 1978.
2.175 K. Hertz, "The Anchorage Capacity of Reinforcing Bars at Normal and High Temperatures," *Magazine of Concrete Research* **34**(121), pp. 213–220, December 1982.
2.176 U. Diederichs and U. Schneider, "Bond Strength at High Temperature," *Magazine of Concrete Research* **33**(115), pp. 75–83, June 1981.
2.177 C-H. Chiang and C-L. Tsai, "Time-Temperature Analysis of Bond Strength of a Rebar After Fire Exposure," *Cement and Concrete Research* **33**, pp. 1651–1654, 2003.
2.178 H. Sager and F.S. Rostasy, "High Temperature Behavior of Reinforcing and Prestressing Steels," *Sonderforschungs-Bereich* **148**, Part II, pp. 51–53, Technical Universität Braunschweig, Germany, 1980.
2.179 C. B. Oland and J. P. Callahan, *Bond Between Concrete and Steel Reinforcement at Temperatures to 149°C (300°F)*, ORNL/TM-6086, Union Carbide Corp., Nucl. Div., Oak Ridge National Laboratory, Oak Ridge, Tennessee, April 1978.
2.180 P.D. Morley and R. Royles, "Response of the Bond in Reinforced Concrete to High Temperatures," *Magazine of Concrete Research* **35**(123), pp. 67-74, June 1983.
2.181 R. Royles and P.D. Morley, "Further Responses to the Bond in Reinforced Concrete to High Temperatures," *Magazine of Concrete Research* **35**(124), pp. 157-163, September 1983.
2.182 R.H. Haddad and L.G. Shannis, "Post-Fire Behavior of Bond Between High Strength Pozzolanic Concrete and Reinforcing Steel," *Construction and Building Materials* **18**, pp. 425-435, 2004.
2.183 J.A. Purkiss, *Fire Safety Engineering Design of Concrete Structures*, Elsevier, 1996.
2.184 G.M. Xie and Z.Z. Qian, "Research on Bond and Tension Behaviour of Concrete After High Temperature," *Journal Zhejiang University* **32**(5), pp. 597-602, 1998.
2.185 B. Zhang, N. Bicanic, C.J. Pearce, and G. Balabanic, "Residual Fracture Properties of Normal- and High-Strength Concrete Subject to Elevated Temperatures," *Magazine of Concrete Research* **52**(2), pp. 123-136, April 2000.

2.186 A. Menou, G. Mounajed, H. Boussa, A. Pineaud, and H. Carre, "Residual Fracture Energy of Cement Paste, Mortar and Concrete Subject to High Temperature," *Theoretical and Applied Fracture Mechanics* **45**, pp. 64-71, 2006.
2.187 H. Abdel-Fattah and S.A. Hamoush, "Variation of the Fracture Toughness of Concrete with Temperature," *Construction and Building Materials* **11**(2), pp. 105-108, 1997.
2.188 D. J. Naus, *Concrete Component Aging and Its Significance Relative to Life Extension of Nuclear Power Plants*, NUREG/CR-4652, Martin Marietta Energy Systems, Inc., Oak Ridge National Laboratory, Oak Ridge, Tennessee, September 1986.
2.189 A. P. Mears, "Long Term Tests on the Effects of Moderate Heating on the Compressive Strength and Dynamic Modulus of Elasticity of Concrete," Paper SP 34-20 in *Concrete for Nuclear Reactors*, pp. 355-375, American Concrete Institute, Farmington Hills, Michigan, 1972.
2.190 C. DeFigh-Price et al., "Effects of Long-Term Exposure to Elevated Temperature on Mechanical Properties of Concrete," ACI Symposium on Concrete and Cementitious Materials for Radioactive Waste Management, New York, November 1, 1984.
2.191 M. P. Gillen et al., *Strength and Elastic Properties of Concrete Exposed to Long-Term Moderate Temperatures and High Radiation Fields*, RHO-RE-SA-55 P, Rockwell Hanford Operations, Richland, Washington, 1984.
2.192 K. W. Nasser and M. Chakraborty, "Temperature Effects on Strength and Elasticity of Concrete Containing Admixtures," *Proceedings of Symposium Temperature Effects on Concrete*, ASTM Special Technical Publication 858, American Society for Testing and Materials, West Conshockon, Pennsylvania, 1985.
2.193 G. G. Carrette and V. M. Malhotra, "Performance of Dolostone and Limestone Concretes at Sustained High Temperatures," *Proceedings of Symposium Temperature Effects on Concrete*, ASTM Special Technical Publication 858, pp. 38–67, American Society for Testing and Materials, West Conshockon, Pennsylvania, 1985.
2.194 T. Suzuki, M. Tabuchi, and K. Nagao, "Study on the Degradation of Concrete Characteristics in the High Temperature Environment," *Concrete Under Severe Conditions: Environment and Loading*, **2**, pp. 1119–1128, E & FN Spon Publishers, 1995.
2.195 T. Kanazu, T. Matsumura, and T. Nishiuchi, *Changes in the Mechanical Properties of Concrete Subjected to Long-Term Exposure to High Temperatures*, Report No. U95037, Abiko Research Laboratory, Central Research Institute of Electric Power Industry, Japan, March 1996.
2.196 H. Etherington, *Nuclear Engineering Handbook*, McGraw-Hill, New York, 1961.
2.197 S. Glasstone and A. Sesonske, *Nuclear Reactor Engineering*, D. Van Nostrand, Princeton, New Jersey, pp. 614–615, 1967.
2.198 E. G. Peterson, *Shielding Properties of Ordinary Concretes as a Function of Temperature*, HW-65572, Hanford Atomic Products Operation, Richland, Washington, August 2, 1960.
2.199 S. Miyasaka, Y. Kanemori, Y. Fukushima, and T. Yamada, "Gamma-Ray Leakage Through Slit in Concrete Shield," *Nippon Genshiryoku Gakkaishi* **11**, pp. 2–8, 1969.
2.200 F. Seboek, "Shielding Effectiveness of Cracked Concrete," *Kerntechnik* **12**, pp. 4496–4501, November 1970.
2.201 H.E. Hungerford, A. Hönig, A.E. Desov, F. Du Bois, and H.S. Davis, "Concretes, Cements, Mortars, and Grouts," *Engineering Compendium on Radiation Shielding*, Vol. II, pg. 117, R.G. Jaeger (Editor), Springer-Verlag, Berlin, Germany, 1975.
2.202 D. J. Naus, *Task 2: Concrete Properties in Nuclear Environment - A Review of Concrete Material Systems for Application to Prestressed Concrete Pressure Vessels,* ORNL/TM-7632, Oak Ridge National Laboratory, Oak Ridge, Tennessee, May 1981.
2.203 F. Bremer, "On a Triaxial Strength Criterion for Concrete," SP-34-14 in *Concrete for Nuclear Reactors*, pp. 283-294, American Concrete Institute, Farmington Hills, Michigan, 1972.
2.204 D. Linse, "Strength of Concrete Under Biaxial Sustained Load" SP-34-17 in *Concrete for Nuclear Reactors*, pp. 327-334, American Concrete Institute, Farmington Hills, Michigan, 1972.
2.205 J. Chinn and R.M. Zimmerman, *Behavior of Plain Concrete Under Various High Triaxial Compression Loading Conditions*, WL TR 64-163, Air Force Weapons Laboratory, August 1965.
2.206 C.D. Goode and M.A. Helmy, "The Strength of Concrete Under Combined Shear and Direct Stress," *Magazine of Concrete Research* **19**(59), June 1967.
2.207 N. J. Gardner, "Triaxial Behavior of Concrete," *Journal American Concrete Institute* **66**(2), Farmington Hills, Michigan, February 1969.

2.208 V. Hansson and K. Schimmelpfennig, "Concrete Strength in Multiaxial Stress States," Paper SP 34-15 in *Concrete for Nuclear Reactors*, pp. 295-312, American Concrete Institute, Farmington Hills, Michigan, 1972.
2.209 G. Schickert and H. Winkler, *Results of Test Concerning Strength and Strain of Concrete Subjected to Multiaxial Compressive Stresses*, Deutscher Auschuss für Stahlbeton, Heft No. 277, Berlin, Germany, 1977.
2.210 R.H. Atkinson and H.Y. Ko, "A Fluid Cushion, Multiaxial Cell for Testing Cubical Rock Specimens," *International Journal of Rock Mechanics and Mineral Sciences* **10**, pp. 35l-361, 1973.
2.211 E. Andrenes, "Response of Mortar to Biaxial Compression," M.S. Thesis, University of Colorado, 1974.
2.212 M.A. Taylor and B.K. Patel, "The Influence of Path Dependency and Moisture Conditions on the Biaxial Compression Envelope for Normal Weight Concrete," *Journal American Concrete Institute* **71**(12), Farmington Hills, Michigan, December 1974.
2.213 H. B. Kupfer, "Nonlinear Behavior of Concrete in Biaxial Stress," *Beton-StahZbetonbau* **11**, pp. 26-74, 1973.
2.214 T.N.W. Akroyd, "Concrete Under Triaxial Stress," *Magazine of Concrete Research* **13**(39), pp. 111-118, November 1961.
2.215 J. Isenberg, "Strength of Concrete Under Combined Stress," *Civil Engineering Publics Works Review*, October 1965.
2.216 R.M. Zimmerman and L.A. Traina, *Strength and Deformation Response of Concrete Under Multiaxial Loadings – Cooperative Project*, Final Report EN676-12097, Engineering Experiment Station, New Mexico State University, May 1977.
2.217 F.K. Garas, "Strength of Concrete Under Different States of Stress," Paper SP 34-18 in *Concrete for Nuclear Reactors*, pp. 335-343, American Concrete Institute, Farmington Hills, Michigan, 1972.
2.218 K.H. Gerstle, D.L. Linse, P. Bertacchi, M.S. Kotosovos, H-Y. Ko, J.B. Newman, P. Rossi, G. Schickert, M.A. Taylor, L.A. Traina, R.M. Zimmerman, and R. Bellotti, "Strength of Concrete Under Multiaxial Stress States," Paper SP 55-5 in *Douglas McHenry International Symposium on Concrete and Concrete Structures*, pp. 103-131, American Concrete Institute, Farmington Hills, Michigan, 1978.
2.219 W. Ren, W. Yang, Y. Zhou, and J. Li, "Behavior of High-Performance Concrete Under Uniaxial and Biaxial Loading," Title No. 105-M62, *ACI Materials Journal*, American Concrete Institute, Farmington Hills, Michigan, November-December 2008.
2.220 S-K. Lee, Y-C. Song, and S-H. Han, "Biaxial Behavior of Plain Concrete of Nuclear Containment Building," *Nuclear Engineering and Design* **227**, pp. 143-153, 2004.
2.221 K.-Ch. Thienel and F. S. Rostásy, "Influences of Concrete Composition on Strength and Deformations Under Uniaxial and Biaxial Loading at Elevated Temperature," Paper H04/6 in *Transactions of the 12th International Conference on Structural Mechanics in Reactor Technology*, pp. 145–150, 1993.
2.222 B.L. Hu, Y.P. Song, and G.F. Zhao, "Test on Strength and Deformation of Concrete Under Complex Stress at Elevated Temperature," *Building Science Research* **20**(1), Sichuan, pp. 47–50, 1994.
2.223 D.J. Hannant, "The Effects of Heat on Concrete Strength," *Engineering* **197**(5105), p. 302, February 21, 1964.
2.224 M. Petkovski, R.S. Crouch, and P. Waldron, "Apparatus of Testing Concrete Under Multiaxial Compression at Elevated Temperature (max^{2T})," *Experimental Mechanics* **46**, pp. 387-398, 2006.
2.225 M. Petkovski and R.S. Crouch, "Strains Under Transient Hygro-Thermal States in Concrete Loaded in Multiaxial Compression and Heated to 250˚C," *Cement and Concrete Research* **38**, pp. 586-596, 2008.
2.226 ACI COMMITTEE 207, "Mass Concrete for Dams and Other Massive Structures," *Proceedings of the Journal of American Concrete Institute* **67**(4), pp. 273–309, April 1970.
2.227 R. Philleo, *Some Physical Properties of Concrete At High Temperature*, Research Department Bulletin 97, Portland Cement Association, Skokie, Illinois, October 1958.
2.228 K.-Y. Shin, J-H. Kim, M. Chung, and P-S. Jung, "Thermo-Physical Properties and Transient Heat Transfer of Concrete at Elevated Temperatures," *Nuclear Engineering and Design* **212**, pp. 233–241, 2002.
2.229 H. Dettling, *The Thermal Expansion of Hardened Cement Paste, Aggregates, and Concrete*, Bulletin No. 164, pp. 1-64, Deutscher Ausschus für Stahlbeton, W. Ernst & Sohn, Berlin, Germany, 1964.
2.230 J.M. Griffiths, *Thermal Expansion of Typical American Rocks*, Bulletin No. 128, Iowa Engineering Experiment Station, Iowa State College, Ames, 1936.
2.231 D.G.R. Bonnell and F.C. Harper, "The Thermal Expansion of Concrete," *National Buildings Studies*, Technical Paper No. 7, Her Majesty's Stationary Office,, London, United Kingdom, 1951.
2.232 *Concrete Manual*, 7th Ed., U.S. Bureau of Reclamation, Denver, Colorado, 1963.

2.233 S.L. Meyers, "Thermal Coefficient of Expansion of Portland Cements – Long-Time Tests," *Industrial and Engineering Chemistry* **32**(8). pp. 1104-1112, 1940.
2.234 C.R. Cruz and M. Gillen, "Thermal Expansion of Portland Cement Paste, Mortar, and Concrete at High Temperature," *Fire and Materials* **4**(2), 1980.
2.235 H. C. Hirth, M. Polivka, and D. Pirtz, *Final Report on Thermal Properties of Concrete at Elevated Temperature*, ORNL/BRP-81/1 (Limited Distribution), Oak Ridge National Laboratory, Oak Ridge, Tennessee, July 1981.
2.236 V.K.R. Kodur and M.A. Sultan, "Effect of Temperature on Thermal Properties of High-Strength Concrete," *Journal of Materials in Civil Engineering* **15**(2), pp. 101-107, American Society of Civil Engineers, New York, New York, April 2003.
2.237 F. Vodak, R. Cerny, J. Drchalová, S. Hosková, O. Kapicková, O. Michalko, P. Semerák, and J. Toman, "Thermophysical Properties of Concrete for Nuclear Safety-Related Structures," *Cement and Concrete Research* **27**(3), pp. 415–426, 1997.
2.238 H. Abe, T. Kawahara, T, Ito, and A. Haraguchi, "Influence Factors of Elevated Temperatures on Thermal Properties and Inelastic Behavior of Concrete," Paper SP 34-40 in *Concrete for Nuclear*, pp. 847-870, American Concrete Institute, Farmington Hills, Michigan, 1972.
2.239 S. L. Meyers, "How Temperature and Moisture Changes May Affect the Durability of Concrete," *Rock Products*, pp. 153–157, August 1951.
2.240 R. Felicetti, P.G. Gambarova, G.P. Rosati, *The Mechanical Properties of High Performance Siliceous Concrete Exposed to High Temperature; "Penly" Concrete; Uniaxial Compression*, Research Project 1794/20-3-95, Milan University of Technology, Milan, Italy, March 1995.
2.241 K-Y. Shin, S-B. Kim, J-H. Kim, M. Chung, and P-S. Jung, "Thermo-Physical Properties and Transient Heat Transfer of Concrete at Elevated Temperatures," *Nuclear Engineering and Design* **212**, pp. 233–241,
2.242 U. Schneider and U. Diederichs, "Physical Properties of Concrete From 20˚C Up To Melting," Parts 1 and 2, *Betonwerk & Fertigteiltechnik*, Heft 3, pp. 141-150, and Heft 4, pp. 223-230, 1981.
2.243 U. Schneider, U. Diederichs, and C. Ehm, "The Behaviour of Concrete Under Attack of Liquid Steel," Paper H3/4 in *7th International Conference on Structural Mechanics in Reactor Technology*, Commission of European Communities, Brussels, Belgium, 1983
2.244 G. Hildenbrand, M. Peeks, A. Skokan, and M. Reimann, *Untersuchung der Wechselvirkung von Kernschmelze und Reaktorbeton*, Abschlussbericht Förderungverhaben BMFT RS 154, KWU, Erlangen, Germany, May 1978.
2.245 Y. Ichikawa and G.L. England, "Prediction of Moisture Migration and Pore Pressure Build-up in Concrete at High Temperatures," Paper #1122, *Proceedings of 16tht International Conference on Structural Mechanics in Reactor Technology*, Elsevier Science Publishers, North-Holland, The Netherlands, 2001.
2.246 P. Kalifa, F-D. Menneteau, and D. Quenard, "Spalling and Pore Pressure in HPC at High Temperatures, *Cement and Concrete Research* **30**(12), pp. 1915-1927, 2000.
2.247 Z.P. Bazant and L.J. Najjar, "Nonlinear Water Diffusion in Nonsaturated Concrete," *Materials and Structures* **5**, pp. 3-20, 1972.
2.248 A.D. Ross, M. Illston, and G.L. England, "Short- and Long-Term Deformations of Concrete Influenced by Its Physical Structure and State," *Proceedings of International Conference on Structural Concrete*, Paper H1, Imperial College, London, United Kingdom, 1965.
2.249 M. Jooss and H.W. Reinhardt, "Permeability and Diffusivity of Concrete as a Function of Temperature," *Cement and Concrete Research* **32**, pp. 1497-504, 2002,
2.250 Z.P. Bazant and W. Thonguthai, "Pore Pressure and Drying of Concrete at High Temperature*," Journal of Engineering Mechanics Division* **4**(EM5), Paper 14077, pp. 1059-1079, Proceedings of American Society of Civil Engineers, New York, New York, 1978.
2.251 L.T. Phan, "Pore Pressure and Explosive Spalling," *Materials and Structures* **41**(10), pp; 1623-1632, 2008.
2.252 G.L. England and T.J. Sharp, "Migration of Moisture and Pore Pressure in Heated Concrete," *Proceedings of 1st International Conference on Structural Mechanics in Reactor Technology*, Elsevier Science Publishers, North-Holland, The Netherlands, 1971.
2.253 *Project on Technology Innovation: Effects of High Temperature on ESBWR Primary Containment*, EPRI 1010071, Electric Power Research Institute, Palo Alto, California, December 2005.
2.254 K.H. Chen, E.L. Glueker, E.L. Lam, and V.S. Shippey, *Comparison of Mechanical Codes for Predicting Water Release from Heated Concrete*, GEFR-00521, General Electric, April 1980.

2.255 G.L. England and A.D. Ross, "Shrinkage, Moisture, and Pore Pressure in Heated Concrete," Paper SP 34-42 in *Concrete for Nuclear Reactors*, pp. 883-907, American Concrete Institute, Farmington Hills, Michigan, 1972.
2.256 J. E. McDonald, *Moisture Migration in Concrete*, Technical Report C-75-l, U.S. Army Waterways Experiment Station, Vicksburg, Mississippi, May 1975.
2.257 T. Takeda, S. Nakane, and K. Nagao, "Experimental Studies on Characteristics of Concrete Members Subjected to High Temperature," *Transactions of 9th International Conference on Structural Mechanics in Reactor Technology*, Vol. H, pp. 195–200, Lausanne, Switzerland, August 17–21, 1987.
2.258 L-O. Nilsson and P. Johansson, "The Moisture Conditions of Nuclear Reactor Containment Walls – An Example for a BWR Reactor," *Proceeding of International Conference on Corrosion and Long Term Performance of Reinforced Concrete in Nuclear Power Plants and Waste Facilities*, NUCPERF 2006, Cadarache, France, 27-30 March 2006.
2.259 Z. P. Bazant and W. Thonuthai, "Pore Pressure in Heated Concrete Walls: Theoretical Prediction," *Magazine of Concrete Research* **31**(107), pp. 67–76, 1979.
2.260 G. L. England and N. Khoylou, "Modeling of Moisture Behaviour in Normal and High Performance Concretes at High Temperatures," *Proceedings of the Fourth Weimar Workshop on High Performance Concrete: Material Properties and Design*, held at Hochschule für Architektur und Bauwesen (HAB), Weimar, Germany, pp. 53–68, October 4–5, 1995.
2.261 G.N. Ahmed and J. P. Hurst, "Modeling the Thermal Behavior of Concrete Slabs Subjected to the ASTM E 119 Standard Fire Condition," *Journal of Fire Protection Engineering* **7**(4), pp. 125–132, 1995.
2.262 L. T. Phan, *Fire Performance of High-Strength Concrete: A Report of the State-of-the-Art*, NISTIR 5934, National Institute of Standards and Technology, Gaithersburg, Maryland, 1996.
2.263 D. Gawin, C.E. Majorana, and B.A. Schrefler, "Numerical Analysis of Hygro-Thermal Behaviour and Damage of Concrete at High Temperature," *Mechanics of Cohesive-Frictional Materials* **4**, pp. 37-74, 1999.
2.264 R.K.K. Yuen, W.K. Kwok, S.M. Lo, and J. Liang, "Heat and Mass Transfer in Concrete at Elevated Temperature," *Numerical Heat Transfer* **51**, Part A, pp. 469-494, 2007.
2.265 A.H. Marchertas, *Experimental Needs in Simulating Concrete Behavior at High Temperatures*, ANL/RAS 84-18, Argonne National Laboratory, Argonne, Illinois, August 1984.
2.266 D.J. Naus, *The Effects of Elevated Temperature on Concrete Materials and Structures – A Literature Review*, NUREG/CR-6900, U.S. Nuclear Regulatory Commission, Washington, DC, March 2006.
2.267 J. P. Callahan, D.A. Canonico, M. Richardson, J.M. Corum, W.G. Dodge, G.C. Robinson, and G.D. Whitman, *Prestressed Concrete Reactor Vessel Thermal Cylinder Model Study*, ORNL/TM-5613, Oak Ridge National Laboratory, June 1977.
2.268 J. Irving, G.D.T. Carmichael, and I.W. Hornby, "A Full Scale Model Test of Hot Spots in the Prestressed Vessels of Oldbury Nuclear Power Station," *Proceedings Institution Civil Engineers* **57**, pp. 795-798, June 1974.

3 RADIATION SHIELDING CONCRETES

3.1 Introduction

Portland cement concrete possesses many of the physical qualities of an ideal radiation shield. It is a polyphase material consisting of particles of aggregate contained in a matrix of Portland cement paste. Gamma rays are absorbed by the high-density aggregate materials and neutrons are attenuated by hydrogen atoms in the cement paste. A concrete shield is exposed to two sources of heat: heat transferred from hot parts of the reactor system and heat produced internally by the attenuation of neutrons and gamma rays [3.1]. Energy captured from slowed down fast neutrons and gamma rays entering the shield from the reactor core is deposited within the shield material and liberated as heat. The total amount of heat generated can be considerable. The heat generated may have detrimental effects on the physical, mechanical, and nuclear properties of the concrete. Different types of concrete perform differently under radiation exposure, although if heated to relatively high temperatures they all will lose waters of crystallization and become somewhat weaker and less effective in neutron attenuation [3.2]. Although limited, some information is available on the effects of elevated temperature on radiation shielding concretes [3.3]. Provided below is a brief summary of the effect of elevated temperature exposure on properties and shielding effectiveness.

3.2 Heavyweight Concretes

Concrete for radiation shielding typically uses ordinary normal weight aggregates, however, special types of aggregate have been used to improve the attenuation properties of concrete or to reduce the thickness of concrete shields. Typically this involves incorporation of heavyweight aggregate materials.

Compared to normal weight aggregate concrete having a typical unit weight of 2400 kg/m^3, heavyweight concretes weigh from 2900 to 6100 kg/m^3. Typical heavyweight aggregate materials for use in production of heavyweight concrete are listed in Table 3.1. Several specifications or standard practice guidelines have been developed that address heavyweight aggregates and heavyweight concretes [3.4-3.12]. More detailed information describing aggregate materials for radiation-shielding concretes and composition and mechanical properties of concretes that have been used for radiation shielding is available elsewhere [3.3].

Table 3.1 Examples of aggregate materials used to produce heavyweight concretes

Type aggregate	Chemical composition of principal mineral	Specific gravity of pure mineral	Typical bulk density (kg/m^3)
Witherite	$BaCO_3$	4.29	2320
Baryte	$BaSO_4$	4.50	2560
Magnetite	Fe_3O_4	5.17	2720
Hematite	Fe_2O_3	4.9-5.3	3040
Lepidocrocite Geothite Limonite	Hydrous iron ores containing 8-12% water	3.4-4.0	2240
Ilmenite	$FeTiO_3$	4.72	2560
Ferrophosphorus	Fe_3P, Fe_2P, FeP	5.7-6.5	3680
Steel aggregate	Fe	7.8	4480

Source: P.K. Mehta and P.J.M. Monteiro, *Concrete – Microstructure, Properties, and Materials*, McGraw Hill, New York, New York, 2006.

Different types of cement have been used in concrete for radiation shielding such as Portland cement, high-alumina cement, gypsum-alumina cement, magnesium oxychloride cement, magnesia cement, phosphate cement, and oxyacid cement [3.3]. Specialty cements, such as gypsum-alumina, have been used to increase the chemically-bound water content to provide additional hydrogen for neutron shielding. Table 3.2 presents examples of ranges of properties that have been reported in the literature for heavyweight aggregate concretes [3.3]. Differences in

properties are due to factors such as proportions and the nature of the materials used in the mixes as well as the test conditions. Additional information on mix constituents and test conditions can be obtained by consulting the references provided in the table.

Table 3.2 Examples of mechanical and physical properties reported in literature for heavyweight aggregate concretes

Property	Type Concrete						
	Baryte	Serpentine	Limonite	Hematite	Ferrophosphous	Magnetite	Limonite-iron
Density ($g\ cm^{-3}$)	3.5-3.7	2.06-2.2	2.96	3.73-4.2	4.65	3.41-4.38	3.62-5.34
Compressive Strength (MPa)	24.8-42.2	13.1-15.8	40.4	16.2-89.3	30.4	19.2-41.8	38.4-78.0
Modulus (GPa)	29.9-35.5		30.7	37.3-69.1	28.2	31.2-62.0	43.4-50.4
Tensile strength (MPa)	2.25-4.9					6.5	3.6-4.0
Thermal expansion ($10^{-6}\ °C^{-1}$)	18	~32			10.35	10.3	6.8-10.0
Thermal Conductivity ($W\ m^{-1}\ °C^{-1}$)	0.961-1.621	0.8			2.914		2.7-3.5
Specific Heat ($cal\ g^{-1}\ °C^{-1}$)	0.123-0.157				0.17		0.17-0.21
Diffusivity ($m^2\ h^{-1}$)	0.002				0.003		0.32
Data Source	3.13-3.17	3.18	3.19,3.20	3.21,3.22	3.23	3.19.3.20, 3.15,3.24	3.20,3.25

Primary source: M.F. Kaplan, *Concrete Radiation Shielding*, Concrete Design and Construction Series, Longman Scientific & Technical, New York, New York, 1989.

3.3 Effect of Elevated Temperature on Properties

Concrete radiation shields may be exposed to external sources of heat as well as heat produced within the shield as a result of attenuation or absorption of gamma and neutron radiation. Generation of heat can produce thermal stresses and affect the mechanical and physical properties of the concrete. Although limited, some data have been assembled on the effects of elevated temperature on the mechanical and physical properties of shielding concretes [3.3]. Information, primarily from this reference, for several of the concretes listed in Table 3.2 will be summarized below.

3.3.1 Serpentine Aggregate-Based Concrete

The effect of elevated temperature on the residual compressive strength of a serpentine and an ophicalcite concrete has been investigated [3.26]. The serpentine concrete mix had a dry density of 2085 kg/m^3 and a 28-day compressive strength of 19.3 MPa. The cylindrical test specimens were 10-cm-diameter by 20-cm-long. The specimens were cured for seven weeks in water at 20˚C, permitted to air dry for several weeks (e.g., 83 to 92 weeks), and then heated to temperatures of 100˚, 200˚, or 600˚C where they remained for 30 minutes. Part of the specimens were immediately removed from the oven and tested and part were permitted to cool to room temperature prior to testing. Figure 3.1 presents the effect of elevated temperature on the strength (% of reference room temperature value) of the serpentine concrete tested hot and the ophicalcite concrete (91-day compressive strength of

30.7 MP) with specimens tested while hot or permitted to cool to room temperature prior to testing. Also shown in the figure is the effect of temperature on the density of the serpentine concrete.

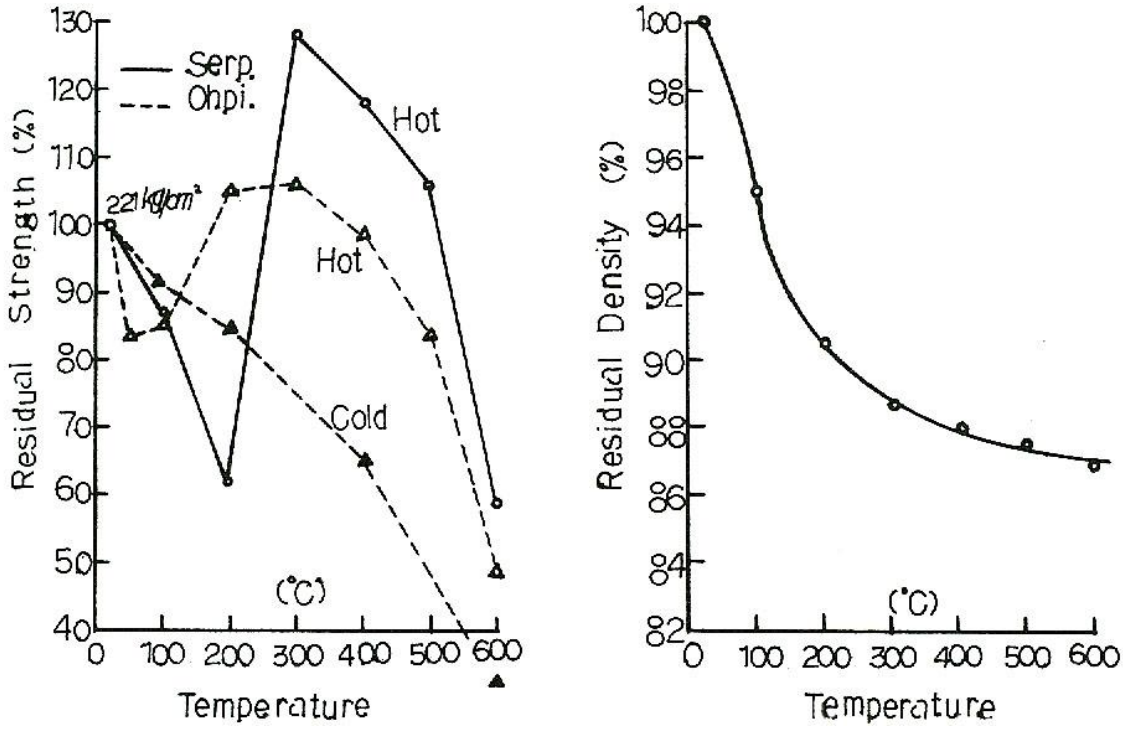

Figure 3.1 Effect of temperature on the compressive strength of a serpentine (tested hot) and ophicalcite (residual and tested hot) aggregate concrete, and on density of a serpentine concrete.

Source: S. Ohgishi, S. Miyasaka, and J. Chida, "On Properties of Magnetite and Serpentine Concrete at Elevated Temperatures for Nuclear Reactor," SP 34-57 in *Concrete for Nuclear Reactors*, pp. 1243-1253, Special Publication 34, American Concrete Institute, 1972.

The effects of elevated temperature on the properties of iron shot, limonite, magnetite, and ferrophosphorous concretes as well as various combinations of these aggregate materials was investigated in conjunction with the N-Production Reactor located at Hanford, Washington [3.23]. Concrete placement was by conventional methods as well as by the preplaced aggregate method. Table 3.3 presents the effect of elevated temperature on selected properties of a serpentine-iron concrete in which the aggregates were preplaced. The effects of elevated temperature on mechanical and physical properties of a magnetite-serpentine aggregate concrete are presented in Table 3.4. Magnetite was used as the coarse aggregate and serpentine as the fine aggregate. Approximately 46% of the total aggregate weight was serpentine. Type II Portland cement was used in the mix and placement was by conventional means. Application of 20 thermal cycles from 40˚ to 200˚ to 40˚C reduced the compressive strength by 11%, and if the peak cycle temperature was increased to 350˚C the reduction was 21%. Modulus of rupture results for the two cycling scenarios were reduced 30% and 77%, respectively. The static modulus of elasticity was reduced by 36% after 20 thermal cycles from 40˚ to 200˚ to 40˚C. Residual compressive strengths of cube specimens soaked in water for two weeks prior to heating to temperatures up to 300˚C were less than results obtained for specimens that had not been soaked prior to heating with the dry specimens exhibiting residual strengths at temperatures up to 350˚C of 98%, or more.

3.3.2 Limonite Aggregate-Based Concrete

Compressive strength ratios for limonite concrete 100-mm cubes tested at elevated temperature have been reported as 94, 88, and 85% the reference room temperature strength after exposure from 3 to 7 hours at 100˚, 150˚, and 200˚C, respectively, [3.27]. Average coefficients of thermal expansion of Portland cement concretes containing

Table 3.3 Effect of temperature on properties of a serpentine-iron concrete

Property	Value	Residual ratio (%)[a]					
	at 90 days[b]	23 °C 28 days[c]	23 °C 90 days[b]	85 °C[d]	140 °C[d]	200 °C[d]	350 °C[d]
Density (g cm^{-3})	3.53	100	100	96	–	96	95
Coefficient of thermal expansion (10^{-6} °C^{-1})	8.66	102	100	109	–	119	127
Compressive strength (MPa)							
Cylinders (15 × 30 cm)	25.1	79	100	–	92	–	–
Modified cubes (15 × 15 × 15 cm)	29.3	–	100	–	–	–	82
	31.2	85	100	53	–	139	–
Modulus of rupture (MPa)	29.9	–	100	–	–	–	122
	3.4	89	100	48	–	29	–
Modulus of elasticity (GPa)	3.6	–	100	–	–	–	11
Static	27.5	90	100	–	–	60	44
Dynamic	32.2	–	100	–	–	–	27
Bond strength (MPa)	37.2	–	100	44	–	42	–
	6.2	91	100	–	–	17	–
Length change[e] (%)	6.5	–	100	–	–	–	3
	+0.011	+0.009	+0.011	−0.036	–	−0.049	−0.021

(*a*) Value of concrete property as a percentage of the value after 28 days moist curing and 62 days air curing at room temperature, i.e total of 90 days.
(*b*) 28 days moist and 62 days in laboratory air.
(*c*) Moist cured for 28 days.
(*d*) As for (*b*) and then heated for two weeks at stated temperature before testing after cooling to room temperature.
(*e*) At room temperature after heat treatment.

Source: H.S. Davis, "N-Reactor Shielding," Paper SP-34-52 in *Concrete for Nuclear Reactors*, pp. 1109-1161, American Concrete Institute, Farmington Hills, Michigan, 1972.

Table 3.4 Effect of temperature on properties of a magnetite-serpentine concrete

Property	Value at 90 days[b]	Residual ratio (%)[a]					
		23 °C 28 days[c]	23 °C 90 days[b]	85 °C[d]	140 °C[d]	200 °C[d]	350 °C[d]
Density (g cm^{-3})	3.05	100	100	95	94	94	95
Coefficient of thermal expansion (10^{-6} °C^{-1})	–	–	–	–	–	–	–
Compressive strength (MPa)							
Cylinders (15 × 30 cm)	39.7	84	100	99	94	89	72
Modified cubes (15 × 15 × 15 cm)	36.1	89	100	109	113	116	98
Modulus of rupture (MPa)	5.3	87	100	110	97	90	61
Modulus of elasticity (GPa)							
Static	34.2	100	100	85	65	57	43
Dynamic	39.0	95	100	80	63	54	35
Bond strength (MPa)	3.2	87	100	67	61	28	11
Length change[e] (%)	+0.007	+0.005	+0.007	−0.041	−0.065	−0.073	−0.149

(*a*) Value of concrete property as a percentage of the value after 28 days moist curing and 62 days air curing at room temperature, i.e. after 90 days.
(*b*) 28 days moist and 62 days in laboratory air.
(*c*) Moist cured for 28 days.
(*d*) As for (*b*) and then heated for two weeks at stated temperature before testing after cooling to room temperature.
(*e*) At room temperature after heat treatment.

Source: H.S. Davis, "N-Reactor Shielding," Paper SP-34-52 in *Concrete for Nuclear Reactors*, pp. 1109-1161, American Concrete Institute, Farmington Hills, Michigan, 1972.

limonite aggregate have been reported as 4.86 x 10^{-6} °C^{-1} for temperatures up to 300°C, 4.5 x 10^{-6}°C^{-1} between 300° and 600°C, and 4.2 x 10^{-6}°C^{-1} between 600° and 800°C [3.28].

Table 3.5 presents results for a hydrous-iron aggregate concrete whose aggregate was a mixture of limonite, magnetite, and haemitite [3.29]. The concrete was made from Type II Portland cement and had a water-cement ratio of 0.43 (by weight). Specimens were moist cured for 28 days at 23°C, stored in laboratory air at about 50% relative humidity for an additional 62 days, heated for a period of two weeks to temperatures of 85°, 200°, or 350°C, and then permitted to cool to room temperature prior to testing.

Table 3.5 Effect of elevated temperature on the physical and mechanical properties of hydrous-iron aggregate concrete

Property	Value	Residual ratio (%)[a]				
	at 90 days[b]	23 °C 28 days[c]	23 °C 90 days[b]	85 °C[d]	200 °C[d]	350 °C[d]
Density (g cm^{-3})	3.59	101	100	99	97	94
Coefficient of thermal expansion (10-6°C^{-1})	9.93	94	100	96	91	83
Compressive strength (MPa)						
Cylinders (15 × 30 cm)	61.4	78	100	–	90	77
Modified cubes (15 × 15 × 15 cm)	73.7	79	100	69	64	65
Modulus of rupture (MPa)	6.4	104	100	109	100	90
Modulus of elasticity (GPa)						
Static at 21 MPa	57.8	89	100	–	70	48
Bond strength (MPa)	8.1	112	100	–	86	34
Length change[e] (%)	−0.006	+0.002	−0.006	−0.020	−0.058	−0.111

(*a*) Value of concrete property as a percentage of the value after 28 days moist curing and 62 days air curing at room temperature, i.e. total of 90 days.
(*b*) 28 days moist and 62 days in laboratory air.
(*c*) Moist cured for 28 days.
(*d*) As for (*b*) and then heated for two weeks at stated temperature before testing after cooling to room temperature.
(*e*) At room temperature after heat treatment.

Source: H.S. Davis and O.E. Borge, "High-Density Concrete Made With Hydrous-Iron Aggregates," *Journal American Concrete Institute* **30**(10), pp. 1141-1147, Farmington Hills, Michigan, 1959.

3.3.3 Magnetite Aggregate-Based Concrete

Tests have been conducted on 10-cm diameter by 20-cm long cylindrical test specimens of magnetite concrete that were initially cured in water at 20°C for twelve weeks and then stored in moist air for 92 weeks prior to heating [3.26]. The specimens were heated to temperatures from 100° to 600°C with the final temperature maintained for 30 minutes. Some of the specimens were tested at temperature and others permitted to cool to room temperature prior to testing. The density of the magnetite concrete was found to decrease approximately linearly as the temperature increased with the decrease being about 4% at 600°C. Figure 3.2 presents the effect of elevated temperature on the compressive strength of the magnetite concrete for specimens tested at temperature and for specimens that returned to room temperature prior to testing. Also shown in the figure are results obtained for a normal weight concrete.

Table 3.6 presents the effect of elevated temperature on the properties of a magnetite concrete used for the radiation shield of the EL4 reactor in France [3.30]. The concrete utilized Portland cement, magnetite fine and coarse aggregate, a water-cement ratio of 0.63 (by weight), and had a 28-day compressive strength of 28.3 MPa and density of 3550 kg/m^3. The specimens were cured in water at 20°C or in air at 20°C and 50% relative humidity and then heated in an oven to 110°C.

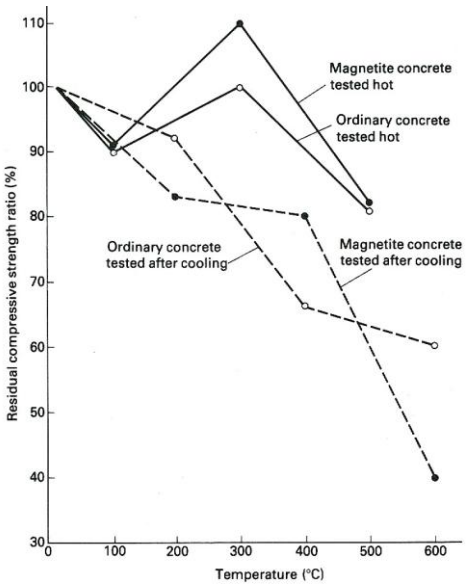

Figure 3.2 Effect of elevated temperature on the compressive strength of a magnetite concrete tested at temperature and after cooling to room temperature.

Source: S. Ohgishi, S. Miyasaka, and J. Chida, "On Properties of Magnetite and Serpentine Concrete at Elevated Temperatures for Nuclear Reactor," SP 34-57 in *Concrete for Nuclear Reactors*, pp. 1243-1253, American Concrete Institute, Farmington Hills, Michigan, 1972.

Table 3.6 Effect of elevated temperature on the physical and mechanical properties of a magnetite aggregate concrete

Conditions of test	Cured in water at 20 °C			Cured in air at 50% R.H. and 20 °C		
	Compressive strength (MPa)	Flexural strength (MPa)	Dynamic *E* (GPa)	Compressive strength (MPa)	Flexural strength (MPa)	Dynamic *E* (GPa)
270 days at 20 °C	41.0	4.2	58.3	35.0	3.1	44.2
150 days at 20 °C followed by 120 days at 110 °C	53.0	4.2	52.0	42.0	3.8	40.5
150 days at 20 °C followed by three thermal cycles from 20 to 110 °C	52.0	3.0	–	35.0	2.75	–

Source: F. Du Bois, "Beton Lourds abase de Mineral de Magnetite de Dielette," Centre d'Etudes Nucleaires de Saclay, Commissariat a l'Energie Atomique, France, June 1964.

3.3.4 Haematite Aggregate-Based Concrete

Mechanical and physical properties of haemitite aggregate concretes are very similar to concrete made with magnetite [3.3]. Coefficients of thermal expansion for Portland cement concretes with haemitite aggregate at temperatures up to 300˚C, between 300˚C and 600˚C, and between 500˚ and 800˚C have been reported as 5.94×10^{-6}°C^{-1}, 11.5×10^{-6}°C^{-1}, and 16.2×10^{-6}°C^{-1}, respectively [3.28]. Residual compressive strength ratios for this concrete were 90, 85, and 150% at temperatures of 100˚, 150˚, and 300˚C, respectively, but when alumina cement was used the ratios were 80, 35, and 55%, respectively.

Investigations have been conducted related to use of haemitite concrete in the thermal shield of a liquid-sodium-cooled fast reactor in Italy [3.31]. The concrete mixes were made using pozzolanic cement or a proprietary cement consisting of a mixture of materials (e.g., Portland cement, plasticizer, expansive cement, and anti-bleeding agent). The pozzolanic concrete with 15-mm-maximum size haematite aggregate had a water-cement ratio of 0.49 (by weight), density of 3850 kg/m^3, 28-day static modulus of elasticity of 37.3 GPa, and 28-day compressive strength of 50.5 MPa. In order to investigate the effect of temperature on compressive strength, 15-cm concrete cube specimens were heated to either 200˚ or 300˚C and tested at temperature or permitted to cool to room temperature prior to testing. The pozzolanic concrete specimens heated to 200˚C and tested at temperature had a compressive strength that was 127% the reference room temperature strength, 138% the reference room temperature strength when tested after cooling to room temperature, and 117% the reference room temperature strength when heated to 300˚C and tested at temperature. Results obtained for the proprietary cement-based mixes ranged from 91 to 141%, 123 to 145%, and 106 to 139% the reference room temperature compressive strengths for the three test conditions. For each of the concrete mixes investigated, residual compressive strengths from specimens permitted to cool to room temperature prior to testing were greater than results obtained from specimens tested at temperature.

3.3.5 Ferrophosphorus Aggregate-Based Concrete

The effect of elevated temperature on mechanical and physical properties of conventionally-placed concrete made with ferrophosphorus aggregates was investigated as part of the study related to the N-Production Reactor located at Hanford, Washington [3.23]. The 4650 kg/m^3 concrete mix utilized Type II Portland cement, 19-mm maximum size ferrophosphorus aggregate, and had a water-cement ratio of 0.53 (by weight). Thermal expansion, thermal diffusivity, thermal conductivity, and specific heat values for the reference concrete were 10.35 x 10^{-6} °C^{-1}, 0.003 m^2 h^{-1}, 2.914 W m^{-1} ˚C^{-1}, and 0.17 cal g^{-1} ˚C^{-1}, respectively. The effect of elevated temperature on mechanical and physical properties of the ferrophosphorus aggregate concrete is presented in Table 3.7. Results obtained from additional specimens that were soaked in water after being heated to 85˚, 200˚, or 350˚C indicated that the residual compressive strengths were 87, 74, and 76%, respectively. It was concluded that residual ratios for compressive strength, flexural strength, bond strength, and modulus of elasticity were comparable to those obtained from a companion ordinary concrete.

Table 3.7 Effect of elevated temperature on the physical and mechanical properties of a ferrophosphorus aggregate concrete

Property	Value at 90 days[b]	Residual ratio (%)[a]					
		23 °C 28 days[c]	23 °C 90 days[b]	85 °C[d]	140 °C[d]	200 °C[d]	350 °C[d]
Density (g cm^{-3})	4.70	101	100	98	–	98	97
Coefficient of thermal expansion (10^{-6} °C^{-1})	10.2	101	100	108	–	118	114
Compressive strength (MPa)							
Cylinders (15 × 30 cm)	53.7	57	100	–	–	97	87
Modified cubes (15 × 15 × 15 cm)	56.8	59	100	99	–	96	80
Modulus of rupture (MPa)	6.2	66	100	125	–	94	75
Modulus of elasticity (GPa)							
Static	28.2	39	100	–	–	65	45
Dynamic	–	–	–	–	–	–	–
Bond strength (MPa)	8.3	68	100	–	–	50	47
Length change[e] (%)	−0.053	+0.013	−0.053	−0.123	–	−0.140	–

(*a*) Value of concrete property as a percentage of the value after 28 days moist curing and 62 days air curing at room temperature, i.e after 90 days.
(*b*) 28 days moist and 62 days in laboratory air.
(*c*) Moist cured for 28 days.
(*d*) As for (*b*) and then heated for two weeks at stated temperature before testing after cooling to room temperature.
(*e*) At room temperature after heat treatment.

Source: H.S. Davis, "N-Reactor Shielding," Paper SP-34-52 in *Concrete for Nuclear Reactors*, pp. 1109-1161, American Concrete Institute, Farmington Hills, Michigan, 1972.

3.3.6 Baryte Aggregate-Based Concrete

A baryte aggregate concrete has been studied under a EURATOM Program to investigate its potential application to fabrication of pressure vessels for nuclear reactors [3.32]. Results were compared to a normal weight limestone aggregate concrete. Reference compressive strength for the two concretes was about 65 MPa. Specimens were heated for a period of 28 days after being cured in water for a period of 28 to 56 days. Coefficients of thermal expansion for the baryte concrete were 13.4 x 10^{-6}°C^{-1}, 13.5 x 10^{-6}°C^{-1}, and 13.5 x 10^{-6}°C^{-1}, for temperatures between 50˚ and 150˚C, 150˚ and 250˚C, and 250˚ and 350˚C, respectively, which were greater than coefficients obtained for the limestone aggregate concrete. Thermal conductivity of the baryte concrete increased from 2.2 W m^{-1} ˚C^{-1} to 2.3 W m^{-1} ˚C^{-1} between 65˚ and 85˚C and then decreased to 1.4 W m^{-1} ˚C^{-1} at 180˚C. The residual compressive strength of the baryte concrete heated to 500˚C and then cooled to room temperature prior to testing was 83%, and after six heating cycles the ratio decreased to 50%. Residual values obtained for these conditions for the limestone aggregate concrete were 65 and 36%, respectively. The residual modulus of elasticity of the baryte concrete after heating to 500˚C was 25% which was about the same as that for the limestone aggregate concrete after heating to 350˚C. Residual modulus of elasticity after six cycles for the baryte aggregate concrete was about the same as that obtained after one cycle. It was concluded that the baryte aggregate concrete retained properties after elevated temperature exposure better than the limestone aggregate concrete because the aggregate thermal expansion coefficient was more compatible with that of the mortar matrix.

The effect of elevated temperature on the physical and mechanical properties of baryte aggregate and quartz aggregate concretes has been investigated [3.33]. Mixes were prepared using either Type I Portland cement or blast furnace slag cement with a water-cement ratio of 0.6 (by weight). Reference room temperature compressive strengths for the limestone aggregate and baryte aggregate concretes were 49 and 52 MPa, respectively. Results were obtained for exposure periods of three hours at temperatures up to 750˚C. Figure 3.3 presents the effect of temperature on the residual ratios of compressive strength and weight loss for two cementitious and two aggregate materials. Reduction in compressive strength and weight loss of baryte aggregate concrete was less than that for

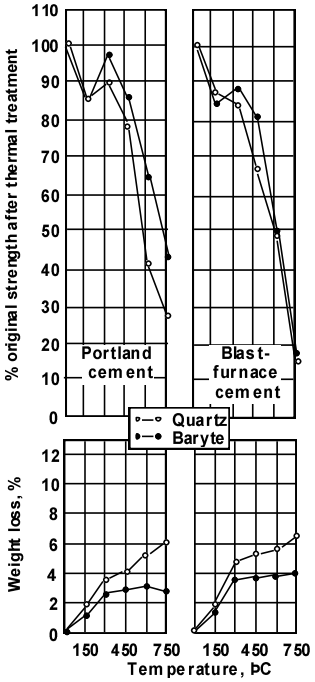

Figure 3.3 Weight loss and residual compressive strength after thermal treatment for baryte and quartz aggregate concretes.

Source: H. Weigler and R. Fischer, "Influence of High Temperatures on Strength and Deformations of Concrete," Paper SP-34-26 in *Concrete for Nuclear Reactors*, pp. 481-493, American Concrete Institute, Farmington Hills, Michigan, 1972.

the quartz aggregate concrete. Compressive strength of specimens tested hot was generally less than that of specimens tested cold. Application of load to about 1/3 the reference compressive strength while heating resulted in no strength loss at elevated temperature for the baryte aggregate concrete while for limestone aggregate concrete the strength was slightly reduced. Thermal cycling to 600˚C did not result in a strength loss for the baryte aggregate concrete but produced a significant strength loss for the quartz aggregate concrete.

The effect of different durations (1, 2, and 3 hours) and temperatures (250˚, 500˚, 750˚, and 950˚C) on the physical and mechanical properties of a baryte aggregate concrete was investigated [3.34]. The baryte aggregate concrete used Portland cement, had a 20-mm maximum aggregate size, water-cement ratio of 0.40 (by weight), and a density of 3250 kg/m^3. Reference compressive strength, tensile strength, flexural strength, and modulus of elasticity values for the baryte aggregate concrete were 47 MPa, 2.85 MPa, 4.42 MPa, and 29.03 GPa, respectively. After two hours exposure to temperatures of 250˚, 500˚, 750˚, or 950˚C, the compressive strength at temperature was reduced 6.5, 39.9, 68.1, and 85.6%, respectively, relative to the 47 MPa reference room-temperature strength. These reductions in compressive strength were less than that obtained for a normal weight gravel concrete. Radiation attenuation coefficient results for a Cobalt 60 source (1330keV) obtained for the baryte aggregate concrete indicate that the attenuation coefficients were reduced 9.5, 13.0, 17.0, and 21.0% after heating for two hours at 250˚, 500˚, 750˚, and 950˚C, respectively. Similar reductions were obtained for a Cesium 127 (660 keV) source. The reductions were attributed to the effect of elevated temperature on concrete properties, especially the density due to loss of water.

The effect of elevated temperature on the compressive and flexural strength and static modulus of elasticity of a baryte aggregate concrete was investigated at the Saclay Nuclear Centre in France [3.35]. Specimens were heated for 28, 90, and 180 days at 150˚ or 250˚C. Table 3.8 summarizes the results and shows that the residual ratios decreased with increasing temperature and exposure period, probably due to cracking resulting from a mismatch in coefficients of thermal expansion between the matrix and aggregate.

Table 3.8 Effect of elevated temperature on mechanical properties of a baryte concrete

Concrete property	Residual ratio (%)					
	150 °C			250 °C		
	28 days[(a)]	90 days	180 days	28 days	90 days	180 days
Compressive strength	112	93	72	97	80	62
Flexural strength	96	81	76	60	54	53
Static E	62	38	38	42	30	27

(*a*) Period of heating.

Source: *Engineering Compendium on Radiation Shielding*, Vol. II, S.9.1.12, p. 156, R.G. Jaeger (Editor), Springer-Verlag, Berlin, Germany, 1975.

3.3.7 Ilmenite Aggregate-Based Concrete

The effect of different durations (1, 2, and 3 hours) and temperatures (250˚, 500˚, 750˚, and 950˚C) on the physical and mechanical properties of an ilmenite aggregate concrete was investigated [3.34]. The ilmenite aggregate concrete used Portland cement, had a 20-mm maximum aggregate size, water-cement ratio of 0.40 (by weight), and a density of 3450 kg/m^3. Reference compressive strength, tensile strength, flexural strength, and modulus of elasticity values for the baryte aggregate concrete were 51 MPa, 3.53 MPa, 5.4 MPa, and 34.43 GPa, respectively. After two hours exposure to temperatures of 250˚, 500˚, 750˚, and 950˚C, the compressive strength at temperature was reduced 6.7, 15.3, 41.3, and 73.7%, respectively, relative to the 51 MPa reference room-temperature strength. These reductions in compressive strength were less than that obtained from a normal weight gravel concrete and the baryte concrete reported earlier. Radiation attenuation coefficient results for a Cobalt 60 source (1330keV) obtained for the ilmenite aggregate concrete indicate that the attenuation coefficients were reduced 11.9, 14.0, 16.0, and 18.0% after heating for two hours at 250˚, 500˚, 750˚, and 950˚C, respectively. Similar reductions were obtained for

a Cesium 127 (660 keV) source. The reductions were attributed to the effect of elevated temperature on concrete properties, especially the density due to loss of water.

3.3.8 Iron/Steel Aggregate-Based Concrete

Average coefficients of thermal expansion for a concrete made with Portland cement, a water-cement ratio of 0.4 (by weight), and steel-shot aggregate have been reported as 4.20 x 10^{-6} $^{\circ}C^{-1}$ up to 300˚C, 8.5 x 10^{-6} $^{\circ}C^{-1}$ between 300˚ and 600˚C, and 16.20 x 10^{-6} $^{\circ}C^{-1}$ between 600˚ and 800˚C [3.36]. Results for concrete using iron and steel scrap were 5.1 x 10^{-6} $^{\circ}C^{-1}$ up to 300˚C, 7.2 x 10^{-6} $^{\circ}C^{-1}$ between 300˚ and 600˚C, and 8.6 x 10^{-6} $^{\circ}C^{-1}$ between 600˚ and 800˚C. Residual ratios of compressive strength for iron-steel aggregate concrete cubes were 83, 113, 133, and 113% at temperatures of 100˚, 150˚, 200˚, and 300˚C, respectively.

3.4 Shielding Effectiveness

The effectiveness of concrete as a shield may be reduced under service conditions (elevated temperature) as drying reduces the hydrogen content or cracking occurs. Figure 3.4 presents results of elevated-temperature exposure on distribution of thermal and fast neutrons in ordinary concrete having a density of 2328 kg/m^3 [3.37]. These results demonstrate how an increase in temperature producing a decrease in concrete water content results in an increase in neutron flux density transmitted through a concrete of given thickness.

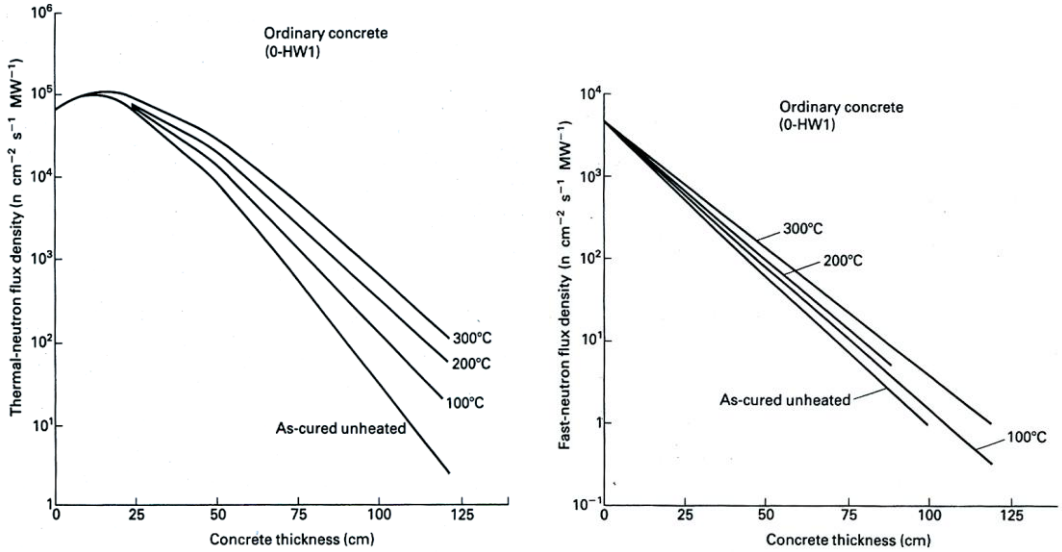

Figure 3.4 Effect of elevated temperature on distribution of thermal and fast neutrons in ordinary concrete.

Source: E. G. Peterson, "Shielding Properties of Ordinary Concretes as a Function of Temperature," HW-65572, Hanford Atomic Products Operation, Richland, Washington, August 2, 1960.

The increase in neutron flux due to a known loss of water can be estimated for different concrete thicknesses [3.38]:

$$R_{\phi} = \left(\frac{\phi}{\phi_0}\right)^{x/122}, \text{ where} \qquad (3.1)$$

R_{ϕ} = increase in neutron flux,
ϕ = flux after water loss in neutrons cm^{-2} s^{-1},
ϕ_0 = flux before water loss in neutrons cm^{-2} s^{-1}, and
x = thickness of shield.

For the case when the water content is not known, the increase in neutron flux through an ordinary concrete shield can be estimated if the densities of concrete before and after water loss are known [3.38]:

$$R_{\phi} = \frac{\phi}{\phi_0} = \exp\left[0.0195 + x(\rho_0 - \rho)\right], \text{ where} \tag{3.2}$$

ρ_0 = density of concrete in shield before water loss in lb ft^{-3},
ρ = density of concrete in shield after water loss in lb ft^{-3}, and
x = thickness of shield.

Estimates for heavyweight-aggregate concretes can be obtained by replacing the constant 0.0195 in the equation by 0.0284, 0.024, 0.0208, 0.0227 for ferrophosphorus concrete, magnetite concrete, limonite concrete, and baryte concrete, respectively.

Gamma dose rates for a ferrophosphorus concrete (4821 kg/m^3) as a function of shield thickness and temperature have been investigated [3.39]. Figure 3.5 presents gamma dose rate versus concrete thickness for this concrete tested in the unheated state and at 320˚C. Results indicate that for a shield thickness of 1.22 m the leakage of gamma rays at a concrete temperature of 320˚C is about 50 times greater than that for unheated concrete. Additional results indicated that the gamma leakage increased by factors of: 1.7 and 20 at temperatures of 100˚ and 320˚C, respectively, for 4231 kg/m^3 limonite-steel aggregate concrete [3.40]; 1.2 and 1.8 at temperatures of 100˚ and 320˚C, respectively, for 4299 kg/m^3 iron-serpentine concrete [3.41]; and 1.3 at a temperature of 320˚C for 3524 kg/m^3 iron-serpentine concrete [3.41].

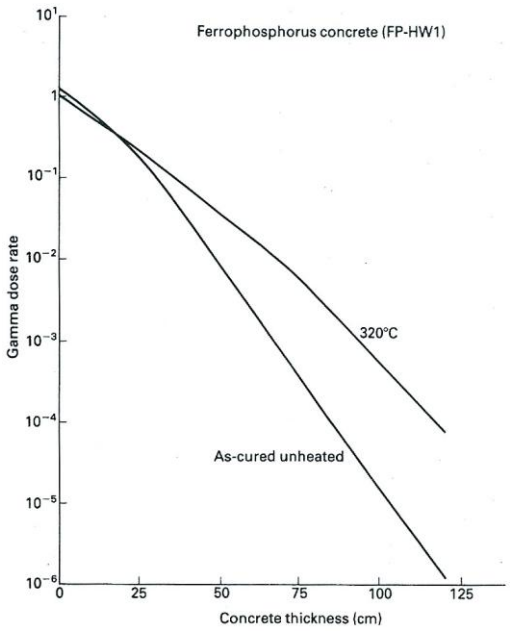

Figure 3.5 Effect of elevated temperature on gamma dose rate distribution in a ferrophosphorus concrete.

Source: E. G. Peterson, "Shielding Properties of Ferrophosphorus Concrete as a Function of Temperature," HW-64774, Hanford Atomic Products Operation, Richland, Washington, 1960.

The effect of different durations (1, 2, and 3 h) of high temperature (250°, 500°, 750°, and 950°C) on the physical, mechanical, and radiation properties of heavyweight concrete has been studied [3.34]. Results showed that ilmenite concrete had the highest density and modulus of elasticity and lowest percent absorption, and it also had higher values of compressive, tensile, bending, and bond strength than that obtained from either the baryte or gravel concretes. Ilmenite also showed the highest attenuation of transmitted gamma rays and was most resistant to elevated temperature. As the magnitude of thermal exposure increased, the attenuation coefficient decreased.

In concrete structures cracks develop due to effects such as thermal stress and heat of hydration and as a result the shielding effectiveness of the concrete can be reduced, especially if through-cracks develop. The effect of straight and crooked cracks through a concrete shield has been investigated [3.42]. In the immediate vicinity of the concrete surface, leakage of gamma rays through a slit contributed significantly to γ-dose rate, but diminished rapidly with distance from the surface as a result of shield thickness and scattering effects. The shielding effectiveness of cracked concrete has been investigated and formulas were developed to define the resulting effects [3.43]. Guidelines developed to compensate for cracking note that it might be economically advantageous to allow a concrete shield to crack and then shield the resulting radiation by other means.

The effect of collinear crack width on γ-ray shielding of concrete has been investigated [3.44]. The concrete specimens were fabricated from the concrete mix used at the Wolsung nuclear power station (i.e., Type V cement, maximum aggregate size of 20 mm, and 30 MPa compressive strength). The test specimen is illustrated in Figure 3.6. Also shown in the figure is the experimental setup used for increasing the crack width from 0 to 2 mm in increments. The basic principal for evaluating the effect of crack width on γ-ray attenuation for concrete samples

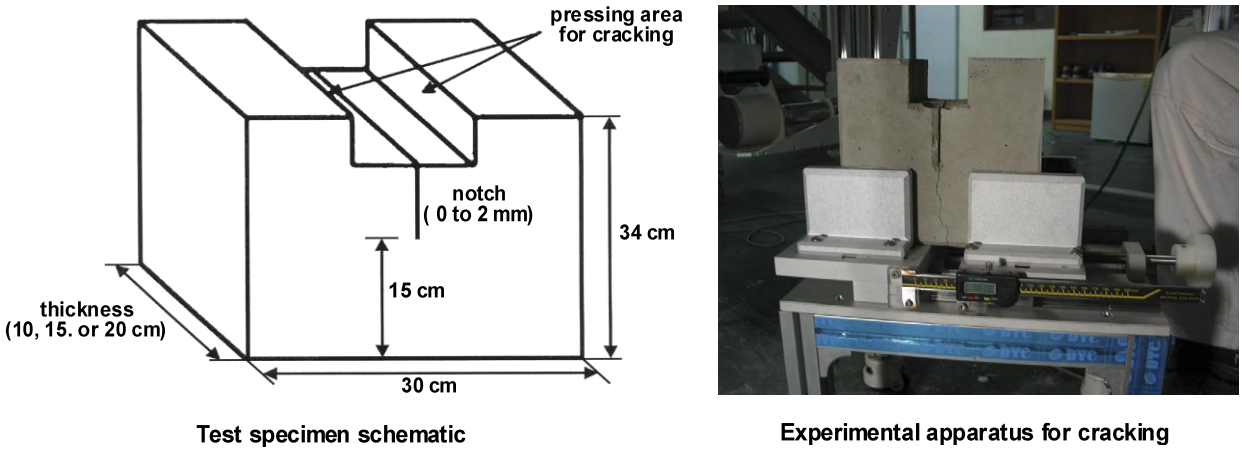

Figure 3.6 Test specimen schematic and experimental setup.

Source: C-M. Lee, Y.H. Lee, and K.J. Lee, "Cracking Effect on Gamma-Ray Shielding Performance in Concrete Structure," *Progress in Nuclear Energy* **49**, pp. 303-312, 2007

that were either 10-, 15-, or 20-cm thick is shown in Figure 3.7. Results are also presented in the figure showing that the relative intensity, as determined by the ratio of the intensity of radiation transmitted to the intensity of radiation before attenuation, increased as the crack width increased and decreased as the specimen thickness increased. Results were utilized to develop a correlation between crack width and intensity for a collinear crack in concrete:

$$\frac{I}{I_0} = e^{-\mu t}\log\left(\frac{bx}{t}+10\right), \text{ where} \qquad (3.3)$$

I = intensity of radiation,
I_0 = intensity of radiation before attenuation,
μ = linear attenuation coefficient for medium,
t = thickness of the medium,
x = crack width, and
b = constant (i.e., 140-150).

The surface dose was found to increase logarithmically with an increase in crack width. It was concluded from the study that if the shielding thickness of the concrete structure exceeds 20 cm and the crack width is 0.4 mm, the effect on shielding effectiveness will be less than 10%. It should be noted that these results were for collinear cracks and in actual concrete structures crack surfaces are irregular.

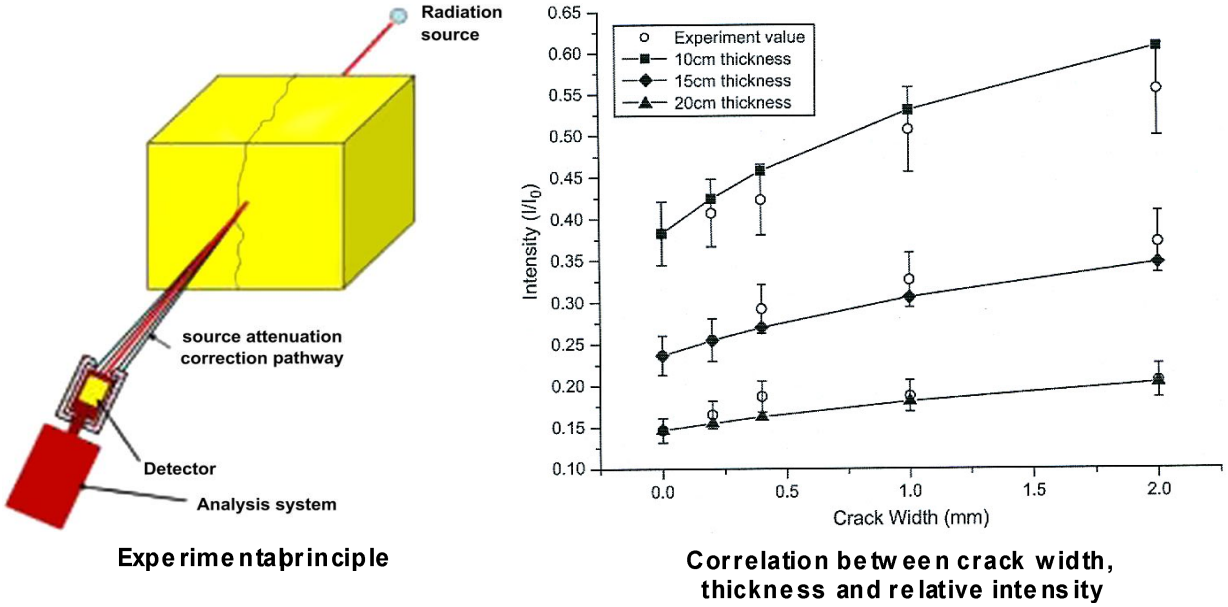

Figure 3.7 Schematic diagram of experimental principle and correlation between crack width and intensity.

Source: C-M. Lee, Y.H. Lee, and K.J. Lee, "Cracking Effect on Gamma-Ray Shielding Performance in Concrete Structure," *Progress in Nuclear Energy* **49**, pp. 303-312, 2007.

3.5 Summary

Results reported in the literature for properties of shielding concretes display wide differences because of factors such as mix proportions, the nature of the materials utilized, and the test conditions. The impact of elevated temperature on the water content of a shielding concrete has a significant effect on its nuclear properties, in particular its neutron radiation attenuation. Mechanical properties of shielding concretes tend to decrease with increasing temperature and exposure period. Thermal cycling can reduce the compressive strength, modulus of rupture, and static modulus of elasticity, with the reduction increasing as the peak cycling temperature increases. Specimens soaked in water prior to testing have lower residual compressive strengths than dry specimens. Specimens loaded while heated retain their residual compressive strength better than specimens that were not loaded during thermal treatment. Concrete density decreases with increasing temperature as evaporable water is removed, with the value becoming relatively stable after evaporable water is lost. As temperature increases (and water content decreases) the neutron flux density transmitted through concrete increases for a given section thickness. The intensity of radiation transmitted through cracked (collinear) concrete increases as the crack width increases and specimen thickness decreases.

3.6 References

3.1 H. Etherington, *Nuclear Engineering Handbook*, McGraw-Hill, New York, pp. 109–111, December 1958.

3.2 S. Glasstone and A. Sesonske, *Nuclear Reactor Engineering*, D. Van Nostrand, Princeton, New Jersey, pp. 614–615, December 1967.

3.3 M.F. Kaplan, *Concrete Radiation Shielding*, Concrete Design and Construction Series, Longman Scientific & Technical. New York, New York, 1989.

3.4 *Standard Specification for Aggregates for Radiation-Shielding Concrete*, ASTM C637-98a, American Society for Testing and Materials, West Conshockon, Pennsylvania, 2003.

3.5 *Standard Descriptive Nomenclature of Constituents of Aggregates for Radiation-Shielding Concrete*, ASTM C638-82, American Society for Testing and Materials, West Conshockon, Pennsylvania, 2002.

3.6 *Guide for Use of Normal Weight and Heavyweight Aggregate in Concrete*, ACI 221R-96, American Concrete Institute, Farmington Hills, Michigan, 2001.

3.7 *Standard Practice for Selecting Proportions for Normal, Heavyweight, and Mass Concrete*, ACI 211.1-91, American Concrete Institute, Farmington Hills, Michigan, 2002.
3.8 *Heavyweight Concrete: Measuring, Mixing, Transporting, and Placing*, ACI 304.3R-96, American Concrete Institute, Farmington Hills, Michigan, 2004.
3.9 *Nuclear Analysis and Design of Concrete Radiation Shielding for Nuclear Power Plants*, ANSI/ANS-6.4-2006, American Nuclear Society, La Grange Park, Illinois, 2006.
3.10 *Specification for Radiation Shielding Materials*, ANSI/ANS-6.4.2-2006, American Nuclear Society, La Grange Park, Illinois, 2006.
3.11 *Specification for Aggregate from Natural Sources for Concrete*," BS 882, British Standards Institute, London, United Kingdom, 1992.
3.12 F. Du Bois, *Specifications Techniques: Betons Tres Lourdes a Base de Riblons, de Fonte, et d'Un Mineral*, Section de Physique de Materiaux Nucleaires, Commissarat a L'Energie Atomique, Saclay, France September 1965.
3.13 R. Walker and M. Grotenhuis, *A Summary of Shielding Constants for Concrete*, USAEC Report ANL-6443, Argonne National Laboratory, November 1961.
3.14 A. Missenard, "Theoretical and Experimental Research on the Heat Conductivity of Concrete," *Annnales de l'Institute Technique du Batiment et des Travaux Publics* **18**, pp. 211-212, July/August 1965.
3.15 M. Tourasse, "The Heavy Concretes – Physical Properties and Mechanical Tests," *Proceedings of Second United Nations Conference on the Peaceful Use of Atomic Energy*, Paper 15/P/1152, 1958.
3.16 R.B. Gallaher and A.S. Kitzes, *Summary Report on Portland Cement Concretes for Shielding*, USAEC Report ORNL-1414, Oak Ridge National Laboratory, Oak Ridge, Tennessee, March 1953.
3.17 H.E. Hungerford, A. Hönig, A.E. Desov, F. Du Bois, and H.S. Davis, "Concretes, Cements, Mortars, and Grouts," *Engineering Compendium on Radiation Shielding*, Vol. II, S.9.1.12.15, p. 153, R.G. Jaeger (Editor), Springer-Verlag, Berlin, Germany, 1975.
3.18 Toledo Testing Laboratory, Inc., Reports 308907 and 308987 (November 1958) and Report 309587, February 1959.
3.19 H.E. Hungerford, A. Hönig, A.E. Desov, F. Du Bois, and H.S. Davis, "Concretes, Cements, Mortars, and Grouts," *Engineering Compendium on Radiation Shielding*, Vol. II, S.9.1.12, R.G. Jaeger (Editor), Springer-Verlag, Berlin, Germany, 1975.
3.20 H.S. Davis, F.L. Brown, and H.C, Winter, "Properties of High-Density Concrete Made With Iron Aggregate," *Journal American Concrete Institute* **27**(7), Farmington Hills, Michigan, March 1956.
3.21 A.N. Komarovskii, *Design of Nuclear Plants*, Chapter 5, Translated from Russian by Israel Progress for Scientific Translation, Jerusalem, 1968.
3.22 G. Massa, R. De Stefano, M. Collepardi, S. Chatterji, and V. Maniscalco, "Shielding Concretes for Liquid Sodium Cooled Nuclear Reactors," Paper H3/8 in *7th International Conference on Structural Mechanics in Reactor Technology*, Chicago, Illinois, North-Holland Publishers, 1983.
3.23 H.S. Davis, "N-Reactor Shielding," Paper SP-34-52 in *Concrete for Nuclear Reactors*, pp. 1109-1161, American Concrete Institute, Farmington Hills, Michigan, 1972.
3.24 J.M. Raphael, "The Structural Properties of Magnetite Concrete," *Journal of the Structural Division* **84**, Proceedings of the American Society of Civil Engineers, No. ST1, Paper 1511, New York, New York, January 1958.
3.25 H.E. Hungerford, A. Hönig, A.E. Desov, F. Du Bois, and H.S. Davis, "Concretes, Cements, Mortars, and Grouts," *Engineering Compendium on Radiation Shielding*, Vol. II, S.9.1.12.18, p. 162, R.G. Jaeger (Editor), Springer-Verlag, Berlin, Germany, 1975.
3.26 S. Ohgishi, S. Miyasaka, and J. Chida, "On Properties of Magnetite and Serpentine Concrete at Elevated Temperatures for Nuclear Reactor," SP 34-57 in *Concrete for Nuclear Reactors*, pp. 1243-1253, American Concrete Institute, Farmington Hills, Michigan, 1972.
3.27 A.E. Desov, K.D. Nekrasov, and A.F. Milovanov, "Cube and Prism Strength of Concrete at Elevated Temperatures," Paper SP-34-23 in *Concrete for Nuclear Reactors*, pp. 423-434, American Concrete Institute, Farmington Hills, Michigan, 1972.
3.28 A.N. Komarovskii, *Design of Nuclear Plants*, Chapter 7, 2nd Edition, Atomizdat, Moscow, Russia, 1965.
3.29 H.S. Davis and O.E. Borge, "High-Density Concrete Made With Hydrous-Iron Aggregates," *Journal American Concrete Institute* **30**(10), pp. 1141-1147, Farmington Hills, Michigan, 1959.
3.30 F. Du Bois, *Beton Lourds abase de Mineral de Magnetite de Dielette*, Centre d'Etudes Nucleaires de Saclay, Commissariat a l'Energie Atomique, France, June 1964.

3.31 G. Massa, R. De Stefano, M. Collepardi, S. Chatterji, and V. Maniscalco, "Shielding Concretes for Liquid Sodium Cooled Nuclear Reactors," Paper H3/8 in *Transactions of the 7th International Conference on Structural Mechanics in Reactor Technology*, pp. 151-158, North-Holland Publishers, 1983.
3.32 E. Crispino, "Studies on the Technology of Concretes Under Thermal Conditions," Paper SP-34-25 in *Concrete for Nuclear Reactors*, pp. 443-479, American Concrete Institute, Farmington Hills, Michigan, 1972.
3.33 H. Weigler and R. Fischer, "Influence of High Temperatures on Strength and Deformations of Concrete," Paper SP-34-26 in *Concrete for Nuclear Reactors*, pp. 481-493, American Concrete Institute, Farmington Hills, Michigan, 1972.
3.34 K. Sakr and E. El-Hakim, "Effect of High Temperature on Heavy Weight Concrete Properties," *Cement and Concrete Research* **35**, pp. 590-596, 2005.
3.35 *Engineering Compendium on Radiation Shielding*, Vol. II, S.9.1.12, p. 156, R.G. Jaeger (Editor), Springer-Verlag, Berlin, Germany, 1975.
3.36 A.N. Komarovskii, *Design of Nuclear Plants*, Chapter 7, Translated from Russian by Israel Progress for Scientific Translation, Jerusalem, 1968.
3.37 E. G. Peterson, *Shielding Properties of Ordinary Concretes as a Function of Temperature*, HW-65572, Hanford Atomic Products Operation, Richland, Washington, August 2, 1960.
3.38 H.E. Hungerford, "Shielding," in *Fast Reactor Technology Plant Design*, Chapter 8, J.G. Yevick Editor, MIT Press Cambridge, Massachusetts, 1966.
3.39 E. G. Peterson, *Shielding Properties of Ferrophosphorus Concrete as a Function of Temperature*, HW-64774, Hanford Atomic Products Operation, Richland, Washington, 1960.
3.40 W.L. Bunch, *Attenuation Properties of High Density Portland Cement Concretes as a Function of Temperature*, HW-54656, Hanford Atomic Products Operation, Richland, Washington, 1958.
3.41 E. G. Peterson, *Shielding Properties of Ordinary Concretes as a Function of Temperature*, HW-73255, Hanford Atomic Products Operation, Richland, Washington, 1962.
3.42 S. Miyasaka, Y. Kanemori, Y. Fukushima, T, Yamada, "Gamma-Ray Leakage Through Slit in Concrete Shield," *Nippon Genshiryaku Gakkaishi* **11**, pp. 2–8, 1969.
3.43 F. Seboek, "Shielding Effectiveness of Cracked Concrete," *Kerntechnik* **12**, pp. 4496–4501, November 1970.
3.44 C-M. Lee, Y.H. Lee, and K.J. Lee, "Cracking Effect on Gamma-Ray Shielding Performance in Concrete Structure," *Progress in Nuclear Energy* **49**, pp. 303-312, 2007.

4 EXAMPLES OF CODES AND STANDARDS THAT ADDRESS CONCRETE UNDER ELEVATED TEMPERATURE CONDITIONS

4.1 Current Practice

The compressive strength influences the load-carrying capacity of concrete components, and the stiffness (modulus of elasticity) impacts the structural deformations and loads that develop at restraints. Current requirements for the design of concrete containments are presented in American Society of Mechanical Engineer's Section III—Division 2, "Code for Concrete Containments – Rules for Construction of Nuclear Facility Components."* Supplemental load combination criteria are presented in Sect. 3.8.1 of the *NRC Standard Review Plan* [4.1].

Table 4.1 presents ASME Code temperature limits for various conditions or load categories in a prestressed concrete reactor vessel (PCRV) for the appropriate conditions (normal operation and abnormal environment). As noted in this table, the temperature in the concrete should not exceed 65°C at the liner-concrete interface and in the bulk concrete. Between cooling tubes (near the liner), 93°C is given as the maximum allowable. Temperature limits for

Table 4.1 Condition categories and temperature limits for concrete and prestressing systems for PCRVs

Load category	Area	Temperature limits, °C
Construction	Bulk concrete	54
Normal	Liner	
	Effective at liner-concrete interface	66
	Between cooling tubes	93
	Bulk concrete	66
	Bulk concrete with nuclear heating	71
	Local hot spots	121
	Distribution asymmetry	10
	At prestressing tendons	66[a]
	Liner interface transients (twice daily) range	38-66
Abnormal and severe environmental	Liner	
	Effective at liner-concrete interface	93
	Between cooling tubes	132
	Bulk concrete	93
	Local hot spots	191
	Distribution asymmetry	38
	At prestressing tendons	79
	Liner interface transients range	38-83
Extreme environmental	Liner	
	Effective at liner-concrete interface	149
	Between cooling tubes	204
	Bulk concrete	154
	Local hot spots	260
	Distribution asymmetry	38
	At prestressing tendons	149
	Liner interface transients range	38-93
Failure	Bulk concrete	
	Unpressurized condition	204
	Pressurized condition	316

[a]Higher temperatures may be permitted as long as the effects on material behavior (e.g., relaxation) are accounted for in design.

Source: "Code for Concrete Reactor Vessels and Containments," Nuclear Power Plant Components, *ASME Boiler and Pressure Vessel Code*, Section III, Division 2, American Society of Mechanical Engineers, New York, New York, July 2003.

* ACI 359-01 is endorsed by U.S. Nuclear Regulatory Guide 1.136 (Rev. 3), "Material for Concrete Containments," March 2007.

concrete safety-related structures other than concrete reactor vessels and concrete containments are contained in Appendix E, "Thermal Considerations," of ACI 349, *Code Requirements for Nuclear Safety-Related Structures and Commentary*." The temperature limitations for: (1) normal operation or any other long-term period are that the concrete surface temperatures shall not exceed 65.6°C except for local areas, such as around penetrations, that are allowed to have increased temperatures not to exceed 93.3°C; (2) for accident or any other short-term period the temperatures shall not exceed 176.7°C for the surface, except, local areas are allowed to reach 343.3°C from steam or water jets in the event of a pipe failure, however, after exposure to these temperatures, the serviceability of the structure needs to be assessed before resuming the operation of the plant with the extent of the assessment determined by the engineer and it may be limited to visual inspection only; and (3) higher temperatures than those given in (1) and (2) above may be allowed if tests are provided to evaluate the reduction in concrete strength and this reduction is applied to design allowables and evidence is provided verifying that the increased temperatures do not cause deterioration of the concrete either with or without load.

The French specification for PCRVs [4.2] limits temperatures in active parts of the concrete to 90°C; the British specification [4.3] states that if the normal operating temperature of any section of the vessel structure is such that the failure strength of the concrete at that temperature is significantly less than at ambient temperature, this will be taken into account. The British specification further notes that most concrete mixes subjected to temperatures above 100°C will suffer a reduction in compressive strength, and concrete with certain aggregates, particularly limestone, may suffer significant losses below that temperature. Figure 4.1 presents the BS 8110 design curves for strength reduction with temperature of unsealed dense concrete and lightweight aggregate concrete. Permissible temperatures for the concrete in PCRVs for gas-cooled reactors has generally been limited to the range of 45 to 80°C [4.4].

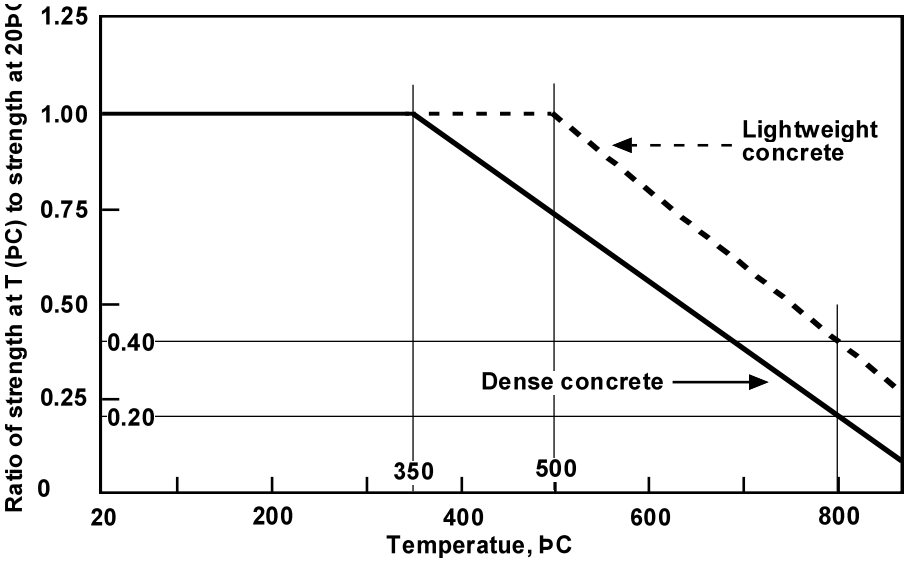

Figure 4.1 BS 8110 design curves for strength variation with the temperature of dense concrete and lightweight concrete.

Source: *Structural Use of Concrete. Code of Practice for Special Circumstances*, Section Four, "Fire Resistance," BS 8110: Part 2, British Standards Institution, London, United Kingdom, 1985.

4.2 Other Code Provisions for Addressing Concrete at Elevated Temperature

The American Concrete Institute in ACI/TMS 216, "Code Requirements for Determining the Fire Resistance of Concrete and Masonry Construction Assemblies," provides guidance on reduction in concrete compressive strength in the zone of flexural behavior that is based on the elevated temperature and coarse aggregate type [4.5]. Figure 4.2 presents information on the compressive strength of different aggregate concretes at elevated temperature and after cooling. Code guidance on the effect of elevated temperature on the strength of flexural reinforcement steel bar and strand is presented in Figure 4.3.

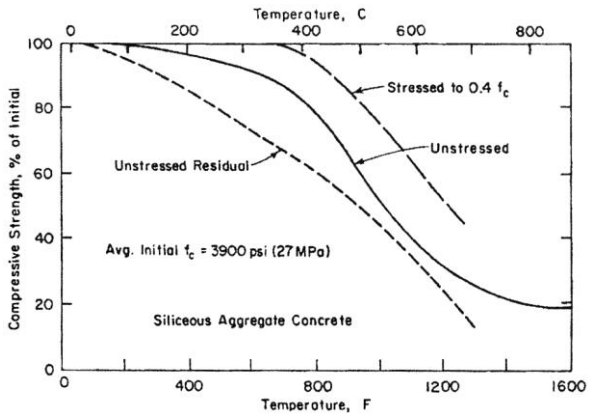

(a) Siliceous aggregate concrete.

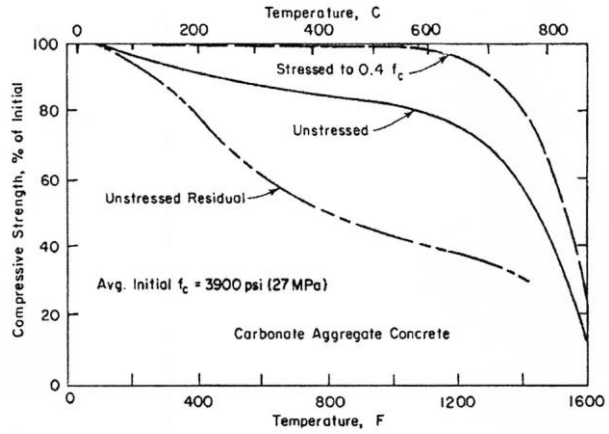

(b) Carbonate aggregate

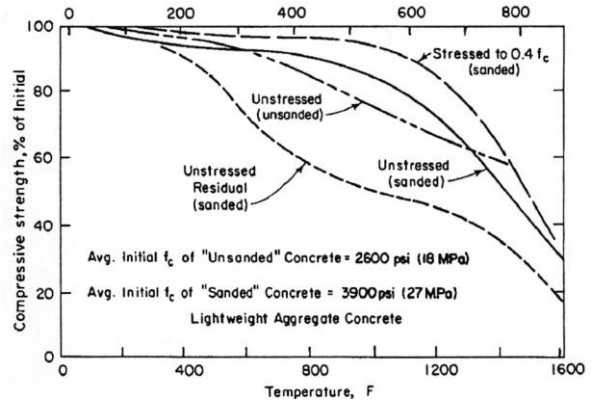

(c) Semi-lightweight aggregate concrete.

Figure 4.2 Compressive strength of different aggregate concretes at elevated temperature and after cooling

Source: *Code Requirements for Determining the Fire Resistance of Concrete and Masonry Construction Assemblies*, ACI 216.1M-07, American Concrete Institute, Farmington Hills, Michigan, 2007.

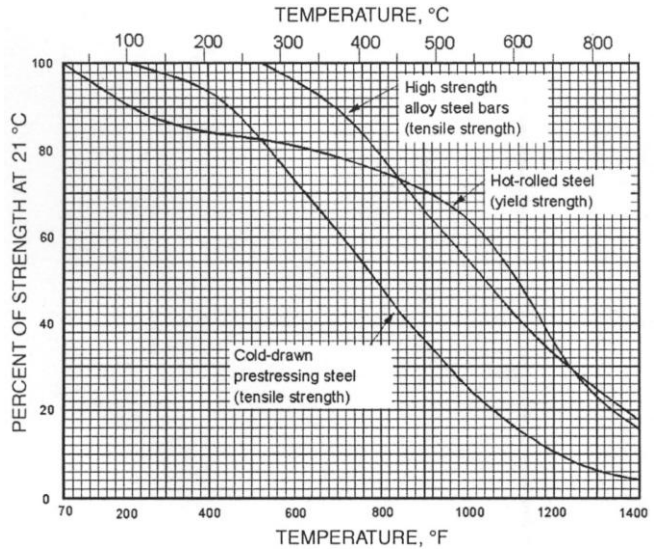

Figure 4.3 Strength of flexural steel bar and strand at elevated temperature.

Source: *Code Requirements for Determining the Fire Resistance of Concrete and Masonry Construction Assemblies*, ACI 216.1M-07, American Concrete Institute, Farmington Hills, Michigan, 2007.

National and international standards are available that provide guidance for computing concrete strength at elevated temperature in their fire design provisions: Comité Europeen de Normalisation (Eurocode 2—Part 1-2, *Structural Fire Design*, Eurocode 4—*Part 1-2, "General Rules for Structural Fire Design*") [4.6], Comites Euro-International du Beton (CEB model code) Bulletin D'Information No. 208, *Fire Design of Concrete Structures* [4.7], and National Building Code of Finland's RakMK B4 [4.8].

Eurocode 2 (CEN) specifies rules for the strength and deformation properties of uniaxially stressed concrete at elevated temperature. Figure 4.4 presents strength reduction factors for concrete with respect to elevated temperature. The Code makes no distinction between normal-strength and high-strength concretes in its fire design provisions. As the Code does not explicitly indicate whether the results are for concrete in service, (i.e., under load) it has been assumed that this is the case since the Code is for design of structural concrete [4.9,4.10].

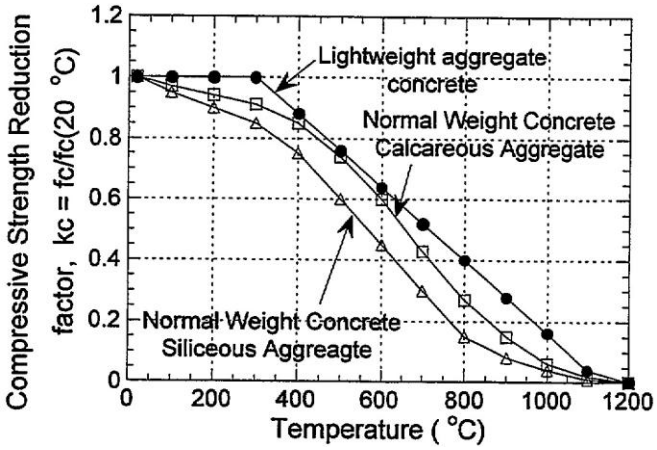

Figure 4.4 CEN compressive strength reduction factor for concrete subjected to elevated temperature.

Source: L.T. Phan, *Fire Performance of High-Strength Concrete: A Report of the State-of-the-Art*, NISTIR 5934, National Institute of Standards and Technology, Gaithersburg, Maryland, December 1966.

Comites Euro-International du Beton (CEB) has provided information on the effect of elevated temperature on concrete compressive strength, modulus of elasticity, and tensile strength. Figure 4.5 presents the recommended design curve for compressive strength of siliceous normal weight concrete at high temperature. Also shown in the figure is a comparison to the design curve of results obtained by several investigators for concretes having a compressive strength of $\leq$ 50MPa. The design curve for compressive strength of lightweight concrete at high temperature is presented in Figure 4.6. Design curves for the effect of elevated temperature on concrete modulus of elasticity and tensile strength are presented in Figures 4.7 and 4.8, respectively. The CEB Code also makes no distinction between normal-strength and high-strength concretes in its fire design provisions and does not indicate whether or not the results are for concrete in service (i.e., under load), but it has been assumed that this is the case [4.9,4.10].

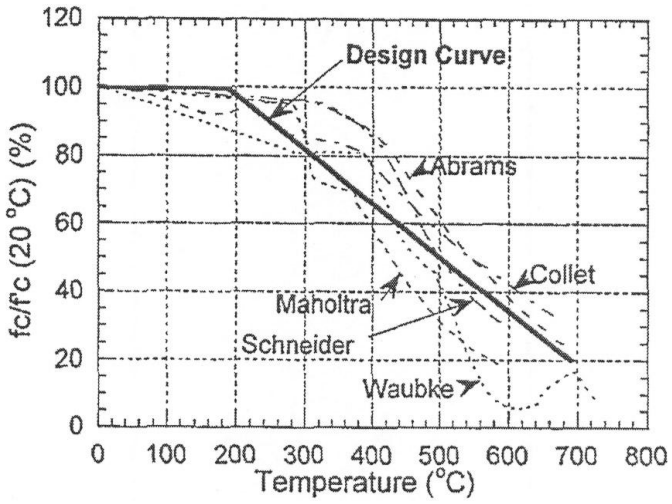

Figure 4.5 CEB design curve for compressive strength of siliceous normal weight concrete subjected to elevated temperature.

Source: L.T. Phan, *Fire Performance of High-Strength Concrete: A Report of the State-of-the-Art*, NISTIR 5934, National Institute of Standards and Technology, Gaithersburg, Maryland, December 1966.

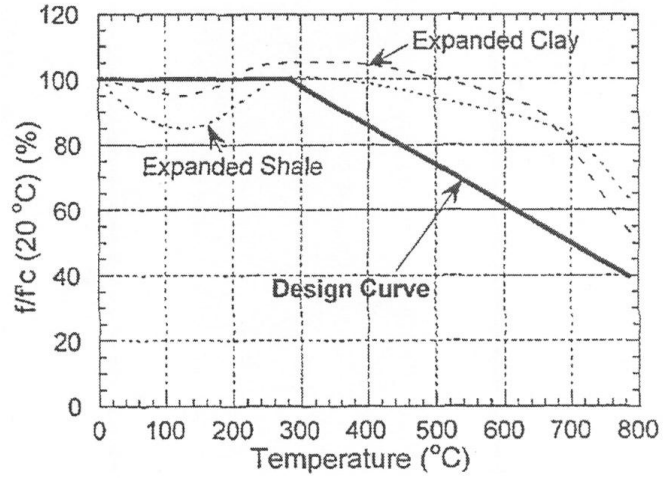

Figure 4.6 CEB design curve for compressive strength of lightweight concrete subjected to elevated temperature.

Source: L.T. Phan, *Fire Performance of High-Strength Concrete: A Report of the State-of-the-Art*, NISTIR 5934, National Institute of Standards and Technology, Gaithersburg, Maryland, December 1966.

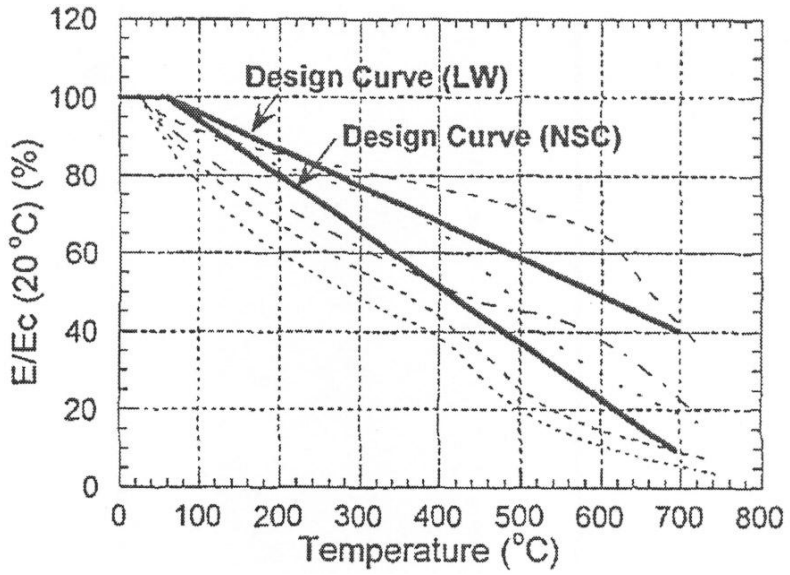

Figure 4.7 CEB design curve for effect of elevated temperature on modulus of elasticity of lightweight and normal-strength concretes.

Source: L.T. Phan, *Fire Performance of High-Strength Concrete: A Report of the State-of-the-Art*, NISTIR 5934, National Institute of Standards and Technology, Gaithersburg, Maryland, December 1966.

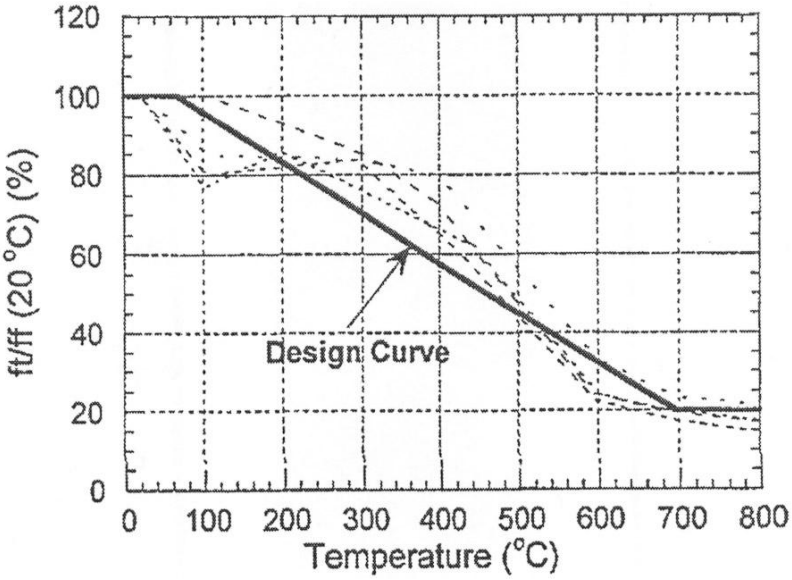

Figure 4.8 CEB design curve for effect of elevated temperature on tensile strength.

Source: L.T. Phan, *Fire Performance of High-Strength Concrete: A Report of the State-of-the-Art*, NISTIR 5934, National Institute of Standards and Technology, Gaithersburg, Maryland, December 1966.

Finland's *RakMK B4* prescribes different design rules for high-strength (70 MPa $\leq f_c' \leq$ 100 MPa, 150-mm cube strength), and normal-strength (10 MPa $\leq f_c' \leq$ 70 MPa, 150-mm cube strength) concretes. The RakMK B4 also prescribes different design rules for concrete in service (stressed, $0.3f_{23^\circ C}$) and for concrete that is not (unstressed). [4.9,4.10]. Figure 4.9 presents the RakMk B4 design code for effect of elevated temperature on concrete relative compressive strength. The RakMK B4's strength prediction for unstressed normal-strength concrete prescribes a

range of no strength loss between room temperature and 220 ºC. Above 220 ºC, RakMK B4 prescribes a strength loss that has a similar rate of strength reduction with temperature as in the case for high-strength concrete. A summary comparison of the design codes for compressive strength is presented in Figure 4.10.*

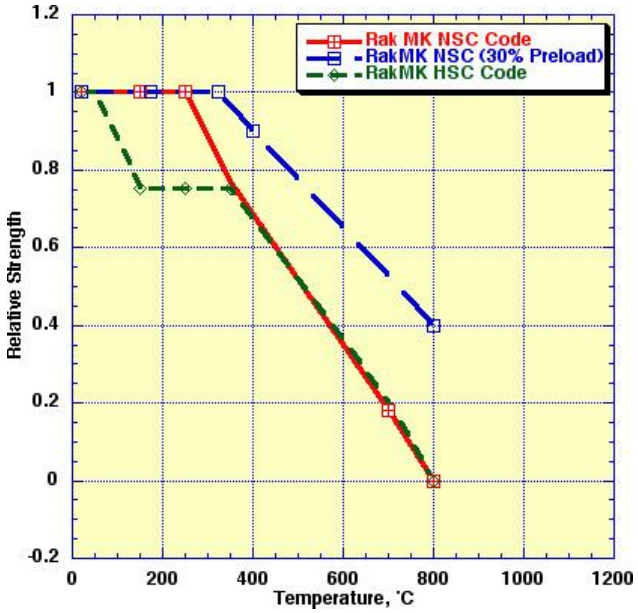

Figure 4.9 RakMK B4 design curves for effect of elevated temperature on concrete compressive strength.

Source: L.T. Phan, *Fire Performance of High-Strength Concrete: A Report of the State-of-the-Art*, NISTIR 5934, National Institute of Standards and Technology, Gaithersburg, Maryland, December 1966.

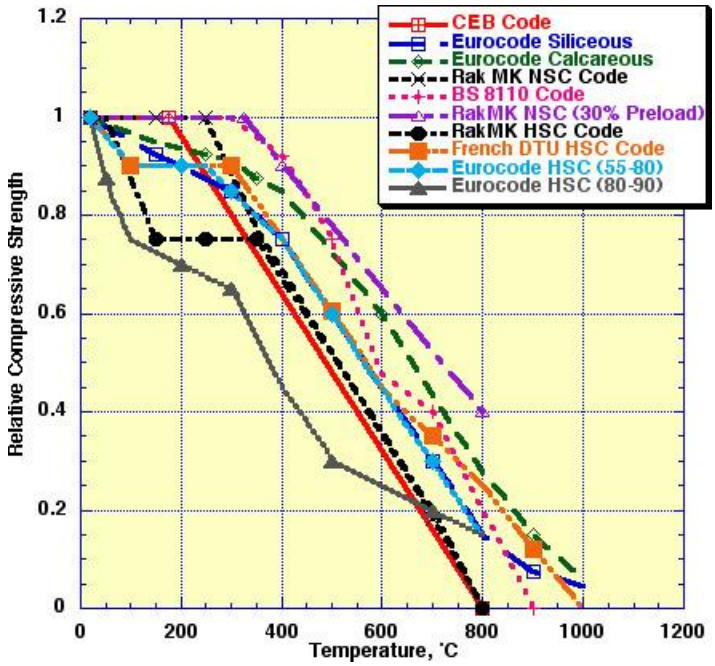

Figure 4.10 Comparison of design curves for effect of elevated temperature on concrete compressive strength.

* Reference [4.11] provides the source of information on the French DTU design code for high-strength concrete.

4.3 References

4.1 U.S. Atomic Energy Commission, "Concrete Containment," Sect. 3.8.1 in *Regulatory Standard Review Plan*, NUREG-0800, Washington, D.C., July 1981.

4.2 "Nuclear Reactor Vessels of Prestressed Concrete with Metal Reinforcements," *J. Offic. Republ. Fr.*, pp. 6119 – 6128, June 1970.

4.3 *Specification for Prestressed Concrete Pressure Vessels for Nuclear Reactors*, BS 4975, British Standards Institution, London, United Kingdom, July 1973

4.4 *Structural Use of Concrete. Code of Practice for Special Circumstances*, Section Four, "Fire Resistance," BS 8110: Part 2, British Standards Institution, London, United Kingdom, 1985.

4.5 *Code Requirements for Determining the Fire Resistance of Concrete and Masonry Construction Assemblies*, ACI 216.1M-07, American Concrete Institute, Farmington Hills, Michigan, 2007.

4.6 Comité Européen de Normalisation, "prENV 1992-1-2: Eurocode 2: Design of Concrete Structures. Part 1 - 2: Structural Fire Design," *CEN/TC 250/SC 2*, 1993.

4.7 Comites Euro-International Du Beton, "Fire Design of Concrete Structures - In Accordance with CEB/FIP Model Code 90," *CEB Bulletin D'Information No.* ***208***, Lausanne, Switzerland, 1991.

4.8 Concrete Association of Finland, *High Strength Concrete Supplementary Rules and Fire Design*, RakMK B4**,** 1991.

4.9 L.T. Phan, *Fire Performance of High-Strength Concrete: A Report of the State-of-the-Art*, NISTIR 5934, National Institute of Standards and Technology, Gaithersburg, Maryland, December 1966.

4.10 L.T. Phan, "High-Strength Concrete at High Temperature – An Overview," *Proceedings of 6th International Symposium on Utilization of High Strength/High Performance Concrete*, Volume 1, pp. 501-518, Leipzig, Germany, June 2002.

4.11 B. Persson, *Self-Compacting Concrete at Fire Temperatures*, TVBM-03/3110, Division of Building Materials, Lund Institute of Technology, Lund University, Sweden, September 2003.

5 POTENTIAL METHODS FOR ASSESSMENT OF CONCRETE EXPOSED TO HIGH TEMPERATURES[+]

5.1 Introduction

Thermal loading of reinforced concrete can result in damage ranging from cosmetic blemishes to more serious effects (e.g., misalignment and distortions). Heating of concrete may result in a variety of structural changes such as cracking, spalling, debonding of aggregate, expansion, and mineralogical or chemical changes such as discoloration, dehydration, and dissociation. With respect to the cement paste, evaporation and dissolution, dehydration and dissociation of ettringite, gypsum, calcium hydroxide, calcium carbonate and other phases such as calcium silicate hydrates may occur [5.1].

Evaluation of the heating history of a structure is important and has three primary purposes: (1) assess the thermal (i.e., fire) resistance of a particular element of a major structure, (2) assist in forensic research of the cause of a thermal excursion by determining the duration of exposure of concrete to elevated temperature, and (3) determine whether the structure is still structurally sound and to assess items such as whether the steel reinforcement has been exposed to high enough temperature to effect its properties [5.2]. One approach for performing an assessment of a reinforced concrete structure following a thermal event is presented in Figure 5.1. A listing of possible approaches for nondestructive assessment of fire-damaged concrete structures is provided in Table 5.1. Information on selected visual assessment approaches, and field and laboratory testing methods is provided below.

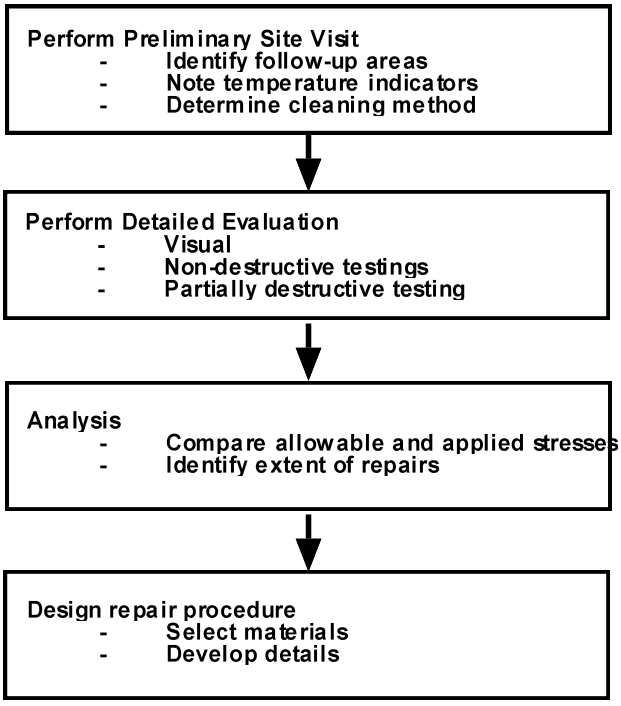

Figure 5.1 Example of evaluation process for structure subjected to thermal excursion such as resulting from a fire.

Source: N.K. Gosain, R.F. Drexler, and P. Choudhuri, "Evaluation and Repair of Fire-Damaged Buildings," *Structure*, 14 pages, September 2008.

[+] Although certain aspects of the information provided in this chapter have application to assessments of long-term effects of thermal loadings (e.g., estimating maximum exposure temperature and in-situ property determinations), the information available in the literature has primarily addressed post-fire damage assessments and thus would have primary application to assessments following postulated design-basis accident scenarios involving rapid thermal excursions in which thermal gradients develop within the structure.

Table 5.1 Listing of possible nondestructive approaches for use in assessment of fire-damaged concrete

Average response of cover concrete	Point-by-point response of small samples	Special interpretation techniques
• Hammer tapping • Schmidt rebound hammer • Windsor probe • Capo test • BRE internal fracture • Ultrasonic pulse velocity	• Small-scale mechanical testing • Differential thermal analysis • Thermogravimetric analysis (TGA) • Dilatometry (TMA) • Thermoluminescense • Porosimetry • Microcrack density analysis • Colorimetry • Petrographic analysis • Chemical analysis	• UPV method • Impact echo • Sonic tomography • Modal analysis of surface waves • Ground-penetrating radar • Electrical resistivity

Source: M. Colombo and R. Felicetti, "New NDT Techniques for the Assessment of Fire-Damaged Concrete Structures," *Fire Safety Journal* **42**, pp. 461-472, 2007.

5.2 Visual Assessment

Information related to the maximum temperature experienced and an assessment of the condition of a concrete structure following a thermal excursion generally starts with an on-site condition assessment.* The first phase of the on-site assessment involves a general visual inspection of the structures for signs of distress (e.g., cracking, spalling, deflections, distortions, misalignment, and exposed steel reinforcement). Table 5.2 provides simplified general guidance for visual concrete fire damage classification [5.5]. Table 5.3 provides more detailed guidance that has been developed to assist in assessing and categorizing damage of individual concrete members [5.6]. Steel reinforcement in flexure members that has not experienced severe distortion usually indicates that the steel has not suffered a significant reduction in yield strength due to thermal exposure, and if concrete spalling does not extend to the depth of steel reinforcement the structural strength is relatively unaffected [5.7]. Columns that contain numerous ties or spiral confinement, however, can reach temperatures high enough to reduce the yield strength without showing signs of severe distortion or buckling. Shear failure of normal weight concrete beams exposed to fire conditions are rare and flexural cracks can form in the negative moment regions over supports to redistribute moments as a result of fire exposure [5.7]. If cracks are not present in the negative moment region, the fire was not

Table 5.2 Simplified visual concrete fire damage classification

Class of damage	Features observed					
	Color	Crazing	Spalling	Reinforcement	Cracks	Deflection
0 (Decoration req'd)	Normal	None	None	None exposed	None	None
1 (Superficial repair req'd)	Normal	Slight	Minor	None exposed	None	None
2 (General repair req'd)	Pink	Moderate	Localized	Up to 25% exposed	None	None
3 (Principal repair req'd)	Whitish gray	Extensive	Considerable	Up to 50% exposed	Minor	None
4 (Major repair req'd)	Buff	Surface lost	Almost total	Up to 50% exposed	Major	Distorted

Source: *Assessment and Repair of Fire-Damaged Concrete Structures*, Technical Report No. 33, Concrete Society, Camberley, United Kingdom, 1990.

* General guidance on conduct of a condition assessment is available [5.3,5.4].

Table 5.3 Initial assessment of damage and probable treatment required

		Damage Class 1	Damage Class 2	Damage Class 3	Damage Class 4
COLUMNS	Soot and smoke deposits	Present	-	-	-
	Color change	-	Pink to buff surface	Buff surface	-
	Spalling	-	Only minor	Local	Extensive
	Steel exposure	-	-	Steel showing	Considerable areas
	Surface separation	Peeling	Substantial	Surface mostly gone. Remainder sounds hollow when struck	-
	Number of main bars buckled	-	-	Not more than one	One or more
	Microcracking	-	Extensive	-	-
	Distortion	-	-	Possible	-
SLABS	Reinforced concrete solid slabs Soot and smoke deposits	Present	General coverage	Completely covered, or color changed	-
	Color change	-	-	Pink	-
	Spalling	Minor	Present	Present	-
	Steel exposure	-	10% or less	Over 10%	-
	Adherence of steel to concrete	-	Adhering	Adhering	Fallen clear
	Plank	Some broken	Substantial damage	-	-
	Ribs	Intact	-	-	-
	Soot and smoke deposits	Present	-	-	-
	Spalling	None	Present	Extensive	-
	Steel exposure	-	Small areas	-	-
	Adherence of steel to concrete	-	-	Generally adhering	Fallen clear
	Suspended ceiling	Extensive damage	-	-	-
	Deflection	-	-	Not severe	Substantial
BEAMS	Soot and smoke deposits	Present	Completely covered or color changed	-	-
	Color change	-	Pink	Buff	Buff to gray
	Spalling	Minor	Substantial but at edges only	Substantial on soffit sides	Extensive on soffit sides
	Steel exposure	Little or none	Outer edges of corner bars	Main bars each about 50%	Almost al lower main bars
	Surface separation	-	Cover concrete of soffit sounds hollow when struck	-	-
	Number of main bars buckled	-	-	Not more than one	Possibly several
	Microcracking	-	Surface	-	-
	Cracking	-	-	Several cracks ~6.4 mm	-
	Deflection or Fracture	-	-	Not severe	Substantial deflection or fracture or both
COLUMNS, BEAMS	Probable treatment required	Cosmetic only	Some replacement	Examination in greater detail. Considerable replacement or reclassification as Class 2 or 4	Removal and replacement or strengthening extensively with additional concrete and reinforcement

Source: "Concrete Structures After Fire," *Concrete Construction* **17**(3), Addison, Illinois, 1972.

significant enough for the concrete's cracking moment strength to be reached and therefore the strength of the steel reinforcement can be considered to be intact. Fire exposure of prestressed concrete members requires a more detailed evaluation as the elevated temperature can result in strength loss, permanent relaxation losses, and a reduction in prestressing force [5.8]. Increased deflection of prestressed concrete members would be an indication of exposure to high temperatures. Critical temperatures for cold-worked steel reinforcement and hot-rolled steel reinforcement at which considerable residual strength is lost have been cited as > 450˚C and > 600˚C, respectively, and prestressing steel exhibits considerable strength loss at 200˚ to 400˚C [5.9][#] Masonry can exhibit distress similar to that of concrete (e.g., cracks, pitting of aggregates, shallow spalling and minor surface damage). Masonry under fire exposure can exhibit some softening of the mortar joints, but the damage is typically confined to within about 19 mm of the fire-exposed wall and excellent structural fire endurance characteristics are maintained [5.7,5.10].

In addition to spalling, loss of chemically combined water, and loss of strength, Portland cement concretes can exhibit changes in color as a result of a sudden thermal excursion such as resulting from a fire.[^] Crazing, cracking, popouts caused by quartz or chert aggregate particles, spalling, and dehydration (crumbling and powder of cement paste) provide general indications of temperatures to which the concrete was exposed. Approximate corresponding temperatures for these occurrences are 300˚, 550˚ (deep cracking), 575˚, 800˚, and 900˚C, respectively [5.12]. Heating can change the color (hue) of concrete that in turn can sometimes provide an indication of the temperature attained and an equivalent fire duration [5.9]. An example of this is presented in Figure 5.2 which shows the presence of cracks in a region of pink discoloration and a partial change of aggregate color from yellow gold to red in upper right of figure.

Figure 5.2 Discoloration and cracking in concrete resulting from elevated temperature exposure.

Source: *Assessing the Condition and Repair Alternatives of Fire-Exposed Concrete and Masonry Members*, Report SR332.01B, National Codes and Standards Council of the Concrete and Masonry Industries, Skokie, Illinois, August 1994.

Concrete made with sedimentary or metamorphic aggregates can show permanent color change on heating [5.13]. Color is normal to 230˚C; goes from pink to red from 290˚ to 590˚C; and from 590˚ to 900˚C color changes to gray and then buff. For temperatures up to about 500˚C temperature distribution is little affected by using carbonate rather than siliceous aggregate. Actual concrete colors observed depend on aggregate type present and are most pronounced for siliceous aggregate and less so for limestone, granite, and Lytag [5.9]. Flint (chert) exhibits the most striking colors as illustrated in Figure 5.3. Colorimeters have been applied directly to the surface of concrete samples as part of the assessment of the Mont Blanc Tunnel fire and the measurements were found to correlate well with the maximum temperature experienced [5.14].

[#] Appendix B presents information on effects of elevated temperature on properties of steel reinforcement and prestressing steels, Chapter 2 discusses effects on concrete's physical and mechanical properties, and spalling has been addressed elsewhere [5.11].
[^] Additional information on color change and temperature is presented in Section 5.4.

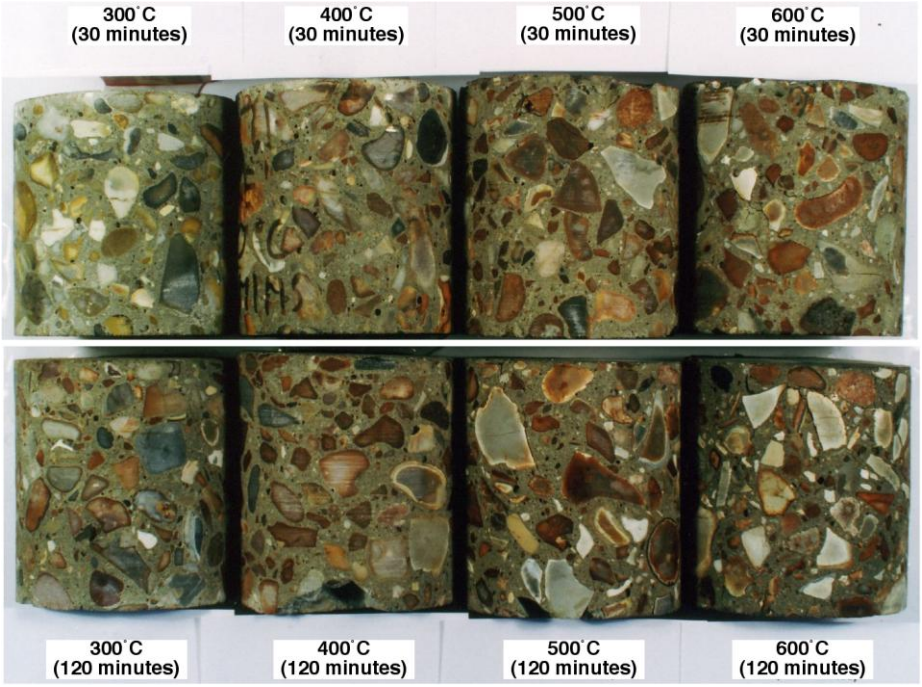

Figure 5.3 Appearance of flint-aggregate concrete after heating.

Source: J.P. Ingham, "Assessment of Fire-Damaged Concrete and Masonry Structures: Application of Petrography," *11th Euroseminar on Microscopy Applied to Building Materials*, 16 pages, Porto, Portugal, 5-9 June 2007.

An overview of the changes in coloration of concrete resulting from temperature exposure has been compiled [5.15]. Presented below is material extracted from this compilation and references cited can be obtained from the main reference.

> "At room temperature, concrete is reported as yellowish [1]. A faint pink hue is observed beginning at either 232° C [90; 96; 98] or at 250° C [95]. This has been attributed to changes in the limestone [98] and/or the iron oxide [95]. Between 250° C and 300° C, a distinct pink hue is reported [1; 69; 74; 90; 95; 96; 98-100].[19] The distinct pink is attributed to iron compounds, sand, and sandstone [1]; to ferric oxide [95][20]; to siliaceous aggregates [74][19]; and to ferrous salts [100]. The pink color at 300° C changes to a brick red at about 600° C. This has been observed by numerous researchers [74; 90; 95; 98; 102].[19] Again, the color change is mostly attributed to limestone [69; 98] and to ferric oxide [95; 102]. The brick red color changes to gray at higher temperatures. This gray color has been reported in the range between 600° C and 900° C [98] and at 900° C [74][19]. Smith [90] found an additional color change, from brick red to black to gray, in the 600° C to 900° C color range. The final color change is to buff. This color has been reported at approximately 1000° C [74][19] and at about 900° C [90; 98]. These color changes are still largely attributed to the iron oxide [95],[102]."

These color changes and their rough temperature ranges are loosely summarized in Table 5.4. Additional information is presented in Table 5.5 covering change in appearance of concrete exposed to very high temperatures ($T \geq 800$˚C) [5.16]. The samples in this study were obtained from two structures in Taiwan and subjected to the temperatures noted in the table for either 10 minutes or one hour and then cooled to room temperature and examined. Results of thermogravimetric analysis, x-ray diffraction, and scanning electron microscopy examinations are also available in the reference. It was noted that 1100˚ to 1200˚C was considered to be critical in that exposure to temperatures below 1000˚C resulted in light color, loose and friable structure, and cracks when cooled to ambient, while exposure to temperatures greater than 1000˚C tended to result in a dark color with glossy appearance, hard structure, and the disappearance of the cracks. Concrete apparently liquefied at temperatures of 1300˚ or 1400˚C.

Table 5.4 Indication of concrete color change on heating

Temp., ˚C	20˚	232˚ - 250˚	300˚	300˚ - 600˚	600˚		600˚ - 900˚	900˚	900˚	1000˚
concrete color	yellow	faint pink	distinct pink	pink changing to brick red	brick red	black	gray	gray	buff	buff

Source: R.K. Schroeder, *Post-Fire Analysis of Construction Materials*, PhD Thesis, University of California, Berkeley, 1999.

Table 5.5 Appearance of concrete after being subjecting to very high temperatures

Thermal exposure condition		Appearance		
		Sample A	Sample B	Sample B-1
800˚C	10 min	Pale red, loose, has small cracks	Gray, loose, has small cracks	Dark brown, glossy, hard (remained unchanged)
	1 hour	Pale red, loose, has small cracks	Gray, loose, has small cracks	-
900˚C	10 min	Pale red, loose, has small cracks	Gray, loose, cracks slightly enlarged	Remained unchanged
	1 hour	Pale red, loose, cracks slightly enlarged	Gray, loose, cracks slightly enlarged	-
1000˚C	10 min	Light red, loose, cracks slightly enlarged	Gray, loose, cracks enlarged	Remained unchanged
	1 hour	Light red, loose, expanded volume with large cracks	Gray, loose, expanded volume with large cracks	-
1100˚C	10 min	Gray, loose, expanded volume with large cracks	Gray, loose, fragile, cracked	Corners become smooth
	1 hour	Gray, loose, expanded volume with large cracks	Brownish yellow, loose, fragile, cracked	-
1200˚C	10 min	Grayish yellow, hard, glossy, has small cracks	Dark brown, hard, glossy, flat	Dark brown, has smooth surface, hard, flat
	1 hour	Partially grayish yellow and partially brown, hard, glossy, no cracks	Dark brown, hard, glossy, flat, partly molten while hot	-
1300˚C	10 min	Brown, hard, glossy, flat, molten while hot	Dark brown, hard, glossy, flat, molten while hot	Dark brown, glossy, hard, liquid-like while hot
	1 hour	Brown, hard, glossy, flat, molten while hot	Dark brown, hard, glossy, flat, liquid-like while hot	-
1400˚C	10 min	Dark brown, glossy, hard, liquid-like while hot	-	Dark brown, glossy, hard, liquid-like while hot
	1 hour	Dark brown, glossy, hard, liquid-like while hot	-	-

Source: W-T. Chang, Y-S. Giang, C-T. Wang, and C-W. Huang, "Concrete at High Temperatures Above 1000˚C," *1993 International Carnahan Conference on Security Technology*, Institute of Electrical and Electronics Engineers, Ottawa, Ontario, Canada, October 1993.

The transition of siliceous aggregate from normal to pink or red at 300˚to 600˚C is considered to be useful in damage assessments in that this is the temperature range at which significant loss of concrete strength occurs [5.17]. The red color change is due to presence of oxidizable iron. The color change from pink to red is less prominent with calcareous and igneous aggregate. Not all aggregates will undergo color changes on heating and consideration should be given to the possibility that the pink/red color may be a feature of the aggregate rather than heat-induced [5.9]. Also surface temperatures usually are quite different from temperatures at different depths in the concrete and thus estimates of strength based on surface color indications of temperature are speculative [5.12].

Visual methods are often complemented by tapping tests with a metallic object such as a hammer or chisel to detect hollow-sounding, delaminated material. Additional information that can be revealed from the tapping tests includes hardness, integrity, depth of damage, seriousness of cracking, and condition of steel [5.12].

5.3 Field-Testing Techniques

A number of non-destructive techniques can be used to provide a more detailed assessment of the material in-situ (e.g., see Table 5.1). Techniques typically utilized include rebound hammer, break-off method, impact echo, and ultrasonics. ACI 364.1R-07, *Guide for Evaluation of Concrete Structures Before Rehabilitation*, in Tables 5.1 and 5.2 provides a listing of test methods to evaluate hardened concrete in existing structures and test methods to determine structural properties and determine the condition of reinforcing steel, respectively. Descriptions and an overview of methods for detection of degradation in reinforced concrete structural members are also available [5.18,5.19]. Discussed below are two relatively recent field-testing techniques that have been proposed for assessment of fire-damaged concrete.

Indirect ultrasonic pulse velocity measurements based on the refraction of longitudinal ultrasonic waves has been investigated [5.20]. The measurement of pulse arrival time is performed by placing the emitting and receiving probes on the same face of the structure. As the maximum depth of the material investigated is a function of the distance between the transmitting and receiving probes, by increasing the separation the structure can be investigated to deeper depths. A plot of distance versus pulse arrival time is developed that is interpreted using numerical methods. Figure 5.4 presents an illustration of application of the method to assessment of damage thickness in a wall. A 20% decrease in the velocity was selected as the threshold for damage in this study. It was noted in the reference that application of this method can be tedious, and a flat surface is required.

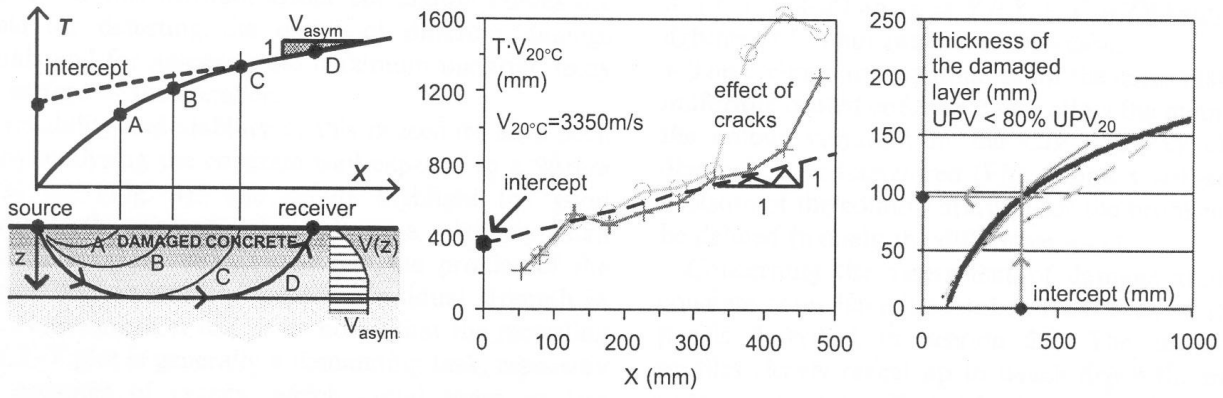

Figure 5.4 Illustration of application of indirect UPV method to identify damage depth (intercept at X = 0 in middle figure is related to thickness of the sizably damaged concrete as shown in right-hand side of figure)

Source: M. Colombo and R. Felicetti, "New NDT Techniques for the Assessment of Fire-Damaged Concrete Structures," *Fire Safety Journal* **42**, pp. 461-472, 2007.

Measurement of drilling resistance has been proposed as a method to ascertain the thermal damage in concrete structures resulting from a fire [5.21]. The approach is based on measurement of either the thrust to be exerted to

drill the material at constant feed rate or the work to drill a unit deep hole (J/mm). A common battery hammer drill that has been modified to monitor power consumption, the bit rotation, and hole depth is utilized. Electrical signals acquired are fed to a laptop computer and processed by dedicated software so the results can be displayed in real time. Figure 5.5 presents an example of results that were obtained from a column that had been severely damaged by fire. The most severely damaged areas were initially selected based on results from rebound hammer tests. Since the rebound hammer results could not indicate the depth of damage, drilling resistance tests were performed to establish a damage depth of slightly over 20 mm. A significant advantage noted for this method is that specific calibration curves do not have to be generated for comparison because the results are compared to the material response of the inner undamaged layer of the member under investigation.

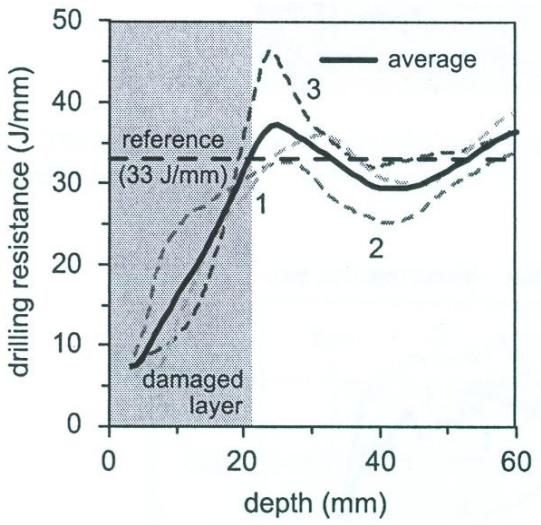

Figure 5.5 Illustration of application of drilling resistance method to fire-damaged concrete column.

Source: M. Colombo and R. Felicetti, "New NDT Techniques for the Assessment of Fire-Damaged Concrete Structures," *Fire Safety Journal* **42**, pp. 461-472, 2007.

5.4 Laboratory Techniques

Removal and testing of concrete cores samples in the laboratory provides the most effective approach for obtaining the comprehensive and detailed information on the mechanical properties and internal condition of concrete following a thermal excursion. Guidance on sampling and material testing is available [5.3,5.4].

Ultrasonic pulse velocity or resonant frequency testing have been noted as a good tool for indicating damage to concrete resulting from elevated temperature exposure, but are not reliable indicators of the concrete compressive strength [5.22]. Examples of other potential lab test methods include thermoluminescence, scanning electron microscopy, x-ray diffraction, differential thermal analysis, thermogravimetric analysis, and derivative thermogravimetric analysis. Figure 5.6 presents an example of use of scanning electron microscopy to examine the change in morphologies of cement hydrates resulting from temperature exposure. It has been noted that these potential lab test methods tend to be somewhat qualitative in nature or have primarily been used in academic research and are not routinely used to investigate thermally-damaged structures [5.9,5.23]. However, concrete petrography provides an approach for examining concrete to characterize and determine any damage caused as a result of a thermal exposure.

Petrographic analysis of extracted concrete core samples can provide information on bond loss between the cement matrix and steel reinforcement, crack orientation and its relationship to the aggregate, microcracking, extent of cement hydration, chemical compositional changes of cementitious materials and aggregates, and temperature distribution within a given concrete depth [5.7]. Petrography is the primary tool for assessing the internal condition of concrete and can be used to determine the depth of damage for reinforced concrete as well as providing a means

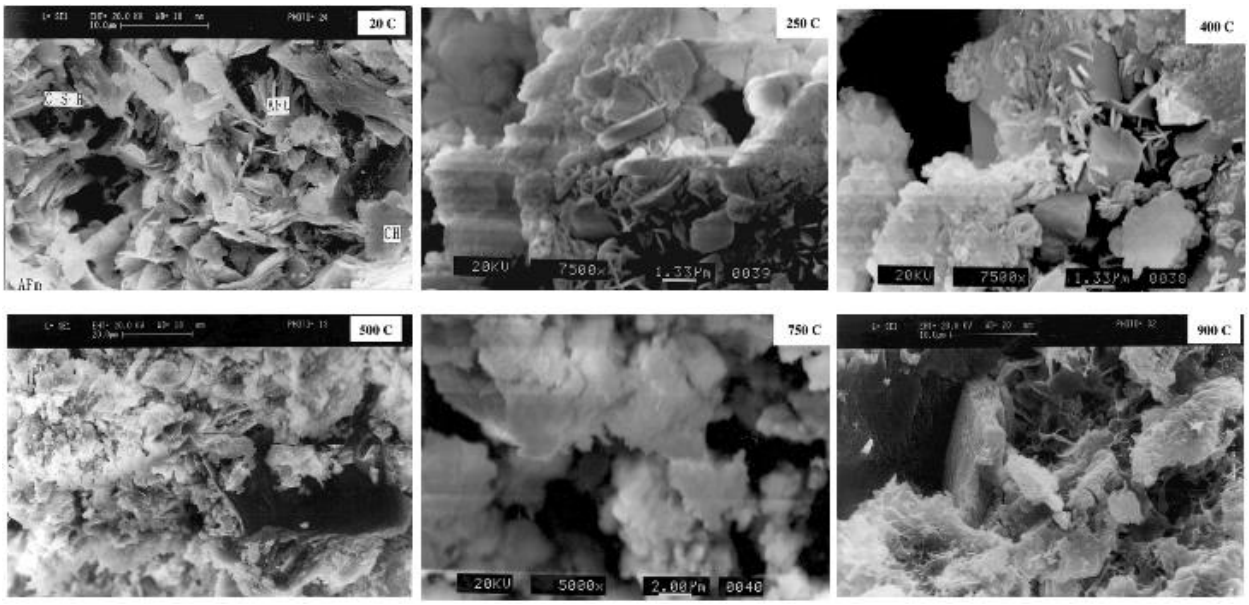

Figure 5.6 Effect of elevated temperature exposure on morphologies of a siliceous aggregate Type I Portland cement concrete.

Source: W-M. Lin, T.D. Lin, and L.J. Powere-Couche, "Microstructures of Fire-Damaged Concrete," *ACI Materials Journal* **93**(3), American Concrete Institute, Farmington Hills, Michigan, September-October 1996.

to determine whether the damage was caused by thermal exposure or some other mechanism. Detailed information on practices for petrographic examination of hardened concrete is available [5.13,5.24]. Two areas related to petrography that can be utilized in assessing the significance of damage resulting from thermal exposure are examinations of phase changes and microcracking occurrence.

Changes in both the cement paste and the aggregate result from elevated temperature exposure and can result in conversion of certain phases into new phases that may alter the concrete color (discussed previously) and the original mineralogical composition of the cement paste so that lines of equal physico-chemical conditions (isograds) can be mapped [5.2]. Since the isograds occur as a result of temperature, they can be used to provide an indication of temperature variations with concrete depth. Table 5.6 provides an indication of results that might be derived by examining the concrete with a hand lens or stereomicroscope. More detailed information (e.g., disappearance or

Table 5.6 Visual indications of elevated temperature effects on concrete

Temperature, ˚C	Indicators
< 300˚	Normal, no apparent macroscopic changes in concrete; color remains gray
300˚ - 350˚	Oxidation of iron hydroxides like FeOOH in aggregate and cement paste to hematite, α-Fe_2O_3, causing a permanent change of color of the concrete from gray to pinkish brown. This isograd is of importance as concrete and steel properties will undergo loss of properties at higher temperatures.
573˚	Transition of α-quartz to β-quartz, accompanied by an instantaneous increase in volume of quartz of about 5%, resulting in a radial cracking pattern around the quartz grains in the aggregate; this phase transition itself is reversible, but the radial cracking provides a diagnostic feature that remains after cooling
> 800˚	Complete disintegration of calcareous constituents of the aggregate and cement paste due to both dissociation and extreme thermal stresses causing a whitish gray coloration of the concrete

Source: T.G. Nijland and J.A. Larbi, "Unraveling the Temperature Distribution in Fire-Damaged Concrete by Means of PFM Microscopy: Outline of Approach and Review of Useful Readings," *HERON* **46**(4), pp. 253-264, 2001.

appearance of cement phases, and secondary phases) can be provided by polarizing and fluorescent microscopy which examines fluorescent thin sections with the aid of a combined polarizing and fluorescent microscope [5.2]. Careful examination of microscopically-observed features allows thermal contours to be plotted through the depth of individual concrete members [i.e., under favorable conditions contours can be plotted for 105˚C (increased porosity of cement matrix), 300˚C (red discoloration of aggregate), 500˚C (cement matrix becomes completely isotropic), 600˚C (α to β quartz transition), 800˚C (calcination of limestone), and 1200˚C (first signs of melting)] [5.9]. By conducting a point by point examination of concrete material constituents and outlines of color profiles using the combination of an optical microscope and a workstation to provide optical magnification and image resolution, it has been shown that locations significantly affected by high temperature can be identified through changes in hue [5.17].

It has been shown that the crack density, residual concrete compressive strength, and temperature can be correlated (e.g., crack density/color change can be used to indicate depth to which compressive strength is likely to have been significantly affected) [5.23]. In this study specimens were fabricated using ordinary Portland cements (OPCs) and blended cements (OPC and 30% fly ash, OPC and 50% blast furnace slag) in conjunction with quartz sand and siliceous gravel. Additional specimens were fabricated using OPC, sand, and either crushed limestone, granite, or Lytag coarse aggregates. After moist curing for 28 days and 32 days air drying, the specimens were heated at 105˚C for 48 hours to provide well-cured specimens and prevent spalling. The beam, cube, and cylindrical test specimens were then heated at temperatures ranging from 175˚ to 700˚C for one hour and then permitted to cool to room temperature. After elevated temperature exposure, 10-mm-thick sections were cut from the center of the cube specimens, vacuum impregnated with low viscosity resin, glued to a slide, polished, and examined using thin-section petrography with the results photographed. Crack densities were then determined in terms of mm of crack length per cm^2 of concrete. Figure 5.7 presents the effect of temperature on crack density for specimens made with siliceous aggregates and OPC and can be used to indicate the temperature at which thermally-induced cracking begins (350˚C). Correlation between this temperature and temperature at which significant reductions in compressive strengths occurred (325˚C) were found to be good. Correlations were also found to be good for the limestone aggregate and granite aggregate with OPC mixes. It was concluded that measurements of crack density after transient heating can be used to identify the depth to which the compressive strength of concrete is likely to have been significantly affected. Table 5.7 presents an example of criteria that have been established to aid in classifying the extent of microcracking in concrete [5.2].

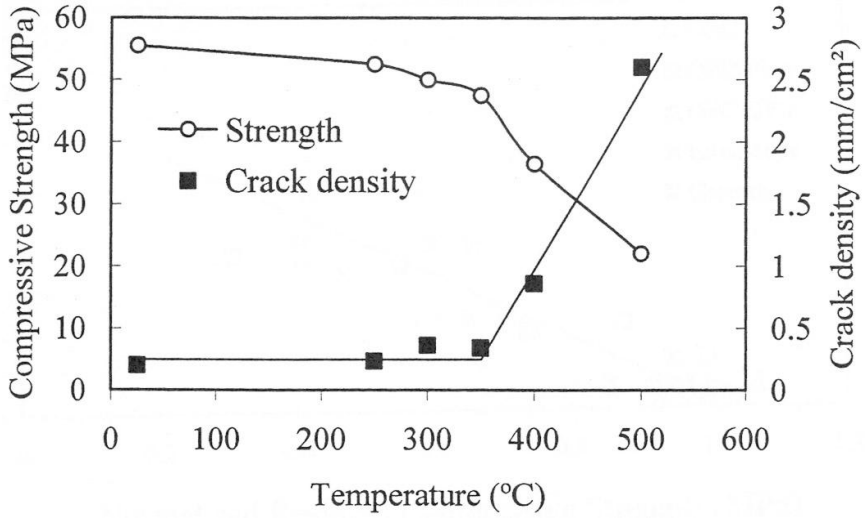

Figure 5.7 Correlation of crack density and residual compressive strength vs temperature.

Source: N. Short and J. Purkiss, "Petrographic Analysis of Fire-Damaged Concrete," *Proceedings of the Workshop Fire Design of Concrete Structures: What now? What next?*, pp. 221-230, Milan University of Technology, Italy, December 2-3, 2004.

Table 5.7 Criteria used to classify the extent of microcracking in concrete

Classification of microcracking	Description of microcracking
Very low	≤ 20% of the cement paste contains more than 5 microcracks/surface unit[1]
Low	20-40% of the cement paste contains more than 5 microcracks/surface unit
Moderate	40-60% of the cement paste contains more than 5 microcracks/surface unit
High	60-80% of the cement paste contains more than 5 microcracks/surface unit
Very high	≥ 80% of the cement paste contains more than 5 microcracks/surface unit

[1]This applies to a specific surface unit area, for example mm^2 or cm^2, as long as the same unit is used throughout the investigation.

Source: T.G. Nijland and J.A. Larbi, "Unraveling the Temperature Distribution in Fire-Damaged Concrete by Means of PFM Microscopy: Outline of Approach and Review of Useful Readings," *HERON* **46**(4), pp. 253-264, 2001.

Without removal of concrete or presence of spalling, assessments of color change in the field can be ineffective in assessing the depth of concrete potentially affected as a result of a thermal excursion where temperature gradients can be large. Utilizing samples removed from the structure in question, modern color measurement systems can be utilized in the laboratory to provide a more detailed and objective inspection of concrete color changes resulting from exposure to elevated temperature [5.17,5.23,5.25].

A simplified approach to colorimetry has been proposed that is based on analysis of a digital camera photograph of a section through the concrete [5.14]. Although it is noted that digital cameras are not that accurate from a colorimetric viewpoint, they are capable of exhibiting color variations from point to point in the same sample. Also as a result of the extensive amount of data available in a single digital image, the mortar and aggregate can be analyzed separately. Color measurement is based on three color-matching functions with each defining a 3-D space (e.g., Commission Internationale de l'Eclairage red-green-blue system). Figure 5.8 presents an example related to digital camera colorimetry evaluation of concrete after exposure to elevated temperature. In Figure 5.8(a) the digital image of a concrete specimen heated to 600˚C is presented. Figure 5.8(b) illustrates the change in chromaticity on heating and for the Mont Blanc tunnel results there is a variation toward the red and yellow directions denoting an increasing temperature. Figure 5.8(c) presents color profiles obtained from four cores removed from a 80-mm-thick panel that had been subjected to a thermal gradient (i.e., > 5˚C/mm). The breakpoint corresponds to the change in color variation profile and when combined with temperature and strength profile results (when available) can indicate the maximum temperature and provide an estimate of residual strength.

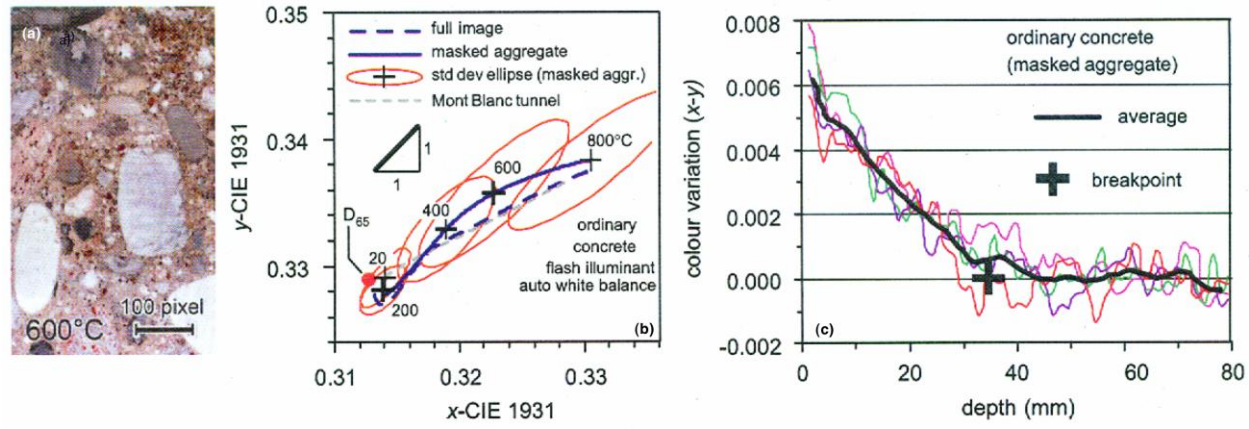

Figure 5.8 Digital camera colorimetry: (a) uniformly heated concrete core, (b) effect of high temperature on chromaticity of ordinary concrete, and (c) color variation profiles with panel depth after exposure to constant thermal gradient.

Source: M. Colombo and R. Felicetti, "New NDT Techniques for the Assessment of Fire-Damaged Concrete Structures," *Fire Safety Journal* **42**, pp. 461-472, 2007.

The fire behavior test (FB Test) has been developed for use in determining the depth of deteriorated concrete in structural elements subjected to fire [5.26]. After removal of concrete cores form the structure, 1.5-cm-thick disks are sliced along the complete length of the core starting from the face that was subjected to the highest temperature (e.g., fire). The disks are then placed into an oven and dried for 24 hours. After drying the disks are permitted to cool to room temperature and weighed to determine the dry weight. The disks are then submerged in water for 48 hours to saturate them, after which the disk's surfaces are dried and the disks reweighed to obtain a saturated weight so that water absorption can be calculated. The disks are then loaded in diametrical compression to obtain a tensile failure stress. Results are used to plot the variation in water absorption and tensile failure stress as a function of depth. Water absorption tends to decrease with depth (or distance from the heated face) until it reaches a constant value. This results because greater porosity and cracking occur at the heated face. Tensile stress also tends to increase with depth until it stabilizes. The lower tensile stress also is the result of the presence of increased porosity and cracking near the heated surface. The interface between deteriorated and sound concrete occurs where the water absorption and tensile stress start to stabilize.

5.5 Summary

Damage to reinforced concrete structural members resulting from thermal loadings can range from cosmetic blemishes to more serious damage (e.g., misalignment and distortions). Heating of concrete can result in a number of changes to its structure that can produce cracking, spalling, debonding of aggregate, expansion, and mineralogical and chemical changes. In the cement paste, evaporation and dissolution, dehydration and dissociation of ettringite, gypsum, calcium hydroxide, calcium carbonate and other phases such as calcium silicate hydrates can occur. Evaluation of a reinforced concrete structure following a thermal excursion is important in order to determine whether the structure is sound structurally or to assess items such as whether the steel reinforcement has been exposed to temperatures high enough to affect its properties. An on-site condition assessment involving a visual inspection is typically the first step in providing information related to the maximum temperature experienced and the suitability of the structure for continued service. Guidance has been developed for conduct of a condition assessment as well as visual classification of concrete fire damage. For concretes containing certain aggregate types (e.g., siliceous), color change can provide important information of the potential structural significance of the fire in that a color change from normal to pink or red will occur in the temperature range of 300˚ to 600˚C which corresponds to the temperature range at which significant loss of concrete strength occurs and steel reinforcement residual strength can decrease. A number of field-testing methods are available for performing a more detailed assessment of the material in-situ (e.g., rebound hammer, impact echo, and ultrasonics). Removal and testing of concrete cores is probably the most effective approach for obtaining detailed information on the mechanical properties and internal condition of the concrete. Petrography is the primary tool for assessing the internal condition of concrete and can be used to determine the depth of damage for reinforced concrete as well as a means to determine whether the damage was caused by thermal exposure or some other mechanism. Petrographic analysis of extracted concrete core samples also can provide information on bond loss between the cement matrix and steel reinforcement, crack orientation and it relationship to the aggregate, microcracking, extent of cement hydration, chemical compositional changes of cementitious material and aggregate, and temperature distribution within a concrete depth. Examples of other potential methods for examining and assessing concrete materials after being subjected to a thermal excursion include crack density determinations, colorimetry using digital cameras, and the fire behavior test.

5.6 References

5.1 D.A. St John, A.W. Poole, and I. Sims, *Concrete Petrography. A Handbook of Investigative Techniques*, 478 pages, Arnold Publishing, London, United Kingdom, 1998.

5.2 T.G. Nijland and J.A. Larbi, "Unraveling the Temperature Distribution in Fire-Damaged Concrete by Means of PFM Microscopy: Outline of Approach and Review of Useful Readings," *HERON* **46**(4), pp. 253-264, 2001.

5.3 *Guide for Evaluation of Concrete Structures before Rehabilitation*, ACI 364.1R-07, American Concrete Institute, Farmington Hills, Michigan, 2007.

5.4 *Guideline for Structural Condition Assessment of Existing Buildings*, SEI/ASCE 11-99, 148 pages, American Society of Civil Engineers, Reston, Virginia, 1999.

5.5 *Assessment and Repair of Fire-Damaged Concrete Structures*, Technical Report No. 33, Concrete Society, Camberley, United Kingdom, 1990.

5.6 "Concrete Structures After Fire," *Concrete Construction* **17**(3), Addison, Illinois, 1972.
5.7 *Assessing the Condition and Repair Alternatives of Fire-Exposed Concrete and Masonry Members*, Report SR332.01B, National Codes and Standards Council of the Concrete and Masonry Industries, Skokie, Illinois, August 1994.
5.8 J. Gales, L.A. Bisby, C. MacDougall, and K. MacLean, "Transient High-Temperature Stress Relaxation of Prestressing Tendons in Unbonded Construction," *Fire Safety Journal* **44**, pp. 570-579, 2009.
5.9 J.P. Ingham, "Assessment of Fire-Damaged Concrete and Masonry Structures: Application of Petrography," *11th Euroseminar on Microscopy Applied to Building Materials*, 16 pages, Porto, Portugal, 5-9 June 2007.
5.10 C.A. Menzel, *Tests of Fire Resistance and Strength of Walls of Concrete Masonry Units*, Portland Cement Association, Skokie, Illinois, 1934.
5.11 K. Willam, Y. Xi, K. Lee, and B. Kim, "Thermal Response Behavior of Reinforced Concrete Structures in Nuclear Power Plants," Department of Civil, Environmental, and Architectural Engineering, University of Colorado, Boulder, 2009.
5.12 B. Erlin, W.G. Hime, and W.H. Kuenning, "Evaluating Fire Damage to Concrete Structures," *Concrete Construction*, Publication #C720154, Aberdeen Group, Addison, Illinois, April 1972.
5.13 *Standard Practice for Petrographic Examination of Hardened Concrete*, ASTM C 856-04, American Society for Testing and Materials, West Conshohocken, Pennsylvania, 2004.
5.14 R. Felicetti, "Digital Camera Colorimetry for the Assessment of Fire-Damaged Concrete," *Proceedings of the Workshop Fire Design of Concrete Structures: What now? What next?*, pp. 211-220, Milan University of Technology, Italy, December 2-3, 2004.
5.15 R.K. Schroeder, *Post-Fire Analysis of Construction Materials*, PhD Thesis, University of California, Berkeley, 1999.
5.16 W-T. Chang, Y-S. Giang, C-T. Wang, and C-W. Huang, "Concrete at High Temperatures Above 1000˚C," *1993 International Carnahan Conference on Security Technology*, Institute of Electrical and Electronics Engineers, Ottawa, Ontario, Canada, October 1993.
5.17 N.R. Short, J.A. Purkiss and S.E. Guise, "Assessment of Fire Damaged Concrete Using Colour Image Analysis," *Construction and Building Materials* 15**(**1), pp. 9-15, February 2001.
5.18 *Handbook of Nondestructive Testing of Concrete*, V.M. Malhotra and N. J. Carino Editors, CRC Press, Boca Raton, Florida, 1991
5.19 D.J. Naus, *Inspection of Nuclear Power Plant Structures – Overview of Methods and Related Applications*, ORNL/TM-2007/191, Oak Ridge National Laboratory, Oak Ridge, Tennessee, May 2009.
5.20 M. Colombo and R. Felicetti, "New NDT Techniques for the Assessment of Fire-Damaged Concrete Structures," *Fire Safety Journal* **42**, pp. 461-472, 2007.
5.21 R. Felicetti, "The Drilling-Resistance Test for Assessment of Thermal Damage in Concrete," *Proceedings of the Workshop Fire Design of Concrete Structures: What now? What next?*, pp. 241-248, Milan University of Technology, Italy, December 2-3, 2004.
5.22 A. Di Maio, G. Giaccio, and R. Zerbino, "Non-Destructive Tests for the Evaluation of Concrete Exposed to High Temperature," *Cement, Concrete, and Aggregates* **24**(2), pp.1-10, 2002.
5.23 N. Short and J. Purkiss, "Petrographic Analysis of Fire-Damaged Concrete," *Proceedings of the Workshop Fire Design of Concrete Structures: What now? What next?*, pp. 221-230, Milan University of Technology, Italy, December 2-3, 2004.
5.24 H.N. Walker, D.S. Lane, and P.E. Stutzman, *Petrographic Methods of Examining Hardened Concrete: A Petrographic Manual*, FHWA-HRT-04-150, Federal Highway Administration, U.S. Department of Transportation, McLean, Virginia, July 2006.
5.25 N. Yüzer, F. Aköz, L.D. Öztürk, "Compressive Strength-Color Change Relation in Mortars at High Temperature," *Cement and Concrete Research* **34**, pp. 1803-1807, 2004.
5.26 J.R. dos Santos, F.A. Branco, and J. de Brito, "Assessment of Concrete Structures Subjected to Fire – The FB Test," *Magazine of Concrete Research* **54**(3), pp. 203-208, June 2002.

6 SUMMARY AND CONCLUSIONS

6.1 Summary

Under normal conditions most concrete structures are subjected to a range of temperature no more severe than that imposed by ambient environmental conditions. However, there are important cases where these structures may be exposed to much higher temperatures (e.g., jet aircraft engine blasts, building fires, chemical and metallurgical industrial applications in which the concrete is in close proximity to furnaces, and some nuclear power-related postulated accident conditions). Of primary interest in the present study is the behavior of reinforced concrete elements in designs of new generation reactor concepts in which the concrete may be exposed to long-term steady-state temperatures in excess of the present ASME Code limit of 65°C. Secondary interests include performance of concrete associated with radioactive waste storage and disposal facilities, and postulated design-basis accident conditions involving unscheduled thermal excursions. Under such applications the effect of elevated temperature on certain mechanical and physical properties may determine whether the concrete will maintain its structural integrity.

Concrete's properties are more complex than for most materials because not only is the concrete a composite material whose constituents have different properties, but its properties also depend on moisture and porosity. Exposure of concrete to elevated temperature affects its mechanical and physical properties. Elements could distort and displace, and, under certain conditions, the concrete surfaces could spall due to the build up of steam pressure. Because thermally induced dimensional changes, loss of structural integrity, and release of moisture and gases resulting from the migration of free water could adversely affect plant operations and safety, a complete understanding of the behavior of concrete under long-term elevated-temperature exposure as well as both during and after a thermal excursion resulting from a postulated design-basis accident condition is essential for reliable design evaluations and assessments. Because the properties of concrete change with respect to time and the environment to which it is exposed, an assessment of the effects of concrete aging is also important in performing safety evaluations.

The objective of this study was to provide a compilation of data and information on the effects of elevated temperature on concrete materials. The effect of elevated temperature exposure on the general behavior of Portland cement pastes including supplementary cementitious materials, aggregate materials, and the bond between cement paste and aggregate is discussed. Data and information is provided on the influence of elevated temperature on the mechanical and physical properties of concrete materials. Mechanical characteristics addressed include: stress and strain characteristics, Poisson's ratio, modulus of elasticity, compressive strength, thermal cycling, tensile strength, shrinkage and creep, concrete-steel reinforcement bond strength, fracture energy and fracture toughness, long-term exposure, radiation shielding effectiveness, and multiaxial conditions. Physical characteristics discussed include: porosity and density, coefficient of thermal expansion, thermal conductivity, thermal diffusivity, specific heat, heat ablation and erosion rates, moisture diffusion, and simulated hot spots. Heavyweight concretes are described and results on the effect of elevated temperature on their properties and shielding effectiveness presented. Examples of design codes and standards that address concrete under elevated temperature applications are identified and described. Methods that can be utilized in assessments of concrete that has been exposed to high temperature are discussed.

6.2 Conclusions

A substantial body of knowledge on the material properties of ordinary Portland cement concretes at elevated temperature is available. The use of these data for a quantitative interpretation of the response of reinforced concrete structural elements in nuclear power plants to long-term moderate elevated-temperature exposure (≥65°C) or design basis and hypothetical severe accident conditions needs to be carefully evaluated. In many of these elevated-temperature tests, neither representative materials nor representative environmental conditions were modeled: (1) samples were tested hot or cold, (2) moisture migration was either free or totally restricted, (3) concrete was either loaded or unloaded while heated, (4) concrete constituents and proportions varied from mix to mix, (5) test specimen size was not consistent, (6) specimens were tested at different degrees of hydration and moisture contents, and (7) heat up rates and thermal stabilization periods varied.

Based on information presented in the report, several observations can be made relative to the behavior of Portland cement concrete materials at elevated temperature:

General Behavior

- Deterioration of concrete's mechanical properties can be attributed to three material factors: (1) physicochemical changes in the cement paste, (2) physicochemical changes in the aggregate, and (3) thermal incompatibility between the aggregate and the cement paste. Concrete properties are influenced by environmental factors such as temperature level, heating rate, applied loading, and external sealing influencing moisture loss.
- Key material features of Portland cement paste that influence properties of concrete at high temperature are its moisture state (i.e., sealed or unsealed), chemical structure (i.e., loss of chemically-combined water from C-S-H in unsealed condition, CaO/SiO_2 ratio of hydrate in sealed condition, and amount $Ca(OH)_2$ crystals in sealed and unsealed condition), and physical structure (i.e., total pore volume, average pore size, and amorphous/crystalline structure of solid).
- Microcracking is a major cause of deterioration when concretes are exposed to high temperatures and is reported to initiate around calcium hydroxide crystals and then around unhydrated cement particles.
- The aggregate-cement paste bond region has been shown to be the weakest link because it is normally weaker that the cement paste which is normally weaker than the aggregate. If the aggregate-cement paste bond fails on heating, chemically, or as a result of thermal incompatibility between the aggregate and cement paste, the concrete will exhibit a significant reduction in strength, even if both the aggregate and surrounding mortar matrix remain intact.
- Aggregate characteristics of importance to behavior of concrete at elevated temperature include physical properties (e.g., thermal conductivity and thermal expansion), chemical properties (e.g., chemical stability at temperature), and thermal stability/integrity.
- Normally aggregates are more stable at elevated temperature than the hardened cement paste when exposed to high temperatures, although decomposition of some less thermally stable aggregates may occur when exposure temperatures are extremely high. Lightweight aggregates exhibit little thermal expansion and therefore little damage to concrete while having small thermal conductivity. It has been noted that the thermal stability of aggregates increases in order of gravel, limestone, basalt, and lightweight.
- In general, for structural applications involving service temperatures in the range of ambient to 300°C or 400°C, provided many temperature cycles of large magnitude are not present, Portland cement concretes are the best materials if heat-resistant aggregates (basalt, limestone, or serpentine) are used. 400˚C appears to be a critical temperature for Portland cement concretes above which concretes would disintegrate on subsequent post-cooling to ambient conditions. Cracking of heated concrete during post-cooling can be ascribed to the rehydration of dissociated calcium hydroxide resulting in a 44% volume increase. Reduced calcium hydroxide in cement paste due to presence of pulverized fly ash that can consume the calcium hydroxide can reduce cracking. At higher temperatures or for prolonged exposure to temperatures around 600°C, special procedures would have to be considered such as removal of the evaporable water by moderate heating.

Mechanical Properties

<u>Stress-Strain Behavior</u>

- Relative to temperature effects on concrete's stress-strain curve, several general observations can be made. The ascending branch of the stress-strain curve consists of three components: (1) an elastic recoverable strain that is temperature dependent and is strongly influenced by the load level during initial heating to the test temperature; (2) an irrecoverable plastic strain component; and (3) a time-dependent creep component that is normally small at room temperature but can be significant at high temperatures, particularly above 550˚C.
- Under steady-state conditions, the original concrete strength, water-cement ratio, heating rate, and type of cement have minor influence on the stress-strain behavior. Aggregate-cement ratio, aggregate type, and presence of a sustained load during heating affect the shape of the stress-strain curve. Harder aggregates

(siliceous, basaltic) exhibit a steeper decrease of initial slope due to elevated temperatures than softer aggregates (lightweight). Other parameters that affect the stress-strain relationship at elevated temperature are the moisture condition and the number of thermal cycles.

- Aggregate type has an effect on ultimate strain under high temperature conditions (i.e., carbonate aggregate concrete strain at peak strength was up to 40% greater than that for siliceous aggregate concrete). Siliceous aggregates expand the most and give the largest damage, and are further damaged on cooling.
- As the temperature increases the ultimate strain increases and the stiffness decreases. Specimens tested at temperature are stiffer than specimens permitted to cool to room temperature prior to testing; type of cement and duration of thermal treatment have a minor effect on slope of stress-strain curve. Compressive peak strain increases almost linearly with temperature. Peak strain after exposure (residual) is higher than peak strain measured at temperature and is greater for concrete cooled rapidly with water than cooled slowly by air.
- Unsealed specimens are stiffer than sealed specimens but strains at ultimate are reduced.
- Mineral additions can improve the elevated temperature stress-strain performance of concrete.
- The mechanical strains in biaxial compression loading were found to be dependent on the stress level, the stress ratio, and the test temperature. When concrete is under a biaxial tension-compression state of stress the capability of concrete to resist cracking is diminished, both the tensile and compressive strengths are found to decrease rapidly with increasing exposure temperature, and the concrete fails abruptly due to tensile stress.

Poisson's Ratio

- Poisson's ratio data at elevated temperature are limited and tend to be inconsistent.
- Poisson's ratio values tend to increase with increasing moisture content at high temperatures and Poisson's ratio values after drying are less than before drying.
- When the specimen is permitted to cool after a given change in state due to heating ($T<400^{\circ}C$), the variation of Poisson's ratio with temperature is slight and negligible when evaporable water has been removed.
- The first few thermal cycles tend to decrease the Poisson's ratio the most with the number of thermal cycles to reach a minimum value decreasing as the concrete strength increases. Poisson's ratio tends to return to the room temperature value with an increase in number of thermal cycles.

Modulus of Elasticity

- Elastic modulus decreases with elevated temperature exposure due to breakage of bonds in the cement paste microstructure with the reduction in modulus increasing as the heating rate increases. Variation of modulus values at temperatures up to 80˚C is considerable, primarily as a result of use of different aggregate materials, and above 100˚C the decrease is linear with increasing temperature up to a critical temperature at which concrete experiences deterioration.
- Type of aggregate has strong influence on modulus with lightweight concrete exhibiting the lowest decrease with temperature and siliceous aggregate concrete the highest. Aggregates that are more compatible with the cement paste and chemically stable provide lower loss of modulus. Concrete containing aggregates with low thermal expansion experience a greater reduction in modulus than those with a higher thermal expansion.
- Modulus after high temperature exposure (residual) is lower than that obtained at temperature.
- Normal strength concretes ($f_c' < 60$ MPa) retain their modulus better at temperature than high strength concretes.
- Sealed (mass concrete) specimen modulus values tend to be more sensitive to elevated temperature than specimens that are unsealed.
- The presence of a preload improves the modulus retention under high temperature exposure.
- The method of cooling after elevated temperature exposure affects the residual modulus of elasticity with rapid cooling (water quenching) producing the lowest values of residual modulus.

Compressive Strength

- Considerable data scatter exists for relative compressive strength (unsealed, hot testing), particularly at the lower exposure temperatures, due to different materials and testing conditions utilized (e.g., constituents and mixture proportions, specimen size and shape, specimens tested at different degrees of hydration and initial moisture contents, and heating rates and thermal stabilization periods). Considerable data scatter

also exists for residual compressive strength (unsealed, cold testing), particularly at lower temperatures due to differences in material and environmental factors.

- Original concrete strength of normal strength concrete, type of cement, aggregate size, heating rate, and water-cement ratio appear to have a minor effect on the relative concrete strength at elevated temperature.
- Type of aggregate appears to be one of main factors influencing concrete compressive strength at high temperature with siliceous aggregate concrete having lower strengths (by percentage) at high temperature than calcareous and lightweight aggregate concretes.
- Concrete in the temperature range of 20°C to 200°C can show a small strength loss. Between 22˚ and 120°C any strength loss that occurs is attributed to the thermal swelling of the physically bound water, that causes disjoint pressures. A regain of strength is often observed between 120°C and 300°C and is attributed to greater van der Waals forces as a result of the cement gel layers moving closer to each other during heating. Between 200°C and 250°C the residual compressive strength is nearly constant. Beyond 350°C there can be a rapid decrease in strength.
- Strength losses for unstressed concretes up to about 300˚C are generally $\leq$ 20% irrespective of type of cement or aggregate. At temperatures > 300˚C strength losses can become relatively great and at temperatures > 450˚C concrete compressive strength drops significantly due to differences in thermal expansion coefficients between aggregate and cement paste (i.e., loss of bond) and decomposition of calcium hydroxide.
- The presence of preload, within reasonable limits, improves retention of compressive strength at elevated temperature for both Portland cement concretes and Portland cement concretes containing supplementary cementitious materials. Although data are limited, a similar conclusion can apparently be derived with respect to residual compressive strength retention. Improved performance has been attributed to densification of the cement paste resulting in a large transient creep component and possibly a reduction in porosity relative to the unloaded state, and precompression can reduce the tensile stresses in the concrete, particularly during cooling.
- Moisture content at time of testing has a significant effect on the strength of concrete at elevated temperature with strength of unsealed concrete being higher than strength of sealed concrete.
- Factors that contribute to the general trend for concrete compressive strength to decrease with increasing temperature are: aggregate damage; weakening of the cement paste-aggregate bond; and weakening of the cement paste due to an increase in porosity on dehydration, partial breakdown of the C-S-H, chemical transformation on hydrothermal reactions, and development of cracking.
- Concrete containing fly ash can exhibit an increase in strength in the temperature range of 121˚ to 149˚C due to the formation of tobermorite which has been reported to be two to three times stronger than C-S-H gel. Although limited, results for concretes containing supplementary cementitious materials indicate that the residual compressive strength retention is highest for concretes containing slag and fly ash, followed by concrete containing metakaoline, with silica fume exhibiting the lowest residual compressive strength at the higher temperatures.
- The higher the cement content the greater the loss in strength. Strength loss in saturated normal strength concrete is greater than dry concrete and higher moisture contents contribute to increased spalling of concrete during significant thermal gradients such as could occur under fire conditions.
- Concrete that is rapidly cooled form elevated temperature (e.g., water quenching) exhibits a lower residual compressive strength than specimens that are gradually cooled from elevated temperature prior to testing. The effect of rapid cooling seems to decrease somewhat at high temperatures, however, the residual compressive strength already has been severely reduced by exposure to these temperatures.
- Concrete containing lightweight/thermally stable aggregates exhibit greater retention of compressive strength at temperature (relative) than those permitted to cool to room temperature (residual) prior to testing.
- Residual and relative compressive strengths of fibrous concretes at temperatures above 200˚C both exhibit a trend for a linear decrease in strength with increasing temperature.

Thermal Cycling

- Thermal cycling, even at relatively low temperatures (e.g., 65˚C) can have a degrading effect on concrete's mechanical properties. Compressive strength, tensile strength, and bond strength to steel reinforcement decrease under thermal cycling.
- The largest percentage decrease in properties for thermal cycling at higher temperatures (e.g., 200˚ to 300˚C) occurs during the first thermal cycle with the extent of damage dependent on the aggregate type and

is associated with loss of bond between the aggregate and cement paste matrix.

Tensile Strength

- Aggregate type and mixture proportions have a significant effect on the tensile strength vs temperature relationship of concrete.
- The effect of elevated temperature on the tensile strength of concrete shows a similar trend to its effect on compressive strength, but tensile strength is more sensitive to deterioration at elevated temperature.
- The decrease in tensile strength of calcareous aggregate concrete with temperature is greater than that of siliceous aggregate concrete at 500˚C, being about twice as much at this temperature.
- Concretes with lower cement contents have lower reduction in tensile strength than those with higher cement contents.
- At relative low temperatures (T < 175˚C) sealed specimens seem to exhibit improved retention of splitting-tensile strength relative to results obtained from unsealed specimens.
- The rate of heating has minimal effect on the tensile strength at high temperature.
- Residual tensile strength (cold testing) is somewhat lower than the tensile strength determined at temperature (hot testing).
- Quenching specimens in water after exposure to high temperatures produces a significant decrease in flexural and splitting-tensile strengths (as well as compressive strength), with the decrease increasing as the maximum exposure temperature increased.

Shrinkage and Creep

- Shrinkage occurs as a result of drying or autogeneous volume change, with drying shrinkage being dominant, resulting from the loss of absorbed water, and increasing with increasing temperature. Autogeneous shrinkage results from continued cement hydration and is more prevalent in mass concrete structures where the total moisture content remains relatively constant.
- Shrinkage at temperatures < 100˚C is not considered to be a significant factor in mass concrete structures over their nominal 30- to 40-year design life.
- Creep of unsealed specimens is less than creep of sealed specimens.
- Creep decreases with increasing concrete maturity and increases with increasing moisture content of the specimen at loading.
- Creep increases as the temperature increases, probably for temperatures at least up to 150˚C. Below 100˚C concrete creep at moderate stress levels originates in the cement paste as a result of the mutual approach of adjacent laminar particles of the cement gel.
- For unsealed specimens the influence of drying becomes significant in the temperature range of 70˚ to 100˚C. At moderate temperature levels hydration accelerates, but as the temperature increases the reverse of this effect takes place as dehydration accelerates creep. Above 100˚C drying of concrete is very rapid with an associated increase in creep rate until a stable moisture condition is reached. After moisture is lost and a stable moisture content at a given temperature is reached, the creep rate becomes less than that before loss of moisture.
- Creep recovery is less than associated creep strain and the degree of creep recovery seems to be independent of temperature but dependent on stress.

Concrete-Steel Reinforcement Bond Strength

- The bond strength between concrete and steel decreases as the temperature increases with the relative reduction in bond strength at elevated temperature being greater than that for the concrete compressive strength.
- Time at temperature affects the bond strength and the bond strength at temperature is higher than residual bond strength.
- Ribbed steel reinforcement bars retain residual bond strength at elevated temperature better than round steel bars. Diameter of ribbed steel reinforcement does not appear to have a significant affect on bond strength.
- The type of aggregate is one of the main factors affecting the elevated temperature bond strength, with the lower the thermal strain of concrete the higher the bond strength.
- Sealed specimens retain bond strength at elevated temperature better than unsealed specimens and prolonged heating at moderate elevated temperatures (T < 175˚C) provides a positive effect on bond strength of sealed specimens.
- Load cycling produces a decrease in maximum bond stress.

- Reduction in bond stress appears to be greater for concretes in which >10% (by weight) of the Portland cement has been replaced by a natural pozzolanic material.
- Incorporation of random discontinuous fiber reinforcement into the concrete mix can improve residual bond strength at elevated temperature by increasing confinement of the steel reinforcement (e.g., reduce concrete cracking and spalling tendencies).

Fracture Energy and Fracture Toughness

- Residual fracture energy of normal- and high-strength concretes can exhibit an increase at temperatures up to about 300˚C or 400˚C due to cement hydration before it decreases with increasing temperature as a result of microcracking and cement dehydration
- Residual fracture toughness decreases with increasing temperature with the decrease being relatively significant at temperatures > 50˚C.
- Heating cycles produce a decrease in fracture toughness with the amount of decrease becoming more significant at temperatures greater than 300˚C.

Long-Term Exposure (Aging)

- Results for exposure of concrete to elevated temperature for relatively long periods of time are limited.
- For moderate exposure periods (e.g., $\leq$ 180 days) and temperatures (e.g., T $\leq$ 232˚C), the concrete compressive strength and modulus of elasticity of sealed specimens tended to decrease with increasing exposure time and temperature, while specimens that were not sealed exhibited an improvement of or very slight reduction in compressive strength and improved retention of the modulus of elasticity relative to sealed specimens. The decreased performance of the sealed specimens was attributed to deterioration in the structural properties of the cement gel resulting from the saturated steam pressure at high temperatures. Modulus of elasticity was affected more than compressive strength as a result of extended exposure at elevated temperature.
- In general, most of the loss of concrete's mechanical properties under elevated temperature exposure for extended exposure periods will occur during the first two or three months exposure for unsealed conditions and at longer periods for sealed conditions as the moisture condition stabilizes (e.g., one to two years).
- There is an indication that partial replacement of Portland cement with fly ash or blast furnace slag imparts improved performance at elevated temperature.

Radiation Shielding Effectiveness

- Drying resulting from elevated temperature exposure reduces the shielding (attenuation) effectiveness of concrete as a result of cracking or reduction in hydrogen content.
- For neutron shields maximum recommended internal and ambient concrete temperatures are 88˚ and 71˚C, respectively, and for gamma shields the corresponding recommended maximum concrete temperatures are 177˚ and 149˚C, respectively.

Multiaxial Conditions

- The platen-interface constraint influences the results for multiaxial loadings (i.e., strength increases as constraint increases).
- Under biaxial compression loading the strength of concrete decreases with increasing temperature with the maximum aggregate size having a significant effect on behavior while the aggregate content and water-cement ratio have a lesser effect.
- Differences between uniaxial and biaxial concrete strength increased as the temperature increased.

Physical Properties and Thermal Effects

Porosity and Density

- As the temperature increases the porosity and average pore size of the concrete increases thus reducing the cement bulk mass density.
- Aggregate type plays an important role in the change in concrete density with increasing temperature (e.g., thermal dilation and dissociation).

Coefficient of Thermal Expansion

- Concrete thermal expansion is a non-linear function of temperature with aggregate type and coarse aggregate volume fraction being the primary factors influencing its value. The coefficient of thermal expansion of concrete increases with temperature even though the cement paste contracts because the aggregate dominates and increases as the temperature increases.
- Moisture content, water-cement ratio, and type of cement only affect the coefficient of thermal expansion at relatively low temperatures (e.g., $T < 200^{\circ}C$).
- Considerable differences exist relative to expansion of aggregate materials with aggregates having the highest percentage of silica by weight exhibiting the largest expansion. Lightweight aggregate materials have lower thermal expansion than naturally-occurring aggregate materials and can show residual contraction after heating.
- Thermal expansion on subsequent cooling is not fully reversible due to irreversible chemical changes and changes in microstructure.
- The presence of load reduces the thermal expansion of concrete with increasing temperature.

Thermal Conductivity

- Primary factors that affect concrete thermal conductivity are moisture content, hardened cement paste, pore volume and distribution, and amount and type of aggregate material. The amount and type of coarse aggregate used have the most influence, however, because aggregates normally occupy 60 to 80% the concrete volume.
- Thermal conductivities of highly crystalline aggregate concretes decrease with increasing temperature up to $1000^{\circ}C$, while amorphous aggregate concretes have thermal conductivity values that are relatively constant.
- In general, at temperatures up to $100^{\circ}C$ the thermal conductivity seems to increase with temperature; at temperatures greater than $100^{\circ}C$ the conductivity decreases; at 300° to $400^{\circ}C$ there is a further decrease as increased cracking occurs; at temperatures greater than $600^{\circ}C$ the thermal conductivity increases slightly; and at temperatures greater than $800^{\circ}C$ up to melting there is only a small change in thermal conductivity.
- Lightweight aggregate concrete's have lower thermal conductivity values because of their porosity and the thermal conductivity is relatively constant or increases slightly for temperatures up to $1000^{\circ}C$.

Thermal Diffusivity

- Thermal diffusivity of concrete is determined by the thermal properties of its constituents and at normal temperatures is mainly governed by the aggregate diffusivity.
- Concrete thermal diffusivity decreases fairly rapidly with an increase in temperature ($T < \sim 200^{\circ}C$) and exhibits a trend to stabilize at high temperatures ($T > 600^{\circ}C$).

Specific Heat

- At room temperature the aggregate type, mix proportions, and age do not have a great effect on the specific heat of concrete, but the moisture content in the concrete at lower temperatures does have an effect.
- Specific heat of concrete increases with increasing temperature and at high temperatures is sensitive to transformations that take place (e.g., water vaporization, dissociation of $Ca(OH)_2$, quartz transformation in aggregates).

Heat of Ablation and Erosion Rates

- Heat of ablation is of interest for hypothetical core disruptive accidents involving a core melt relative to how much energy is dissipated by the concrete structures that are designed to contain the core melt.
- Erosion rate refers to the velocity at which concrete subjected to high temperatures is decomposed by mechanical disintegration and by the melting process.
- For a heat flow between 20 and 200 $W \bullet cm^2$ the heat of ablation of concrete has been estimated to be in the range of 1474 to 6000 $kJ \bullet kg^{-1}$.
- The amount of heat required to transform a given volume of concrete to a molten state is about twice as much for limestone aggregate as for quartzitic aggregate concrete due to the additional heat required to decarbonate the limestone aggregate.
- Erosion rates determined experimentally for limestone, quartzitic, and basalt aggregate concretes are about 20 to 66, 30 to 44, and 10 to 22 mm/min, respectively.

Moisture Diffusion and Pore Pressure

- Heating of concrete can produce large pore pressures that are functions of temperature, temperature history, and size of specimen.
- Transfer of free moisture in concrete can affect the concrete strength, thermal expansion, shrinkage, and creep, as well as potentially affect the concrete durability and radiation shielding capability.
- Under normal operating conditions in a nuclear plant (i.e., $T \leq 65^{\circ}C$) moisture migration in mass concrete structures is a very slow process and drying is not likely to be an important factor in thick-section concrete structures.
- Limited data on moisture distribution in a nuclear power plant containment wall indicates that even after 30 years the walls were still drying, with the drying being extremely slow due to the large thickness and one-sided drying; drying was different in different parts of the containment due to different temperature levels and climatic conditions, and the concrete continued to mature because moisture conditions in the inner parts of the wall permitted further cement hydration.
- In unsealed specimens diffusion and eventual drying leads to lower pore pressures than obtained for sealed specimens at the same temperature level.
- Pore pressures in concrete do not increase significantly until the concrete temperature reaches about $105^{\circ}C$.

Simulated Hot Spot Tests

- Results of tests designed to simulate hot spots that could develop in the vicinity of hot penetrations of a localized failure of a liner cooling system indicate that the effect is localized, some loss of concrete strength would occur, but not significant enough to affect structural integrity, and pressure build up behind a liner may not be significant due to pressure relief along the liner-concrete interface.

Radiation Shielding Concretes

- Thermal cycling can reduce the compressive strength, modulus of rupture, and static modulus of elasticity of radiation shielding concretes.
- Specimens loaded while heated retain their residual compressive strength better than specimens that were not loaded during thermal treatment.
- Concrete density decreases with increasing temperature as evaporable water is removed, with the value becoming relatively stable after evaporable water is lost.
- The impact of elevated temperature on the water content of a shielding concrete has a significant effect on its nuclear properties, in particular its neutron radiation attenuation. As temperature increases the neutron flux density transmitted through concrete increases for a given section thickness.
- The intensity of radiation transmitted through cracked (collinear) concrete increases as the crack width increases and specimen thickness decreases.

Codes and Standards

- Codes and standards for concrete technology recognize that concrete strength tends to decrease with increasing temperature. Consequently, current design procedures specify concrete temperature limits to ensure predictable concrete behavior.
- Analytical models for accurately predicting the response of a structure to thermal loadings for practical design considerations, where thermal environments exceed the limits contained in the code, are very complex. As a result, most existing methods utilize various types and degrees of simplification that affect the accuracy of results. Current designs for nuclear structures cover these shortcomings by appropriate conservatism in designs.
- When design conditions exceed established temperature limits, experimental investigations for characteristic mechanical and physical properties data and for design verification may be required to avoid undue and impractical conservatism in design.

Methods for Assessment of Concrete Exposed to High Temperatures

- Damage to concrete structural members resulting from thermal loadings can range from cosmetic blemishes to more serious damage (e.g., misalignments and distortions).

- Evaluation of a reinforced concrete structure following a thermal excursion is important in order to determine whether the structure is structurally sound or to assess items such as whether the steel reinforcement has been exposed to temperatures high enough to affect its properties.
- For concretes containing certain aggregate types (e.g., siliceous), color change can provide important information on the potential structural significance of a thermal excursion (i.e., peak temperature reached).
- A number of field testing methods (e.g., rebound hammer, impact echo, and ultrasonics) are available for performing assessments of reinforced concrete structures after being subjected to thermal excursions.
- Removal and testing (e.g., compressive strength and petrography) of concrete cores is probably the most effective approach for obtaining detailed information on the mechanical properties and internal condition of the concrete (e.g., depth affected and cause of damage).
- Other methods having potential for assessing concrete materials after being subjected to a thermal excursion include crack density determinations, colorimetry using digital cameras, fire behavior test, and drilling resistance test.

APPENDIX A – REFERENCES NOTED IN DATA PLOTS AND CITED IN FIGURES OR TABLES

A.1 References Noted in Data Plots

Data Sheet #	Reference
1.	T. Suzuki, M. Tabuchi, and K.Nagao, "Study on the Degradation of Concrete Characteristics in the High Temperature Environment," *Concrete Under Severe Conditions: Environment and Loading*, Vol. 2, pp. 1119–1128, E & FN Spon Publishers, 1995.
2.	D. Campbell-Allen and P. M. Desai, "The Influence of Aggregate on the Behavior of Concrete at Elevated Temperature," *Nuclear Engineering and Design* **6**(1), pp. 65–77, August 1967.
3.	J. C. Saeman and G. W. Washa, "Variation of Mortar and Concrete Properties with Temperature," *J. American Concrete Institute* **29**(5), pp. 385–395, 1957.
4.	C.R. Cruz, "Elastic Properties of Concrete at High Temperatures," Department Bulletin 191, *Journal of the Portland Cement Association Research and Development Laboratories* 8(1), pp. 37-45, January 1966.
5.	J. Xiao and G. König, "Study of Concrete at High Temperature in China—An Overview," *Fire Safety Journal* 39, pp. 89–103, 2004.
6.	G.G. Carette, K.E. Painter, and V.M. Malhotra, "Sustained High Temperature Effects on Concretes Made with Normal Portland Cement, Normal Portland Cement and Slag, or Normal Portland Cement and Fly Ash," *Concrete International* **4**(7), 41–51 (July 1982).
7.	J. Guo and P. Waldron, "Deterioration of PCPV Concrete," *Nuclear Engineering and Design* **198**, pp. 211-226, 2000.
8.	T. Yagashita, K. Shirai, C. Ito, and H. Shiojiri, "Effect of Strain Rate on Concrete Strength Under High Temperature," *International Conference on Structures Under Shock & Impact VI*, pp. 539-548, Cambridge, United Kingdom, WIT Press, July 2000.
9.	I. Hager and P. Pimienta, "Mechanical Properties of HPC at High Temperature," *Proceedings of the Workshop - Fire Design of Concrete Structures: What now? What Next?*, pp. 95-100, Milan, Italy, December 2-3, 2004.
10.	P.J.E. Sullivan, "Chapter 1, The Effects of Temperature on Concrete," in *Developments in Concrete Technology -1*, Applied Science Publishers, Ltd., London, 1979.
11.	H. Tanyildizi and A. Coskun, "Performance of Lightweight Concrete with Silica Fume After High Temperature," *Construction and Building Materials* **22**, pp. 2124-2129, 2008.
12.	E. Tolentino, F.S. Lameiras, A.M. Gomes, C.A.R. de Silva, and W.L. Vasconcelos, "Effects of High Temperature on the Residual Performance of Portland Cement Concretes," *Materials Research* **5**(3), pp. 301-307, July/September 2002.
13.	E. Sancak, Y.D. Sari, and O. Simsek, "Effects of Elevated Temperature on Compressive Strength and Weight Loss of the Light-Weight Concrete with Silica Fume and Superplasticizer," *Cement and Concrete Composites* **30**(8), pp. 715-721, 2008.
14.	C-S. Poon, S. Azhar, M. Anson, Y-L. Wong, "Performance of Metakaolin Concrete at Elevated Temperature," *Cement and Concrete Composites* **25**, pp. 83-89, 2003.
15.	S.K. Handoo, S. Agarwal, and S.K. Agarwall, "Physiochemical, Mineralogical, and Morphological Characteristics of Concrete Exposed to Elevated Temperatures," *Cement and Concrete Research* **32**, pp. 1009-1018, 2002.
16.	G.T.G. Mohamedbhai, "Effect of Exposure Time and Rates of Heating and Cooling on Residual Strength of Heated Concrete," *Magazine of Concrete Research* **38**(136), pp. 151-158, September 1986.
17.	A.N. Noumowe and C. Galle, "Study of High Strength Concretes at Raised Temperatures up to 200˚C: Thermal Gradient and Mechanical Behaviour," *Transactions of 16th International Conference on Structural Mechanics in Reactor Technology*, Paper #1580, Washington, DC, August 2001.
18.	A.N. Noumowe, P. Clastres, G. Debocki, and J.-L. Costaz, "Transient Heating Effect on High Strength Concrete, " *Nuclear Engineering and Design* **166**, pp. 99-108, 1996.
19.	G.C. Hoff, A. Bilodeau, and V.M. Malhotra, "Elevated Temperature Effects on HSC Residual Strength," *Concrete International* 2**2**(4), pp. 41-47, April 2000.
20.	M. Li, C.X. Quian, and W. Sun, "Mechanical Properties of High-Strength Concrete After Fire," *Cement and Concrete Research* **34**, pp. 1001-1005, 2004.

21. Y.N. Chan, G.F. Peng, and M. Anson, "Residual Strength and Pore Structure of High-Strength Concrete and Normal Strength Concrete After Exposure to High Temperatures," *Cement and Concrete Research* **21**, pp. 23-27, 1999.
22. R.S. Ravindrarajah, R. Lopez, and H. Reslan, "Effect of Elevated Temperature on the Properties of High-Strength Concrete Containing Cement Supplementary Materials," *9th International Conference on Durability of Building Materials and Components*, Brisbane, Australia, March 17-20, 2002.
23. B. Zhang, N. Bicanic, C.J. Pearce, and D.V. Phillips, "Relationship Between Brittleness and Moisture Loss of Concrete Exposed to High Temperatures," *Cement and Concrete Research* **32**, pp. 363-371, 2002.
24. C-S. Poon, S. Azhar, M. Anson, and Y-L Wong, "Comparison of the Strength and Durability Performance of Normal- and High-Strength Pozzolanic Concretes at Elevated Temperatures," *Cement and Concrete Research* **31**, pp. 1291-1300, 2001.
25. K.W. Nasser and H.M. Marzouk, "Properties of Mass Concrete Containing Fly Ash at High Temperatures," Title 76-25, *ACI Journal* 7**6**(4), pp. 537-550, April 1979.
26. M. Husem, "The Effects of High Temperature on Compressive and Flexural Strengths of Ordinary and High-Performance Concrete," *Fire Safety Journal* **41**, pp. 55-163, 2006.
27. M.S. Abrams, *Behavior of Inorganic Materials in Fire*, Research and Development Bulletin RD067.01M, Portland Cement Association, Skokie, IL, 1979.
28. J. Papayianni and T. Valiasis, "Residual Mechanical Properties of Heated Concrete Incorporating Different Pozzolanic Materials," *Materials and Structures* **24**, pp. 115-121, 1991.
29. Y. Xu, Y.L. Wong, C.S. Poon, and M. Anson, "Impact of High Temperature on PFA Concrete," *Cement and Concrete Research* **31**, pp. 1065-1073, 2001.
30. C. Castillo and A. J. Durrani, "Effect of Transient Temperature on High-Strength Concrete," *ACI Materials Journal* **87**(10), pp. 47-53, January-February 1990.
31. N.A. Noumowe, P. Clastres, A.M. Shekarchi, and G. Debicki, "Thermal Stability of Concrete Under Accidental Situation," *Transactions of 14th International Conference on Structural Mechanics in Reactor Technology*, Paper H02/5, Lyon, France, August 17-22, 1997.
32. T. Jávor, "Durability of Concrete in Nuclear Plants Under Temperature Extremes," *Transactions of 15th International Conference on Structural Mechanics in Reactor Technology*, Paper H10/02, Seoul, Korea, August 15-20, 1999.
33. K. Nagao and S. Nakane, "Influences of Various Factors on Physical Properties of Concretes Heated to High Temperatures," *Transactions of 11th International Conference on Structural Mechanics in Reactor Technology*, Paper H03/1, Tokyo, Japan, 1991.
34. K. Hirano, K. Ohmatsuzawa, T. Takeda, S. Nakane, T. Kawaguchi, and K. Nagao, *Physical Properties of Concrete Subjected to High Temperature for "Monju*, P2-25, Private Communication, Power Reactor and Nuclear Fuel Development Corporation, Tokyo, Japan.
35. A.P. Mears, "Long Term Tests on the Effect of Moderate Heating on the Compressive Strength and Dynamic Modulus of Elasticity," Paper SP-34-20 in *Concrete for Nuclear Reactors*, pp. 355-375, American Concrete Institute, Farmington Hills, Michigan, 1972.
36. V.V. Bertero and M. Polivka, "Influence of Thermal Exposures on Mechanical Characteristics of Concrete," Paper SP-34-28 in *Concrete for Nuclear Reactors*, pp. 505-531, American Concrete Institute, Farmington Hills, Michigan, 1972.
37. N. Nishizawa and H. Okamura, "Strength and Inelastic Properties of Concrete at Elevated Temperature," Paper SP-34-22 in *Concrete for Nuclear Reactors*, pp. 407-421, American Concrete Institute, Farmington Hills, Michigan, 1972.
38. H. Weigler and R. Fischer, "Influence of High Temperature on Strength and Deformation of Concrete," Paper SP-34-26 in *Concrete for Nuclear Reactors*, pp. 481-493, American Concrete Institute, Farmington Hills, Michigan, 1972.
39. T. Harada, J. Takeda, S. Yamane, and F. Furumura, "Strength, Elasticity and Thermal Properties of Concrete Subjected to Elevated Temperatures," Paper SP-34-21 in *Concrete for Nuclear Reactors*, pp. 377-406, American Concrete Institute, Farmington Hlls, Michigan, 1972.
40. M.S. Abrams, "Compressive Strength of Concrete at Temperatures to 1,600˚F," *PCA Research and Development Bulletin RD016.01T*, Portland Cement Association, Skokie, IL, 1973.
41. R. Kottas, J. Seeberger, and H.K. Hilsdorf, "Strength Characteristics of Concrete in the Temperature Range of 20˚ to 200˚C," *Transactions of the 5th International Conference on Structural Mechanics in Reactor Technology*, Paper H 1/2, Berlin, Germany 13-17 August 1979.

42. M. Mahdy, P.R.S. Speare, and A.H. Abdel-Reheem, "Effect of Transient High Temperature on Heavyweight, High Strength Concrete," *15th ASCE Engineering Mechanics Conference*, Columbia University, New York, New York, 2-5 June 2002.
43. S. Ghosh ad K.W. Nasser, "Effects of Temperature and Pressure on Strength and Elasticity of Lignite Fly Ash and Silica Fume Concrete," *ACI Materials Journal*, Title No. 93-M7, American Concrete Institute, Farmington Hills, Michigan, January-February 1996.
44. K.-CH. Thienel and F.S. Rostasy, "Strength of Concrete Subjected to High Temperature and Biaxial Stress; Experiments and Modelling," *Materials and Structures* **28**, pp. 575-581, 1995.
45. F. Furumura, T. Abe, and Y. Shinohara, "Mechanical Properties of High strength Concrete at High Temperatures," *Proceedings of Fourth Weimar Workshop on High Performance Concrete: Material Properties and Design*, held at Hochschule für Architektur und Bauwesen (HAB), Weimar, Germany, pp. 237-254, October 4-5, 1995.
46. U. Diederichs, U.M. Jumppanen, and V. Penttala, *Behavior of High Strength Concrete at High Temperatures*, Report #92, Helsinki University of Technology, Department of Structural Engineering, Finland, 1988.
47. T.A. Hammer, *High-Strength Concrete Phase 3, Compressive Strength and E-modulus at Elevated Temperatures: SP6 Fire Resistance*, Report 6.1, SINTEF Structures and Concrete, STF70, A95023, February 1995.
48. T. Morita, H. Saito, and H. Kumajai, "Residual Mechanical Properties of High Strength Concrete Members Exposed to High Temperature – Part 1. Test of Material Properties," *Summaries of Technical Papers of Annual Meeting*, Architectural Institute of Japan, Niigata, August 1992.
49. F. Vodák, K. Trtík, O. Kapicková, S. Hisková, and P. Demo, "The Effect of Temperature on Strength – Porosity Relationship of Concrete," *Construction and Building Materials* **18**, pp. 529-534, 2004.
50. G.G. Carette and V.M. Malhotra, "Performance of Dolostone and Limestone Concretes at Sustained High Temperatures," ASTM STP 858, *Temperature Effects on Concrete*, pp. 38-67, American Society for Testing and Materials, West Conshohocken, Pennsylvania, 1985.
51. G.A. Khoury, *Performance of Heated Concrete – Mechanical Properties* Imperial College, Contract NUC/56/3604A, London, United Kingdom, August 1996.
52. R. Felicetti and P.G. Gambarova, "Effects of High Temperature on the Residual Compressive Strength of High-Strength Siliceous Concretes," *ACI Materials Journal* **95**(4), pp. 395-406, American Concrete Institute, Farmington Hills, Michigan, May-June 1999.
53. P.J.E. Sullivan and R. Sharshar, "The Performance of Concrete at Elevated Temperatures (as Measured by the Reduction in Compressive Strength)," *Fire Technology*, pp. 240-250, August 1992.
54. L.T. Phan, J.R. Lawson and F.L. Davis, "Effects of Elevated Temperature Exposure on Heating Characteristics, Spalling, and Residual Properties of High Performance Concrete," *Materials and Structures* **34**, pp. 83-91, March 2001.
55. R. Sarshar and G.A. Khoury, "Material and Environmental Factors Influencing the Compressive Strength of Unsealed Cement Paste and Concrete at High Temperature," *Magazine of Concrete Research* **45**(162), pp. 51-61, March 1993.
56. J. Xiao, M. Xie, and C. Zhang, "Residual Compressive Behaviour of Pre-Heated High-Performance Concrete with Blast-Furnace-Slag," *Fire Safety Journal* **41**, pp. 91-98, 2006.
57. B. Zhang and N. Bicanic, "Fracture Energy of High-Performance Concrete at High Temperatures up to 450˚C: the Effects of Heating Temperatures and Testing Conditions (Hot and Cold)," *Magazine of Concrete Research* **58**(5), pp. 277-288, June 2006.
58. Y.F. Fu, Y.L. Wong, C.S. Poon and C.A. Tang. "Stress-Strain Behaviour of High-Strength Concrete at Elevated Temperature," *Magazine of Concrete Research* **57**(9), pp. 535-544, November 2005.
59. O. Arioz, "Effects of Elevated Temperatures on Properties of Concrete," *Fire Safety Journal* **42**, pp. 516-522, 2007.
60. M. Kanema, M.V.G. de Morris, A. Noumowe, J.L. Gallias, and R. Cabrillac, "Experimental and Numerical Studies of Thermo-Hydrous Transfers in Concrete Exposed to High Temperature," *Heat Mass Transfer* **44**, pp. 149-164. 2007.
61. E. Sancak, Y.D. Sari, and O. Simsek, "Effects of Elevated Temperature on Compressive Strength and Weight Loss of the Light-Weight Concrete with Silica Fume and Superplasticizer," *Cement and Concrete Composites* **30**(8), pp. 715-721, September 2008.

62. C. Gallé, J. Sercombe, M. Pin, G. Arcier, and P. Bouniol, "Behavior of High Performance Concrete Under High Temperature (60-450˚C) for Surface Long-Term Storage: Thermo-Hydro-Mechanical Residual Properties," *Materials Research Symposium Proceedings* **663**, Materials Research Society, 8 p., 2001.
63. D.R. Lankard, D.L. Birkimer, F.F. Fondriest, and M.J. Snyder, "Effects of Moisture Content on the Structural Properties of Portland Cement Concrete Exposed to Temperatures up to 500F," Paper SP 25-3, ACI Special Publication 25, *Temperature and Concrete*, pp. 59-102, American Concrete Institute, Farmington Hills, Michigan, 1971.
64. F-P. Cheng, V.K.R. Kodur, and T-C. Wang, "Stress-Strain Curves for High Strength Concrete at Elevated Temperatures," *Journal of Materials in Civil Engineering* **16**(1), pp. 84-94, January 1, 2004.
65. M. Takeuchi, M. Hiramoto, N. Kumagai, N. Yamazaki, A. Kodaira, and K. Sugiyama, "Material Properties of Concrete and Steel Bars at Elevated Temperature*," Proceedings of 12th International Conference on Structural Mechanics in Reactor Technology*, Paper H04/5, pp. 133-138, 1993.
66. K.-Ch. Thienel and F.S. Rostasy, "Influences of Concrete Composition on Strength and Deformation Under Uniaxial and Biaxial Loading at Elevated Temperature," *Proceedings of 12th International Conference on Structural Mechanics in Reactor Technology*, Paper H04/6, pp. 145-150, 1993.
67. L.T. Phan and N.J. Carino, "Effects of Test Conditions and Mixture Proportions on Behavior of High-Strength Concrete Exposed to High Temperatures," *ACI Materials Journal*, Title No. 99-M8, pp. 54-66, American Concrete Institute, Farmington Hills, Michigan, January-February 2002.
68. G. Khoury and S. Algar, "Mechanical Behavior of HPC and UHPC Concretes at High Temperatures in Compression and Tension," *ACI International Conference on State-of-the-Art in High-Performance Concrete*, Chicago, Illinois, March 1999.
69. G.A. Khoury, C.E. Majorana, F. Pesavento, and B.A. Schrefler, "Modelling of Heated Concrete," *Magazine of Concrete Research* **54**(2), pp. 77-101, April 2002.
70. I. Janotka, T. Nürnbergerová, and L. Nad, "Behaviour of High-Strength Concrete with Dolomitic Aggregate at High Temperatures," *Magazine of Concrete Research* **52**(6), pp. 399-409, December 2000.
71. G.T.G. Mohamedbhai, "The Residual Strength of Concrete Subjected to Elevated Temperatures," *Concrete* **17**(12), December 1983.
72. A. Savva, P. Manita, and K.K. Sideris, "Influence of Elevated Temperature on the Mechanical Properties of Blended Cement Concretes Prepared with Limestone and Siliceous Aggregates," *Cement and Concrete Composites* **27**, pp. 239-248, 2005.
73. H. Kasami, T. Okuno, and S. Yamane, "Properties of Concrete Exposed to Sustained Elevated Temperature," *Proceedings of 3rd International Conference on Structural Mechanics in Reactor Technology*, Volume 3, Part G-H, London, United Kingdom, September 1-5, 1975.
74. K. Ichise, T. Kawaguchi, and K. Nagao, "Influence of Aggregate in High-Strength Concrete for Mechanical Properties Subjected to High Temperature Heating," *Transactions of Architectural Institute of Japan*, Paper No. 3026, pp. 51-54, Tokyo, 2002.
75. L.T. Phan, *Fire Performance of High-Strength Concrete: A Report of the State-of-the-Art*, NISTIR 5934, National Institute of Standards and Technology, Gaithersburg, Maryland, December 1996.
76. H. Tanyildizi and A. Coskun, "The Effect of High Temperature on Compressive Strength and Splitting Tensile Strength of Structural Lightweight Concrete Containing Fly Ash," *Construction and Building Materials* **22**, pp. 2269-2275, 2008.
77. T.Z. Harmathy and J.E. Berndt, "Hydrated Portland Cement and Lightweight Concrete At Elevated Temperatures, " *Journal of American Concrete Institute*, Title No. 63-4, pp. 93-112, Farmington Hills, Michigan, January 1966.
78. N.G. Zoldners and H.S. Wilson, "Effect of Sustained and Cyclic Temperature Exposures on Lightweight Concrete, Paper SP 39-9 in *Behavior of Concrete Under Temperature Extremes*, ACI SP-39, pp. 149-178, American Concrete Institute, Farmington Hills, Michigan, 1973.
79. R.H. Haddad, R.J. Al-Saleh, and N.M. Al-Akhras, "Effect of Elevated Temperature on the Bond Between Steel Reinforcement and Fiber Reinforced Concrete," *Fire Safety Journal* **43**(5), pp. 334-343, July 2008.
80. F.J. Roux, *Concrete at Elevated Temperatures*, Doctoral Thesis, University of Capetown, South Africa, August 1974.
81. S. Ohgishi, S. Miyasaka, and J. Chida, "On Properties of Magnetite and Serpentine Concrete at Elevated Temperatures for Nuclear Reactor," SP 34-57 in *Concrete for Nuclear Reactors*, pp. 1243-1253, American Concrete Institute, Farmington Hills, Michigan, 1972.

82. D. A. Campbell-Allen, E.W.E. Roper, and H. Roper, "An Investigation of the Effect of Elevated Temperatures on Concrete for Reactor Vessels," *Nuclear Structural Engineering* **2**(4), pp. 382–388, 1965.

83. J.C. Marechal, "Variations in the Modulus of Elasticity and Poisson's Ratio with Temperature," Paper SP 34-27 in *Concrete for Nuclear Reactors*, pp. 495-503, American Concrete Institute, Farmington Hills, Michigan, 1972.

A.2 References Cited by Others in Figures

Figure Number	Reference(s)[+]
2.50	ZhD Lu, *A Research on Fire Response of Reinforced Concrete Beams*, PhD Thesis, Tongji University,1989 [in Chinese]. Y.X. Yao, *Research on Fire Response of Reinforced Concrete Frames and Determination of Temperature Reached During a Fire*, Master Thesis, Tongji University, 1991 [in Chinese]. Y.K. Yang and ShE Zhen, "Fire damage assessment of concrete structures. *Build Sci Res Sichuan* **17**(4), pp. 22–26, 1991 [in Chinese]. W. Li and ZhH Guo, "Experimental Investigation on Strength and Deformation of Concrete Under High Temperature," *Chin J Build Struct* **14**(1), pp. 8–16, 1993 [in Chinese]. JZh Xiao, P. Wang, M. Xie and J. Li, "Experimental Study on Compressive Constitutive Relationship of HPC at Elevated Temperature," *J Tongji Univ* **31**(2), pp. 186–90, 2003; [in Chinese].
2.54	F.J. Roux, Concrete at Elevated Temperatures, Doctoral Thesis, University of Capetown, South Africa, August 1974. T. Harada, T. Takeda, S, Yamane, and F, Furumura, "Strength, Elasticity and Thermal Properties of Concrete Subjected to Elevated Temperatures," Paper SP-34-21 in *Concrete for Nuclear Reactors*, pp. 377-406, American Concrete Institute, Farmington Hills, Michigan, 1972. D. T. Lankard, D.L. Birkimer, F.F. Fondriest, and M.J. Snyder, "Effects of Moisture Content on the Structural Properties of Portland Cement Concrete Exposed to Temperatures Up to 500°F," SP-25 *Temperature and Concrete*, pp. 59–102, American Concrete Institute, Farmington Hills, Michigan, 1971. J.C. Marechal, "Variations in the Modulus of Elasticity and Poisson's Ratio with Temperature," Paper SP 34-27 in *Concrete for Nuclear Reactors*, pp. 495-503, American Concrete Institute, Farmington Hills, Michigan, 1972. S. Ohgishi, S. Miyasaka, and J. Chida, "On Properties of Magnetite and Serpentine Concrete at Elevated Temperatures for Nuclear Reactor," SP 34-57 in *Concrete for Nuclear Reactors*, pp. 1243-1253, American Concrete Institute, Farmington Hills, Michigan, 1972.
2.80	K.B. Hickey, *Creep, Strength and Elasticity of Concrete at Elevated Temperatures*, Report No. C-1257, U.S. Bureau of Reclamation, 1967. J. C. Saeman and G. W. Washa, "Variation of Mortar and Concrete Properties with Temperature," *J. American Concrete Institute* **29**(5), pp. 385–395, 1957. H. Kasami, T. Okuno, and S. Yamane, "Properties of Concrete Exposed to Sustained Elevated Temperature," Paper Hl/5 in *Proceedings of 3rd International Conference on Structural Mechanics in Reactor Technology*, Elsevier Science Publishers, North-Holland, The Netherlands, 1975. H. Steege, HHT – Demo Betonversuchsprogramme, Abschlüssbericht, HRB GmbH, Mannheim, Germany, 1981 (unpublished).
2.81	K.W. Nasser and R.P. Lothia, "Mass Concrete Properties at High Temperatures," *Journal American Concrete Institute* **68**(3), pp. 180-181, March 1971. D. A. Campbell-Allen, E.W.E. Roper, and H. Roper, "An Investigation of the Effect of Elevated Temperatures on Concrete for Reactor Vessels," *Nuclear Structural Engineering* **2**(4), pp. 382–388, 1965.

[+]All references cited by an author may not be listed.

S. Ohgishi, S. Miyasaka, and J. Chida, "On Properties of Magnetite and Serpentine Concrete at Elevated Temperatures for Nuclear Reactor," SP 34-57 in *Concrete for Nuclear Reactors*, pp. 1243-1253, American Concrete Institute, Farmington Hills, Michigan, 1972.
D.J. Hannant, "The Effects of Heat on Concrete Strength," *Engineering* **197**(5105), p. 302, February 21, 1964.
N.G. Zoldners, "Effect of High Temperatures on Concrete Incorporating Different Aggregates," *ASTM Proceedings* **60**, pp. 1087-1080, American Society for Testing and Materials, 1960.
H.L. Malhotra, "The Effect of Temperature on the Compressive Strength of Concrete," *Magazine of Concrete Research* **8**(2), pp.382-388, 1965.
M. S. Abrams, "Compressive Strength of Concrete at Temperatures to 1600°F," SP-25, *Temperature and Concrete*, American Concrete Institute, pp. 33–58, 1971.
Portland Cement Association (Miller and Faulkner), "Effect of Long Exposure of Concrete to High Temperatures," *Concrete Information ST 32-3-53*, 1953.

2.82 S. Ohgishi, S. Miyasaka, and J. Chida, "On Properties of Magnetite and Serpentine Concrete at Elevated Temperatures for Nuclear Reactor," SP 34-57 in *Concrete for Nuclear Reactors*, pp. 1243-1253, American Concrete Institute, Farmington Hills, Michigan, 1972.
F.J. Roux, *Concrete at Elevated Temperatures*, Doctoral Thesis, University of Capetown, South Africa, August 1974.
T. Harada, T. Takeda, S, Yamane, and F, Furumura, "Strength, Elasticity and Thermal Properties of Concrete Subjected to Elevated Temperatures," Paper SP-34-21 in *Concrete for Nuclear Reactors*, pp. 377-406, American Concrete Institute, Farmington Hills, Michigan, 1972.
D. T. Lankard, D.L. Birkimer, F.F. Fondriest, and M.J. Snyder, "Effects of Moisture Content on the Structural Properties of Portland Cement Concrete Exposed to Temperatures Up to 500°F," SP-25 *Temperature and Concrete*, pp. 59–102, American Concrete Institute, Farmington Hills, Michigan, 1971.
H.L. Malhotra, "The Effect of Temperature on the Compressive Strength of Concrete," *Magazine of Concrete Research* **8**(2), pp.382-388, 1965.
M. S. Abrams, "Compressive Strength of Concrete at Temperatures to 1600°F," SP-25, *Temperature and Concrete*, American Concrete Institute, pp. 33–58, 1971.

2.1155 G.L. England and A.D. Ross, "Reinforced Concrete Under Thermal Gradients," *Magazine of Concrete Research* **14**(40), pp. 5-12, March 1962.
K.B. Hickey, Creep, Strength, and Elasticity of Concrete at Elevated Temperature, Report No. C-1257, Bureau of Reclamation, Washington, DC, December 1967.
J.C. Marechal, "Causes Physiques et Chimiques du Fluage et du Retrait du Béton," RILEM Colloquim on the Physical and Chemical Causes of Creep and Shrinkage of Concrete, Munich, Germany, April 1968.

2.1156 K.B. Hickey, *Creep, Strength, and Elasticity of Concrete at Elevated Temperature*, Report No. C-1257, Bureau of Reclamation, Washington, DC, December 1967.
J.C. Marechal, "Causes Physiques et Chimiques du Fluage et du Retrait du Béton," RILEM Colloquim on the Physical and Chemical Causes of Creep and Shrinkage of Concrete, Munich, Germany, April 1968.
G.L. England and A.D. Ross, "Reinforced Concrete Under Thermal Gradients," *Magazine of Concrete Research* **14**(40), pp. 5-12, March 1962.
K.W. Nasser and A.M. Neville, "Creep of Concrete at Elevated Temperatures," *Journal of the American Concrete Institute*, Title 62-87, pp. 1567-1579, Farmington Hills, Michigan, December 1965.
S. Arthanari and C.W. Yu, "Creep of Concrete Under Uniaxial and Biaxial Stresses at Elevated Temperatures," *Magazine of Concrete Research* **19**(60), pp. 149-156, September 1967.

2.240 T. Harada, T. Takeda, S, Yamane, and F, Furumura, "Strength, Elasticity and Thermal Properties of Concrete Subjected to Elevated Temperatures," Paper SP-34-21 in *Concrete for Nuclear Reactors*, pp. 377-406, American Concrete Institute, Farmington Hills, Michigan, 1972.
C.R. Cruz and M. Gillen, "Thermal Expansion of Portland Cement Paste, Mortar, and Concrete at High Temperature," *Fire and Materials* **4**(2), 1980.
R. Philleo, *Some Physical Properties of Concrete At High Temperature*, *Research Department Bulletin 97*, Portland Cement Association, Skokie, Illinois, October 1958.

M.S. Crowley, "Initial Thermal Expansion Characteristics of Insulating Refractory Concretes," *Bulletin of the American Ceramic Society* **35**(12), pp. 465-468, 1956.

2.244 T. Z Harmathy. and L.W. Allen, "Thermal Properties of Selected Masonry Unit Concretes," *Journal of American Concrete Institute* **70**, pp. 132–142, 1973.
T. Harada, *The Thermal Expansion of Concrete at High Temperatures*, Part 1.2, Dissertation, Tokyo Institute of Technology, Japan, 1962
U. Schneider and U. Diederichs, *Physikalische Eigenschaften von Beton und Stahl im Bereich 20˚C bis zum Schmelzen*, Bericht des Instituts für Baustoffe, Massivbau und Brandschutz TU Braunschweig, Germany, 1980.

2.245 T.Z Harmathy. and L.W. Allen, "Thermal Properties of Selected Masonry Unit Concretes," *Journal of American Concrete Institute* **70**, pp. 132–142, 1973.
T. Harada, *The Thermal Expansion of Concrete at High Temperatures*, Part 1.2, Dissertation, Tokyo Institute of Technology, Japan, 1962
U. Schneider and U. Diederichs, *Physikalische Eigenschaften von Beton und Stahl im Bereich 20˚C bis zum Schmelzen*, Bericht des Instituts für Baustoffe, Massivbau und Brandschutz TU Braunschweig, Germany, 1980.
G. Hillenbrand et al., *Untersuchung der Wechselwirkung von Kernschmelze und Reaktorbeton*, Abschlussbericht – Förderungsvorhaben BMFT RS 154, KWU, Erlangen, Germany, May 1978.

2.249 T. Harada, T. Takeda, S, Yamane, and F, Furumura, "Strength, Elasticity and Thermal Properties of Concrete Subjected to Elevated Temperatures," Paper SP-34-21 in *Concrete for Nuclear Reactors*, pp. 377-406, American Concrete Institute, Farmington Hills, Michigan, 1972.
T.Z. Harmathy, *Thermal Properties of Concrete at Elevated Temperatures,* Research Paper No. 426 of the Division of Building Research, Ottawa, Canada, March 1970.
U. Schneider and K. Kordina, *Bestimmung der Wärmeleitfähigkeit des "Konstruktonsbetons 2.3" des Kernkraftwerkes SNR-Kalkar*, Gutachtliche Stellungnahme, Institut for Baustoffe, Massivbau und Brandschutz, TU Braunschweig, Germany, 1976.
E. Crispino, "Studies on the Technology of Concretes Under Thermal Conditions," Paper SP-34-25 in *Concrete for Nuclear Reactors*, pp. 443-479, American Concrete Institute, Farmington Hills, Michigan, 1972.
J. F. Muir, *Response of Concrete Exposed to High Heat Flux on Surface*, Research Paper SAND 77-1467, Sandia National Laboratories, Albuquerque, New Mexico, 1977.
J. Hundt, *Wärme und Feuchtigkeitsleitung in Beton unter Einwirkung eines Temperaturgefälles*, DAfStB, Heft 256, 1975.

2.250 T. Harada, T. Takeda, S, Yamane, and F, Furumura, "Strength, Elasticity and Thermal Properties of Concrete Subjected to Elevated Temperatures," Paper SP-34-21 in *Concrete for Nuclear Reactors*, pp. 377-406, American Concrete Institute, Farmington Hills, Michigan, 1972.

2.251 J.P. Moore, J.G. Stradley, R.S. Graves, J.H. Hanna, D.L. and McElroy, *Some Thermal Transport Properties of a Limestone Concrete*, ORNL/TM-2644, Oak Ridge National Laboratory, Oak Ridge, Tennessee, 1969.
H.W.Brewer, "General Relation of Heat Flow Factors to the Unit Weight of Concrete," *Journal of Portland Cement Association* **9**(1), pp. 48–60, Research and Development Laboratories, Skokie, Illinois, 1967.
R.C. Valore, Jr., "Cellular Concretes, Part 2 Physical Properties," *Journal of the American Concrete Institute* **50**(6), pp. 817-836, June 1954.
M. Tyner, "Effect of Moisture on Thermal Conductivity of Limerock Concrete," *Journal of the American Concrete Institute* **43**(9), Document JL43-02, September 1946.

2.254 J. F. Muir, *Response of Concrete Exposed to High Heat Flux on Surface*, Research Paper SAND 77-1467, Sandia National Laboratories, Albuquerque, New Mexico, 1977.
G. Hillenbrand et al., *Untersuchung der Wechselwirkung von Kernschmelze und Reaktorbeton*, Abschlussbericht – Förderungsvorhaben BMFT RS 154, KWU, Erlangen, Germany, May 1978.
T.Z Harmathy. and L.W. Allen, "Thermal Properties of Selected Masonry Unit Concretes," *Journal of American Concrete Institute* **70**, pp. 132–142, 1973.

T.Z Chu, *Radiant Heat Evolution of Concrete – A Study of the Erosion of Concrete Due to Surface Heating*, SAND 77-0922, Sandia National Laboratory, Albuquerque, New Mexico, 1978.

2.255 G. Hillenbrand et al., *Untersuchung der Wechselwirkung von Kernschmelze und Reaktorbeton*, Abschlussbericht – Förderungsvorhaben BMFT RS 154, KWU, Erlangen, Germany, May 1978.
T.Z Harmathy. and L.W. Allen, "Thermal Properties of Selected Masonry Unit Concretes," *Journal of American Concrete Institute* **70**, pp. 132–142, 1973.
T. Harada, T. Takeda, S, Yamane, and F, Furumura, "Strength, Elasticity and Thermal Properties of Concrete Subjected to Elevated Temperatures," Paper SP-34-21 in *Concrete for Nuclear Reactors*, pp. 377-406, American Concrete Institute, Farmington Hills, Michigan, 1972.

J.A. Pogorzelski, *Thermal Properties of Some Building Materials*, Report to RILEM Committee 44-PHT, Warsaw, Poland, 1979.

2.257 T. Harada, T. Takeda, S, Yamane, and F, Furumura, "Strength, Elasticity and Thermal Properties of Concrete Subjected to Elevated Temperatures," Paper SP-34-21 in *Concrete for Nuclear Reactors*, pp. 377-406, American Concrete Institute, Farmington Hills, Michigan, 1972.

2.261 G. Hillenbrand et al., *Untersuchung der Wechselwirkung von Kernschmelze und Reaktorbeton*, Abschlussbericht – Förderungsvorhaben BMFT RS 154, KWU, Erlangen, Germany, May 1978.
T.Z Harmathy and L.W. Allen, "Thermal Properties of Selected Masonry Unit Concretes," *Journal of American Concrete Institute* **70**, pp. 132–142, 1973.
T.Z Chu, *Radiant Heat Evolution of Concrete – A Study of the Erosion of Concrete Due to Surface Heating*, SAND 77-0922, Sandia National Laboratory, Albuquerque, New Mexico, 1978.
Y. Collet and E. Tavernier, *Etude des Propiétés du Béton Soumis a des Témperatures Élevés*, Group de Travail, Comportement du Matériau Béton en Fonction de la Température, Brussels, Belgium, November 1976.

2.262 G. Hillenbrand et al., *Untersuchung der Wechselwirkung von Kernschmelze und Reaktorbeton*, Abschlussbericht – Förderungsvorhaben BMFT RS 154, KWU, Erlangen, Germany, May 1978.
T.Z Harmathy and L.W. Allen, "Thermal Properties of Selected Masonry Unit Concretes," *Journal of American Concrete Institute* **70**, pp. 132–142, 1973.
Y. Collet and E. Tavernier, *Etude des Propiétés du Béton Soumis a des Témperatures Élevés*, Group de Travail, Comportement du Matériau Béton en Fonction de la Température, Brussels, Belgium, November 1976.
J.A. Pogorzelski, *Thermal Properties of Some Building Materials*, Report to RILEM Committee 44-PHT, Warsaw, Poland, 1979.
K. Ödeen and A. Nordström, "Termiska Egenskaper hos Beton vid Höga Temperaturer, "*Cement och Beton* **1**, Stockholm, Sweden, 1972.

A.3 References Cited by Others in Tables

Table Number	Reference(s)
2.15	J. F. Muir, *Response of Concrete Exposed to High Heat Flux on Surface*, Research Paper SAND 77-1467, Sandia National Laboratories, Albuquerque, New Mexico, 1977. G. Hillenbrand et al., *Untersuchung der Wechselwirkung von Kernschmelze und Reaktorbeton*, Abschlussbericht – Förderungsvorhaben BMFT RS 154, KWU, Erlangen, Germany, May 1978. T.Z Chu, *Radiant Heat Evolution of Concrete – A Study of the Erosion of Concrete Due to Surface Heating*, SAND 77-0922, Sandia National Laboratory, Albuquerque, New Mexico, 1978 U. Schneider and U. Diederichs, "Physical Properties of Concrete From 20˚C Up To Melting," Parts 1 and 2, *Betonwerk & Fertigteiltechnik*, Heft 3, pp. 141-150, and Heft 4, pp. 223-230, 1981.
2.17	H.J. Sutherland, "Acoustic Measurement of the Penetration of a Molten Metallic Pool into Concrete," *Nuclear Technology* **46**, ISO-355, December 1979.

D. Perinic et al., *Betontiegelversuche mit Thermitschmelzen*, Kernforschungszentrum Karlsruhe, KfK 2572, Germany, July 1979.
M. Peehs , A. Skokan and M. Reimann, "Investigations in Germany of the Barrier Effect of Reactor Concrete Against Propagating Molten Corium in the Case of a Hypothetical Core Meltdown Accident of a LWR," *ENS/ANS International Topical Meeting on Nuclear Power Reactor Safety* **1**, Brussels, Belgium 9-16 October 1978.
J. F. Muir, *Response of Concrete Exposed to High Heat Flux on Surface*, Research Paper SAND 77-1467, Sandia National Laboratories, Albuquerque, New Mexico, 1977.
C. Ehm et al., *Verhalten von Beton unter Einwirkung Flüssiger Metalle*, Report of Institute für Baustoffe, Massivbau und Brandschutz der Technischen Universität Braunschweig, Germany, 1981.

APPENDIX B - TEMPERATURE-DEPENDENT PROPERTIES OF MILD STEEL AND PRESTRESSING MATERIALS FOR USE WITH PORTLAND CEMENT CONCRETES

Bonded reinforcement (i.e., deformed bars) is provided to control the extent and width of cracks at operating temperatures, resist tensile stresses and computed compressive stresses for elastic design, and provide structural reinforcement where required by limit condition design procedures. Bonded reinforcement in nuclear power plant structures is often used in conjunction with prestressed steel. The prestressed steel provides the structural rigidity and the major part of the strength while the bonded reinforcement distributes cracks, increases ultimate strength and reinforces those areas not adequately strengthened by the prestressed steel, and provides additional safety for unexpected conditions of loading.

The elevated temperature response of a reinforced concrete member depends on the mechanical and thermal properties of the materials of which it is composed. Structural elements fabricated from reinforced concrete, because of their typical size, have a high thermal inertia that results in relatively slow rates of temperature increase through the cross section. As a result, the steel reinforcement temperatures generally are kept sufficiently low to avoid significant softening. In addition, due to the monolithic nature of construction, the existence of alternate load paths, and compartmentalazation of fires (i.e., conventional civil engineering construction), reinforced concrete structures generally perform well under elevated-temperature conditions such as fires. However, under certain scenarios (e.g., rapid heat build up) spalling of the concrete could occur to expose the steel reinforcement to the effects of elevated temperature, or the thermal event could last for a prolonged period of time (e.g., hot spot). As a result the strength of steel can decrease and deformations and other property changes may occur under prolonged exposure. Primary mechanical properties of steel that affect the response of structural members to thermal events are the strength, modulus of elasticity, coefficient of thermal expansion, and creep. Primary thermal properties are those that influence the temperature rise and its distribution in the member (i.e., thermal conductivity, specific heat, and density). Although this report primarily addresses cementitious materials, for completeness limited information is provided below on effects of elevated temperature on selected properties of mild steel and steel reinforcing materials. More detailed information on properties of steel materials at elevated temperatures has been compiled elsewhere [B1].

B.1 Mechanical Properties

Stress-Strain. Strength characteristics and mechanical properties of steels depend on several factors: amount and type of alloying constituents, heat treatment during manufacture, and retreatment in cold state (e.g., cold drawing). Figures B.1 and B.2 presents examples of the effect of elevated temperature on the stress-strain curve of a typical structural steel.

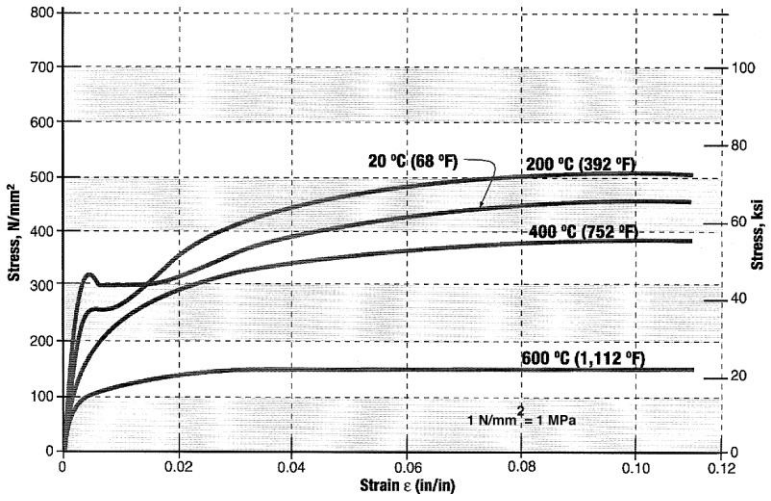

Figure B.1 Stress-strain curves for structural steel (ASTM A36).

Source: *SFPE Engineering Guide to Performance Based Fire Protection Analysis and Design of Buildings*, Society of Fire Protection Engineers, Bethesda, Maryland, March 2000.

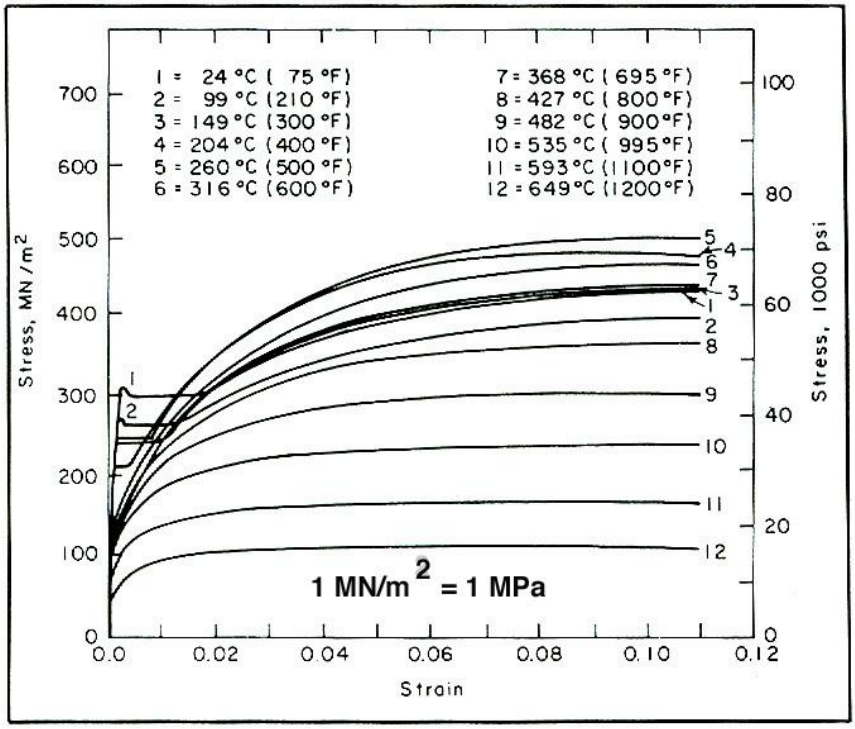

Figure B.2 Stress-strain curves for structural steel (ASTM A36) at high temperatures.

Source: T.Z. Harmathy and W.W. Stanzak, "Elevated-Temperature Tensile and Creep Properties of Some Structural and Prestressing Steels," *Fire Test Performance*, STP 464, American Society for Testing and Materials, West Conshohocken, Pennsylvania, pp. 186-208, 1970.

Stress-strain curves for hot-rolled 220 and 420 MPa ribbed steel rebars having diameters of 10 and 16 mm that were tested at room temperature after exposure to temperatures up to 950˚C for 3 hours are presented in Figures B.3. Additional information presenting results for a 343 MPa 51-mm diameter steel rebar tested at temperatures up to 600˚C are presented in Figure B.4.

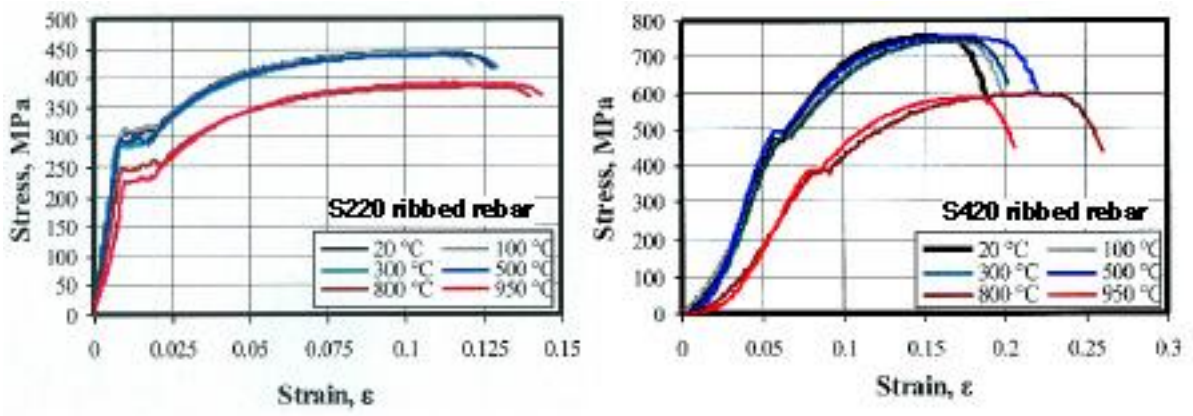

Figure B.3 Stress-strain curves for steel reinforcement (S220 and S420).

Source: I.B. Topçu and C. Karakurt, "Properties of Reinforced Concrete Steel Rebars Exposed to High Temperatures," Research Letter in *Materials Science*, Article ID 814137, Hindawi Publishing Co., 4 p., 2008.

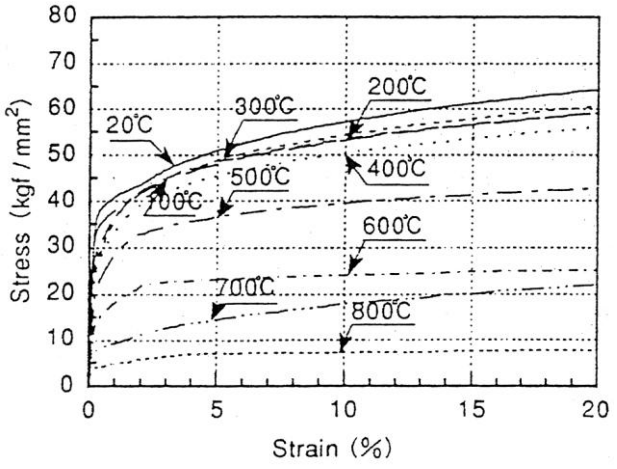

Figure B.4 Stress-strain relationships of reinforcing bars at elevated temperature.

Source: M. Takeuchi, M. Hiramoto, N. Kumagai, N. Yamazaki, A. Kodaira, and K. Sugiyama, "Material Properties of Concrete and Steel Bars at Elevated Temperatures," *12th International Conference on Structural Mechanics in Reactor Technology*, Paper H04/4, pp. 133–138, Elsevier Science Publishers, North-Holland, The Netherlands, 1993.

The effect of elevated temperature exposure on the stress-strain curves for uncoated stress-relieved steel wire (ASTM A421) has been investigated [B.2]. Results are presented in Figure B.5. The specimens were tested at temperature about 60 to 90 minutes after heating was initiated by loading at a rate of 0.635 mm/min. Additional specimens were tested at rates of 1.905 and 19.05 mm/min to evaluate the rate effect. For the strain rates investigated, the rate did not have a considerable effect on the shape of the stress-strain curves until the temperatures reached 371 ˚C. Figure B.6 presents a comparison of stress-strain curves obtained at high temperature and after

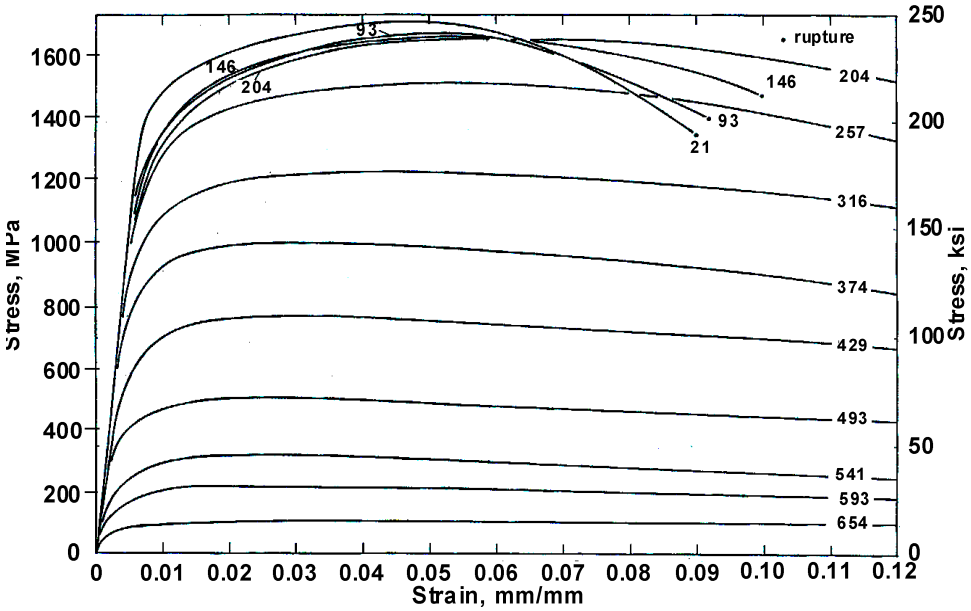

Figure B.5 Effect of temperature on stress-strain curves of a prestressing steel (ASTM A421).

Source: T.Z. Harmathy and W.W. Stanzak, "Elevated-Temperature Tensile and Creep Properties of Some Structural and Prestressing Steels," *Fire Test Performance*, STP 464, American Society for Testing and Materials, West Conshohocken, Pennsylvania, pp. 186-208, 1970.

cooling to room temperature for 1770 MPa 5-mm-diameter low-relaxation prestressing steel wire [B.3]. Specimens tested at temperature were loaded at 1/mm/min until the strain reached 0.012 at which the loading rate was increased to 5 mm/min causing a slight step increase in the results obtained at high temperature. Specimens tested at room temperature were subjected to the desired test temperature for 1 hour prior to permitting them to cool to room temperature. A comparison of results indicates that up to 300˚C the results for specimens tested at temperature and after cooling to room temperature were similar.

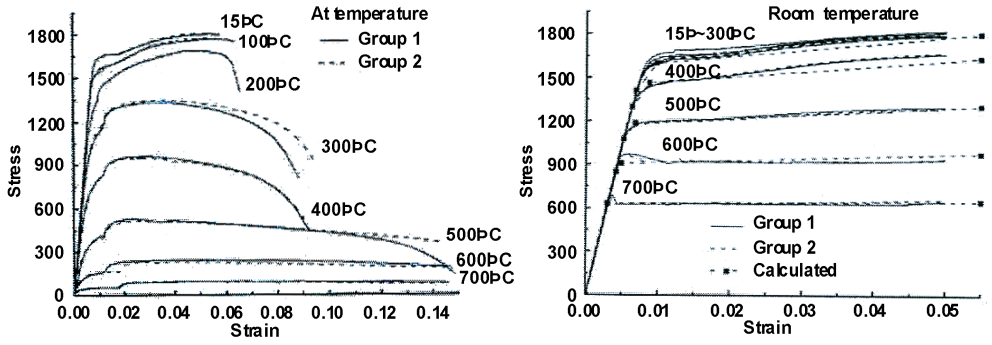

Figure B.6 Stress-strain curve for 1770 MPa 5-mm-diameter low-relaxation prestressing steel wire tested at temperature and at room temperature.

Source: W. Zheng, Q. Hu, and H. Zhang, "Experimental Research on the Mechanical Property of Prestressing Steel Wire During and After Heating," *Frontiers in Architecture and Civil Engineering in China* 1(2), pp. 247-254, 2007.

It has been noted that the critical temperatures for reinforcing steel and prestressing steel are 593˚C and 426˚C, respectively [B.4]. The critical temperature is defined as the temperature at which the reinforcement loses much of its strength and can no longer support applied load.

Modulus of Elasticity. Figure B.7 presents the effect of elevated temperature on the modulus of elasticity for structural steel and steel reinforcing bars. The results have been normalized relative to room temperature results (i.e., $E_0 = 210 \times 10^3$ MPa). These results indicate that at a temperature of 550˚C the modulus of elasticity is reduced to about half of the value at ambient temperature. Figure B.8 presents the effect of temperature on elongation and Young's modulus for a 343 MPa 51-mm diameter steel rebar tested at temperatures up to 800˚C [B.5]. Modulus

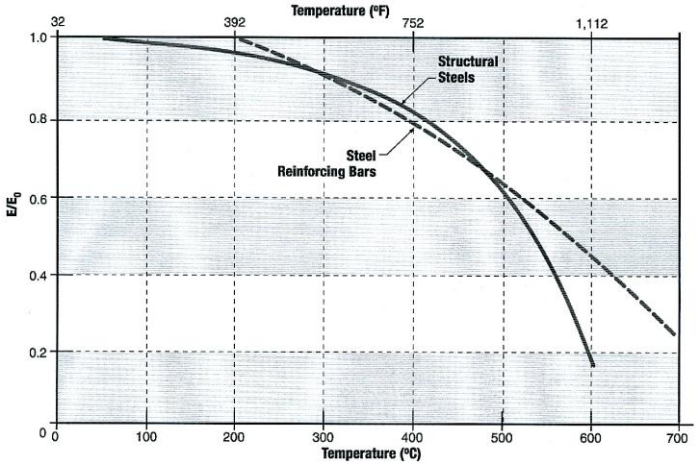

Figure B.7 Modulus of elasticity at elevated temperatures for structural steel and steel reinforcing bars.

Source: *SFPE Engineering Guide to Performance Based Fire Protection Analysis and Design of Buildings*, Society of Fire Protection Engineers, Bethesda, Maryland, March 2000.

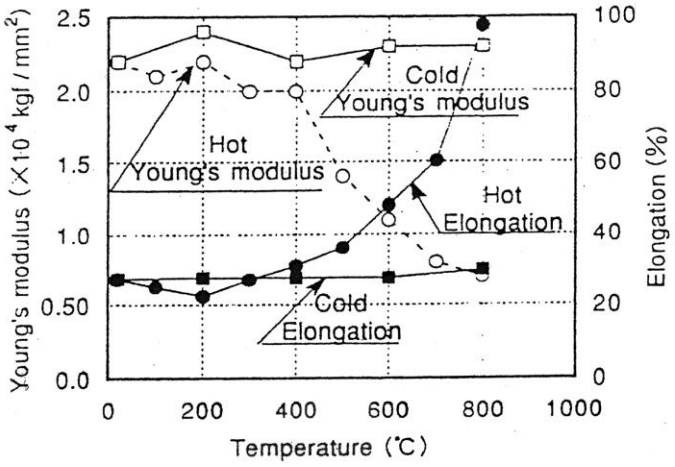

Figure B.8 Influence of temperature on Young's modulus and elongation of reinforcing bars.

Source: M. Takeuchi, M. Hiramoto, N. Kumagai, N. Yamazaki, A. Kodaira, and K. Sugiyama, "Material Properties of Concrete and Steel Bars at Elevated Temperatures," *12th International Conference on Structural Mechanics in Reactor Technology*, Paper H04/4, pp. 133–138, Elsevier Science Publishers, North-Holland, The Netherlands, 1993.

data for 1770 MPa 5-mm-diameter low-relaxation prestressing steel wire tested at temperature are presented in Figure B.9. The results have been normalized relative to the room-temperature modulus. Also shown in the figure are calculated results for modulus as a function of temperature determined from:

$$E_S(T) = \frac{E_S}{1.03 + 32x(T+108)^6 x10^{-18}}, \qquad \text{(B.1)}$$

where $E_s(T)$ is the elastic modulus of steel wire at T˚C, T is temperature in ˚C, and E_s is the elastic modulus of steel wire at room temperature. Modulus results for the steel prestressing wire after permitting it to cool to room temperature were similar to the reference room temperature value. It was therefore recommended that the room temperature modulus value for prestressing wire be used as the residual modulus value after heating.

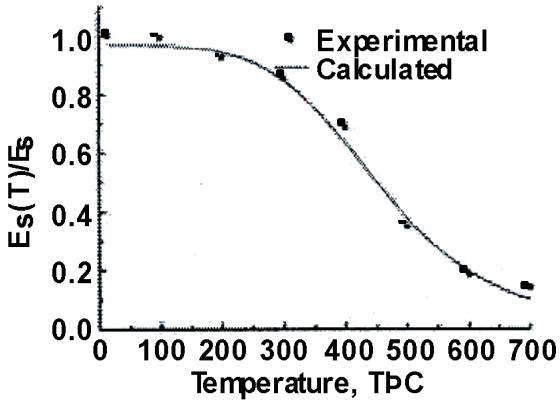

Figure B.9 Normalized modulus of elasticity results for 1770 MPa 5-mm-diameter low-relaxation prestressing steel wire tested at temperature.

Source: W. Zheng, Q. Hu, and H. Zhang, "Experimental Research on the Mechanical Property of Prestressing Steel Wire During and After Heating," *Frontiers in Architecture and Civil Engineering in China* 1(2), pp. 247-254, 2007.

Yield and Ultimate Strengths. The effect of elevated temperature on the strength of a typical structural steel (ASTM A36) is presented in Figure B.10. Normalized yield strength results for hot-rolled and cold-worked reinforcing steel at temperature and after cooling to room temperature are presented in Figure B.11. The loss of yield strength is significant while the steel remains hot but, except for cold-worked steel, the recovery is practically complete after cooling to room temperature from temperatures up to 700˚C for the hot-rolled steel. The yield strength of cold-worked steel does not recover as well as that of hot-rolled steel due to release of sessile dislocations created initially by the amount of prior cold working of the crystal structure [B.6]. Strength data for hot-rolled steel, cold-drawn

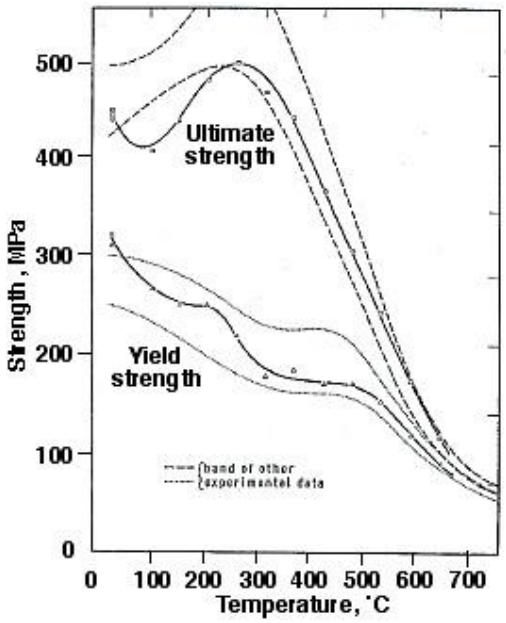

Figure B.10 Effect of elevated temperature on yield and ultimate strength of a typical structural steel (ASTM A36).

Source: T.Z. Harmathy and W.W. Stanzak, "Elevated-Temperature Tensile and Creep Properties of Some Structural and Prestressing Steels," *Fire Test Performance*, STP 464, American Society for Testing and Materials, West Conshohocken, Pennsylvania, pp. 186-208, 1970.

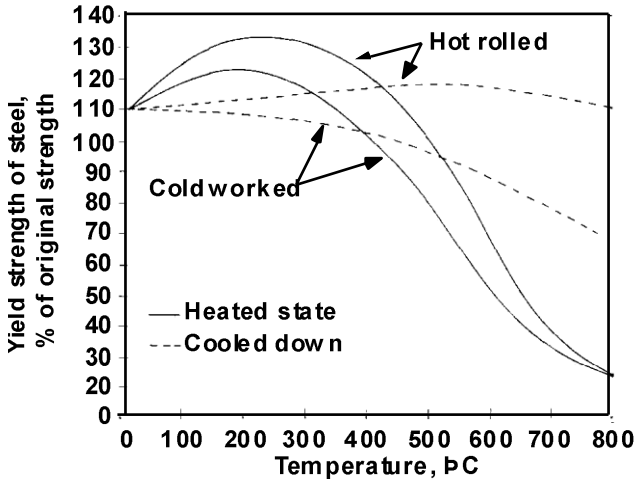

Figure B.11 Yield strength of steel reinforcement vs temperature.

Source: "Assessment of Fire-Damaged Concrete Structures and Repair by Gunite," *Technical Report No. 15*, Concrete Society, London, United Kingdom May 1978.

wire or strand, and high strength alloy bars are presented in Figure B.12. Residual tensile strength and elongation at failure results for #4 Grade 60 ASTM A615 steel rebar heated to temperatures from 500˚ to 802˚C, held at temperature for 1 hour, and then permitted to slowly cool to room temperature prior to testing are presented in Figure B.13. Yield and ultimate strength results for hot-rolled 220 and 420 MPa ribbed steel rebars having

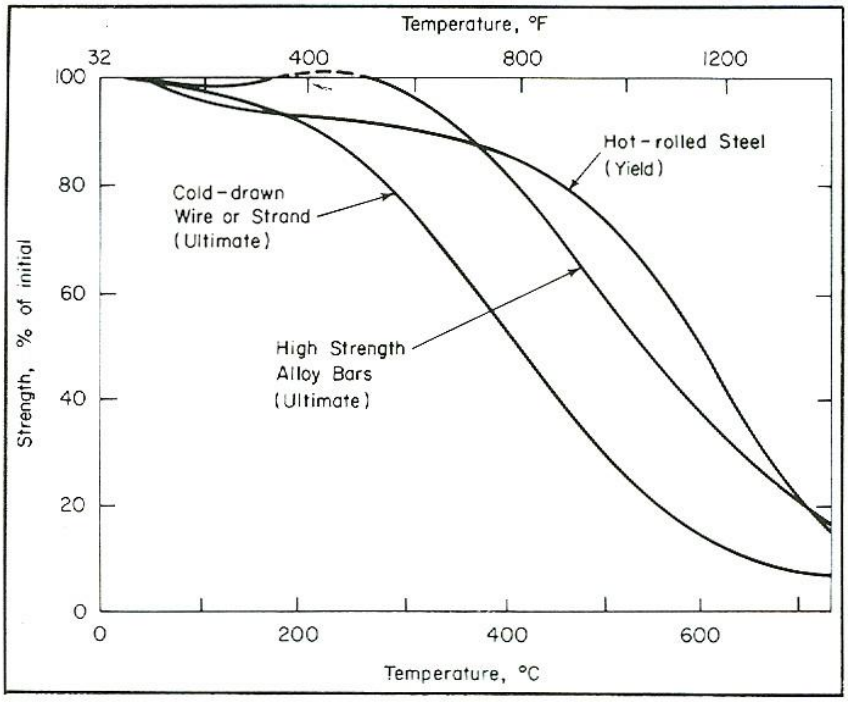

Figure B.12 Strength of selected steels at high temperature.

Source: *Guide for Determining the Fire Endurance of Concrete Elements*, ACI 216R-81, American Concrete Institute, Farmington Hills, Michigan, November 1982.

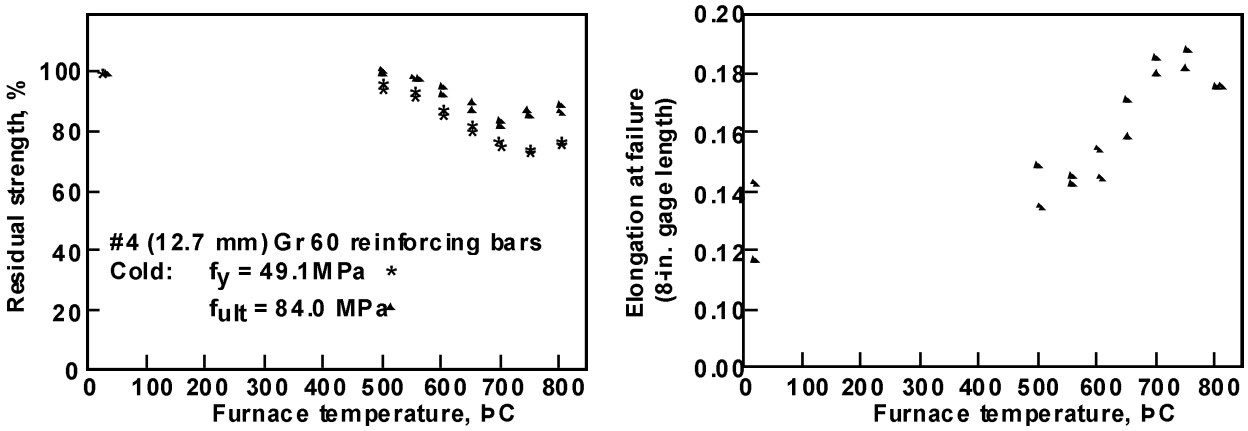

Figure B.13 Effect of elevated temperature on residual yield and ultimate strength, and elongation of ASTM A615 steel rebar.

Source: W.T. Edwards and W.L. Gamble, "Strength of Grade 60 Reinforcing Bars After Exposure to Fire Temperatures," *Concrete International* **8**(10), pp. 17-19, American Concrete Institute, Farmington Hills, Michigan, October 1986.

diameters of 10 and 16 mm that were tested at room temperature after exposure to temperatures up to 950˚C for 3 hours are presented in Figures B.14 and B.15, respectively. Also shown in the figures are relations developed to fit the data.

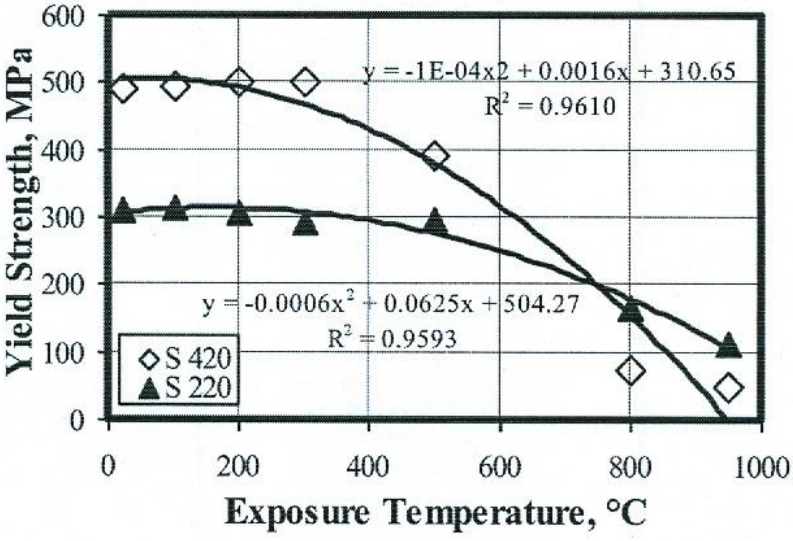

Figure B.14 Effect of exposure temperature on residual yield strength of steel reinforcement (S220 and S420).

Source: I.B. Topçu and C. Karakurt, "Properties of Reinforced Concrete Steel Rebars Exposed to High Temperatures," Research Letter in *Materials Science*, Article ID 814137, Hindawi Publishing Co., 4 p., 2008.

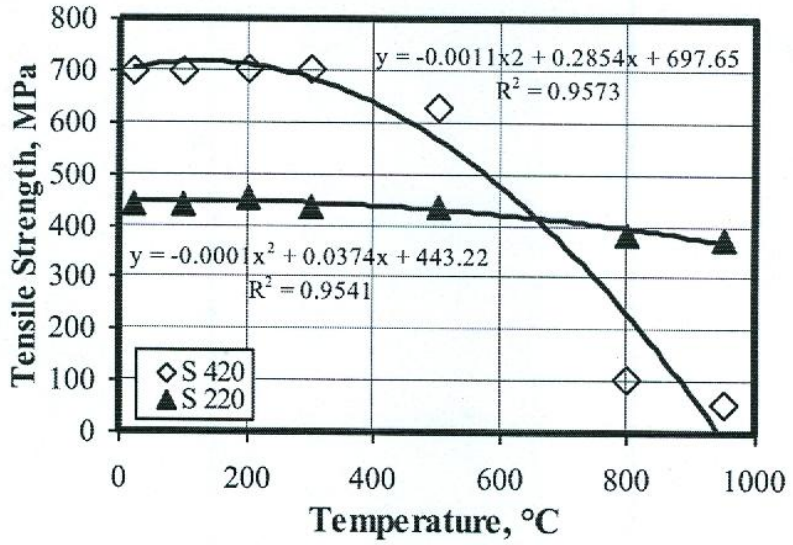

Figure B.15 Effect of exposure temperature on residual tensile strength of steel reinforcement (S220 and S420).

Source: I.B. Topçu and C. Karakurt, "Properties of Reinforced Concrete Steel Rebars Exposed to High Temperatures," Research Letter in *Materials Science*, Article ID 814137, Hindawi Publishing Co., 4 p., 2008.

Hot and cold (residual) yield and ultimate tensile strength results for a 343 MPa 51-mm diameter steel rebar are presented in Figure B.16.

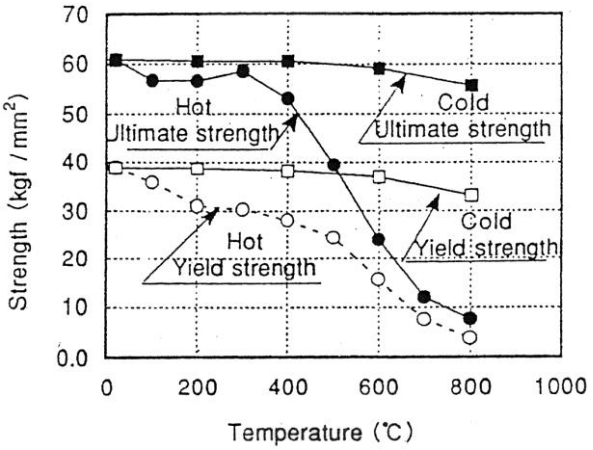

Figure B.16 Yield strength and ultimate tensile strength of reinforcing bars at elevated temperature.

Source: M. Takeuchi, M. Hiramoto, N. Kumagai, N. Yamazaki, A. Kodaira, and K. Sugiyama, "Material Properties of Concrete and Steel Bars at Elevated Temperatures," *12th International Conference on Structural Mechanics in Reactor Technology*, Paper H04/4, pp. 133–138, Elsevier Science Publishers, North-Holland, The Netherlands, 1993.

The effect of elevated temperature on the residual yield and ultimate strength of high-strength (500 MPa) weldable 8- and 12-mm diameter steel reinforcement was investigated [B.7]. The steels were produced by the Temcore process (thermochemical strengthening process), microalloying with vanadium, and work hardening. Reference room temperature yield and ultimate strengths for the steel ranged from 531 to 640 MPa and 655 to 740 MPa, respectively. The steels were subjected to the designated heat-soak temperature for 1 hour and then permitted to slowly cool to room temperature prior to testing. The effect of temperature on the residual yield and tensile strengths of the steels is presented in Figure B.17. Heating of the microalloyed steel resulted in a coarsening of the

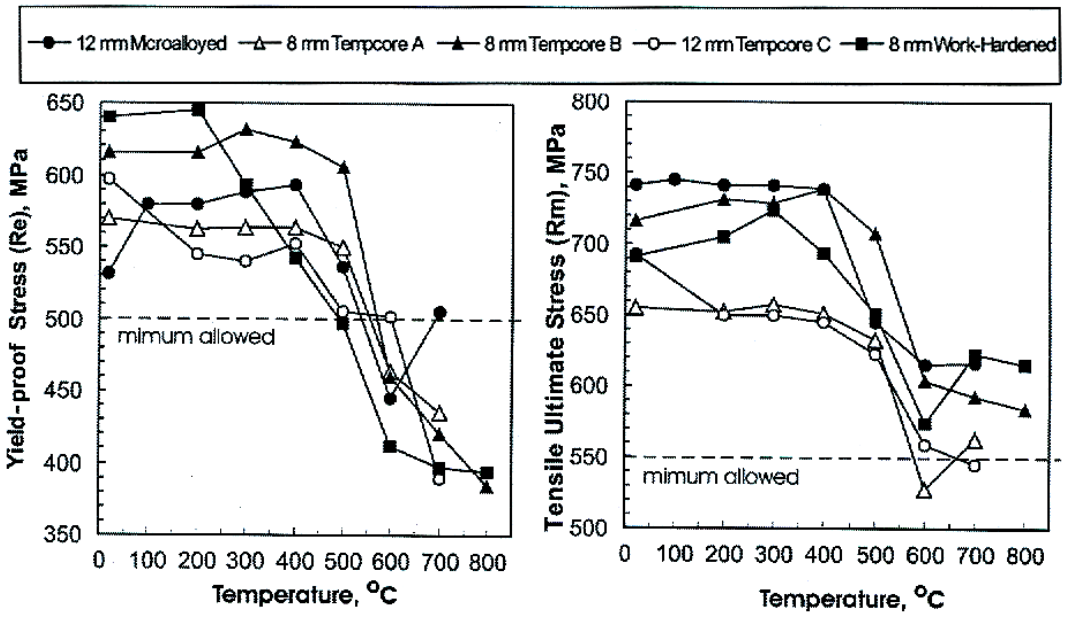

Figure B.17 Residual yield and ultimate strength of high-strength weldable rebars.

Source: J. Nikolaou and G.D. Papadimitriou, "Microstrnctures and Mechanical Properties After Heating of Reinforcing 500 MPa Class Weldable Steels Produced by Various Processes (Temcore, Microalloyed With Vanadium and Work-Hardened)," *Construction and Building Materials* **18**, pp. 243-254, 2004.

existing precipitates along the ferritic grain boundaries leading to a slight increase in yield strength at temperatures between 100˚ and 400˚C. Work-hardened steel bars exhibited a continuous drop in yield and ultimate strength starting at 200˚C and 300˚C, respectively. The weakening of mechanical properties of the Tempcore was attributed to tempering that occurred at high temperatures.

Yield and ultimate strength data for uncoated stress-relieved steel wire (ASTM A421) tested at temperature are provided in Figure B.18.

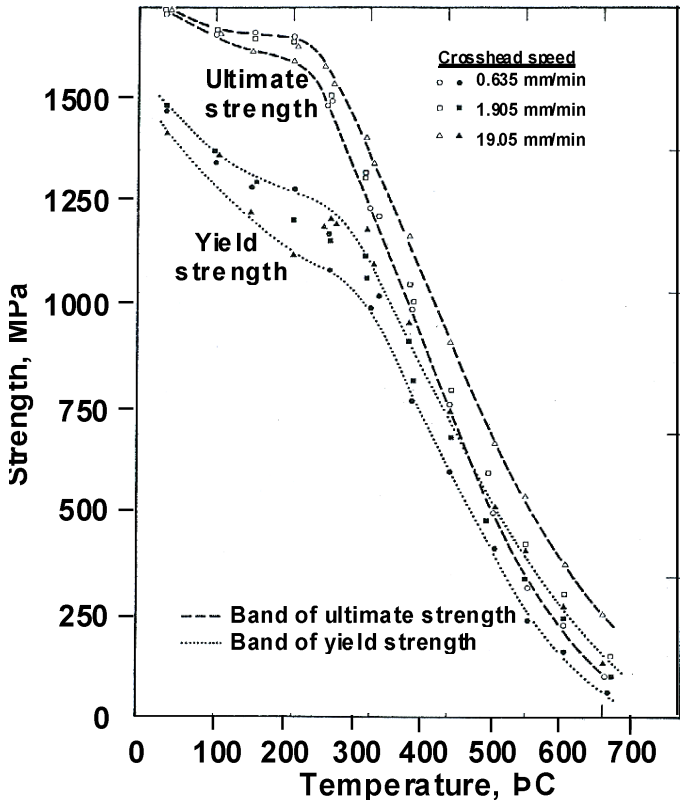

Figure B.18 Effect of elevated temperature on yield and ultimate strength of a prestressing steel (ASTM A421).

Source: T.Z. Harmathy and W.W. Stanzak, "Elevated-Temperature Tensile and Creep Properties of Some Structural and Prestressing Steels," *Fire Test Performance*, STP 464, American Society for Testing and Materials, West Conshohocken, Pennsylvania, pp. 186-208, 1970.

Yield and tensile strength data for 1770 MPa 5-mm-diameter low-relaxation prestressing steel wire tested at temperature are presented in Figure B.19. The results have been normalized relative to the room-temperature values. Also shown in the figure are calculated results for yield and tensile strengths as a function of temperature [B.3]. Yield strength was determined from:

$$f_{0.2}(T)/f_{0.2} = 1.013 - 8.47\text{x}10^{-4}\,\text{x}T + 1.269\text{x}10^{-7}\,\text{x}T^2 - 7.8\text{x}10^{-9}\,\text{x}T^3 + 9.24\text{x}10^{-12}\,\text{x}T^4, \quad \text{(B.2)}$$

where $f_{0.2}$ (T) is yield strength of steel wire at T ˚C, $f_{0.2}$ is the yield strength of steel wire at room temperature, and T is temperature in ˚C. Tensile strength was determined from:

$$f_b(T)/f_b = 0.99 + 4.75\text{x}10^{-4}\,\text{x}T - 5.57\text{x}10^{-6}\,\text{x}T^2 + 1.02\text{x}10^{-9}\,\text{x}T^3 + 4.55\text{x}10^{-12}\,\text{x}T^4, \quad \text{(B.3)}$$

where $f_b(T)$ is the tensile strength limit of steel wire at T ˚C, f_b is the tensile strength limit at room temperature and T is the temperature in ˚C. Residual yield and tensile strength data for the 1770 MPa 5-mm-diameter low-relaxation

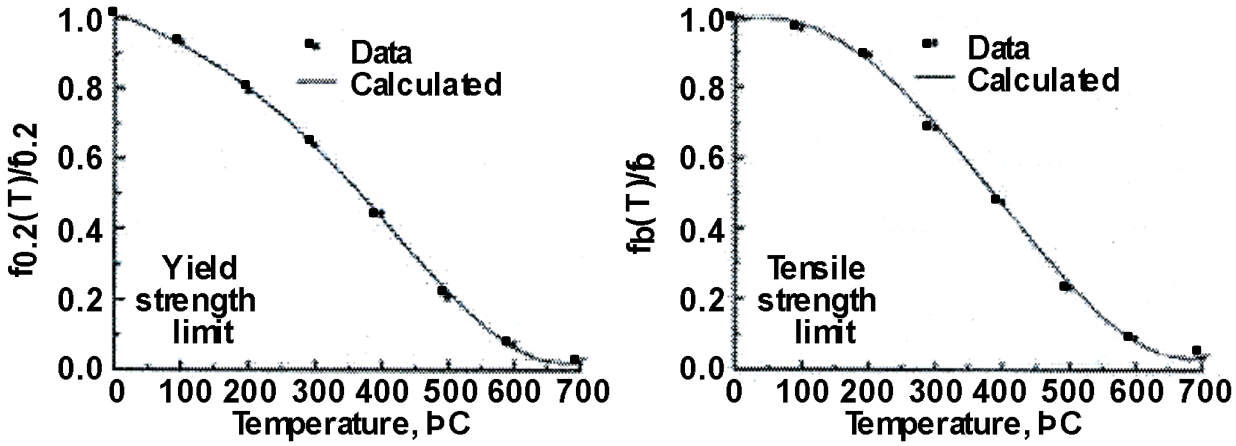

Figure B.19 Normalized yield and tensile strength results for 1770 MPa 5-mm-diameter low-relaxation prestressing steel wire tested at temperature.

Source: W. Zheng, Q. Hu, and H. Zhang, "Experimental Research on the Mechanical Property of Prestressing Steel Wire During and After Heating," *Frontiers in Architecture and Civil Engineering in China* 1(2), pp. 247-254, 2007.

prestressing steel wire obtained at room temperature are presented in Figure B.20. The results have been normalized relative to the room-temperature values. Also shown in the figure are calculated results for the residual yield and tensile strengths as a function of exposure temperature [B.3]. Yield strength was determined from:

$$f_y'(T)/f_y = 0.98 \qquad 0^\circ C \le T \le 300^\circ C, \tag{B.4}$$

$$f_y'(T)/f_y = 1.25 - 9x10^{-4}xT \qquad 300^\circ C < T \le 400^\circ C, \tag{B.5}$$

$$f_y'(T)/f_y = 1.565 - 0.0017xT \qquad 400^\circ C < T \le 700^\circ C, \tag{B.6}$$

where $f_y'(T)$ is yield strength of steel wire after T ˚C and T is temperature in ˚C. Tensile strength was determined from:

$$f_b(T)/f_b = 1, \qquad 0^\circ C \le T \le 300^\circ C, \tag{B.7}$$

$$f_b(T)/f_b = 1.19 - 6.48x10^{-4}xT \qquad 300^\circ C < T \le 400^\circ C, \tag{B.8}$$

$$f_b(T)/f_b = 1.75 - 0.00203xT \qquad 400^\circ C < T \le 700^\circ C \tag{B.9}$$

where $f_b'(T)$ is the tensile strength of steel wire after T ˚C and T is the temperature in ˚C.

The relationship between and tensile strength normalized to the room-temperature value and temperature for a cold-drawn 7-wire prestressing strand is shown in Figure B.21. Also shown in the figure are normalized results obtained for a 25.4-mm diameter hot-rolled reinforcing steel alloy bar. It has been noted that special care must be taken when dealing with prestressing steel due to loss of tension caused by relaxation effects when creep occurs, with about 50% of normal yield strength likely achieved at 400˚C [B.8]. Additional results for 30 types of prestressing steels having strengths from 1500 to 2200 MPa and tested at temperature are presented in Figure B.22.

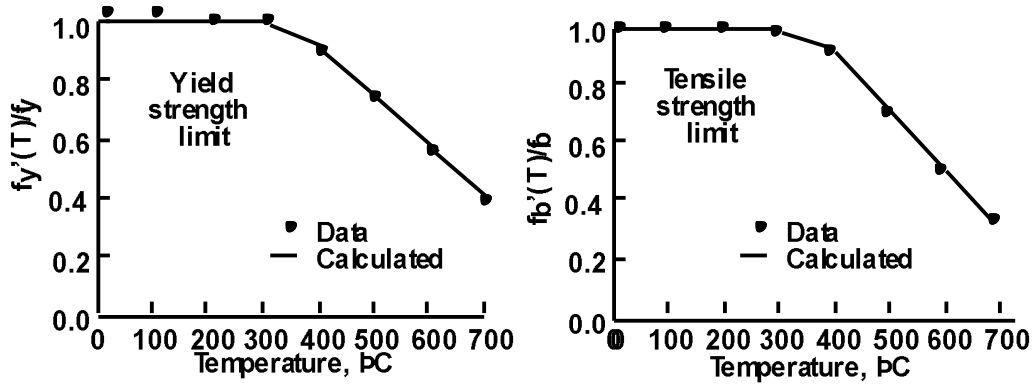

Figure B.20 Normalized residual yield and tensile strength results for 1770 MPa 5-mm-diameter low-relaxation prestressing steel wire tested after heating.

Source: W. Zheng, Q. Hu, and H. Zhang, "Experimental Research on the Mechanical Property of Prestressing Steel Wire During and After Heating," *Frontiers in Architecture and Civil Engineering in China* 1(2), pp. 247-254, 2007.

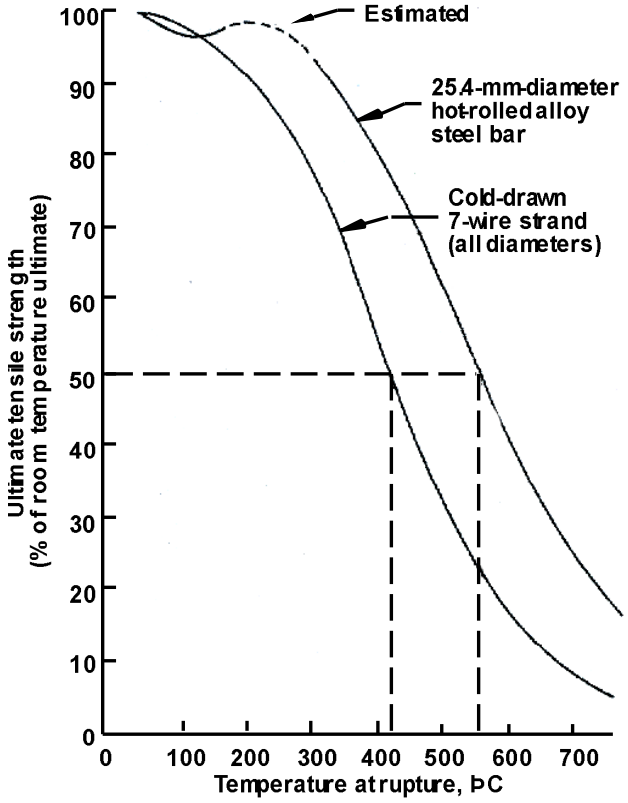

Figure B.21 Relationship between temperature and normalized tensile strength for hot-rolled reinforcing steel bar and cold-drawn prestressing steel wire.

Source: M.S. Abrams and C.R. Cruz, "The Behavior at High Temperature of Steel Strand for Prestressed Concrete," *Journal of PCA Research and Development Laboratories* **3**(3), pp. 8-19, September 1961.

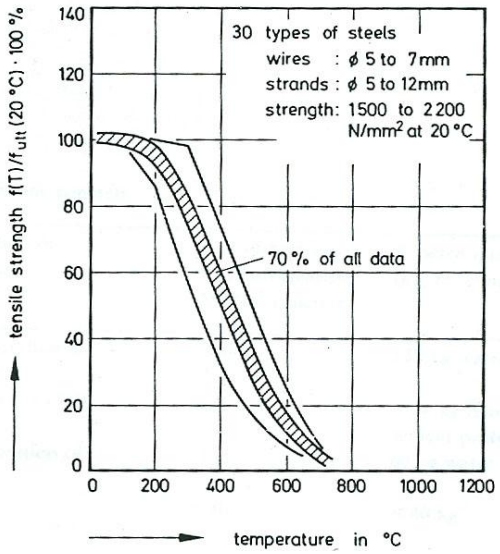

Figure B.22 Tensile strength results of different prestressing steels in the heated state.

Source: U. Schneider, C. Diererichs, and C. Ehm, "Effect of Temperature on Steel and Concrete for PCRV's," *Nuclear Engineering and Design* **67**, pp. 245–258, 1981.

Toughness. Residual toughness results for hot-rolled 220 and 420 MPa ribbed steel rebars having diameters of 10 and 16 mm that were tested at room temperature after exposure to temperatures up to 950˚C for 3 hours are presented in Figure B.23. Also shown in the figure are relations developed to fit the data. Results show that toughness values for both steel types decreased after elevated temperature exposure. However up to about 300˚C the toughness values increased somewhat due to the increased ductility of the steels.

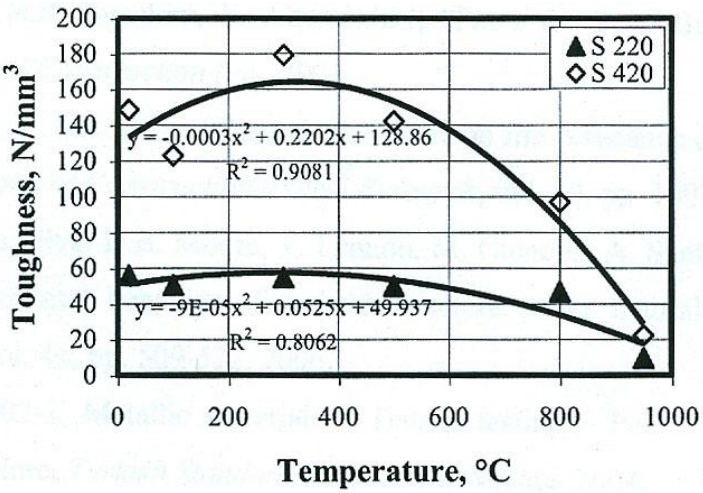

Figure B.23 Effect of exposure temperature on toughness of steel reinforcement (S220 and S420).

Source: I.B. Topçu and C. Karakurt, "Properties of Reinforced Concrete Steel Rebars Exposed to High Temperatures," Research Letter in *Materials Science*, Article ID 814137, Hindawi Publishing Co., 4 p., 2008.

The effect of elevated temperature on the residual toughness (Chapry V-notch energy) for high-strength (500 MPa) weldable 8- and 12-mm diameter steel reinforcement was investigated [B.7]. The steels were produced by the Tempcore process (thermochemical strengthening process), microalloying with vanadium, and work hardening.

Reference room temperature yield and ultimate strengths for the steel ranged from 531 to 640 MPa and 655 to 740 MPa, respectively. The steels were subjected to the designated heat-soak temperature for 1 hour and then permitted to slowly cool to room temperature prior to testing. Figure B.24 presents residual normalized Chapry V-notch absorbed energy of the steels after heating.

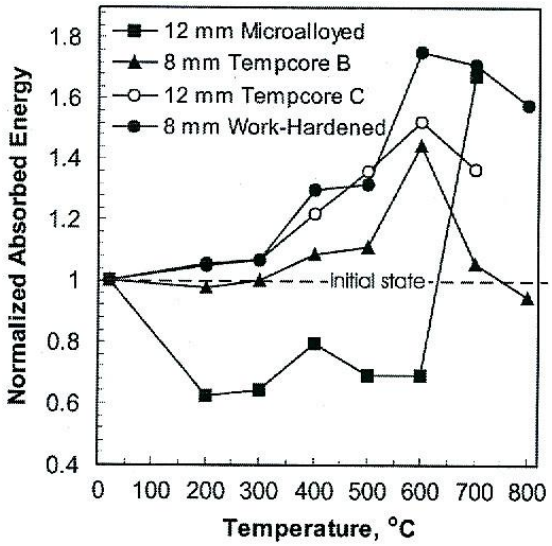

Figure B.24 Residual normalized absorbed energy of high-strength weldable rebars.

Source: J. Nikolaou and G.D. Papadimitriou, "Microstrnctures and Mechanical Properties After Heating of Reinforcing 500 MPa Class Weldable Steels Produced by Various Processes (Temcore, Microalloyed With Vanadium and Work-Hardened)," *Construction and Building Materials* 18, pp. 243-254, 2004.

B.2 Physical Properties

Information on the density, mean specific heat, thermal conductivity, thermal diffusivity, and coefficient of thermal expansion of different steels is presented in Figures B.25-B.29, respectively [B.8]. Average thermal expansion data

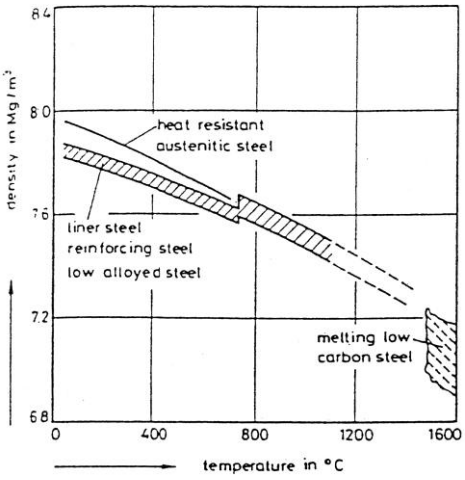

Figure B.25 Density of different steels.

Source: U. Schneider, C. Diererichs, and C. Ehm, "Effect of Temperature on Steel and Concrete for PCRV's," *Nuclear Engineering and Design* **67**, pp. 245–258, 1981.

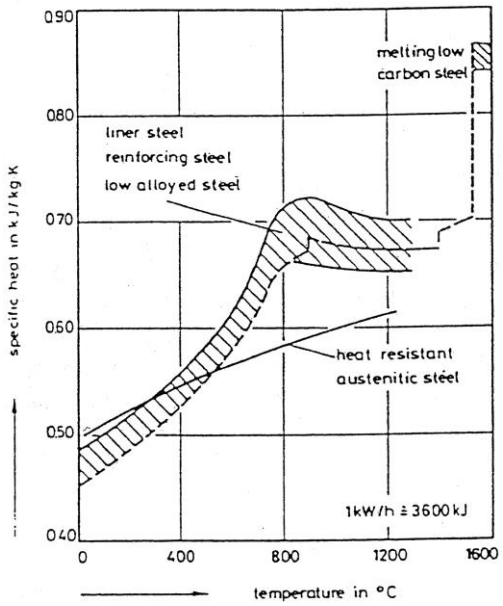

Figure B.26 Mean specific heat of different steels.

Source: U. Schneider, C. Diererichs, and C. Ehm, "Effect of Temperature on Steel and Concrete for PCRV's," *Nuclear Engineering and Design* **67**, pp. 245–258, 1981.

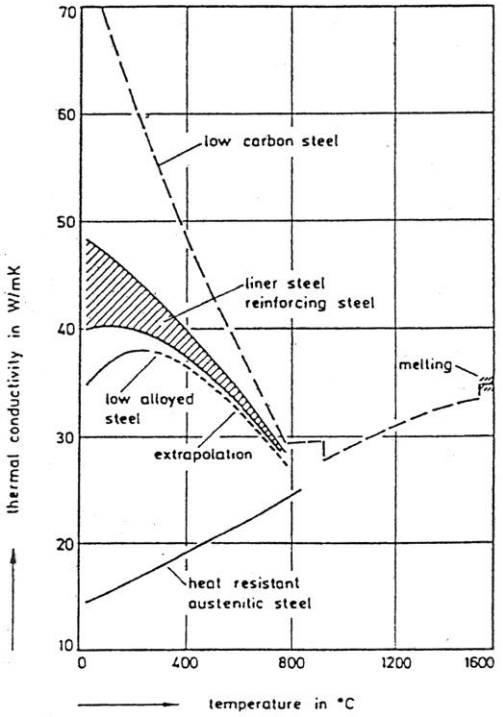

Figure B.27 Thermal conductivity of different steels.

Source: U. Schneider, C. Diererichs, and C. Ehm, "Effect of Temperature on Steel and Concrete for PCRV's," *Nuclear Engineering and Design* **67**, pp. 245–258,1981.

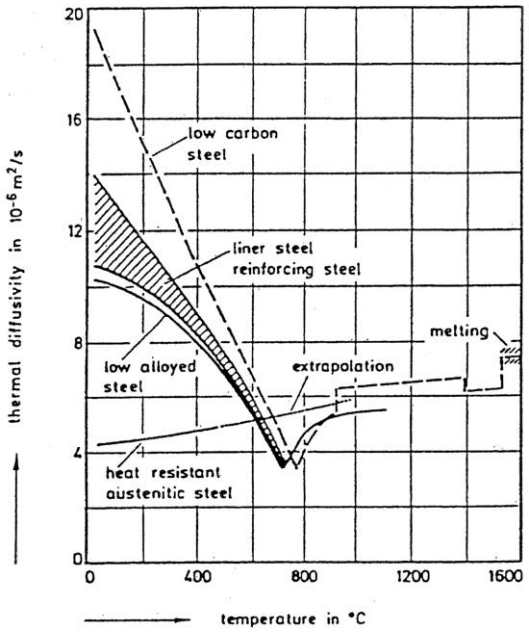

Figure B.28 Thermal diffusivity of different steels.

Source: U. Schneider, C. Diererichs, and C. Ehm, "Effect of Temperature on Steel and Concrete for PCRV's," *Nuclear Engineering and Design* **67**, pp. 245–258, 1981.

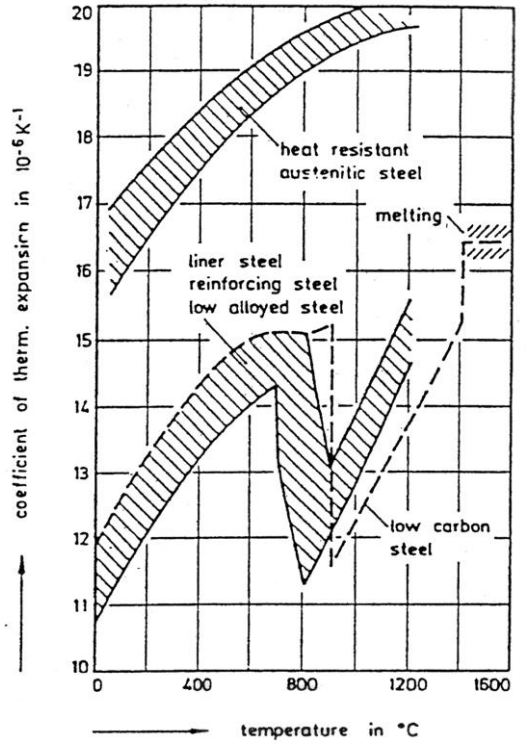

Figure B.29 Coefficient of expansion of different steels.

Source: U. Schneider, C. Diererichs, and C. Ehm, "Effect of Temperature on Steel and Concrete for PCRV's," *Nuclear Engineering and Design* **67**, pp. 245–258, 1981.

for ferritic steels over the temperature range of 200˚ to 650˚C is presented in Figure B.30. For this data the coefficient of thermal expansion can be approximated by [B.9]:

$$\alpha = (11 + 0.0036\ \theta_1) \times 10^{-6}/^{\circ}C$$

where θ_1 is the temperature in degrees C.

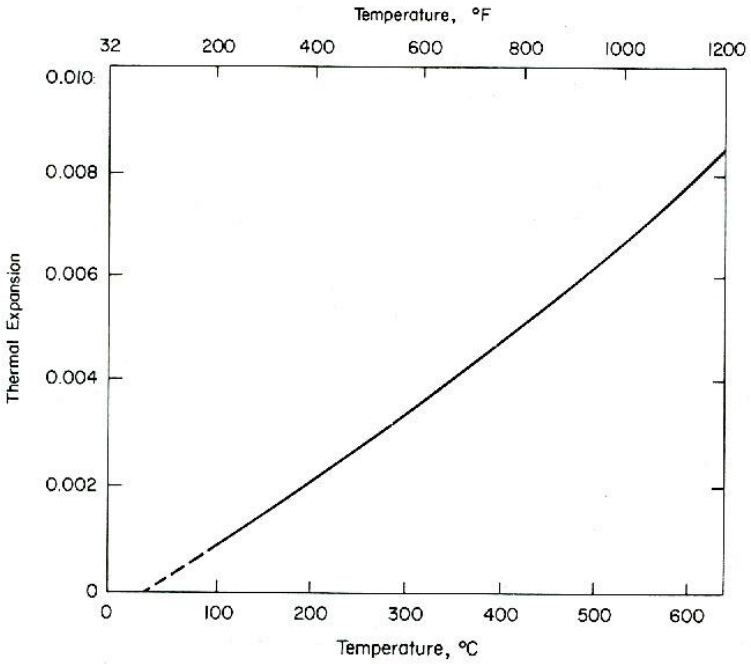

Figure B.30 Thermal expansion of ferritic steel at high temperature.

Source: *Manual of steel Construction*, 7th Edition, American Institute of Steel Construction, New York, New York, 1970.

B.3 Examples of Constitutive Relations at Elevated Temperature

Relations for the effect of elevated temperature on modulus of elasticity of rebars have been proposed [B.10]. The elastic modulus at elevated temperature can be estimated from:

$$E_s^T = E_s/[1.03 + 7(T-20)^6 x 10^{-7}] \tag{B.10}$$

where E_s^T and E_s are the elastic modulus of rebar at elevated and room temperature, respectively. The elastic modulus after high temperature exposure can be estimated from [B.10]:

$$E_s^T = (1.0011 - 0.0249T/100)E_s. \tag{B.11}$$

Stress-strain relationships for rebars at high temperatures have been proposed [B.10]:

$$\varepsilon^T(\sigma, T) = \left(a + b\sigma/f_y\right)(T-20)^{1.15} \tag{B.12}$$

where a and b are parameters related to different types of rebar, and f_y is the yield strength of the rebar at room temperature. A relationship has also been proposed for the nominal yield strength of high strength wires at high temperatures [B.11]:

$$f_{0.2}^{T} = [1 - 5.07(T-20)x10^{-4}]f_{0.2} \qquad 20^{\circ} < T \leq 300^{\circ}C \qquad (B.13)$$

$$f_{0.2}^{T} = [1.56 - 2.51(T-20)x10^{-3}]f_{0.2} \qquad 300^{\circ} < T < 600^{\circ}C \qquad (B.14)$$

where $f_{0.2}^{T}$ and $f_{0.2}$ are the nominal yield strength corresponding to 0.2% residual strain at elevated and room temperature, respectively.

Eurocode ENV 1993-1-2 provides the following relation for thermal conductivity (λ_a) (W/m $^{\circ}$C), thermal diffusivity (a_a) (m^2/hr), and specific heat (c_a) (J/kg$^{\circ}$C) of steel [B.12]:

$$\lambda_a = 54 - 3.33x10^{-2}\theta_a \quad \text{for } \theta_a \leq 800^{\circ}C, \qquad (B.15)$$

$$\lambda_a = 27.3 \quad \text{for } \theta_a > 800^{\circ}C, \qquad (B.16)$$

$$a_a = 0.87 - 0.84x10^{-3}\theta_a \quad \text{for } \theta_a \leq 750^{\circ}C, \qquad (B.17)$$

$$c_a = 425 + 0.773\,\theta_a - 1.69 \times 10^{-3}\,\theta_a^{2} + 2.22 \times 10^{-6}\,\theta_a^{3} \quad \text{for } 20^{\circ} < \theta_a \leq 600^{\circ}C, \qquad (B.18)$$

$$c_a = 666 + \frac{13002}{738 - \theta_a} \quad \text{for } 600^{\circ} < \theta_a \leq 735^{\circ}C, \qquad (B.19)$$

$$c_a = 545 + \frac{17820}{\theta_a - 731} \quad \text{for } 735^{\circ} < \theta_a \leq 900^{\circ}C, \text{ and} \qquad (B.20)$$

$$c_a = 650, \quad \text{for } 900^{\circ} < \theta_a \leq 1200^{\circ}C. \qquad (B.21)$$

B.4 References

B.1 *Properties of Materials at High Temperatures – Steel*, Y. Anderberg (Editor), Report LUTVDG/(TVBB-2008), Lund Institute of Technology, Sweden, February 1983.

B.2 T.Z. Harmathy and W.W. Stanzak, "Elevated-Temperature Tensile and Creep Properties of Some Structural and Prestressing Steels," *Fire Test Performance*, STP 464, American Society for Testing and Materials, West Conshohocken, Pennsylvania, pp. 186-208, 1970.

B.3 W. Zheng, Q. Hu, and H. Zhang, "Experimental Research on the Mechanical Property of Prestressing Steel Wire During and After Heating," *Frontiers in Architecture and Civil Engineering in China* **1**(2), pp. 247-254, 2007.

B.4 *Structural Fire Protection*, Manuals and Reports on Engineering Practice, No. 78, T.T. Lie (Editor), American Society of Civil Engineers, New York, New York, 1992.

B.5 M. Takeuchi, M. Hiramoto, N. Kumagai, N. Yamazaki, A. Kodaira, and K. Sugiyama, "Material Properties of Concrete and Steel Bars at Elevated Temperatures," *12th International Conference on Structural Mechanics in Reactor Technology*, Paper H04/4, pp. 133–138, Elsevier Science Publishers, North-Holland, The Netherlands, 1993.

B.6 P.D. Morley and R. Royles, "The Influence of High Temperature on the Bond in Reinforced Concrete," *Fire Safety Journal* **2**, pp. 243-255, 1979/1980.

B.7 J. Nikolaou and G.D. Papadimitriou, "Microstructures and Mechanical Properties After Heating of Reinforcing 500 MPa Class Weldable Steels Produced by Various Processes (Temcore, Microalloyed With Vanadium and Work-Hardened)," *Construction and Building Materials* **18**, pp. 243-254, 2004.

B.8 U. Schneider, C. Diererichs, and C. Ehm, "Effect of Temperature on Steel and Concrete for PCRV's," *Nuclear Engineering and Design* **67**, pp. 245–258, 1981.

B.9 *Manual of steel Construction*, 7th Edition, American Institute of Steel Construction, New York, New York, 1970.

B.10 T.G. Lv, *Experimental Investigation on Strength and Deformation of Steel Bars at Elevated Temperature*, Masters Thesis, Tsinghua University, 1996.

B.11 Y.J. Hua, *Research on Response and Resistance of Prestressed Concrete Structure in Fire*, PhD Thesis, Tongji University, 2000.

B.12 "Design of Steel Structures, General Rules, Structural Fire Design," *Eurocode 3*, ENV 1993-1-2, British Standards Institution, London, United Kingdom, 2005.